

UCLA

UCLA Electronic Theses and Dissertations

Title

Synthesis of Biodegradable Polymers via Metal Complexes Supported by Ferrocene Derived Schiff Base Ligands

Permalink

<https://escholarship.org/uc/item/9b51k8tf>

Author

Quan, Stephanie Mary

Publication Date

2017

Peer reviewed|Thesis/dissertation

UNIVERSITY OF CALIFORNIA

Los Angeles

Synthesis of Biodegradable Polymers
via Metal Complexes Supported
by Ferrocene Derived Schiff Base Ligands

A dissertation submitted in partial satisfaction of the
requirements for the degree Doctor of Philosophy
in Chemistry

by

Stephanie Mary Quan

2017

© Copyright by
Stephanie Mary Quan
2017

ABSTRACT OF THE DISSERTATION

Synthesis of Biodegradable Polymers
via Metal Complexes Supported
by Ferrocene-Derived Schiff Base Ligands

by

Stephanie Mary Quan

Doctor of Philosophy in Chemistry

University of California, Los Angeles, 2017

Professor Paula Loredana Diaconescu, Chair

In the last few decades, biodegradable plastics have become more common, however, their application is restricted by their limited range of physical properties. To address this issue, new methods and catalysts are required to synthesize variations in the polymer microstructure. Ferrocene-derived Schiff base ligands can provide a redox switch to alter the selectivity of catalysts toward monomers to produce block copolymers. Here, we discuss the synthesis of (salfen)In(O^tBu) (salfen = 1,1'-di(2,4-di-*tert*-butyl-6-iminephenoxy)ferrocene) and its high activity with lactone monomers. Its polymerization rate of ϵ -caprolactone, δ -valerolactone and β -butyrolactone is currently among the fastest rates of group 13 catalysts (Chapter 1). The study of (salfan)Zr(O^tBu)₂ (salfan = 1,1'-di(2-*tert*-butyl-6-*N*-methylmethylenephenoxy)ferrocene) demonstrated redox-switchable copolymerization toward lactide and cyclohexene oxide. Using

$^{Ac}FeBAR^F$ as a chemical oxidant and $CoCp_2$ as a chemical reductant, ABA and BAB triblock copolymers were synthesized. The protons at the junctions of these blocks were carefully characterized using 2D NMR spectroscopy methods (Chapter 2). A more detailed study of $(salfan)Zr(O^tBu)_2$'s copolymerization mechanism with regard to its selectivity of monomers and propensity for side reactions was carried out experimentally and supported by DFT calculations by Junnian Wei (Chapter 3). The side reaction between oxidant and cyclohexene oxide was found to be significant in one-pot reaction conditions and an unusual temperature dependent polymerization of lactide by $[(salfan)Zr(O^tBu)_2][BAR^F]$ was found to occur after the polymerization of cyclohexene oxide. Initial investigations into the application of bulk electrolysis to circumvent the need for chemical oxidants and reductants are reported (Chapter 4). And through a collaboration with Spokoyny and coworkers, dodecaborate clusters were found to synthesize extremely high molecular weight polymers of cyclohexene oxide (Chapter 5). Finally, a number of small projects down tangential lines of inquiry surrounding this work are discussed (Appendix F).

The dissertation of Stephanie Mary Quan is approved.

Andrea Kasko

Heather Maynard

Paula Loredana Diaconescu, Committee Chair

University of California, Los Angeles

2017

This thesis is dedicated to my glovebox AMLES
who despite its multiple owners, undergraduates, and one small explosion
has been a dependable friend.

TABLE OF CONTENTS

Introduction	1
Chapter 1: Ring-opening Polymerization of Cyclic Esters by (salphen)In(O^tBu)	
1.1 Introduction	14
1.2 Results and Discussion	14
1.3 Conclusions	27
1.4 Experimental	27
1.5 Appendix A	33
References	62
Chapter 2: Redox-switchable Copolymerization of Cyclic Esters and Ethers by a Zirconium Complex	
2.1 Introduction	65
2.2 Results and Discussion	67
2.3 Conclusions	106
2.4 Experimental	107
2.5 Appendix B	116
References	193
Chapter 3: Mechanistic and Kinetic Observations of Redox-Switchable Copolymerization by (salfan)Zr(O^tBu)₂	
3.1 Introduction	197
3.2 Results and Discussion	198
3.3 Conclusions	211
3.4 Experimental	211
3.5 Appendix C	218
References	236
Chapter 4: Applications of Bulk Electrolysis to Redox-Switchable Catalysis	
4.1 Introduction	238
4.2 Results and Discussion	239
4.3 Conclusions	246
4.4 Experimental	247
4.5 Appendix D	250
References	252
Chapter 5: Polymerization of Epoxides by Dodecaborate	
5.1 Introduction	254
5.2 Results and Discussion	254
5.3 Conclusions	264
5.4 Experimental	264
5.5 Appendix E	267
References	320
Conclusions and Outlook	324

LIST OF TABLES AND FIGURES

Introduction

Figure 1. Degradation times of common plastic items (noaa.gov).	1
Figure 2. Polylactic acid life cycle.	2
Figure 3. Two methods to make PLA.	3
Figure 4. Redox-switchable polymerization of lactide by Long and coworkers.	4
Figure 5. Redox-switchable ROMP catalysts developed by the Plenio and Bielawski.	5
Figure 6. Redox-switchable ring-opening polymerization catalysts by Okuda and Byers.	6
Figure 7. Redox switchable behavior of (phosfen)Y(OtBu) and (phosfen)In(OPh).	7
Figure 8. In situ redox-switchable copolymerization of LA and CL by (thiolfan*)Ti(O ⁱ Pr) ₂ .	8
Figure 9. Palladium and aluminum redox-switchable catalysts published by the Diaconescu and coworkers.	9
Figure 10. Redox-switchable copolymerization of CHO and LA by Fe(PDI)(4-methoxyphenoxide) ₂ .	10

Chapter 1

Scheme 1.1. Synthesis of (salfen)In(O ^t Bu).	15
Figure 1.1. Thermal-ellipsoid (50% probability) representation of (salfen)InCl.	16
Figure 1.2. Cyclic voltammogram of 1.0 mM (salfen)InCl.	17
Figure 1.3. Cyclic voltammogram of 1.0 mM (salfen)In(O ^t Bu).	17
Table 1.1. Polymerization of L-lactide (LLA), <i>rac</i> -lactide (DLLA), and trimethylene carbonate (TMC) by (salfen)In(O ^t Bu).	18
Figure 1.4. ¹ H{ ¹ H} NMR spectrum of PLA and calculation of P _m .	19
Table 1.2. Polymerization of ε-caprolactone by (salfen)In(O ^t Bu).	21
Table 1.3. Polymerization of δ-valerolactone (VL) by (salfen)In(O ^t Bu).	22
Table 1.4. Polymerization of β-butyrolactone by (salfen)In(O ^t Bu).	23
Figure 1.5. ¹³ C NMR spectrum of PHB and calculation of P _m .	24
Table 1.5. Polymerization of ε-caprolactone (CL) and δ-valerolactone (VL) by (salfen)In(O ^t Bu) at different temperatures.	25
Figure 1.6. Polymerization of 50 equivalents of <i>rac</i> -lactide over 200 minutes.	26
Figure 1.7. Polymerization of 50 equivalents of <i>rac</i> -lactide, first 50 minutes.	26

Chapter 2

Equation 2.1. One-pot polymerization of LA and CL by thiolfan* titanium complex.	66
Table 2.1. Polymerization of different monomers with (salfan)Zr(O ^t Bu) ₂ (red) and [(salfan)Zr(O ^t Bu) ₂][BAR ^F ₄] (ox).	68
Figure 2.1. Polymerization of cyclohexene oxide by (salfan)Zr(OtBu) ₂ . Polymerization is switched off by the addition of ^{Ac} FcBAR ^F and switched on by the addition of CoCp ₂ .	69
Figure 2.2. Conversion of L-lactide versus M _n by (salfan)Zr(OtBu) ₂ .	70
Figure 2.3. Conversion of cyclohexene oxide versus M _n by [(salfan)Zr(O ^t Bu) ₂][BAR ^F ₄].	71
Figure 2.4. Conversion of 100 equivalents of L-lactide to PLA vs time with (blue) and without (orange) 100 equivalents of cyclohexene oxide.	72
Figure 2.5. Conversion of 100 equivalents of cyclohexene oxide to PCHO vs time with (blue) and without (orange) 100 equivalents of L-lactide.	72

Table 2.2. One-pot copolymerization of two different monomers by (salfan)Zr(O ^t Bu) ₂ (red) or [(salfan)Zr(O ^t Bu) ₂][BAr ^F ₄] (ox).	73
Figure 2.1. Comparison of GPC traces for a PCHO homopolymer (Table 2.2, entry 11) and a PCHO-PLA copolymer (Table 2.2, entry 12).	74
Scheme 2.1. Possible side reactions during the oxidation of (salfan)Zr(O ^t Bu) ₂ in the presence of CHO.	75
Table 2.3. Screening of oxidants for in situ switching between (salfan)Zr(O ^t Bu) ₂ and [(salfan)Zr(O ^t Bu) ₂][BX ₄].	77
Table 2.4. Formation of block copolymers by redox switchable catalysis using (salfan)Zr(O ^t Bu) ₂ (red) or [(salfan)Zr(O ^t Bu) ₂][BAr ^F ₄] (ox).	78
Table 2.5. Comparison of PLA and PCHO homopolymers and block copolymers.	80
Table 2.6. Results of selective precipitation of a PLA-PCHO diblock copolymer.	82
Table 2.7. Results of selective precipitation of a PLA-PCHO-PLA triblock copolymer.	83
Table 2.8. Results of selective precipitation of a PCHO-PLA diblock copolymer.	84
Table 2.9. Results of selective precipitation of a PCHO-PLA-PCHO triblock copolymer.	85
Figure 2.7. DOSY maps of a mixture of PLA and PCHO homopolymers, PLA-PCHO diblock copolymer, PLA-PCHO-PLA triblock copolymer, PCHO-PLA diblock copolymer, PCHO-PLA-PCHO triblock copolymer.	87
Table 2.10. Formation of low weight block copolymers by redox switchable catalysis using (salfan)Zr(O ^t Bu) ₂ (red) or [(salfan)Zr(O ^t Bu) ₂][BAr ^F ₄] (ox) and sequential monomer addition.	88
Figure 2.8. Top: ¹ H NMR (300 MHz, 25 °C, C ₆ D ₆) spectrum of the purified PLA-PCHO polymer obtained by polymerization of 100 equivalents of L-lactide and cyclohexene oxide, monomers added sequentially, using initiator redox switch “red-ox”. Bottom: Magnified peaks to show the assignment of the protons corresponding to the junction between blocks.	89
Figure 2.9. Top: ¹ H NMR (300 MHz, 25 °C, C ₆ D ₆) spectrum of the purified PLA-PCHO-PLA polymer obtained by polymerization of 100 equivalents of L-lactide and cyclohexene oxide, monomers added sequentially, using initiator redox switch “red-ox-red”. Bottom: Magnified peaks to show the assignment of the protons corresponding to the junction between blocks.	90
Figure 2.10. Top: ¹ H NMR (300 MHz, 25 °C, C ₆ D ₆) spectrum of the purified PCHO-PLA polymer obtained by polymerization of 100 equivalents of cyclohexene oxide and L-lactide monomers added sequentially, using initiator redox switch “ox-red”. Bottom: Magnified peaks to show the assignment of the protons corresponding to the junction between blocks. *unable to assign. Some of the peaks showed correlations to LA methine carbons. HMBC inconclusive.	91
Figure 2.11. Top: ¹ H NMR (300 MHz, 25 °C, C ₆ D ₆) spectrum of the purified PCHO-PLA-PCHO polymer obtained by polymerization of 100 equivalents of cyclohexene oxide and L-lactide monomers added sequentially, using initiator redox switch “ox-red-ox”. Bottom: Magnified peaks to show the assignment of the protons corresponding to the junction between blocks. *unable to assign. Some of the peaks showed correlations to LA methine carbons. HMBC inconclusive.	92
Figure 2.12. Table 2.5, entry 1. Low molecular weight PLA-PHB copolymer. ¹ H NMR.	93
Figure 2.13. Table 2.5, entry 1. Low molecular weight PLA-PHB copolymer. ¹³ C NMR.	94

Figure 2.14. Table 2.5, entry 1. Low molecular weight PLA-PHB copolymer. HMBC ^1H - ^{13}C NMR.	94
Figure 2.15. Table 2.5, entry 1. Low molecular weight PLA-PHB copolymer. HSQC ^1H - ^{13}C NMR.	95
Figure 2.16. Table 2.5, entry 2. Low molecular weight PHB-PCHO. ^1H NMR.	96
Figure 2.17. Table 2.5, entry 2. Low molecular weight PHB-PCHO. ^{13}C NMR.	96
Figure 2.18. Table 2.5, entry 2. Low molecular weight PHB-PCHO. HMBC ^1H - ^{13}C NMR.	97
Figure 2.19. Table 2.5, entry 2. Low molecular weight PHB-PCHO. HSQC ^1H - ^{13}C NMR.	97
Figure 2.20. Table 2.5, entry 3. Low molecular weight PCHO-PLA. ^1H NMR.	99
Figure 2.21. Table 2.5, entry 3. Low molecular weight PCHO-PLA. ^{13}C NMR.	99
Figure 2.22. Table 2.5, entry 3. Low molecular weight PCHO-PLA. HMBC ^1H - ^{13}C NMR.	100
Figure 2.23. Table 2.5, entry 3. Low molecular weight PCHO-PLA. HSQC ^1H - ^{13}C NMR.	100
Figure 2.24. Table 2.5, entry 4. Low molecular weight PLA-PCHO. ^1H NMR.	101
Figure 2.25. Table 2.5, entry 4. Low molecular weight PLA-PCHO. ^{13}C .	102
Figure 2.26. Table 2.5, entry 4. Low molecular weight PLA-PCHO. HMBC ^1H - ^{13}C NMR.	102
Figure 2.27. Table 2.5, entry 4. Low molecular weight PLA-PCHO. HSQC ^1H - ^{13}C NMR.	103
Figure 2.28. Table 2.5, entry 5. Low molecular weight PLA-PCHO-PHB. ^1H NMR.	104
Figure 2.29. Table 2.5, entry 5. Low molecular weight PLA-PCHO-PHB. ^{13}C NMR.	104
Figure 2.30. Table 2.5, entry 5. Low molecular weight PLA-PCHO-PHB. HMBC ^1H - ^{13}C NMR.	105
Figure 2.31. Table 2.5, entry 5. Low molecular weight PLA-PCHO-PHB. HSQC ^1H - ^{13}C NMR.	105

Chapter 3

Figure 3.1. One-pot versus sequential monomer addition copolymerization.	198
Table 3.1. Selective precipitation of PLA-PCHO-PLA copolymer synthesized by the one-pot method.	199
Table 3.2. Selective precipitation of PCHO-PLA-PCHO copolymer synthesized by the one-pot method.	199
Table 3.3. Polymerization of LA and CHO by [(salfan)Zr(O ^t Bu) ₂][BAr ^F].	201
Figure 3.2. Potential reaction scheme of CHO cationic polymerization. “Zr” represents (salfan)Zr(O ^t Bu) ₂ , “Zr ⁺ ” represents [(salfan)Zr(O ^t Bu) ₂][BAr ^F].	201
Figure 3.3. Potential energy surfaces of the ROP of CHO by [(salfan)Zr(O ^t Bu) ₂][BAr ^F].	202
Figure 3.4. Polymerization of LA and CHO by [(salfan)Zr(O ^t Bu) ₂][BAr ^F].	203
Figure 3.5. Potential energy surfaces of the ROP of LA by (salfan)Zr(O ^t Bu) ₂ and [(salfan)Zr(O ^t Bu) ₂][BAr ^F].	204
Table 3.4 LA and CHO diblock copolymers synthesized by redox switchable catalysis.	206
Table 3.5. Conversion of LA or CHO and percentage of residual monomer in tetrablock copolymer.	207
Figure 3.6. Percent conversion versus time, with position in tetrablock copolymer for LA (top) and CHO (bottom).	208
Figure 3.7. Comparison of polymerization rates of LA (top) and CHO (bottom) with and without the presence of the other monomer.	209
Figure 3.8. Comparison of LA and CHO polymerization rates as first and second blocks in the synthesis of diblock copolymers made of 100 equivalents (top), 100 equivalents	

concentrated (upper middle), 50 equivalents (lower middle), and 25 equivalents (bottom) of each monomer. 210

Chapter 4

Figure 4.1. Electrolyte solution after nafion was immersed in it for 24 hours.	240
Figure 4.2. Cyclohexene oxide in the presence of TBAPF ₆ for 5.25 hours.	241
Figure 4.3. Polymerization of lactide by (salfan)Zr(O ^t Bu) ₂ under bulk electrolysis conditions.	241
Figure 4.4. Background scan of 100 mM TPABAr ^F in <i>o</i> -F ₂ C ₆ H ₄ .	242
Figure 4.5. Cyclohexene oxide and lactide in 100 mM TPABAr ^F in <i>o</i> -F ₂ C ₆ H ₄ .	242
Figure 4.6. Color change from yellow to brown to yellow as (salfan)Zr(O ^t Bu) ₂ (a) was oxidized (b) and reduced (c).	243
Table 4.1. Bulk electrolysis of (salfan)Zr(O ^t Bu) ₂ in the presence of LA and CHO.	245
Figure 4.7. Polymerization of LA and CHO by (salfan)Zr(O ^t Bu) ₂ oxidized and reduced by bulk electrolysis.	245
Figure 4.8. ¹ H NMR of H ₂ salfan-Me and LLA after 2 days at 100 °C. ¹ H	246

Chapter 5

Figure 5.1. Dodecaborate derivatives described in this chapter.	255
Figure 5.2. ¹ H NMR spectrum of (salfan)Zr(O ^t Bu) ₂ . Oxidation of (salfan)Zr(O ^t Bu) ₂ by 0.5 equivalents of F ₃₆ , then reduction by 0.5 equivalents of CoCp ₂ and then another 0.5 equivalents of CoCp ₂ . ¹¹ B NMR spectrum F ₃₆ ⁻¹ , F ₃₆ ⁻² .	256
Table 5.1. Polymerization of CHO by F ₃₆ .	258
Table 5.2. Polymerization of epoxide monomers by F ₃₆ .	259
Table 5.3. Polymerization of cyclic ethers by F ₆₀ .	260
Table 5.4. Polymerization of cyclic ethers with functionalized dodecaborates.	261
Figure 5.2. Conversion of CHO to PCHO over time by F ₃₆ .	262
Figure 5.3. Molecular weight of PCHO versus conversion.	263
Table 5.5. Aliquots from polymerization of CHO by F ₃₆ .	263

ACKNOWLEDGEMENTS

“If your Nerve, deny you / Go above your Nerve” –Emily Dickinson

As this is may be the most permanent published document I will probably ever get to write, I obviously put it to the last minute and wrote too much.

First, I'd like to thank my labmates Mark Abubekero and Jon Brosmer. Our camaraderie is a hard one to explain, and a weird one, but it is the glue that holds together my workdays. 1210 has become a place with many great memories, jokes, and shenanigans. Mark, thank you for being you and challenging me on a day to day basis. Your commiseration, humor, graciousness, and pep talks have been a great help. Jon, thank you for being the joy and frenzy that we all need. Our lab Summer Fridays and dance parties have been the highlights of my time here. Your playlists are on fire!

Over the years, I've had the opportunity to work closely with two fantastic undergraduate students. Jun Gao brought a wonderful spirit and meticulous style to our research. I hope you find that car ride that never ends. RJ Zhang always had the best questions and kept the glovebox running. His positivity and quick work will be missed. Best of luck with medical school!

Our current crop of undergraduates includes Yi Shen, Miranda Lowe, Madeline Riffel, James Ro, Alex Laughlin, Kevin Swartz, and Tate Reuter. Past undergraduates/visiting students have included Scott Shepard, Bianca Ramirez, Shisheng Shu, Tianyu Zhang, Nima Adhami, Arnaud Savoy, Arnaud Thevenon, Cindy Cao, Fawad Janjua and many others. Thank you for all of the laughs and questions. Thanks especially for abiding by the “Do not disturb. Thesis writing in progress” sign.

The 1st and 2nd year graduate students (and future of the lab) are Amy Lai, Ruxi Dai, and Zach Hern. Thanks for bringing in a fresh new energy. Take care of each other and the undergraduates. Also, the centrifuge in 1210 with the spinning metal top has tried to kill itself a few times by running into its own cord. You may want to tape it down.

Many former Diaconescu students have shaped the scientist I have become. Selma Duhovic taught me how to ask for space to focus and that all things are transient. Kevin Miller jammed and began dance parties when group meeting got cancelled. Wenliang Huang encouraged me to keep my head up and keep working through the tough times. Xinke (Kirk) Wang inspired me with his skill and believed in my ability to grow as a scientist. Junnian Wei made all problems feel somehow multifaceted and trivial with his lighthearted attitude and intelligence.

The person who has been most formative to my training has been, of course, Paula Diaconescu. Her tough style has reshaped me, unwillingly at times, to become a more rigorous scientist. As a mentor, she has also evolved tremendously over the past 6 years and has become a great source of encouragement, trusting and giving me the space to pursue my own lines of inquiry.

My sisters Trisha and Eva have been an unending source of support and love. Our group conversations are always the best and I don't know what I would do without you two. No one

else seems to want debate tax reform loudly in an Argentinian airport or send endless cat pictures.

I'd like to thank my mom and dad who tolerated me through what has been a rather incomprehensible process for them. Between offering grocery money and words of encouragement, your consistent efforts to help are wonderful. I am happy to have you two on my side.

Robert Jordan, thank you for cheering the loudest when I am climbing my hardest. Your open-mindedness and passion for science have been such positive force in my life. I look forward to talking more science and climbing more mountains with you.

Tristin Rose is many things: brilliant chemist, roommate, cyclist, and fellow donut enthusiast. Her guidance on chemistry matters and insights have been invaluable over the last two years. And we still have money in the slush fund.

To my climbing friends Cait Decker, Michael Harrison, Kelsey Scharnhorst, Miles Painter, John Klopfer, Jen Fox, April McGuire, Byron Boon, Matt Kowal, Robert Thompson, Devan Schwartz, I am grateful to have share some of the greatest views and the best adventures with you. Nothing puts life into perspective quite like dangling off a rock face or enjoying the stars in a beautiful remote place.

This thesis would also not have been possible without support from my friend family: Sarah Donner, Sam Roberts, Rachel Lowdermilk, Matt Jacobs, Rob Trump, Adrienne Ho, Matt Thorton, Henning Fog, Kelley-Malyshev family, Sarah Agor, Kimi Traube, Danielle Wilmot, Emma Jacobs, Rachel Gibbons, Morgan Midgley, Morgan Whitcomb, Jessica Taboada, Juliana Lewis, Isaac Silverman, Richard Jordan, Nanette Jaranwattananon, Jannette Bloom, Dahlia Goldfeld, Tanya Brown, Manoj Dayaram and many others. The last 9 years in LA have been so massive, I can't process it all. Thank you for providing the couch I could sleep on, the afternoon of board games to distract me from research, the letters to take me to a new place, and the weekend beach days to remind me that there is so much more outside of chemistry grad school.

To Nanette Jaranwattananon, Byron Boon, Courtney Roberts, Graciela Negri, Eric Gharakhanian, Tejas Shah, and the other folks who started at UCLA in 2011: I'm a little late to this party, but I'm happy to have made it. Thanks for checking in and cheering me on! And Nanette, they should have never let us into those town halls.

Ana Ribas at CAPS who has been a great resource for the last few years. Our sporadic sessions have been wonderful for venting, rehashing and reframing all issues. Thank you.

Specific acknowledgements for this work:

Initial GPC characterizations were done at UCSB's Materials Research Laboratory. Rachel Behrens was extremely helpful in training me and assisting with GPC characterization.

Chapter 1 is a version of [S. M. Quan, P. L. Diaconescu, *Chem. Commun.*, 2015, **51**, 9643-9646. DOI: 10.1039/C5CC01312G].

Chapter 2 is a version of [S. M. Quan, X. Wang, R. Zhang, P. L. Diaconescu, *Macromolecules*, 2016, **49**, 6768-6778. DOI: 10.1021/acs.macromol.6b00997].

Chapter 2's idea and initial experiments were carried out by Xinke (Kirk) Wang. His pioneering work in new ligand design and endless work ethic set a very high standard for all of us to meet. For this publication, Rongjia Zhang was invaluable in the synthesis of salfan ligand as well as the characterization of the polymers by DSC and TGA.

Junnian Wei's calculations helped fill the gaps in story of (salfan)Zr(O^tBu)₂'s unique mechanism and increased our understanding of how our compounds initiate polymerization. Madeline Riffel assisted with the kinetic portion of this work and will be taking on the revisions.

Chapter 4's foray into electrochemistry would not have been possible without guidance from Brian Lydon of the Yang group. Their bulk electrolysis set up was a testing ground for many of the initial ideas. Ruxi Dai has since taken on some of the work and I look forward to seeing where he takes it. Good luck!

The dodecaborate polymerization work in Chapter 5 was initiated by Alex Spokoyny, Jon Axtell, and Marco Messina. Jon Axtell is particularly contributory in synthesizing the dodecaborate complexes and organizing meetings to share data. This data may be incorporated into a future publication.

The work as a whole was reviewed over countless hours and under less than desirable conditions by the wonder women of my committee: Paula Diaconescu, Heather Maynard, and Andrea Kasko. Thank you for all of your helpful and constructive comments.

Given the number of hours I spend any given week in the NMR room or MCTP lab, none of the 200 or so pages of supporting information in this dissertation would have been possible without the UCLA-MIC. Jane Strouse, Bob Taylor, Dafni Amirsakis, and Ignacio Martini have been "instrumental" in keeping these facilities running, teaching us new experimental methods, and supporting our research.

This work was financially supported by the NSF (CAREER Grant 0847735 and 1362999 to PLD and CHE-1048804 for NMR spectroscopy) and the John Simon Guggenheim Memorial Foundation. Some of the polymers from Chapter 1 were characterized by GPC at the MRL Shared Experimental Facilities in UCSB that is supported by the MRSEC Program of the National Science Foundation under award NSF DMR 1121053; a member of the NSF-funded Material Research Facilities Network.

VITA

EDUCATION

Columbia University 2008
B.A. Biochemistry

RESEARCH EXPERIENCE

University of California, Los Angeles 2011 – present
Advisor: Professor Paula Diaconescu

Columbia University, New York, NY
Advisor: Professor Scott Snyder 2007 – 2008
Advisor: Professor Gerard Parkin 2006 – 2007

AWARDS

Ralph and Charlene Bauer Research Award 2016
Hansen Dow Teaching Award 2012
Pfizer SURF-DOC Fellowship 2007

PUBLICATIONS

Stephanie M. Quan, Xinke Wang, Rhongjia Zhang, and Paula L Diaconescu, “**Redox-switchable Copolymerization of Cyclic Esters and Ethers by a Zirconium Complex**” *Macromolecules*, 2016, 49, 6768-6778.

Stephanie M. Quan and Paula L. Diaconescu, “**High activity of an indium alkoxide complex toward ring opening polymerization of cyclic esters**” *Chem. Commun.*, 2015, 51, 9643-9646.

Victoria K. Landry, Keliang Pang, Stephanie M. Quan and Gerard Parkin, “**Tetrahedral nickel nitrosyl complexes with tripodal [N₃] and [Se₃] donor ancillary ligands**” *Dalton Trans.*, 2007, 820-824.

Keliang Pang, Stephanie M. Quan, Gerard Parkin, “**Palladium complexes with Pd→B dative bonds**” *Chemical Commun.*, 2006, 5015-5017

PRESENTATIONS

American Chemical Society Spring National Meeting 2017
Southern California Organometallics Meeting 2016
American Chemical Society Spring National Meeting 2016
Southern California Organometallics Meeting 2015
American Chemical Society Spring National Meeting 2015
Southern California Organometallics Meeting 2013
American Chemical Society Undergraduate Poster Session 2008
Pfizer Summer Undergraduate Research Fellowship Ceremony
2007
Columbia University Summer Research Seminar
2007

TEACHING EXPERIENCE

University of California- Los Angeles

2011 – present

Teaching Assistant – 21 quarters

Mentor – 6 years

Harvard Westlake School

2008 – 2011

Columbia University

2006 – 2008

VOLUNTEERING

CNSI Nanoscience High School Outreach Program

2014 – 2015

Diaconescu Lab Safety Officer

2012 – 2015

Chandler Society for Undergraduate Chemistry- President

2004 – 2008

Introduction

1. Biodegradable plastics

In the last 100 years, plastic materials changed our standard of living. These polymers comprise a number of everyday objects from Styrofoam food containers to polyvinylchloride pipes. Despite their variety of structure and uses, most plastics are similar in two respects. Most are made from petroleum feedstocks and most outlive their intended lifetime (Figure 1).¹



Figure 1. Degradation times of common plastic items (noaa.gov).

Biodegradable plastics have emerged as a means to help shorten the degradation lifetimes of these items. There are generally two categories: traditional plastics infused with additives to help degradation, and bioplastics derived from biomass. The former was recently shown to be far less degradable than purported.² The latter has been shown to degrade readily within months.³ Bioplastics typically feature an ester linkage which provides a starting point for ring-opening polymerization as well as weak point for enzymatic or acid degradation. The most common bioplastic in production is polylactic acid (PLA, Figure 2). 800,000 tons of PLA were produced in 2013 and this number is projected to grow over the next few years.⁴

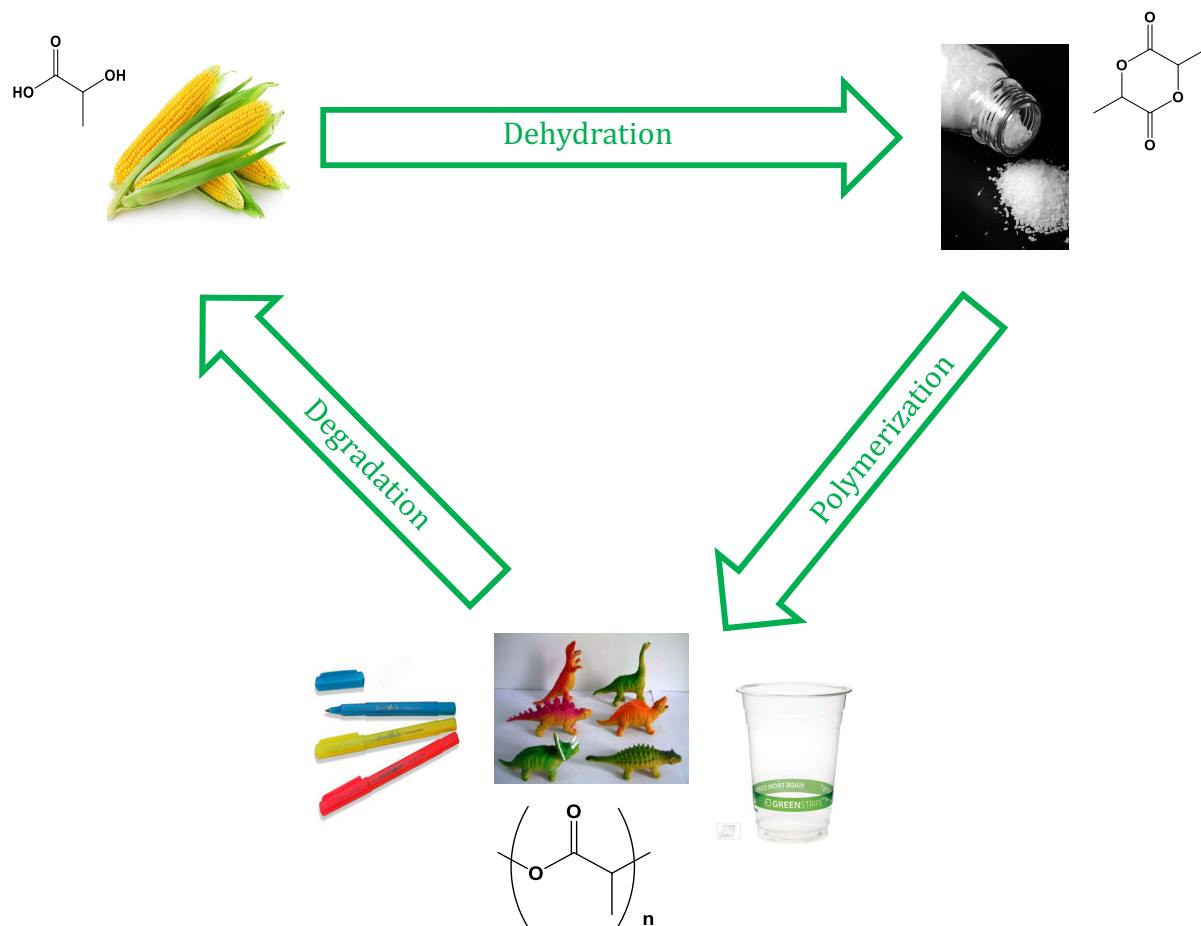


Figure 2. Polylactic acid life cycle. Lactic acid is derived from corn (top left) and dehydrated to form lactide monomer (top right). Lactide is then ring-open polymerized to form polylactic acid (PLA), which can be used for a variety of purposes (bottom). When PLA is discarded, it can be enzymatically or acid degraded into water, carbon dioxide, and other small molecules, which can be used toward future plant growth.

Despite the advantages of biodegradable plastics, these polyesters have a limited range of properties. PLA has a glass transition temperature between 60-65 °C,⁵ meaning it becomes rubbery when in contact with boiling water. Given the wide range of applications of traditional

petroleum based plastics, the restricted properties of PLA (as well as its cost) are barriers to this material becoming widespread.

There are several methods for tuning the properties of a polymer.⁶ On a molecular level, one can incorporate branching in the structure, alter the tacticity, or introduce another monomer to create alternating, block, gradient, or random copolymers. Block copolymers⁷ are of particular interest because their architecture is fundamentally separated from the reactivity of monomers. Furthermore, they can be altered both in block length and number of blocks to generate endless possibilities in structure.

Current industrial methods to make PLA utilize $\text{Sn}(\text{oct})_2$ (oct = 2-ethylhexanoate), an FDA⁸ approved catalyst for PLA food containers (Figure 3). Its moderate activity⁹ generates PLA with broad dispersity, which is advantageous in molding. For more specific uses of PLA, such as drug delivery or tissue scaffolding, more complex catalysts are employed. Aluminum salen (salen = *N,N'*-Ethylenebis(salicylimine)) complexes can synthesize isotactic PLA with high activity and low dispersity.¹⁰ The specificity of the generated polymeric structure in these systems helps make plastic materials with certain physical properties.

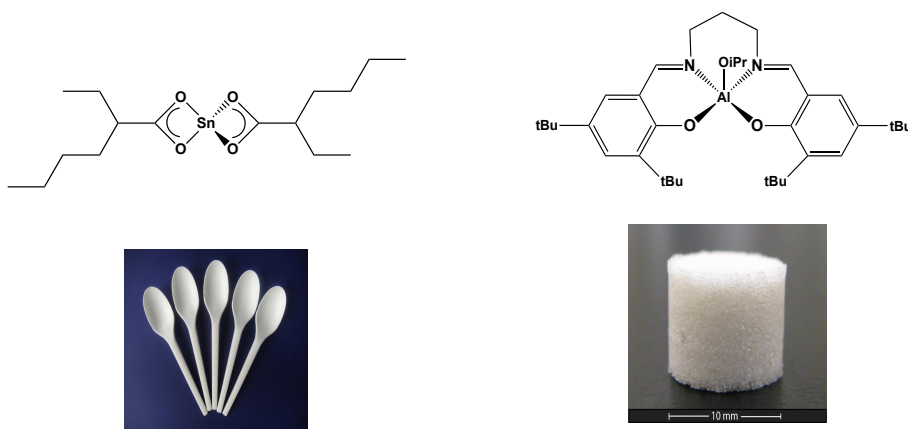


Figure 3. Two methods to make PLA. Industrially used $\text{Sn}(\text{oct})_2$ synthesizes atactic PLA for utensils (left) and $(\text{salen})\text{Al}(\text{O}^i\text{Pr})$ synthesizes syndiotactic PLA for tissue scaffolding (right).

2. Redox-switchable catalysis

To create block copolymer structures with biodegradable polymers, our group has focused its efforts on redox-switchable catalysis. The first reported examples of a redox-switchable polymerization was in 2006 by Long and coworkers.¹¹ Their titanium complex supported by an ethynylferrocene-substituted salicylaldimine ligand showed activity toward lactide in its reduced form. Upon the addition of silver triflate (AgOTf), the polymerization slowed down by an order of magnitude. Afterwards, when decamethylferrocene (Cp₂*Fe) reduced the complex, the polymerization rate returned to approximately the same proportion (Figure 4).

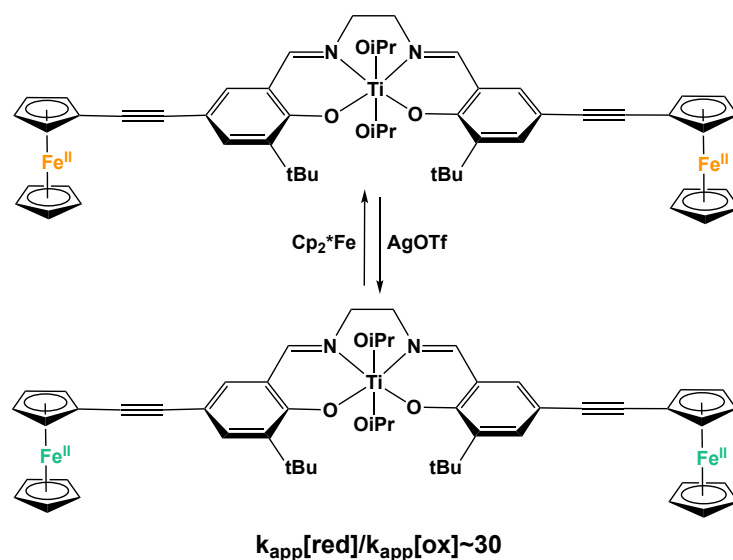


Figure 4. Redox-switchable polymerization of lactide by Long and coworkers.

Other notable examples in the last two decades include redox-switchable ring-opening metathesis polymerization (ROMP) catalysts by Plenio¹² and Bielawski¹³ (Figure 5). Plenio and coworkers synthesized *N*-Hoveyda-type ruthenium complexes with ferrocene support to demonstrate the responsiveness of the complex toward the polymerization of cis-cyclooctene (COE). For two of their new compounds, oxidation of the ferrocene could activate ROMP of

COE. Bielawski and coworkers found a similar phenomenon with their *N,N'*-dimethyldiaminocarbeneferrocenophane iridium and ruthenium Grubbs type catalysts. Oxidation of the iron center by 2,3-dichloro-5,6-dicyanoquinone lowered the ROMP rate of *cis,cis*-1,5-cyclooctadiene from 0.045 s^{-1} to 0.0012 s^{-1} . Reduction with decamethylferrocene returned ROMP rates to 0.016 s^{-1} .

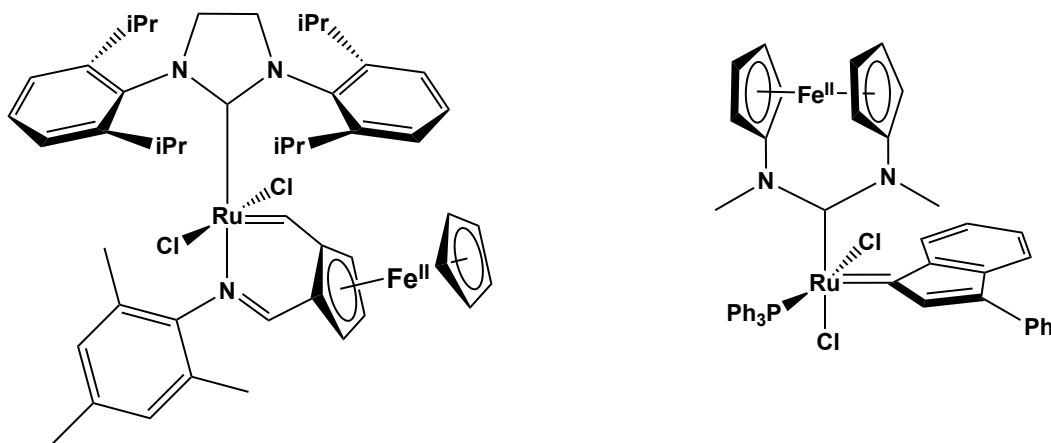


Figure 5. Redox-switchable ROMP catalysts developed by the Plenio (left) and Bielawski (right).

In the area of redox-switchable ring-opening polymerization, Okuda¹⁴ and coworkers synthesized cerium complexes with bis(phenolate)ligands (OSSO type) (Figure 6) that could change their activity toward lactide polymerization upon reduction of the cerium from a +4 to +3 oxidation state. This switch could be performed up to three times. Byers and coworkers¹⁵ developed a bis(imino)pyridine iron alkoxide complex (Figure 6) that performed redox-switchable copolymerizations with cyclic esters and cyclic ethers, expanding the range of possible monomers beyond lactones (see section below). For more information on switchable polymerization, please see the the Bielawski and coworkers' comprehensive review on the topic.¹⁶

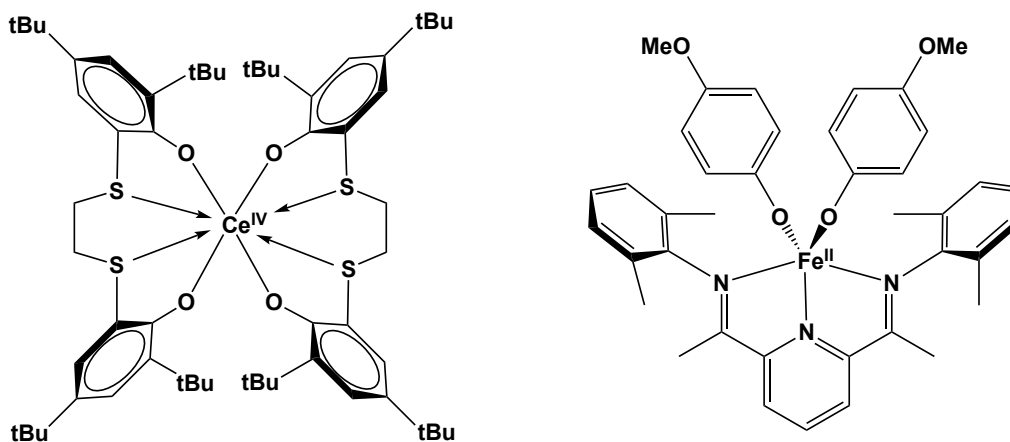


Figure 6. Redox-switchable ring-opening polymerization catalysts by Okuda (left) and Byers (right).

3. Ferrocene containing ligands

Ferrocene is an iron sandwich complex that was first discovered Kealy and Pauson¹⁷ in 1951 and characterized by Woodward, Wilkinson, and Fischer in 1952.¹⁸ Its robust and reversible oxidation and reduction have made it an ideal candidate for redox chemistry. One can utilize this redox event as a switch to turn on and off the reactivity of a reaction or alter the selectivity of a metal center. Fortunately, its relatively easy synthesis as well as its mass production led to a wealth of chemistry surrounding its alteration and incorporation into metal complexes¹⁹ that we could use toward developing redox-switchable polymerization catalysts.

4. Previous work by the Diaconescu lab

Erin Broderick initiated the redox-switchable polymerization project in 2009²⁰ with her synthesis of cerium ferrocene containing metal complexes based on Arnold's salfen ligand (salfen = 1,1'-di(2,4-di-tert-butyl-6-iminephenoxy)ferrocene).²¹ (salfen)Ce(O^tBu)₂ was found to polymerize lactide (LA).²² This polymerization rate could be modified by switching between the

cerium (III) and cerium (IV) species.²³ She also developed a new phosfen (1,1'-di(2-tert-butyl-6-diphenylphosphiniminophenoxy)ferrocene) ligand based on salfen that utilized a phosphimine bond in place of the imine in salfen. This ligand proved to be instrumental in finding another redox-switchable pair of catalysts.²⁴ (phosfen)Y(O^tBu) was shown to polymerize lactide (LA), cease activity when chemically oxidized by ^{Ac}FcBAr^F and return activity when chemically reduced by CoCp₂. On the other hand, (phosfen)In(OPh) polymerized trimethylene carbonate (TMC) in its oxidized state, but not in its reduced state. With these compounds, Broderick was able to show for the first time a true on/off switch with polymerization and orthogonal reactivity between two metal complexes and two monomers (Figure 7). This work was instrumental to the project described in Chapter 1 that although did not yield a redox-switchable catalyst, allowed us to discover a highly active catalyst for lactone polymerization.

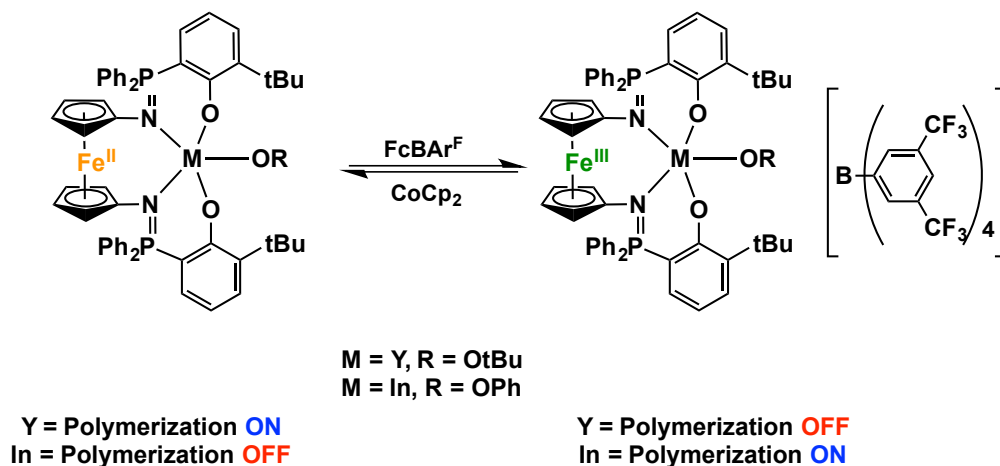


Figure 7. Redox-switchable behavior of (phosfen)Y(O^tBu) and (phosfen)In(OPh).

Xinke Wang continued this project by synthesizing three new variations of the salfen ligand and screening a number of various metal ligand combinations. His extensive work was summarized in a paper in 2014 that reported the first *in situ* redox switch for the polymerization of two different monomers.²⁵ In the presence of ϵ -caprolactone (CL) and lactide (LA), (thiofan*)Ti(OⁱPr)₂ (thiofan* = 1,1'-di(2,4-di-tert-butyl-6-thiohenol)ferrocene) polymerized LA

in the reduced state and, upon the addition of $\text{AcFcBAR}^{\text{F}}$, polymerized CL (Figure 8). This represented a big step toward a truly redox-reversible copolymerization. This work also revealed that one of the complexes, $(\text{salfan})\text{Zr}(\text{O}^t\text{Bu})_2$ ($\text{salfan} = 1,1'$ - di(2,4-di-tert-butyl-6-*N*-methylmethylenepheno)ferrocene), showed activity toward tetrahydrofuran, which led to a study of $(\text{salfan})\text{Zr}(\text{O}^t\text{Bu})_2$'s activity toward cyclic ethers as described in Chapter 2.

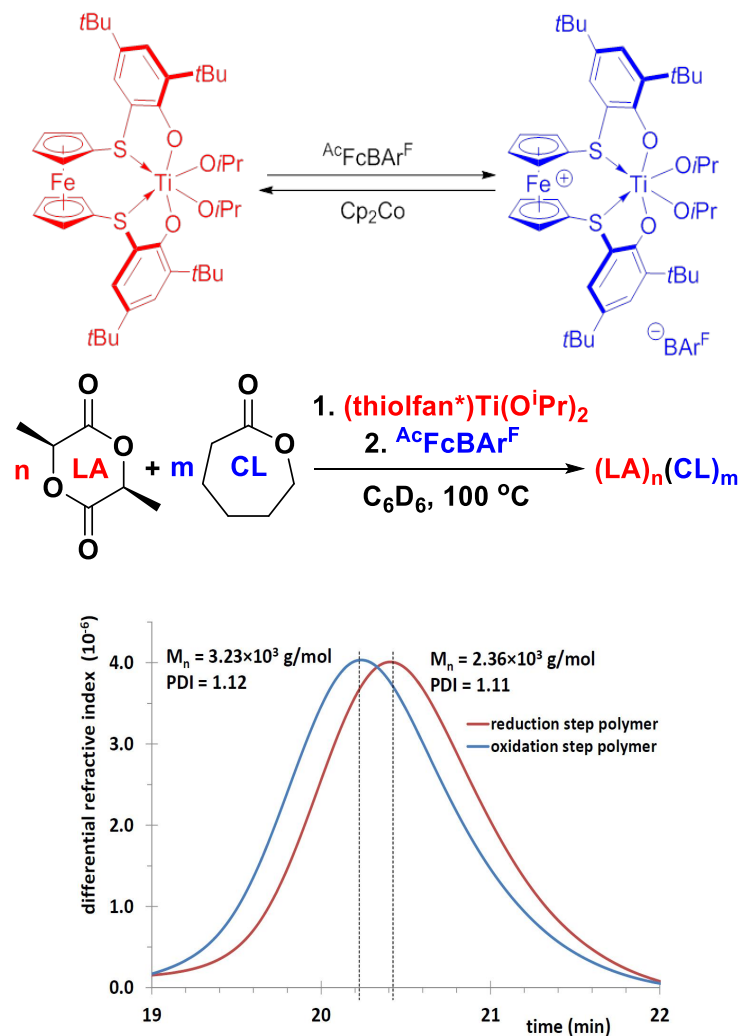


Figure 8. *In situ* redox-switchable copolymerization of LA and CL by $(\text{thiofanz}^*)\text{Ti}(\text{O}^i\text{Pr})_2$.

Concurrent to this work, several other publications on redox-switchable polymerization were published. From our own group, a Pd(II) heteroscorpionate complex was found to show switchable polymerization activity toward norbornene²⁶ and $(\text{thiofanz}^*)\text{Al}(\text{O}^t\text{Bu})_3$'s redox-

switchable activity toward lactones was examined using a combination of experimental and DFT methods (Figure 9).²⁷

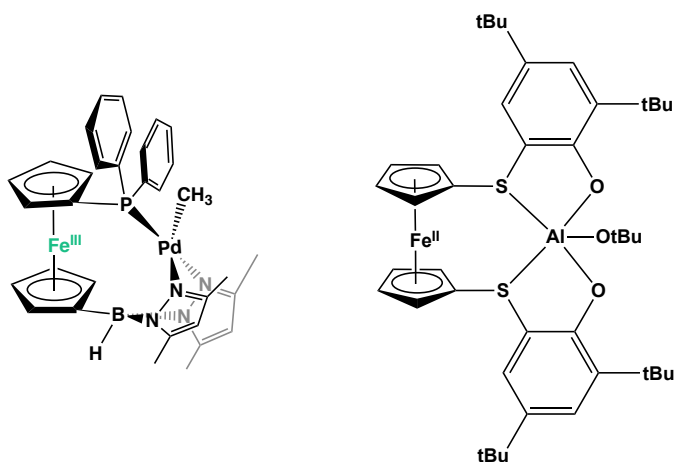


Figure 9. Palladium and aluminum redox-switchable catalysts published by the Diaconescu and coworkers.

More closely related to our work with (salfan)Zr(O^tBu)₂, Byers and coworkers in 2013 reported the redox-switchable polymerization activity of Fe(PDI)(4-methoxyphenoxy)₂ (PDI = 2,6-(2,6-Me₂-C₆H₃N=CMe)₂C₅H₃N).²⁸ Using ferrocenium hexafluorophosphate (FcPF₆) as an oxidant, and cobaltacene (CoCp₂) as a reductant, the bis(imino)pyridine iron alkoxide compound demonstrated polymerization growth with up to fifteen redox switches and sequential additions of monomer. The versatility of this catalyst was further demonstrated in 2016 when they described the first *in situ* redox-switchable copolymerization between cyclohexene oxide (CHO) and LA (Figure 10)²⁹ and applied this concept to an epoxide-functionalized cyclic diester to furnish cross-linking degradable polymers.³⁰

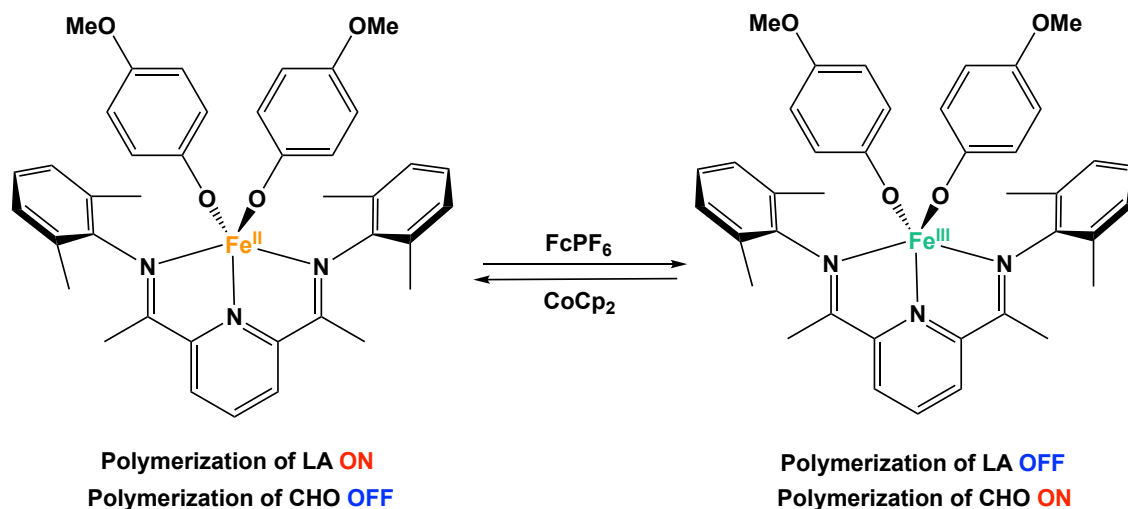


Figure 10. Redox-switchable copolymerization of CHO and LA by Fe(PDI)(4-methoxyphenoxide)₂.

5. This work

Herein, (salfen)In(O^tBu)'s remarkably high activity with cyclic esters and (salfan)Zr(O^tBu)₂'s redox-switchable polymerization with cyclic esters and cyclic ethers are described in Chapters 1 and 2. Both of these studies were published in 2014³¹ and 2016.³² An extension of the mechanism of the copolymerization activity of (salfan)Zr(O^tBu)₂ is elucidated in Chapter 3 and preliminary work in the application of bulk electrolysis methods toward redox-switchable catalysis is reported in Chapter 4. Chapter 5 is a departure from ferrocene-containing ligands and describes the high activity of dodecaborates toward cyclohexene oxide. This project was done in collaboration with the Spokoyny and coworkers at UCLA and was tangential to the oxidant screenings described in Chapter 2. Lastly, Appendix F has a number of small successful reactions, which may be interesting starting points for future directions of study.

References

1. (a) J. R. Jambeck, R. Geyer, C. Wilcox, T. R. Siegler, M. Perryman, A. Andrady, R. Narayan, K. L. Law, *Science*, 2015, **347**, 768-771.
(b) B. Gewert, M. M. Plassmann, M. MacLeod, *Environ. Sci: Processes Impacts*, 2015, **17**, 1513-1521.
2. S. Selk, R. Auras, T. A. Nguyen, D. C. Aguirre, R. Cheruvathur, Y. Liu, *Environ. Sci. Technol.*, 2015, **49**, 3769-3777.
3. (a) G. Gorrası, R. Pantani, *Polym. Degrad. Stab.*, 2013, **98**, 1006-1014.
(b) L. Xu, K. Crawford, C. B. Gorman, *Macromolecules*, 2011, **44**, 4777-4782.
(c) Y. Tokiwa, B. P. Calabia, C. U. Ugwu, S. Aiba, *Int. J. Mol. Sci.*, 2009, **10**, 3722-3742.
(d) M. Agarwal, K. W. Koelling, J. J. Chalmers, *Biotech. Prog.*, 1998, **14**, 517-526.
4. Global and China Lactic Acid and Derivative Industry Report 2014-2016, Research in China, 2014.
5. A. Sodergard, M. Stolt, *Prog. Polym. Sci.*, 2002, **27**, 1123-116.
6. (a) I. Campbell, *Introduction to Synthetic Polymers, 2nd Ed.*, Oxford University Press, 2000.
(b) R. J. Young, P. A. Lovell, *Introduction to Polymers, 3rd Ed.*, CRC Press, 2011.
(c) M. P. Stevens, *Polymer Chemistry, An Introduction 3rd Ed.*, Oxford University Press, 1998.
(d) J. E. Mark, *Physical Properties of Polymers Handbook*, Springer New York, 2007.
(e) J. Brandrup, E. H. Immergut, E. A. Grulke, *Polymer Handbook, 4th Ed.*, Wiley, 2003.
7. (a) N. Hadjichristidis, M. Pitikalis, H. Iatrou, *Synthesis of Block Copolymers, Advances in Polymer Science*, 2005, **189**.
(b) V. Abetz, *Block Copolymers I, Advances in Polymer Science*, 2005, **189**.
(c) V. Abetz, *Block Copolymers II, Advances in Polymer Science*, 2005, **190**.
8. <https://www.accessdata.fda.gov>

9. P. DuBois, O. Coulembier, J. Raquez, *Handbook of Ring-Opening Polymerization*, Wiley-VCH, 2009.
10. H. Nomura, R. Ishii, M. Akajura, K. Aoi, *J. Am. Chem. Soc. Comm.*, 2002, **124**, 5938-5939.
11. C. K. A. Gregson, V. C. Gibson, N. J. Long, E. L. Marshall, P. J. Oxford, A. J. P. White, *J. Am. Chem. Soc.*, 2006, **128**, 7410–7411.
12. R. Savka, S. Foro, M. Gallei, M. Rehahn, H. Plenio, *Chem. - Eur. J.*, 2013, **19**, 10655–10662.
13. C. D. Varnado Jr., E. L. Rosen, M. S. Collins, V. M. Lynch, C. W. Bielawski, *Dalton Trans.* 2013, **42**, 13251–13264.
14. A. Sauer, J.-C. Buffet, T. P. Spaniol, H. Nagae, K. Mashima, J. Okuda, *Chem. Cat. Chem.*, 2013, **5**, 1088–1091.
15. A. B. Biernesser, B. Li, J. A. Byers, *J. Am. Chem. Soc.*, 2013, **135**, 16553–16560.
16. A. J. Teator, D. N. Lastovickova, C. W. Bielawski, *Chem. Rev.*, 2016, **116**, 1969-1992.
17. T. J. Kealy, P. L. Pauson, *Nature*, 1951, **168**, 1039.
18. (a) G. Wilkinson, M. Rosenblum, M.C. Whiting, R. B. Woodward, *J. Am. Chem. Soc.*, 1952, **74**, 2125-2126.
(b) E. O. Fischer, W. Pfab, *Zeitschrift fur Naturforschung*, 1952, **7**, 377-379.
19. (a) A. Togni, *Ferrocene: Homogeneous Catalysis, Organic Synthesis, Materials Science*, John Wiley and Sons, 2008.
(b) P. Stepnicka, *Ferrocene: Ligands, Materials and Biomolecules*, John Wiley and Sons, 2008.
20. E. M. Broderick, P. S. Thuy-Boun, N. Guo, C. S. Vogel, J. Sutter, J. T. Miller, K. Meyer, P. L. Diaconescu, *Inorg. Chem.*, 2011, **50**, 2870-2877.
21. A. Shafir, D. Fiedler, J. Arnold, *J. Chem. Soc., Dalton Trans.*, 2002, **0**, 555-560.
22. E. M. Broderick, P. L. Diaconescu, *Inorg. Chem.*, 2009, **48**, 4701-4706.
23. E. M. Broderick, N. Guo, T. Wu, C. S. Vogel, C. Xu, J. Sutter, J. T. Miller, K. Meyer, T. Cantat, P. L. Diaconescu, *Chem. Commun.*, 2011, **47**, 9897-9899.

24. E. M. Broderick, N. Guo, C. S. Vogel, C. Xui, J. Sutter, J. T. Miller, K. Meyer, P. Mehrkhodavandi, P. L. Diaconescu, *J. Am. Chem. Soc.*, 2011, **133**, 9278-9281.
25. X. Wang, A. Thevenon, J. L. Brosmer, I. Yu, S. I. Khan, P. Mehrkhodavandi, P. L. Diaconescu, *J. Am. Chem. Soc.*, 2014, **136**, 11264-11267.
26. M. Abubekеров, S. M. Shepard, P. L. Diaconescu, *Eur. J. Inorg. Chem.*, 2016, **15**, 2634-2640.
27. J. Wei, M. N. Riffel, P. L. Diaconescu, *Macromolecules*, 2017, **50**, 1847-1861.
28. A. B. Biernesser, B. Li, J. A. Byers, *J. Am. Chem. Soc.*, 2013, **135**, 16553-16560.
29. A. B. Biernesser, K. R. Delle Chiaie, J. B. Curley, J. A. Byers, *Angew. Chem.*, 2016, **55**, 5251-5254.
30. K. R. Delle Chiaie, L. M. Yablon, A. B. Biernesser, G. R. Michalowski, A. W. Sudyn, J. A. Byers, *Polym. Chem.*, 2016, **7**, 4675-4681.
31. S. M. Quan, P. L. Diaconescu, *Chem. Commun.* 2015, **51**, 9643-9646.
32. S. M. Quan, X. Wang, R. Zhang, P. L. Diaconescu, *Macromolecules*, 2016, **49**, 6768-6778.

CHAPTER 1. Ring-opening Polymerization of Cyclic Esters by (salphen)In(O^tBu)

1.1 Introduction

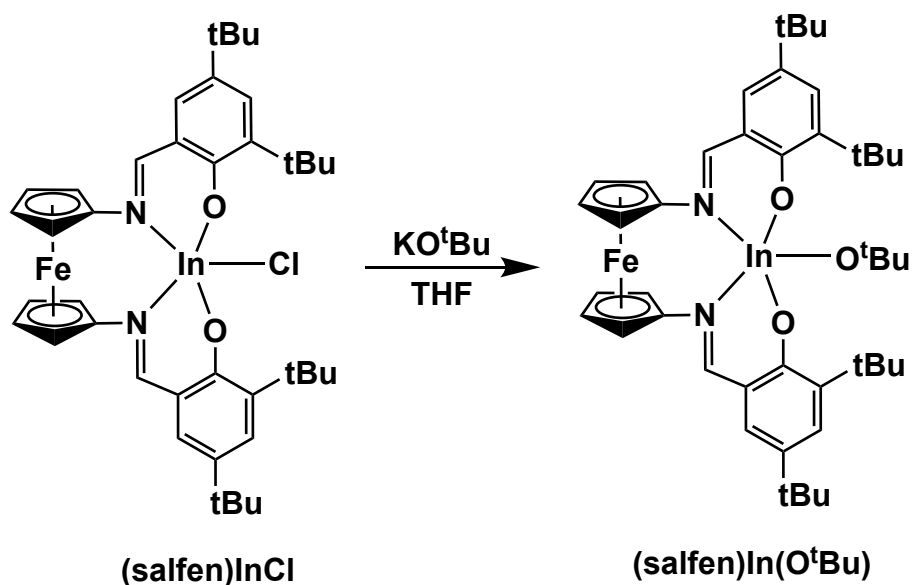
Over the past two decades, the ring-opening polymerization of cyclic esters has been increasingly studied because of its potential to produce biodegradable polymers from biomass.¹ Industrial applications of these polymers range from disposable plastic utensils to 3D printing and biomedical tissue scaffolding.² Of the numerous initiators developed toward this end, indium complexes have demonstrated high activity and stereoselectivity for a number of monomers.^{3–}¹³ Lactide polymerizations have been particularly well examined, but many of the initiators^{14–}²⁰ often require co-initiators. β -Butyrolactone,^{8,21} ϵ -caprolactone,²⁰ and trimethylene carbonate²² polymerizations have also been achieved using indium initiators. Though less studied, low initiator loadings²¹ and the potential range of monomers²³ make lactone and carbonate polymerizations a promising area toward finding new biodegradable polymers.

In our recent studies, a cerium complex supported by a Schiff base ligand with a ferrocene backbone polymerized L-lactide in a controlled fashion.²⁴ Phosphinimine analogues with yttrium and indium also demonstrated good activity in lactide and trimethylene carbonate polymerizations.²² Therefore, we decided to combine indium's activity with the Schiff base, a ferrocene-derived ligand in order to study the activity of the resulting complexes toward a broad range of cyclic ester polymerizations. Additional motivation was found from recent studies that point to the biocompatibility, robustness, and high activity of indium initiators in the ring opening polymerization of cyclic esters.^{10,25}

Herein, we report a ferrocene-derived Schiff base indium complex that possesses a remarkable range of activities toward cyclic esters and exceptionally fast polymerization rates

with lactones. Compound $(\text{salfen})\text{In}(\text{O}^t\text{Bu})$ ($\text{salfen} = 1,1'$ -di(2,4-di-*tert*-butyl-6-iminephenoxy)ferrocene) represents the first indium initiator capable of δ -valerolactone polymerization and the most active indium initiator to date in the polymerization of β -butyrolactone and ϵ -caprolactone. The polymerization rates of ϵ -caprolactone are even competitive with those of current industrial initiators.

1.2 Discussion



Scheme 1.1. Synthesis of $(\text{salfen})\text{In}(\text{O}^t\text{Bu})$.

Compound $(\text{salfen})\text{In}(\text{O}^t\text{Bu})$ was synthesized from the reaction of $(\text{salfen})\text{InCl}$ and freshly sublimed KO^tBu (Scheme 1.1). In turn, $(\text{salfen})\text{InCl}$ was synthesized by combining InCl_3 with $\text{K}_2(\text{salfen})$, which was generated from $\text{H}_2(\text{salfen})$ and two equivalents of KH . Needle crystals of $(\text{salfen})\text{InCl}$ were isolated from a diethyl ether solution. The solid state molecular

structure (Fig. 1.1) shows a distorted octahedral indium center and a THF molecule coordinated trans to the chloride ligand. Similar to the phosphinimine indium chloride analogue previously reported by us,²² a long In–Fe distance (3.98 Å) and a staggered configuration of the Cp rings were apparent. Elongation of the In–heteroatom distances compared to other compounds, such as (salen)InCl (salen = *N,N'*-bis(3,5-di-*tert*-butylsalicylidene)-1,2-cyclohexanediamine (*rac*- or (*R,R*)-H₂(ONNO)))⁹ and (phosfen)In(OPh) (phosfen = 1,1'-di(2-*tert*-butyl-6-diphenylphosphiniminophenoxy)ferrocene),²² by about 0.25 Å possibly compensates for the distortion caused by the staggered Cp rings.

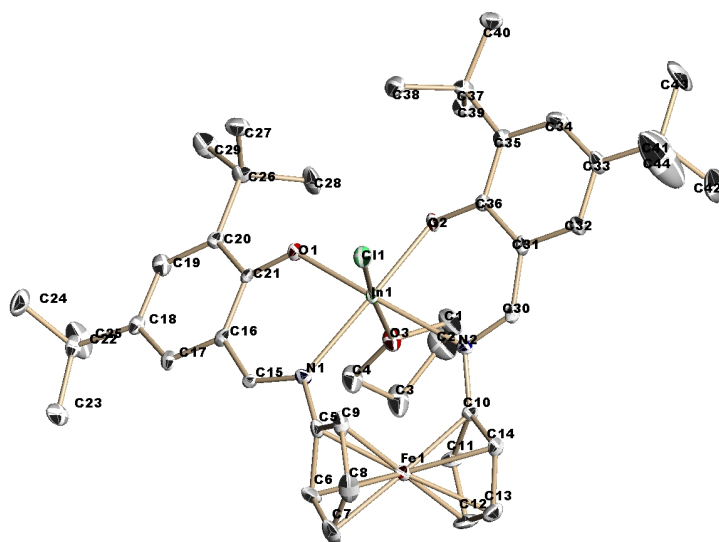


Figure 1.1. Thermal-ellipsoid (50% probability) representation of (salfen)InCl, hydrogen, disordered counterparts, and solvent atoms were removed for clarity.

Cyclic voltammograms of (salfen)InCl and (salfen)In(O^{*t*}Bu) revealed the compounds' redox events to be quasi-reversible and irreversible respectively (Figures 1.2 and 1.3).

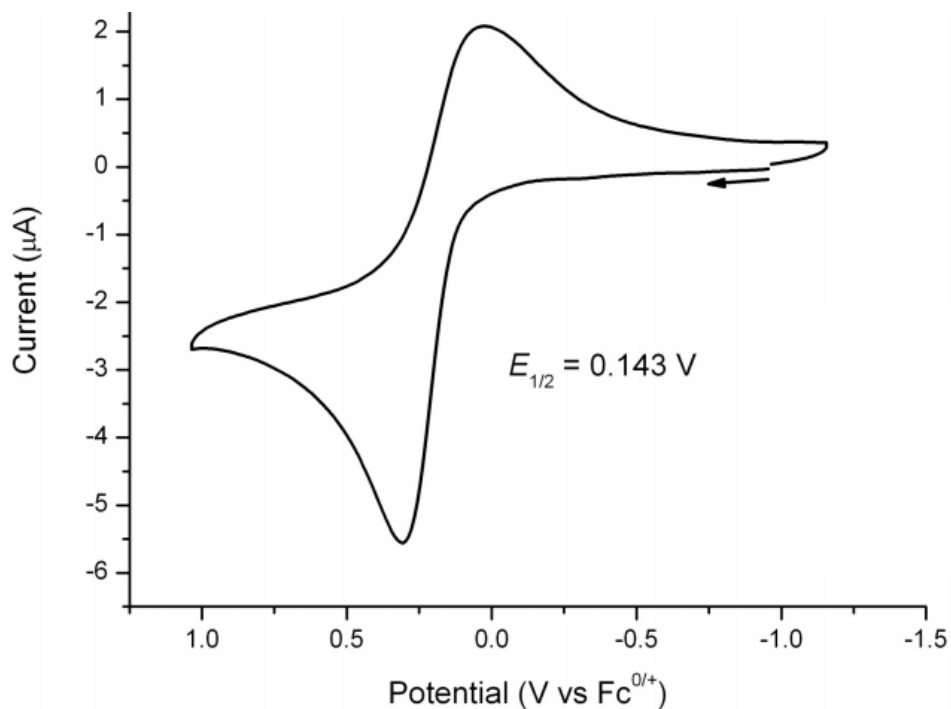


Figure 1.2. Cyclic voltammogram of 1.0 mM (salfen)InCl recorded with a glassy carbon electrode at 100 mV/s in THF, 0.010 M [(C₃H₇)₄N][BAR^F₄].

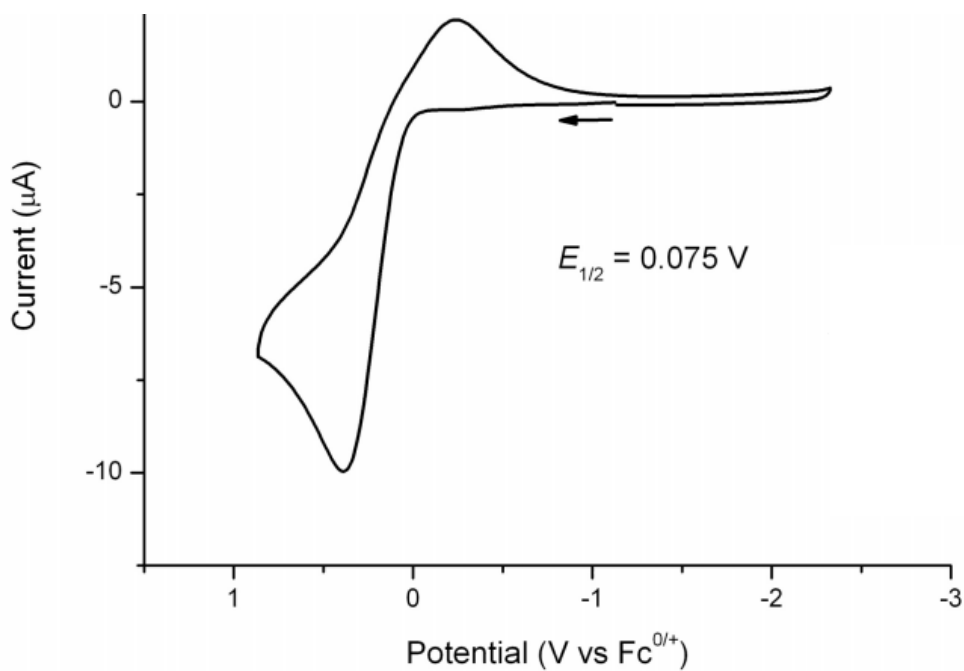
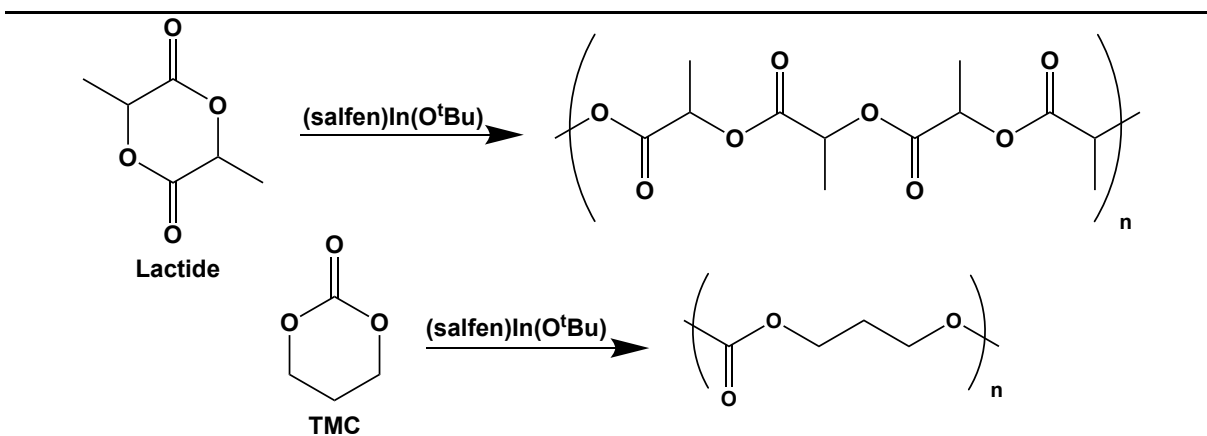


Figure 1.3. Cyclic voltammogram of 1.0 mM (salfen)In(O^tBu) recorded with a glassy carbon electrode at 100 mV/s in THF, 0.010 M [(C₃H₇)₄N][B[3,5-(CF₃)₂C₆H₃]₄].

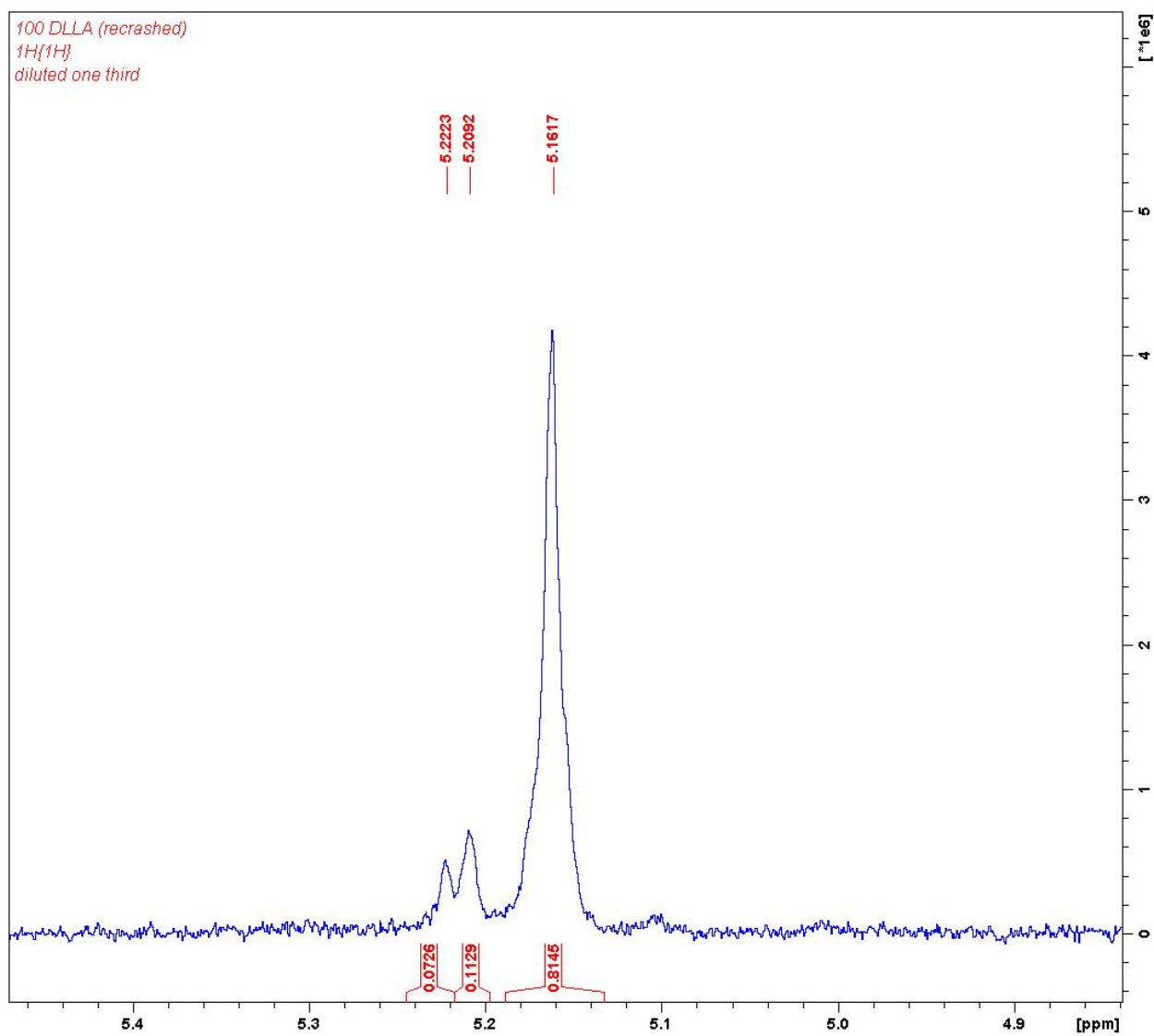
Compound (salfen)In(O^tBu) was evaluated for polymerization activity toward L-lactide, D,L-lactide, trimethylene carbonate, ε-caprolactone, δ-valerolactone, and β-butyrolactone. Reacting (salfen)In(O^tBu) with 100 equivalents of L-lactide led to 95% conversion of the monomer in 270 min (Table 1.1, entry 2); *D* values ranged from 1.06–1.16. D,L-Lactide showed a similar activity attaining 98% conversion in 280 minutes (Table 1.1, entry 4). A selectivity of $P_m = 0.52$ was determined using homodecoupled ¹H NMR spectroscopy and Bernoullian statistics (Figure 1.4) that is higher than that obtained for our previously reported (phosfen)Y(O^tBu) complex.²²

Table 1.1. Polymerization of L-lactide (LLA), *rac*-lactide (DLLA), and trimethylene carbonate (TMC) by (salfen)In(O^tBu).



Entry	Monomer	[M]/[I]	Time (min)	Conversion ^a (%)	$M_{n,theo}$ ^b	$M_{n,exp}$ ^c	D^d
1	LLA	50	120	97	8.4	15.9	1.12
2	LLA	100	270	95	15.1	32.8	1.16
3	DLLA	50	150	96	8.7	15.4	1.07
4	DLLA	100	280	98	17.5	32.2	1.06
5	TMC	50	5	95	4.0	28.1	1.75
6	TMC	100	10	94	6.8	39.7	1.70

Conditions: [I] = 0.005 M, room temperature, 1,3,5-trimethoxybenzene as the internal standard, and toluene as the solvent. ^a Conversion determined by ¹H NMR spectroscopy. ^b M_n reported in 10^3 g mol⁻¹. ^c Determined by GPC in chloroform calibrated *versus* polystyrene standards. See the note in the Appendix A about TMC. ^d $D = M_w/M_n$.



mmr/rmr = 5.22 ppm, 0.0726
 rmm = 5.21 ppm, 0.1129

$$[\text{rmr}] = P_r^2/2$$

$$[\text{mmr}] = (P_r P_m)/2$$

$$P_m = 0.59$$

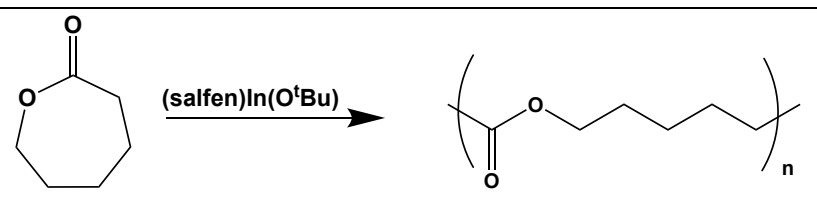
$$P_r = 0.38$$

Figure 1.4. $^1\text{H}\{^1\text{H}\}$ NMR (500 MHz, 25 °C, C_6D_6) spectrum of PLA and calculation of P_m .

Trimethylene carbonate was polymerized rapidly, reaching a full conversion of 100 equivalents in less than 10 minutes (Table 1.1, entry 6). Higher \bar{D} values (1.70–1.75) were observed though. Compared with our previous indium complex,²² which reached 49% conversion in one day, the present results represent considerable improvement. Aluminum initiators have achieved similar activity^{26–29} albeit at high temperatures. The highest conversions have been obtained using lanthanide complexes³⁰ and organoinitiators.²⁹

The polymerization of ϵ -caprolactone was particularly impressive. Compound (salfen)In(O^tBu) polymerized 1500 equivalents in five minutes (Table 1.2, entry 4), trapping the stir bar in a matrix of polymers. However, at higher monomer : initiator ratios, a plateauing of the polymer molecular weight was observed (Table 1.2, entries 4–7). Also, the polymerization of 2000 equivalents of ϵ -caprolactone took 20 minutes to reach completion. \bar{D} values ranged from 1.15 to 1.28 (Table 1.2). The activity of (salfen)In(O^tBu), which is capable of polymerizing 1500 equivalents in five minutes, is much faster than that of industrially used Sn(oct)₂.^{31,32}

Table 1.2. Polymerization of ϵ -caprolactone by (salfen)In(O^tBu).



Entry	[M]/[I]	Time (min)	Conversion ^a (%)	$M_{n,theo}$ ^b	$M_{n,exp}$ ^c	\bar{D} ^d
1	100	2	99	13.0	109.7	1.28
2	250	2	99	25.7	148.1	1.25
3	500	5	99	76.0	232.7	1.19
4	750	5	99	95.8	266.3	1.22
5	1000	5	99	106.3	298.1	1.16
6	1500	5	99	184.8	310.0	1.18
7	2000	20	99	233.6	322.5	1.15

Conditions: $[I] = 0.005$ M, room temperature, 1,3,5-trimethoxybenzene as the internal standard, and toluene as the solvent. ^a Conversion determined by ¹H NMR spectroscopy. ^b M_n reported in 10^3 g mol⁻¹. ^c Determined by GPC in chloroform calibrated *versus* polystyrene standards. ^d $\bar{D} = M_w/M_n$.

Encouraged by the ϵ -caprolactone polymerization results, (salfen)In(O^tBu) was tested for activity toward other lactone monomers. The polymerization of 100 equivalents of δ -valerolactone at room temperature in toluene reached over 90% conversion in a few minutes (Table 1.3, entry 1). Lowering the initiator loading to 0.1 mol% did not decrease the polymerization time (Table 1.3, entry 5). Like in the case of ϵ -caprolactone, the newly generated polymer locked the stir bar in a gel-like substance. \bar{D} values ranged from 1.38 to 1.46. Although aluminum alkoxide,^{33,34} thiolate,³⁵ and porphyrin³⁶ complexes have been known to polymerize δ -valerolactone since the 1990s, polymerizing over 200 equivalents within several hours has been rarely achieved. A recent aluminum complex has shown great promise, polymerizing up to 1250 equivalents in 30 minutes, albeit with \bar{D} values ranging between 1.93 and 4.89.³⁷ Organoinitiators have also demonstrated good activity with moderate control.³⁸ Our current initiator is the first indium complex capable of δ -valerolactone polymerization and

achieves faster activity and greater control than many current initiators. It should be noted that while the polymerization of other monomers proceeds under greater control, it is not necessarily a detriment to have slightly broad molecular weight distributions. Less controlled polymer mixtures exhibit elastic mechanical properties that can make them easier to produce and process.^{39,40}

Table 1.3. Polymerization of δ -valerolactone (VL) by (salfen)In(O^tBu).

Entry	[M]/[I]	Time (min)	Conversion ^a (%)	$M_{n,theo}$ ^b	$M_{n,exp}$ ^c	\mathcal{D} ^d
1	100	5	99	11.9	31.8	1.46
2	250	5	99	27.7	77.5	1.46
3	500	5	99	46.7	112.6	1.38
4	750	5	99	64.4	218.5	1.43
5	1000	5	99	87.7	190.3	1.43

Conditions: [I] = 0.005 M, room temperature, 1,3,5-trimethoxybenzene as the internal standard, and toluene as the solvent. ^a Conversion determined by ¹H NMR spectroscopy. ^b M_n reported in 10^3 g mol⁻¹. ^c Determined by GPC in chloroform calibrated *versus* polystyrene standards. ^d $\mathcal{D} = M_w/M_n$.

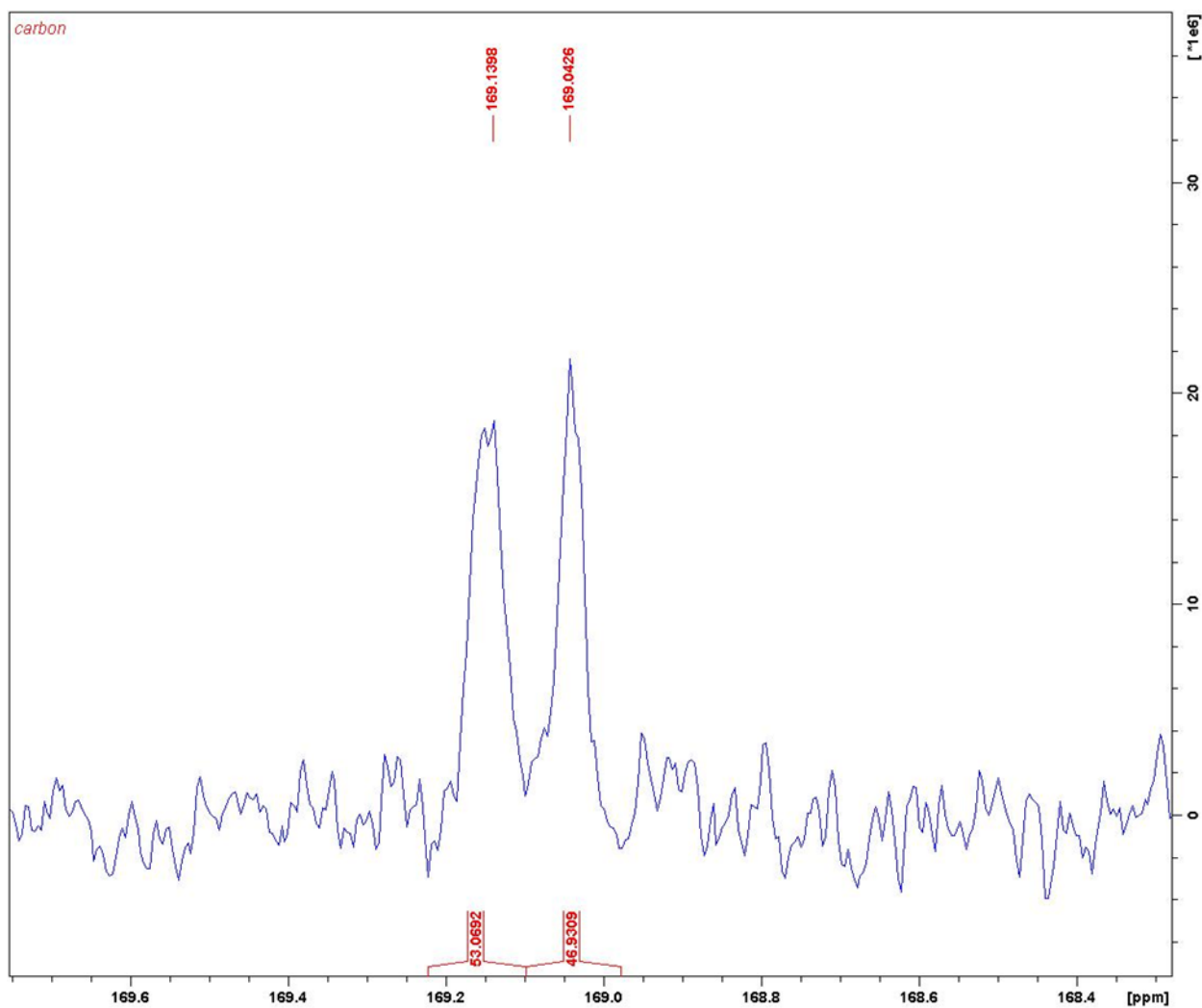
On the other hand, γ -butyrolactone showed no signs of polymerization after 4 days. Calculations by the Houk group have demonstrated that despite γ -butyrolactone having a strain energy of 8 kcal, the smaller geometric distortion in the ester group and the unusual stability of coiled polyhydroxybutyrate often renders γ -butyrolactone less likely to polymerize than δ -valerolactone.⁴¹

Furthermore, (salfen)In(O^tBu) showed an excellent polymerization activity with β -butyrolactone: 100 equivalents were polymerized in 30 minutes (Table 1.4, entry 1). Increasing the monomer amount to 500 equivalents resulted in a slower reaction, taking 60 minutes to reach full conversion. A similar decrease in activity has been observed using yttrium initiators.⁴² Most promisingly, these results indicate that (salfen)In(O^tBu) is the fastest among a group of 13 initiators for the polymerization of β -butyrolactone.^{43–46} Bernouillian statistics and NMR techniques were used to determine the selectivity of the process. The P_m value was found to be 0.47 (Figure 1.5), comparable to the value reported for other indium initiators.²¹ Low \mathcal{D} values ranging from 1.07 to 1.12 were found.

Table 1.4. Polymerization of β -butyrolactone by (salfen)In(O^tBu).

Entry	[M]/[I]	Time (min)	Conversion ^a (%)	$M_{n,theo}$ ^b	$M_{n,exp}$ ^c	\mathcal{D} ^d
1	100	30	99	10.4	15.1	1.08
2	200	45	99	17.3	27.8	1.07
3	300	45	99	27.2	31.2	1.10
4	400	60	99	34.4	43.9	1.08
5	500	60	99	42.8	47.2	1.12

Conditions: [I] = 0.005 M, room temperature, 1,3,5-trimethoxybenzene as the internal standard, and toluene as the solvent. ^a Conversion determined by ¹H NMR spectroscopy. ^b M_n reported in 10^3 g mol⁻¹. ^c Determined by GPC in chloroform calibrated *versus* polystyrene standards. ^d $\mathcal{D} = M_w/M_n$.



$r = 169.1$ ppm, 53.1
 $m = 169.0$ ppm, 46.9

$P_m = m/(r+m)$
 $P_m = 0.47$

For more detail on methods used see reference.⁵⁴

Figure 1.5. ^{13}C NMR (500 MHz, 25 °C, C_6D_6) spectrum of PHB and calculation of P_m .

Although the D values were low for all investigated monomers, there was a substantial difference between theoretical and experimental M_n values, though this difference diminished at high monomer/initiator ratios. It is possible that this difference is a consequence of using a

standard that is a different polymer (polystyrene) than the sample being tested.^{37,47–50} However, the large disparities between the theoretical and experimental molecular weights in the ϵ -caprolactone and δ -valerolactone polymerizations prompted further examination. Consequently, the polymerization of ϵ -caprolactone and δ -valerolactone was carried out at low temperatures. The resulting polymers yielded even larger molecular weights and \mathcal{D} values (Table 1.5). This indicated that some inhibition or retardation has led to the polymerization of just a few chains of very long polymers. Lowering the temperature likely prolonged the retardation period, initiating fewer chains, and amplifying the effect. A kinetic study of *rac*-lactide polymerization further confirmed a retardation period of the polymerization prior to the initiation and propagation of the polymer (Figures 1.6 and 1.7).

Table 1.5. Polymerization of ϵ -caprolactone (CL) and δ -valerolactone (VL) by (salphen)In(O^tBu) at different temperatures.

Entry	M	[M]/[I]	Temp. (°C)	Time (min)	Conversion ^a (%)	$M_{n,theo}$ ^b	$M_{n,exp}$ ^c	\mathcal{D} ^d
1	CL	100	22	2	99	13.0	109.7	1.28
2	CL	100	0	2	99	12.9	116.2	1.38
3	VL	100	22	5	99	11.9	31.8	1.46
4	VL	100	0	10	99	10.0	124.5	1.65

Conditions: [I] = 0.005 M, 1,3,5-trimethoxybenzene as the internal standard, and toluene as the solvent. ^a Conversion determined by ¹H NMR spectroscopy. ^b M_n reported in 10^3 g mol^{-1} . ^c Determined by GPC in chloroform calibrated *versus* polystyrene standards. ^d $\mathcal{D} = M_w/M_n$.

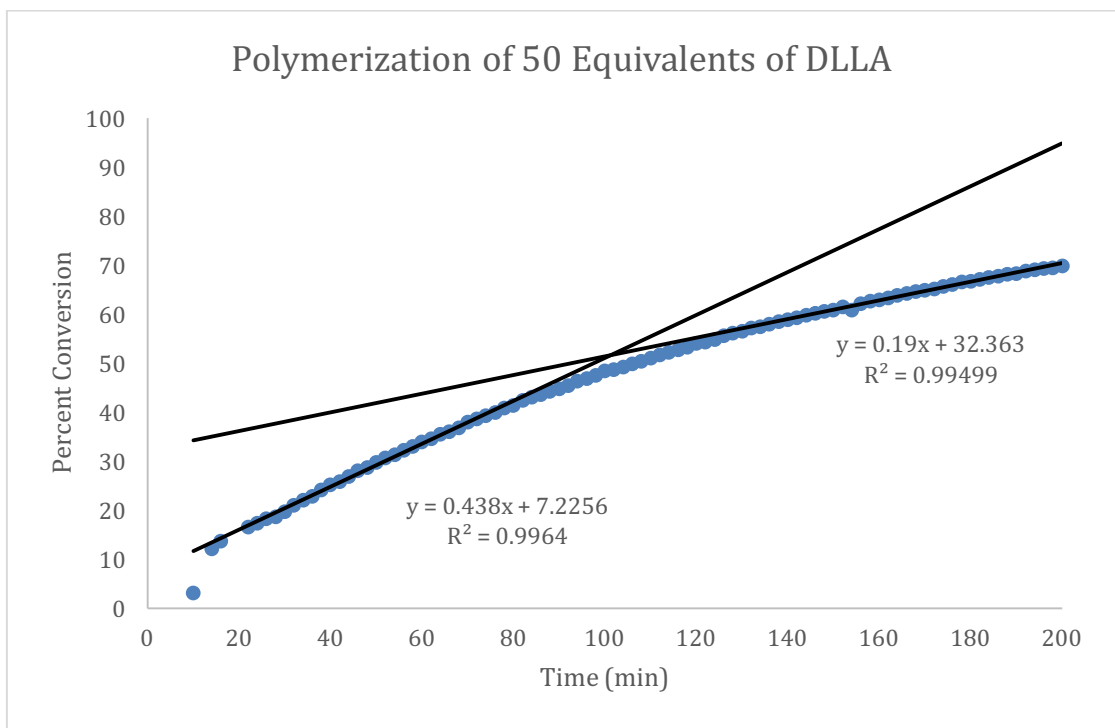


Figure 1.6. Polymerization of 50 equivalents of rac-lactide over 200 minutes

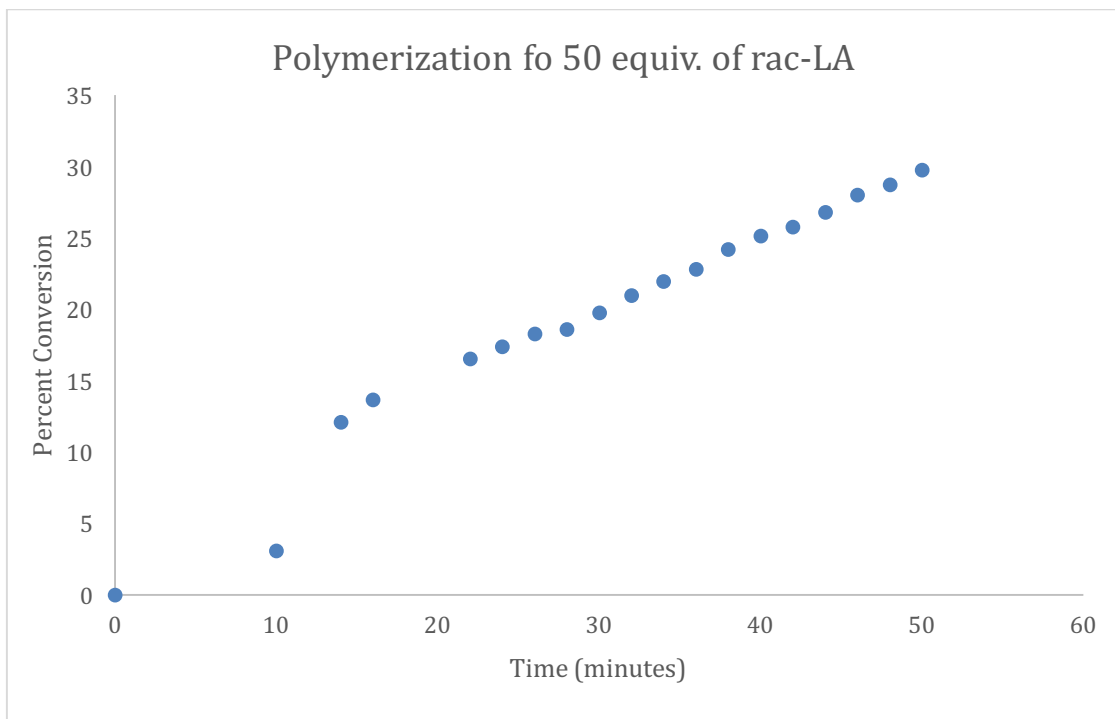


Figure 1.7. Polymerization of 50 equivalents of rac-lactide, first 50 minutes

1.3 Conclusions

In conclusion, two ferrocene-derived Schiff base indium complexes, (salfen)InCl and (salfen)In(O^tBu), were synthesized and characterized. Compound (salfen)In(O^tBu) was particularly impressive with lactone polymerizations in addition to being highly active toward lactide and carbonate polymerizations. Our results indicate that (salfen)In(O^tBu) showed unprecedented activity toward ϵ -caprolactone, δ -valerolactone, and β -butyrolactone leading to extremely high molecular weight polymers in minutes. To our knowledge, (salfen)In(O^tBu) is the fastest indium initiator for ϵ -caprolactone, δ -valerolactone, and β -butyrolactone and the first indium initiator for δ -valerolactone polymerization.

1.4 Experimental

General Considerations

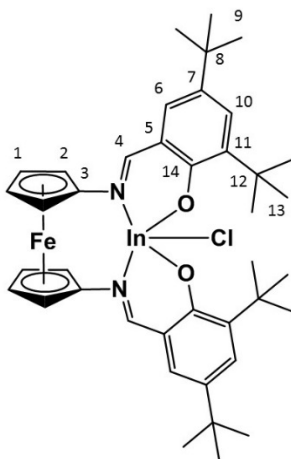
All experiments were performed under a dry nitrogen atmosphere using standard Schlenk techniques or an MBraun inert-gas glovebox. Solvents were purified using a two-column solid-state purification system by the method of Grubbs⁵¹ and transferred to the glove box without exposure to air. Liquid monomers were distilled over CaH₂ and brought into the glove box without exposure to air. Solid monomers and 1,3,5-trimethylbenzene were recrystallized from toluene at least twice before use. 2,4-di-*tert*-butylphenol, *n*-BuLi were purchased from Sigma Aldrich and used as received. InCl₃ was purchased from Alfa Aesar and used as received. H₂(salfen)⁵² was synthesized following previously published procedures. NMR solvents were obtained from Cambridge Isotope Laboratories, degassed and stored over activated molecular sieves prior to use. ¹H NMR spectra were recorded on Bruker 300, Bruker 400 or Bruker 500 spectrometers at room

temperature in C_6D_6 or $CDCl_3$. Chemical shifts are reported with respect to internal solvent, 7.16 ppm (C_6D_6) and 7.26 ppm ($CDCl_3$) for 1H NMR spectra. CHN analyses were performed on an Exeter Analytical, Inc. CE-440 Elemental Analyzer. Cyclic voltammetric studies were carried out in a 25 mL three neck round bottom flask with electrodes fixed in position by rubber stoppers, in a 0.10M [nPr_4N][BAR^F_4] ($Ar^F = 3,5-(CF_3)_2C_6H_3$) solution in tetrahydrofuran. A glassy carbon working electrode (planar circular area = 0.071 cm^2), a platinum reference electrode (planar circular area = 0.031 cm^2), and a silver-wire pseudo-reference electrode were purchased from CH Instruments. Cyclic voltammograms were acquired with a CH Instruments CHI630D potentiostat and recorded with CH Instruments software (version 13.04) with data processing on Origin 9.1. All potentials are given with respect to the ferrocene-ferrocenium couple. Molecular weights of the polymers were determined by GPC-LLS (Gel Permeation Chromatography, Laser Light Scattering). GPC-LLS uses an Agilent liquid chromatograph equipped with an Agilent 1200 series pump and autosampler, three Phenogel 5 μm Narrow Bore columns, a Wyatt Optilab differential refractometer, Wyatt Tristar miniDAWN and a Wyatt Viscostar viscometer. A flow rate of 1.0 mL/min was used and samples were dissolved in chloroform with 0.25% triethylamine. Results were calibrated to a narrow molecular weight polystyrene standards.

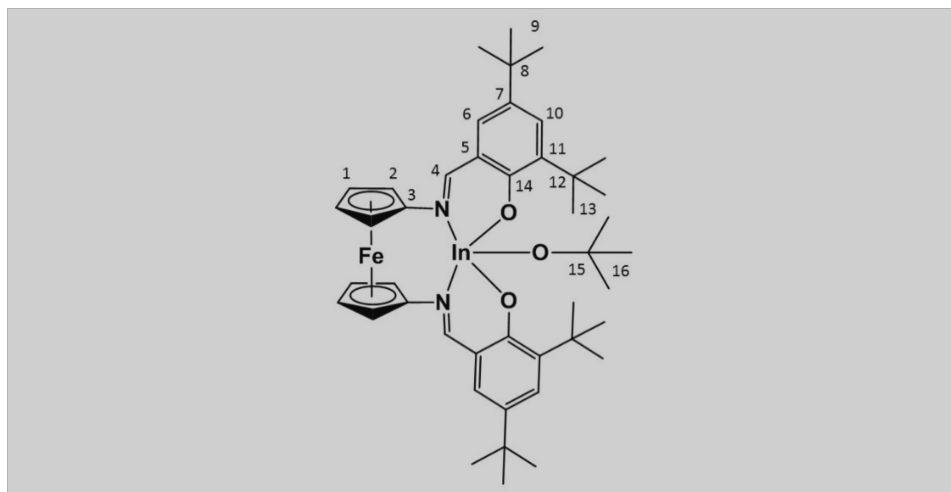
Synthesis of K_2 (salfen). A saturated THF solution of H_2 (salfen)⁵² (1.00 g, 1.54 mmol) was added dropwise to a THF slurry of KH (132 mg, 3.18 mmol) (2 equiv, 57% oil dispersion). Some bubbles were formed indicating the release of hydrogen gas. The solution was stirred for two h and then filtered through Celite. The volatiles were removed under reduced pressure. The obtained red solid was washed with hexanes over a

medium frit until the resulting liquid was clear. Yield: 1.02 g, 89%. ^1H NMR (300 MHz, 25 °C, C_6D_6), δ (ppm): 8.58 (s, 2H, PhH), 7.70 (s, 2H, PhH), 4.09 (t, 4H, CpH), 3.97 (t, 4H, CpH), 3.42 (s, 2H, CpH), 1.79 (s, 18H, CH_3), 1.48 (s, 18H, CH_3). A ^{13}C NMR spectrum could not be obtained due to solubility issues.

Synthesis of (salfen)InCl. A THF solution of $\text{K}_2(\text{salfen})$ (117 mg, 0.161 mmol) was added dropwise to a THF solution of InCl_3 (35.7 mg, 0.161 mmol). The solution was stirred for one hour. Volatiles were removed under reduced pressure. The crude product was dissolved in diethyl ether, the resulting solution filtered through Celite and cooled to -36 °C overnight. An orange solid precipitate was collected over a medium frit, washed with hexanes (2×2.5 mL) and then dried. The solid was dissolved in diethyl ether and recrystallized at -36 °C before further use. Additional product can be precipitated by concentrating the mother liquor and placing in the freezer. Yield: 97.5 mg, 79.5%. ^1H NMR (300 MHz, 25 °C, C_6D_6), δ (ppm): 7.80 (s, 2H, PhH), 7.77 (s, 2H, PhH), 6.75 (s, 2H, PhH), 4.71 (t, 4H, CpH), 3.97 (t, 4H, CpH), 3.64 (s, 2H, CpH), 1.85 (s, 18H, CH_3), 1.34 (s, 18H, CH_3). ^{13}C NMR (500 MHz, 25 °C, C_6D_6), δ (ppm): *see figure below* 173.52 (4), 171.00 (14), 143.24, 130.04, 117.91, 106.28 (3, 5, 7, or 11), 137.95 (6), 131.88 (10), 69.75, 67.99, 65.86, 64.99 (1, 2), 36.20 (12), 34.13 (8), 30.32 (13), 25.76 (9). Analysis for $\text{C}_{40}\text{H}_{50}\text{N}_2\text{O}_2\text{FeInCl}$: Calcd.: C, 60.28%; H, 6.32%; N, 3.52%. Found: C, 60.78%; H, 6.72%; N, 3.06 %.



Synthesis of (salfen)In(O^tBu). A THF solution of freshly sublimed KO^tBu (137.6 mg, 1.11 mmol) was added dropwise to a THF solution of (salfen)InCl (787 mg, 0.99 mmol). The solution was stirred for one hour. Volatiles were removed under reduced pressure. The crude product was dissolved in hexanes, filtered through Celite, and dried. The compound was recrystallized from hexanes twice before polymerization studies. Yield: 560 mg, 68%. ¹H NMR (300 MHz, 25 °C, C₆D₆), δ (ppm): 7.84 (s, 2H, PhH), 7.66 (s, 2H, PhH), 6.70 (s, 2H, PhH), 5.35 (t, 4H, CpH), 3.86 (t, 4H, CpH), 3.75 (s, 2H, CpH), 1.74 (s, 9H, OCH₃), 1.69 (s, 18H, CH₃) 1.27 (s, 18H, CH₃). ¹³C NMR (500 MHz, 25 °C, C₆D₆), δ (ppm): 173.30 (4), 170.77 (14), 142.52, 137.12, 118.12, 105.72 (3, 5, 7, 11), 130.99 (6), 129.72 (10), 69.26, 68.74, 67.91, (1, 2), 62.37 (15), 36.08 (12), 34.00 (8), 35.07 (16), 31.46 (13), 30.36 (9). Analysis for C₄₄H₅₉N₂O₃FeIn: Calcd.: C, 63.32%; H, 7.13%; N, 3.36%. Found: C, 63.60%; H, 7.21 %; N, 3.06%.



General Polymerization Procedure. In the glovebox, 1.5 mL of a 0.033 M monomer solution and 1.0 mL of a 0.010 M standard solution were added to a 20 mL scintillation vial. 1.0 mL of a 0.010 M initiator solution was added to the stirring solution. To monitor the polymerizations, 0.05 mL aliquots were taken and quenched with two drops of wet hexanes. Volatiles were removed under reduced pressure. Progress was monitored by ^1H NMR spectroscopy until conversion reached 95%. The polymerization was quenched with cold MeOH outside the box. The solution was stirred for ten minutes and filtered over a medium frit to collect solid polymer. The crude polymer was then dissolved in a minimum amount of CH_2Cl_2 and precipitated with cold MeOH until a pure white solid was obtained.

To increase $[\text{M}]:[\text{I}]$, larger amounts of monomer were used while maintaining 1.0 mL of 0.010M standard solution and 1.0 mL of 0.010M initiator solution. It should be noted that increasing the $[\text{M}]:[\text{I}]$ ratio was also attempted by decreasing the amount of standard and initiator solution. However issues with measuring small volumes accurately as well rapidly decreasing activity were encountered.

Large Scale Polymerization (CL, VL, BBL). 1.0 mL of a 0.010 M standard solution, followed by the addition of 1.0 mL of a 0.010 M initiator solution was added to neat monomer in a 20 mL scintillation vial. The rest of the procedure follows the general procedure given above.

Notes of valerolactone work up. Valerolactone polymers were precipitated with cold hexanes instead of cold methanol.

Notes on β -butyrolactone work up. Polyhydroxybutyrate was quenched with 0.5 mL of 1.5 M HCl in diethyl ether. Volatiles were removed under reduced pressure. The polymer was precipitated by methanol as an oily substance. The vial was dipped in liquid nitrogen quickly to solidify the polymer before decanting the supernatant liquid and drying under vacuum.

Kinetic study of rac-LA polymerization. NMR scale polymerization was prepared on a 1/10th scale in a J-young tube with C₆D₆ as a solvent. The sample tube was inserted into the probe of a DRX500 Bruker spectrometer. The command “multi_zgvd” was applied to collect one scan automatically every two min. The data was processed with the Topspin 3.0 program. The product concentration was measured by ¹H NMR (comparing the methylene peak adjacent to oxygen of the monomer to methylene peak adjacent to the oxygen of the polymer). The polymerization was monitored to about 70% conversion.

1.5 Appendix A

NMR Spectroscopy

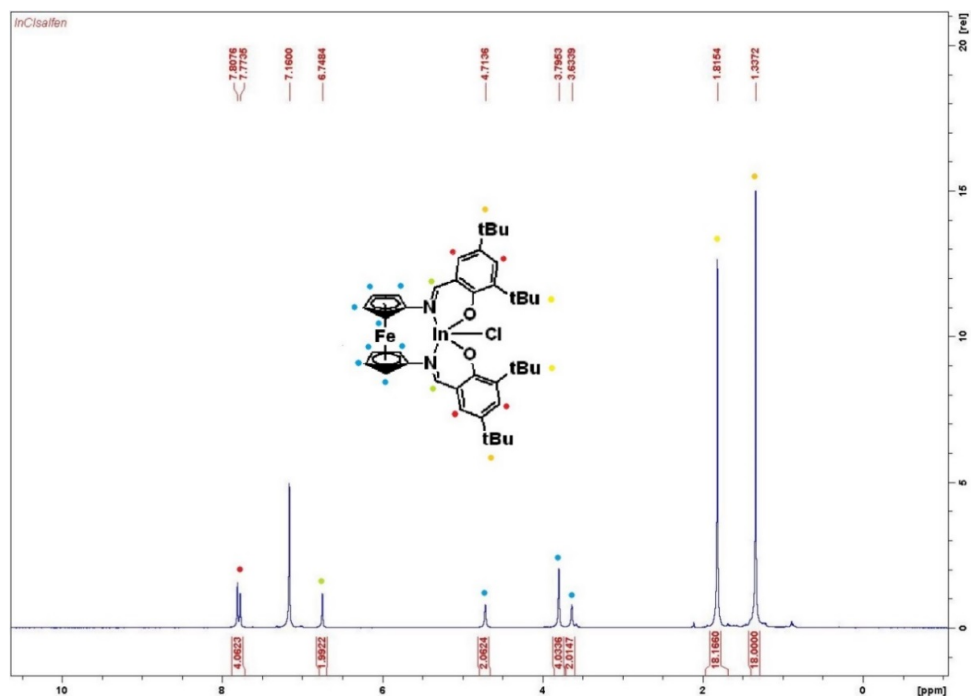


Figure A1. ^1H NMR (300 MHz, 25 °C, C_6D_6) spectrum of (salfen)InCl.

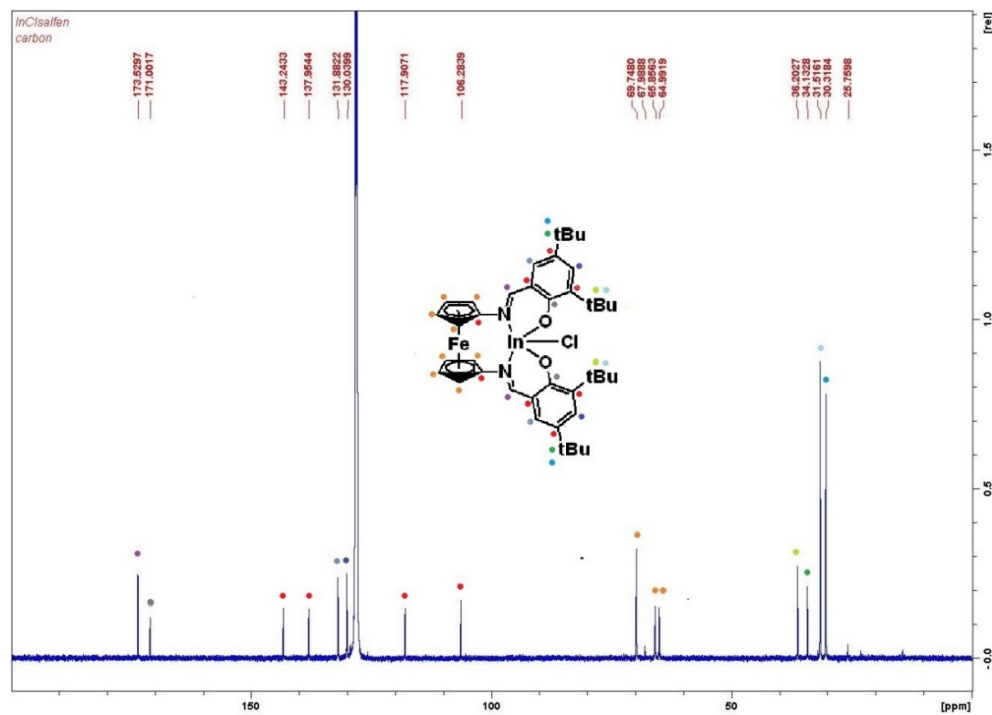


Figure A2. ^{13}C NMR (500 MHz, 25 °C, C_6D_6) spectrum of (salfen)InCl. Peak assignments were based on ^{13}C APT spectra below and previously published NMR spectra of similar compounds.³

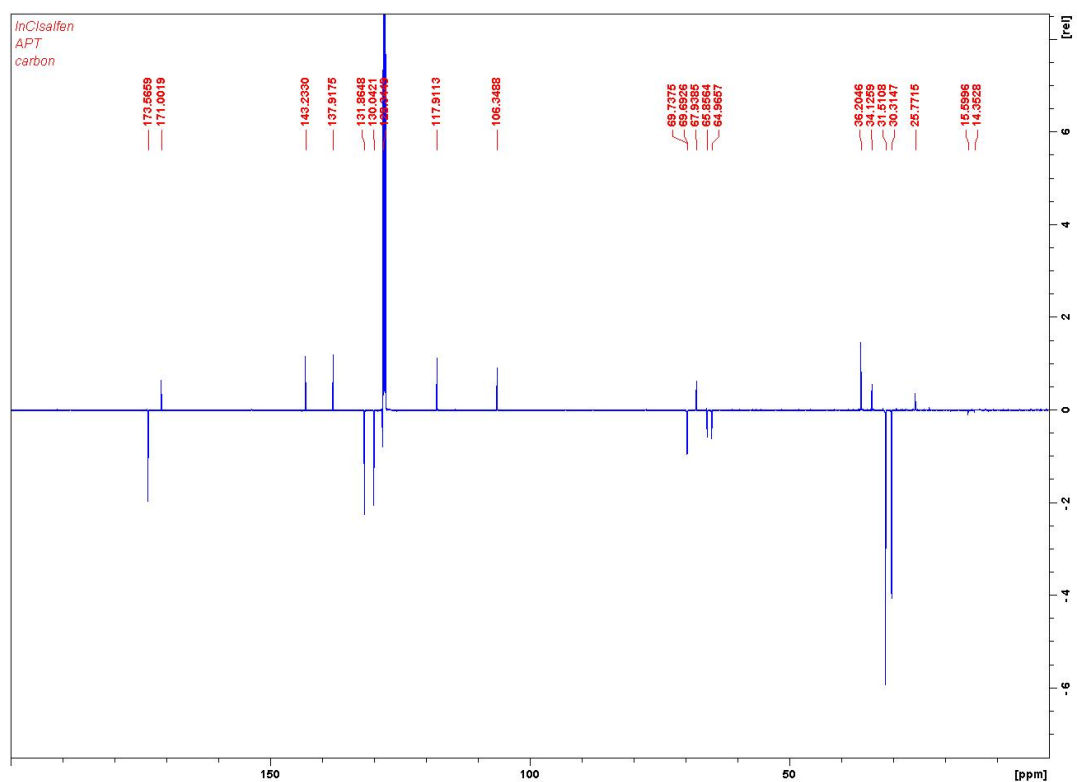


Figure A3. ^{13}C APT (attached proton test, 500 MHz, 25 °C, C_6D_6) spectrum of (salfen)InCl.

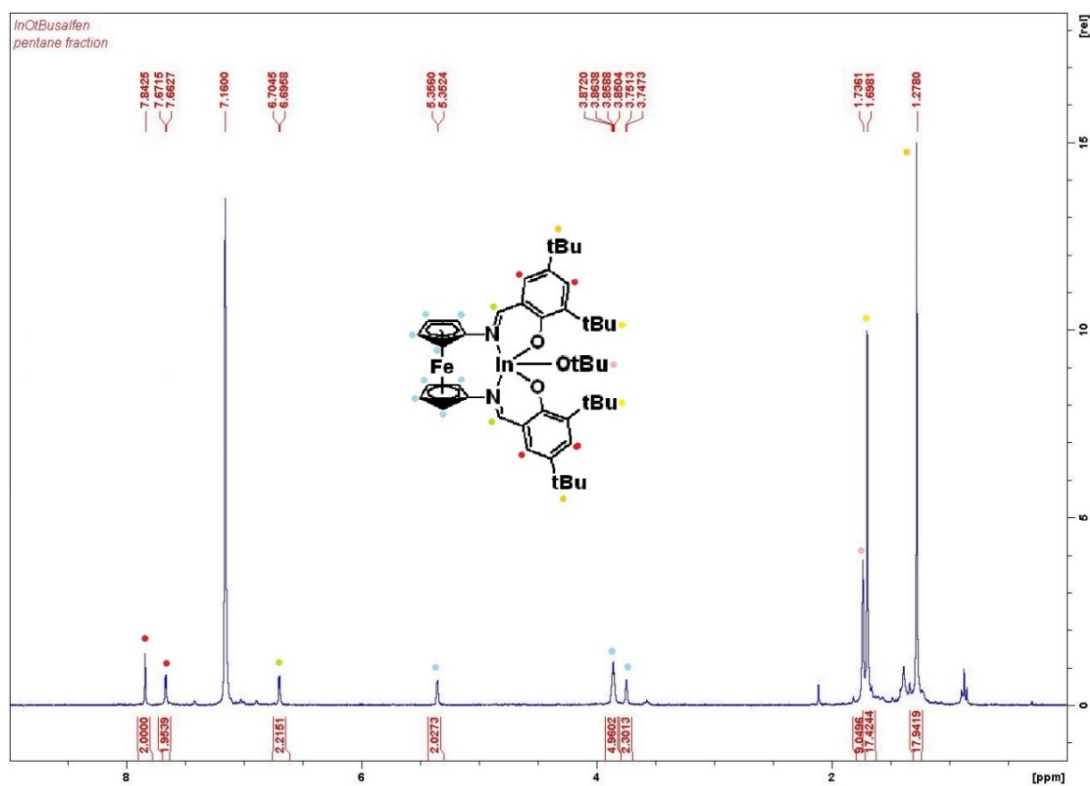


Figure A4. ^1H NMR (300 MHz, 25 °C, C_6D_6) spectrum of (salfen)In(O t Bu).

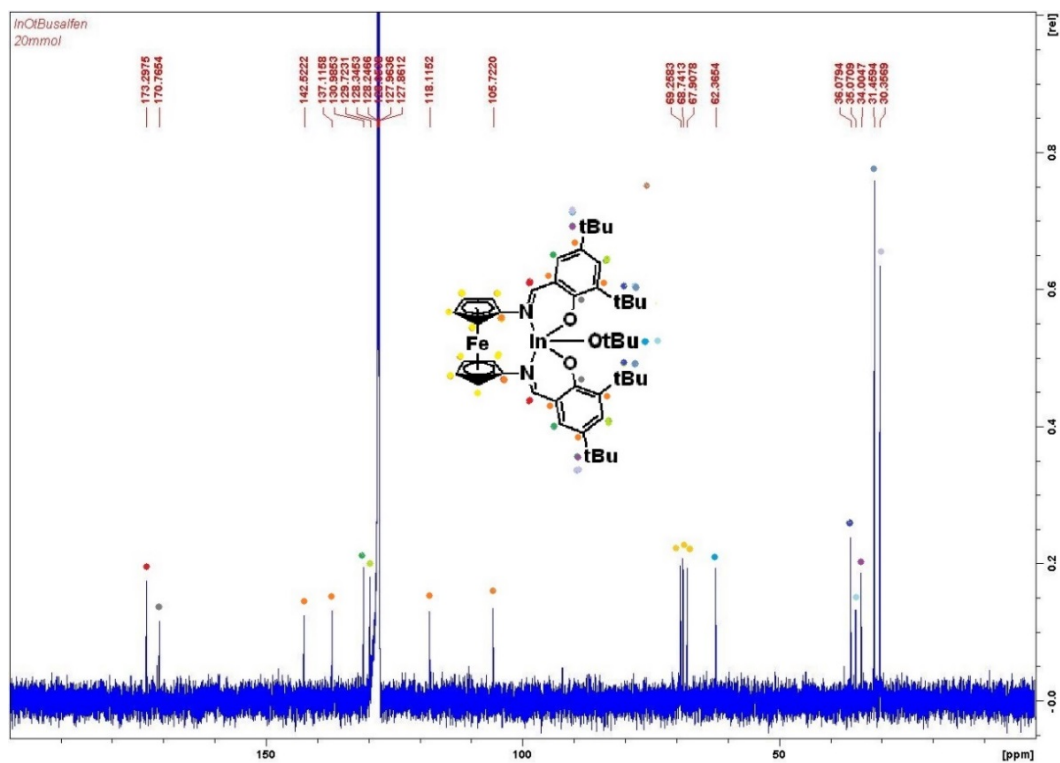


Figure A5. ^{13}C NMR (500 MHz, 25 °C, C_6D_6) spectrum of $(\text{salphen})\text{In}(\text{O}^t\text{Bu})$. Peak assignments were based on ^{13}C APT spectra below and previously published NMR spectra of similar compounds.⁵³

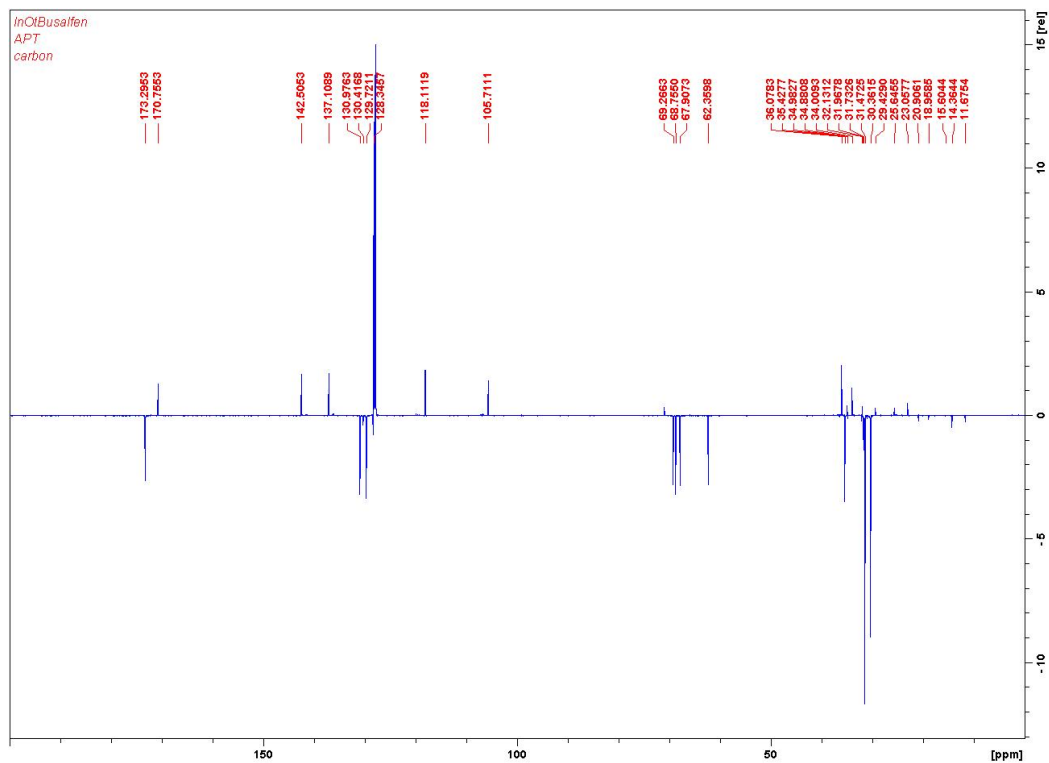


Figure A6. ^{13}C APT NMR (500 MHz, 25 °C, C_6D_6) spectrum of $(\text{salphen})\text{In}(\text{O}^t\text{Bu})$.

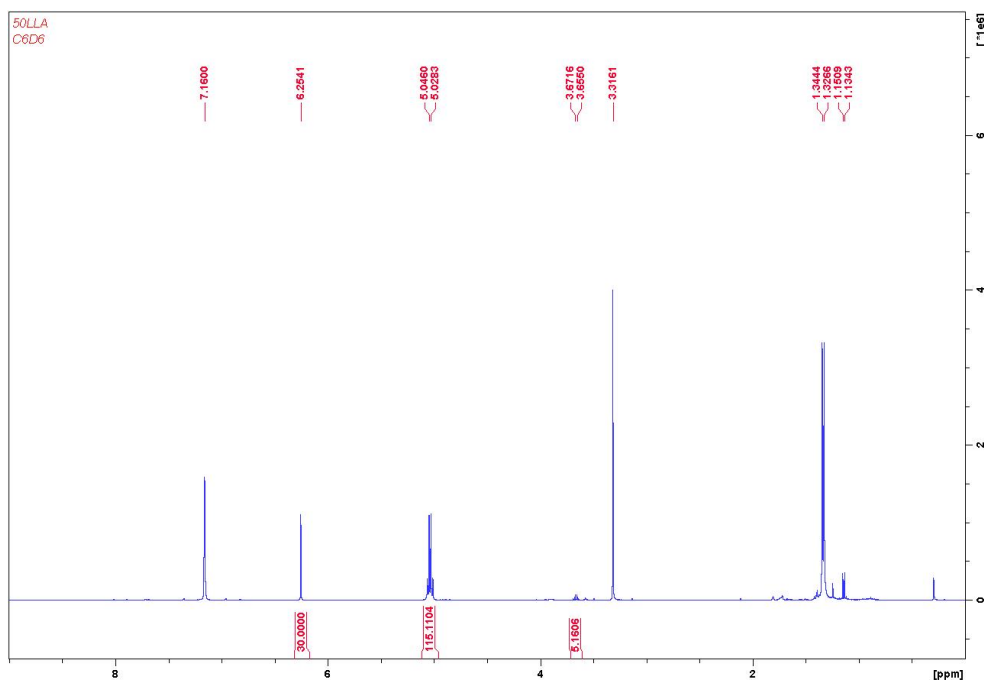


Figure A7. ^1H NMR (400 MHz, 25 $^\circ\text{C}$, C_6D_6) spectrum of L-lactide polymerization. Standard is 1,3,5-trimethoxybenzene (TMB). Initiator: TMB: L-lactide ratio is 1: 10: 50. δ (ppm): 6.25 (s, 3H, PhH TMB), 5.04 (q, 2H, CHCH_3 PLA), 3.60 (q, 2H, CHCH_3 L-lactide), 3.32 (s, 9H, CH_3 TMB), 1.34 (d, 6H, CHCH_3 PLA), 1.14 (d, 6H, CHCH_3 L-lactide).

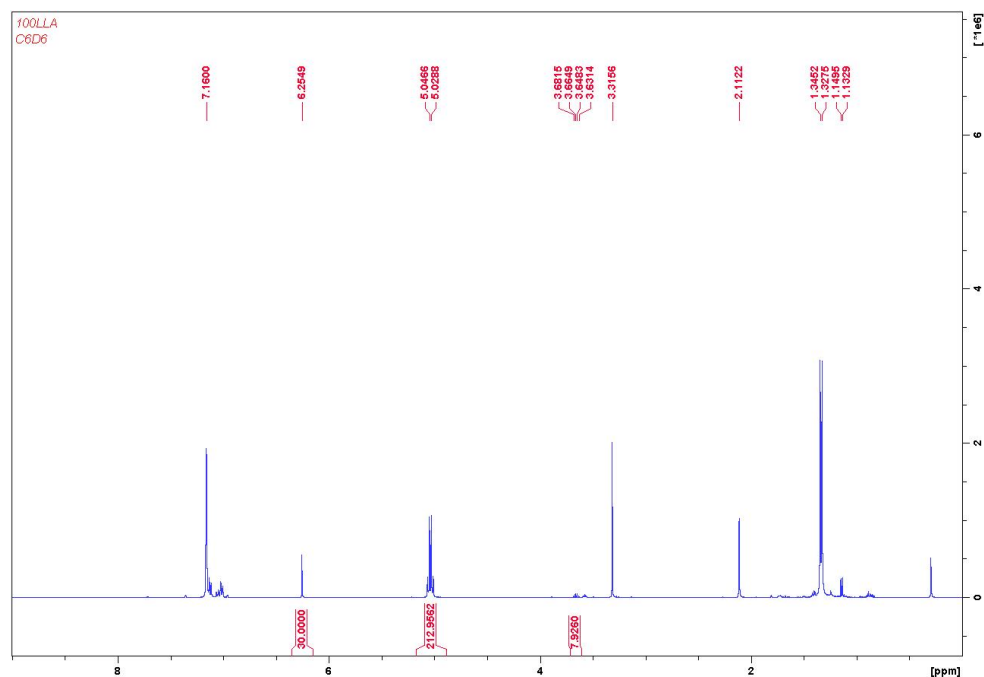


Figure A8. ^1H NMR (400 MHz, 25 $^\circ\text{C}$, C_6D_6) spectrum of L-lactide polymerization. Standard is 1,3,5-trimethoxybenzene (TMB). Initiator: TMB: L-lactide ratio is 1:10:100. δ (ppm): 6.25 (s, 3H, PhH TMB), 5.04 (q, 2H, CHCH_3 PLA), 3.60 (q, 2H, CHCH_3 L-lactide), 3.32 (s, 9H, CH_3 TMB), 1.34 (d, 6H, CHCH_3 PLA), 1.14 (d, 6H, CHCH_3 L-lactide).

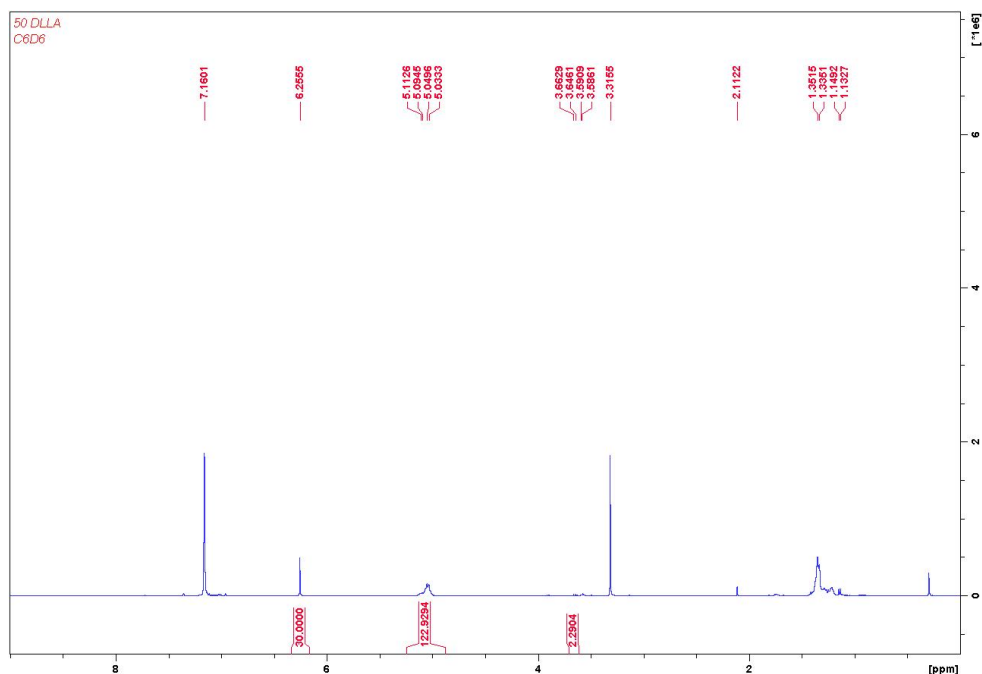


Figure A9. ^1H NMR (400 MHz, 25 °C, C_6D_6) spectrum of D,L-lactide polymerization. Standard is 1,3,5-trimethoxybenzene (TMB). Initiator: TMB: D,L-lactide ratio is 1:10:50. δ (ppm): 6.25 (s, 3H, PhH TMB), 5.04 (m, 2H, CHCH_3 PLA), 3.60 (q, 2H, CHCH_3 D,L-lactide), 3.32 (s, 9H, CH_3 TMB), 1.34 (m, 6H, CHCH_3 PLA), 1.14 (d, 6H, CHCH_3 D,L-lactide).

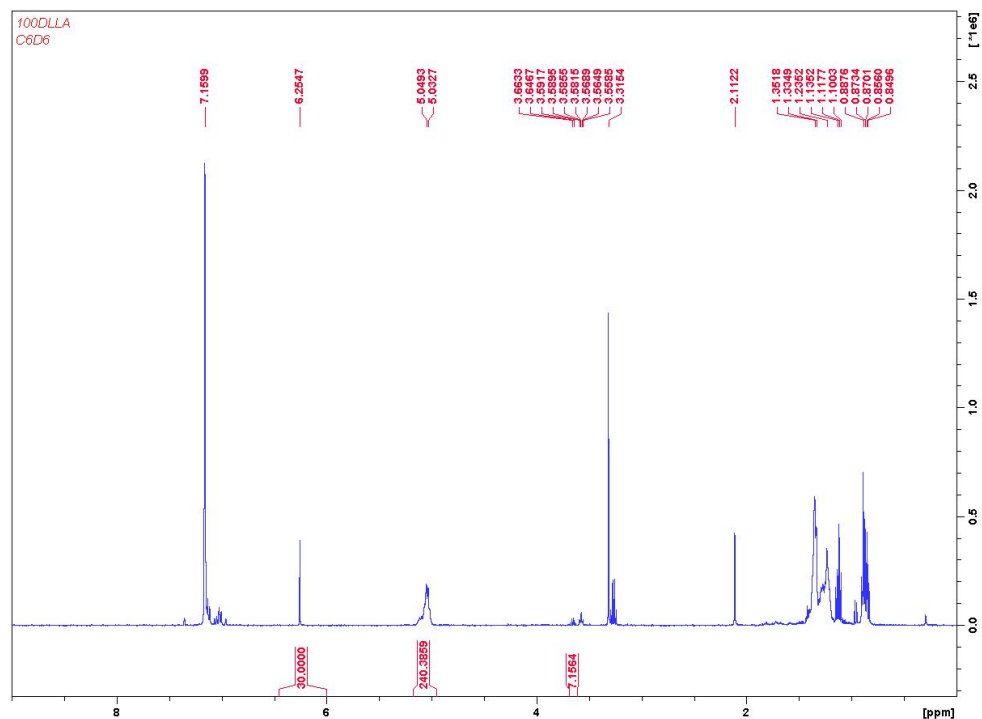


Figure A10. ^1H NMR (400 MHz, 25 °C, C_6D_6) spectrum of D,L-lactide polymerization. Standard is 1,3,5-trimethoxybenzene (TMB). Initiator: TMB: D,L-lactide ratio is 1:10:100. δ (ppm): 6.25 (s, 3H, PhH TMB), 5.04 (m, 2H, CHCH_3 PLA), 3.60 (q, 2H, CHCH_3 D,L-lactide), 3.32 (s, 9H, CH_3 TMB), 1.34 (m, 6H, CHCH_3 PLA), 1.14 (d, 6H, CHCH_3 D,L-lactide).

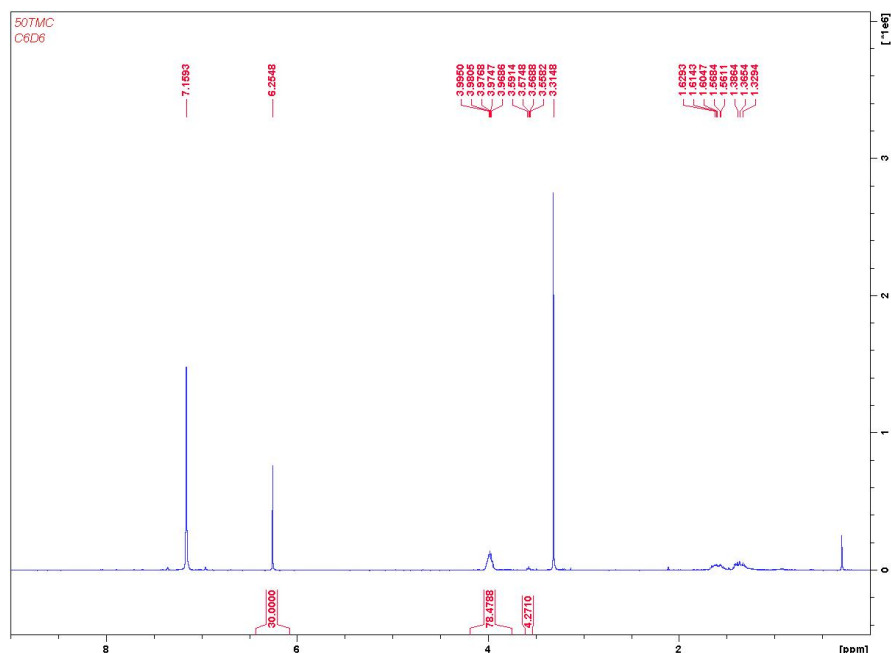


Figure A11. ^1H NMR (400 MHz, 25 °C, C_6D_6) spectrum of trimethylene carbonate (TMC) polymerization. Standard is 1,3,5-trimethoxybenzene (TMB). Initiator: TMB: TMC ratio is 1:10:50. δ (ppm): 6.25 (s, 3H, PhH TMB), 3.98 (m, 4H, CH_2 PTMC), 3.57 (m, 4H, CH_2 TMC), 3.32 (s, 9H, CH_3 TMB), 1.34 (m, 2H, CH_2 PTMC), 1.14 (m, 2H, CH_2 TMC). *Note:* Aliquots were difficult to extract from the heterogeneous mixture of solid polymer and polymerization solution.

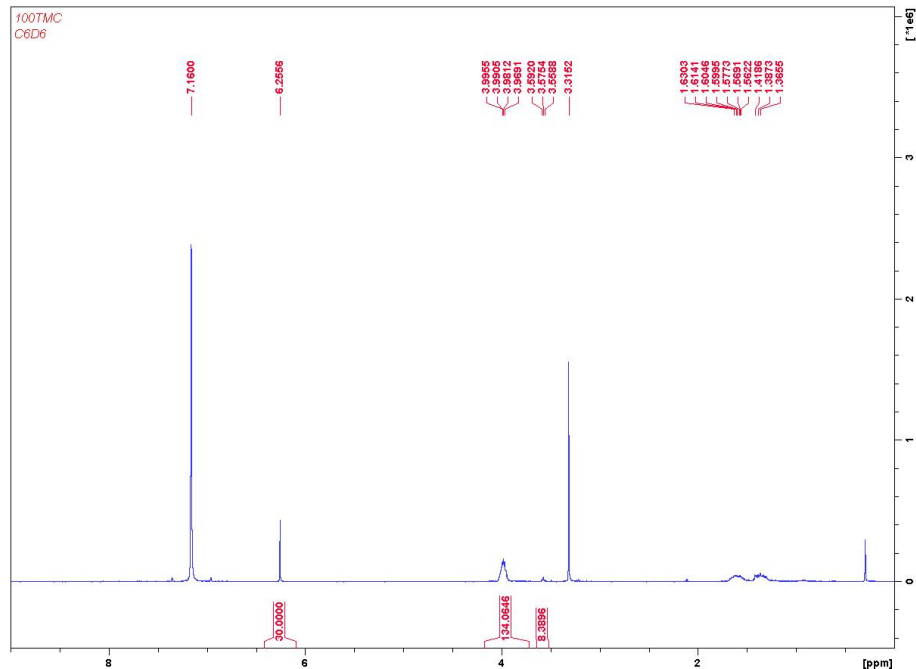


Figure A12. ^1H NMR (400 MHz, 25 °C, C_6D_6) spectrum of trimethylene carbonate (TMC) polymerization. Standard is 1,3,5-trimethoxybenzene (TMB). Initiator: TMB: TMC ratio is 1:10:100. δ (ppm): 6.25 (s, 3H, PhH TMB), 3.98 (m, 4H, CH_2 PTMC), 3.57 (m, 4H, CH_2 TMC), 3.32 (s, 9H, CH_3 TMB), 1.34 (m, 2H, CH_2 PTMC), 1.14 (m, 2H, CH_2 TMC). Aliquots were difficult to extract from the heterogeneous mixture of solid polymer and polymerization solution.

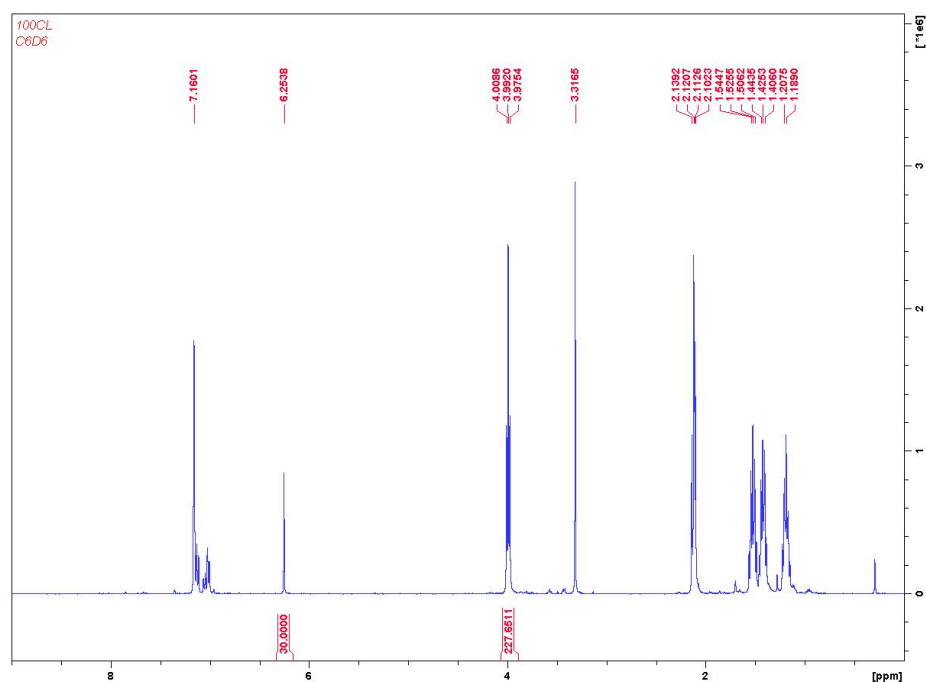


Figure A13. ^1H NMR (400 MHz, 25 °C, C_6D_6) spectrum of ϵ -caprolactone (CL) polymerization. Standard is 1,3,5-trimethoxybenzene (TMB). Initiator: TMB: CL ratio is 1:10:100. δ (ppm): 6.25 (s, 3H, PhH TMB), 3.99 (t, 2H, OCH_2 PCL), 3.32 (s, 9H, CH_3 TMB), 2.12 (t, 2H, COCH_2 , PCL), 1.53 (q, 2H, CH_2 PCL), 1.43 (q, 2H, CH_2 PCL), 1.19 (q, 2H, CH_2 PCL).

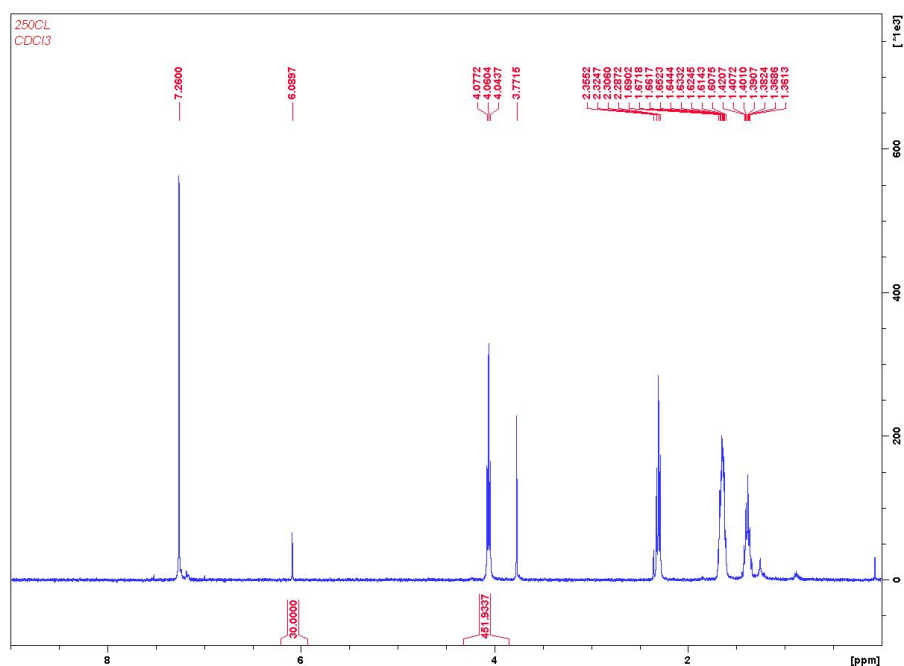


Figure A14. ^1H NMR (400 MHz, 25 °C, CDCl_3) spectrum of ϵ -caprolactone (CL) polymerization. Standard is 1,3,5-trimethoxybenzene (TMB). Initiator: TMB: CL ratio is 1:10:250. δ (ppm): 6.09 (s, 3H, PhH TMB), 4.06 (t, 2H, OCH_2 PCL), 3.77 (s, 9H, CH_3 TMB), 2.31 (t, 2H, COCH_2 , PCL), 1.65 (m, 4H, $\text{CH}_2\text{CH}_2\text{CH}_2$ PCL), 1.39 (q, 2H, $\text{CH}_2\text{CH}_2\text{CH}_2$ PCL).

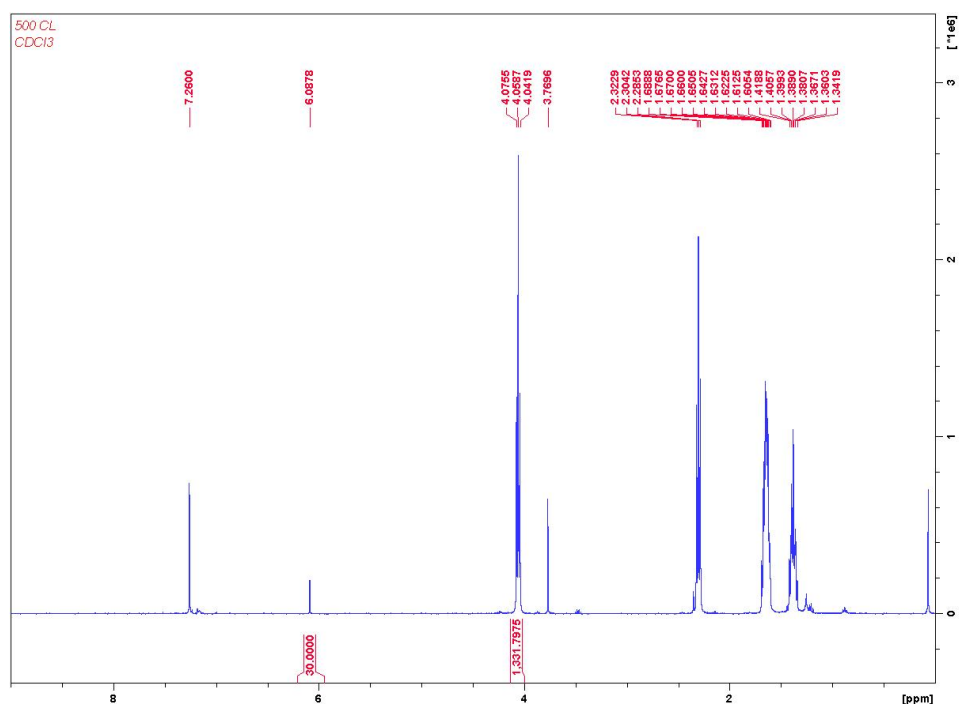


Figure A15. ¹H NMR (400 MHz, 25 °C, CDCl₃) spectrum of ε-caprolactone (CL) polymerization. Standard is 1,3,5-trimethoxybenzene (TMB). Initiator: TMB: CL ratio is 1:10:500. δ (ppm): 6.09 (s, 3H, PhH TMB), 4.06 (t, 2H, OCH₂ PCL), 3.77 (s, 9H, CH₃ TMB), 2.31 (t, 2H, COCH₂ PCL), 1.65 (m, 4H, CH₂CH₂CH₂ PCL), 1.39 (q, 2H, CH₂CH₂CH₂ PCL).

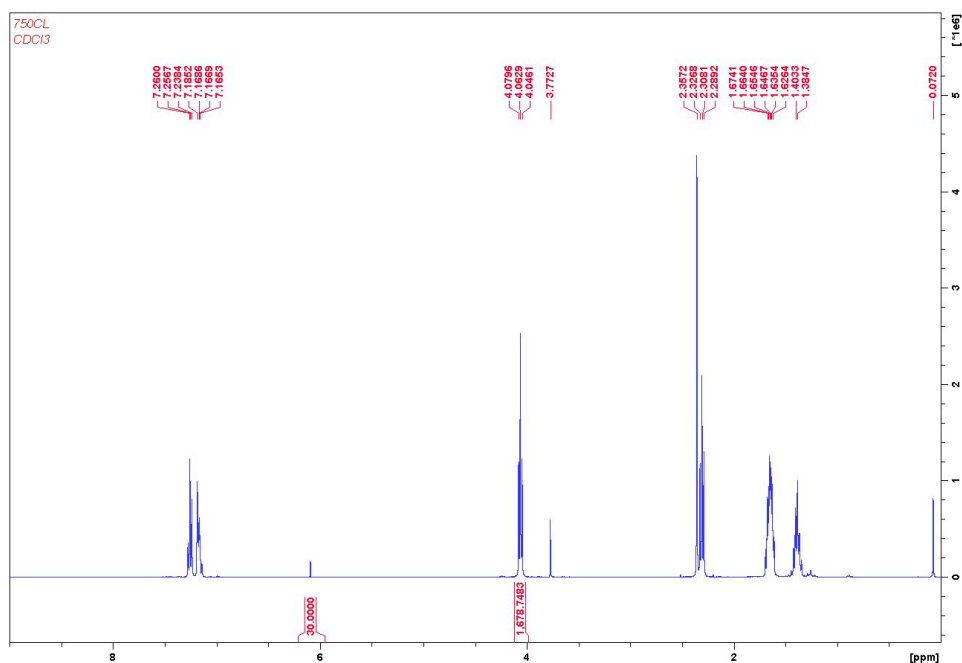


Figure A16. ¹H NMR (400 MHz, 25 °C, CDCl₃) spectrum of ε-caprolactone (CL) polymerization. Standard is 1,3,5-trimethoxybenzene (TMB). Initiator: TMB: CL ratio is 1:10:750. δ (ppm): 6.09 (s, 3H, PhH TMB), 4.06 (t, 2H, OCH₂ PCL), 3.77 (s, 9H, CH₃ TMB), 2.31 (t, 2H, COCH₂, PCL), 1.65 (m, 4H, CH₂CH₂CH₂ PCL), 1.39 (q, 2H, CH₂CH₂CH₂ PCL).

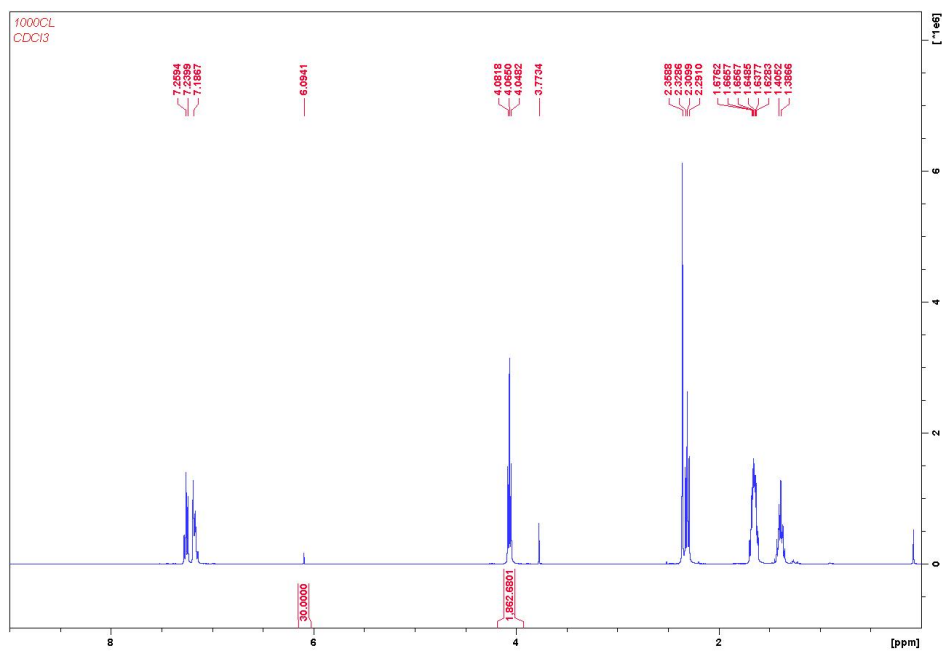


Figure A17. ¹H NMR (400 MHz, 25 °C, CDCl₃) spectrum of ε -caprolactone (CL) polymerization. Standard is 1,3,5-trimethoxybenzene (TMB). Initiator: TMB: CL ratio is 1:10:1000. δ (ppm): 6.09 (s, 3H, PhH TMB), 4.06 (t, 2H, OCH₂ PCL), 3.77 (s, 9H, CH₃ TMB), 2.31 (t, 2H, COCH₂, PCL), 1.65 (m, 4H, CH₂CH₂CH₂ PCL), 1.39 (q, 2H, CH₂CH₂CH₂ PCL).

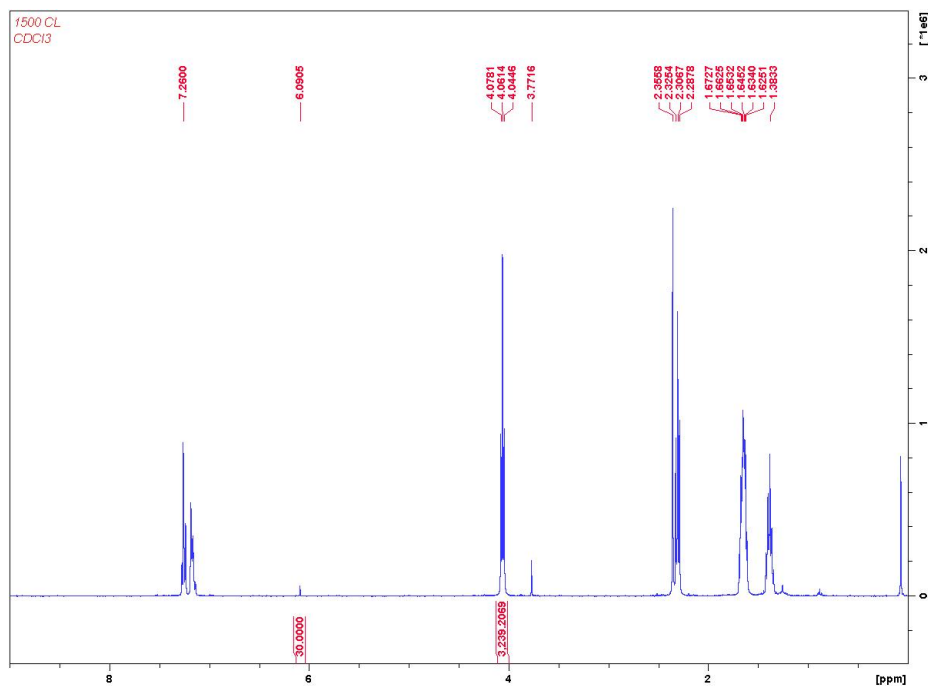


Figure A18. ¹H NMR (400 MHz, 25 °C, CDCl₃) spectrum of ε -caprolactone (CL) polymerization. Standard is 1,3,5-trimethoxybenzene (TMB). Initiator: TMB: CL ratio is 1:10:1500. δ (ppm): 6.09 (s, 3H, PhH TMB), 4.06 (t, 2H, OCH₂ PCL), 3.77 (s, 9H, CH₃ TMB), 2.31 (t, 2H, COCH₂, PCL), 1.65 (m, 4H, CH₂CH₂CH₂ PCL), 1.39 (q, 2H, CH₂CH₂CH₂ PCL).

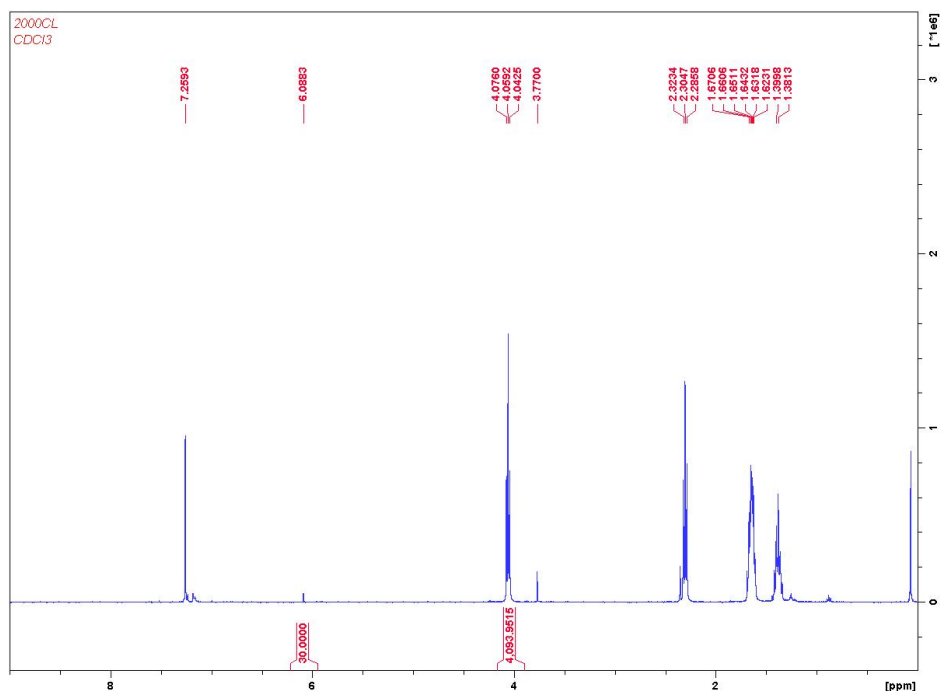


Figure A19. ^1H NMR (400 MHz, 25 °C, CDCl_3) spectrum of ϵ -caprolactone (CL) polymerization. Standard is 1,3,5-trimethoxybenzene (TMB). Initiator: TMB: CL ratio is 1:10:2000. δ (ppm): 6.09 (s, 3H, PhH TMB), 4.06 (t, 2H, OCH_2 PCL), 3.77 (s, 9H, CH_3 TMB), 2.31 (t, 2H, COCH_2 PCL), 1.65 (m, 4H, $\text{CH}_2\text{CH}_2\text{CH}_2$ PCL), 1.39 (q, 2H, $\text{CH}_2\text{CH}_2\text{CH}_2$ PCL).

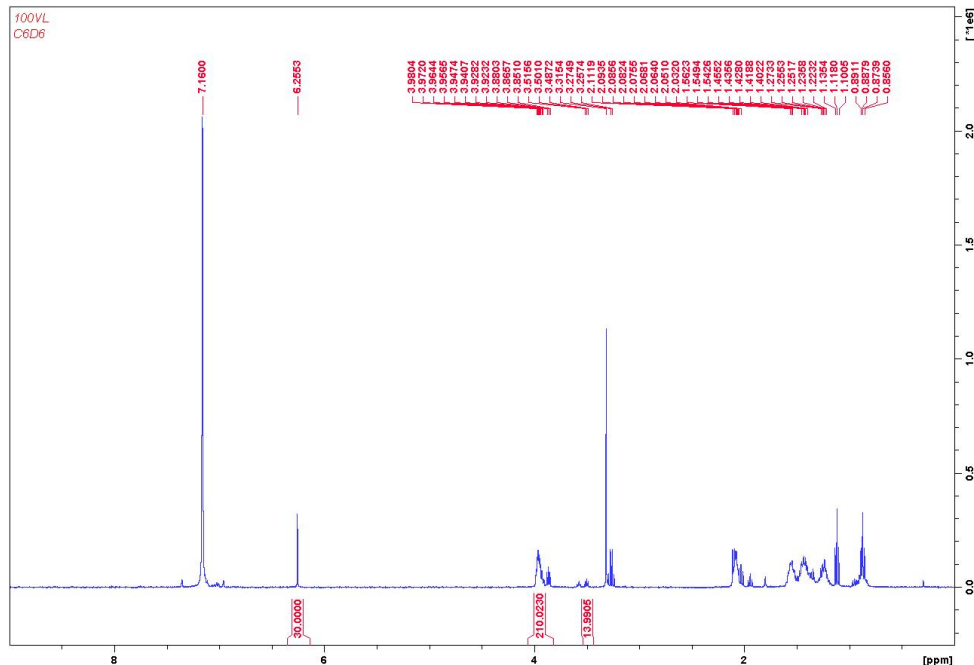


Figure A20. ^1H NMR (400 MHz, 25 °C, C_6D_6) spectrum of δ -valerolactone (VL) polymerization. Standard is 1,3,5-trimethoxybenzene (TMB). Initiator: TMB: VL ratio is 1:10:100. δ (ppm): 6.26 (s, 3H, PhH TMB), 3.96 (m, 2H, OCH_2 PVL), 3.50 (t, 2H, OCH_2 VL), 3.32 (s, 9H, CH_3 TMB), 2.08 (m, 2H, COCH_2 , PVL), 1.55 (m, 2H, CH_2 PVL), 1.43 (m, 2H, CH_2 PVL), 1.23 (m, 2H, CH_2 PVL).

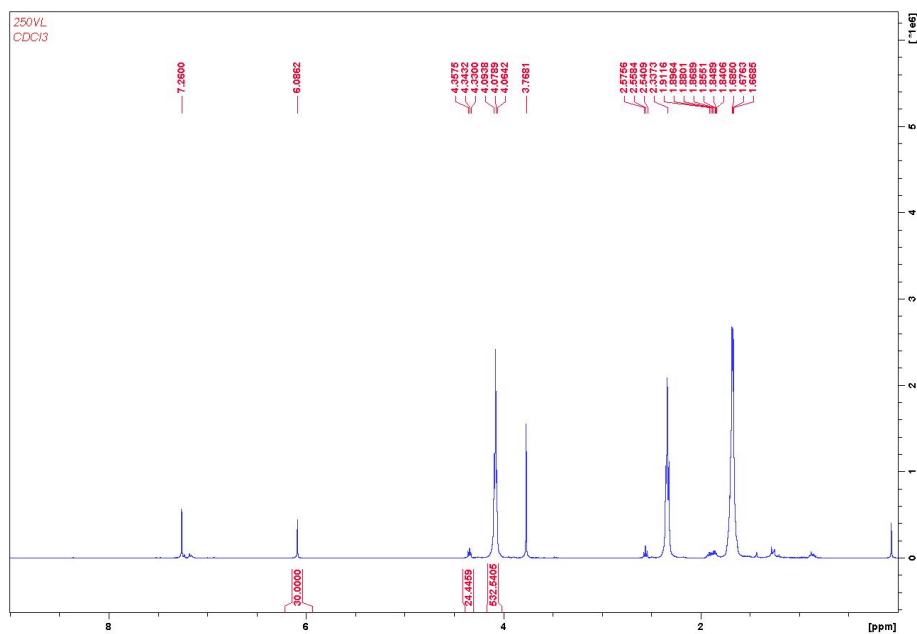


Figure A21. ¹H NMR (400 MHz, 25 °C, CDCl₃) spectrum of δ -valerolactone (VL) polymerization. Standard is 1,3,5-trimethoxybenzene (TMB). Initiator: TMB: VL ratio is 1:10:250. δ (ppm): 6.09 (s, 3H, PhH TMB), 4.34 (t, 2H, OCH₂ VL), 4.07 (t, 2H, OCH₂ PVL), 3.77 (s, 9H, CH₃ TMB), 2.56 (t, 2H, COCH₂, VL), 2.34 (t, 2H, COCH₂, PVL), 1.88 (m, 4H, CH₂ VL), 1.67 (m, 4H, CH₂ PVL).

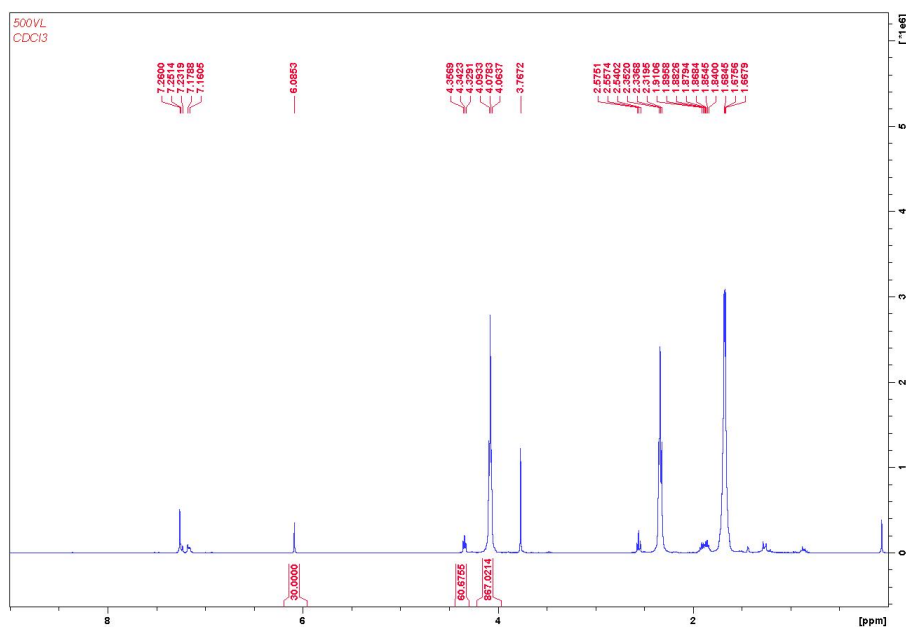


Figure A22. ¹H NMR (400 MHz, 25 °C, CDCl₃) spectrum of δ -valerolactone (VL) polymerization. Standard is 1,3,5-trimethoxybenzene (TMB). Initiator: TMB: VL ratio is 1:10:500. δ (ppm): 6.09 (s, 3H, PhH TMB), 4.34 (t, 2H, OCH₂ VL), 4.07 (t, 2H, OCH₂ PVL), 3.77 (s, 9H, CH₃ TMB), 2.56 (t, 2H, COCH₂, VL), 2.34 (t, 2H, COCH₂, PVL), 1.88 (m, 4H, CH₂ VL), 1.67 (m, 4H, CH₂ PVL).

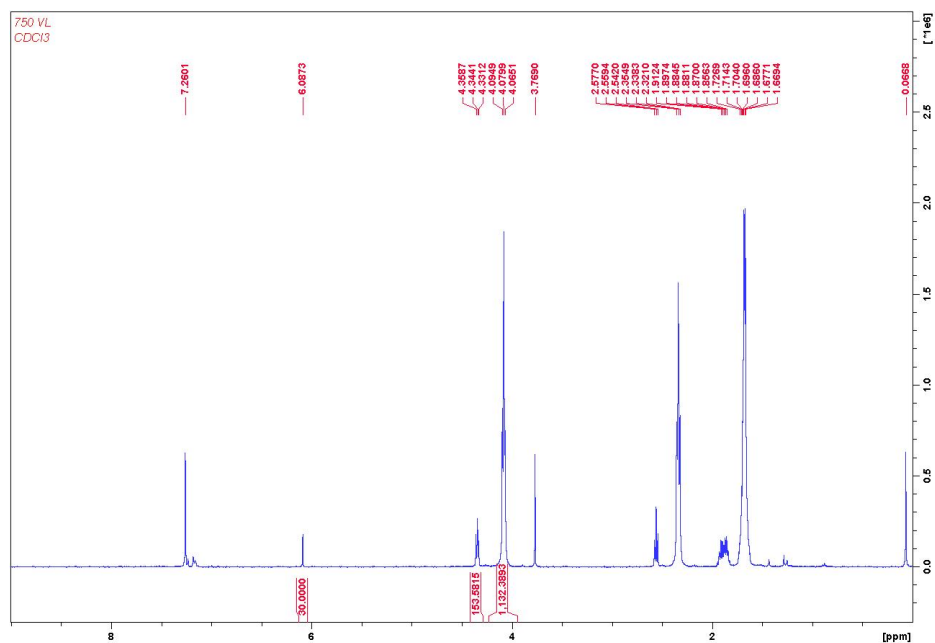


Figure A23. ^1H NMR (400 MHz, 25 °C, CDCl_3) spectrum of δ -valerolactone (VL) polymerization. Standard is 1,3,5-trimethoxybenzene (TMB). Initiator: TMB: VL ratio is 1:10:750. δ (ppm): 6.09 (s, 3H, PhH TMB), 4.34 (t, 2H, OCH_2 VL), 4.07 (t, 2H, OCH_2 PVL), 3.77 (s, 9H, CH_3 TMB), 2.56 (t, 2H, COCH_2 , VL), 2.34 (t, 2H, COCH_2 , PVL), 1.88 (m, 4H, CH_2 VL), 1.67 (m, 4H, CH_2 PVL).

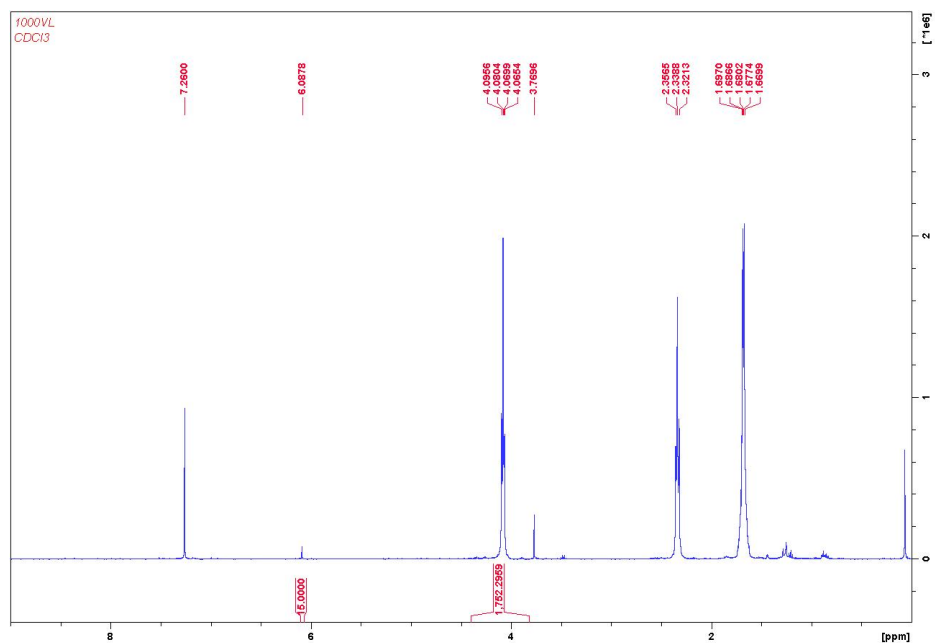


Figure A24. ^1H NMR (400 MHz, 25 °C, CDCl_3) spectrum of δ -valerolactone (VL) polymerization. Standard is 1,3,5-trimethoxybenzene (TMB). Initiator: TMB: VL ratio is 1:10:1000. δ (ppm): 6.09 (s, 3H, PhH TMB), 4.34 (t, 2H, OCH_2 VL), 4.07 (t, 2H, OCH_2 PVL), 3.77 (s, 9H, CH_3 TMB), 2.56 (t, 2H, COCH_2 , VL), 2.34 (t, 2H, COCH_2 , PVL), 1.88 (m, 4H, CH_2 VL), 1.67 (m, 4H, CH_2 PVL).

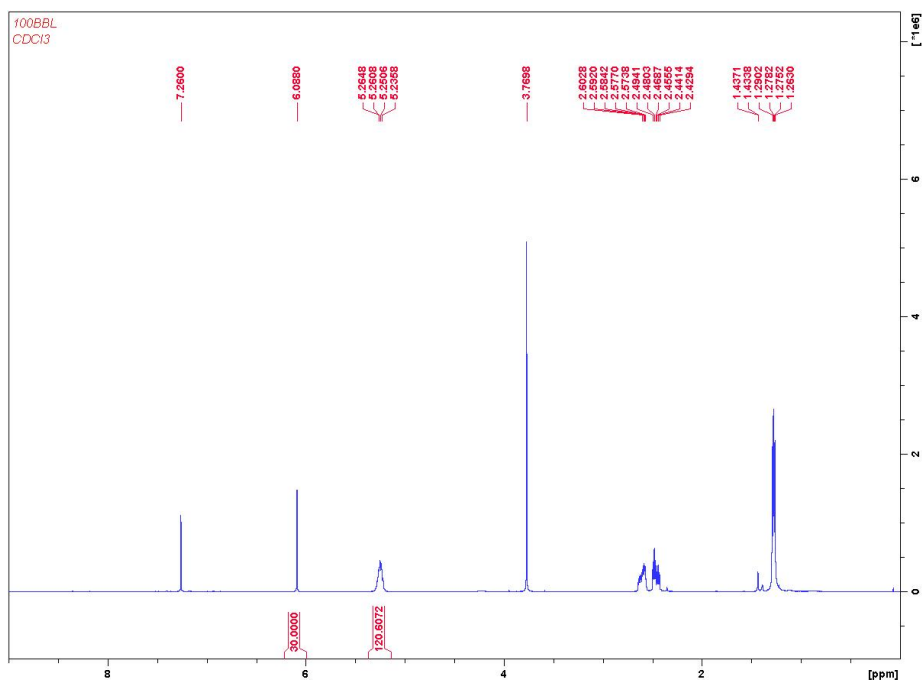


Figure SA5. ^1H NMR (400 MHz, 25 °C, CDCl_3) spectrum of β -butyrolactone (BBL) polymerization. Standard is 1,3,5-trimethoxybenzene (TMB). Initiator: TMB: BBL ratio is 1:10:100. δ (ppm): 6.09 (s, 3H, PhH TMB), 5.26 (m, 1H, OCHCH_3 PHB), 3.77 (s, 9H, CH_3 TMB), 2.53 (m, 2H, COCH_2 PHB), 1.28 (t, 3H, OCHCH_3 PHB).

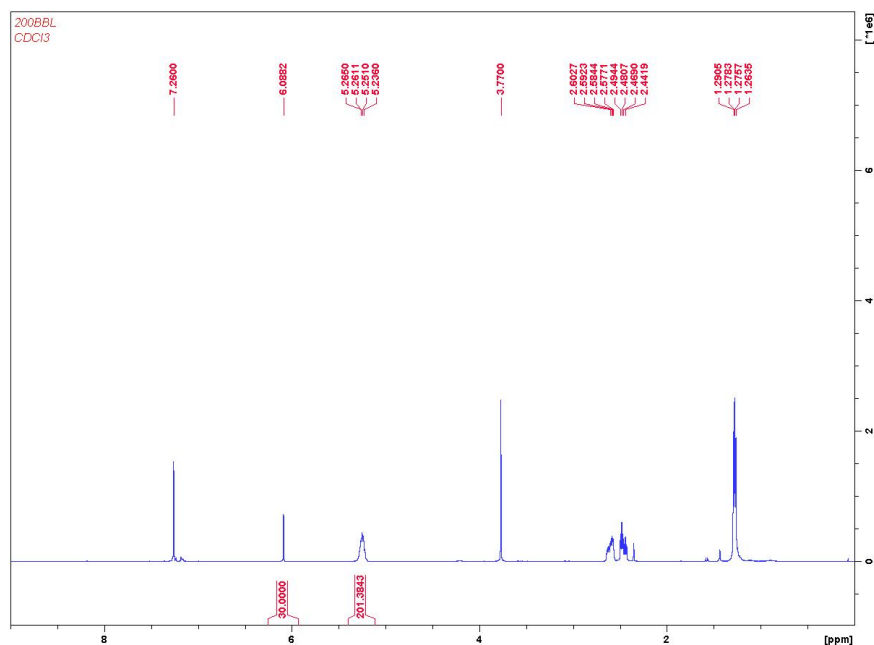


Figure A26. ^1H NMR (400 MHz, 25 °C, CDCl_3) spectrum of β -butyrolactone (BBL) polymerization. Standard is 1,3,5-trimethoxybenzene (TMB). Initiator: TMB: BBL ratio is 1:10:200. δ (ppm): 6.09 (s, 3H, PhH TMB), 5.26 (m, 1H, OCHCH_3 PHB), 3.77 (s, 9H, CH_3 TMB), 2.53 (m, 2H, COCH_2 PHB), 1.28 (t, 3H, OCHCH_3 PHB).

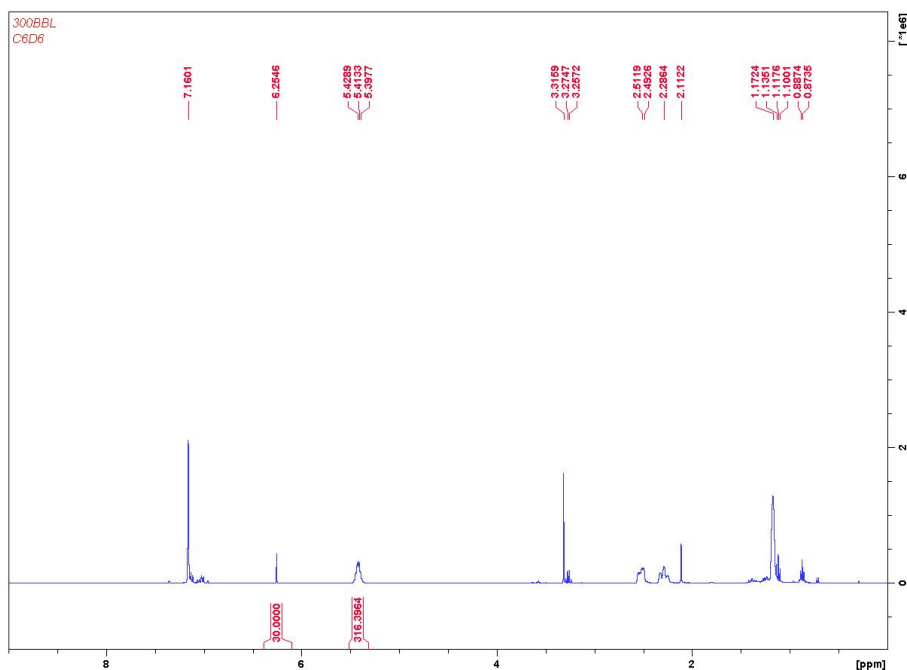


Figure A27. ^1H NMR (400 MHz, 25 °C, CDCl_3) spectrum of β -butyrolactone (BBL) polymerization. Standard is 1,3,5-trimethoxybenzene (TMB). Initiator: TMB: BBL ratio is 1:10:300. δ (ppm): 6.09 (s, 3H, PhH TMB), 5.26 (m, 1H, OCHCH_3 PHB), 3.77 (s, 9H, CH_3 TMB), 2.53 (m, 2H, COCH_2 PHB), 1.28 (t, 3H, OCHCH_3 PHB).

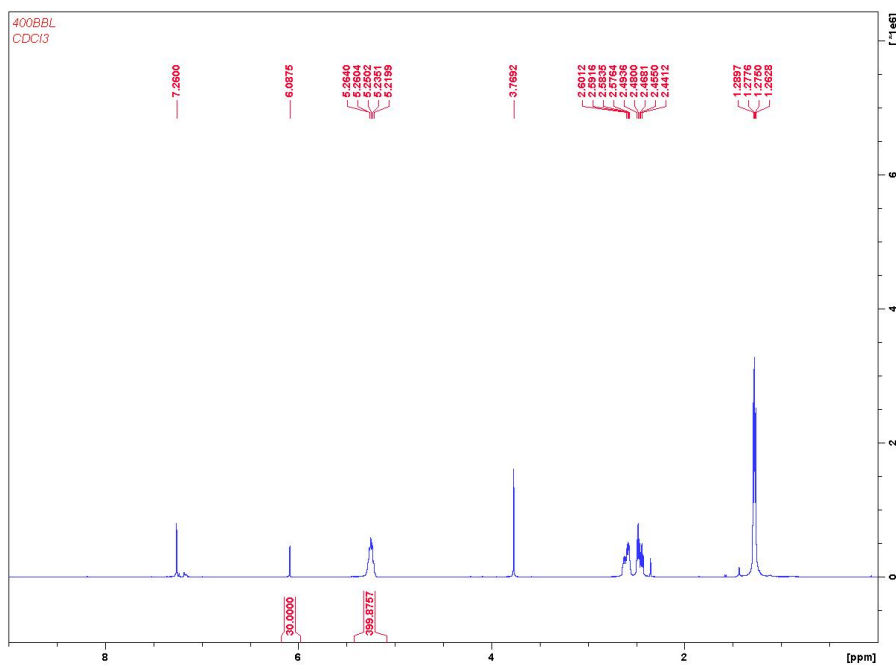


Figure A28. ^1H NMR (400 MHz, 25 °C, CDCl_3) spectrum of β -butyrolactone (BBL) polymerization. Standard is 1,3,5-trimethoxybenzene (TMB). Initiator: TMB: BBL ratio is 1:10:400. δ (ppm): 6.09 (s, 3H, PhH TMB), 5.26 (m, 1H, OCHCH_3 PHB), 3.77 (s, 9H, CH_3 TMB), 2.53 (m, 2H, COCH_2 PHB), 1.28 (t, 3H, OCHCH_3 PHB).

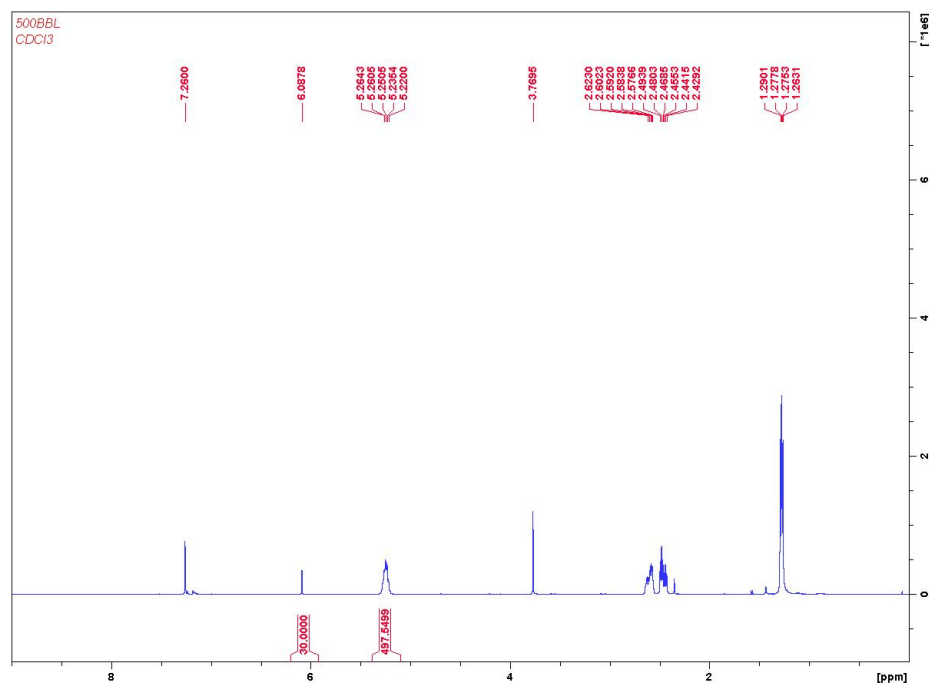


Figure A29. ^1H NMR (400 MHz, 25 °C, CDCl_3) spectrum of β -butyrolactone (BBL) polymerization. Standard is 1,3,5-trimethoxybenzene (TMB). Initiator: TMB: BBL ratio is 1:10:500. δ (ppm): 6.09 (s, 3H, PhH TMB), 5.26 (m, 1H, OCHCH₃ PHB), 3.77 (s, 9H, CH₃ TMB), 2.53 (m, 2H, COCH₂, PHB), 1.28 (t, 3H, OCHCH₃, PHB).

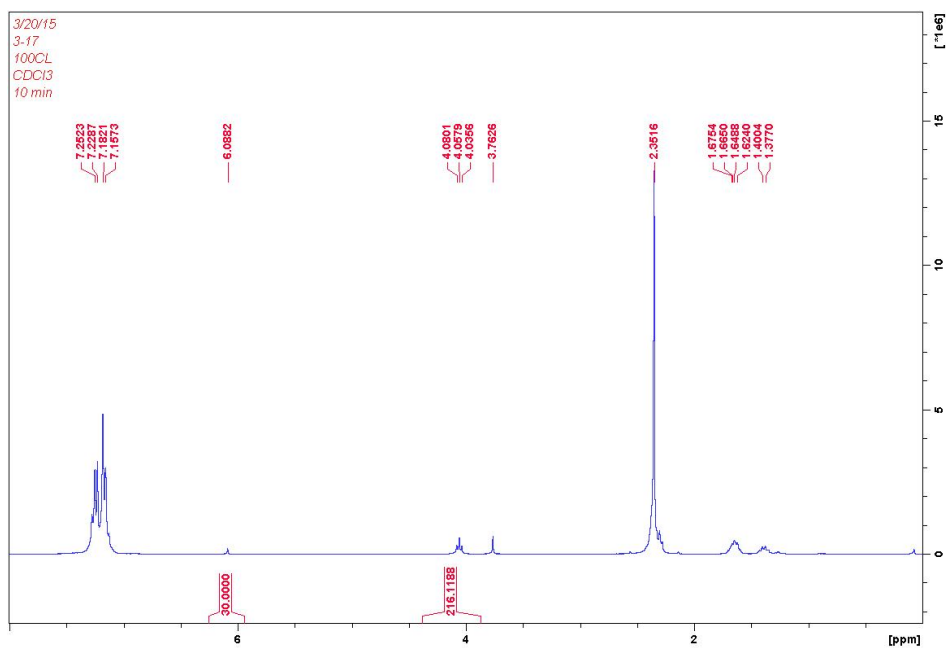


Figure A30. ^1H NMR (300 MHz, 0 °C, CDCl_3) spectrum of ϵ -caprolactone (CL) polymerization. Standard is 1,3,5-trimethoxybenzene (TMB). Initiator: TMB: CL ratio is 1:10:100. δ (ppm): 6.25 (s, 3H, PhH TMB), 3.99 (t, 2H, OCH₂ PCL), 3.32 (s, 9H, CH₃ TMB), 2.12 (t, 2H, COCH₂, PCL), 1.53 (q, 2H, CH₂ PCL), 1.43 (q, 2H, CH₂ PCL), 1.19 (q, 2H, CH₂ PCL).

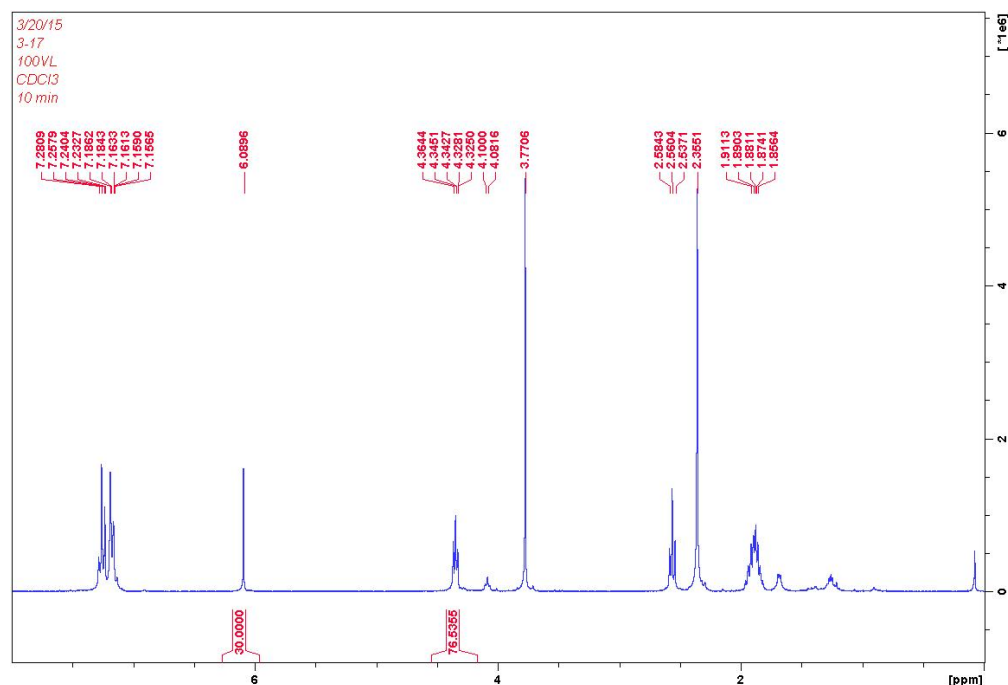


Figure A31. ^1H NMR (300 MHz, 0°C , CDCl_3) spectrum of δ -valerolactone (VL) polymerization. Standard is 1,3,5-trimethoxybenzene (TMB). Initiator: TMB: VL ratio is 1:10:100. δ (ppm): 6.26 (s, 3H, PhH TMB), 3.96 (m, 2H, OCH_2 PVL), 3.50 (t, 2H, OCH_2 VL), 3.32 (s, 9H, CH_3 TMB), 2.08 (m, 2H, COCH_2 , PVL), 1.55 (m, 2H, CH_2 PVL), 1.43 (m, 2H, CH_2 PVL), 1.23 (m, 2H, CH_2 PVL). Aliquots were difficult to extract from the heterogeneous mixture of solid polymer and polymerization solution.

Gel Permeation Chromatography

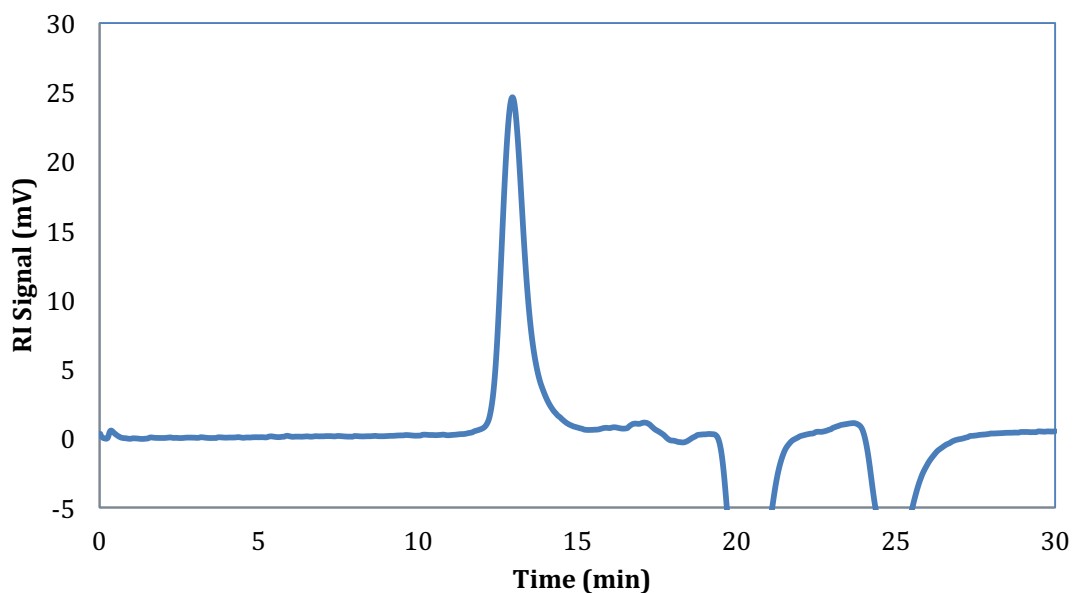


Figure A32. Polymerization of 50 equivalents of L-lactide; $M_n = 15900$, $M_w = 18900$, $D = 1.19$.

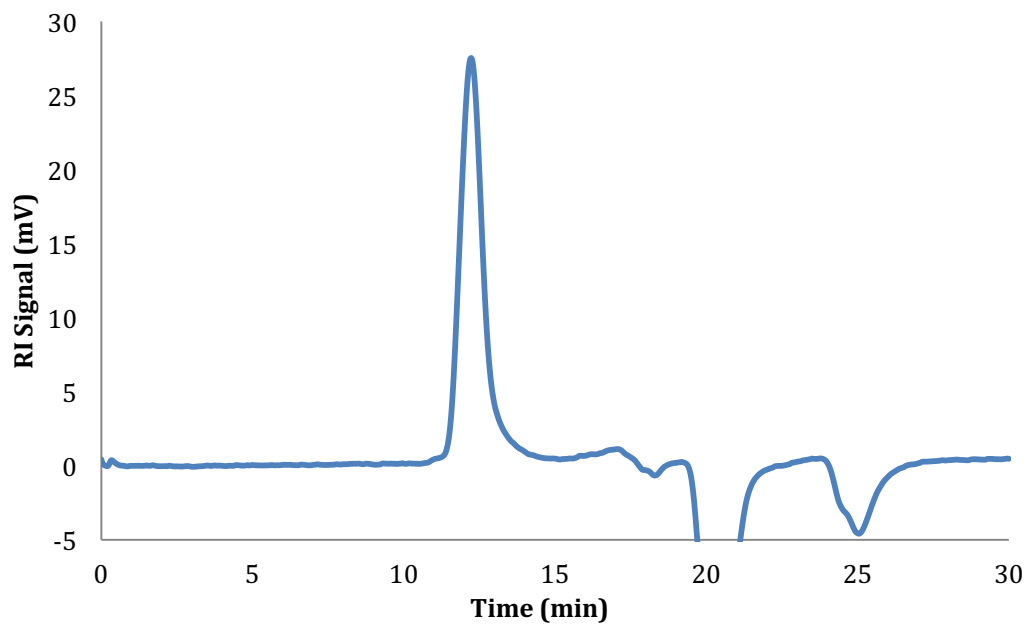


Figure A33. Polymerization of 100 equivalents of L-lactide; $M_n = 32800$, $M_w = 38200$, $D = 1.16$.

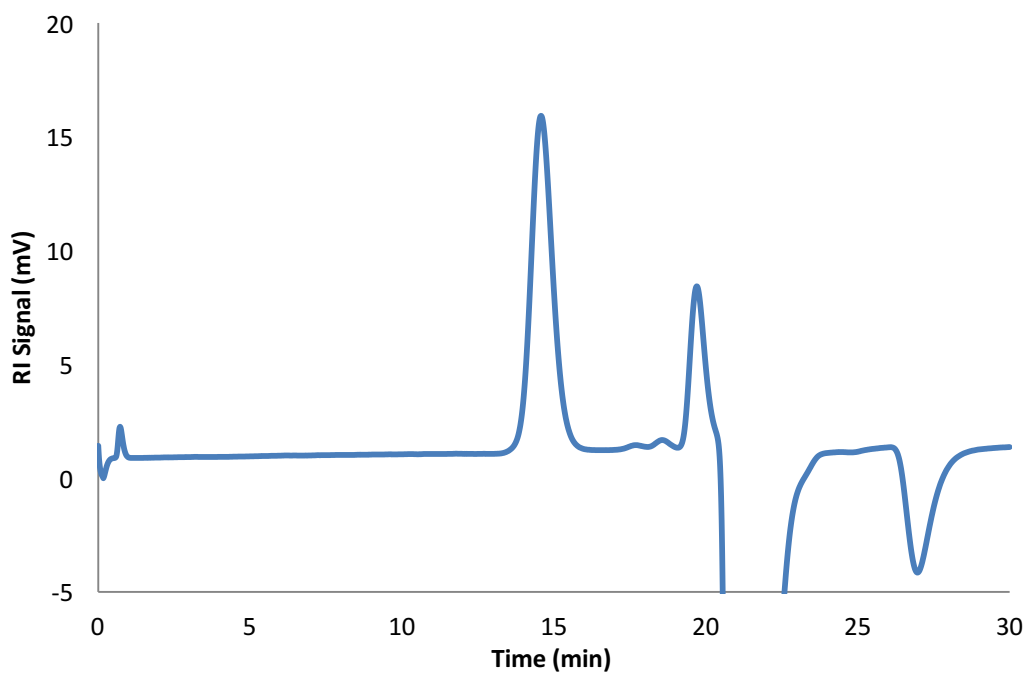


Figure A34. Polymerization of 50 equivalents of D,L-lactide; $M_n = 15400$, $M_w = 16600$, $D = 1.07$.

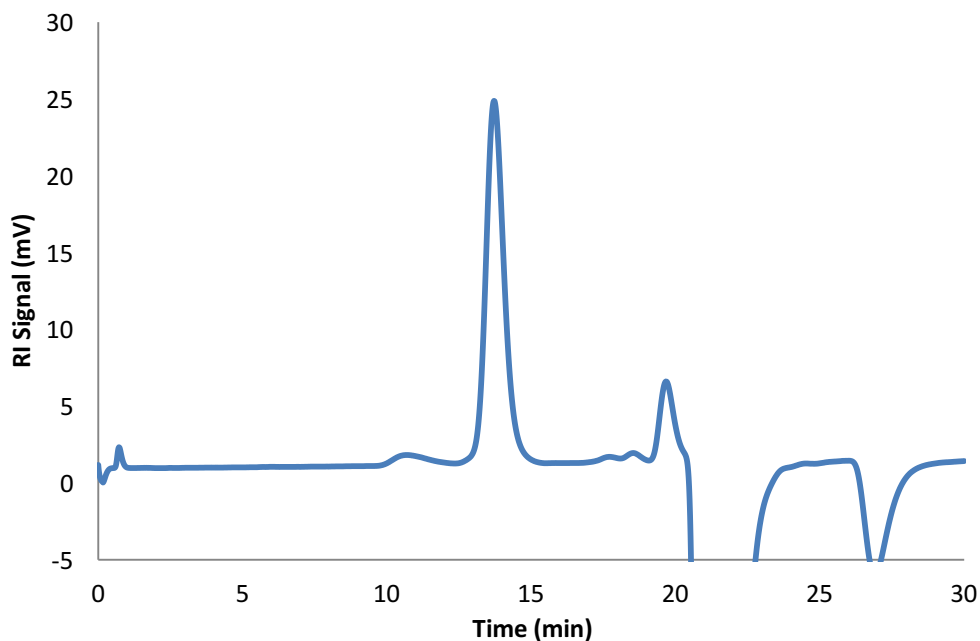


Figure A35. Polymerization of 100 equivalents of D,L-lactide; $M_n = 32200$, $M_w = 34100$, $D = 1.06$. Dispersity was calculated for large peak around 14 minutes and does not include small peak at 11 minutes.

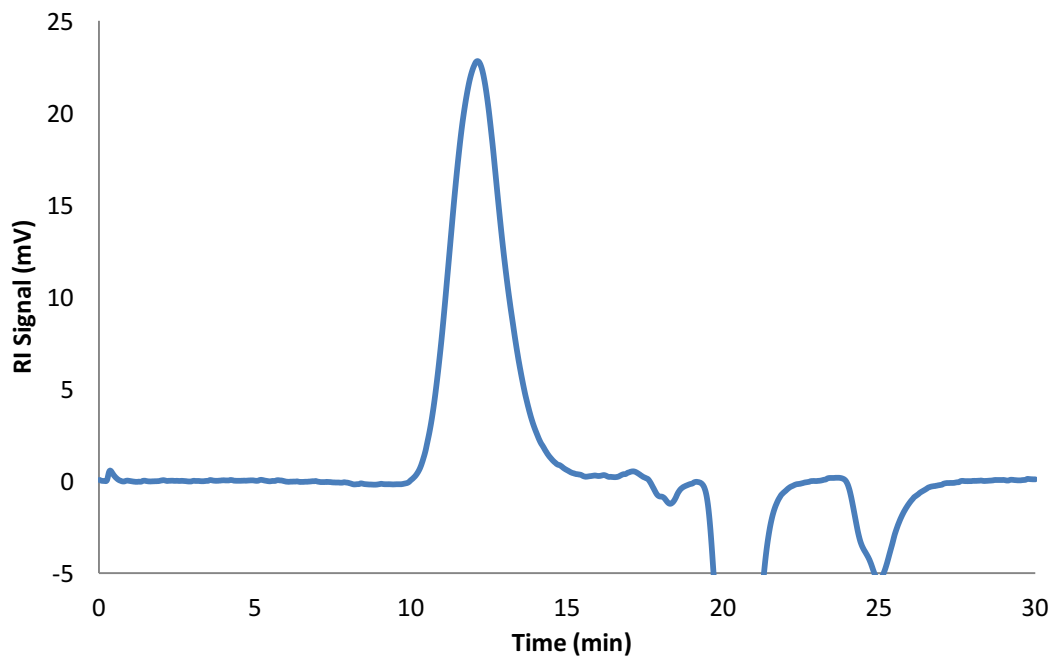


Figure A36. Polymerization of 50 equivalents of TMC; $M_n = 28100$, $M_w = 49200$, $D = 1.75$.

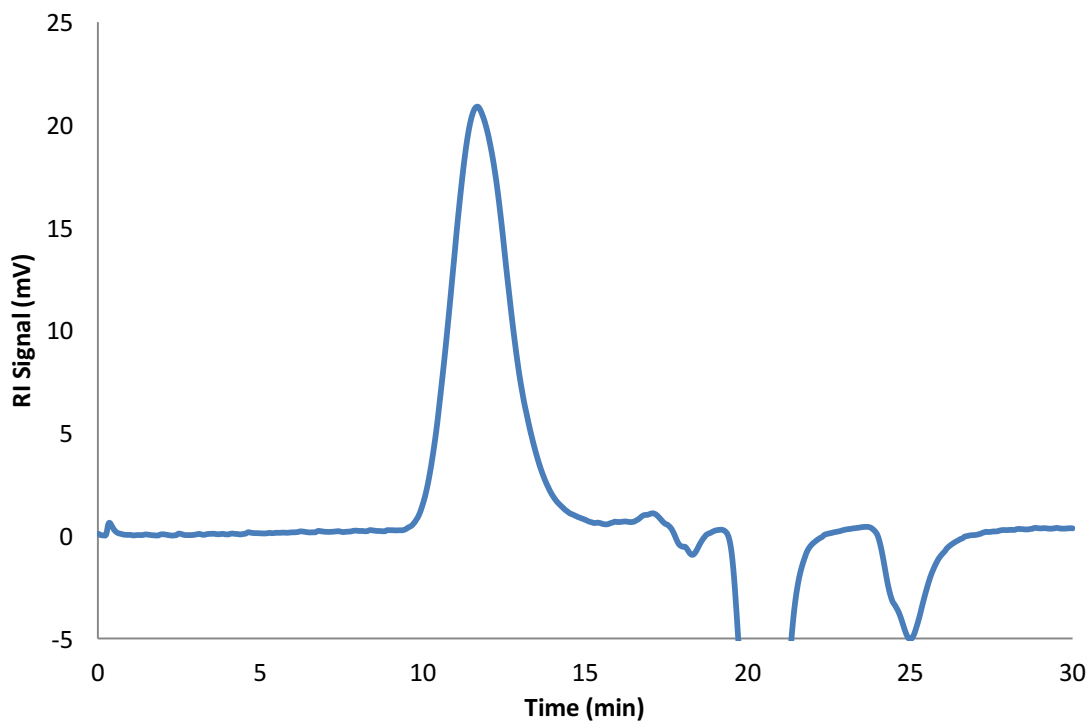


Figure A37. Polymerization of 100 equivalents of TMC; $M_n = 39800$, $M_w = 67600$, $D = 1.70$.

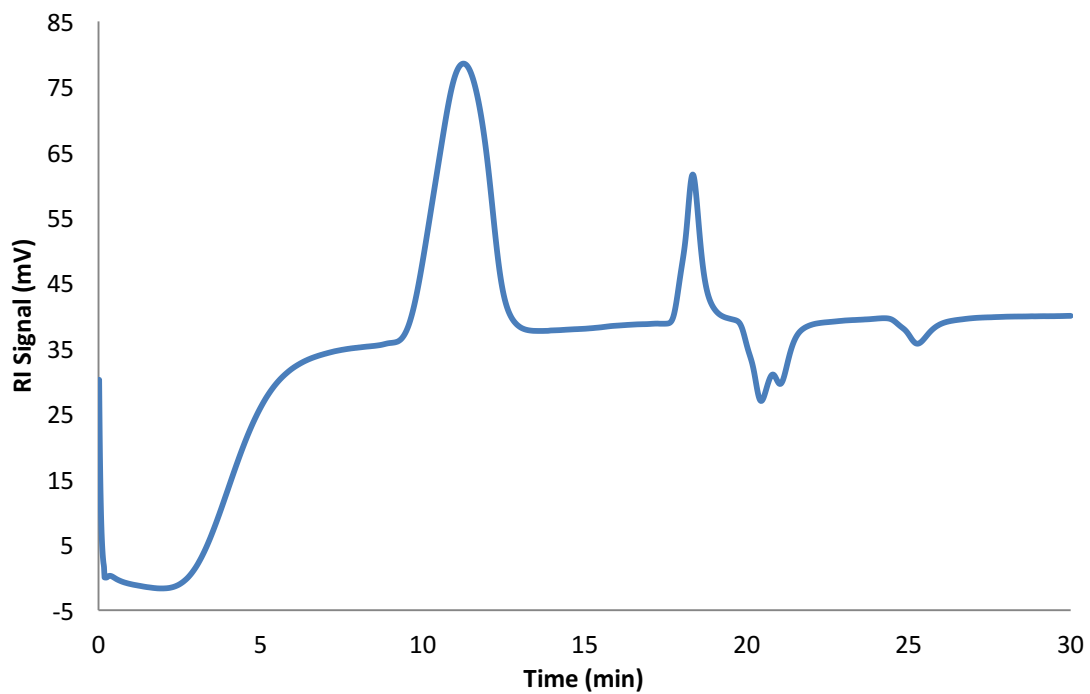


Figure A38. Polymerization of 100 equivalents of CL; $M_n = 79800$, $M_w = 108600$, $D = 1.36$.

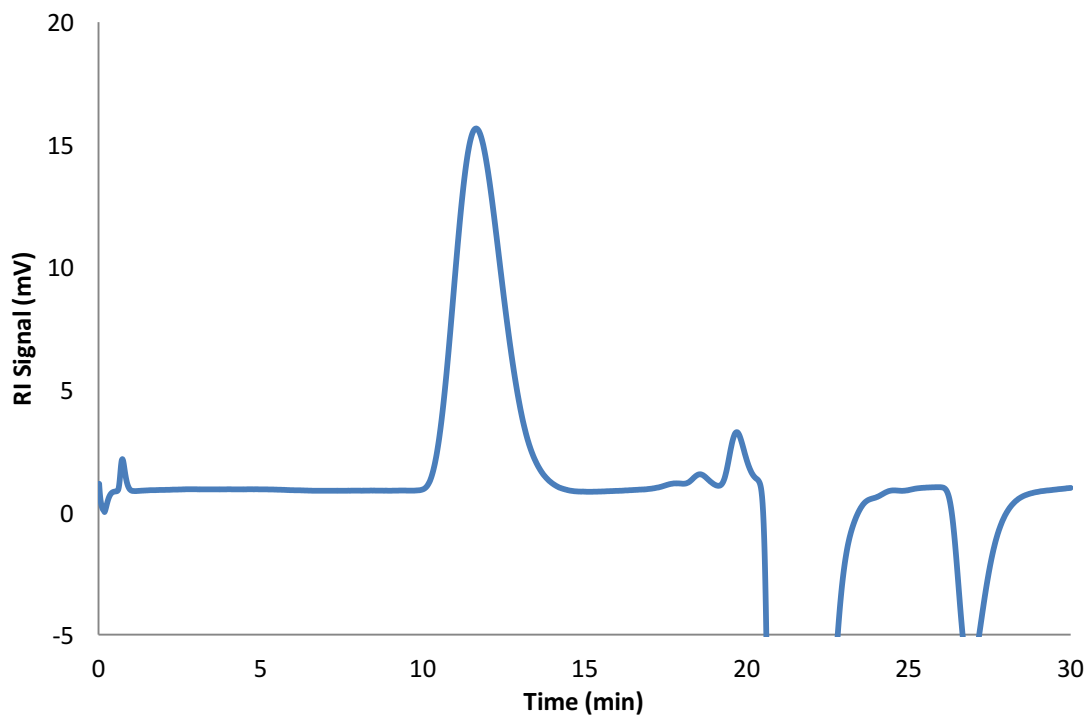


Figure A39. Polymerization of 250 equivalents of CL; $M_n = 148100$, $M_w = 184500$, $D = 1.25$.

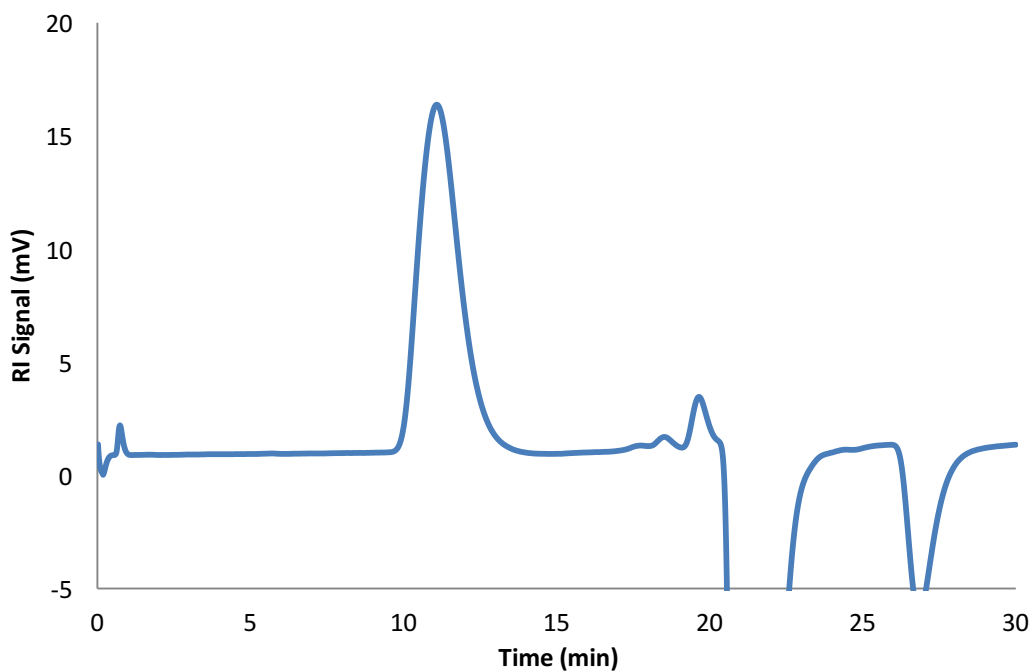


Figure A40. Polymerization of 500 equivalents of CL; $M_n = 232700$, $M_w = 276100$, $D = 1.19$.

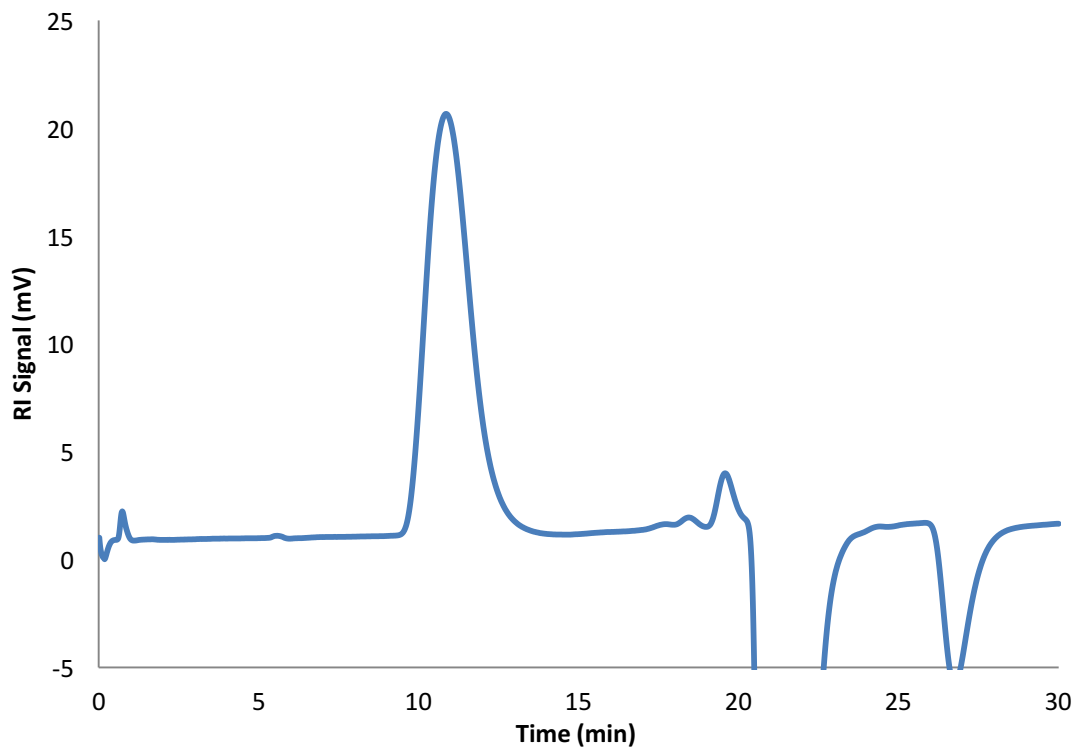


Figure A41. Polymerization of 750 equivalents of CL; $M_n = 266300$, $M_w = 323600$, $\mathcal{D} = 1.21$.

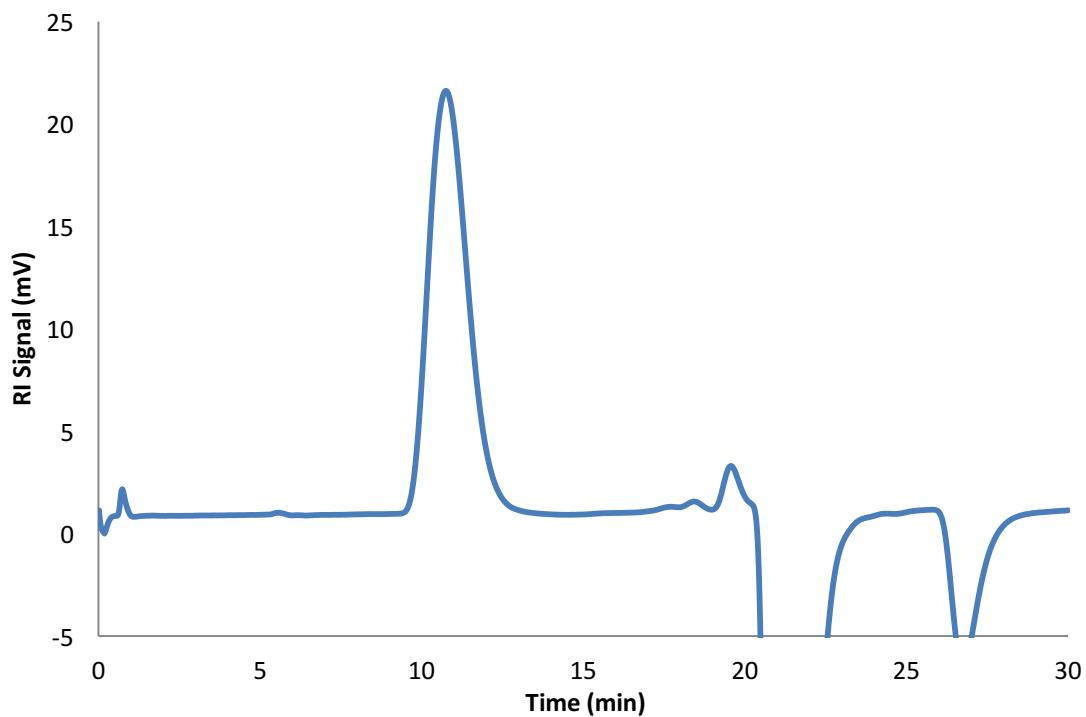


Figure A42. Polymerization of 1000 equivalents of CL; $M_n = 298100$, $M_w = 346400$, $\mathcal{D} = 1.16$.

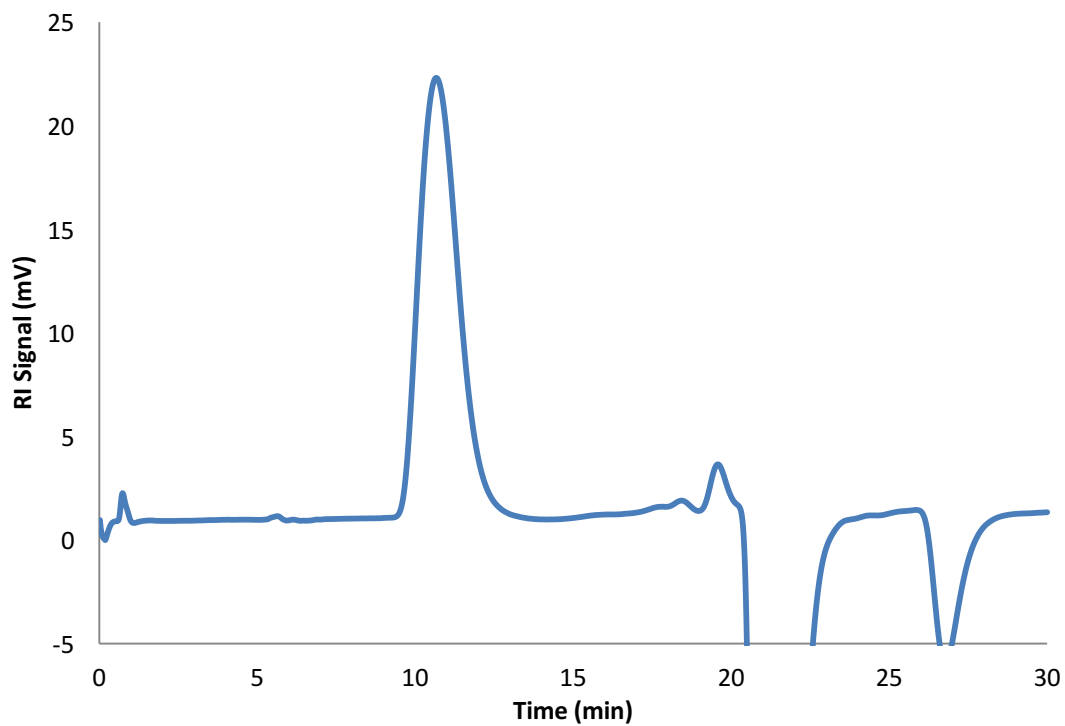


Figure A43. Polymerization of 1500 equivalents of CL; $M_n = 310000$, $M_w = 364400$, $D = 1.17$.

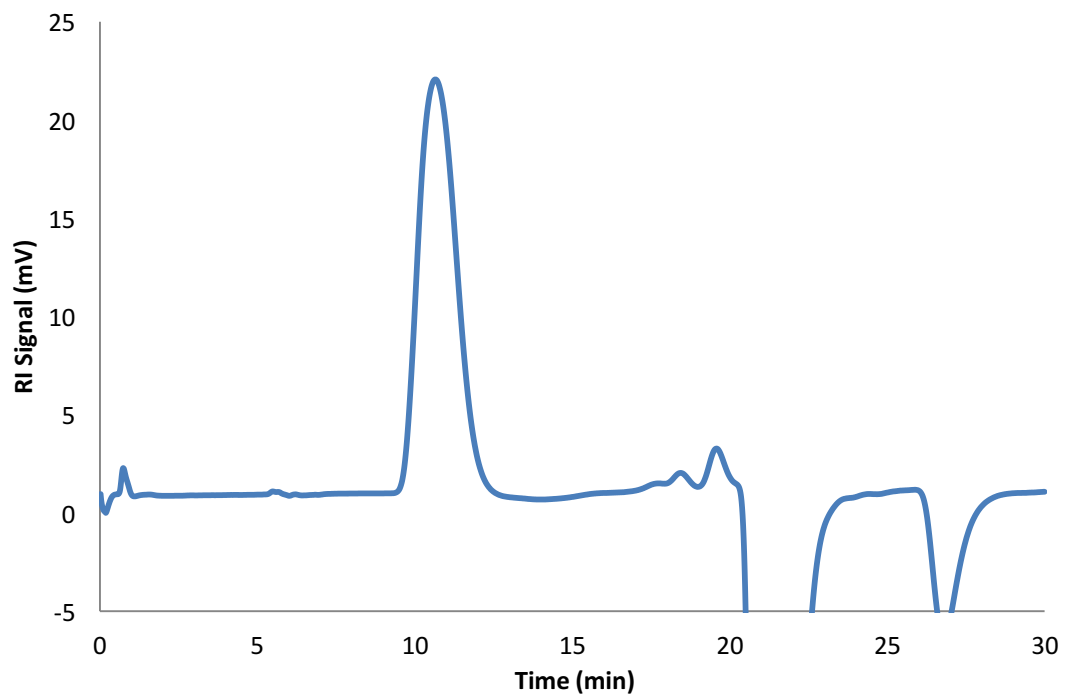


Figure A44. Polymerization of 2000 equivalents of CL; $M_n = 322500$, $M_w = 371700$, $D = 1.15$.

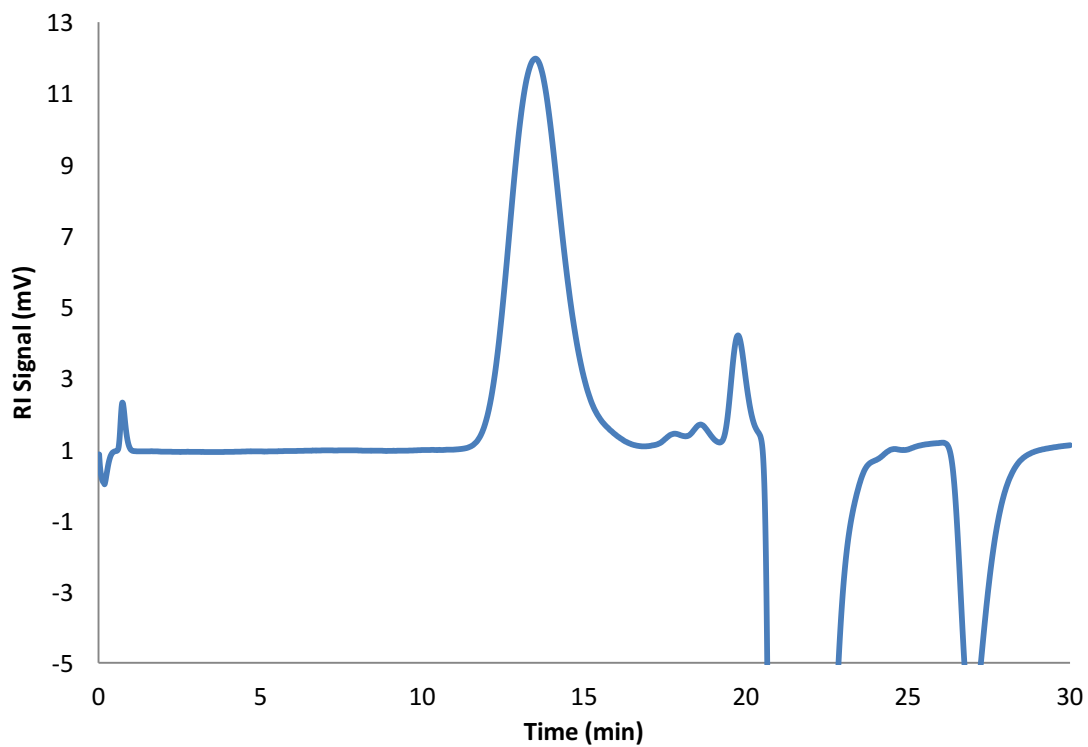


Figure A45. Polymerization of 100 equivalents of VL; $M_n = 31800$, $M_w = 46500$, $D = 1.46$.

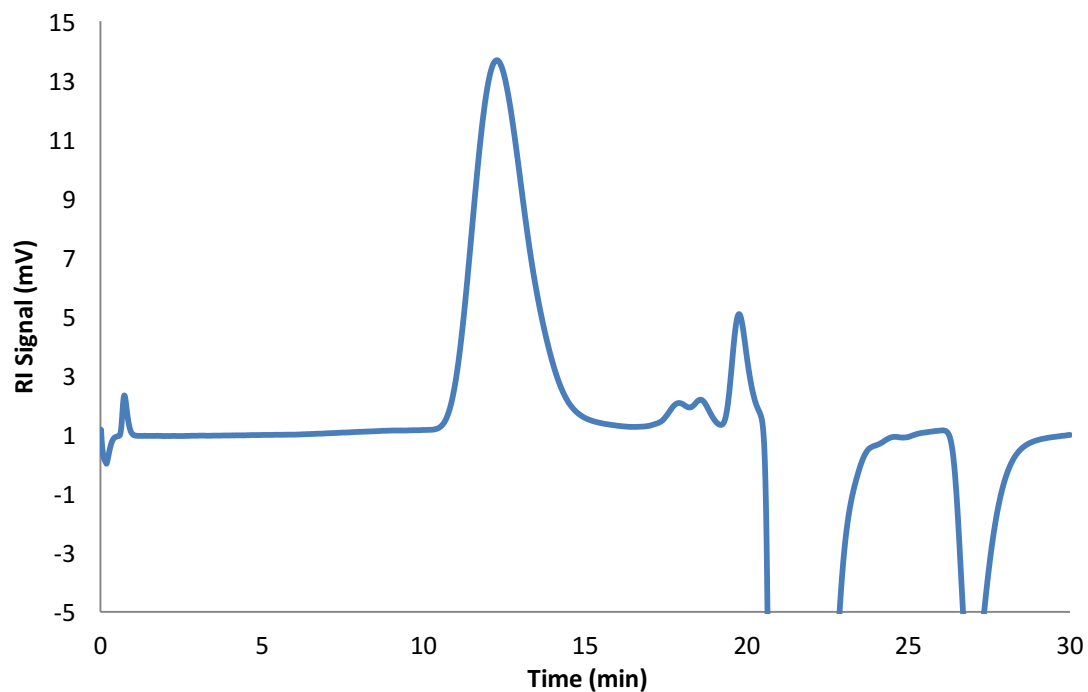


Figure A46. Polymerization of 250 equivalents of VL; $M_n = 77500$, $M_w = 113300$, $D = 1.46$.

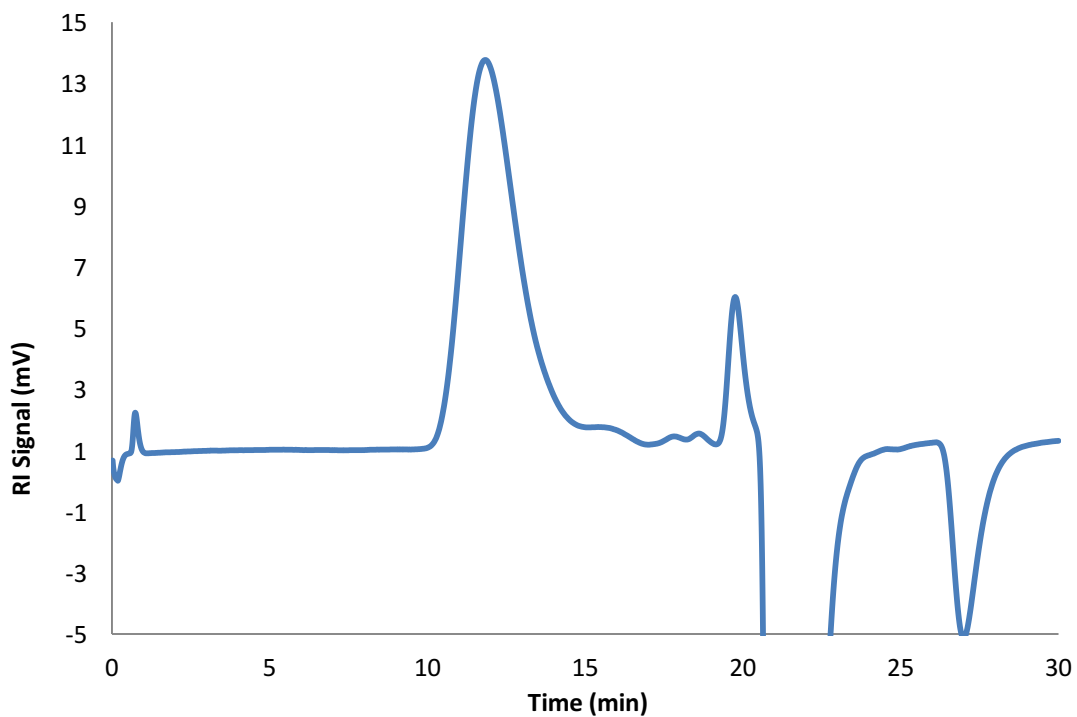


Figure A47. Polymerization of 500 equivalents of VL; $M_n = 112600$, $M_w = 156200$, $D = 1.39$.

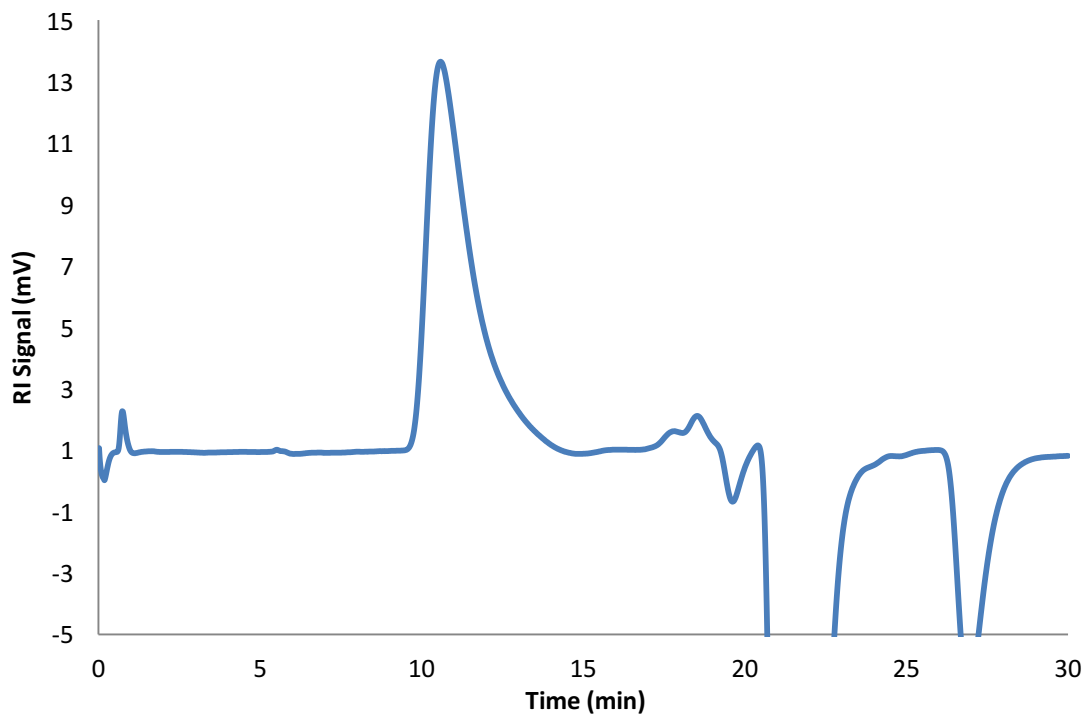


Figure A48. Polymerization of 750 equivalents of VL; $M_n = 218500$, $M_w = 312900$, $D = 1.43$.

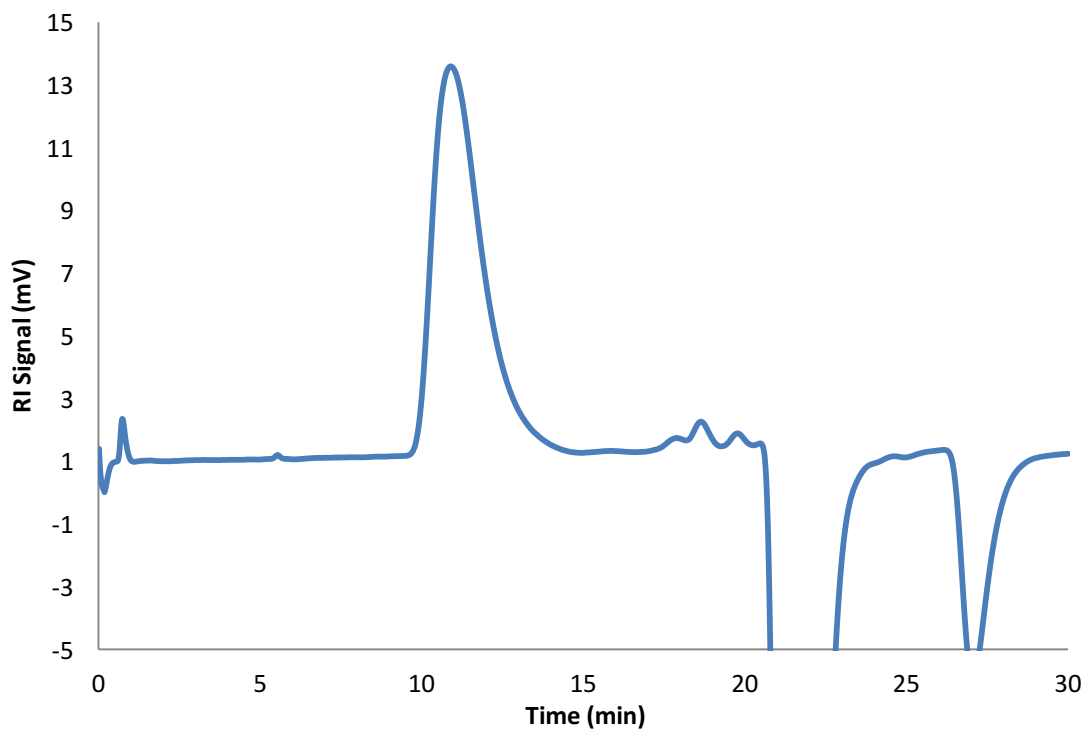


Figure A49. Polymerization of 1000 equivalents of VL; $M_n = 190300$, $M_w = 272300$, $D = 1.43$.

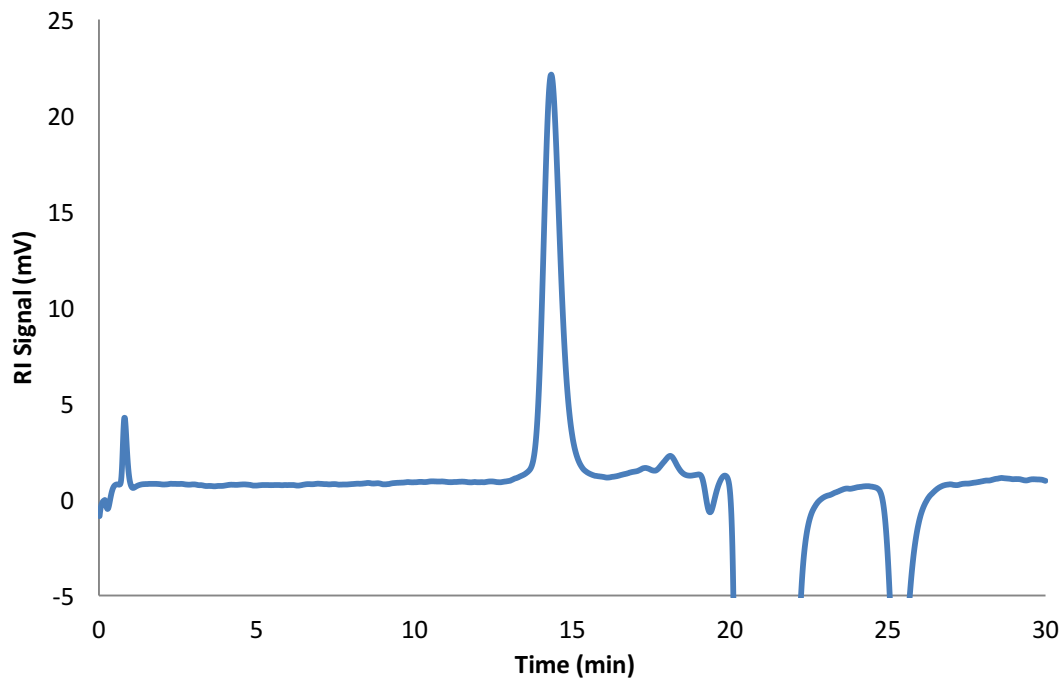


Figure A50. Polymerization of 100 equivalents of BBL; $M_n = 15000$, $M_w = 16400$, $D = 1.09$.

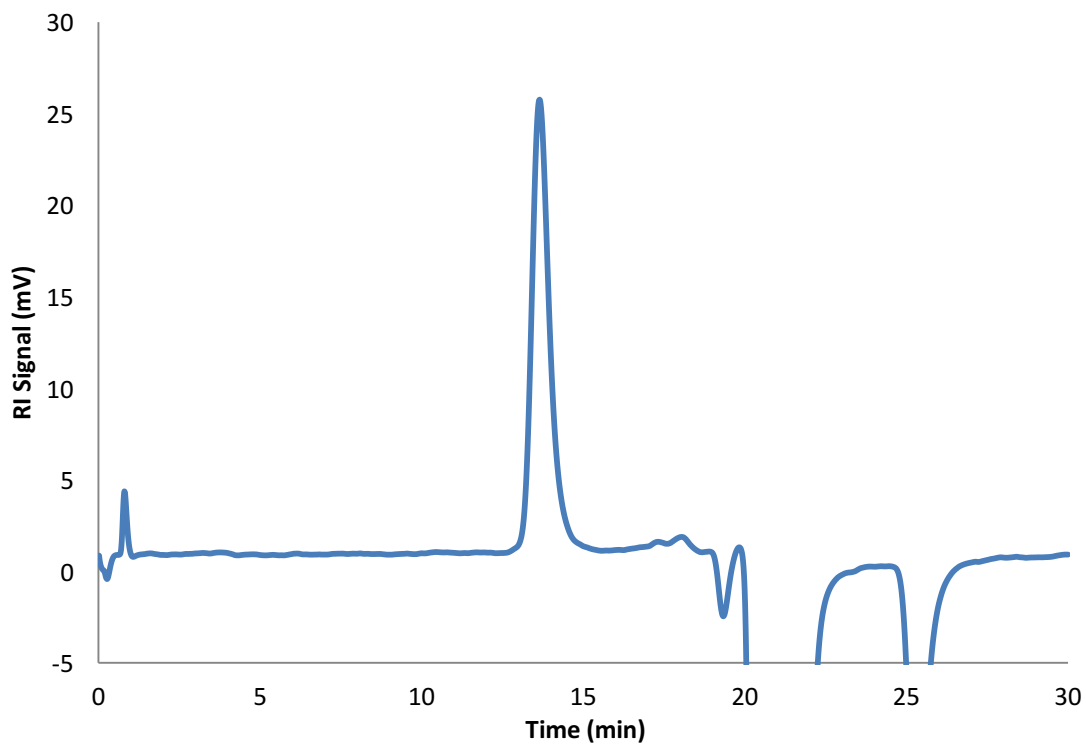


Figure A51. Polymerization of 200 equivalents of BBL; $M_n = 27800$, $M_w = 29700$, $D = 1.07$.

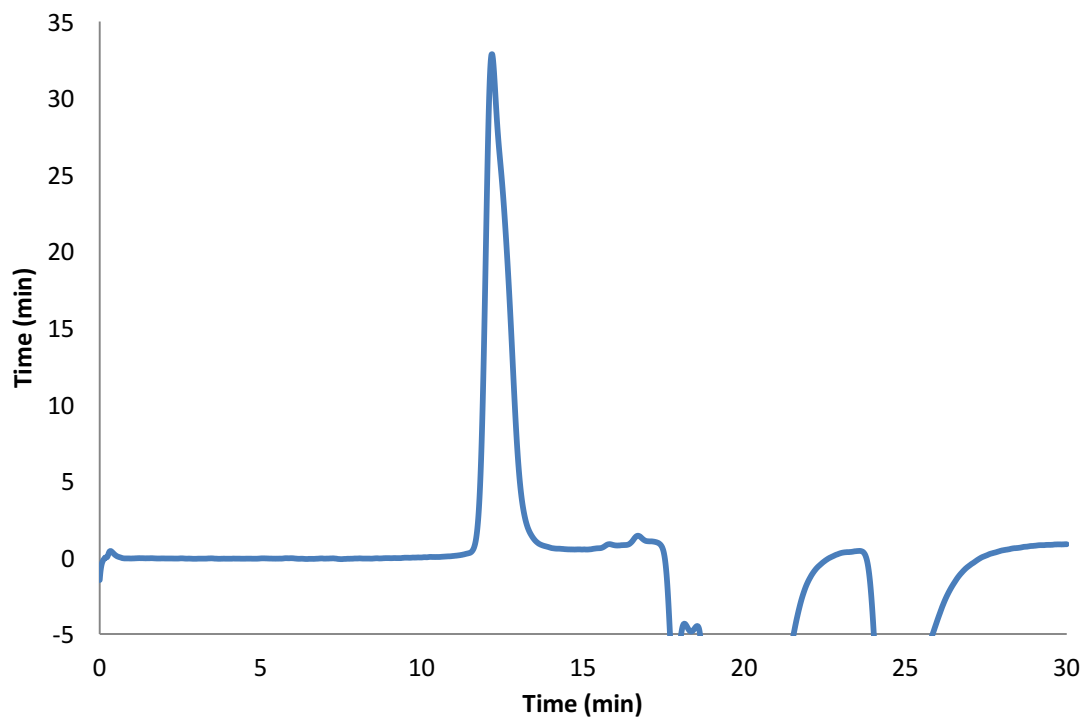


Figure A52. Polymerization of 300 equivalents of BBL; $M_n = 31200$, $M_w = 34400$, $D = 1.10$.

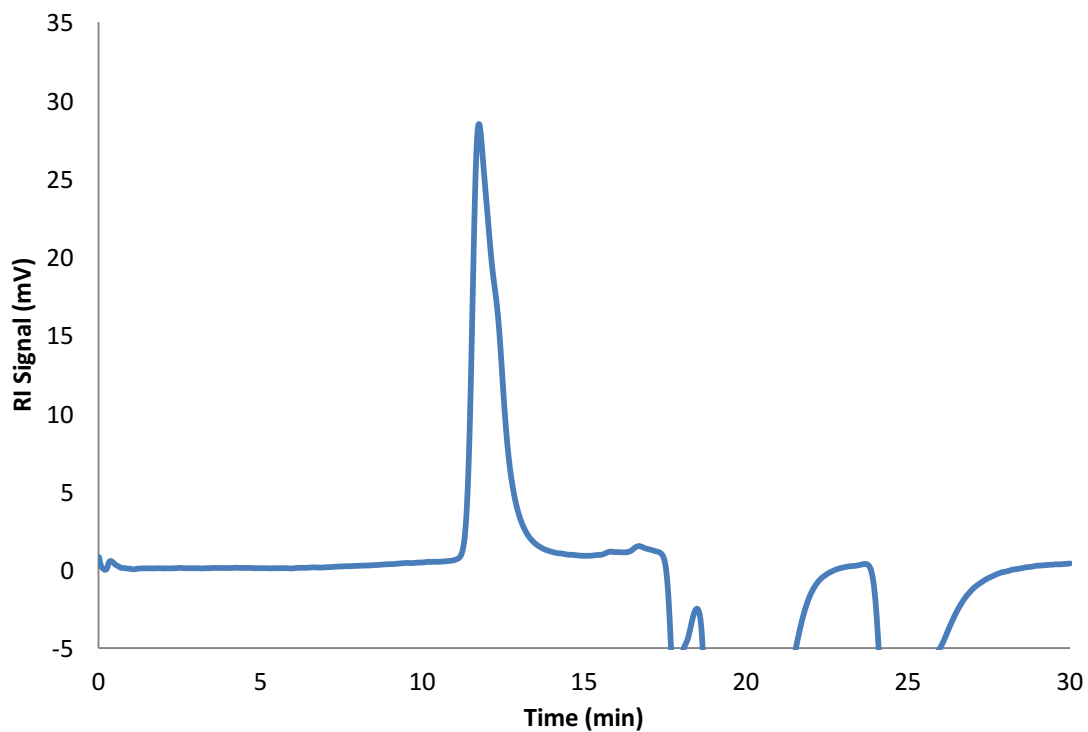


Figure A53. Polymerization of 400 equivalents of BBL; $M_n = 42400$, $M_w = 48100$, $D = 1.13$.

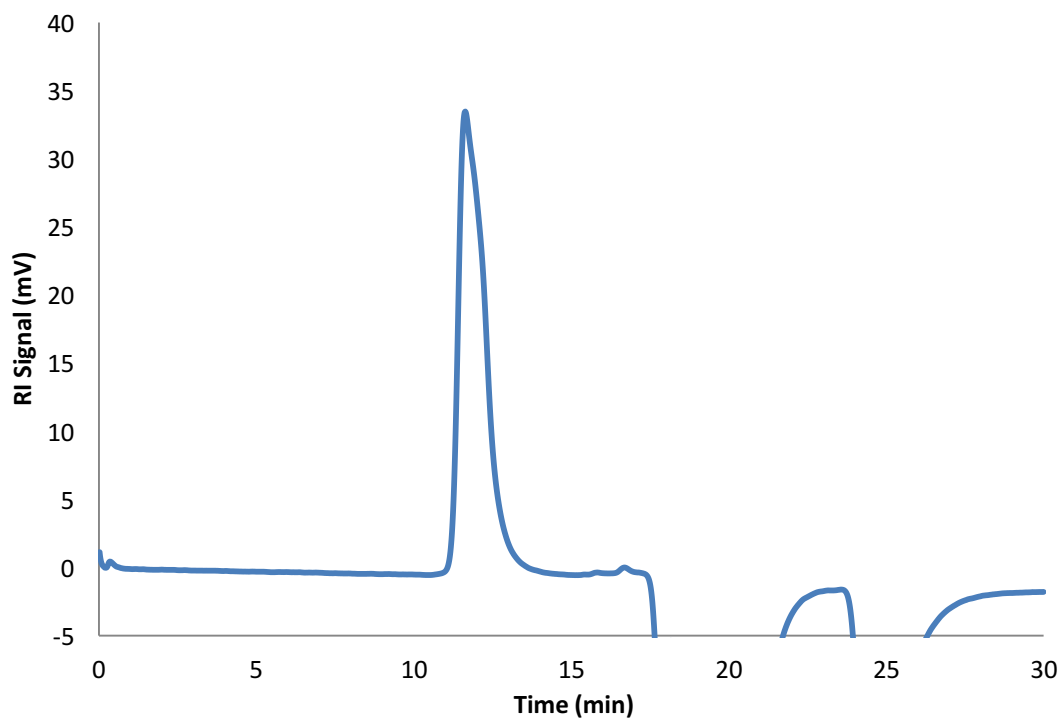


Figure A54. Polymerization of 500 equivalents of BBL; $M_n = 47200$, $M_w = 53300$, $D = 1.13$.

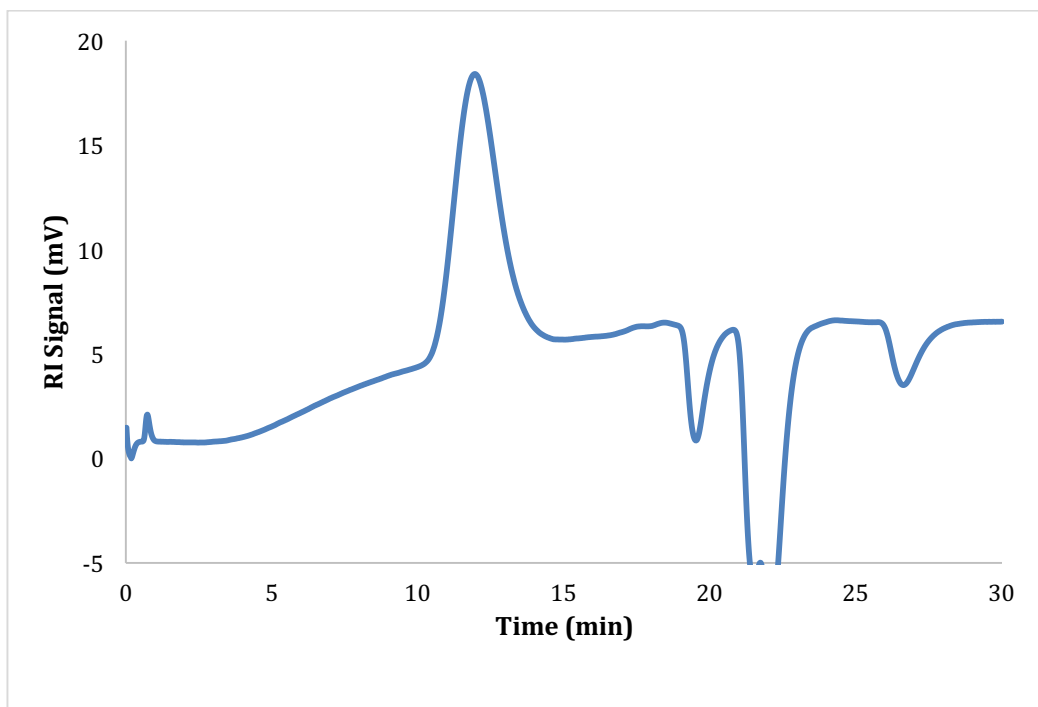


Figure A55. Polymerization of 100 equivalents of CL at 0 °C; $M_n=116300$, $M_w=160200$, $D=1.38$.

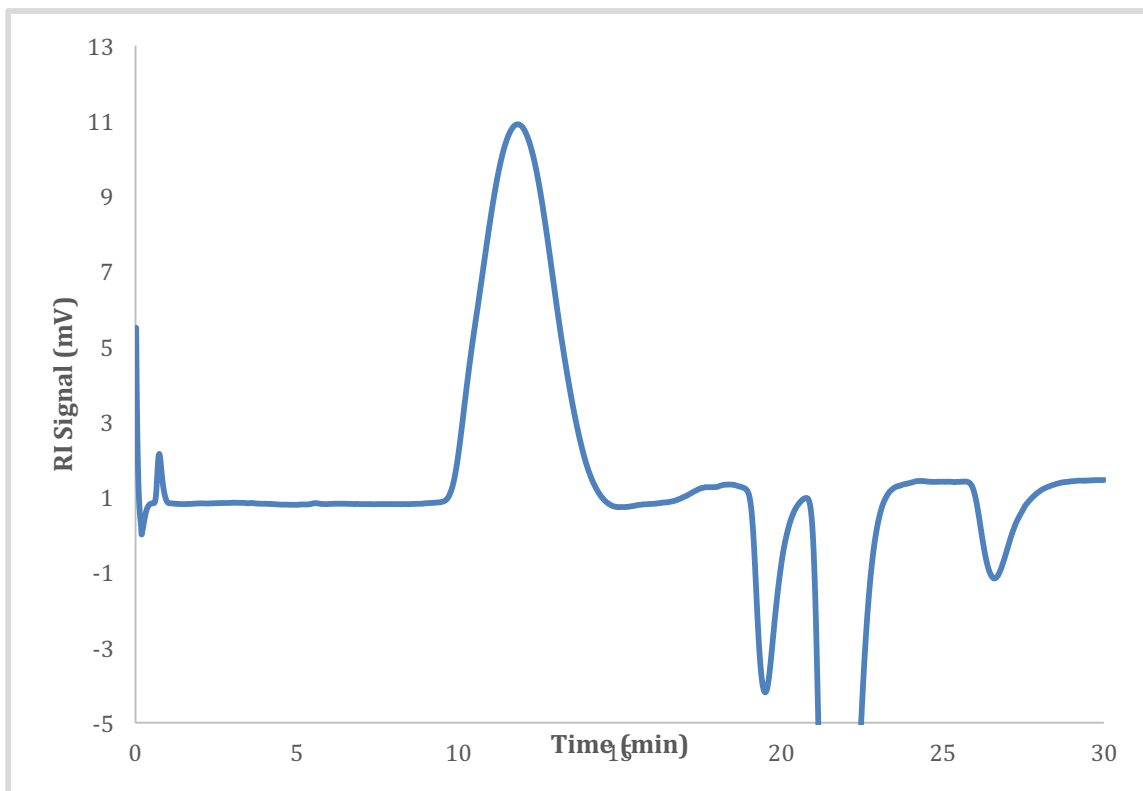


Figure A56. Polymerization of 100 equivalents of VL at 0 °C; $M_n=124500$, $M_w=205400$, $D=1.65$.

X-ray Structure Data

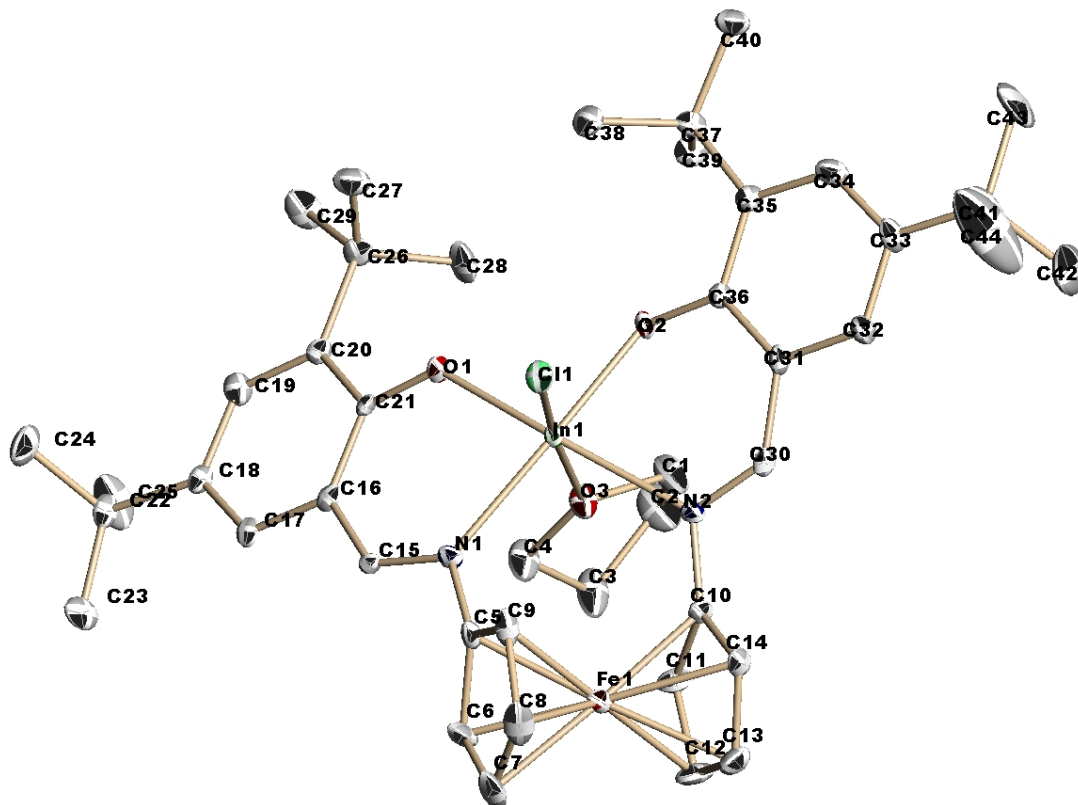


Figure A57. Thermal-ellipsoid (50% probability) representation of (salfen)InCl. Hydrogen atoms were omitted for clarity.

Single crystals suitable for X-ray diffraction were grown from a concentrated diethyl ether solution at $-35\text{ }^{\circ}\text{C}$. Crystal data for $\text{C}_{48}\text{H}_{68}\text{ClFeInN}_2\text{O}_4$; $M_r = 943.16$; orthorhombic; space group $\text{P}2(1)2(1)2(1)$; $a = 10.3658(10)\text{ \AA}$; $b = 18.6942(18)\text{ \AA}$; $c = 23.794(2)\text{ \AA}$; $\alpha = 90^{\circ}$; $\beta = 90^{\circ}$; $\gamma = 90^{\circ}$; $V = 4610.8(8)\text{ \AA}^3$; $Z = 4$; $T = 120(2)\text{ K}$; $\lambda = 0.71073\text{ \AA}$; $\mu = 0.916\text{ mm}^{-1}$; $d_{\text{calc}} = 1.359\text{ g.cm}^{-3}$; 50963 reflections collected; 9383 unique ($R_{\text{int}} = 0.0289$) giving $R_1 = 0.0225$, $wR_2 = 0.0506$ for 9156 data with $[I > 2\sigma(I)]$ and $R_1 = 0.0234$, $wR_2 = 0.0510$ for all 9383 data. Residual electron density ($\text{e}^{-}.\text{\AA}^{-3}$) max/min: 0.623/-0.727.

References

1. B. J. O'Keefe, M. A. Hillmyer and W. B. Tolman, *J. Chem. Soc., Dalton Trans.*, 2001, 2215
2. O. Dechy-Cabaret, B. Martin-Vaca and D. Bourissou, *Chem. Rev.*, 2004, **104**, 6147–6176
3. K. M. Osten, D. C. Aluthge, B. O. Patrick and P. Mehrkhodavandi, *Inorg. Chem.*, 2014, **53**, 9897–9906
4. N. Maudoux, T. Roisnel, J.-F. Carpentier and Y. Sarazin, *Organometallics*, 2014, **33**, 5740–5748
5. D. C. Aluthge, E. X. Yan, J. M. Ahn and P. Mehrkhodavandi, *Inorg. Chem.*, 2014, **53**, 6828–6836
6. M. Normand, T. Roisnel, J. F. Carpentier and E. Kirillov, *Chem. Commun.*, 2013, **49**, 11692–11694
7. J. Fang, I. Yu, P. Mehrkhodavandi and L. Maron, *Organometallics*, 2013, **32**, 6950–6956
8. D. C. Aluthge, C. Xu, N. Othman, N. Noroozi, S. G. Hatzikiriakos and P. Mehrkhodavandi, *Macromolecules*, 2013, **46**, 3965–3974
9. D. C. Aluthge, B. O. Patrick and P. Mehrkhodavandi, *Chem. Commun.*, 2013, **49**, 4295–4297
10. M. Normand, V. Dorcet, E. Kirillov and J.-F. Carpentier, *Organometallics*, 2013, **32**, 1694–1709
11. I. Yu, A. Acosta-Ramírez and P. Mehrkhodavandi, *J. Am. Chem. Soc.*, 2012, **134**, 12758–12773
12. K. M. Osten, I. Yu, I. R. Duffy, P. O. Lagaditis, J. C. C. Yu, C. J. Wallis and P. Mehrkhodavandi, *Dalton Trans.*, 2012, **41**, 8123–8134
13. M. Normand, E. Kirillov, T. Roisnel and J.-F. Carpentier, *Organometallics*, 2011, **31**, 1448–1457
14. J.-C. Buffet, J. Okuda and P. L. Arnold, *Inorg. Chem.*, 2010, **49**, 419–426
15. A. Pietrangelo, S. C. Knight, A. K. Gupta, L. J. Yao, M. A. Hillmyer and W. B. Tolman, *J. Am. Chem. Soc.*, 2010, **132**, 11649–11657
16. M. Hu, M. Wang, P. Zhang, L. Wang, F. Zhu and L. Sun, *Inorg. Chem. Commun.*, 2010, **13**, 968–971
17. M. P. Blake, A. D. Schwarz and P. Mountford, *Organometallics*, 2011, **30**, 1202–1214

18. A. Kapelski and J. Okuda, *J. Polym. Sci., Part A: Polym. Chem.*, 2013, **51**, 4983–4991
19. I. Peckermann, A. Kapelski, T. P. Spaniol and J. Okuda, *Inorg. Chem.*, 2009, **48**, 5526–5534
20. L. E. N. Allan, G. G. Briand, A. Decken, J. D. Marks, M. P. Shaver and R. G. Wareham, *J. Organomet. Chem.*, 2013, **736**, 55–62
21. C. Xu, I. Yu and P. Mehrkhodavandi, *Chem. Commun.*, 2012, **48**, 6806–6808
22. E. M. Broderick, N. Guo, C. S. Vogel, C. Xu, J. Sutter, J. T. Miller, K. Meyer, P. Mehrkhodavandi and P. L. Diaconescu, *J. Am. Chem. Soc.*, 2011, **133**, 9278–9281
23. D. M. Stevens, H. A. Watson, M.-A. LeBlanc, R. Y. Wang, J. Chou, W. S. Bauer and E. Harth, *Polym. Chem.*, 2013, **4**, 2470–2474
24. E. M. Broderick and P. L. Diaconescu, *Inorg. Chem.*, 2009, **48**, 4701–4706
25. S. Dagherne, M. Normand, E. Kirillov and J.-F. Carpentier, *Coord. Chem. Rev.*, 2013, **257**, 1869–1886
26. C. Romain, C. Fliedel, S. Bellemin-Laponnaz and S. Dagherne, *Organometallics*, 2014, **33**, 5730–5739
27. P. Brignou, J.-F. o. Carpentier and S. M. Guillaume, *Macromolecules*, 2011, **44**, 5127–5135
28. M. Helou, O. Miserque, J.-M. Brusson, J.-F. Carpentier and S. M. Guillaume, *ChemCatChem*, 2010, **2**, 306–313
29. M. Helou, O. Miserque, J.-M. Brusson, J.-F. Carpentier and S. M. Guillaume, *Chem. – Eur. J.*, 2010, **16**, 13805–13813
30. M. Schmid, S. M. Guillaume and P. W. Roesky, *Organometallics*, 2014, **33**, 5392–5401
31. A. Stjerndahl, A. Finne-Wistrand, A. C. Albertsson, C. M. Bäckesjö and U. Lindgren, *J. Biomed. Mater. Res., Part A*, 2008, **87**, 1086–1091
32. G. Jiang, I. A. Jones, C. D. Rudd and G. S. Walker, *J. Appl. Polym. Sci.*, 2009, **114**, 658–662
33. K. Shimasaki, T. Aida and S. Inoue, *Macromolecules*, 1987, **20**, 3076–3080
34. M. Isoda, H. Sugimoto, T. Aida and S. Inoue, *Macromolecules*, 1997, **30**, 57–62
35. H. Sugimoto, T. Aida and S. Inoue, *Macromolecules*, 1990, **23**, 2869–2875
36. C.-H. Huang, F.-C. Wang, B.-T. Ko, T.-L. Yu and C.-C. Lin, *Macromolecules*, 2001, **34**, 356–361
37. J. Koller and R. G. Bergman, *Organometallics*, 2011, **30**, 3217–3224

38. S. Kan, Y. Jin, X. He, J. Chen, H. Wu, P. Ouyang, K. Guo and Z. Li, *Polym. Chem.*, 2013, **4**, 5432–5439
39. M. Akay, *Introduction to Polymer Science and Technology*, Ventus Publishing, 2012
40. F. Cogswell, *Polymer Melt Rheology: A Guide for Industrial Practice*, Woodhead Publishing Ltd., 2003
41. K. N. Houk, A. Jabbari, H. K. Hall and C. Alemán, *J. Org. Chem.*, 2008, **73**, 2674–2678
42. A. Amgoune, C. M. Thomas and J.-F. Carpentier, *Macromol. Rapid Commun.*, 2007, **28**, 693–697
43. C. Agatemor, A. E. Arnold, E. D. Cross, A. Decken and M. P. Shaver, *J. Organomet. Chem.*, 2013, **745–746**, 335–340
44. E. D. Cross, L. E. N. Allan, A. Decken and M. P. Shaver, *J. Polym. Sci., Part A: Polym. Chem.*, 2013, **51**, 1137–1146
45. D. J. Darensbourg, O. Karroonnirun and S. J. Wilson, *Inorg. Chem.*, 2011, **50**, 6775–6787
46. P. Kurcok, P. Dubois and R. Jérôme, *Polym. Int.*, 1996, **41**, 479–485
47. R. Potzsch, B. C. Stahl, H. Komber, C. J. Hawker and B. I. Voit, *Polym. Chem.*, 2014, **5**, 2911–2921
48. D. Mecerreyes, P. Dubois, R. Jérôme, J. L. Hedrick and C. J. Hawker, *J. Polym. Sci., Part A: Polym. Chem.*, 1999, **37**, 1923–1930
49. B. M. Chamberlain, M. Cheng, D. R. Moore, T. M. Ovitt, E. B. Lobkovsky and G. W. Coates, *J. Am. Chem. Soc.*, 2001, **123**, 3229–3238
50. L. R. Rieth, D. R. Moore, E. B. Lobkovsky and G. W. Coates, *J. Am. Chem. Soc.*, 2002, **124**, 15239–15248
51. A. B. Pangborn, M. A. Giardello, R. H. Grubbs, R. K. Rosen and F. J. Timmers, *Organometallics*, 1996, **15**, 1518–1520.
52. E. M. Broderick, P. S. Thuy-Boun, N. Guo, C. S. Vogel, J. Sutter, J. T. Miller, K. Meyer and P. L. Diaconescu, *Inorg. Chem.*, 2011, **50**, 2870–2877.
53. X. Wang, A. Thevenon, J. L. Brosmer, I. Yu, S. I. Khan, P. Mehrkhodavandi and P. L. Diaconescu, *J. Am. Chem. Soc.*, 2014, **136**, 11264–11267.
54. M. H. Chisholm, S. S. Iyer and M. E. Matison, *Chem. Commun.*, **20**, 1997, 1999–2000.

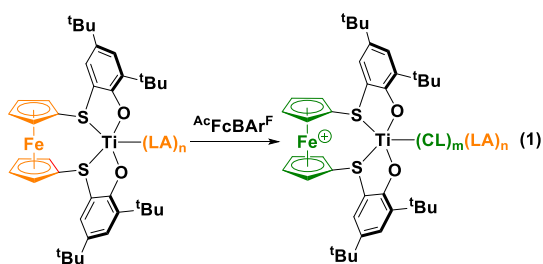
Chapter 2: Redox-switchable Copolymerization of Cyclic Esters and Ethers by a Zirconium Complex

2.1 Introduction

Synthetic polymers are ubiquitous in today's world. Their applications range from everyday items such as molded car interiors and plastic utensils to specialty objects like absorbable medical sutures and drug delivery materials.¹ Most plastics are derived from petroleum feedstocks and are non-biodegradable, but there is a growing sector of bio-sourced and biodegradable materials that is beginning to replace environmentally hostile substances.² Aliphatic polyesters and polyethers are particularly appealing because they can be prepared in a highly controlled fashion by the ring-opening polymerization of bio-derived lactones, lactides, and epoxides.^{1a, 2a} In general, the properties of polyesters and polyethers formed from only one monomer (homopolymers) are not as diverse as those of polymers made from multiple monomers (copolymers).^{1c, 3} Various copolymer structures exist and can be envisioned, ranging from a random sequence of monomers (A and B) to precisely controlled positions along the polymer chain.⁴

AB diblock and ABA triblock copolymers have emerged as some of the most common types of copolymers due to the number of methods available for their preparation. Living polymerization mechanisms such as atom transfer free radical polymerization, reversible addition fragmentation chain transfer, coordination-insertion, and anionic or cationic ring opening polymerization combined with step-growth techniques such as telechelic polymerization,⁵ end-group modification,⁶ and multi-functional initiator⁷ have allowed a greater degree of control over polymer block lengths than ever before.

However, few methods exist that do not require additional modification steps in order to achieve a precise control of the copolymer structure.⁸ Our group's aim is to design initiator systems that can create block copolymer^{8b, 9} by selectively polymerizing monomers in different oxidation states.^{9a, 9b, 10}



Equation 2.1 One-pot ring-opening polymerization of LA and CL by (thiolfan*)Ti(OⁱPr)₂ (thiolfan* = 1,1'-di(2-*tert*-butyl-6-thiophenoxy)ferrocene).

Xinke Wang reported the first example of switching *in situ* between the reduced ((salfan)Zr(OⁱBu)₂, salfan = 1,1'-di(2-*tert*-butyl-6-*N*-methylmethylenephenoxy)ferrocene) and oxidized ([((salfan)Zr(OⁱBu)₂)]₂[BAR^F₄]) forms of a metal complex that resulted in a change in the rate of polymerization of L-lactide (LA) and ε-caprolactone (CL), respectively.^{8b} One-pot copolymerization of the two monomers (Equation 2.1) to give a block copolymer was also achieved by using a titanium complex, (thiolfan*)Ti(OⁱPr)₂ (thiolfan* = 1,1'-di(2-*tert*-butyl-6-thiophenoxy)ferrocene). Unfortunately, the activity was low and the incorporation of ε-caprolactone was only about 17% before both monomers were polymerized at comparable rates by the oxidized initiator. Herein, we report the redox-switchable copolymerization^{8b, 11} of L-lactide or β-butyrolactone (A) and epoxides (B) and the formation of ABA or BAB type copolymers by using a zirconium alkoxide complex supported by a ferrocene-based ligand, (salfan)Zr(OⁱBu)₂. The synthesis of diblock polylactide/polycyclohexene oxide copolymers using

a bis(imino)pyridine iron complex was recently reported by using a redox switch at the metal performing the polymerization reactions.¹¹ For more detailed mechanistic discussions of the copolymerizations examined in this paper, please see Chapter 3.

2.2 Results and discussion

The synthesis of (salfan)Zr(O^tBu)₂ was reported previously.^{8b} While studying the influence that the solvent has on polymerization activity, we noticed that [(salfan)Zr(O^tBu)₂][BAR^F₄] can polymerize THF (Figure B1). Therefore, we reasoned that [(salfan)Zr(O^tBu)₂][BAR^F₄] may also ring-open polymerize other cyclic ethers (Table 2.1). Cyclohexene oxide (CHO) stood out as a highly active orthogonal partner for L-lactide since no conversion is observed with (salfan)Zr(O^tBu)₂ after 24 h (Table 2.1, entry 7), while [(salfan)Zr(O^tBu)₂][BAR^F₄] polymerizes 95% of it in an hour and a half (Table 2.1, entry 8). Although in low conversion, propylene oxide (Table 2.1, entry 10) and oxetane (Table 2.1, entry 12) showed slightly higher activity with [(salfan)Zr(O^tBu)₂][BAR^F₄] than (salfan)Zr(O^tBu)₂. A similar selectivity to that previously reported for L-lactide^{8b} (Table 2.1, entry 1) was observed for β-butyrolactone: (salfan)Zr(O^tBu)₂ polymerizes 96% of the monomer (Table 2.1, entry 3), while [(salfan)Zr(O^tBu)₂][BAR^F₄] converts only 11% of it (Table 2.1, entry 4). Almost no reactivity was observed toward succinic anhydride in the presence of either preinitiator (Table 2.1, entries 5-6).

Several studies were conducted to probe the possibility of carrying out redox-switchable copolymerizations. Conversion studies were carried out to determine CHO and LA's potential for a controlled redox-switchable copolymerization. The reversibility of the CHO polymerization was demonstrated by an “on-off-on” polymerization (Figure 2.1), where the polymerization was turned “off” by the addition of a reductant (CoCp₂) and turned back “on” by the addition of an

oxidant (${}^{\text{Ac}}\text{FcBAR}^{\text{F}}$). The corresponding LA “on-off-on” polymerization was previously reported.^{8b} Since living polymerizations are important toward controlling the molecular weight and structure of multi-block copolymers, the possibility of living character in LA and CHO homopolymerizations was determined by plotting M_n versus percent conversion. The polymerization of LA by (salfan)Zr(O^tBu)₂ was found to not exhibit any chain transfer (Figure 2.2), while the polymerization of CHO by [(salfan)Zr(O^tBu)₂][BAR^F₄] was found to be not living (Figure 2.3). Furthermore, while probing the effect that the presence of the other monomer has on polymerization rates, it was found that the polymerization of LA is faster in the presence of CHO (Figure 2.4), while the polymerization of CHO is faster in the absence of LA (Figure 2.5).

Table 2.1. Polymerization of different monomers with (salfan)Zr(O^tBu)₂ (red) and [(salfan)Zr(O^tBu)₂][BAR^F₄] (ox).

Entry	Initiator	Monomer	Time	Conversion ^a
1	red	LA	3 h	93%
2	ox	LA	24 h	0
3	red	BBL	24 h	94%
4	ox	BBL	24 h	11%
5	red	SA	24 h	<5%
6	ox	SA	24 h	0
7	red	CHO	24 h	0
8	ox	CHO	1.5 h	95%
9	red	PO	24 h	0
10	ox	PO	24 h	16%
11	red	OX	24 h	0
12	ox	OX	24 h	10%

Conditions: [M]/[I] = 100, [I] = 0.01 mM, 100 °C, C₆D₆ as a solvent, 1,3,5- trimethoxybenzene as an internal standard, ${}^{\text{Ac}}\text{FcBAR}^{\text{F}}$ as oxidant. LA = L-lactide, BBL = β-butyrolactone, PO = propylene oxide, OX = oxetane, SA = succinic anhydride, CHO = cyclohexene oxide, SO = styrene oxide. ^a Conversion calculated by integration of polymer peaks versus internal standard.

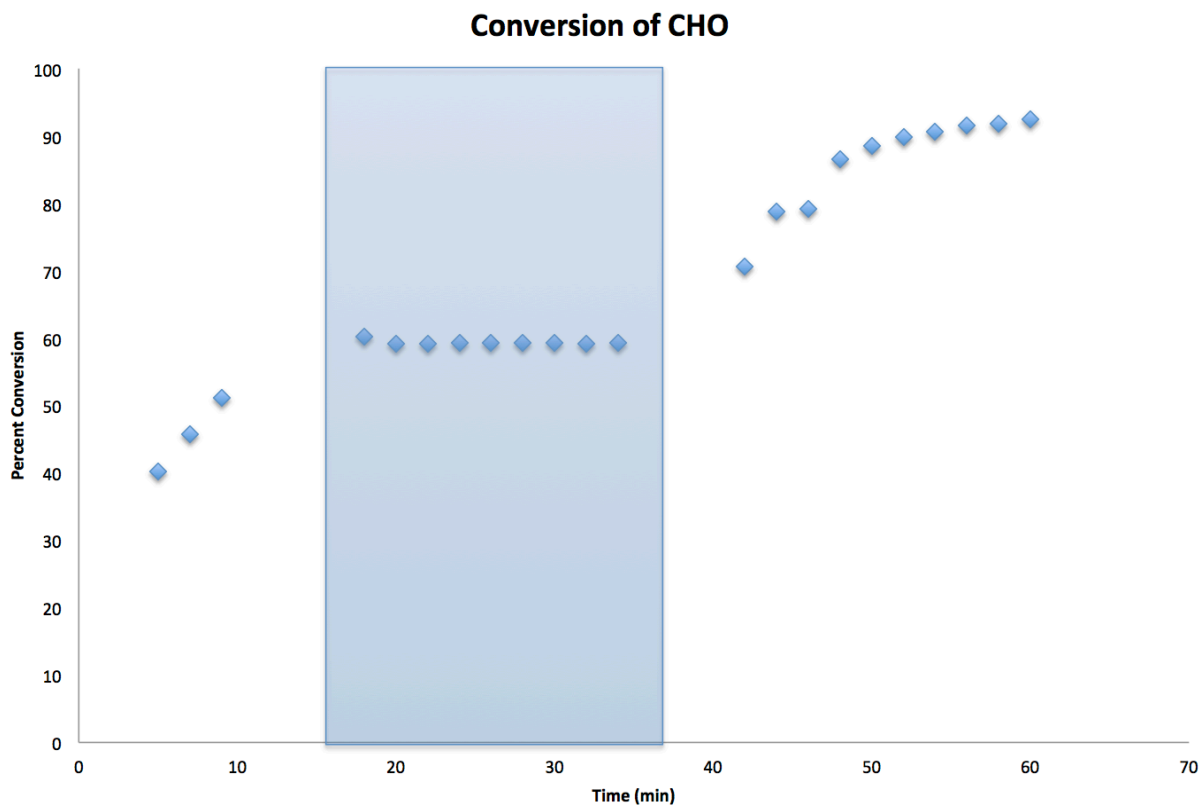
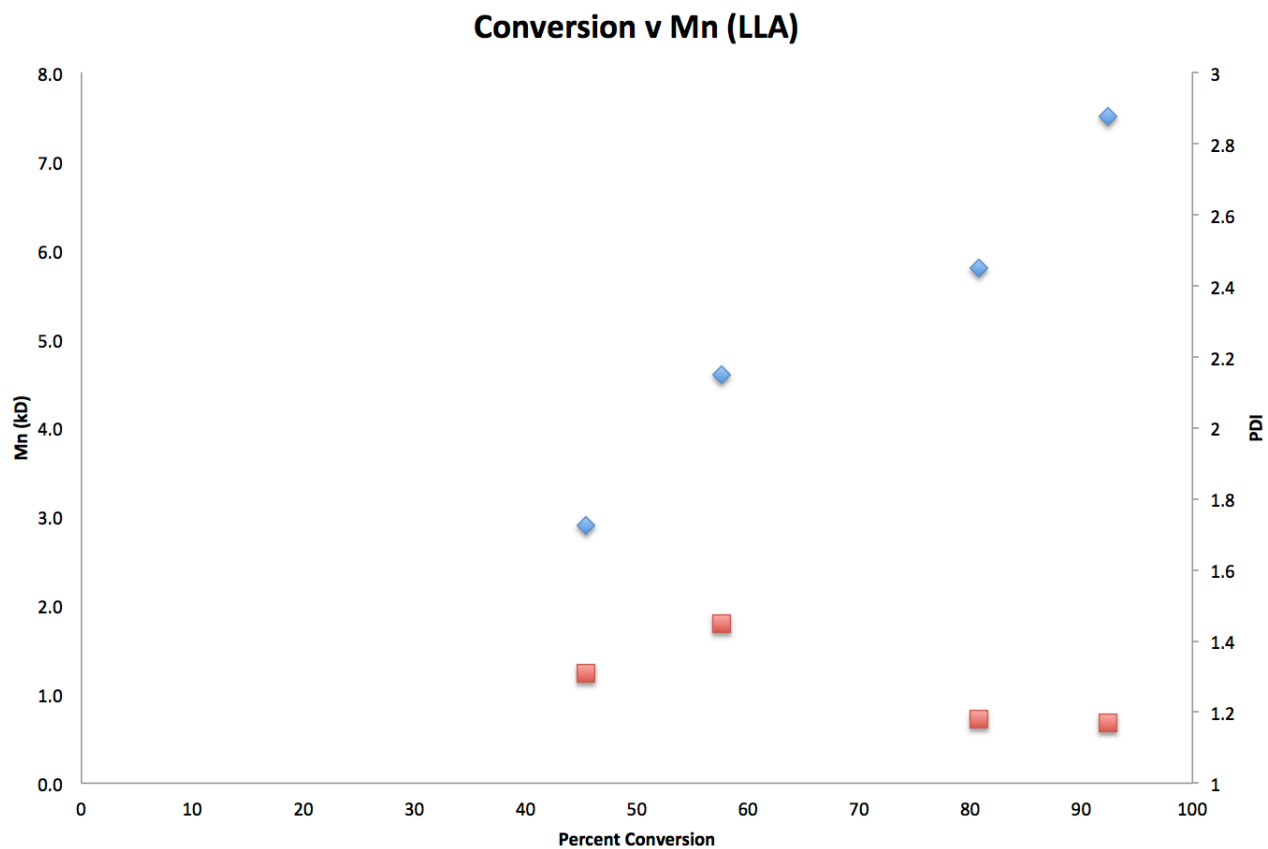
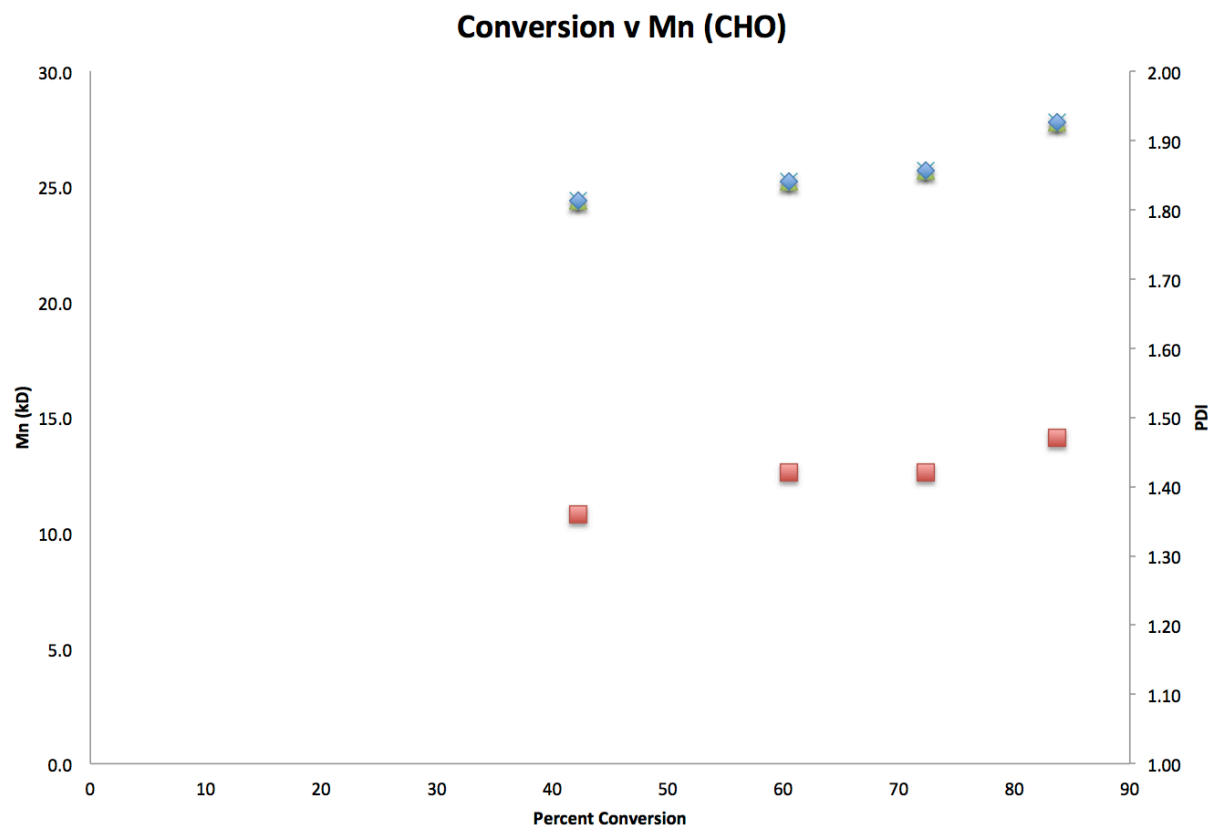


Figure 2.1. Polymerization of cyclohexene oxide by (salfan)Zr(O^tBu)₂. Polymerization is switched off by the addition of ^{Ac}FcBAR^F and switched on by the addition of CoCp₂. The corresponding lactide polymerization diagram can be found at DOI: 10.1021/ja505883u.



Time	Conversion	M_{n,NMR}	M_{n,GPC}	<i>D</i>
60	45.4	3.3	2.9	1.31
50	57.6	4.1	4.6	1.45
140	80.8	5.8	5.8	1.18
440	92.4	6.7	7.5	1.17

Figure 2.2. Conversion of L-lactide versus M_n by (salfan)Zr(O^tBu)₂.



Time (min)	Conversion	M_n, NMR	M_n, GPC	<i>D</i>
13	42.2	4.1	24.4	1.36
28	60.5	5.9	25.2	1.42
42	72.3	7.1	25.7	1.42
71	83.7	8.2	27.8	1.47

Figure 2.3. Conversion of cyclohexene oxide versus M_n by [(salfan)Zr(O^tBu)₂][BAr^F₄]. See experimental for conditions.

Conversion vs. Time (LA)

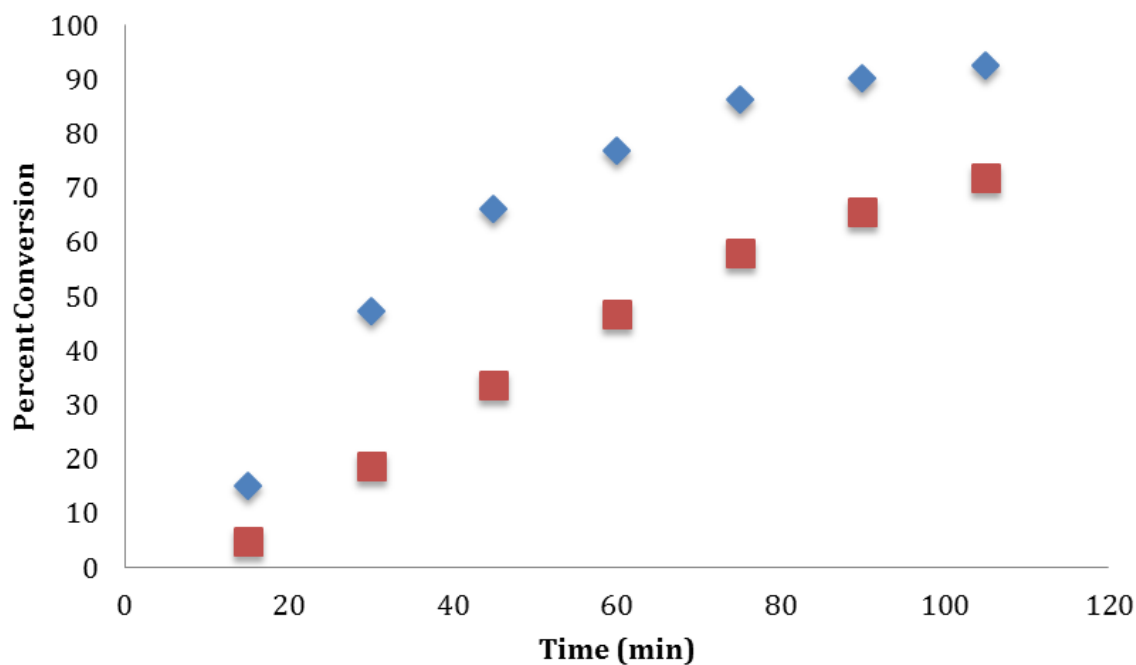


Figure 2.4. Conversion of 100 equivalents of L-lactide to PLA vs time with (blue) and without (orange) 100 equivalents of cyclohexene oxide (0.66 M) in 4 : 1 C_6D_6 : $o\text{-}F_2C_6H_4$.

Conversion vs. Time (CHO)

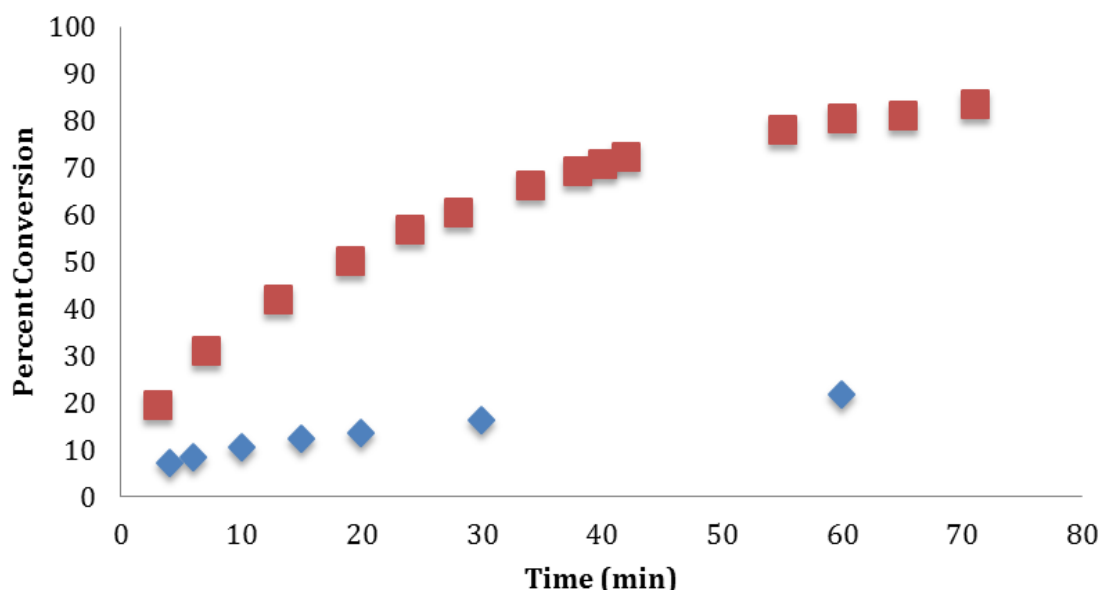


Figure 2.5. Conversion of 100 equivalents of cyclohexene oxide to PCHO vs time with (blue) and without (orange) 100 equivalents of L-lactide (0.66 M) in 4 : 1 C_6D_6 : $o\text{-}F_2C_6H_4$.

Table 2.2. One-pot copolymerization of two different monomers by (salfan)Zr(O^tBu)₂ (red) or [(salfan)Zr(O^tBu)₂][BAR^F₄] (ox).

Entry	Monomer 1	Monomer 2	Initiator	Conversion ^a	M _n ^b	<i>D</i> ^c	Appendix Figures ^d
1	BBL	CHO	red	78%-0%	4.8	1.22	B14, B85
2	BBL	CHO	red-ox	86%-92%	4.2	1.44	B15, B86
3	BBL	CHO	ox	0%-97%	8.3	1.51	B16, B87
4	BBL	CHO	ox-red	69%-97%	9.7	1.55	B17, B88
5	LA	PO	ox	9%-trace	-	-	B18
6	LA	PO	ox-red	95%-trace	16.4	1.65	B19, B89
7	LA	OX	ox	9%-trace	-	-	B20
8	LA	OX	ox-red	88%-trace	14.1	1.66	B21, B90
9	LA	CHO	red	45%-0%	8.0	1.13	B22, B91
10	LA	CHO	red-ox	45%-75%	7.6	1.29	B23, B92
11	LA	CHO	ox	trace-54%	5.5	1.54	B24, B93
12	LA	CHO	ox-red	85%-70%	12.3	1.44	B25, B94

Conditions: [M]/[I] = 100, [I] = 0.01 mM, 100 °C, (4:1) benzene-d₆: 1,2-difluorobenzene as solvent, 1,3,5-trimethoxybenzene as an internal standard, ^{Ac}FcBAR^F as oxidant. LA = L-lactide, BBL = β-butyrolactone, PO = propylene oxide, OX = oxetane, CHO = cyclohexene oxide, SO = styrene oxide. ^a Conversion calculated by integration of polymer peaks versus internal standard. The first number indicates conversion of Monomer 1, while the second number indicates conversion of Monomer 2. ^b M_n values are reported in 10³ g/mol. Narrow molecular weight polystyrene standards were used for calibration purposes, but reported M_n values were not corrected. ^c *D* = M_w/M_n ^d ¹H NMR spectrum, GPC trace

In order to determine whether the orthogonal behavior would persist in a polymerization with both monomers present, we evaluated several combinations of epoxides and L-lactide or β-butyrolactone (Table 2.2). For example, the combination of L-lactide with propylene oxide or oxetane showed similar activity in the presence of the two monomers as their individual polymerizations, incorporating small percentages of the epoxide and L-lactide during the oxidized phase, and polymerizing L-lactide rapidly in the reduced state (Table 2.2, entries 5-8). Since the polymerization of the cyclic ethers was low, no significant change in molecular weight was observed compared to the polymerization of just L-lactide. Importantly, β-butyrolactone

with cyclohexene oxide demonstrated significant conversions by ^1H NMR spectroscopy. The oxidized initiator polymerized 100 equivalents of cyclohexene oxide in about one hour (Table 2.2, entry 3). Once reduced, the initiator polymerized the same number of equivalents of β -butyrolactone overnight (Table 2.2, entry 4). The copolymerization rate for β -butyrolactone was slower than the homopolymerization rate, decreasing from 94% in 20 hours to 69% in 24 hours. A similar trend was found for cyclohexene oxide in the presence of L-lactide (Table 2.2, entries 1-2). Although polymer weights might be expected to increase with each redox switch, GPC data only indicated an increase in polymer weight from the oxidized state to the reduced state, i.e., when incorporating additional LA but not CHO (see below for discussion). It is important to mention that no distinctly multimodal distribution was observed by GPC, consistent with the possible formation of one type of block copolymer (Figures 2.6 and B85-B94).

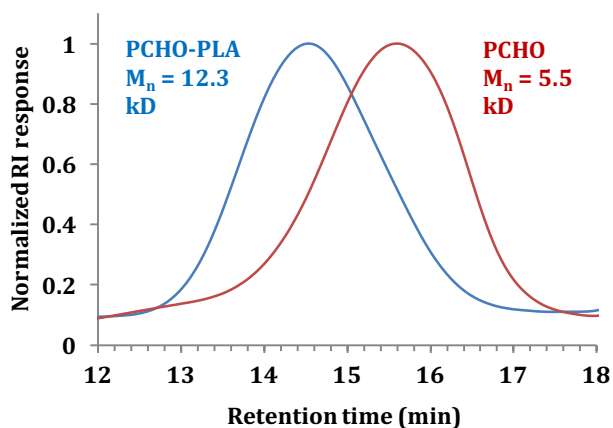
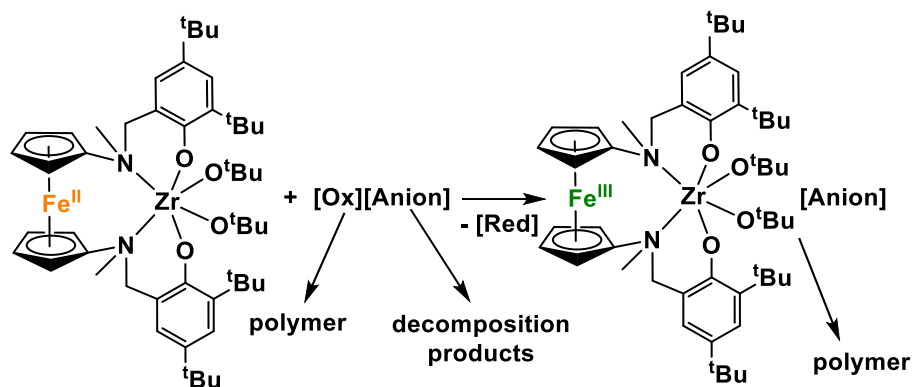


Figure 2.6. Comparison of GPC traces for a PCHO homopolymer (Table 2.2, entry 11) and a PCHO-PLA copolymer (Table 2.2, entry 12). The PCHO homopolymer sample was obtained from a PCHO-PLA copolymerization without employing the switch.



Scheme 2.1. Possible side reactions during the oxidation of (salfan)Zr(O^tBu)₂ in the presence of CHO.

The decreased rate of CHO incorporation after an *in situ* oxidation of the initiator could have resulted from an incomplete oxidation of the initiator and/or activity of the oxidant with CHO. Although the former reason would prevent an increase in polymer molecular weight, the latter is in line with control experiments that show that ^{Ac}FcBAR^F polymerized CHO quickly at room temperature (Table 2.3, entry 1). Therefore, we evaluated the activity of the oxidant (Scheme 2.1) toward cyclic ethers.¹² Screening a number of oxidants led to disappointing results. NOBF₄ has a higher oxidation potential than ^{Ac}FcBAR^F, but its oxidation of the initiator was not reversible (Table 2.3, entry 2). AgOTf was not very active with CHO and it oxidized (salfan)Zr(O^tBu)₂ reversibly, but the oxidized initiator was inactive toward CHO polymerization (Table 2.3, entry 3), likely because OTf coordination inhibited its activity. The addition of NaBAR^F to the mixture initiated CHO polymerization. However, as sodium compounds have been known to initiate ring-opening polymerization of epoxides,¹³ it was tested separately (Table 2.3, entry 4). Like ^{Ac}FcBAR^F, NaBAR^F rapidly polymerized CHO. To determine whether the combination of silver and weakly coordinating borate ions could yield a competent oxidant, several silver borate salts were synthesized and tested. Unfortunately, the larger borates AgBPh₄

and AgBAR^{F} did not oxidize the initiator and, in the latter case, led to some decomposition of the initiator (Table 2.3, entries 6 and 7). The oxidation with $\text{Ag}[\text{B}(\text{C}_6\text{F}_5)_4]$ was also not clean (Table 2.3, entry 8). Other solvents that were utilized to assess the solubility of $(\text{salfan})\text{Zr}(\text{O}^t\text{Bu})_2$ were dichloromethane and chlorobenzene. The former decomposed the initiator after one hour at ambient temperature, while the latter did so after 1.5 h at 100 °C (Figures B53-B54).

Control experiments were performed for the polymerization of CHO with $^{\text{Ac}}\text{FcBAR}^{\text{F}}$ (Figures B55, B102) and $[\text{H}_2(\text{salfan})][\text{BAR}^{\text{F}}]$ (Figures B56, B101) in order to compare the resulting polymers with those obtained when $(\text{salfan})\text{Zr}(\text{O}^t\text{Bu})_2/{}^{\text{Ac}}\text{FcBAR}^{\text{F}}$ was used. For $^{\text{Ac}}\text{FcBAR}^{\text{F}}$, the polymerization proceeded rapidly and reached completion in less than a half hour at room temperature. The molecular weight of the resulting polymer, $M_n = 111400$ Da, was extremely large. Although this molecular weight is not comparable to that of the polymers obtained in the presence of $(\text{salfan})\text{Zr}(\text{O}^t\text{Bu})_2/{}^{\text{Ac}}\text{FcBAR}^{\text{F}}$ (bimodal distribution described above), it is still possible that some of the polymer was generated by $^{\text{Ac}}\text{FcBAR}^{\text{F}}$ since $^{\text{Ac}}\text{FcBAR}^{\text{F}}$ would be present in different concentrations in the two reactions, i.e., in the presence and absence of $(\text{salfan})\text{Zr}(\text{O}^t\text{Bu})_2$. The polymerization of CHO by $[\text{H}_2(\text{salfan})][\text{BAR}^{\text{F}}]$ was slower than that by $[(\text{salfan})\text{Zr}(\text{O}^t\text{Bu})_2][\text{BAR}^{\text{F}}]$, requiring four and a half hours to reach 69% conversion. This experiment is also inconclusive since the electronic properties of iron in $[(\text{salfan})\text{Zr}(\text{O}^t\text{Bu})_2][\text{BAR}^{\text{F}}]$ and $[\text{H}_2(\text{salfan})][\text{BAR}^{\text{F}}]$ are different.

Table 2.3. Screening of oxidants for *in situ* switching between (salfan)Zr(O^tBu)₂ and [(salfan)Zr(O^tBu)₂][BX₄].

En-try	Oxidant	Polymerization of CHO (initial 20 °C)	Polymerization of CHO (1 h at 100 °C)	Reversible oxidation	Polymerization of CHO by [(salfan)Zr(O ^t Bu) ₂][BR ₄]
1	[^{Ac} Fc][BAr ^F ₄]	90%+	-	yes	yes
2	NOBF ₄ *	-	-	irreversible	-
3	AgOTf	0%	0%	yes	no
4	NaBAr ^F	14%	83%	-	-
5	AgBF ₄	1%	13%	irreversible	-
6	AgBPh ₄ *	0%	2%	no reaction	-
7	Ag[BAr ^F ₄]*	0%	70%	no reaction	-
8	Ag[B(C ₆ F ₅) ₄]	90%+	-	irreversible	-
9	AgNO ₃	0%	0%	decomp.	-

Conditions: [M]/[I] = 100, [I] = 0.01 mM, 1,2-difluorobenzene as solvent, 1,3,5-trimethoxybenzene as an internal standard, CoCp₂ as reductant.

Table 2.4. Formation of block copolymers by redox-switchable catalysis using (salfan)Zr(O^tBu)₂ (red) or [(salfan)Zr(O^tBu)₂][BAr^F₄] (ox).

En-try	Monomer 1	Monomer 2	Monomer 3	Initiator	Conversion ^a	Time (h)	M _n ^b	<i>D</i> ^c	Figures ^d
1	LA	CHO	-	red-ox	91-89	4-18	11.4	1.32	B57, B95
2	LA	CHO	LA	red-ox-red	91-92-99	4-18-8	16.9	1.25	B58, B96
3	CHO	LA	-	ox-red	94-99	3-12	13.8	1.66	B59, B97
4	CHO	LA	CHO	ox-red-ox	94-80-82	3-12-8	13.3	1.53	B60, B98
5	CHO	LA	PO	ox-red-ox	91-99-trace	3-12-5	8.9	1.51	B61, B99
6	LA	CHO	BBL	red-ox-red	99-97-30	4-18-15	9.0	1.53	B62, B100

Conditions: [M]/[I] = 100, [I] = 0.01 mM, 100 °C, (4:1) benzene-d₆: 1,2-difluorobenzene as solvent, 1,3,5-trimethoxybenzene as an internal standard, ^{Ac}FcBAr^F as oxidant, CoCp₂ as reductant. LA = L-lactide, BBL = β-butyrolactone, PO = propylene oxide, CHO = cyclohexene oxide. ^a Conversion calculated by integration of polymer peaks versus internal standard. The first number indicates conversion of Monomer 1, while the second number indicates conversion of Monomer 2, etc. For entries 2 and 4, the first number indicates total conversion of Monomer 1/3. ^b M_n values are reported in 10³ g/mol. Narrow molecular weight polystyrene standards were used for calibration purposes, but reported M_n values were not corrected. Polymers from entries 1-4 were analyzed on a GPC-MALS instrument. ^c *D* = M_w/M_n. ^d ¹H NMR spectrum, GPC trace

In order to avoid a competition between CHO polymerization and the oxidation of (salfan)Zr(O^tBu)₂, sequential monomer additions were employed for the formation of block copolymers that did not start with the oxidized initiator (Table 2.4). In this way, the concomitant presence of the oxidant and CHO can be avoided. Although these methods limit the applicability of our system for one-pot reactions, this limitation might be overcome by employing electrochemical switches, an avenue we are currently researching, or by finding different chemical oxidants. Furthermore, the principle of synthesizing block copolymers by using redox-switchable catalysis still applies. Solubility issues with the oxidant and oxidized species were corrected with the addition of 1,2-difluorobenzene. The polymers were purified by precipitation in methanol and characterized by ¹H NMR spectroscopy and gel permeation chromatography (GPC).

Copolymers composed of three different monomers were also synthesized and characterized (Table 2.4, entries 5 and 6). PCHO-PLA-PPO contained a small amount of PO, as reflected in a similar molecular weight to that of the PCHO-PLA diblock polymer (Table 2.4, entry 5). The composition of PLA-PCHO-PBBL determined by ¹H NMR spectroscopy indicated that 30% of the initial BBL amount was incorporated in the last block after 15 h, although the homopolymerization of BBL proceeded to 94% conversion with (salfan)Zr(O^tBu)₂ in 24 hours (Table 2.1, entry 3). We noticed that after the polymerization of the first monomer, each subsequent oxidation/reduction and monomer addition proceeded more slowly. For L-lactide and CHO, a similar pattern was found: the time required for high conversion increased after the first block was synthesized.

In the case of LA and CHO, the molecular weight of the corresponding triblock copolymer, PLA-PCHO-PLA, increased after reduction and LA monomer addition (i.e., from

11.4 for PLA-PCHO to 16.9 kDa for PLA-PCHO-PLA, Table 2.4, entries 1 and 2). However, the same trend was not observed following chemical oxidation and CHO addition, i.e., the molecular weights for PCHO-PLA and PCHO-PLA-PCHO are similar (13.8 and 13.3 kDa, respectively, Table 2.4, entries 3 and 4). The same observation was made by Byers et al. with respect to the molecular weight of diblock copolymers.¹¹ To help determine the composition of the copolymers, a comparison was drawn between the polymers obtained by homopolymerization and copolymerization reactions (Table 2.5). As mentioned above, despite the percentage of conversion indicated by ¹H NMR spectroscopy, the molecular weight measurements by GPC only increased after each reduction and subsequent LA addition. Oxidations followed by CHO addition gave polymers of the same or slightly decreased weight.

Table 2.5. Comparison of PLA and PCHO homopolymers and block copolymers.

Entry	(co)Polymer	$M_{n, GPC}^a$	\bar{D}	%PLA ^b
1	LA	12.2	1.30	100
2	LA-CHO	11.4	1.32	53
3	LA-CHO-LA	16.9	1.25	69
4	CHO	4.0	1.38	0
5	CHO-LA	13.9	1.66	47
6	CHO-LA-CHO	13.3	1.53	34

^a M_n values are reported in 10^3 g/mol. Narrow molecular weight polystyrene standards were used for calibration purposes, but reported M_n values were not corrected. Samples for entries 2, 3, 5, and 6 were analyzed on a GPC-MALS instrument. ^b As determined by ¹H NMR spectroscopy of the purified polymer.

The lack of distinctly multimodal distributions in GPC traces (Figures B95-B100) suggests that only one type of polymer is present and that the oxidant did not create a separate polymer chain. Furthermore, the molecular weights of PLA-PCHO and PCHO-PLA diblock copolymers that were obtained from high conversions of each monomer were similar (Table 2.5, entries 2 and 5) even though they represented a decrease or increase from their previous

homopolymer blocks (Table 2.5, entries 1 and 4). In addition, ^1H NMR spectra of the purified polymers indicate an increased ratio of LA to CHO from PLA-PCHO to PLA-PCHO-PLA (Table 2.5, entries 2 and 3). Likewise, from PCHO-PLA to PCHO-PLA-PCHO, the percentage of protons corresponding to CHO increased (Table 2.5, entries 5 and 6). The triblock copolymers PLA-PCHO-PLA and PCHO-PLA-PCHO had reversed compositions, as expected: PLA-CHO-PLA had 69% PLA to 31% PCHO, while PCHO-PLA-PCHO had 66% PCHO to 34% PLA.

Inspired by the selective precipitation procedures developed by Byers and coworkers to remove homopolymer fragments from the copolymeric material,¹¹ we applied these methods to our PLA/PCHO diblock and triblock copolymers synthesized by sequential addition (Tables 2.6-2.9, Figures B63-78, B103-112). There was one rather notable difference that was found during the sequential polymerization procedure. The copolymers developed by Byers et al. were largely composed of PLA, even when sequential monomer addition was used. In their sequential precipitations, their copolymers easily dissolved into acetone and precipitated in hexanes. This was reflected in the mass balance of their experiments, where most of the copolymer mass was found in the acetone filtrate and then the hexanes precipitate. Compared to the iron system developed by Byers and coworkers, our initiator incorporated a greater percentage of PCHO into its copolymers. Therefore, the copolymer was largely insoluble in both solvents. The mass balance reflects this fact, with most of the copolymer being found in both the acetone and hexanes precipitates. In contrast to the copolymers studied by Byers and coworkers, there is a small loss of PCHO and even a smaller loss of PLA during the precipitation procedures, suggesting that most of the PCHO and PLA sequences are part of the copolymer rather than of individual homopolymeric chains. The resulting GPC traces showed, in general, higher molecular weights after successive precipitation processes, but no significant change in D values

(Tables 2.6-2.9, Figures B63-78, B103-112). The copolymers achieved by sequential addition are therefore likely predominantly block copolymers.

Table 2.6. Results of selective precipitation of a PLA-PCHO diblock copolymer as obtained below.

	PLA : PCHO	Mass (mg)	M_n	\bar{D}
Crude	1:0.89	100	11.4	1.32
Acetone filtrate	1:0.33	28	-	-
Acetone precipitate	1:0.98	67	12.9	1.33
Hexanes filtrate	1:579	17	-	-
Hexanes precipitate	1:0.38	35	12.7	1.25

Copolymerization of LA and CHO by (salfan)Zr(O^tBu)₂ (red-ox). To a C₆D₆ (0.15 mL) solution of (salfan)Zr(O^tBu)₂ (4.6 mg, 5 μmol) in a J-Young NMR tube, a solution of 1,3,5-trimethoxybenzene (16.8 mg, 50 μmol) in C₆D₆ (0.15 mL), 0.10 mL of F₂C₆H₄ and L-lactide (72.0 mg, 0.500 mmol) were added. The reaction was heated to 100 °C and analyzed every 30 min by ¹H NMR spectroscopy until completion. A solution of [^{Ac}Fc][BAR^F₄] (5.5 mg, 5 μmol) in F₂C₆H₄ (0.10 mL) was then added and the reaction was left at room temperature for two hours. A solution of cyclohexene oxide (49.0 mg, 0.500 mmol) in C₆D₆ (0.10 mL) was added. The reaction was heated to 100 °C and analyzed every 30 min by ¹H NMR spectroscopy until completion. At the end, the reaction mixture was dissolved in CH₂Cl₂ and poured into methanol at ambient temperature; a white solid precipitated briefly and was filtered. Yield: 350 mg, 96.8%.

Table 2.7. Results of selective precipitation of a PLA-PCHO-PLA triblock copolymer as obtained below.

	PLA : PCHO	Mass (mg)	M_n	D
Crude	1:0.55	100	16.9	1.25
Acetone filtrate	1:0.22	12	-	-
Acetone precipitate	1:0.43	69	17.4	1.23
Hexanes filtrate	1:79	5	-	-
Hexanes precipitate	1:0.36	56	18.1	1.38

Copolymerization of LA and CHO by (salfan)Zr(O^tBu)₂ (red-ox-red). To a C₆D₆ (0.15 mL) solution of (salfan)Zr(O^tBu)₂ (4.6 mg, 5 μmol) in a J-Young NMR tube, a solution of 1,3,5-trimethoxybenzene (16.8 mg, 50 μmol) in C₆D₆ (0.15 mL), 0.10 mL of F₂C₆H₄ and L-lactide (72.0 mg, 0.500 mmol) were added. The reaction was heated to 100 °C and analyzed every 30 min by ¹H NMR spectroscopy until completion. A solution of [^{Ac}Fc][BAR^F₄] (5.5 mg, 5 μmol) in F₂C₆H₄ (0.10 mL) was then added and the reaction was left at room temperature for two hours. A solution of cyclohexene oxide (49.0 mg, 0.500 mmol) in C₆D₆ (0.10 mL) was added. The reaction was heated to 100 °C and analyzed every 30 min by ¹H NMR spectroscopy until completion. A solution of CoCp₂ (5.5 mg, 5 μmol) in C₆D₆ (0.10 mL) was then added and the reaction was left at room temperature for two hours. L-lactide (72.0 mg, 0.500 mmol) was added. The reaction was heated to 100 °C and analyzed every 30 min by ¹H NMR spectroscopy until completion. At the end, the reaction mixture was dissolved in CH₂Cl₂ and poured into methanol at ambient temperature; a white solid precipitated briefly and was filtered. Yield: 350 mg, 96.8%.

Table 2.8. Results of selective precipitation of a PCHO-PLA diblock copolymer as obtained below.

	PLA : PCHO	Mass (mg)	M_n	\bar{D}
Crude	1:1.15	100	13.8	1.66
Acetone filtrate	1:0.40	25	-	-
Acetone precipitate	1:1.38	68	18.6	1.48
Hexanes filtrate	1:1.45	6	-	-
Hexanes precipitate	1:1.29	47	15.8	1.60

Copolymerization of LA and CHO by [(salfan)Zr(O^tBu)₂][BAr^F₄] (ox-red). To a C₆D₆ (0.15 mL) solution of (salfan)Zr(O^tBu)₂ (4.6 mg, 5 μmol) in a J-Young NMR tube, a solution of 1,3,5-trimethoxybenzene (16.8 mg, 50 μmol) in C₆D₆ (0.15 mL), 0.10 mL of F₂C₆H₄ and a solution of [^{Ac}Fc][BAr^F₄] (5.5 mg, 5 μmol) in F₂C₆H₄ (0.10 mL) were added and the reaction was left at room temperature for 2 h. A solution of cyclohexene oxide (49.0 mg, 0.500 mmol) in C₆D₆ (0.10 mL) was added. The reaction was heated to 100 °C and analyzed every 30 min by ¹H NMR spectroscopy until completion. A solution of CoCp₂ (5.5 mg, 5 μmol) in C₆D₆ (0.10 mL) was then added and the reaction was left at room temperature for two hours. A C₆D₆ solution of L-lactide solution (72.0 mg, 0.500 mmol) was added. After being heated at 100 °C for 2 h, the reaction was monitored by ¹H NMR spectroscopy until completion. At the end, the reaction was dissolved in CH₂Cl₂ and poured into methanol at ambient temperature; a white solid precipitated briefly and was filtered. Yield: 280 mg, 91.3%.

Table 2.9. Results of selective precipitation of a PCHO-PLA-PCHO triblock copolymer as obtained below.

	PLA : PCHO	Mass (mg)	M_n	\bar{D}
Crude	1:1.99	100	13.3	1.53
Acetone filtrate	1:0.23	Trace	-	-
Acetone precipitate	1:2.41	99	14.0	1.47
Hexanes filtrate	1:214	17	-	-
Hexanes precipitate	1:1.43	59	16.8	1.49

Copolymerization of LA and CHO by [(salfan)Zr(O^tBu)₂][BAR^F₄] (ox-red-ox). To a C₆D₆ (0.15 mL) solution of (salfan)Zr(O^tBu)₂ (4.6 mg, 5 μmol) in a J-Young NMR tube, a solution of 1,3,5-trimethoxybenzene (16.8 mg, 50 μmol) in C₆D₆ (0.15 mL), 0.10 mL F₂C₆H₄ and a solution of [¹³C][BAR^F₄] (5.5 mg, 5 μmol) in F₂C₆H₄ (0.10 mL) was added and the reaction was left at room temperature for 2 h. A solution of cyclohexene oxide (49.0 mg, 0.500 mmol) in C₆D₆ (0.10 mL) was added. The reaction was heated to 100 °C and analyzed every 30 min by ¹H NMR spectroscopy until completion. A solution of CoCp₂ (5.5 mg, 5 μmol) in C₆D₆ (0.10 mL) was then added and the reaction was left at room temperature for two hours. A C₆D₆ solution of L-lactide solution (72.0 mg, 0.500 mmol) was added. After being heated at 100 °C for 2 h, the reaction was monitored by ¹H NMR spectroscopy until completion. A solution of [¹³C][BAR^F₄] (5.5 mg, 5 μmol) in F₂C₆H₄ (0.10 mL) was then added and the reaction was left at room temperature for 2 h. A solution of cyclohexene oxide (49.0 mg, 0.500 mmol) in C₆D₆ (0.10 mL) was added. After being heated at 100 °C for two hours, the reaction was monitored by ¹H NMR spectroscopy until completion. At the end, the reaction was dissolved in CH₂Cl₂ and poured into methanol at ambient temperature; a white solid precipitated briefly and was filtered. Yield: 280 mg, 91.3%.

DOSY experiment⁴ of the homopolymers and copolymers provided further evidence of copolymer formation. A mixture of PLA and PCHO homopolymers gave a distinct spectrum with PCHO diffusing at a slightly slower rate than PLA (Figure 2.7.a). Their respective values ($1.27 \times 10^{-10} \text{ m}^2/\text{s}$ and $1.53 \times 10^{-10} \text{ m}^2/\text{s}$) were similar to those obtained by Byers and coworkers in a recent report.¹¹ In contrast, the diblock copolymers exhibited higher diffusion rates and altered diffusion patterns. The PLA block of PLA-PCHO ($D = 1.76 \times 10^{-10} \text{ m}^2/\text{s}$) diffused more slowly than the PCHO block, possibly due to its attachment to PCHO and the O'Bu end group (Figure 2.7.b). The PCHO and PLA blocks of PCHO-PLA ($D = 1.57 \times 10^{-10} \text{ m}^2/\text{s}$) diffused at the same rate (Figure 2.7.d). The corresponding triblock copolymers, PLA-PCHO-PLA ($D = 1.18 \times 10^{-10} \text{ m}^2/\text{s}$) and PCHO-PLA-PCHO ($D = 1.31 \times 10^{-10} \text{ m}^2/\text{s}$), shared similar patterns to their diblock precursors and showed a decrease in diffusion rate (Figure 2.7.c and 2.7.e, respectively). Neither diblock nor triblock copolymers contained traces of the homopolymer blocks, indicating the formation of only one type of polymeric species.

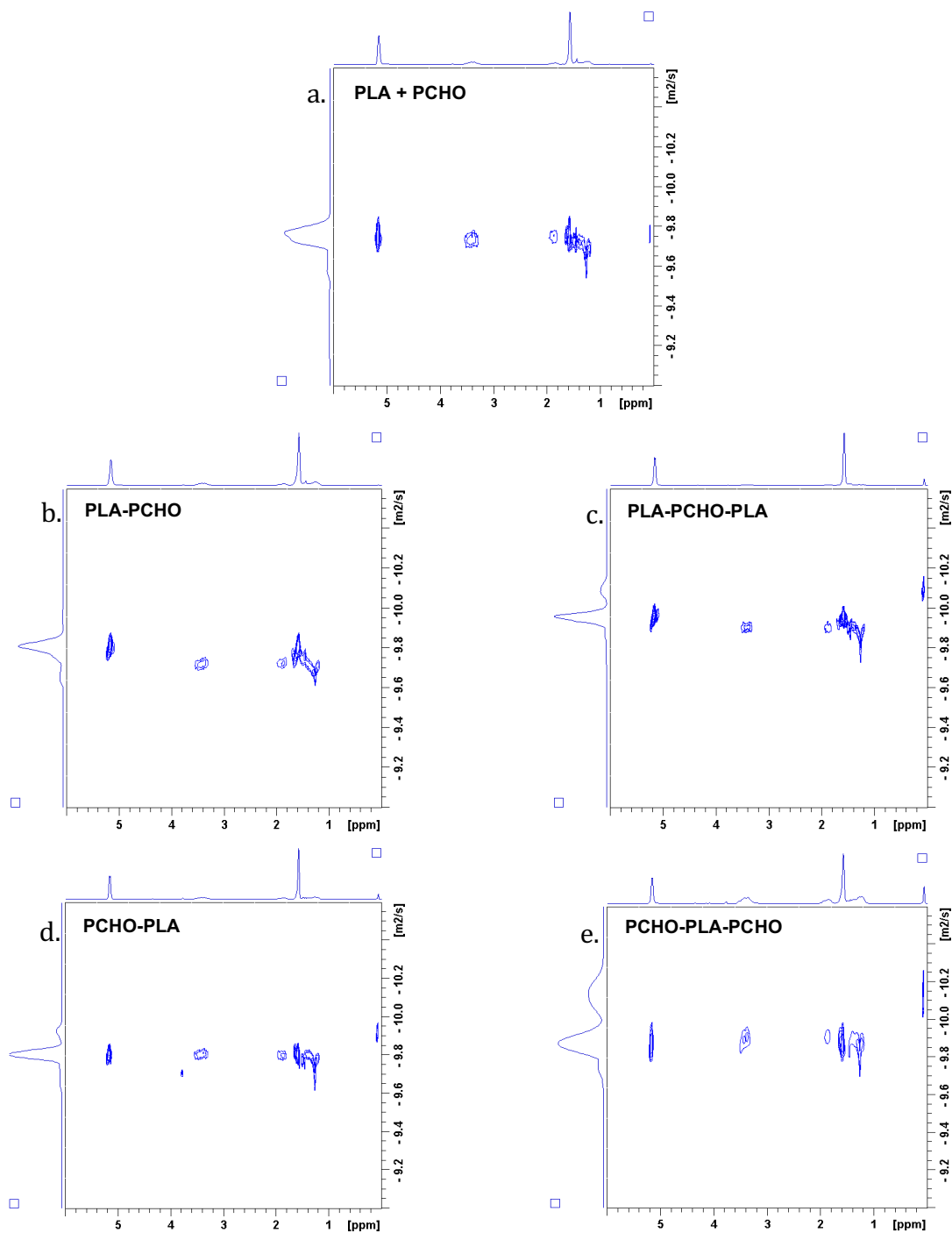


Figure 2.7. DOSY map of a mixture of PLA and PCHO homopolymers (a); DOSY maps of PLA-PCHO diblock copolymer (b) and subsequent PLA-PCHO-PLA triblock copolymer (c); and DOSY maps of PCHO-PLA diblock copolymer (d) and subsequent PCHO-PLA-PCHO triblock copolymer (e).

Since end group analysis could not be accurately obtained due to the overlap between the O^tBu methyl peaks and PCHO methyl peaks, low molecular weight copolymers were synthesized and analyzed by ¹H NMR spectroscopy (Table 2.10).

Table 2.10. Formation of low weight block copolymers by redox-switchable catalysis using (salfan)Zr(O^tBu)₂ (red) or [(salfan)Zr(O^tBu)₂][BAr^F₄] (ox) and sequential monomer addition.

Entry	Monomer 1	Monomer 2	Monomer 3	Initiator	Conversion ^a	Composition ^b	Figures ^c
1	LA	BBL	-	red	92-65	8:10	2.12-2.15
2	BBL	CHO	-	red-ox	70-90	3:25	2.16-2.19
3	CHO	LA	-	ox-red	96-95	17:8	2.20-2.23
4	LA	CHO	-	red-ox	92-87	13:7	2.24-2.27
5	LA	CHO	BBL	red-ox-red	92-88-50	5:20:3	2.28-2.31

Conditions: [M]/[I] = 25, [I] = 0.01 mM, 100 °C, (4:1) benzene-d₆: 1,2-difluorobenzene as solvent, 1,3,5-trimethoxybenzene as an internal standard, ^{Ac}FcBAr^F as oxidant, CoCp₂ as reductant. LA = L-lactide, BBL = β-butyrolactone, CHO = cyclohexene oxide. Samples could not be analyzed by GPC due to their low molecular weight. ^a Conversion calculated by integration of polymer peaks versus internal standard in crude mixture. The first number indicates conversion of Monomer 1, while the second number indicates conversion of Monomer 2, etc. ^b Conversion calculated by integration of polymer peaks versus internal standard in purified polymer. The first number indicates the estimated number of units of Monomer 1 per polymer chain, while the second number indicates the estimated units of Monomer 2, etc. ^c ¹H NMR spectrum, GPC trace

The low integration of protons corresponding to junctions or to the ends of blocks is consistent with a block¹⁵ and not a random¹⁶ copolymer structure (Figures 2.8-2.11). 2D Heteronuclear multiple bond correlation (HMBC) and heteronuclear single quantum coherence (HSQC) ¹H-¹³C experiments were utilized to assign some of these peaks.

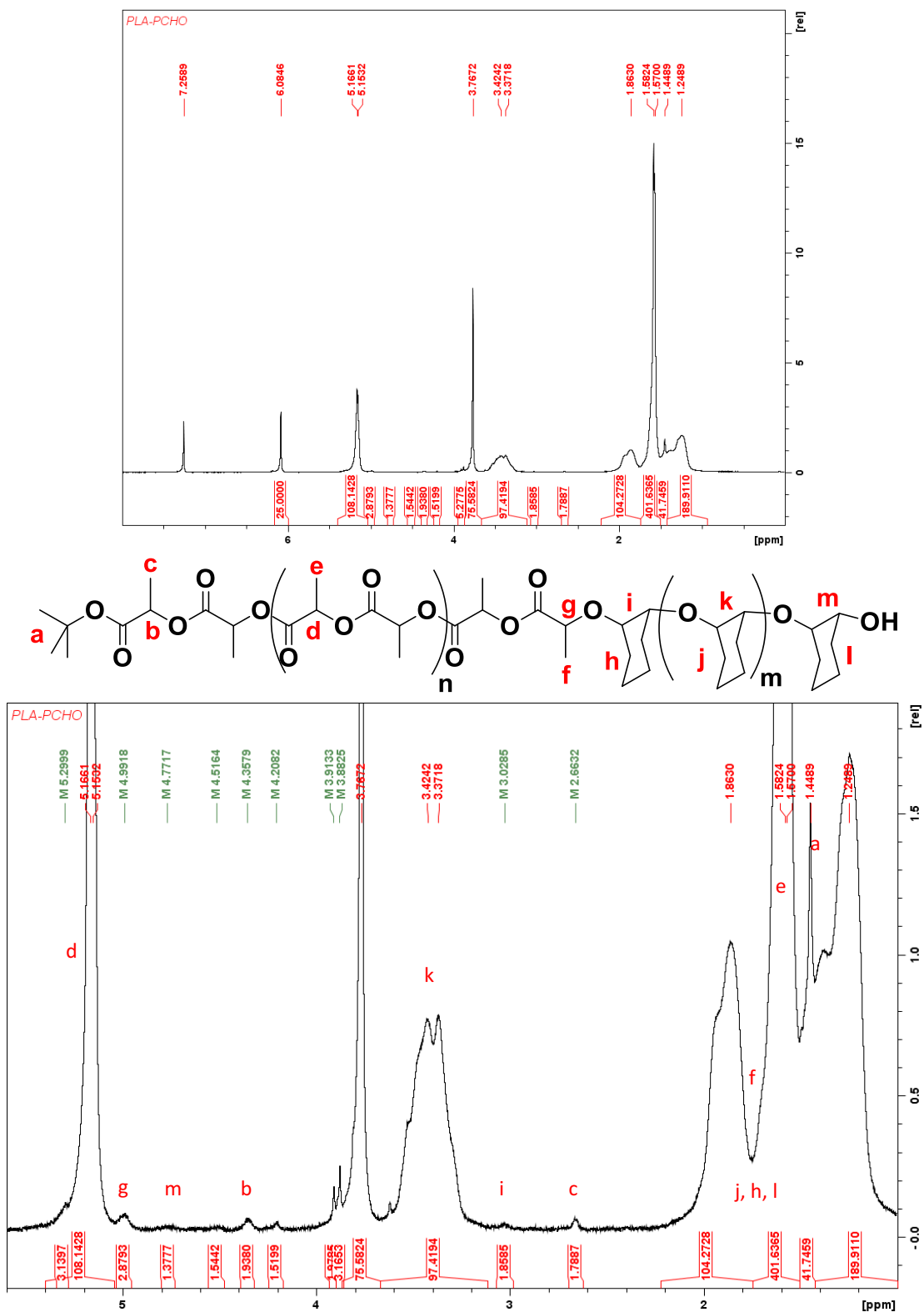


Figure 2.8. Top: ^1H NMR (300 MHz, 25 °C, C_6D_6) spectrum of the purified PLA-PCHO polymer obtained by polymerization of 100 equivalents of L-lactide and cyclohexene oxide, monomers added sequentially, using initiator redox switch “red-ox”. Bottom: Magnified peaks to show the assignment of the protons corresponding to the junction between blocks.

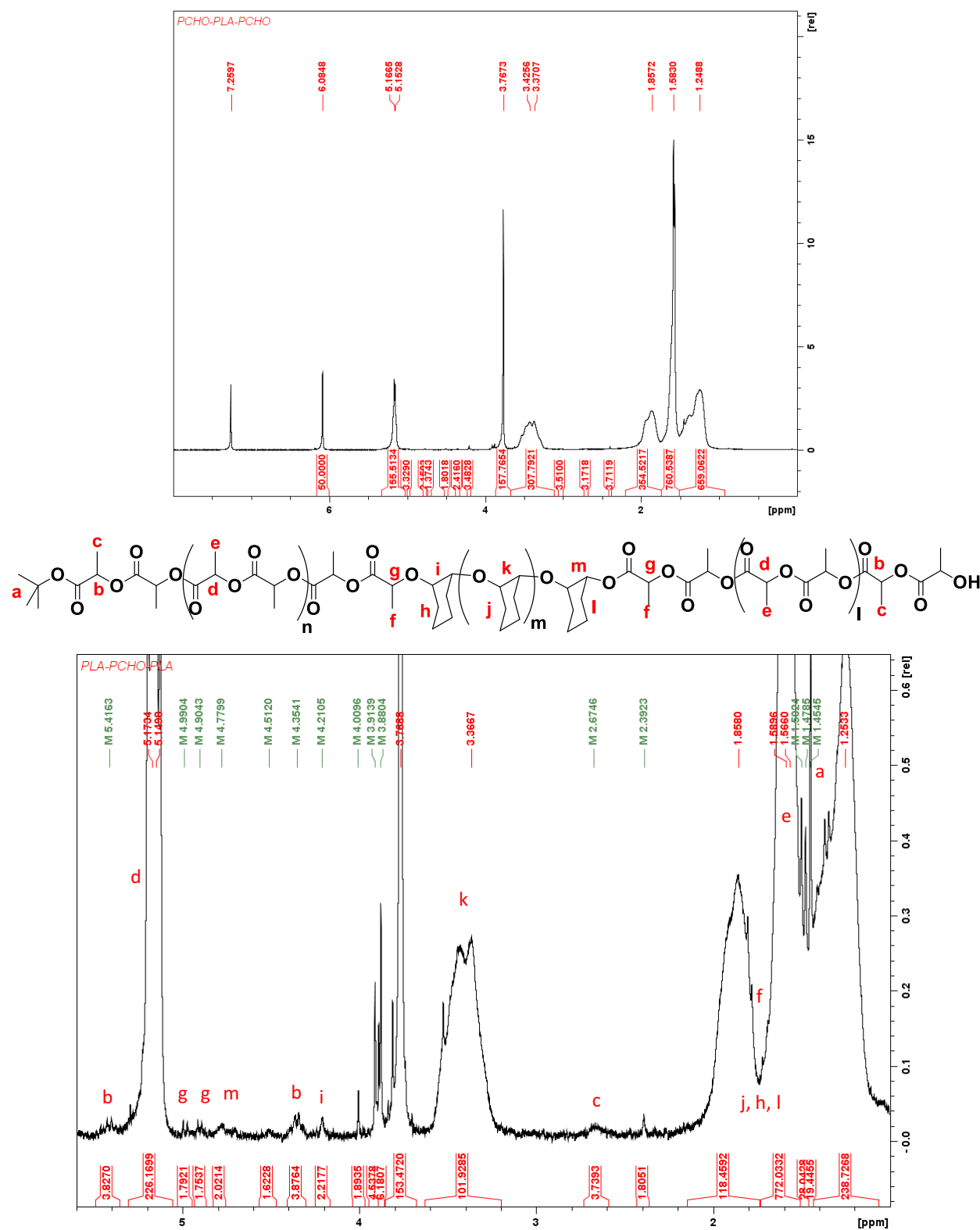


Figure 2.9. Top: ^1H NMR (300 MHz, 25 °C, C_6D_6) spectrum of the purified PLA-PCHO-PLA polymer obtained by polymerization of 100 equivalents of L-lactide and cyclohexene oxide, monomers added sequentially, using initiator redox switch “red-ox-red”. Bottom: Magnified peaks to show the assignment of the protons corresponding to the junction between blocks.

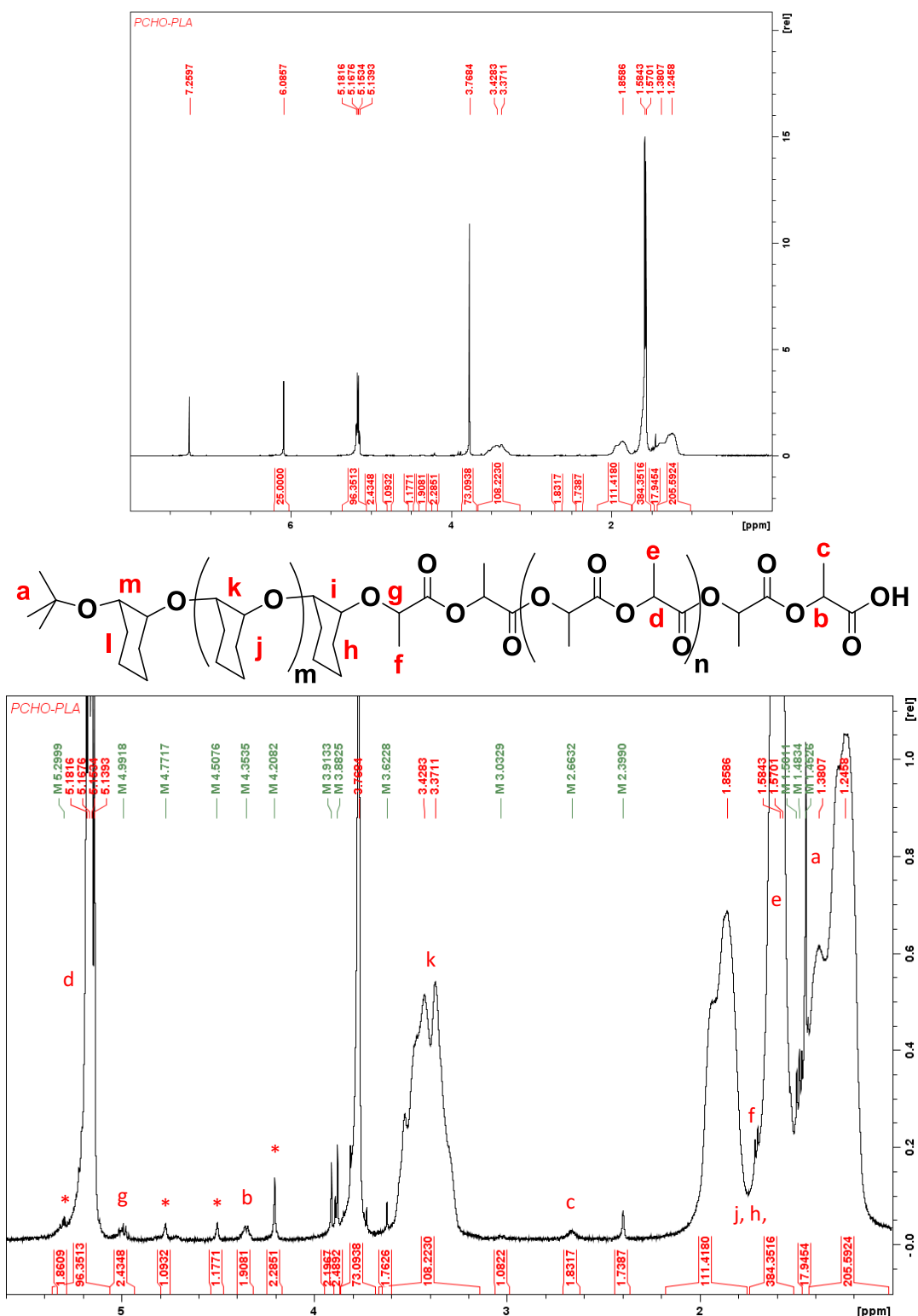


Figure 2.10. Top: ¹H NMR (300 MHz, 25 °C, C₆D₆) spectrum of the purified PCHO-PLA polymer obtained by polymerization of 100 equivalents of cyclohexene oxide and L-lactide monomers added sequentially, using initiator redox switch “ox-red”. Bottom: Magnified peaks to show the assignment of the protons corresponding to the junction between blocks. *unable to assign. Some of the peaks showed correlations to LA methine carbons. HMBC inconclusive.

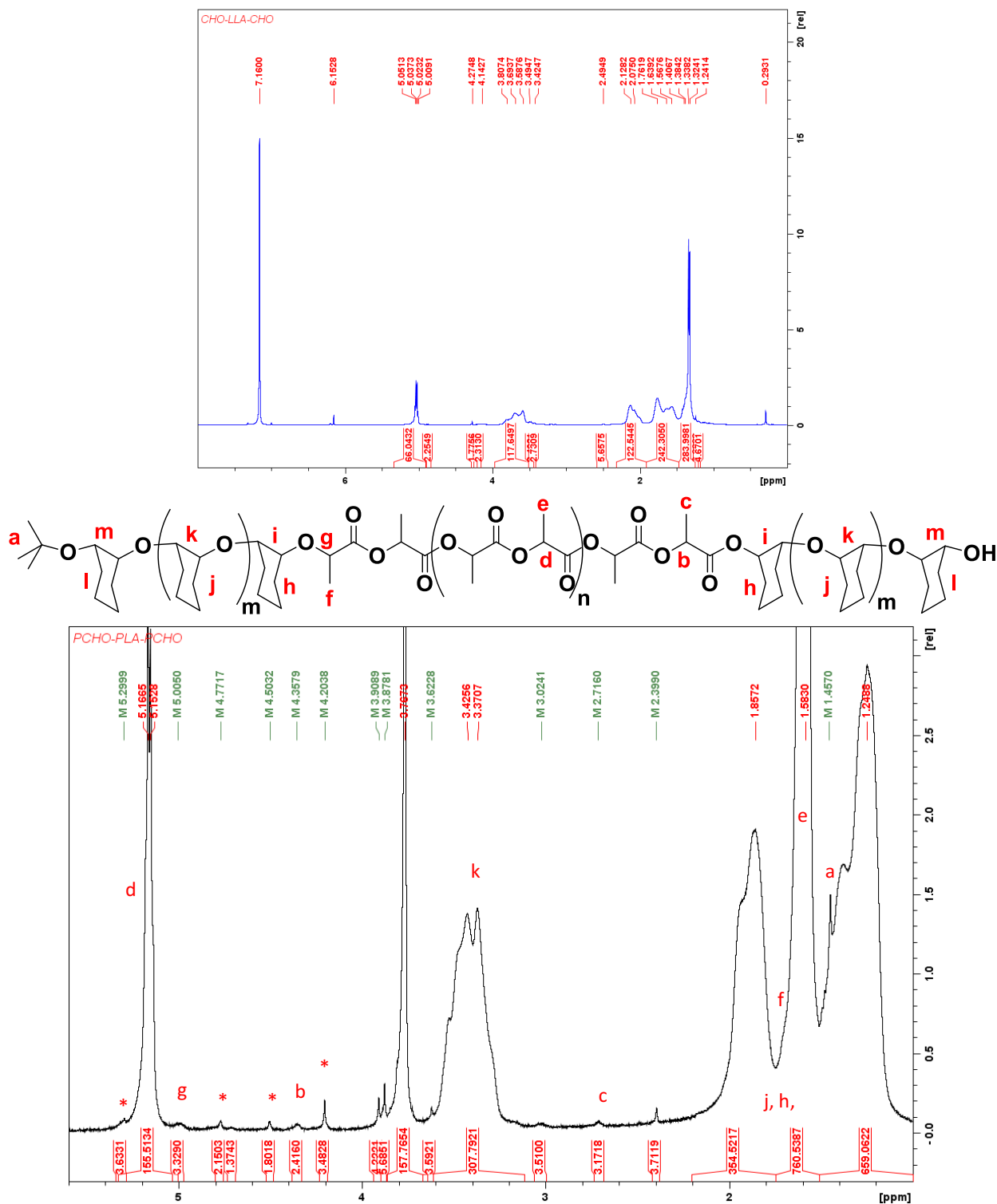


Figure 2.11. Top: ^1H NMR (300 MHz, 25 °C, C_6D_6) spectrum of the purified PCHO-PLA-PCHO polymer obtained by polymerization of 100 equivalents of cyclohexene oxide and L-lactide monomers added sequentially, using initiator redox switch “ox-red-ox”. Bottom: Magnified peaks to show the assignment of the protons corresponding to the junction between blocks. *unable to assign. Some of the peaks showed correlations to LA methine carbons. HMBC inconclusive.

For a PLA-PHB copolymer, low incorporation of BBL was observed, in line with BBL's low reactivity with (salfan)Zr(O^tBu)₂ in sequential addition copolymerizations. It was previously reported that PHB methylene protons are sensitive to BBL-LA junctions.¹⁶ In the case of LA₈-BBL₁₀ obtained by us, integrations of the BBL methylene protons in a BBL-LA environment (2.70 ppm) versus a BBL-BBL environment (2.50 ppm) indicated that despite using a sequential addition of the monomers, there was some competitive behavior between the leftover LA and the newly added BBL with the reduced initiator. Correlations of BBL methylene ¹H peaks to LA methine ¹³C peaks, as well as LA methine ¹H peaks to BBL carbonyl ¹³C peaks, also presented evidence of BBL-LA heterosequences (Figures 2.12-2.15).

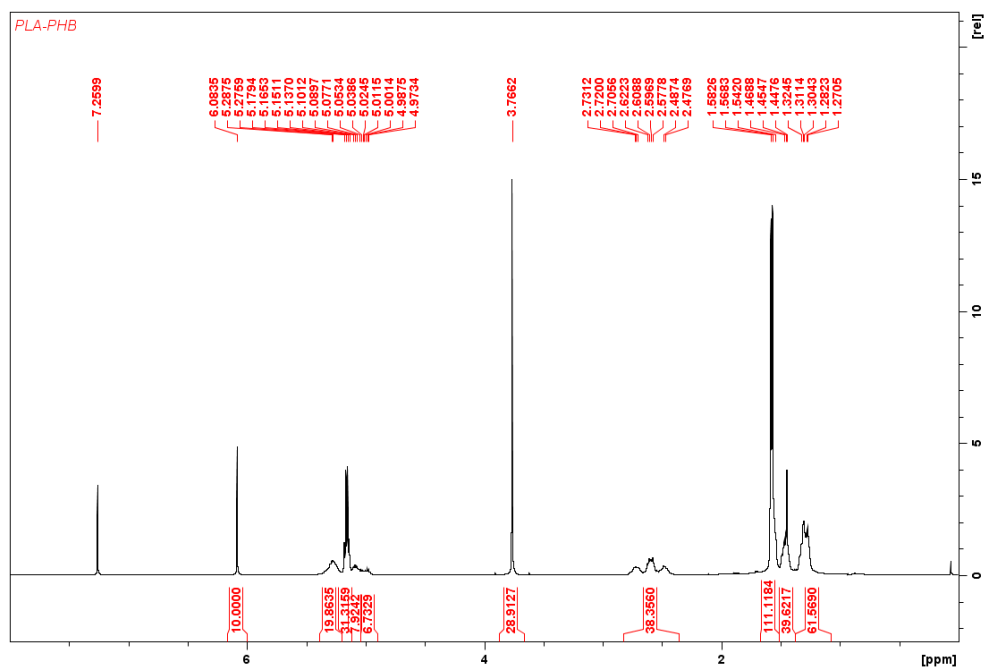


Figure 2.12. Table 2.5, entry 1. Low molecular weight PLA-PHB copolymer. ¹H NMR (500 MHz, 25 °C, CDCl₃), δ (ppm): 6.08 (s, 3H, PhH TMB), 5.27 (m, 1H, OCHCH₃ PHB), 5.16-5.00 (m, 2H, CHCH₃ PLA), 3.77 (s, 9H, CH₃ TMB), 2.60 (m, 2H, COCH₂ PHB), 1.57 (d, 6H, CHCH₃ PLA), 1.30 (t, 3H, OCHCH₃ PHB).

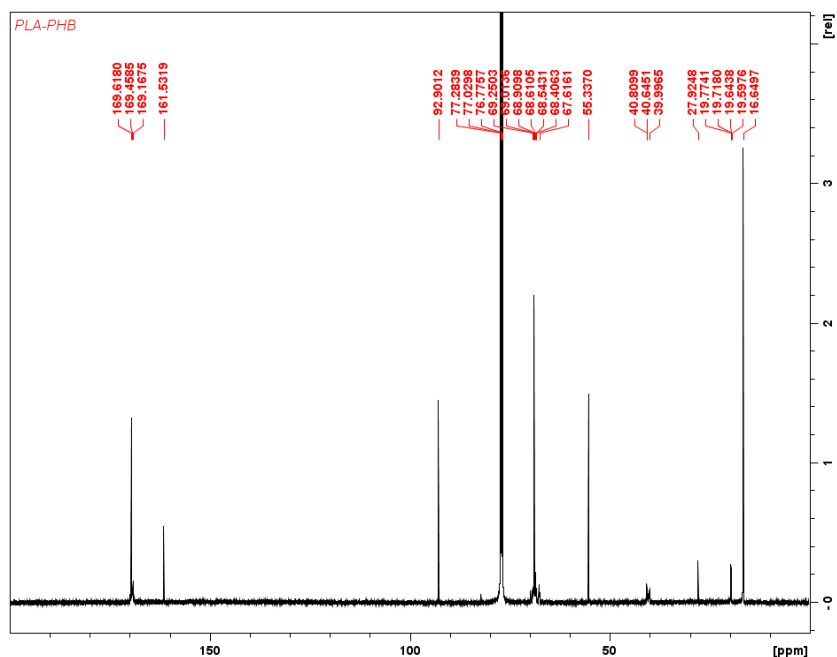


Figure 2.13. Table 2.5, entry 1. Low molecular weight PLA-PHB copolymer. ^{13}C NMR (500 MHz, 25 °C, CDCl_3), δ (ppm): 169.6 (C=O, PLA), 169.2 (C=O, PHB), 161.5 (C-OMe, TMB), 92.9 (CH, TMB), 77.0 (CDCl_3), 68.6 (CH, PLA), 67.6 (CH, PHB), 55.3 (OCH_3 , TMB), 40.6 (CH_2 , PHB), 27.9 (CH_3 , O'Bu), 19.6 (CH_3 , PHB), 16.6 (CH_3 , PLA).

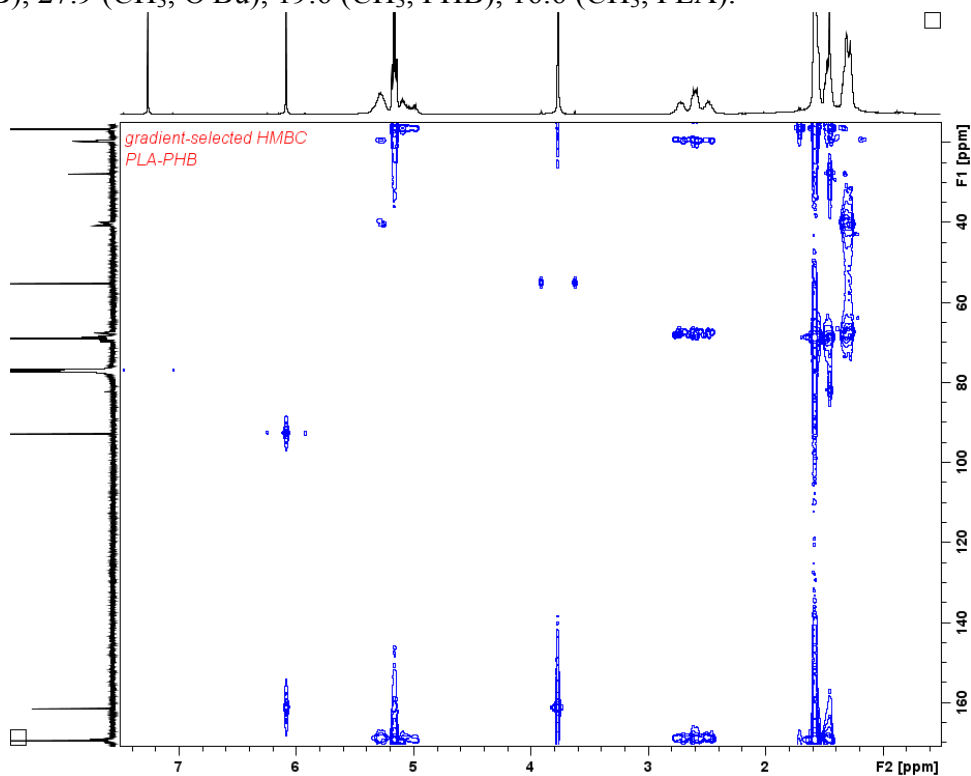


Figure 2.14. Table 2.5, entry 1. Low molecular weight PLA-PHB copolymer. HMBC ^1H - ^{13}C NMR (500 MHz, 25 °C, CDCl_3).

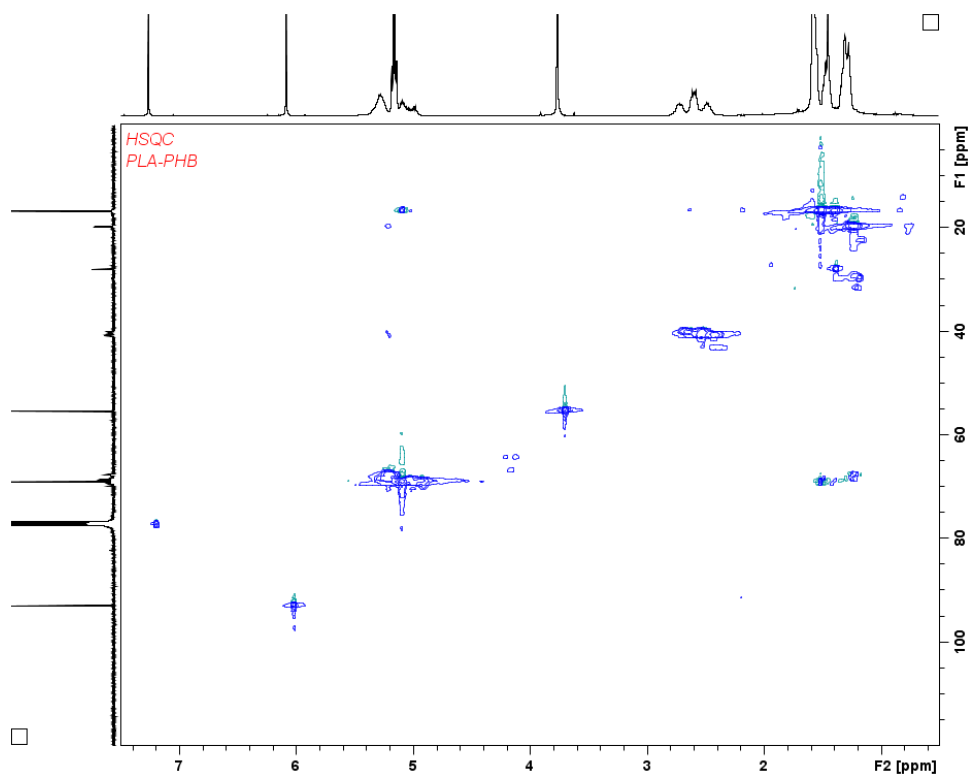


Figure 2.15. Table 2.5, entry 1. Low molecular weight PLA-PHB copolymer. HSQC ^1H - ^{13}C NMR (500 MHz, 25 °C, CDCl_3).

Copolymers with PCHO were more difficult to interpret due to PCHO's broad signals. BBL's methylene protons in $\text{BBL}_3\text{-CHO}_{25}$ did not show a third set of peaks outside the 2.50 ppm region (BBL methylene protons in a PHB homopolymer sequence) or correlations to CHO, suggesting a lack of heterosequences. Small peaks, which are proposed to be related to junctions or end groups, were analyzed. The proton peaks near 4.10 ppm were assigned as BBL methine ^{13}C peaks by HSQC and correlated to BBL methine ^{13}C peaks by HMBC. Small alkyl peaks near the broad regions of 1.00-1.50 ppm could not be assigned definitively to BBL, CHO, or the O'Bu end group (Figures 2.16-2.19).

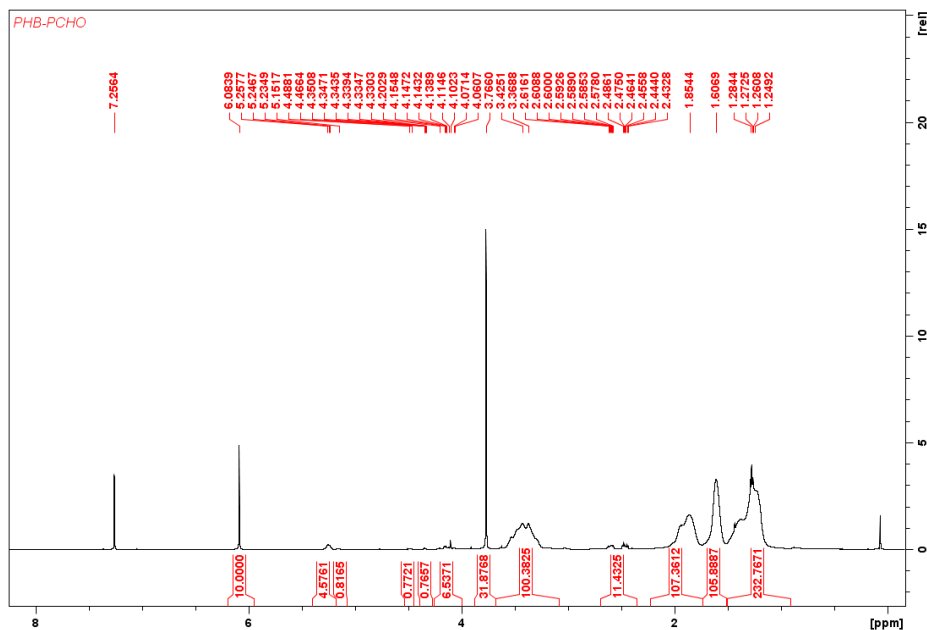


Figure 2.16. Table 2.5, entry 2. Low molecular weight PHB-PCHO. ^1H NMR (500 MHz, 25 °C, CDCl_3), δ (ppm): 6.08 (s, 3H, PhH TMB), 5.25 (m, 1H, OCHCH_3 PHB), 3.77 (s, 9H, CH_3 TMB), 3.39 (m, 2H, COCH PCHO), 2.53 (m, 2H, COCH_2 PHB), 1.85 (m, 2H, COCHCH_2 PCHO), 1.61 (m, 2H, COCHCH_2 PCHO), 1.30 (t, 3H, OCHCH_3 PHB), 1.26 (m, 2H, $\text{COCHCH}_2\text{CH}_2$ PCHO).

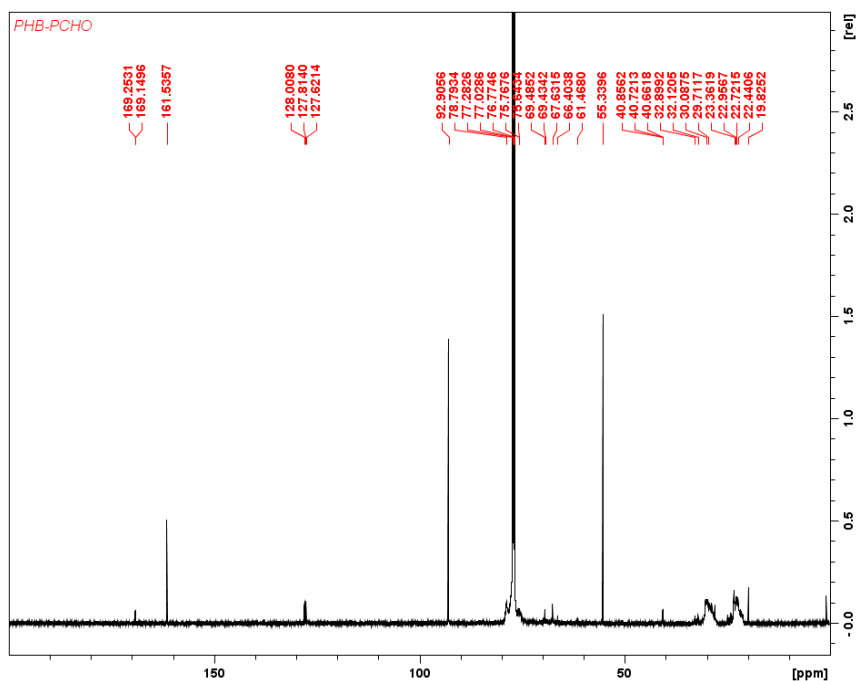


Figure 2.17. Table 2.5, entry 2. Low molecular weight PHB-PCHO. ^{13}C NMR (500 MHz, 25 °C, CDCl_3), δ (ppm): 169.2 ($\text{C}=\text{O}$, PHB), 161.5 ($\text{C}-\text{OMe}$, TMB), 127.8 (residual C_6D_6), 92.9 (CH , TMB), 77.0 (broad, CH , PCHO), 77.0 (CDCl_3), 67.6 (CH , PHB), 55.3 (OCH_3 , TMB), 40.6 (CH_2 , PHB), 32.1 (broad, CHCH_2 , PCHO), 27.9 (CH_3 , O^tBu), 22.7 (broad, CH_2 , PCHO), 19.8 (CH_3 , PHB).

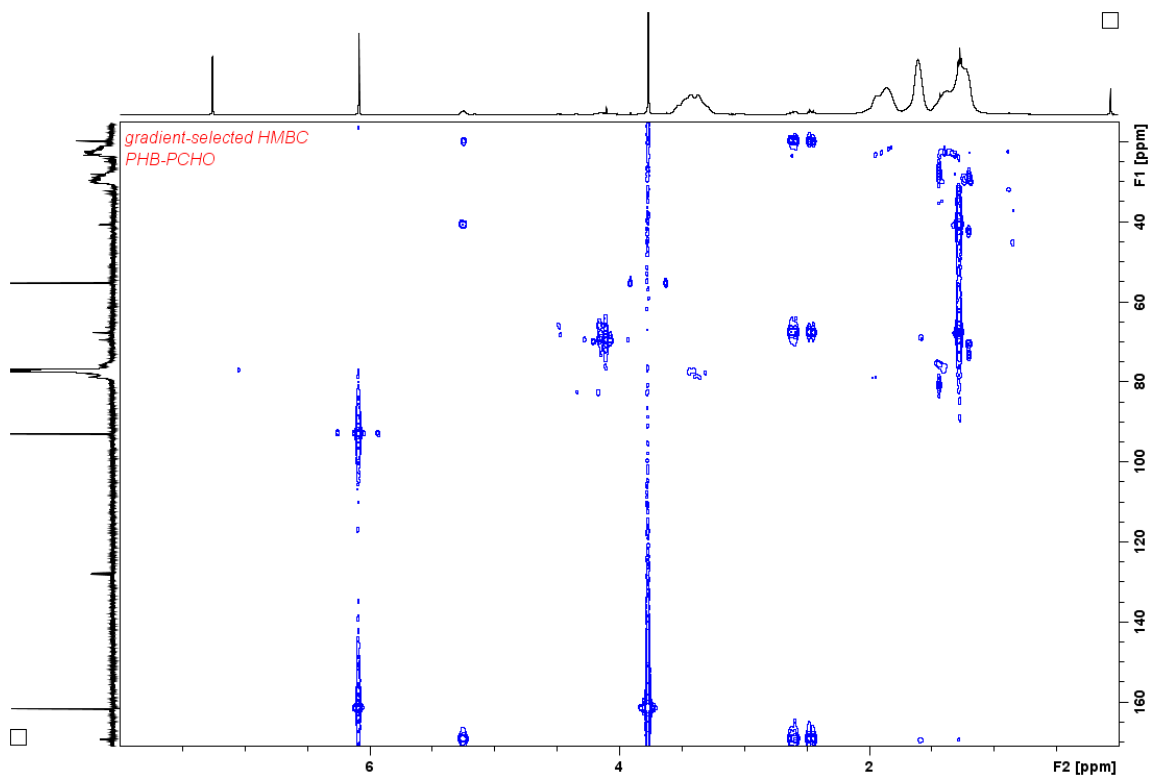


Figure 2.18. Table 2.5, entry 2. Low molecular weight PHB-PCHO. HMBC ^1H - ^{13}C NMR (500 MHz, 25 °C, CDCl_3).

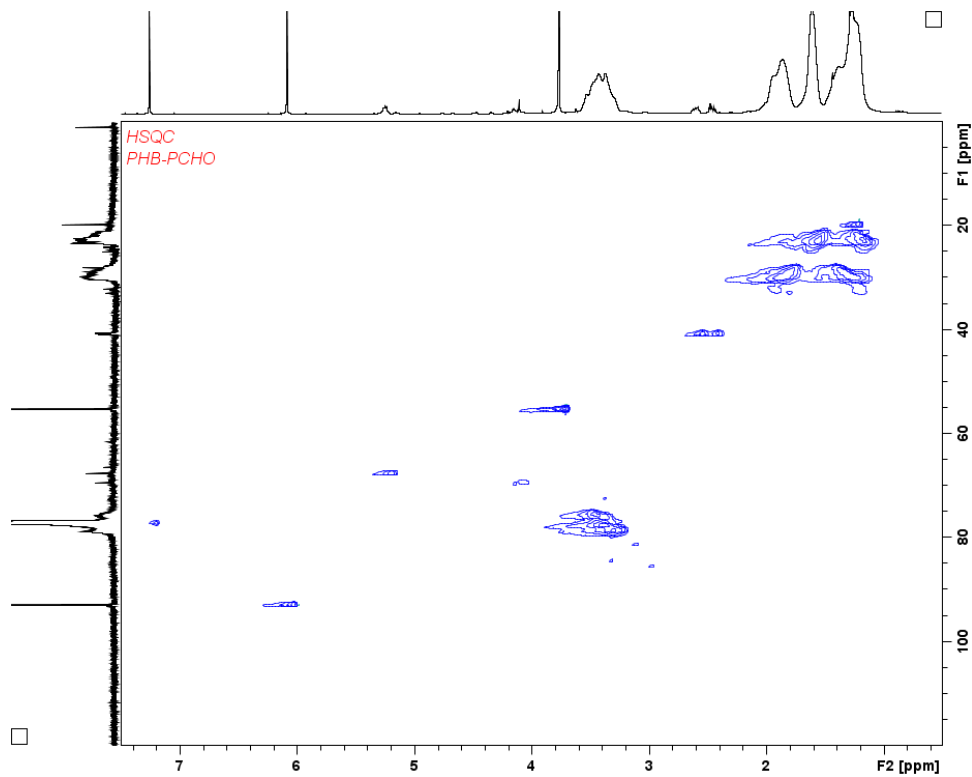


Figure 2.19. Table 2.5, entry 2. Low molecular weight PHB-PCHO. HSQC ^1H - ^{13}C NMR (500 MHz, 25 °C, CDCl_3).

The diblock PLA₁₃-PCHO₇ copolymer had several small LA methine proton signals (5.17, 4.98, and 4.34 ppm) located near the main PLA methine signal (5.15 ppm). The signals at 5.17 ppm and 4.98 ppm were correlated to the bulk LA methyl ¹³C signal at 16.7 ppm, suggesting that these are the methines of the LA units closest to the bulk of the PLA polymer. The LA methine signal at 4.98 ppm is related to the LA methyl peak at 1.70 ppm and a doublet at 1.46 ppm. The LA methine proton peak at 4.34 ppm is correlated to the LA methyl peak at 2.68 ppm and a doublet at 1.49 ppm (possibly corresponding to an adjoining LA methyl group). The O⁴Bu proton peak at 1.44 ppm can be correlated to a methyl ¹³C peak at 27.9 ppm and a quaternary ¹³C peak at 82.3 ppm, however, neither of these peaks correlates to any other peaks. Although there was no definitive evidence of direct correlations by 2D NMR spectroscopy, these LA monomer units show a relationship to the main PLA signals yet altered microstructures. Therefore, we propose that the peaks at 4.98 and 4.34 ppm, along with their related peaks, most likely correspond to the LA monomer units closest to the junction with PCHO and O⁴Bu, respectively (Figures 2.20-2.23).

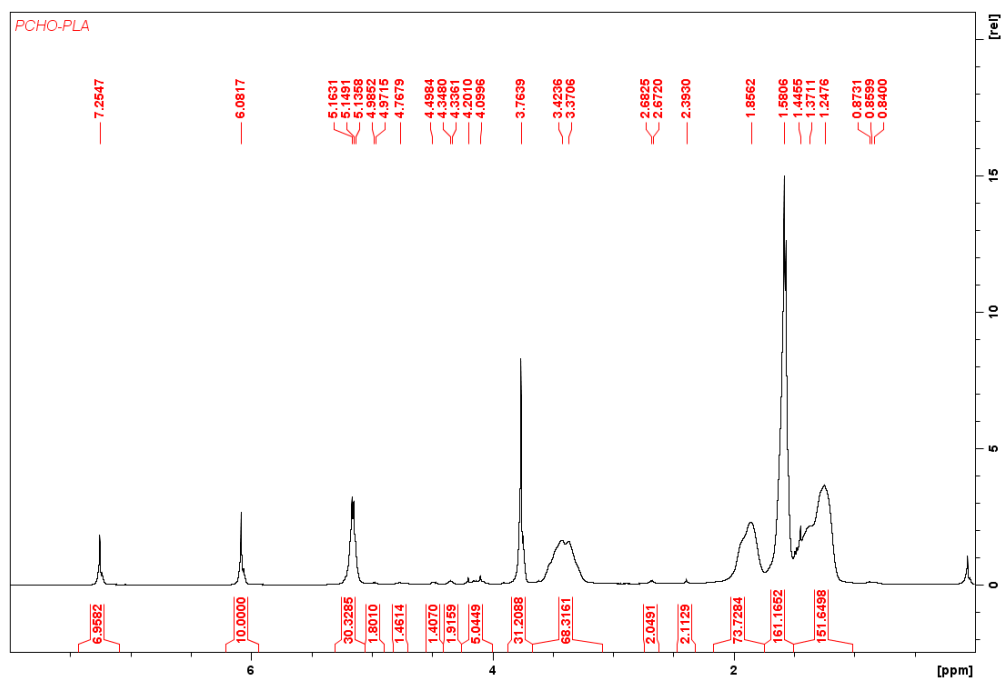


Figure 2.20. Table 2.5, entry 3. Low molecular weight PCHO-PLA. ^1H NMR (500 MHz, 25 °C, CDCl_3), δ (ppm): 6.08 (s, 3H, PhH TMB), 5.15 (q, 2H, CHCH₃ PLA), 3.77 (s, 9H, CH₃ TMB), 3.40 (m, 2H, COCH PCHO), 1.86 (m, 2H, COCHCH₂ PCHO), 1.58 (d, 6H, CHCH₃ PLA), 1.25 (m, 2H, COCHCH₂CH₂ PCHO).

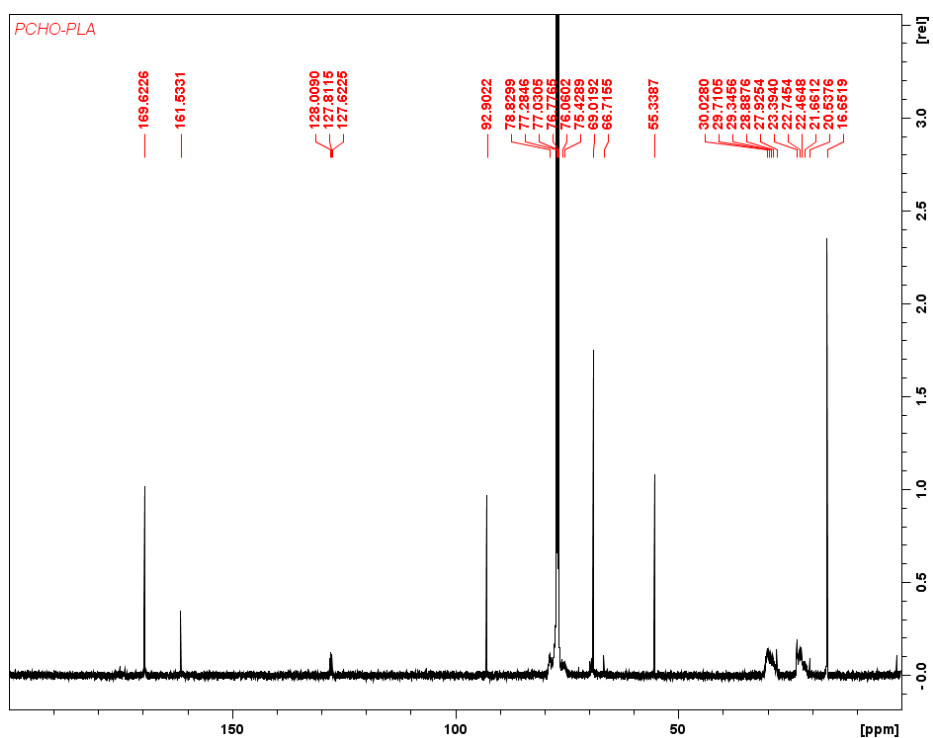


Figure 2.21. Table 2.5, entry 3. Low molecular weight PCHO-PLA. ^{13}C NMR (500 MHz, 25 °C, CDCl_3), δ (ppm): 169.6 (C=O, PLA), 161.5 (C-OMe, TMB), 127.8 (residual C_6D_6), 92.9 (CH, TMB), 77.0 (broad, CH, PCHO), 77.0 (CDCl_3), 68.6 (CH, PLA), 55.3 (OCH₃, TMB), 29.3 (broad, CHCH₂, PCHO), 27.9 (CH₃, O^tBu), 22.7 (broad, CH₂, PCHO), 16.6 (CH₃, PLA).

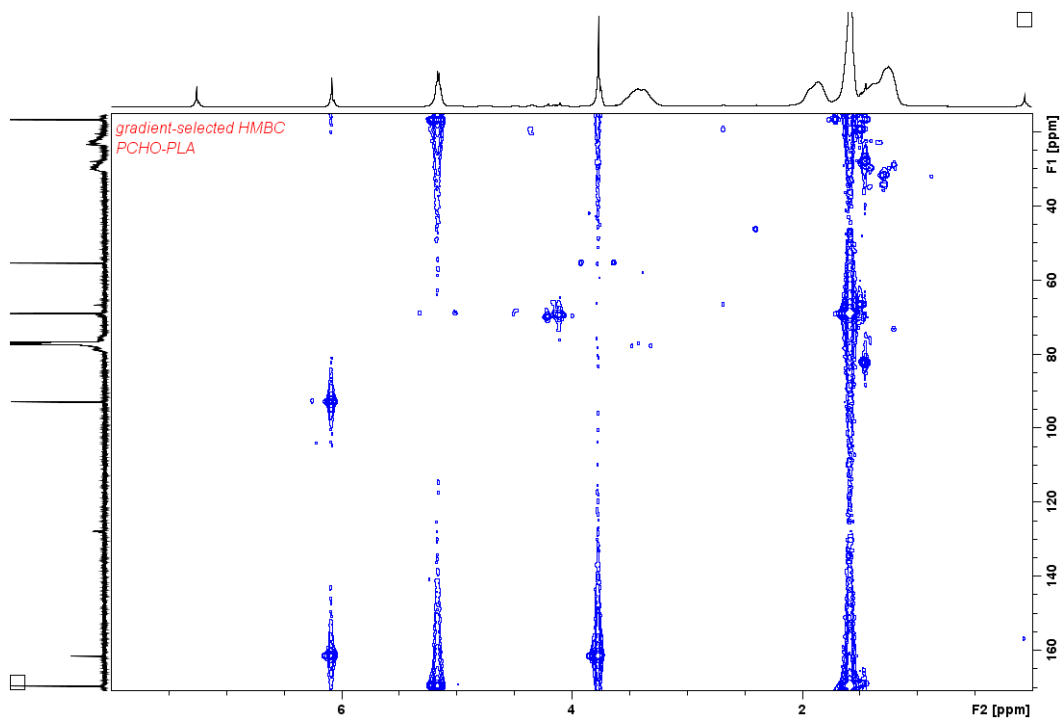


Figure 2.22. Table 2.5, entry 3. Low molecular weight PCHO-PLA. HMBC ^1H - ^{13}C NMR (500 MHz, 25 °C, CDCl_3).

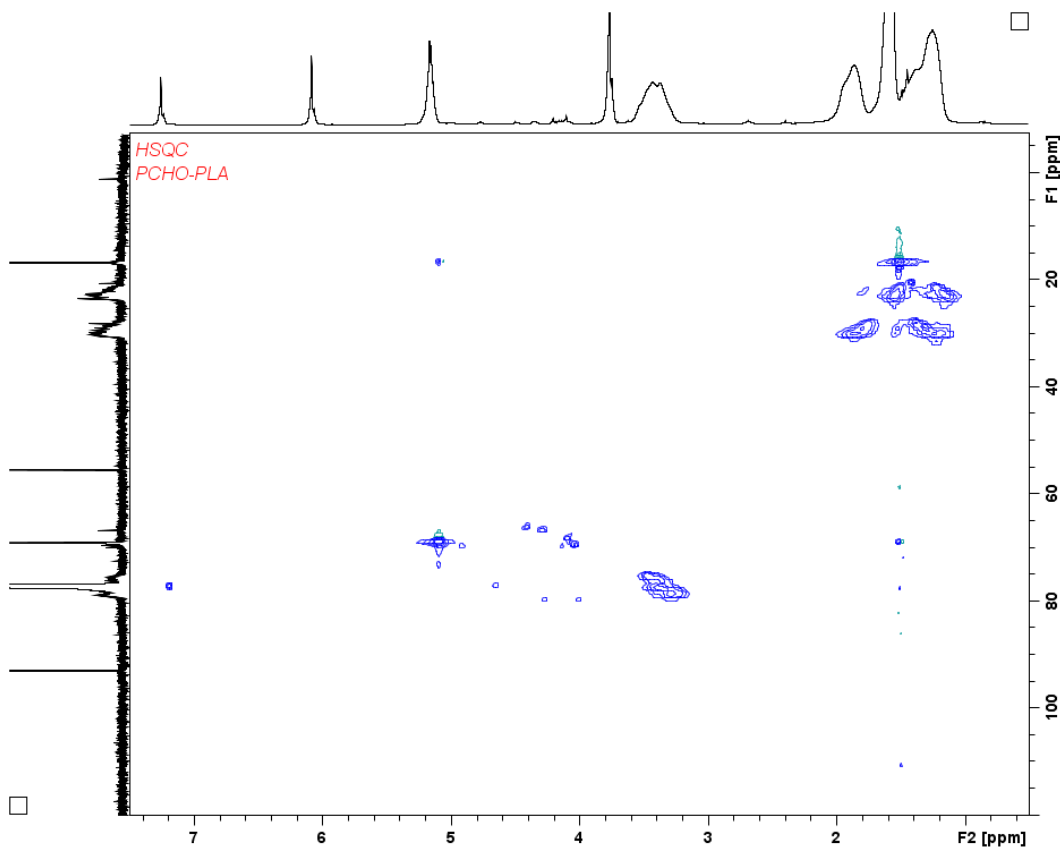


Figure 2.23. Table 2.5, entry 3. Low molecular weight PCHO-PLA. HSQC ^1H - ^{13}C NMR (500 MHz, 25 °C, CDCl_3).

The diblock CHO₁₇-LA₈ showed similar peaks as PLA-PCHO, with a few additional small peaks at 4.77, 4.50, 4.20, and 4.10 ppm, which were identified as being related to LA and CHO methine ¹³C peaks by HSQC. HMBC, however, was only helpful in identifying the peaks at 4.50, 4.20, and 4.10 ppm as being nearby LA methine ¹³C peaks (Figures 2.24-2.27). The presence of numerous small peaks between 4.00 - 5.00 ppm may be due to differences in the junction environment (i.e., PCHO-PLA has an ester linkage, while PLA-PCHO has an ether linkage).

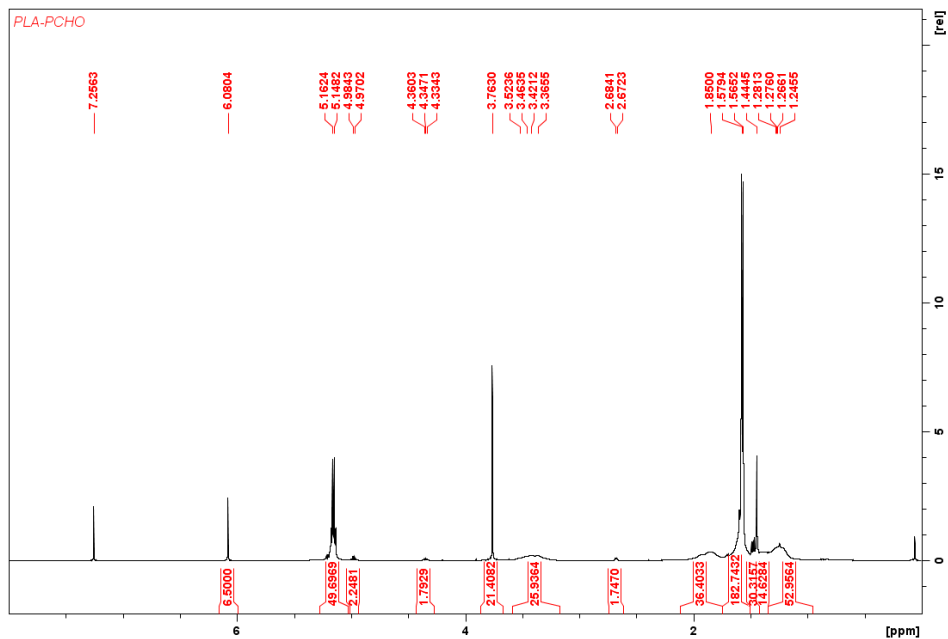


Figure 2.24. Table 2.5, entry 4. Low molecular weight PLA-PCHO. ¹H NMR (500 MHz, 25 °C, CDCl₃), δ (ppm): 6.08 (s, 3H, PhH TMB), 5.15 (q, 2H, CHCH₃ PLA), 3.77 (s, 9H, CH₃ TMB), 3.40 (m, 2H, COCH PCHO), 1.86 (m, 2H, COCHCH₂ PCHO), 1.58 (d, 6H, CHCH₃ PLA), 1.25 (m, 2H, COCHCH₂CH₂ PCHO).

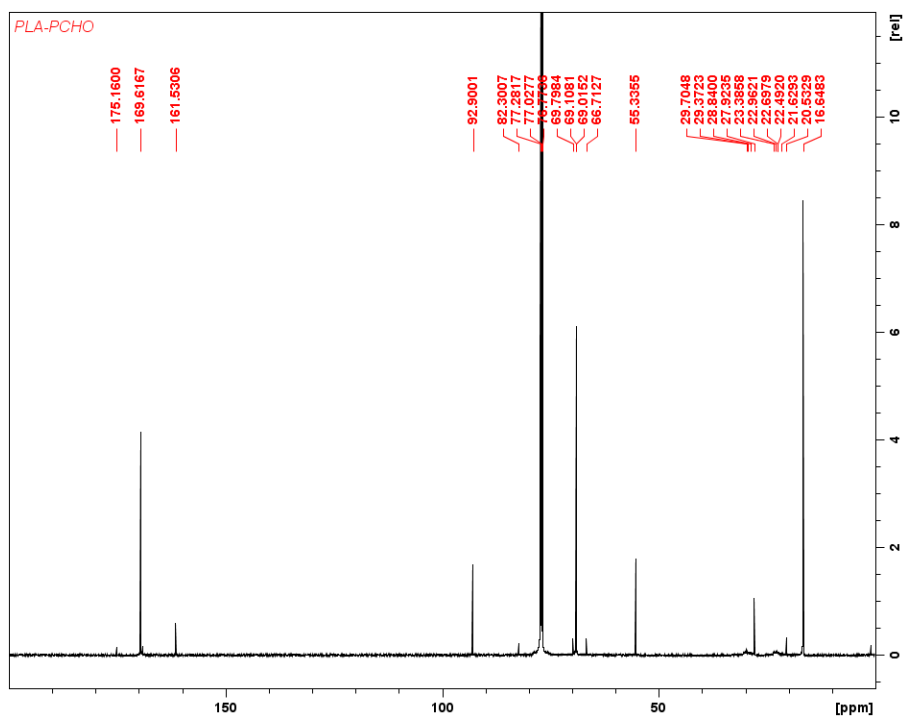


Figure 2.25. Table 2.5, entry 4. Low molecular weight PLA-PCHO. ^{13}C NMR (500 MHz, 25 °C, CDCl_3), δ (ppm): 175.1 (C=O, PLA), 169.6 (C=O, PLA), 161.5 (C=O, PLA), 161.5 (C-OMe, TMB), 92.9 (CH, TMB), 82.3 ($\text{C}(\text{CH}_3)_3$, O^tBu), 77.0 (broad, CH, PCHO), 77.0 (CDCl_3), 68.6 (CH, PLA), 55.3 (OCH_3 , TMB), 29.3 (broad, CHCH_2 , PCHO), 27.9 (CH_3 , O^tBu), 22.7 (broad, CH_2 , PCHO), 16.6 (CH_3 , PLA).

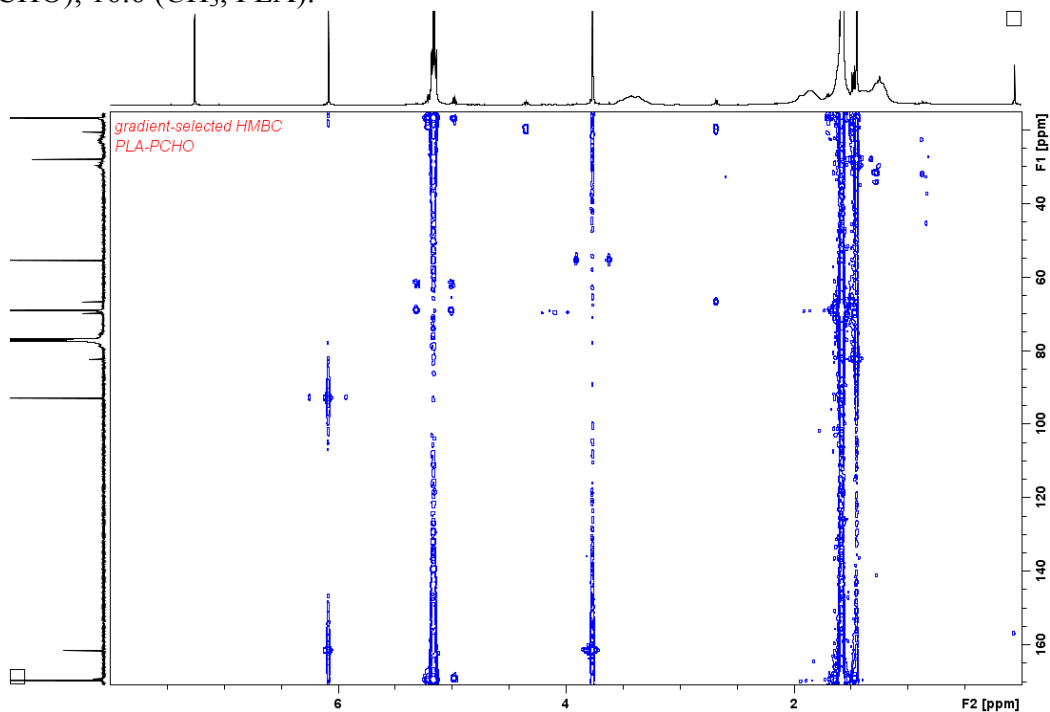


Figure 2.26. Table 2.5, entry 4. Low molecular weight PLA-PCHO. HMBC ^1H - ^{13}C NMR (500 MHz, 25 °C, CDCl_3).

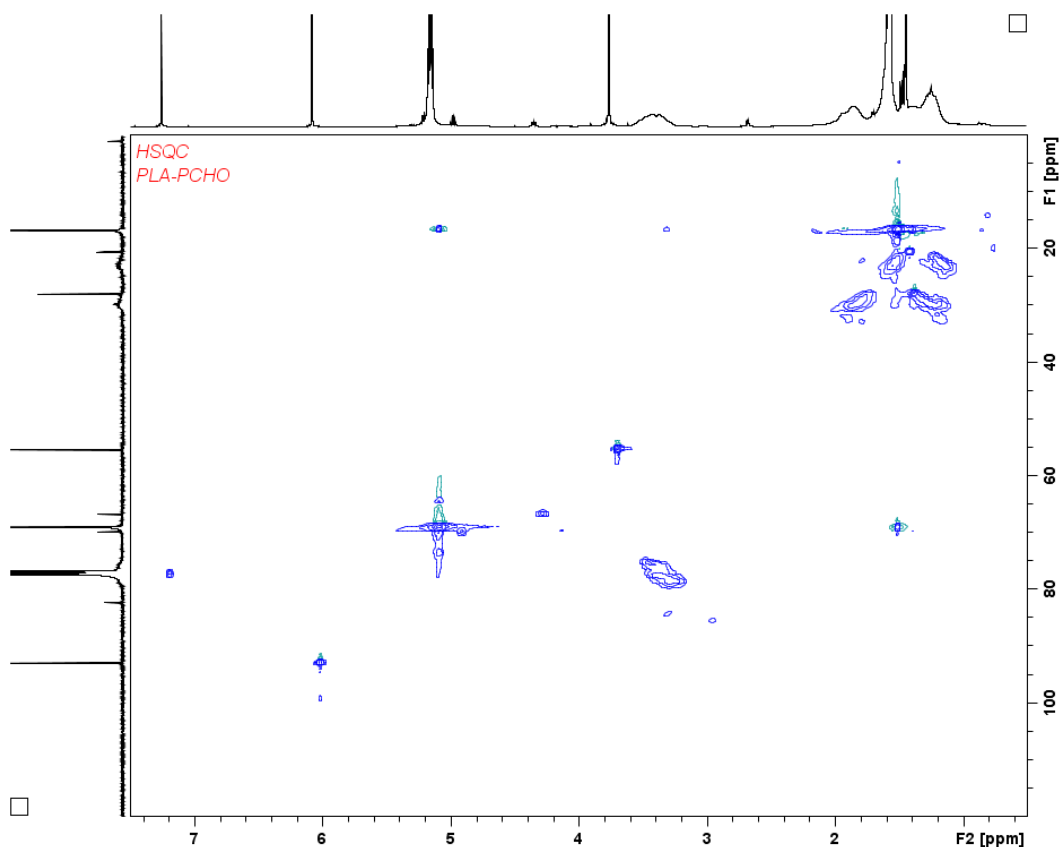


Figure 2.27. Table 2.5, entry 4. Low molecular weight PLA-PCHO. HSQC ^1H - ^{13}C NMR (500 MHz, 25 °C, CDCl_3).

The low weight copolymer $\text{LA}_5\text{-CHO}_{20}\text{-PHB}_3$ showed little incorporation of BBL (around two monomers per initiator). The BBL's methylene peaks showed correlations with LA's methine ^{13}C peaks exclusively, indicating that the “third block” of the copolymer was in reality a heterosequence of BBL and leftover LA in solution. Like $\text{CHO}_{17}\text{-LA}_8$, a number of small peaks were present on the HSQC and HMBC maps, but none of them could be identified definitively as junction protons (Figures 2.28-2.31).

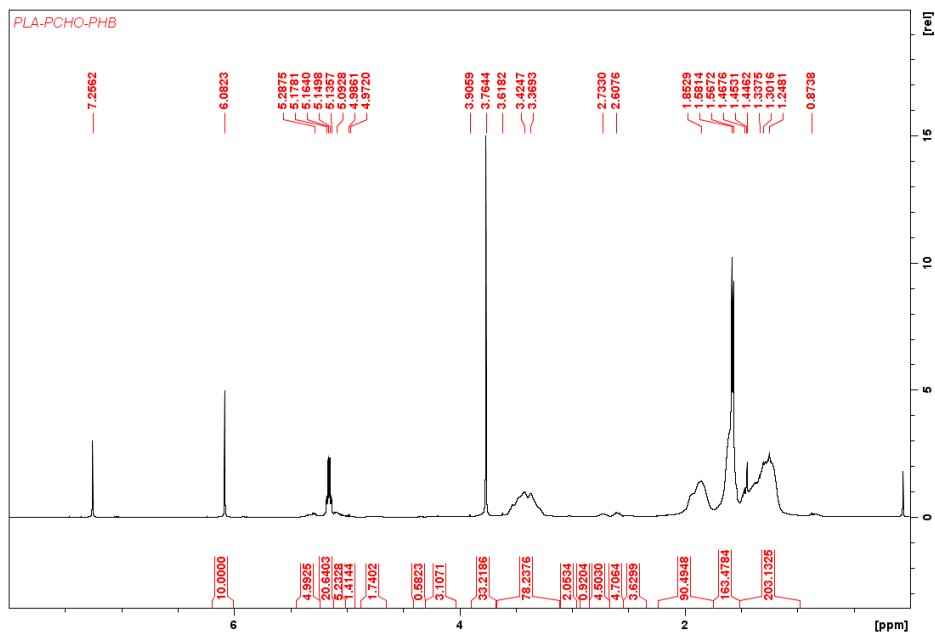


Figure 2.28. Table 2.5, entry 5. Low molecular weight PLA-PCHO-PHB. ^1H NMR (500 MHz, 25 °C, CDCl_3), δ (ppm): 6.08 (s, 3H, PhH TMB), 5.29 (m, 1H, OCHCH₃ PHB), 5.15 (q, 2H, CHCH₃ PLA), 3.76 (s, 9H, CH₃ TMB), 3.40 (m, 2H, COCH PCHO), 2.73-2.61 (m, 2H, COCH₂ PHB), 1.85 (m, 2H, COCHCH₂ PCHO), 1.57 (d, 6H, CHCH₃ PLA), 1.24 (m, 2H, COCHCH₂CH₂ PCHO).

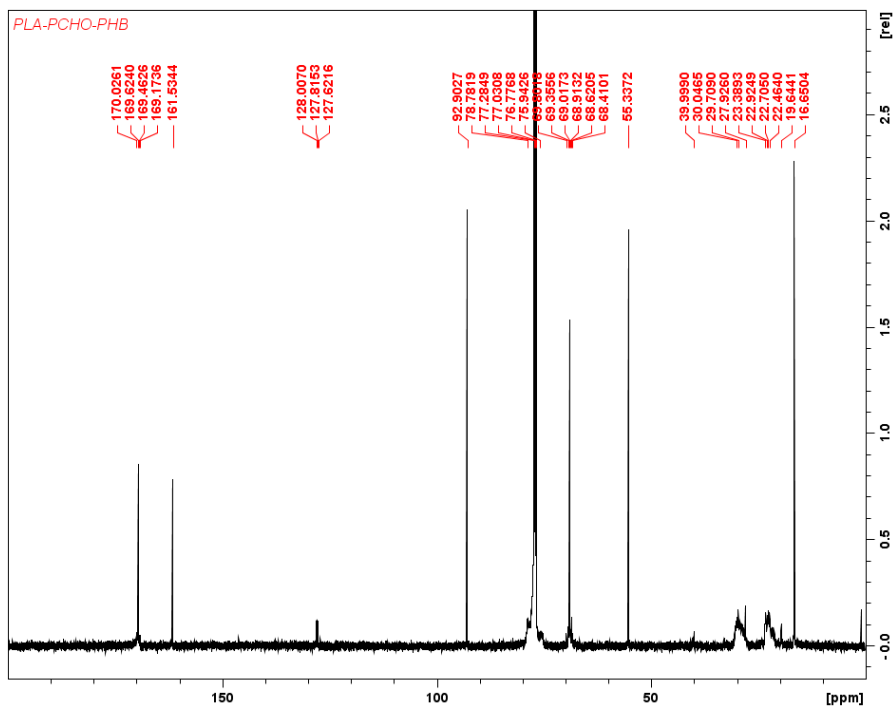


Figure 2.29. Table 2.5, entry 5. Low molecular weight PLA-PCHO-PHB. ^{13}C NMR (500 MHz, 25 °C, CDCl_3), δ (ppm): 169.6 (C=O, PLA), 169.2 (C=O, PHB), 161.5 (C-OMe, TMB), 127.8 (residual C_6D_6), 92.9 (CH, TMB), 77.0 (broad, CH, PCHO), 77.0 (CDCl_3), 68.6 (CH, PLA), 67.6 (CH, PHB), 55.3 (OCH₃, TMB), 40.0 (CH₂, PHB), 29.7 (broad, CHCH₂, PCHO), 27.9 (CH₃, O'Bu), 22.7 (broad, CH₂, PCHO), 19.6 (CH₃, PHB), 16.6 (CH₃, PLA).

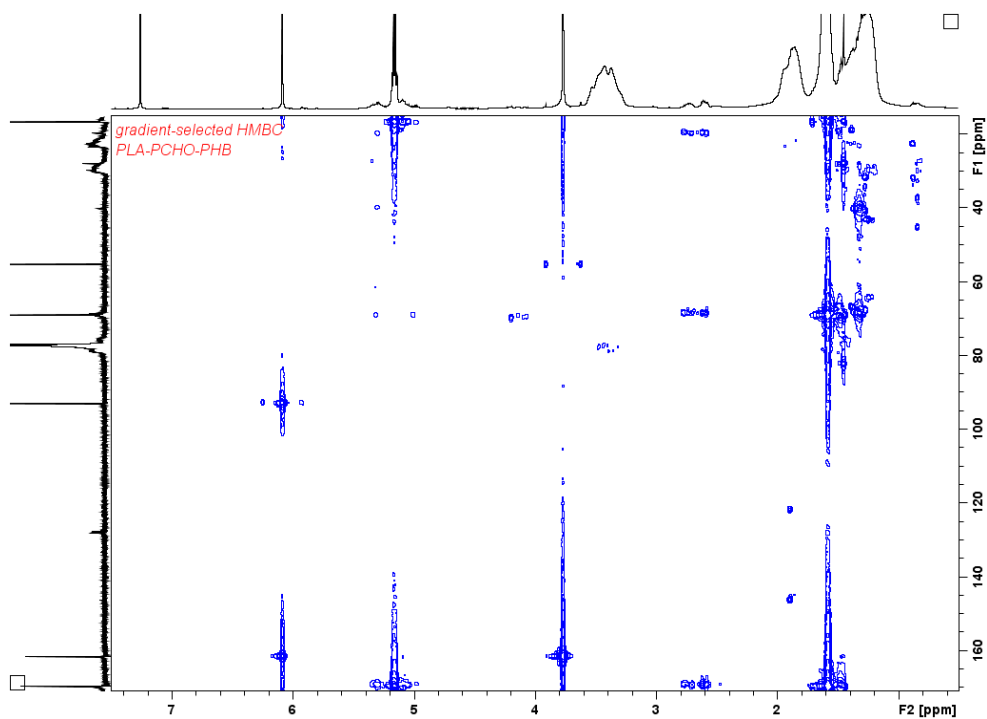


Figure 2.30. Table 2.5, entry 5. Low molecular weight PLA-PCHO-PHB. HMBC ^1H - ^{13}C NMR (500 MHz, 25 °C, CDCl_3).

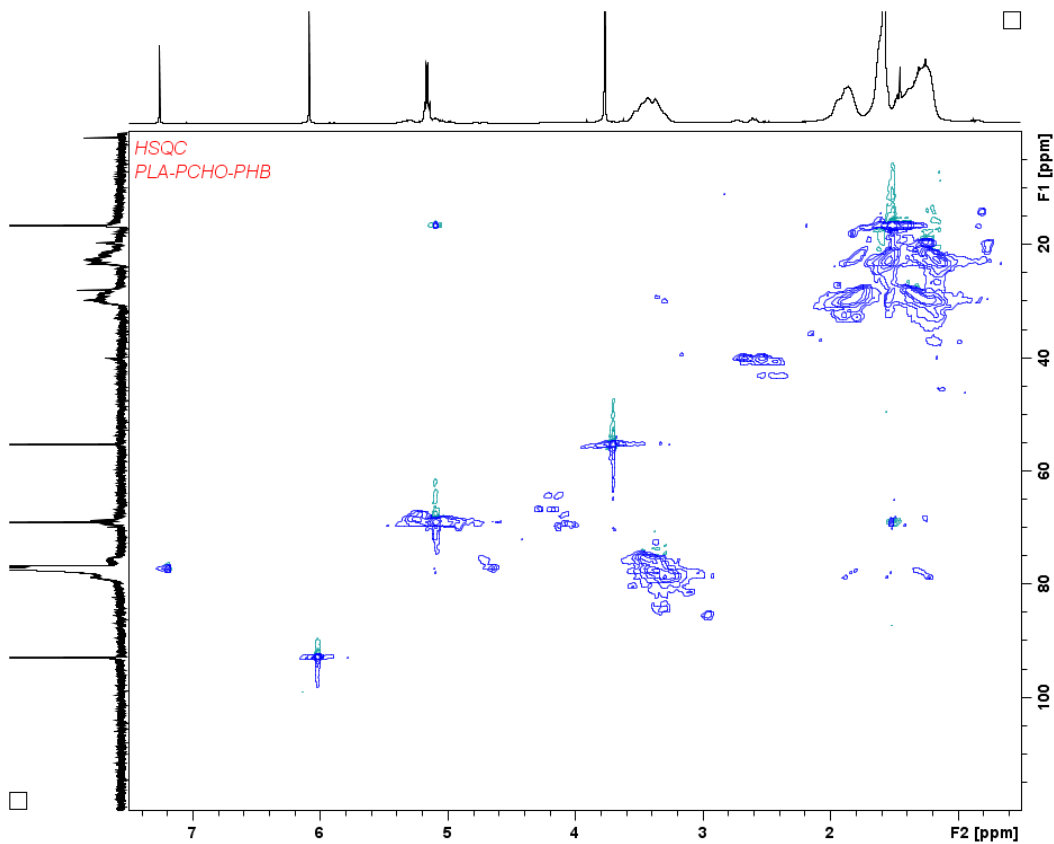


Figure 2.31. Table 2.5, entry 5. Low molecular weight PLA-PCHO-PHB. HSQC ^1H - ^{13}C NMR (500 MHz, 25 °C, CDCl_3).

Reexamination of the ^1H NMR spectra for the larger block copolymers in this light yields some information on the microstructure of these copolymers. For LA/CHO copolymers, some of the small peaks present in the ^1H NMR spectra between 3.76-5.15 ppm and 1.85-3.37 ppm could now be identified as LA monomer units closest to the end groups or junctions. Their relatively low integration (less than three protons in most cases) compared to the bulk polymer peaks (100-300 protons), indicates few junctions or heterosequences. For the LA/CHO/BBL copolymers, given the number of heterosequences found in the low weight polymers with LA and BBL, it is likely that the BBL block is heavily contaminated with LA monomers, thus not forming a true block copolymer in this case. We have tentatively assigned some of these peaks in Figures 2.8-2.11.

2.3 Conclusions

We achieved the redox-switchable copolymerization of L-lactide/ β -butyrolactone and cyclohexene oxide both in one pot and by sequential additions. Difficulties in achieving multiple redox switches in a one-pot polymerization underscored the necessity of choosing an effective yet otherwise innocent oxidant. The complex role of the oxidant was revealed through chemical oxidant screenings. Sequential monomer additions were employed to achieve multi-block copolymers. GPC analysis indicated an increase in the hydrodynamic volume of the copolymers after the addition of a PLA block and a decrease after the addition of a PCHO block. However, sequential precipitations, 2D NMR experiments, and DOSY experiments confirmed the formation of block copolymers and indicated that no significant homopolymer impurities are present. In addition, a clear decrease in the diffusion coefficient of the diblock to the triblock copolymers was observed.

2.4 Experimental

General considerations

All experiments were performed under a dry nitrogen atmosphere using standard Schlenk techniques or an MBraun inert-gas glovebox. Solvents were purified using a two-column solid-state purification system by the method of Grubbs²¹ and transferred to the glove box without exposure to air. NMR solvents were obtained from Cambridge Isotope Laboratories, degassed and stored over activated molecular sieves prior to use. ¹H NMR spectra were recorded on Bruker 300, Bruker 400 or Bruker 500 spectrometers at room temperature in C₆D₆ or CDCl₃. Chemical shifts are reported with respect to internal solvent, 7.16 ppm (C₆D₆) and 7.26 ppm (CDCl₃) for ¹H NMR spectra. All 2D NMR spectroscopy was performed on a Bruker 500 MHz spectrometer. The target block copolymer (10 mg) was dissolved in CDCl₃ (ca. 0.5 mL). Spectra were acquired with the ledbpgp2s pulse program from the Bruker topspin software. The gradient strength was logarithmically incremented in 32 steps from 2% up to 95% of the maximum gradient strength.¹⁴ Liquid monomers and 1,2-difluorobenzene were distilled over CaH₂ and brought into the glove box without exposure to air. Solid monomers and 1,3,5-trimethoxybenzene were recrystallized from toluene at least twice before use. 2,4-di-*tert*-butylphenol, *n*-BuLi, cobaltocene, and Zr(O^{*t*}Bu)₄ were purchased from Sigma Aldrich and used as received. Na[BAr^F₄], [^{Ac}Fc][BAr^F₄], Ag[BAr^F₄],²² AgB(C₆F₅)₄,²³ and (salfan)Zr(O^{*t*}Bu)₂^{8b} were synthesized following previously published procedures. Molecular weights of the polymers were determined by GPC (Gel Permeation Chromatography) at MRL Shared Experimental Facilities in UCSB that is supported by the MRSEC Program of the National Science Foundation under award NSF DMR 1121053; a member of the NSF-funded Material Research Facilities Network. GPC uses an Agilent liquid chromatograph equipped with a Waters Alliance HPLC System 2690

Separation Module and autosampler, two Agilent PLGEL 5 μm MIXED-D, $300 \times 7.5\text{mm}$ columns, a Waters 2410 Differential Refractometer and Water 2998 Photodiode Array Detector. The column temperature was set at $25\text{ }^\circ\text{C}$. A flow rate of 1.0 mL/min was used and samples were dissolved in chloroform with 0.25% triethylamine. GPC results were calibrated to narrow molecular weight polystyrene standards. Where indicated, molecular weights were also determined by a GPC-MALS instrument at UCLA. GPC-MALS uses a Shimadzu Prominence-i LC 2030C 3D equipped with an autosampler, two MZ Analysentechnik MZ-Gel SDplus LS $5\text{ }\mu\text{m}$, $300 \times 8\text{mm}$ linear columns, Wyatt DAWN HELEOS-II and Wyatt Optilab T-rEX. The column temperature was set at $40\text{ }^\circ\text{C}$. A flow rate of 0.70 mL/min was used and samples were dissolved in chloroform. dn/dc values were calculated for PLA and PCHO by creating five solutions of increasing concentration ($0.1 - 1.0\text{ mg/mL}$), directly injecting them into the RI detector sequentially, and using the batch dn/dc measurement methods in the Astra software. The dn/dc value for PLA and PCHO were calculated to be 0.024 mL/g and 0.086 mL/g over three trials.

Decomposition study of (salfan)Zr(O'Bu)₂ in CH₂Cl₂. To a J-Young NMR tube, a solution of (salfan)Zr(O'Bu)₂ (4.6 mg , $5\text{ }\mu\text{mol}$) in C₆D₆ (0.15 mL) was added, followed by 0.5 mL of CH₂Cl₂. After 20 min , the volatiles were removed under reduced pressure and the solid was analysed by ¹H NMR spectroscopy.

Decomposition study of (salfan)Zr(O'Bu)₂ in C₆H₅Cl. To a J-Young NMR tube, a solution of (salfan)Zr(O'Bu)₂ (4.6 mg , $5\text{ }\mu\text{mol}$) in C₆D₆ (0.15 mL) was added, followed by 0.5 mL of C₆H₅Cl. After heating for one hour at $100\text{ }^\circ\text{C}$, the volatiles were removed under reduced pressure and the solid was analysed by ¹H NMR spectroscopy.

Procedure for determining the reversibility of (salfan)Zr(O^tBu)₂ oxidation. To a C₆D₆ (0.15 mL) solution of (salfan)Zr(O^tBu)₂ (4.6 mg, 5 μmol) in a J-Young NMR tube, a solution of 1,3,5-trimethoxybenzene (16.8 mg, 50 μmol) in C₆D₆ (0.15 mL), 0.10 mL of F₂C₆H₄, and a solution of [^{Ac}Fc][BAr^F₄] (5.5 mg, 5 μmol) in F₂C₆H₄ (0.10 mL) were added and the reaction was left at room temperature for two hours. The reaction was monitored by ¹H NMR spectroscopy. A solution of CoCp₂ (5.5 mg, 5 μmol) in C₆D₆ (0.10 mL) was then added and the reaction was left at room temperature for another two hours. The reaction was monitored by ¹H NMR spectroscopy.

General polymerization procedures

General procedure for polymerization of one monomer by (salfan)Zr(O^tBu)₂. To a J-Young NMR tube, a solution of (salfan)Zr(O^tBu)₂ (4.6 mg, 5 μmol) in C₆D₆ (0.15 mL) was added, followed by a solution of 1,3,5-trimethoxybenzene (16.8 mg, 50 μmol) in C₆D₆ (0.15 mL), 0.10 mL of C₆D₆, and 0.10 mL of F₂C₆H₄. The solution was shaken. 0.5 mmol monomer was added. The reaction was monitored to completion or for 24 hours.

General procedure for polymerization of one monomer by [(salfan)Zr(O^tBu)₂][BAr^F₄]. To a J-Young NMR tube, a solution of (salfan)Zr(O^tBu)₂ (4.6 mg, 5 μmol) in C₆D₆ (0.15 mL) was added, followed by a solution of 1,3,5-trimethoxybenzene (16.8 mg, 50 μmol) in C₆D₆ (0.15 mL), 0.10 mL of C₆D₆, and 0.10 mL of F₂C₆H₄. The solution was shaken. 0.10 mL of a [^{Ac}Fc][BAr^F₄] solution (5.5 mg, 5 μmol) was added. After two hours, 0.5 mmol monomer was added. The reaction was monitored to completion or for 24 h.

General procedure for the polymerization of two monomers by (salfan)Zr(O^tBu)₂ or [(salfan)Zr(O^tBu)₂][BAr^F₄] with one redox switch (one pot)

Copolymerization of LA and CHO by (salfan)Zr(O'Bu)₂ (red-ox). To a C₆D₆ (0.15 mL) solution of (salfan)Zr(O'Bu)₂ (4.6 mg, 5 μmol) in a J-Young NMR tube, a solution of 1,3,5-trimethoxybenzene (16.8 mg, 50 μmol) in C₆D₆ (0.15 mL), 0.10 mL of F₂C₆H₄ and a C₆D₆ (0.10 mL) solution of cyclohexene oxide (49.0 mg, 0.5 mmol) and L-lactide (72.0 mg, 0.5 mmol) were added. The reaction was heated to 100 °C and periodically removed from the oil bath every 30 min to be analyzed by ¹H NMR spectroscopy. A solution of [^{Ac}Fc][BAR^F₄] (5.5 mg, 5 μmol) in F₂C₆H₄ (0.10 mL) was added. After two hours, the reaction was heated to 100 °C again and removed from the oil bath every hour to be analyzed by ¹H NMR spectroscopy. At the end, the reaction mixture was dissolved in CH₂Cl₂ and poured into cold methanol; a white solid precipitated briefly and was filtered.

Copolymerization of LA and CHO by (salfan)Zr(O'Bu)₂ (ox-red). To a C₆D₆ (0.15 mL) solution of (salfan)Zr(O'Bu)₂ (4.6 mg, 5 μmol) in a J-Young NMR tube, a solution of 1,3,5-trimethoxybenzene (16.8 mg, 50 μmol) in C₆D₆ (0.15 mL), 0.10 mL of F₂C₆H₄ and a solution of [^{Ac}Fc][BAR^F₄] (5.5 mg, 5 μmol) in F₂C₆H₄ (0.10 mL) was added. After two hours, a C₆D₆ (0.10 mL) solution of cyclohexene oxide (49.0 mg, 0.5 mmol) and L-lactide (72 mg, 0.5 mmol) was added. The reaction was heated to 100 °C and removed from the bath every 30 min to be analyzed by ¹H NMR spectroscopy. A solution of CoCp₂ (0.95 mg, 5 μmol) in C₆D₆ (0.10 mL) was added. The reaction was heated to 100 °C again and removed from the oil bath every hour to be analyzed by ¹H NMR spectroscopy. At the end, the reaction mixture was dissolved in CH₂Cl₂ and poured into cold methanol; a white solid precipitated briefly and was filtered.

General procedure for the sequential polymerization of LA and CHO by (salfan)Zr(O'Bu)₂ or [(salfan)Zr(O'Bu)₂][BAR^F₄] with two redox switches (sequential addition of monomers)

Copolymerization of LA and CHO by (salfan)Zr(O^tBu)₂ (red-ox-red). To a C₆D₆ (0.15 mL) solution of (salfan)Zr(O^tBu)₂ (4.6 mg, 5 μmol) in a J-Young NMR tube, a solution of 1,3,5-trimethoxybenzene (16.8 mg, 50 μmol) in C₆D₆ (0.15 mL), 0.10 mL of F₂C₆H₄ and L-lactide (72.0 mg, 0.5 mmol) were added. The reaction was heated to 100 °C and removed from the oil bath every 30 min to be analyzed by ¹H NMR spectroscopy. A solution of [¹⁹Fc][BAR^F₄] (5.5 mg, 5 μmol) in F₂C₆H₄ (0.10 mL) was then added and the reaction was left at room temperature for two hours. A solution of cyclohexene oxide (49.0 mg, 0.5 mmol) in C₆D₆ (0.10 mL) was added. The reaction was heated to 100 °C and removed from the oil bath every 30 min to be analyzed by ¹H NMR spectroscopy. A solution of CoCp₂ (5.5 mg, 5 μmol) in C₆D₆ (0.10 mL) was then added and the reaction was left at room temperature for two hours. L-lactide (72.0 mg, 0.5 mmol) was added. The reaction was heated to 100 °C and removed from the oil bath every 30 min to be monitored by ¹H NMR spectroscopy until completion. At the end, the reaction mixture was dissolved in CH₂Cl₂ and poured into cold methanol; a white solid precipitated briefly and was filtered. Yield: PLA-PCHO, 174 mg, 81.8%; PLA-PCHO-PLA 350 mg, 96.8%.

Copolymerization of LA and CHO by [(salfan)Zr(O^tBu)₂][BAR^F₄] (ox-red-ox). To a C₆D₆ (0.15 mL) solution of (salfan)Zr(O^tBu)₂ (4.6 mg, 5 μmol) in a J-Young NMR tube, a solution of 1,3,5-trimethoxybenzene (16.8 mg, 50 μmol) in C₆D₆ (0.15 mL), 0.10 mL F₂C₆H₄ and a solution of [¹⁹Fc][BAR^F₄] (5.5 mg, 5 μmol) in F₂C₆H₄ (0.10 mL) was added and the reaction was left at room temperature for two hours. A solution of cyclohexene oxide (49.0 mg, 0.5 mmol) in C₆D₆ (0.10 mL) was added. The reaction was heated to 100 °C and removed from the oil bath every 30 minutes to be analyzed by ¹H NMR spectroscopy. A solution of CoCp₂ (5.5 mg, 5 μmol) in C₆D₆ (0.10 mL) was then added and the reaction was left at room temperature for 2h.

L-lactide (72.0 mg, 0.5 mmol) was added. The reaction was heated to 100 °C and removed from the oil bath every hour to be analyzed by ^1H NMR spectroscopy. A solution of $[\text{AcFc}][\text{BAr}^{\text{F}}_4]$ (5.5 mg, 5 μmol) in $\text{F}_2\text{C}_6\text{H}_4$ (0.10 mL) was then added and the reaction was left at room temperature for two hours. A solution of cyclohexene oxide (49.0 mg, 0.5 mmol) in C_6D_6 (0.10 mL) was added. The reaction was heated at 100 °C and removed from the oil bath every hour to be analyzed by ^1H NMR spectroscopy until completion. At the end, the reaction was dissolved in CH_2Cl_2 and poured into cold methanol; a white solid precipitated briefly and was filtered. Yield: PCHO-PLA, 211 mg, 93.9%. PCHO-PLA-PCHO, 280 mg, 91.3%.

Procedure for CHO conversion study with two redox switches. To a J-Young NMR tube, a solution of (salfan) $\text{Zr}(\text{O}^t\text{Bu})_2$ (4.6 mg, 5 μmol) in C_6D_6 (0.15 mL) was added, followed by a solution of 1,3,5-trimethoxybenzene (16.8 mg, 50 μmol) in C_6D_6 (0.15 mL), and a solution of $[\text{AcFc}][\text{BAr}^{\text{F}}_4]$ (5.5 mg, 5 μmol) in $\text{F}_2\text{C}_6\text{H}_4$ (0.10 mL). The mixture was left at room temperature for two hours. 1.00 mL of C_6D_6 was layered on top followed by 0.20 mL of a cyclohexene oxide (98 mg, 1.0 mmol) solution in C_6D_6 . The tube was shaken to mix the contents and a timer was started. NMR spectra were taken two minutes apart until 50% conversion was reached. The tube was brought back to the glovebox and a solution of CoCp_2 (5.5 mg, 5 μmol) in C_6D_6 (0.10 mL) was added. The reaction was monitored for 15 minutes by ^1H NMR spectroscopy then brought back into the glovebox and 0.10 mL of a $[\text{AcFc}][\text{BAr}^{\text{F}}_4]$ solution in $\text{F}_2\text{C}_6\text{H}_4$ (5.5 mg, 5 μmol) was added. Polymerization was monitored by ^1H NMR spectroscopy every two minutes until 90% conversion was reached.

Procedure for CHO conversion study with and without LA. To two J-Young NMR tubes, a solution of (salfan) $\text{Zr}(\text{O}^t\text{Bu})_2$ (4.6 mg, 5 μmol) in C_6D_6 (0.15 mL) was added, followed by a solution of 1,3,5-trimethoxybenzene (16.8 mg, 50 μmol) in C_6D_6 (0.15 mL), 0.10 mL of

C₆D₆, 0.10 mL of F₂C₆H₄ and a solution of [^{Ac}Fc][BAR^F₄] (5.5 mg, 5 μmol) in F₂C₆H₄ (0.10 mL). The resulting solution was shaken. To one J-Young NMR tube, L-lactide (72 mg, 0.5 mmol) was added. To both NMR tubes, a solution of cyclohexene oxide (49.0 mg, 0.5 mmol) in C₆D₆ (0.10 mL) was added. NMR tubes were monitored every five minutes until one of them reached over 90% conversion.

Procedure for LA conversion study with and without CHO. To two J-Young NMR tubes, a solution of (salfan)Zr(O^tBu)₂ (4.6 mg, 5 μmol) in C₆D₆ (0.15 mL) was added, followed by a solution of 1,3,5-trimethoxybenzene (16.8 mg, 50 μmol) in C₆D₆ (0.15 mL), 0.10 mL of C₆D₆, and 0.10 mL of F₂C₆H₄. The solution was shaken. To one J-Young NMR tube, a solution of cyclohexene oxide (49.0 mg, 0.25 mmol) in C₆D₆ (0.10 mL) was added. To both NMR tubes, L-lactide (72.0 mg, 0.5 mmol) was added. NMR tubes were heated to 100 °C. The reactions were removed from the oil bath and analyzed every 15 minutes by ¹H NMR spectroscopy until one of them reached over 90% conversion.

Procedure for conversion versus M_n study. To 4 J-Young NMR tubes, a solution of (salfan)Zr(O^tBu)₂ (4.6 mg, 5 μmol) in C₆D₆ (0.15 mL) was added, followed by a solution of 1,3,5-trimethoxybenzene (16.8 mg, 50 μmol) in C₆D₆ (0.15 mL), 0.10 mL of C₆D₆, and 0.10 mL of F₂C₆H₄. The resulting solution was shaken. To all NMR tubes, L-lactide (72.0 mg, 0.5 mmol) was added. NMR tubes were heated to 100 °C in an oil bath and a timer was started. An NMR tube was taken out every 15 minutes and the polymerizations were monitored until 40% conversion. The contents of the first tube were poured into a vial of cold methanol. Spectra were taken every 15 minutes afterward. Once significant changes in conversion were observed (about 10% more than the previous data point), the contents of the tube were poured into a vial of cold

methanol. Conversion vs. Mn studies for CHO were conducted at room temperature and at half the concentration for LA to slow down polymerization times.

Procedure for polymerization of CHO by $[\text{H}_2(\text{salfan})][\text{BAr}^{\text{F}}]$. To a J-Young NMR tube, a solution of $\text{H}_2(\text{salfan})$ (3.4 mg, 5 μmol) in C_6D_6 (0.15 mL) was added, followed by a solution of 1,3,5-trimethoxybenzene (16.8 mg, 50 μmol) in C_6D_6 (0.15 mL), 0.10 mL of C_6D_6 , 0.10 mL of $\text{F}_2\text{C}_6\text{H}_4$, and a solution of $[\text{AcFc}][\text{BAr}^{\text{F}}_4]$ (5.5 mg, 5 μmol) in $\text{F}_2\text{C}_6\text{H}_4$ (0.10 mL); the mixture was left at room temperature for two hours. A solution of cyclohexene oxide (49.0 mg, 0.5 mmol) in C_6D_6 (0.10 mL) was added. The reaction was monitored to completion or for 24 h.

Procedure for polymerization of CHO by $^{\text{Ac}}\text{FcBAR}^{\text{F}}$. To a J-Young NMR tube, a solution of $[\text{AcFc}][\text{BAr}^{\text{F}}]$ (5.5 mg, 5 μmol) in $\text{F}_2\text{C}_6\text{H}_4$ (0.10 mL) was added, followed by a solution of 1,3,5-trimethoxybenzene (16.8 mg, 50 μmol) in C_6D_6 (0.15 mL), 0.10 mL of C_6D_6 , and 0.10 mL of $\text{F}_2\text{C}_6\text{H}_4$. The solution was shaken. A solution of cyclohexene oxide (49 mg, 0.5 mmol) in C_6D_6 (0.10 mL) was added. The reaction was monitored to completion.

Modifications for the synthesis of low weight diblock and triblock copolymers. The same polymerization procedures as above were followed, but with the following modifications. Quantities of $(\text{salfan})\text{Zr}(\text{O}^t\text{Bu})_2$, 1,3,5-trimethoxybenzene and $[\text{AcFc}][\text{BAr}^{\text{F}}_4]$ were doubled from 5 μmol to 10 μmol . Quantities of monomer were halved from 0.50 mmol to 0.25 mmol, with the exception of BBL, which was otherwise difficult to observe by ^1H NMR spectroscopy.

Procedure for precipitation of homopolymers from copolymers. A polymerization reaction mixture was dissolved in minimal CH_2Cl_2 and poured into 10 mL of cold methanol. The mixture was centrifuged and the supernatant was poured off. The resulting crude polymer was dried, dissolved in minimal CH_2Cl_2 , and precipitated in 10 mL cold methanol two more times. To isolate the copolymer from any resulting homopolymer fragments selectively, 100 mg of the

crude polymer was dissolved in minimal CH_2Cl_2 and poured into 10 mL of cold acetone. The mixture was centrifuged and filtered through a 0.20 micron FTPE filter. The isolated precipitate was dried, dissolved in minimal CH_2Cl_2 and poured into 10 mL of cold hexanes. The mixture was centrifuged and then filtered through a 0.20 micron FTPE filter. Filtrates and precipitates from each precipitation were dried, weighed, and analyzed by ^1H NMR spectroscopy and GPC.

2.5 Appendix B

^1H NMR Spectroscopy

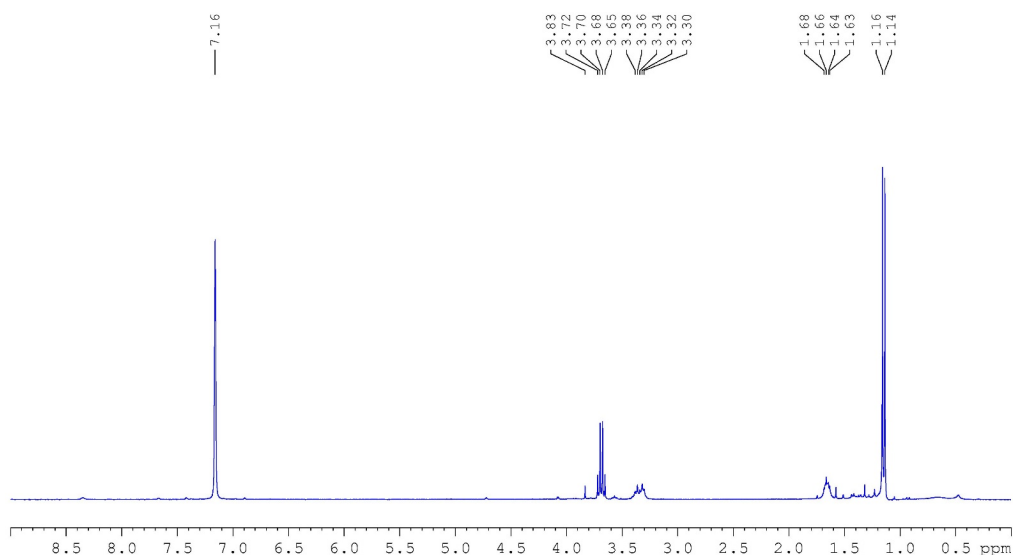


Figure B1. Polymerization of THF by *in situ* generated $[(\text{salfan})\text{Zr}(\text{O}^t\text{Bu})_2][\text{BAR}^{\text{F}}_4]$. ^1H NMR (300 MHz, 25 °C, C_6D_6) δ (ppm): 3.69 (m, 4H, OCH_2 THF), 3.33 (m, 4H, OCH_2 PTHF), 1.65 (m, 4H, OCH_2CH_2 PTHF), 1.15 (m, OCH_2CH_2 , THF).

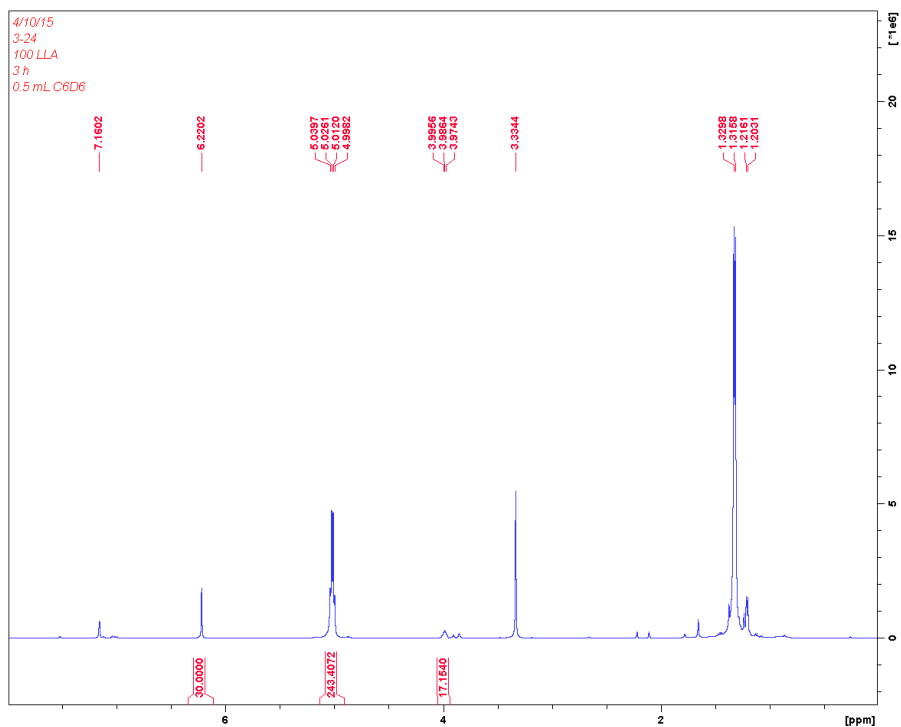


Figure B2. Polymerization of L-lactide by $(\text{salfan})\text{Zr}(\text{O}^t\text{Bu})_2$. ^1H NMR (300 MHz, 25 °C, C_6D_6), δ (ppm): 6.22 (s, 3H, PhH TMB), 5.02 (q, 2H, CHCH_3 PLA), 3.99 (q, 2H, CHCH_3 LLA), 3.33 (s, 9H, CH_3 TMB), 1.32 (d, 6H, CHCH_3 PLA), 1.20 (d, 6H, CHCH_3 LLA).

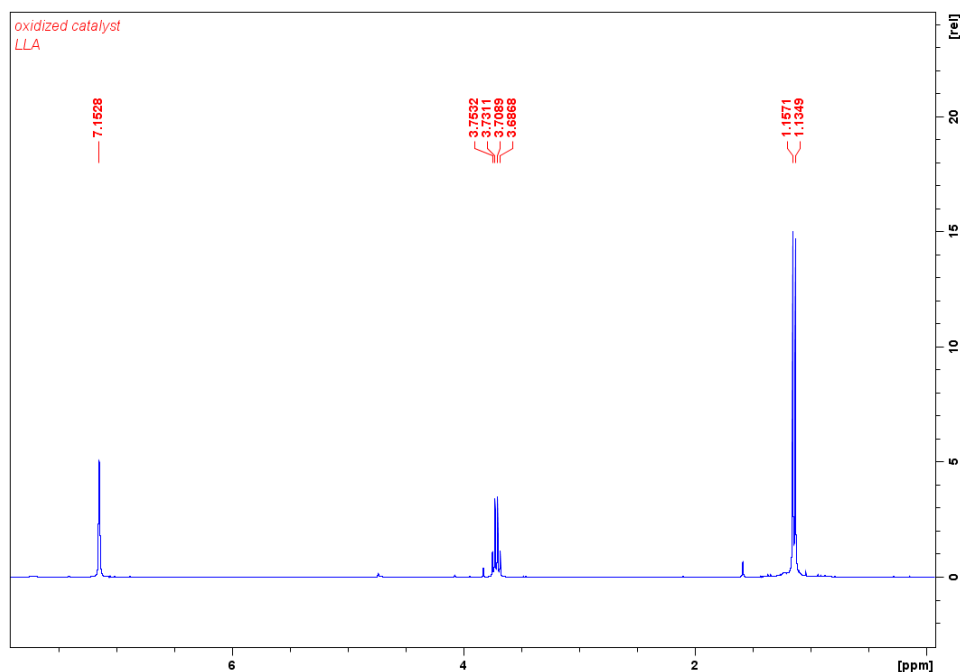


Figure B3. Polymerization of L-lactide by $[(\text{salfan})\text{Zr}(\text{O}^i\text{Bu})_2][\text{BAR}^{\text{F}}_4]$. ^1H NMR (300 MHz, 25 °C, C_6D_6), δ (ppm): 3.72 (q, 2H, CHCH_3 LA), 1.14 (d, 6H, CHCH_3 LA).

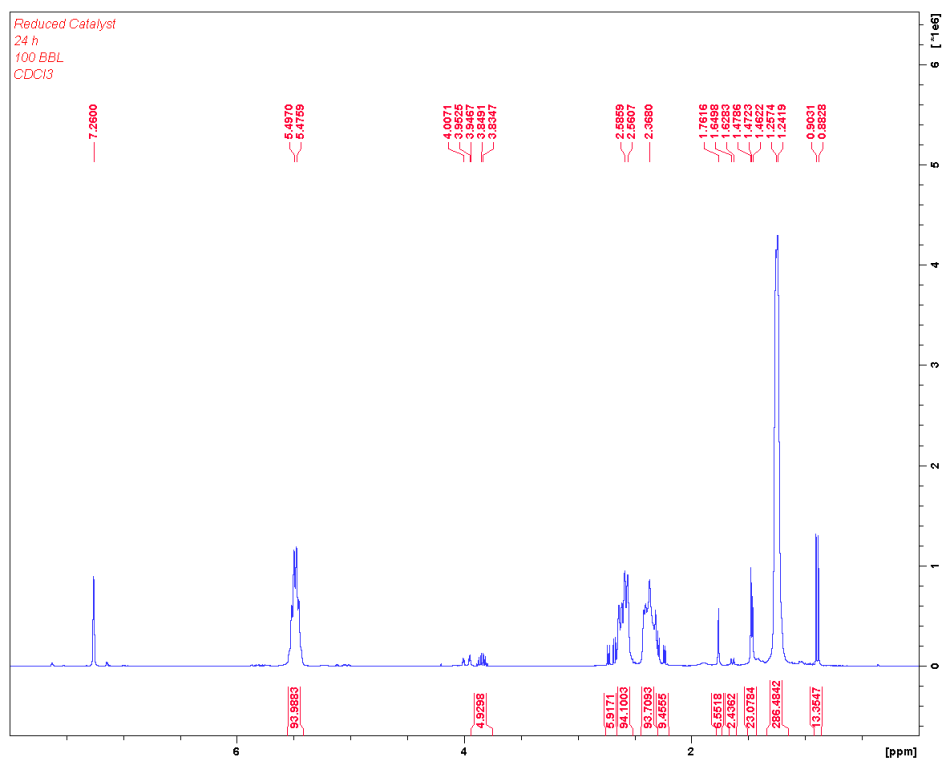


Figure B4. Polymerization of β -butyrolactone by $(\text{salfan})\text{Zr}(\text{O}^i\text{Bu})_2$. ^1H NMR (300 MHz, 25 °C, CDCl_3), δ (ppm): 5.48 (m, 1H, OCHCH_3 PHB), 3.84 (m, 1H, OCHCH_3 BBL), 2.58-2.37 (m, 2H, COCH_2 PHB), 1.25 (t, 3H, OCHCH_3 PHB), 0.89 (t, 3H, OCHCH_3 BBL).

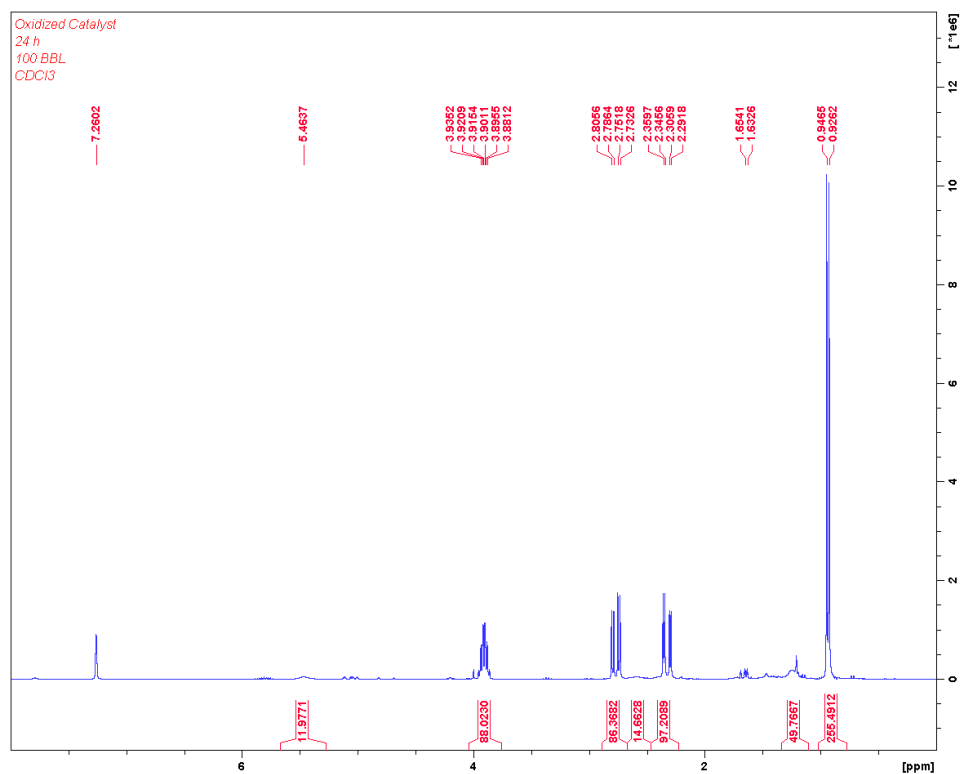


Figure B5. Polymerization of β -butyrolactone by $[(\text{salfan})\text{Zr}(\text{O}^t\text{Bu})_2][\text{BAR}^{\text{F}}_4]$. ^1H NMR (300 MHz, 25 °C, CDCl_3), δ (ppm): 5.46 (m, 1H, OCHCH_3 PHB), 3.90 (m, 1H, OCHCH_3 , BBL), 2.77-2.32 (m, 2H, COCH_2 BBL), 0.93 (t, 3H, OCHCH_3 BBL).

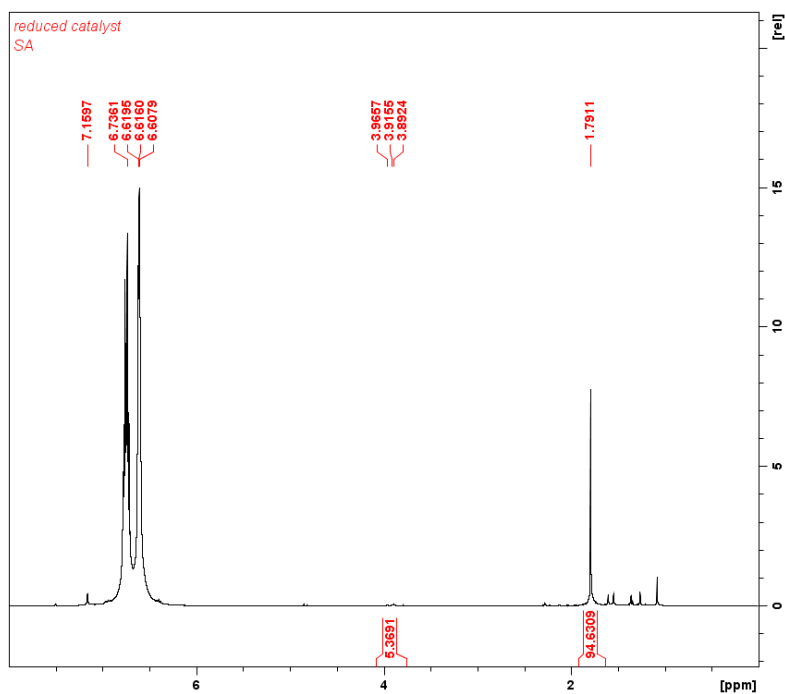


Figure B6. Polymerization of succinic anhydride by $(\text{salfan})\text{Zr}(\text{O}^t\text{Bu})_2$. ^1H NMR (300 MHz, 25 °C, C_6D_6), δ (ppm): 6.74 (CFCH 1,2-difluorobenzene), 6.62 (CFCHCH 1,2-difluorobenzene), 3.91 (m, CH_2 , PSA), 1.79 (s, CH_2 , SA).

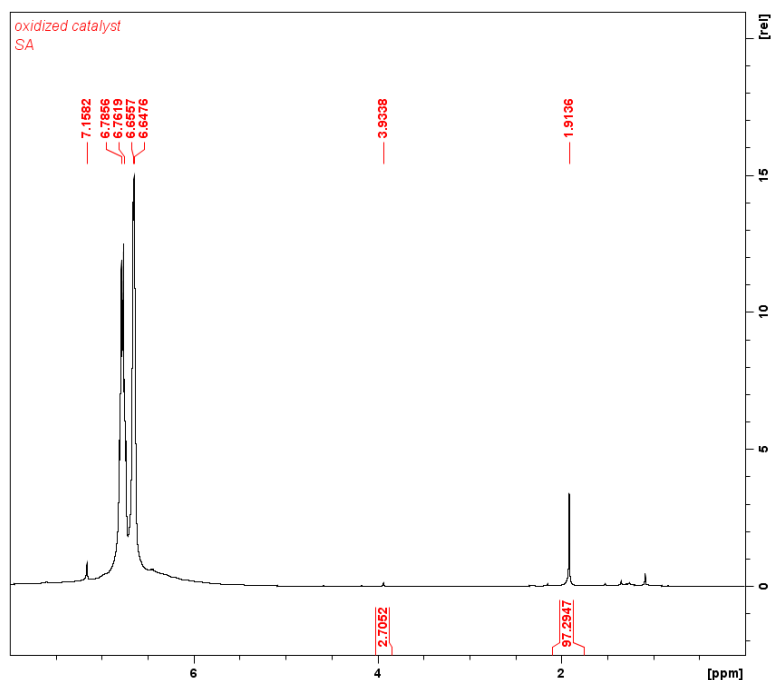


Figure B7. Polymerization of succinic anhydride by [(salfan)Zr(O^tBu)₂][BAr^F₄]. ¹H NMR (300 MHz, 25 °C, C₆D₆), δ (ppm): 6.74 (CFCH 1,2-difluorobenzene), 6.62 (CFCHCH 1,2-difluorobenzene), 3.91 (m, CH₂, PSA), 1.79 (s, CH₂, SA).

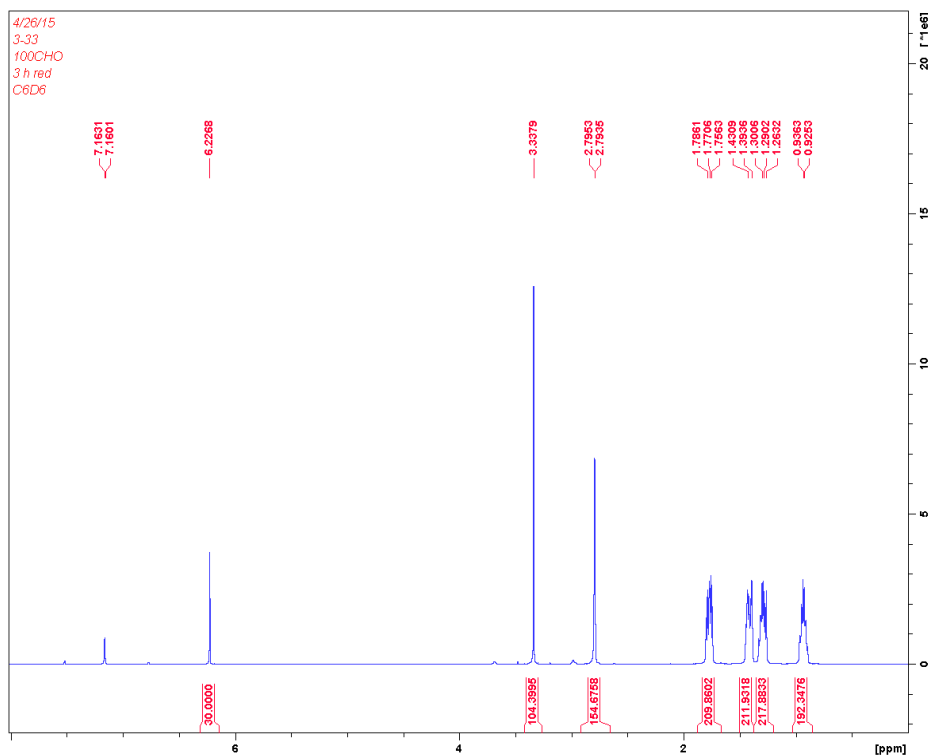


Figure B8. Polymerization of cyclohexene oxide by (salfan)Zr(O^tBu)₂. ¹H NMR (300 MHz, 25 °C, C₆D₆), δ (ppm): 6.22 (s, 3H, PhH TMB), 3.33 (s, 9H, CH₃ TMB), 2.79 (s, 2H, COCH CHO), 1.77 (m, 2H, COCHCH₂ CHO), 1.39 (m, 2H, COCHCH₂ CHO), 1.29 (m, 2H, COCHCH₂CH₂ CHO), 0.93 (m, 2H, COCHCH₂CH₂ CHO).

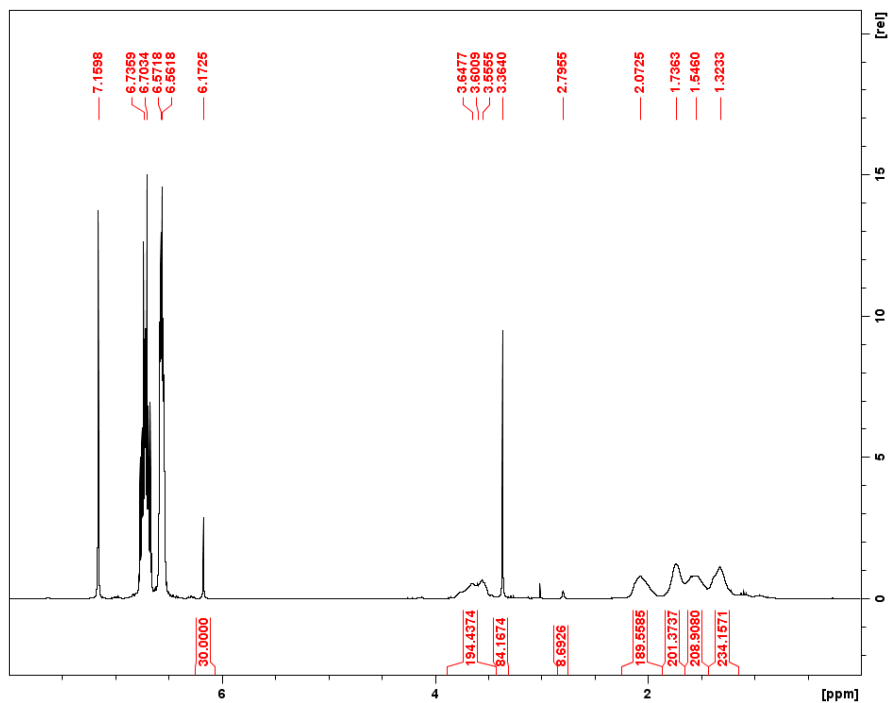


Figure B9. Polymerization of cyclohexene oxide by $[(\text{salfan})\text{Zr}(\text{O}^t\text{Bu})_2][\text{BAR}^{\text{F}}_4]$. ^1H NMR (300 MHz, 25 °C, C_6D_6), δ (ppm): 6.72 (CFCH 1,2-difluorobenzene), 6.57 (CFCHCH 1,2-difluorobenzene), 6.17 (s, 3H, PhH TMB), 3.60 (m, 2H, COCH PCHO), 3.36 (s, 9H, CH_3 TMB), 2.80 (s, 2H, COCH CHO), 2.07 (m, 2H, COCH CH_2 PCHO), 1.74 (m, 2H, COCH CH_2 PCHO), 1.54 (m, 2H, COCH CH_2CH_2 PCHO), 1.32 (m, 2H, COCH CH_2CH_2 PCHO).

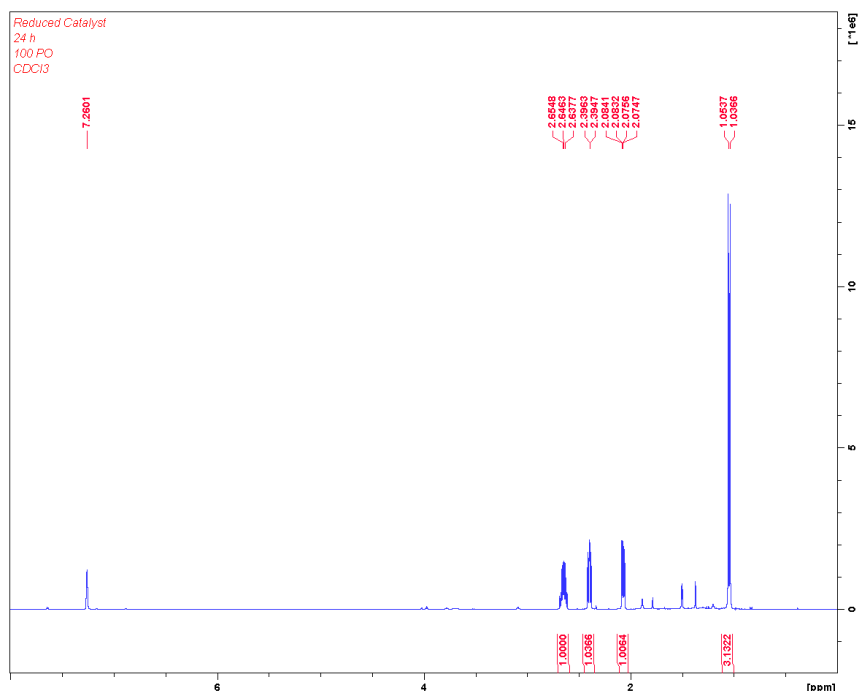


Figure B10. Table 2.1, entry 9. Polymerization of propylene oxide by $(\text{salfan})\text{Zr}(\text{O}^t\text{Bu})_2$. ^1H NMR (300 MHz, 25 °C, C_6D_6), δ (ppm): 2.65 (m, 1H, COCH CH_3 PO), 2.39 (m, 1H, COCH $_2$ PO), 2.07 (m, 1H, COCH $_2$ PO), 1.04 (d, 3H, COCH CH_3 PO).

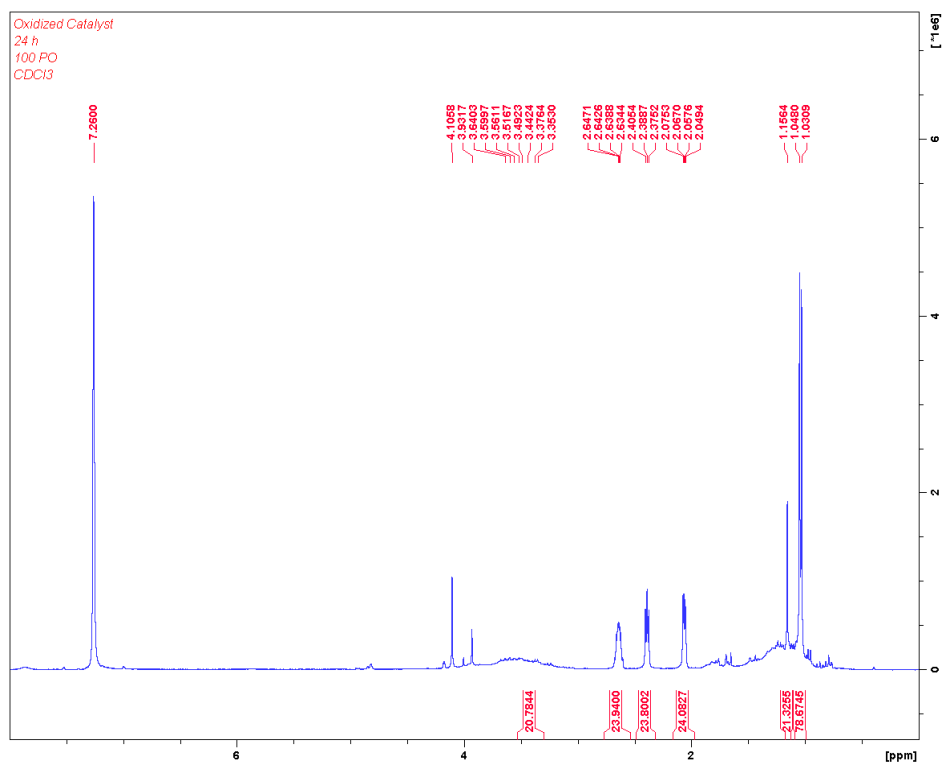


Figure B11. Table 2.1, entry 10. Polymerization of propylene oxide by [(salfan)Zr(O^tBu)₂][BAR^F₄]. ¹H NMR (300 MHz, 25 °C, CDCl₃), δ (ppm): 3.49 (m, 1H, COCHCH₃ PPO), 2.64 (m, 1H, COCHCH₃ PO), 2.38 (m, 1H, COCH₂ PO), 2.06 (m, 1H, COCH₂ PO), 1.56 (d, 3H, COCHCH₃ PPO), 1.04 (d, 3H, COCHCH₃ PO).

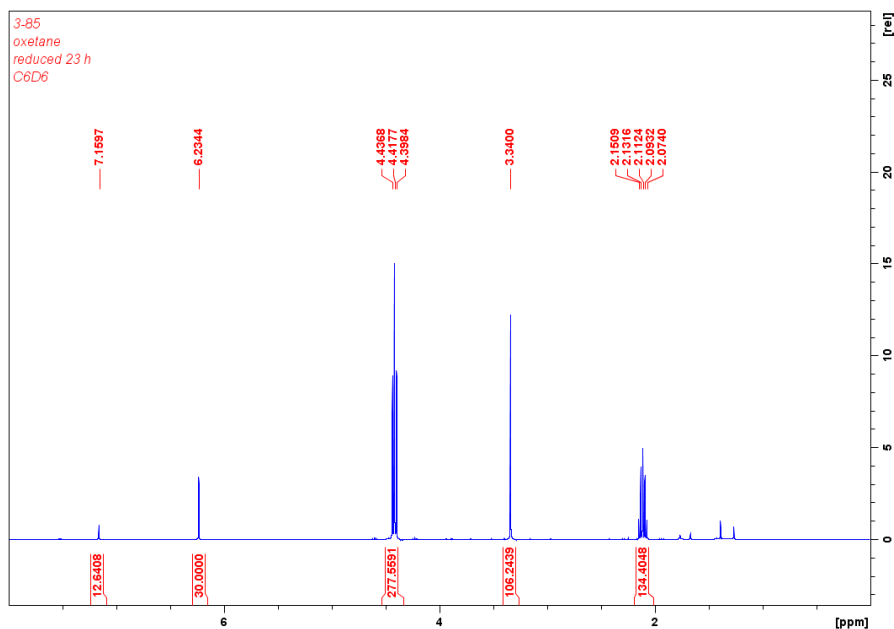


Figure B12. Table 2.1, entry 11. Polymerization of oxetane by (salfan)Zr(O^tBu)₂. ¹H NMR (300 MHz, 25 °C, C₆D₆), δ (ppm): 6.23 (s, 3H, PhH TMB), 4.42 (t, 4H, OCH₂ OX), 3.34 (s, 9H, CH₃ TMB), 2.11 (m, 2H, OCH₂CH₂ OX).

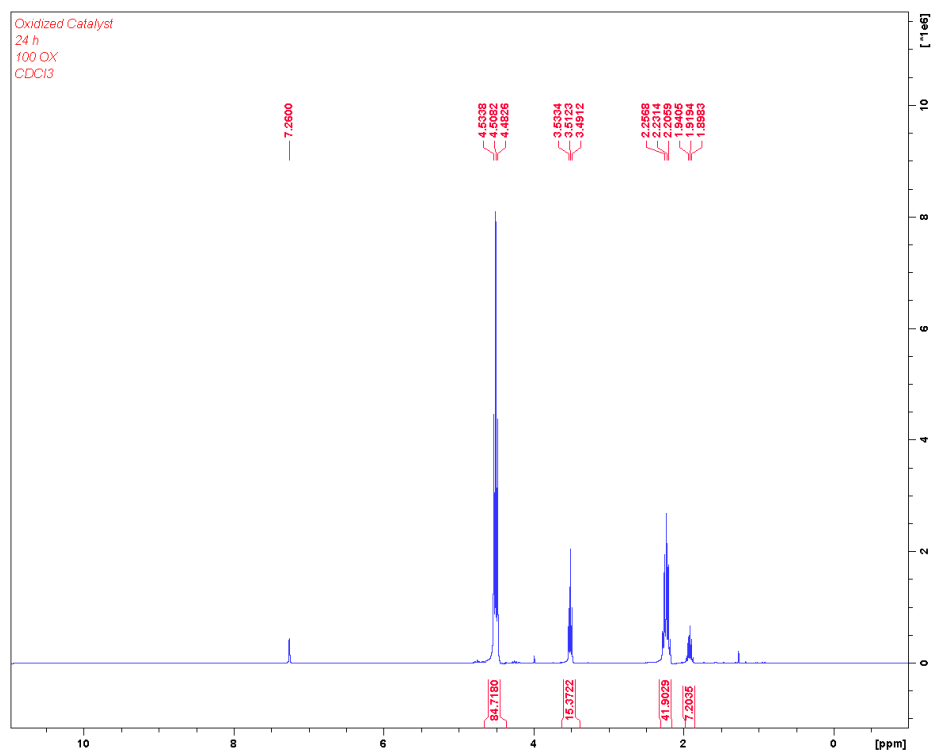


Figure B13. Table 2.1, entry 12. Polymerization of oxetane by $[(\text{salfan})\text{Zr}(\text{O}^t\text{Bu})_2][\text{BAR}^{\text{F}}_4]$. ^1H NMR (300 MHz, 25 °C, CDCl_3), δ (ppm): 4.51 (t, 4H, OCH_2OX), 3.51 (t, 4H, OCH_2POX), 2.23 (m, 2H, $\text{OCH}_2\text{CH}_2\text{OX}$), 1.92 (m, 2H, $\text{OCH}_2\text{CH}_2\text{OX}$).

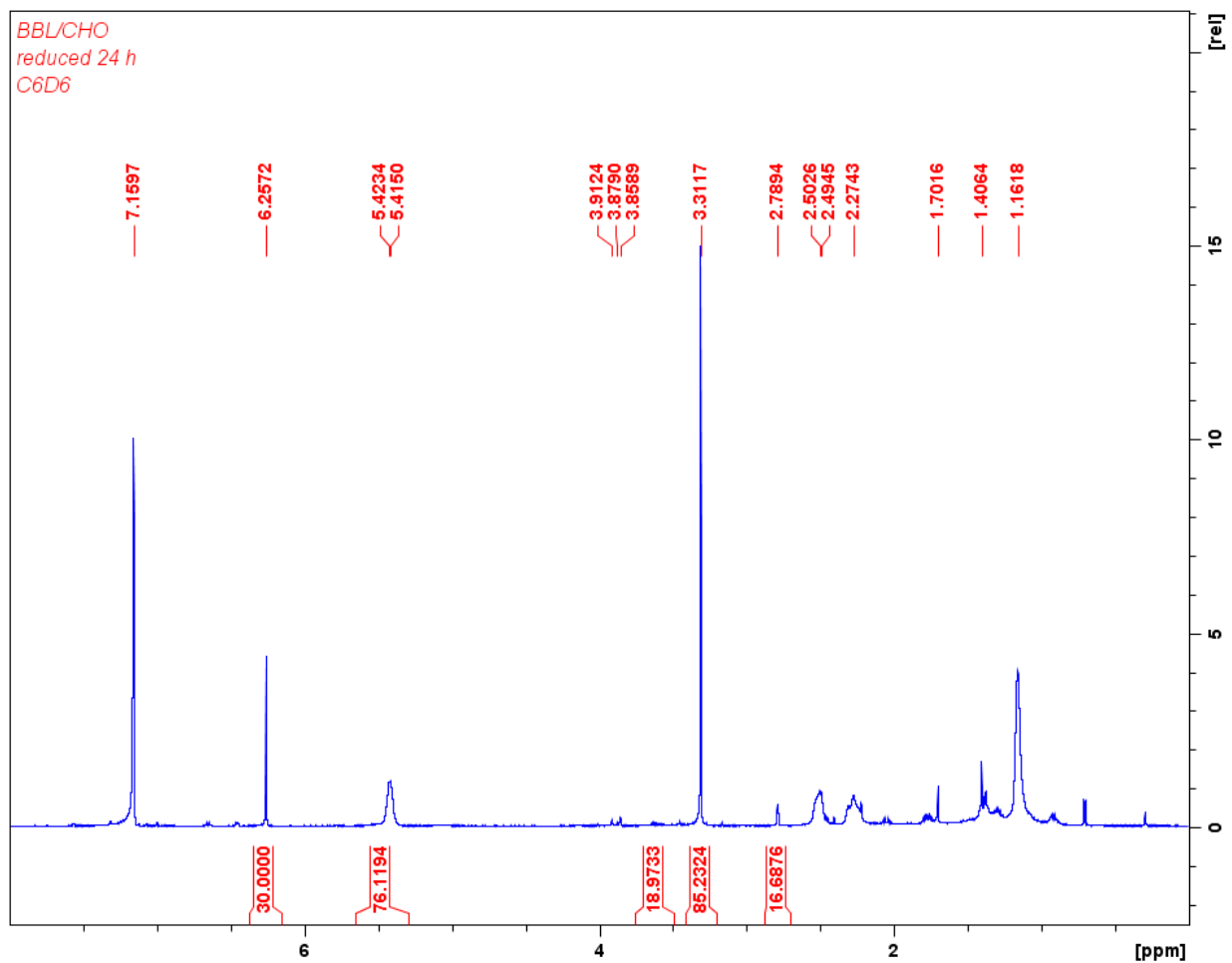


Figure B14. Table 2.2, entry 1. Polymerization of 100 equivalents of β -butyrolactone in the presence of 100 equivalents of cyclohexene oxide with initiator in the reduced state. ^1H NMR (300 MHz, 25 $^\circ\text{C}$, C_6D_6), δ (ppm): 6.26 (s, 3H, PhH TMB), 5.42 (m, 1H, OCHCH₃ PHB), 3.87 (m, 1H, OCHCH₃ BBL), 3.62 (m, 2H, COCH PCHO), 3.31 (s, 9H, CH₃ TMB), 2.79 (s, 2H, COCH₂ CHO), 2.50-2.27 (m, 2H, COCH₂ PHB), 1.70 (m, 2H, COCHCH₂ PCHO), 1.40 (m, 2H, COCHCH₂CH₂ PCHO), 1.31 (m, 2H, COCHCH₂CH₂ PCHO), 1.16 (t, 3H, OCHCH₃ PHB), 0.89 (t, 3H, OCHCH₃ BBL).

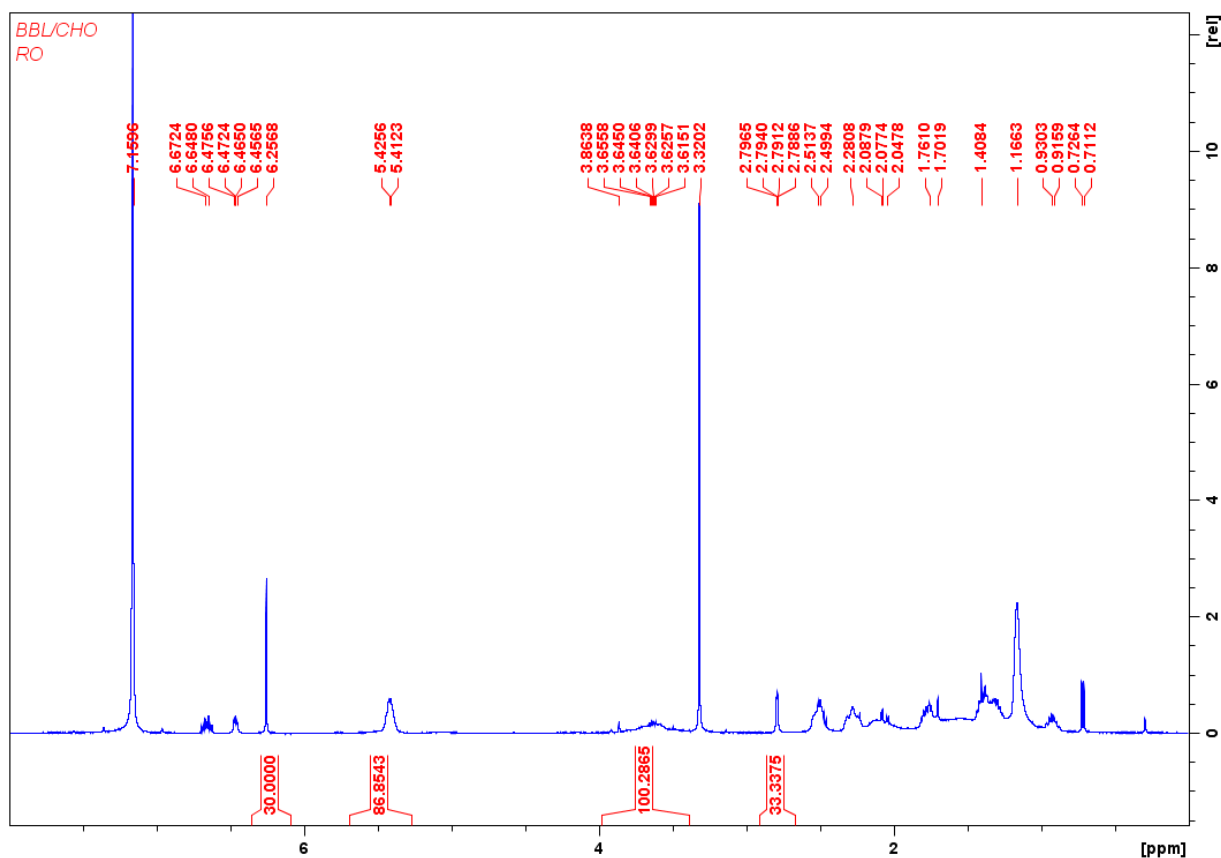


Figure B15. Table 2.2, entry 2. Polymerization of 100 equivalents of β -butyrolactone in the presence of 100 equivalents of cyclohexene oxide with initiator in the reduced state and subsequently oxidized. ^1H NMR (300 MHz, 25 °C, C_6D_6), δ (ppm): 6.65 (CFCH 1,2-difluorobenzene), 6.47 (CFCHCH 1,2-difluorobenzene), 6.26 (s, 3H, PhH TMB), 5.42 (m, 1H, OCHCH₃ PHB), 3.62 (m, 2H, COCH PCHO), 3.32 (s, 9H, CH₃ TMB), 2.79 (s, 2H, COCH₂ CHO), 2.50-2.28 (m, 2H, COCH₂ PHB), 2.07 (m, 2H, COCHCH₂ PCHO), 1.76 (m, 2H, COCHCH₂ PCHO), 1.41 (m, 2H, COCHCH₂CH₂ PCHO), 1.17 (m, 2H, OCHCH₃ PHB), 0.93 (m, 2H, COCHCH₂CH₂ CHO), 0.71 (t, 3H, OCHCH₃ BBL).

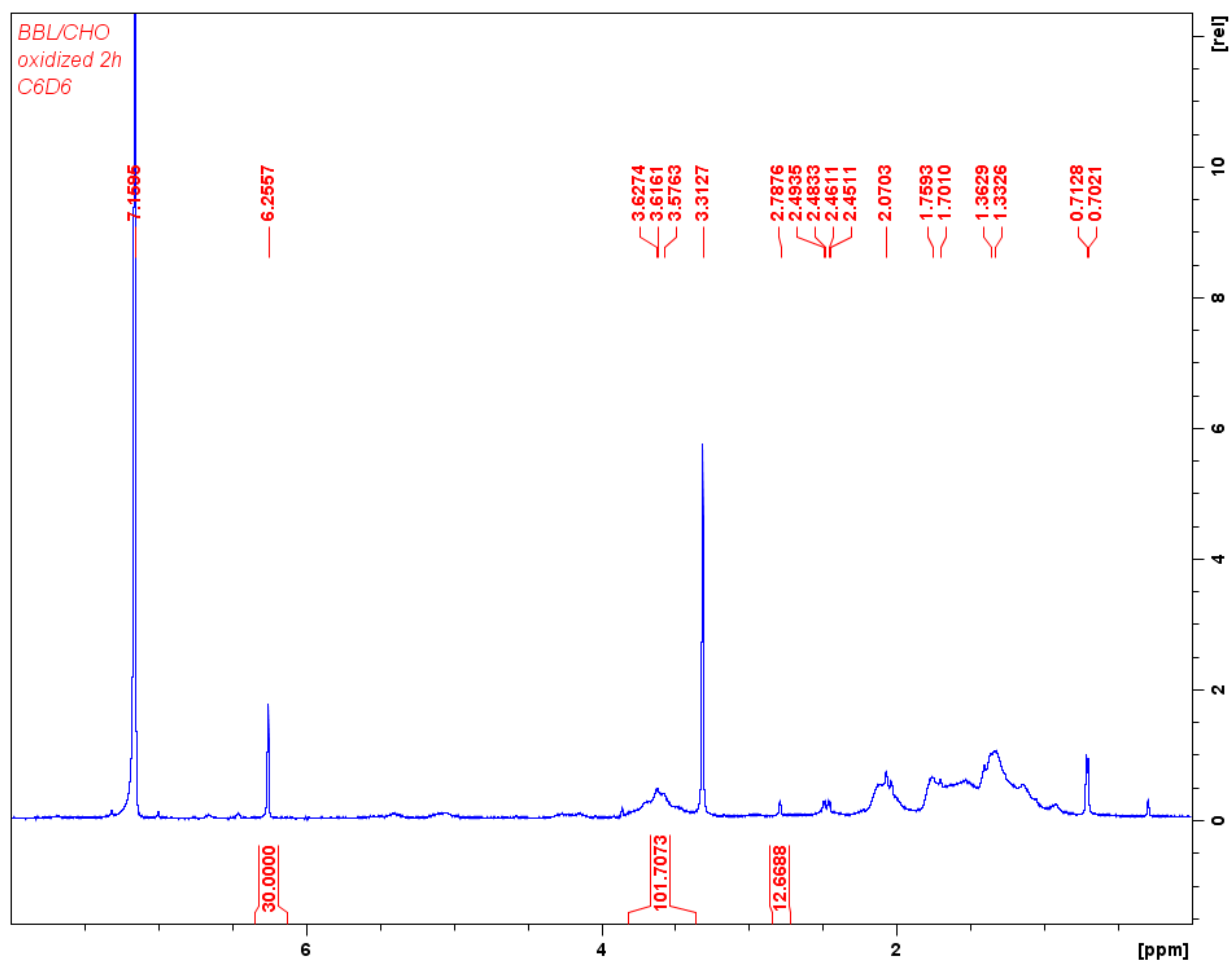


Figure B16. Table 2.2, entry 3. Polymerization of 100 equivalents of β -butyrolactone in the presence of 100 equivalents of cyclohexene oxide with initiator in the oxidized state. ^1H NMR (300 MHz, 25 $^\circ\text{C}$, C_6D_6), δ (ppm): 6.26 (s, 3H, PhH TMB), 3.62 (m, 2H, COCH PCHO), 3.31 (s, 9H, CH_3 TMB), 2.78 (s, 2H, COCH₂ CHO), 2.47 (m, 2H, COCH₂ BBL), 2.07 (m, 2H, COCHCH₂ PCHO), 1.74 (m, 2H, COCHCH₂ PCHO), 1.34 (m, 2H, COCHCH₂CH₂ PCHO), 0.71 (t, 3H, OCHCH₃ BBL).

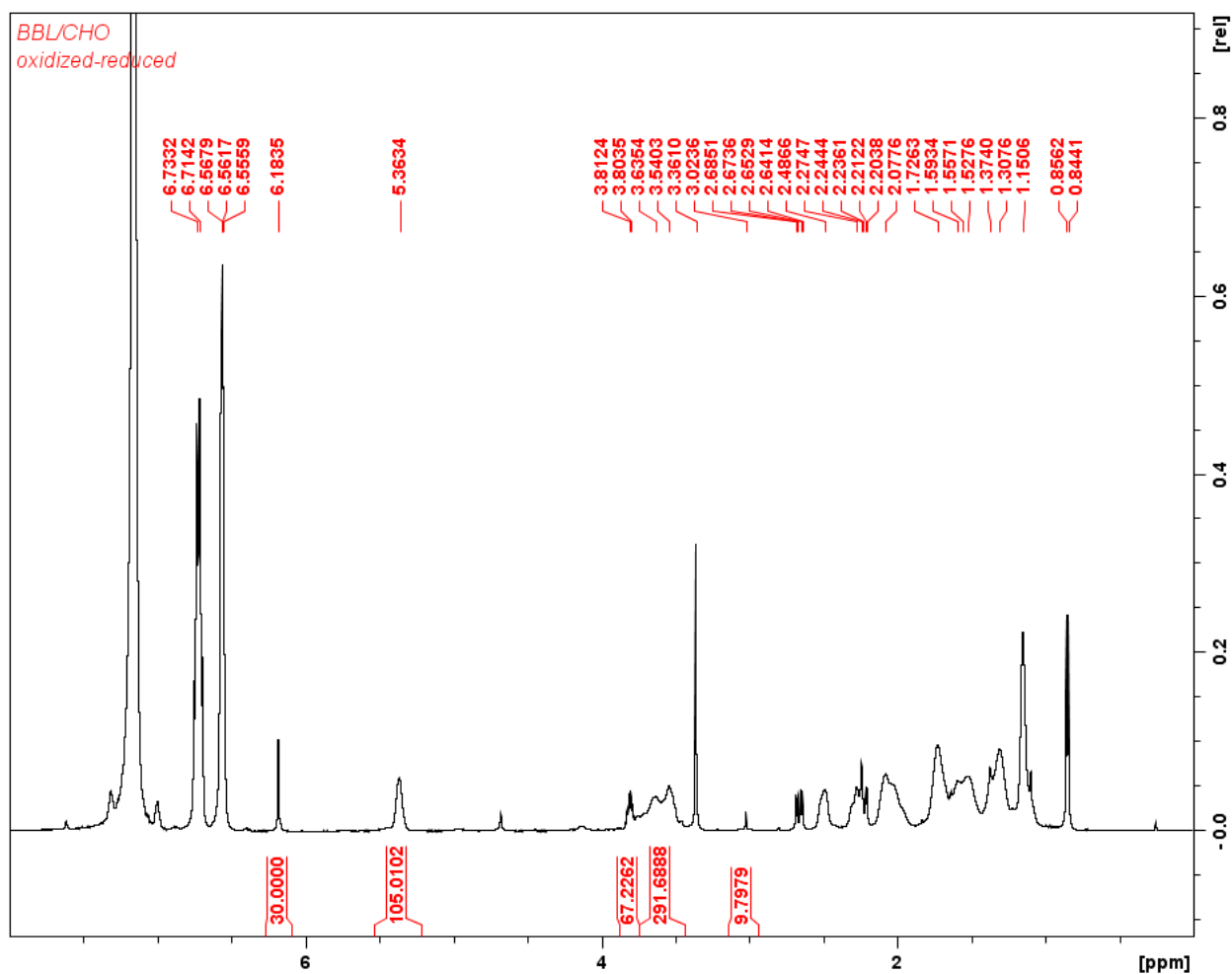


Figure B17. Table 2.2, entry 4. Polymerization of 100 equivalents of β -butyrolactone in the presence of 100 equivalents of propylene oxide with initiator in the oxidized state and subsequently reduced. ^1H NMR (300 MHz, 25 $^\circ\text{C}$, C_6D_6), δ (ppm): 6.71 (CFCH 1,2-difluorobenzene), 6.55 (CFCHCH 1,2-difluorobenzene), 6.18 (s, 3H, PhH TMB), 5.36 (m, 1H, OCHCH₃ PHB), 3.81 (m, 1H, OCHCH₃ BBL), 3.58 (m, 2H, COCH PCHO), 3.36 (s, 9H, CH₃ TMB), 3.02 (s, 2H, COCH₂ CHO), 2.67-2.24 (m, 2H, COCH₂ BBL), 2.48-2.27 (m, 2H, COCH₂ PHB), 2.07 (m, 2H, COCHCH₂ PCHO), 1.73 (m, 2H, COCHCH₂ PCHO), 1.37 (m, 2H, COCHCH₂CH₂ PCHO), 1.31 (m, 2H, COCHCH₂CH₂ PCHO), 1.15 (t, 3H, OCHCH₃ PHB), 0.85 (t, 3H, OCHCH₃ BBL).

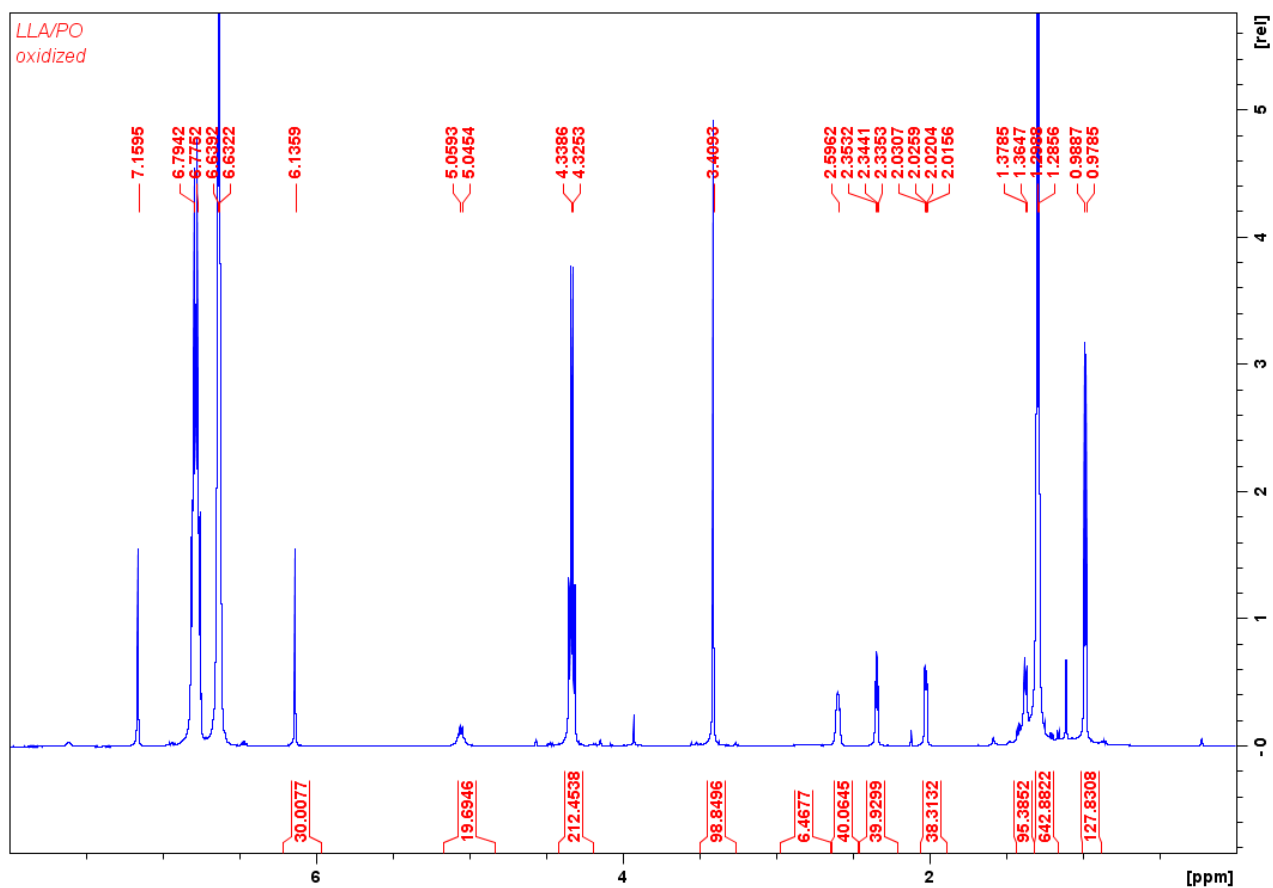


Figure B18. Table 2.2, entry 5. Polymerization of 100 equivalents of L-lactide in the presence of 100 equivalents of propylene oxide with initiator in the oxidized state. ^1H NMR (300 MHz, 25 $^\circ\text{C}$, C_6D_6), δ (ppm): 6.78 (CFCH 1,2-difluorobenzene), 6.63 (CFCHCH 1,2-difluorobenzene), 6.14 (s, 3H, PhH TMB), 5.04 (q, 2H, CHCH₃ PLA), 4.33 (q, 2H, CHCH₃ LLA), 3.60 (m, 1H, COCHCH₃ PPO), 3.40 (s, 9H, CH₃ TMB), 2.60 (m, 1H, COCHCH₃ PO), 2.34 (m, 1H, COCH₂ PO), 2.02 (m, 1H, COCH₂ PO), 1.36 (d, 3H, CHCH₃ PLA), 1.29 (d, 6H, CHCH₃ LA), 0.98 (d, 3H, COCHCH₃ PO).

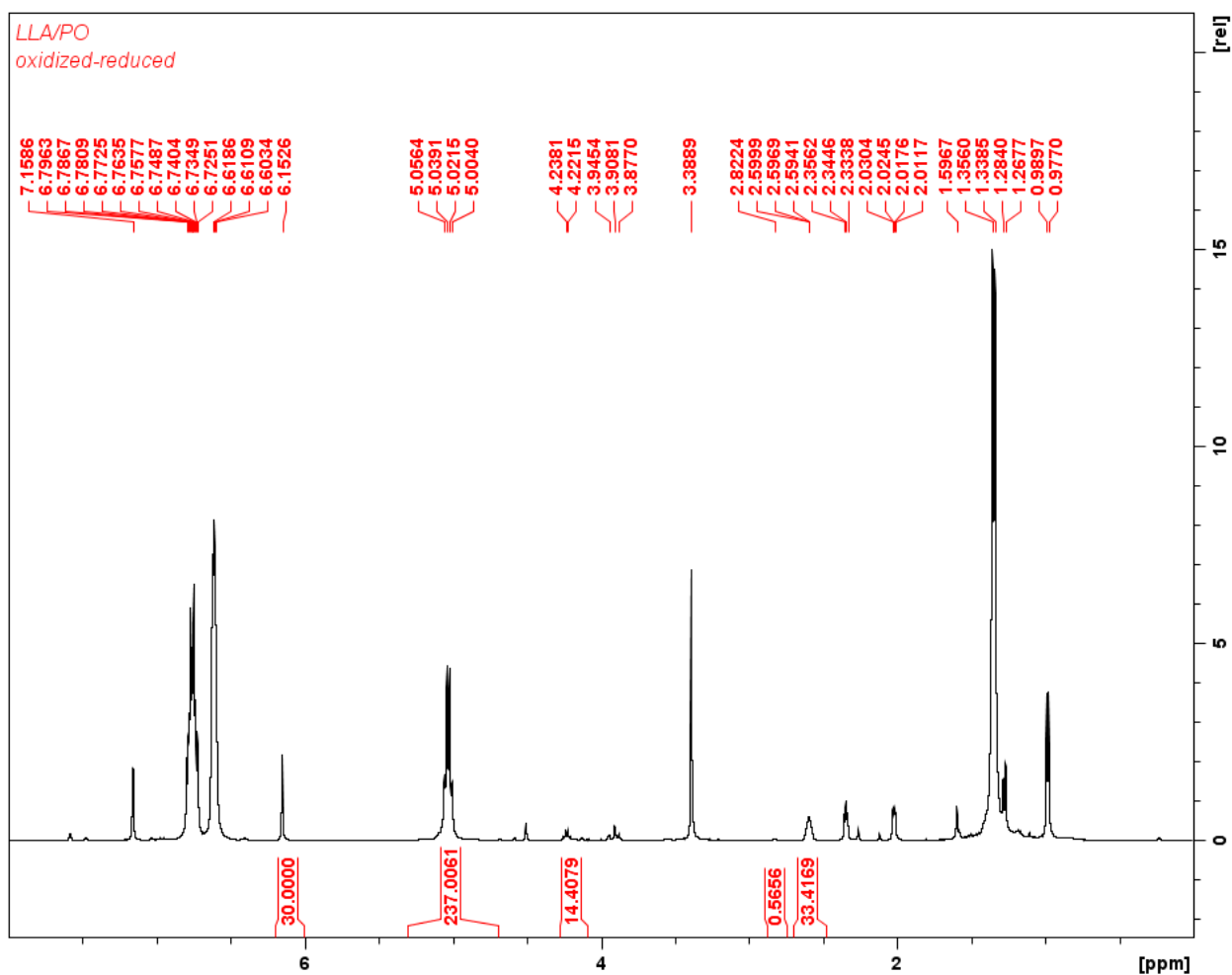


Figure B19. Table 2.2, entry 6. Polymerization of 100 equivalents of L-lactide in the presence of 100 equivalents of propylene oxide with initiator in the oxidized state and subsequently reduced. ^1H NMR (300 MHz, 25 °C, C_6D_6), δ (ppm): 6.76 (CFCH 1,2-difluorobenzene), 6.60 (CFCHCH 1,2-difluorobenzene), 6.15 (s, 3H, PhH TMB), 5.03 (q, 2H, CHCH₃ PLA), 4.23 (q, 2H, CHCH₃ LLA), 3.39 (s, 9H, CH₃ TMB), 2.82 (m, 1H, COCHCH₃ PPO), 2.60 (m, 1H, COCHCH₃ PO), 2.34 (m, 1H, COCH₂ PO), 2.02 (m, 1H, COCH₂ PO), 1.60 (d, 3H, COCHCH₃ PPO), 1.34 (d, 6H, CHCH₃ PLA), 1.27 (d, 6H, CHCH₃ L-lactide), 0.98 (d, 3H, COCHCH₃ PO).

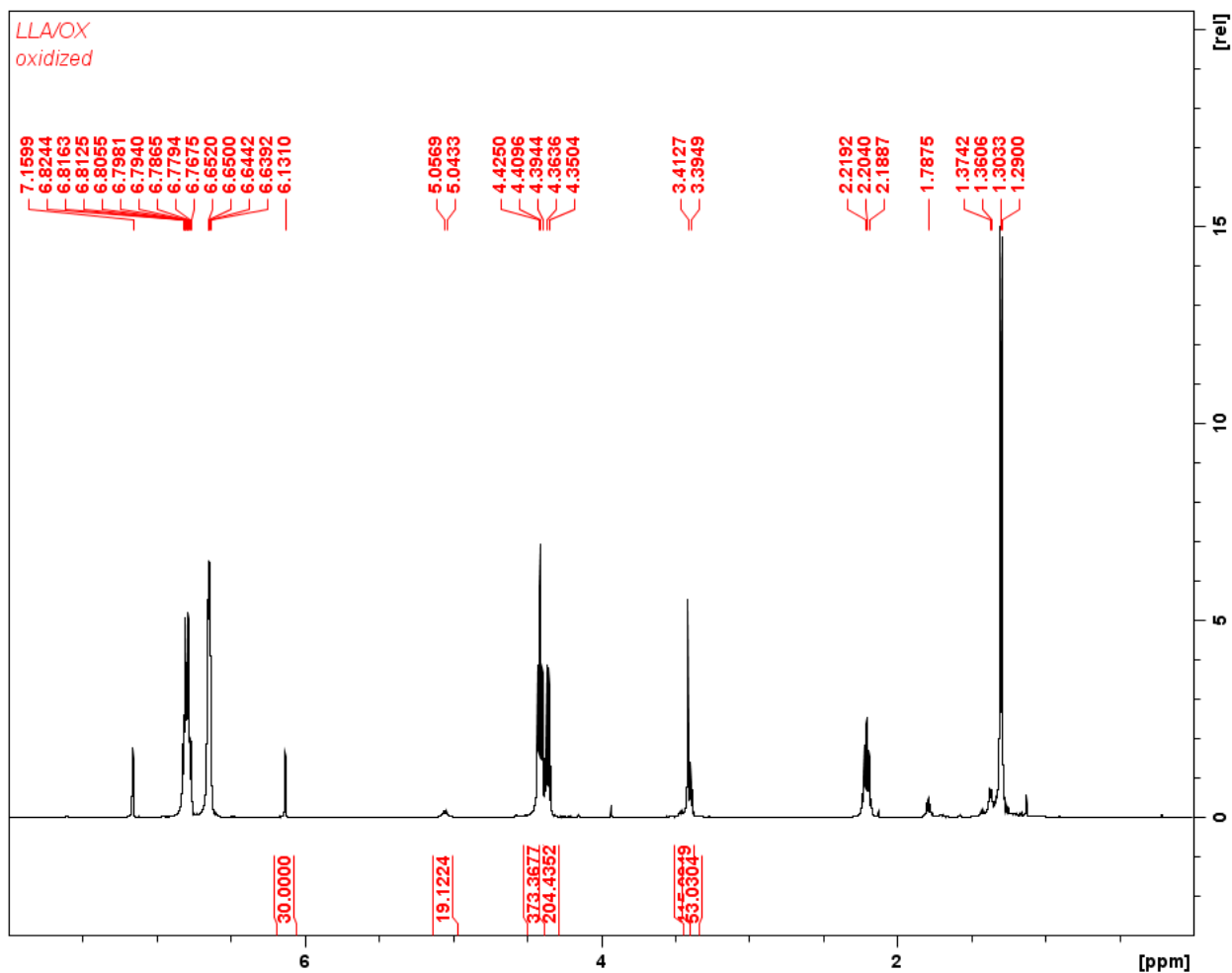


Figure B20. Table 2.2, entry 7. Polymerization of 100 equivalents of L-lactide in the presence of 100 equivalents of oxetane with initiator in the oxidized state. ^1H NMR (300 MHz, 25 °C, C_6D_6), δ (ppm): 6.77 (CFCH 1,2-difluorobenzene), 6.65 (CFCHCH 1,2-difluorobenzene), 6.13 (s, 3H, PhH TMB), 5.04 (q, 2H, CHCH_3 PLA), 4.41 (t, 4H, OCH_2 OX), 4.36 (q, 2H, CHCH_3 LA), 3.40 (s, 9H, CH_3 TMB), 3.39 (t, 4H, OCH_2 POX), 2.20 (m, 2H, OCH_2CH_2 OX), 1.79 (m, 2H, OCH_2CH_2 POX), 1.37 (d, 6H, CHCH_3 PLA), 1.30 (d, 6H, CHCH_3 LA).

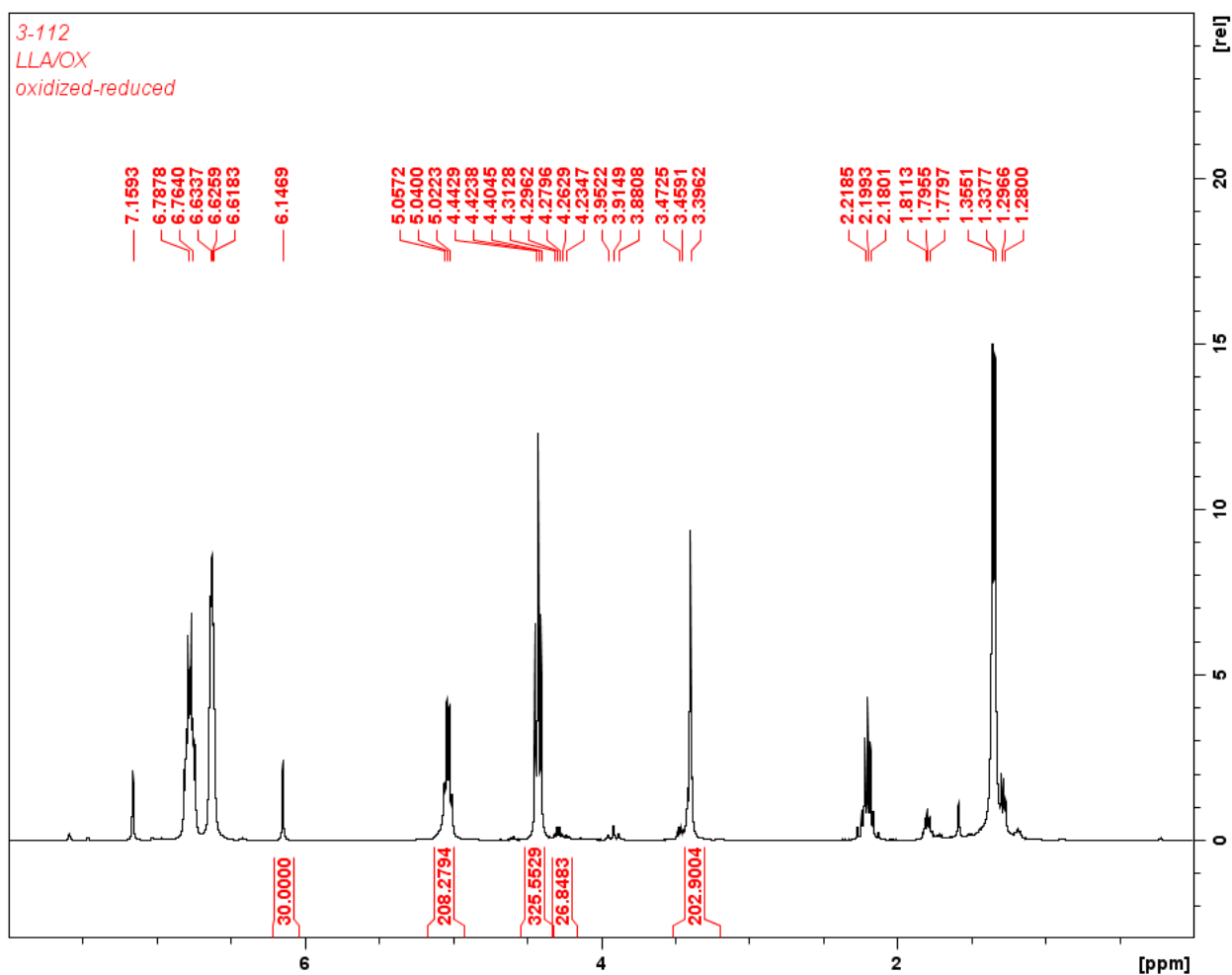


Figure B21. Table 2.2, entry 8. Polymerization of 100 equivalents of L-lactide in the presence of 100 equivalents of oxetane with initiator in the oxidized state and subsequently reduced. ^1H NMR (300 MHz, 25 °C, C_6D_6), δ (ppm): 6.77 (CFCH 1,2-difluorobenzene), 6.62 (CFCHCH 1,2-difluorobenzene), 6.15 (s, 3H, PhH TMB), 5.04 (q, 2H, CHCH₃ PLA), 4.42 (t, 4H, OCH₂ OX), 4.27 (q, 2H, CHCH₃ LA), 3.47 (t, 4H, OCH₂ POX), 3.39 (s, 9H, CH₃ TMB), 2.20 (m, 2H, OCH₂CH₂ OX), 1.79 (m, 2H, OCH₂CH₂ OX), 1.34 (d, 6H, CHCH₃ PLA), 1.29 (d, 6H, CHCH₃ LA).

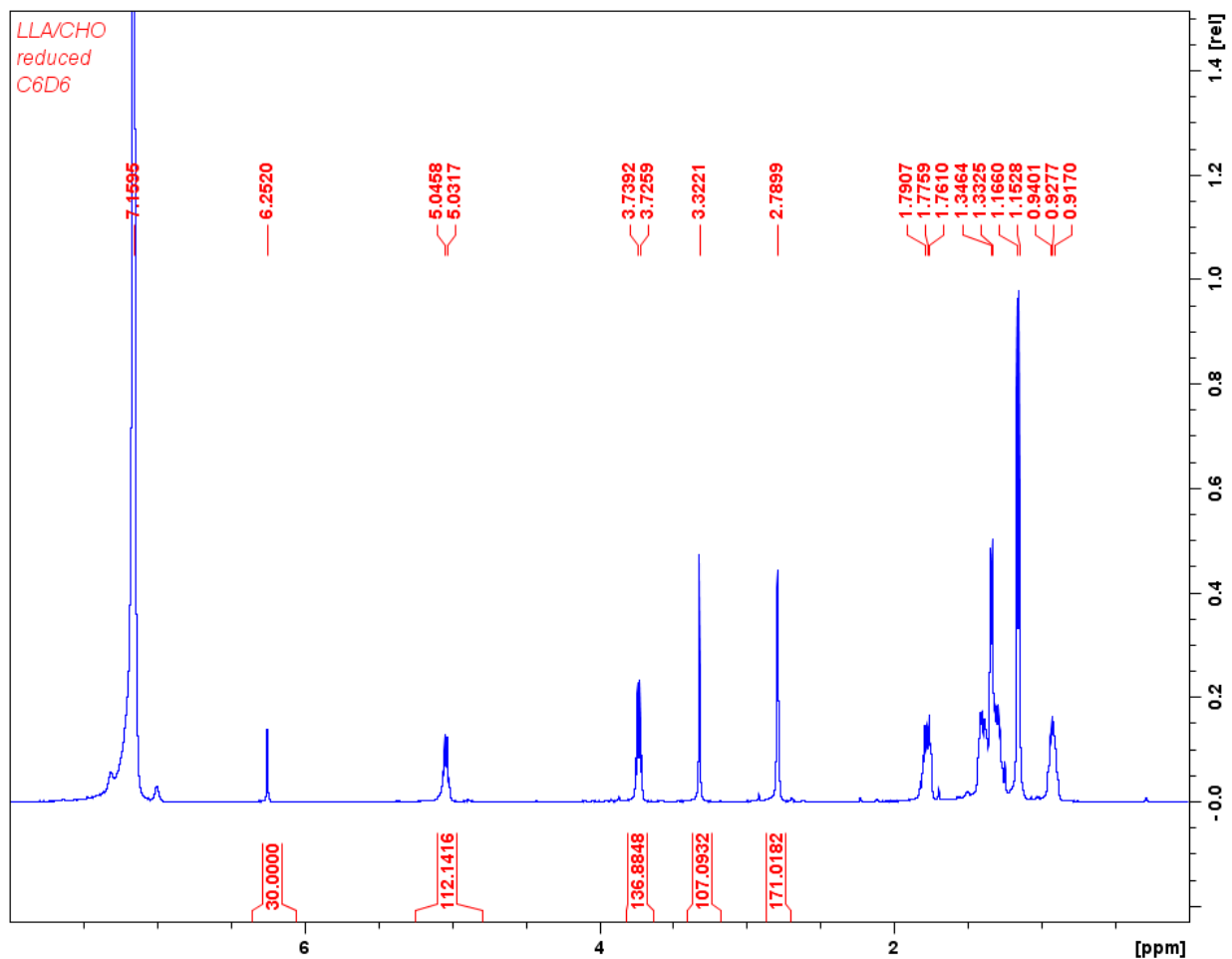


Figure B22. Table 2.2, entry 9. Polymerization of 100 equivalents of L-lactide in the presence of 100 equivalents of cyclohexene oxide with initiator in the reduced state. ^1H NMR (300 MHz, 25 $^\circ\text{C}$, C_6D_6), δ (ppm): 6.25 (s, 3H, PhH TMB), 5.04 (q, 2H, CHCH_3 PLA), 3.73 (q, 2H, CHCH_3 LA), 3.32 (s, 9H, CH_3 TMB), 2.79 (s, 2H, COCH_2 CHO), 1.77 (m, 2H, COCHCH_2 CHO), 1.39 (m, 2H, COCHCH_2 CHO), 1.33 (d, 6H, CHCH_3 PLA), 1.29 (m, 2H, $\text{COCHCH}_2\text{CH}_2$ CHO), 1.15 (d, 6H, CHCH_3 LA), 0.93 (m, 2H, $\text{COCHCH}_2\text{CH}_2$ CHO).

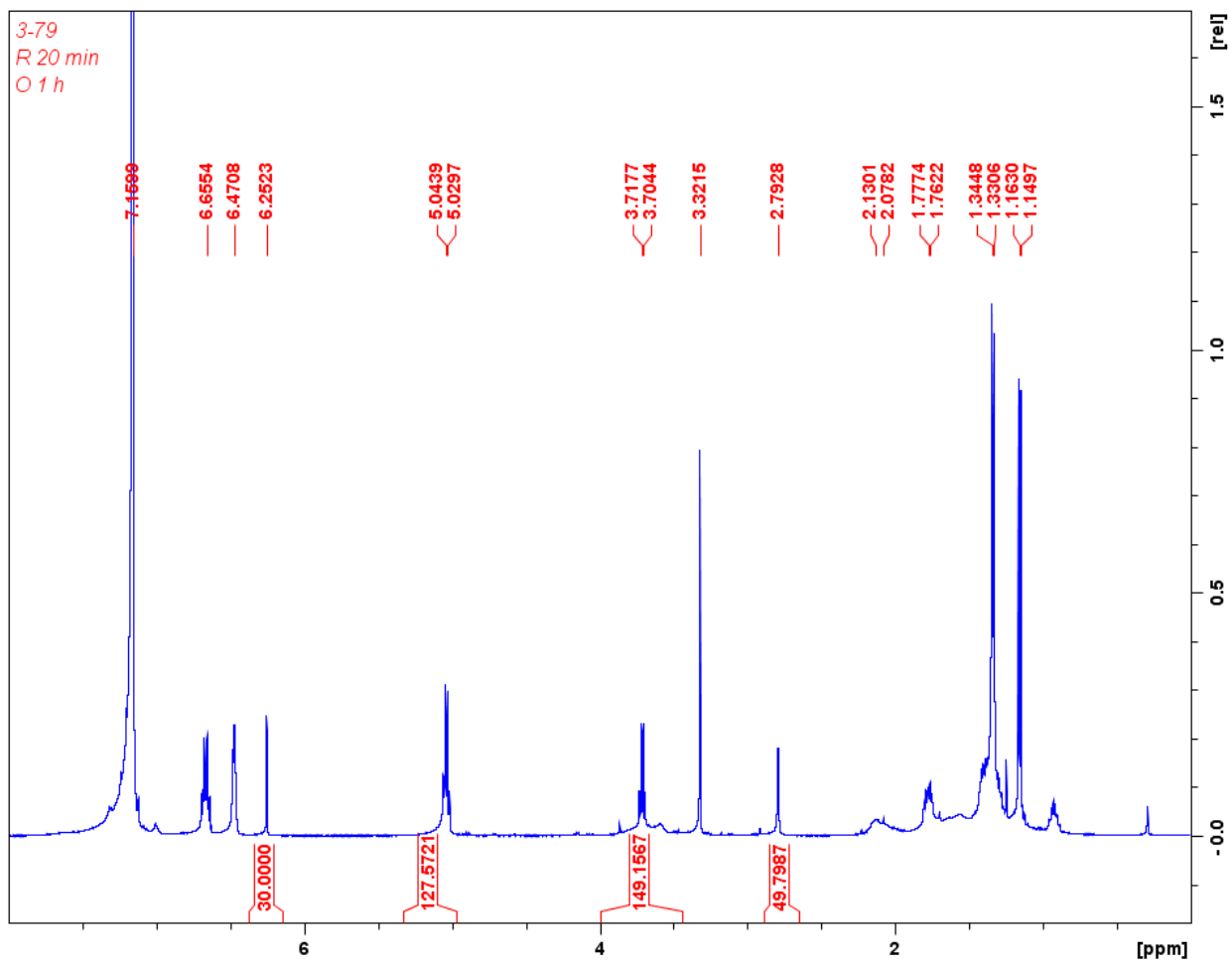


Figure B23. Table 2.2, entry 10. Polymerization of 100 equivalents of L-lactide in the presence of 100 equivalents of cyclohexene oxide with initiator in the reduced state and subsequently oxidized. ^1H NMR (300 MHz, 25 °C, C_6D_6), δ (ppm): 6.65 (CFCH 1,2-difluorobenzene), 6.47 (CFCHCH 1,2-difluorobenzene), 6.25 (s, 3H, PhH TMB), 5.04 (q, 2H, CHCH_3 PLA), 3.71 (q, 2H, CHCH_3 LLA), 3.62 (m, 2H, COCH PCHO), 3.32 (s, 9H, CH_3 TMB), 2.79 (s, 2H, COCH₂ CHO), 2.07 (m, 2H, COCHCH₂ PCHO), 1.77 (m, 2H, COCHCH₂ CHO), 1.33 (d, 6H, CHCH_3 PLA), 1.15 (d, 6H, CHCH_3 LLA).

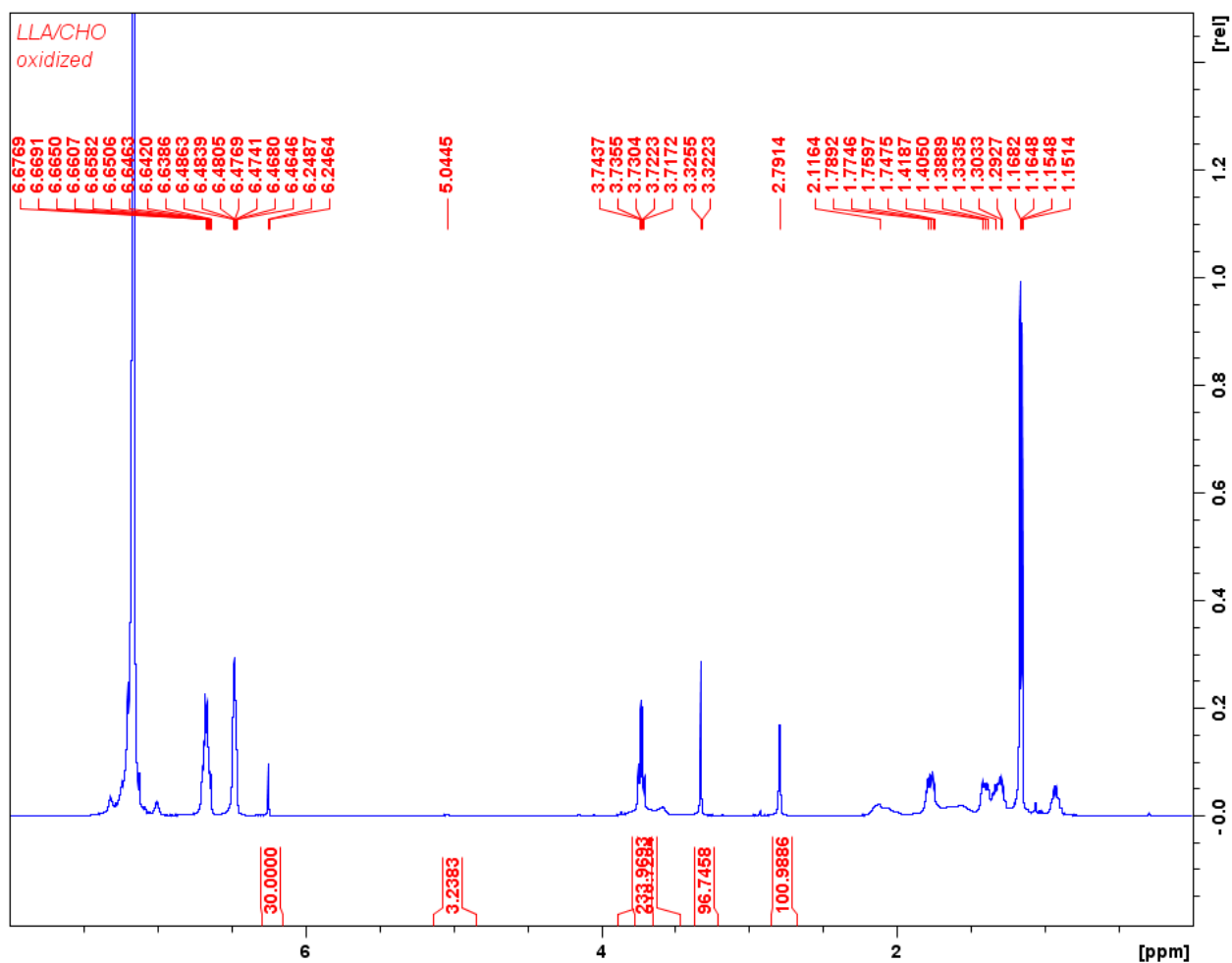


Figure B24. Table 2.2, entry 11. Polymerization of 100 equivalents of L-lactide in the presence of 100 equivalents of cyclohexene oxide with initiator in the oxidized state. ^1H NMR (300 MHz, 25 °C, C_6D_6), δ (ppm): 6.65 (CFCH 1,2-difluorobenzene), 6.47 (CFCHCH 1,2-difluorobenzene), 6.25 (s, 3H, PhH TMB), 5.04 (q, 2H, CHCH₃ PLA), 3.73 (q, 2H, CHCH₃ LLA), 3.62 (m, 2H, COCH PCHO), 3.32 (s, 9H, CH₃ TMB), 2.79 (s, 2H, COCH₂ CHO), 2.11 (m, 2H, COCHCH₂ PCHO), 1.77 (m, 2H, COCHCH₂ CHO), 1.39 (m, 2H, COCHCH₂ CHO), 1.31 (m, 2H, COCHCH₂CH₂ PCHO), 1.29 (m, 2H, COCHCH₂CH₂ CHO), 1.15 (d, 6H, CHCH₃ LLA).

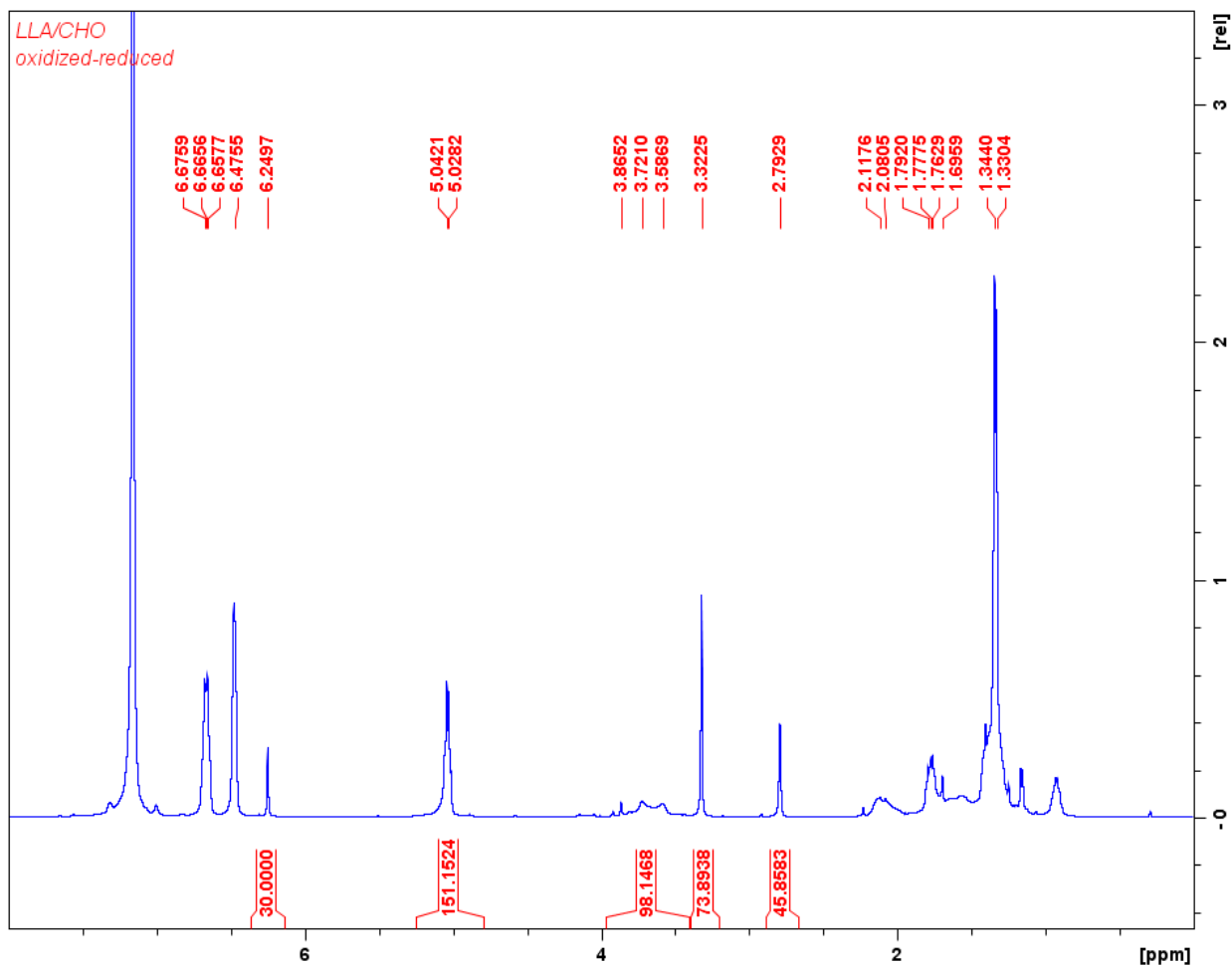


Figure B25. Table 2.2, entry 12. Polymerization of 100 equivalents of L-lactide in the presence of 100 equivalents of cyclohexene oxide with initiator in the oxidized state and subsequently reduced. ^1H NMR (300 MHz, 25 °C, C_6D_6), δ (ppm): 6.66 (CFCH 1,2-difluorobenzene), 6.48 (CFCHCH 1,2-difluorobenzene), 6.25 (s, 3H, PhH TMB), 5.03 (q, 2H, CHCH₃ PLA), 3.65 (m, 2H, COCH PCHO), 3.32 (s, 9H, CH₃ TMB), 2.79 (s, 2H, COCH₂ CHO), 2.08 (m, 2H, COCHCH₂ PCHO), 1.77 (m, 2H, COCHCH₂ CHO), 1.70 (m, 2H, COCHCH₂ CHO), 1.33 (d, 6H, CHCH₃ PLA), 1.31 (m, 2H, COCHCH₂CH₂ PCHO).

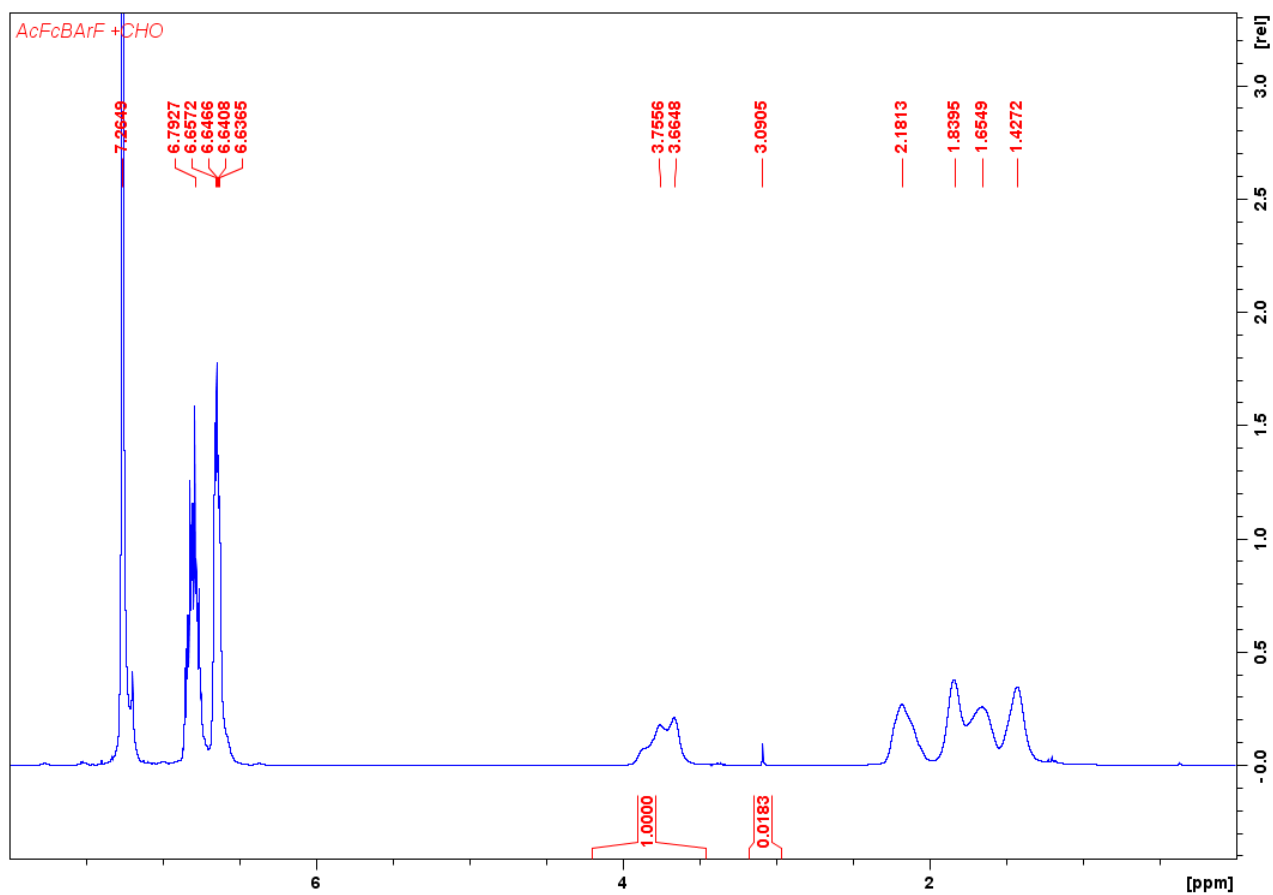


Figure B26. Table 2.3, entry 1. Polymerization of 100 equivalents of cyclohexene oxide by $^{Ac}FcBAR^F$. 1H NMR (300 MHz, 25 °C, $CDCl_3$), δ (ppm): 6.79 (CFCH 1,2-difluorobenzene), 6.65 (CFCHCH 1,2-difluorobenzene), 3.70 (m, 2H, COCH PCHO), 3.09 (s, 2H, COCH₂ CHO), 2.18 (m, 2H, COCHCH₂ PCHO), 1.84 (m, 2H, COCHCH₂ PCHO), 1.65 (m, 2H, COCHCH₂CH₂ PCHO), 1.43 (m, 2H, COCHCH₂CH₂ PCHO).

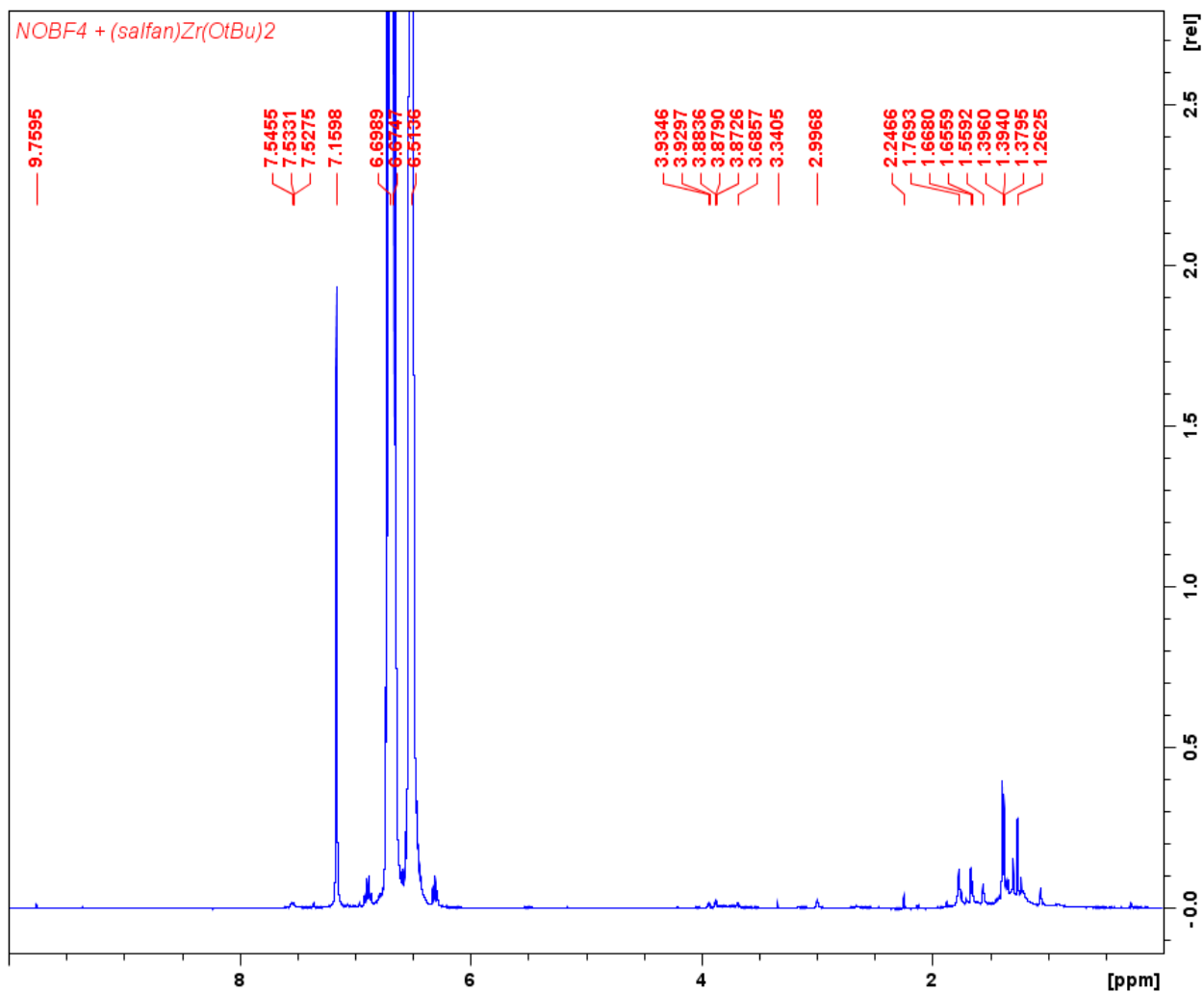


Figure B27. Table 2.3, entry 2. Oxidation of (salfan)Zr(O^tBu)₂ by NOBF₄. ¹H NMR (300 MHz, 25 °C, C₆D₆), δ (ppm): 9.76 (s, 2H, OH), 7.53 (m, 2H, PhH), 6.68 (CFCH 1,2-difluorobenzene), 6.51 (CFCHCH 1,2-difluorobenzene), 3.93 (m, 2H, CpH), 3.88 (m, 2H, CpH), 3.68 (m, 4H, CpH), 3.34 (s, 4H, NCH₂), 3.00 (s, 6H, NCH₃), 2.25 (s, 6H, NCH₃), 1.77 (s, 18H, C(CH₃)₃), 1.66 (s, 18H, C(CH₃)₃), 1.56 (s, 18H, C(CH₃)₃), 1.39 (s, 18H, C(CH₃)₃), 1.38 (s, 18H, C(CH₃)₃), 1.26 (s, 18H, C(CH₃)₃).

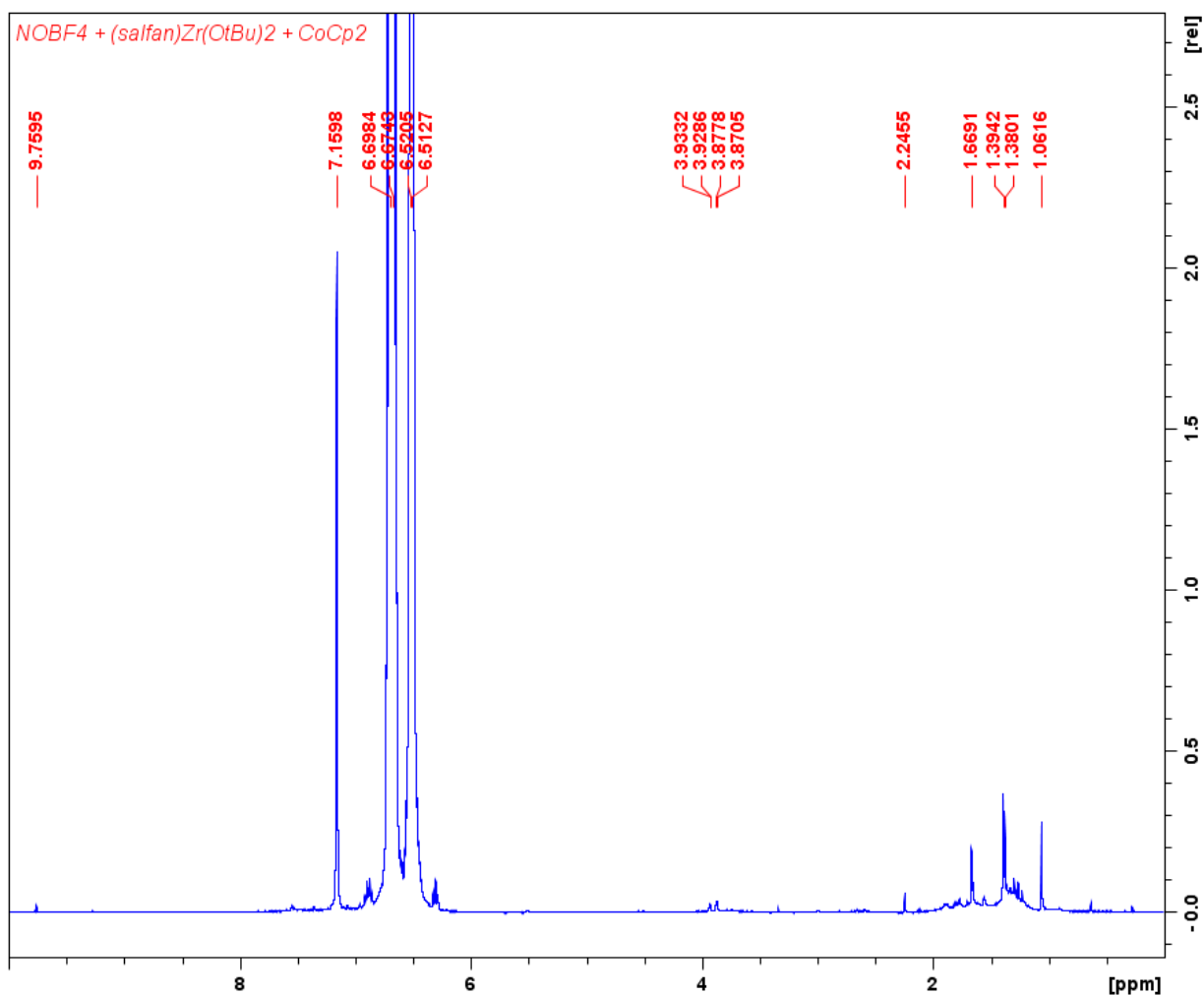


Figure B28. Table 2.3, entry 2. Oxidation of (salfan)Zr(O^tBu)₂ by NOBF₄ and subsequent reduction by CoCp₂. ¹H NMR (300 MHz, 25 °C, C₆D₆), δ (ppm): 9.76 (s, 2H, OH), 7.53 (m, 2H, PhH), 6.68 (CFCH 1,2-difluorobenzene), 6.51 (CFCHCH 1,2-difluorobenzene), 3.93 (m, 2H, CpH), 3.88 (m, 2H, CpH), 2.25 (s, 6H, NCH₃), 1.66 (s, 18H, C(CH₃)₃), 1.39 (s, 18H, C(CH₃)₃), 1.38 (s, 18H, C(CH₃)₃), 1.06 (s, 18H, C(CH₃)₃).

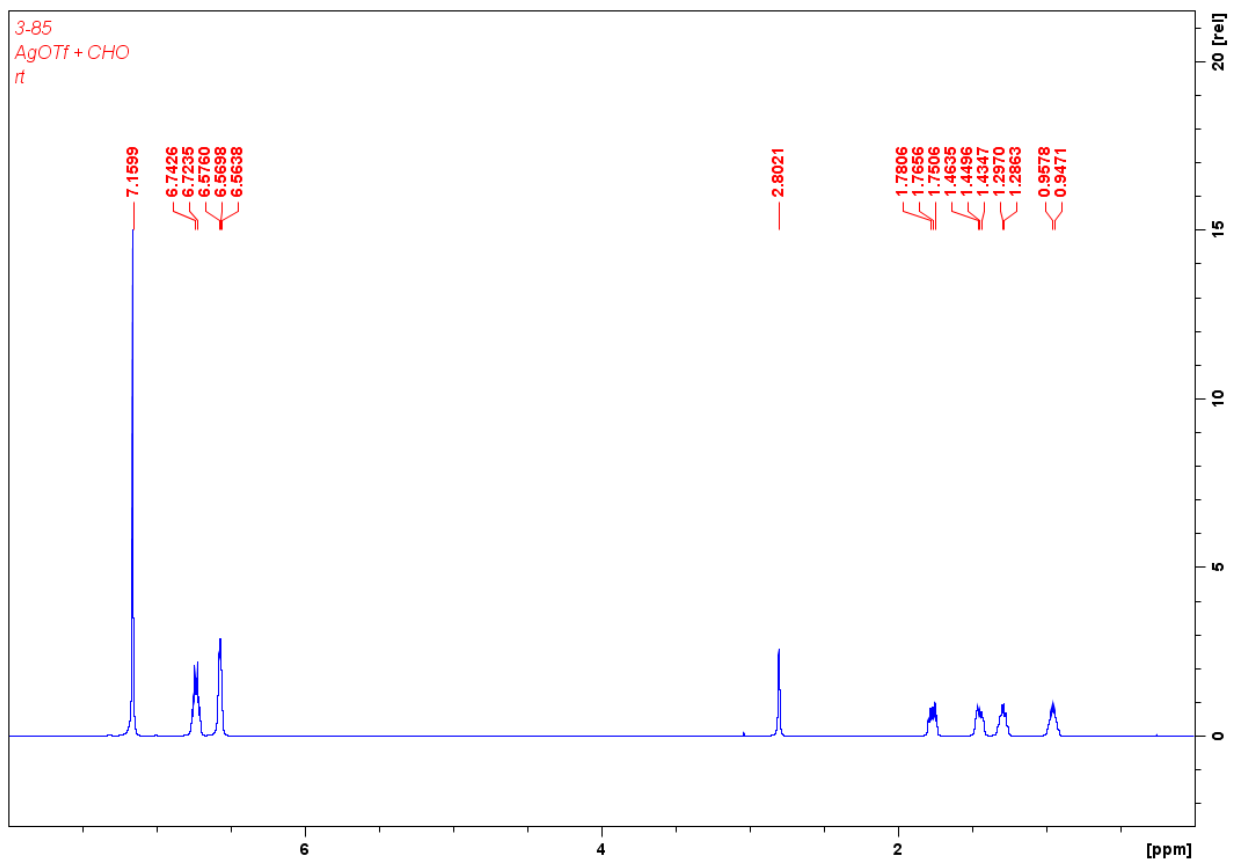


Figure B29. Table 2.3, entry 3. Polymerization of 100 equivalents of cyclohexene oxide by AgOTf at room temperature. ^1H NMR (300 MHz, 25 °C, C_6D_6), δ (ppm): 6.73 (CFCH 1,2-difluorobenzene), 6.55 (CFCHCH 1,2-difluorobenzene), 2.80 (s, 2H, COCH₂ CHO), 1.77 (m, 2H, COCHCH₂ CHO), 1.48 (m, 2H, COCHCH₂ CHO), 1.29 (m, 2H, COCHCH₂CH₂ CHO), 0.93 (m, 2H, COCHCH₂CH₂ CHO).

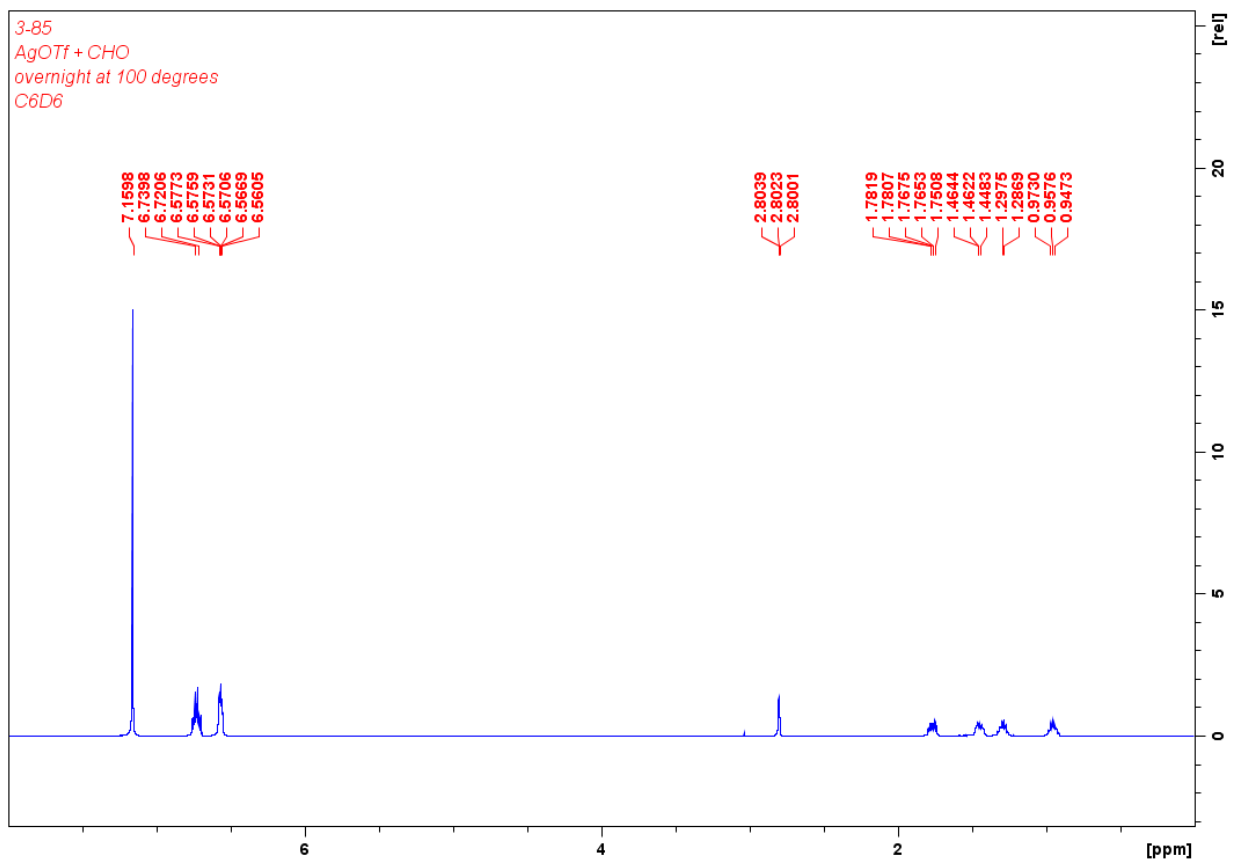


Figure B30. Table 2.3, entry 3. Polymerization of 100 equivalents of cyclohexene oxide by AgOTf at 100 °C overnight. ^1H NMR (300 MHz, 25 °C, C_6D_6), δ (ppm): 6.72 (CFCH 1,2-difluorobenzene), 6.57 (CFCHCH 1,2-difluorobenzene), 2.80 (s, 2H, COCH₂ CHO), 1.77 (m, 2H, COCHCH₂ CHO), 1.48 (m, 2H, COCHCH₂ CHO), 1.29 (m, 2H, COCHCH₂CH₂ CHO), 0.94 (m, 2H, COCHCH₂CH₂ CHO).

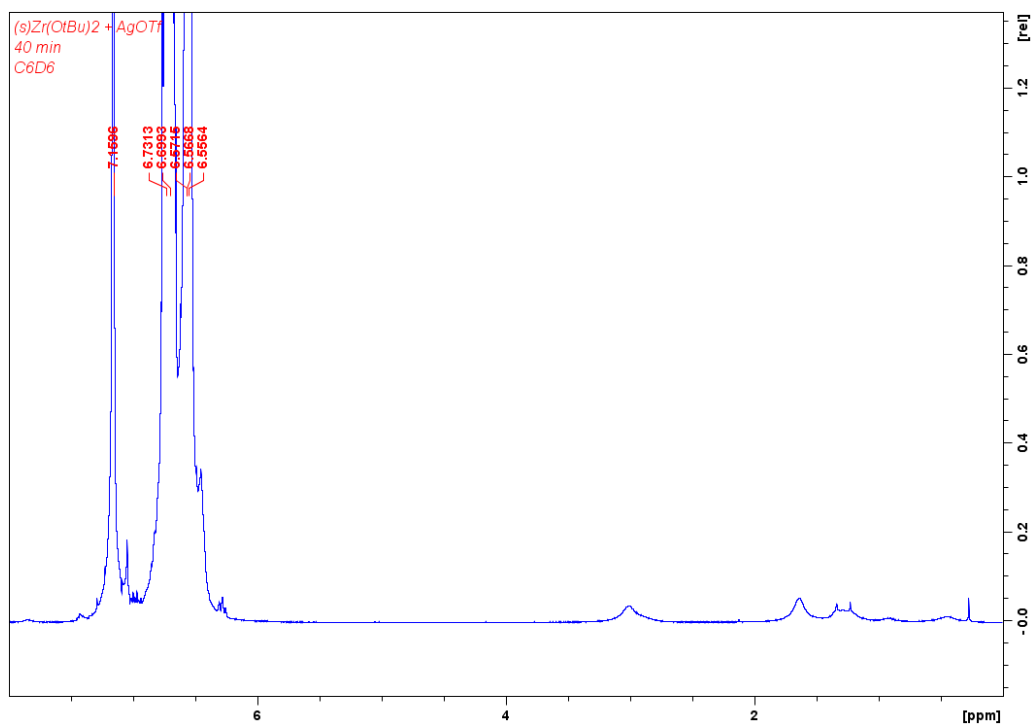


Figure B31. Table 2.3, entry 3. ^1H NMR (300 MHz, 25 °C, C_6D_6) spectrum of the oxidation of $(\text{salfan})\text{Zr}(\text{O}^t\text{Bu})_2$ by AgOTf .

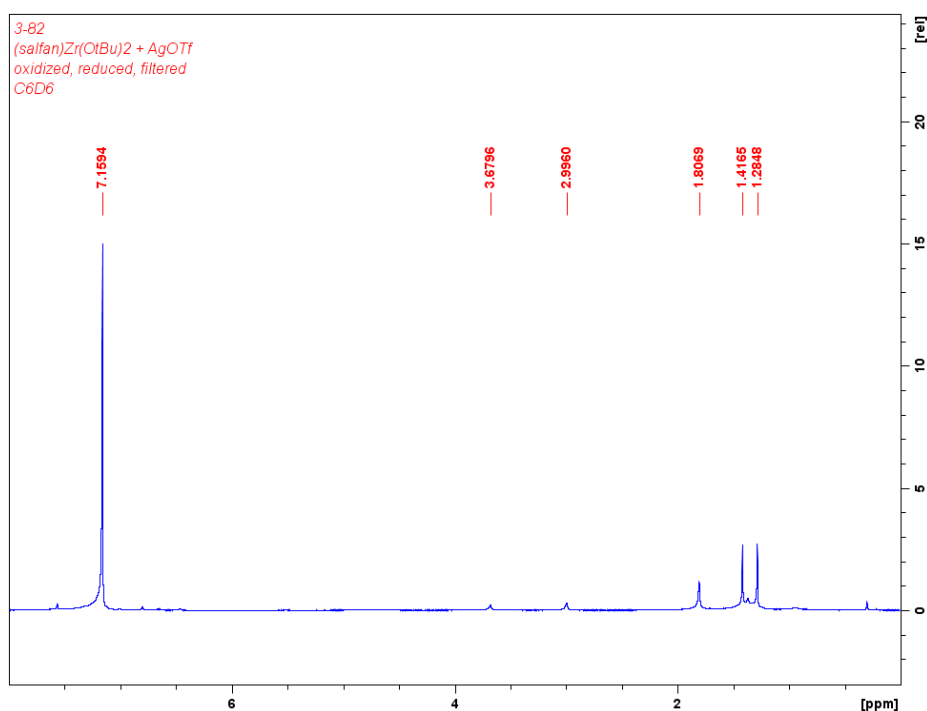


Figure B32. Table 2.3, entry 3. Oxidation of $(\text{salfan})\text{Zr}(\text{O}^t\text{Bu})_2$ by AgOTf and subsequent reduction by CoCp_2 . ^1H NMR (300 MHz, 25 °C, C_6D_6), δ (ppm): 3.67 (s, 4H, NCH_2), 2.99 (s, 6H, NCH_3), 1.80 (s, 18H, $\text{C}(\text{CH}_3)_3$), 1.41 (s, 18H, $\text{C}(\text{CH}_3)_3$), 1.28 (s, 18H, $\text{C}(\text{CH}_3)_3$).

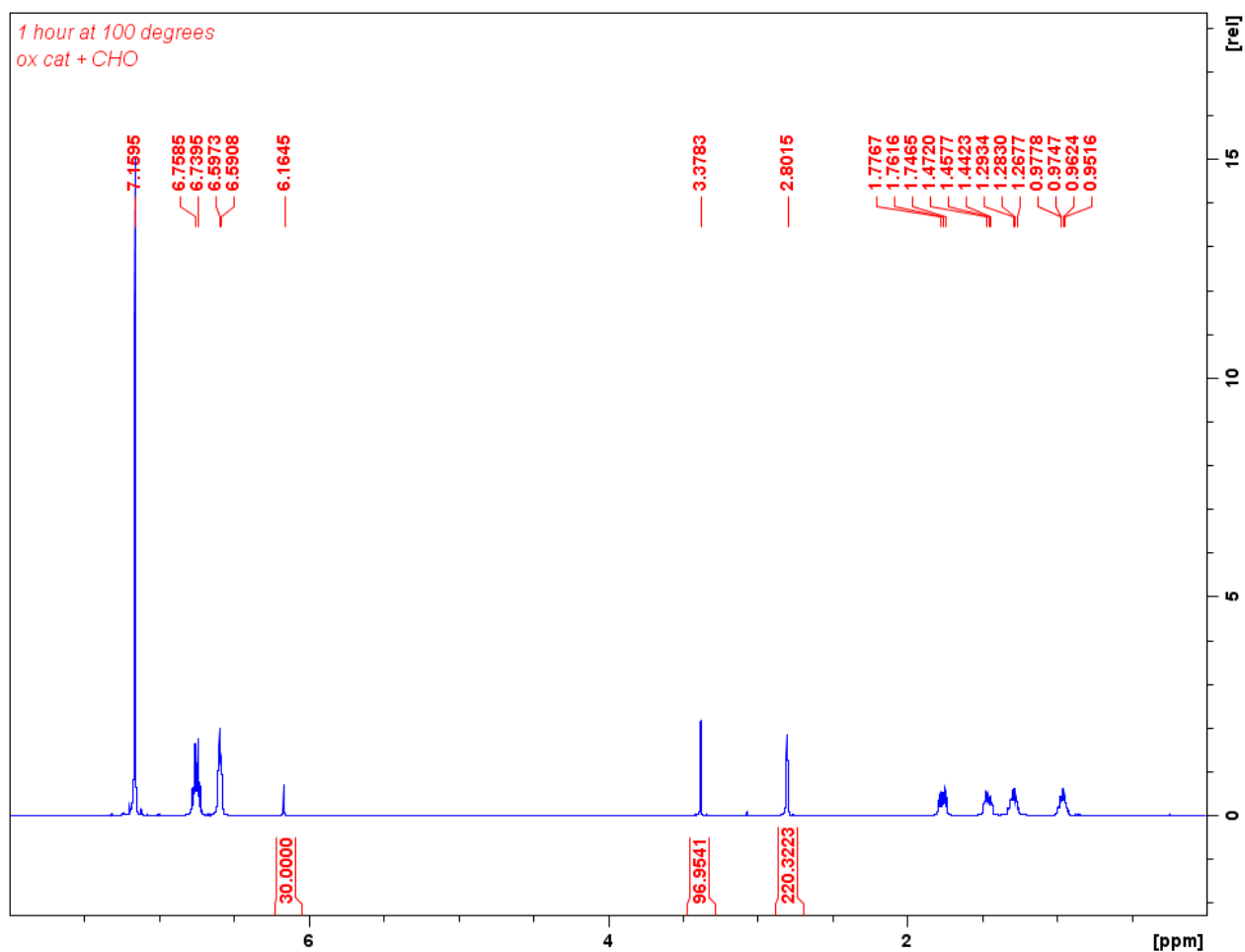


Figure B33. Table 2.3, entry 3. Polymerization of 100 equivalents of cyclohexene oxide by *in situ* generated [(salfan)Zr(O^tBu)₂][OTf] using AgOTf. ¹H NMR (300 MHz, 25 °C, C₆D₆), δ (ppm): 6.74 (CFCH 1,2-difluorobenzene), 6.59 (CFCHCH 1,2-difluorobenzene), 6.16 (s, 3H, PhH TMB), 3.38 (s, 9H, CH₃ TMB), 2.80 (s, 2H, COCH₂ CHO), 1.77 (m, 2H, COCHCH₂ CHO), 1.48 (m, 2H, COCHCH₂ CHO), 1.28 (m, 2H, COCHCH₂CH₂ CHO), 0.93 (m, 2H, COCHCH₂CH₂ CHO).

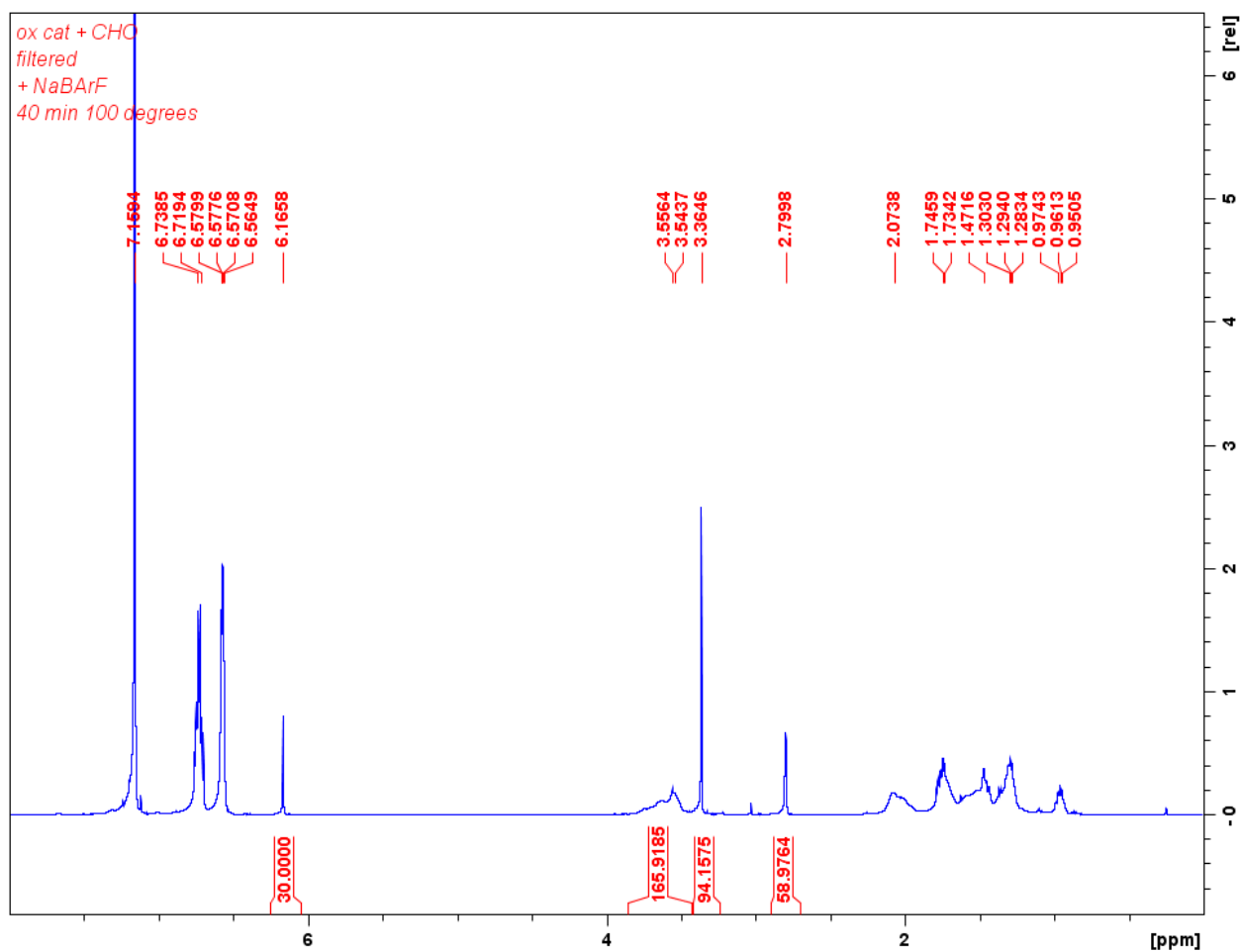


Figure B34. Table 2.3, entry 3. Polymerization of 100 equivalents of cyclohexene oxide by *in situ* generated [(salfan)Zr(O^tBu)₂][OTf] using AgOTf in the presence of Na[BAR^F₄]. ¹H NMR (300 MHz, 25 °C, C₆D₆), δ (ppm): 6.71 (CFCH 1,2-difluorobenzene), 6.58 (CFCHCH 1,2-difluorobenzene), 6.17 (s, 3H, PhH TMB), 3.55 (m, 2H, COCH PCHO), 3.36 (s, 9H, CH₃ TMB), 2.80 (s, 2H, COCH₂ CHO), 2.07 (m, 2H, COCHCH₂ PCHO), 1.74 (m, 2H, COCHCH₂ CHO), 1.47 (m, 2H, COCHCH₂CH₂ CHO), 1.30 (m, 2H, COCHCH₂CH₂ CHO), 0.93 (m, 2H, COCHCH₂CH₂ CHO).

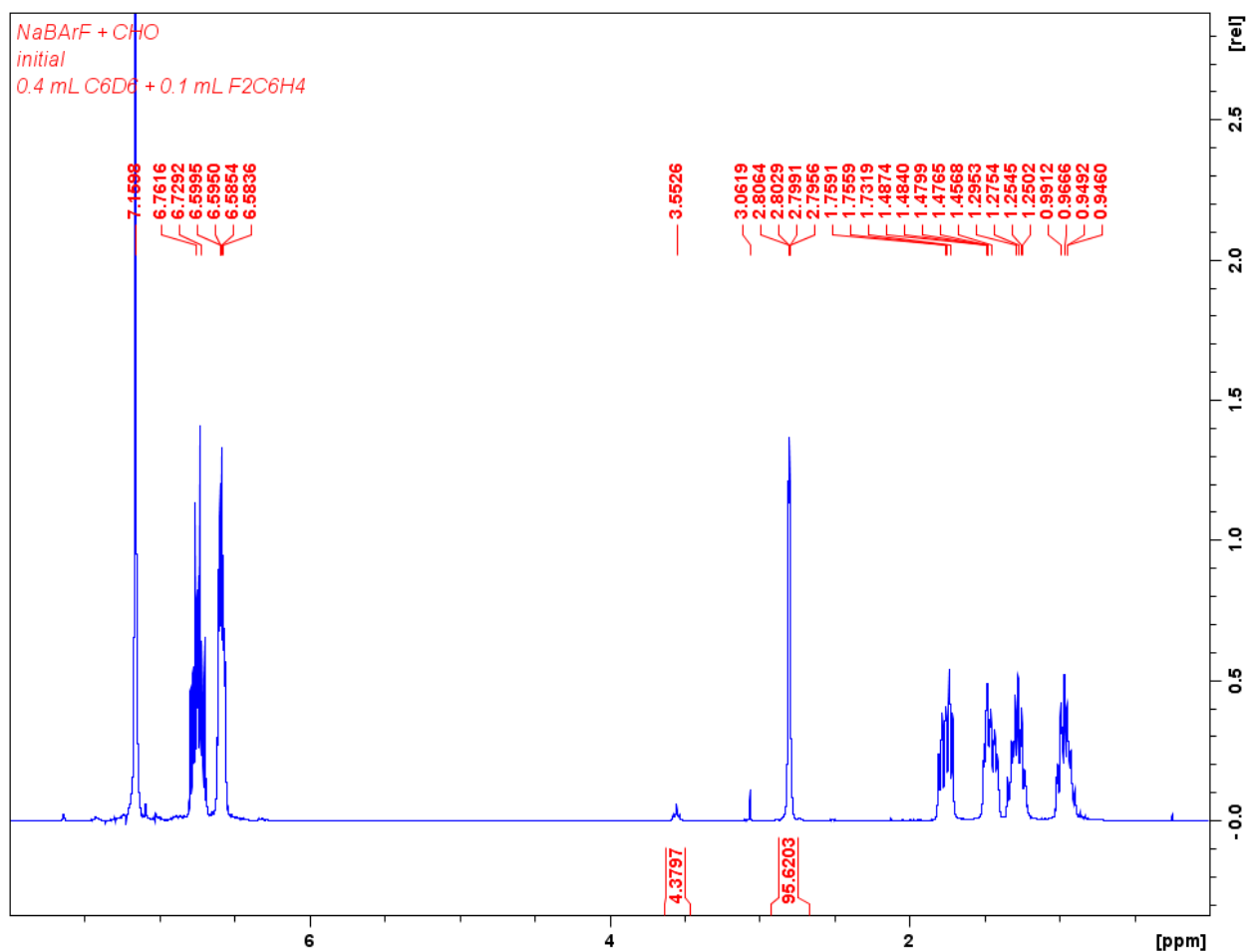


Figure B35. Table 2.3, entry 4. Polymerization of 100 equivalents of cyclohexene oxide by Na[BARF₄] at ambient temperature. ¹H NMR (300 MHz, 25 °C, C₆D₆), δ (ppm): 6.73 (CFCH 1,2-difluorobenzene), 6.59 (CFCHCH 1,2-difluorobenzene), 3.55 (m, 2H, COCH PCHO), 2.80 (s, 2H, COCH₂ CHO), 1.75 (m, 2H, COCHCH₂ CHO), 1.48 (m, 2H, COCHCH₂ CHO), 1.28 (m, 2H, COCHCH₂CH₂ CHO), 0.95 (m, 2H, COCHCH₂CH₂ CHO).

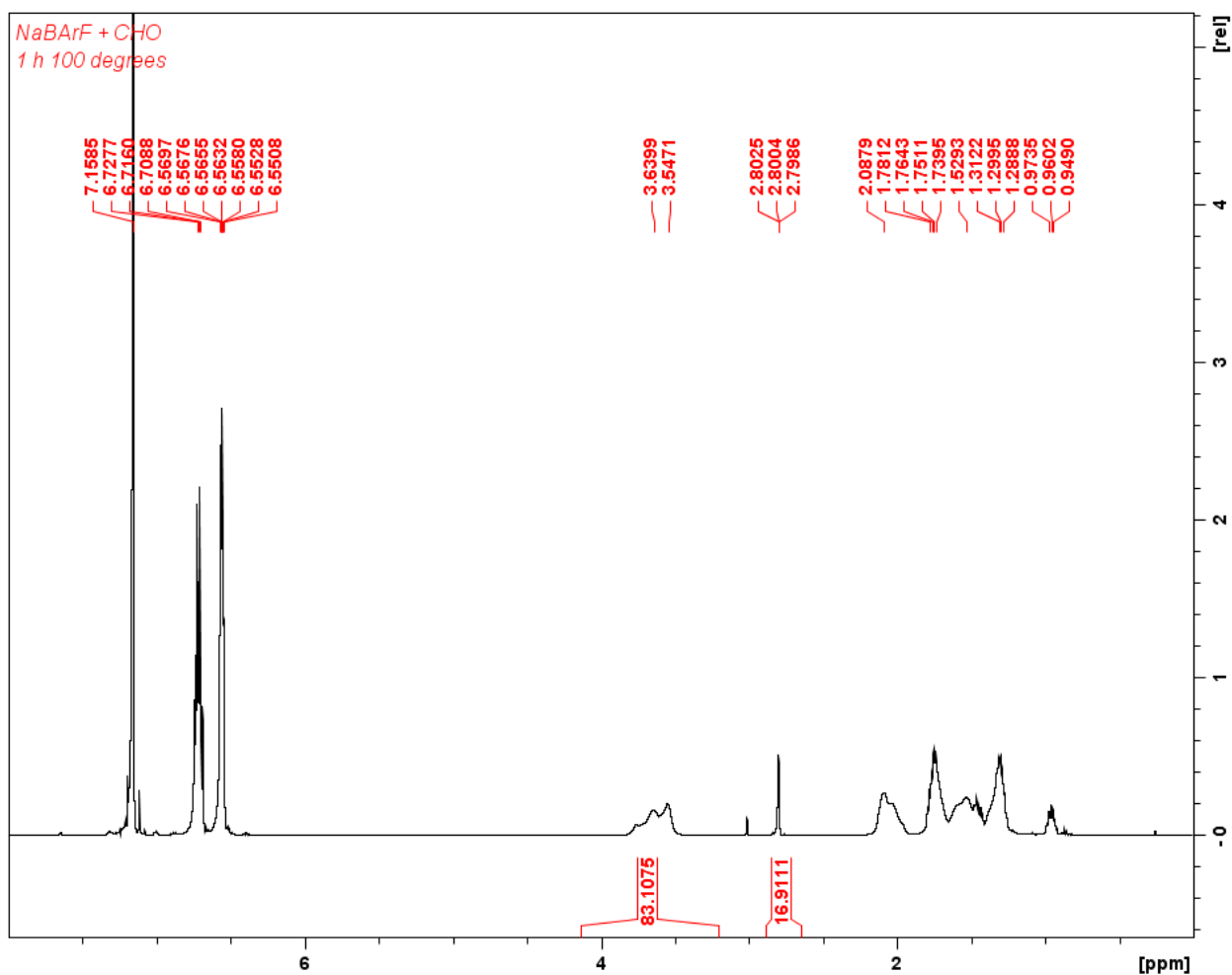


Figure B36. Table 2.3, entry 4. Polymerization of 100 equivalents of cyclohexene oxide by Na[BAR₄^F] after 1 h at 100 °C. ¹H NMR (300 MHz, 25 °C, C₆D₆), δ (ppm): 6.71 (CFCH 1,2-difluorobenzene), 6.55 (CFCHCH 1,2-difluorobenzene), 3.56 (m, 2H, COCH PCHO), 2.80 (s, 2H, COCH₂ CHO), 2.08 (m, 2H, COCHCH₂ PCHO), 1.74 (m, 2H, COCHCH₂ PCHO), 1.53 (m, 2H, COCHCH₂ CHO), 1.47 (m, 2H, COCHCH₂ CHO), 1.30 (m, 2H, COCHCH₂CH₂ PCHO), 0.96 (m, 2H, COCHCH₂CH₂ PCHO).

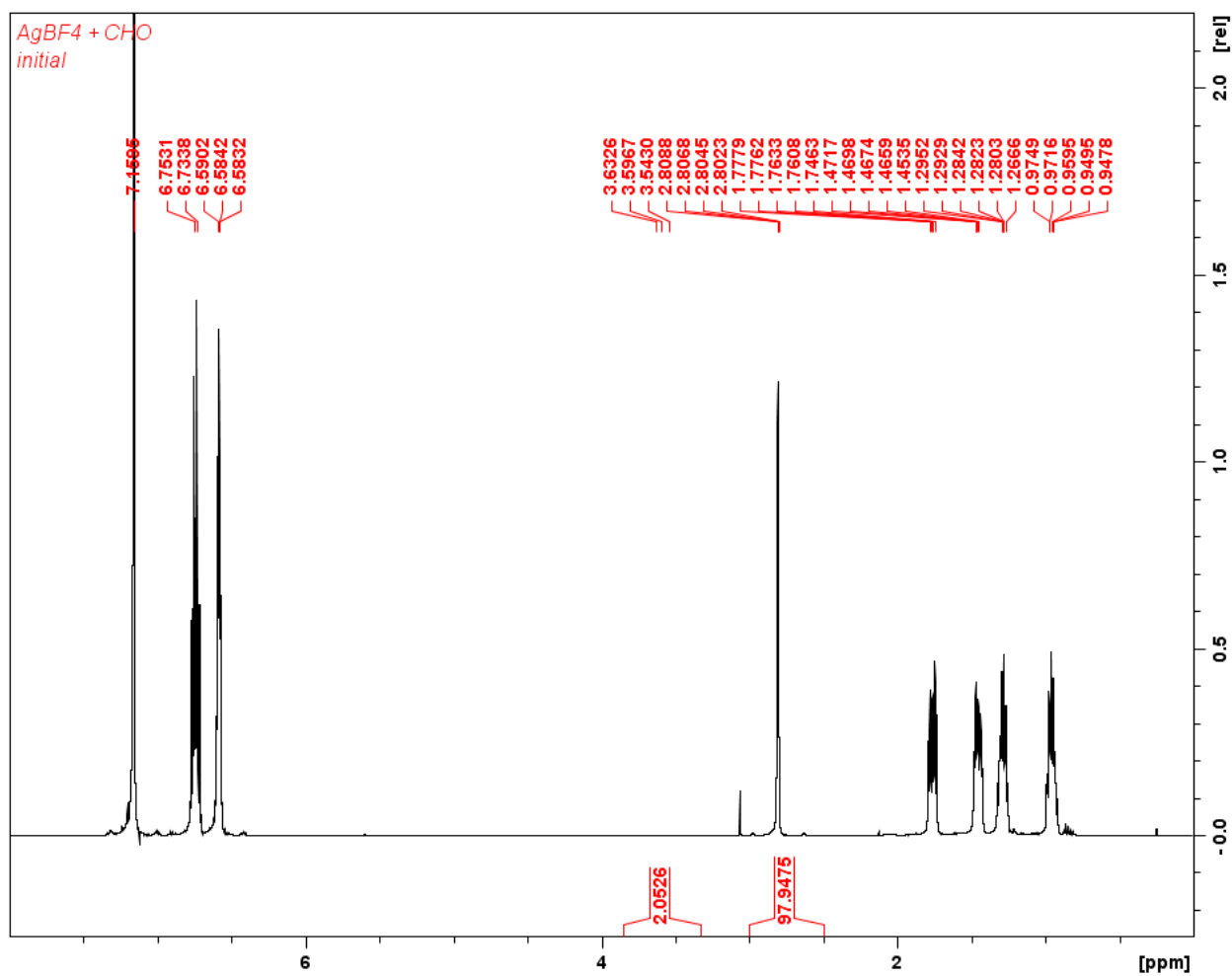


Figure B37. Table 2.3, entry 5. Polymerization of 100 equivalents of cyclohexene oxide by AgBF₄ at ambient temperature. ¹H NMR (300 MHz, 25 °C, C₆D₆), δ (ppm): 6.74 (CFCH 1,2-difluorobenzene), 6.58 (CFCHCH 1,2-difluorobenzene), 3.60 (m, 2H, COCH PCHO), 2.81 (s, 2H, COCH₂ CHO), 1.77 (m, 2H, COCHCH₂ CHO), 1.48 (m, 2H, COCHCH₂ CHO), 1.28 (m, 2H, COCHCH₂CH₂ CHO), 0.95 (m, 2H, COCHCH₂CH₂ CHO).

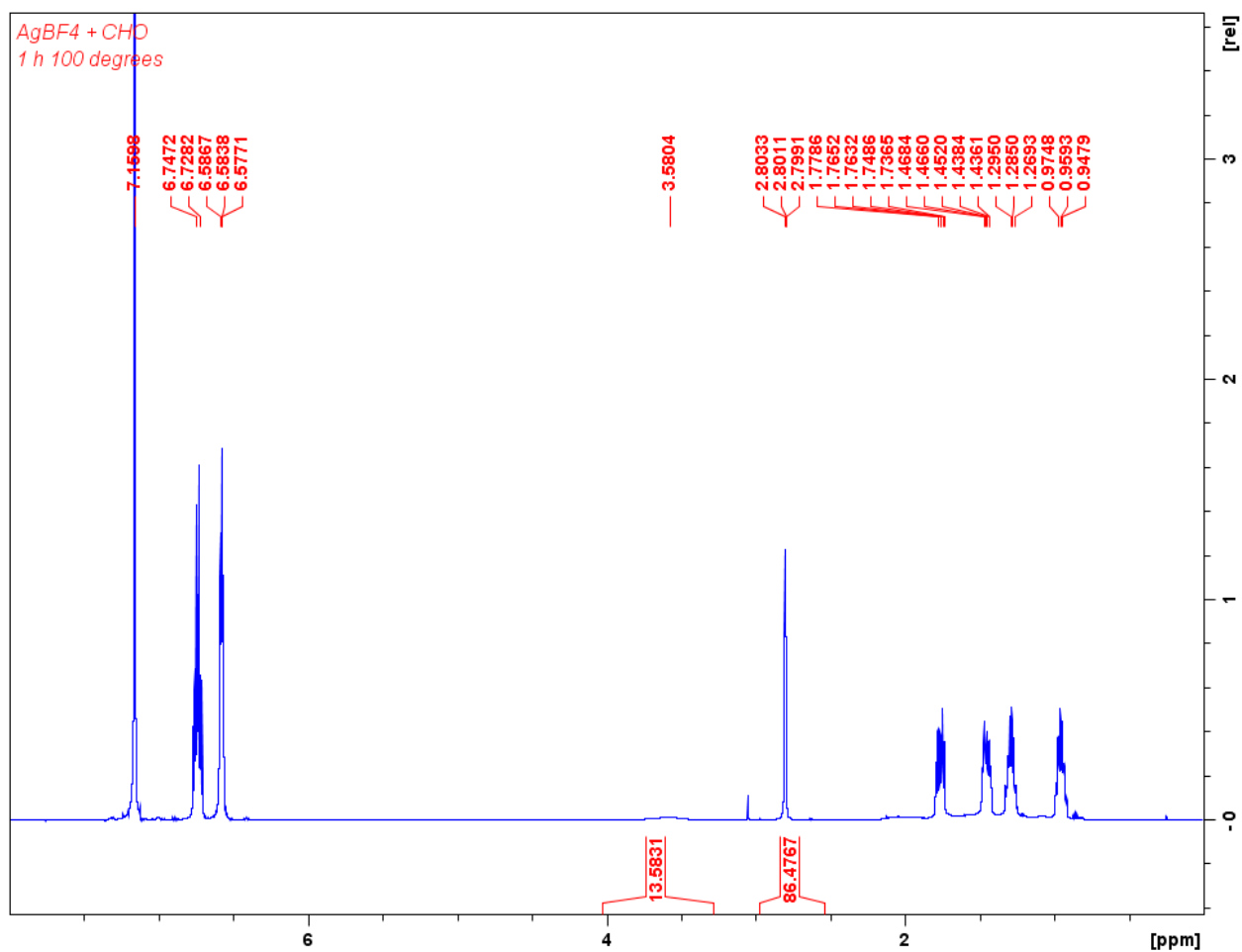


Figure B38. Table 2.3, entry 5. Polymerization of 100 equivalents of cyclohexene oxide by AgBF₄ after 1 h at 100 °C. ¹H NMR (300 MHz, 25 °C, C₆D₆), δ (ppm): 6.73 (CFCH 1,2-difluorobenzene), 6.58 (CFCHCH 1,2-difluorobenzene), 3.58 (m, 2H, COCH PCHO), 2.80 (s, 2H, COCH₂ CHO), 1.77 (m, 2H, COCHCH₂ PCHO), 1.47 (m, 2H, COCHCH₂ CHO), 1.29 (m, 2H, COCHCH₂CH₂ CHO), 0.95 (m, 2H, COCHCH₂CH₂ CHO).

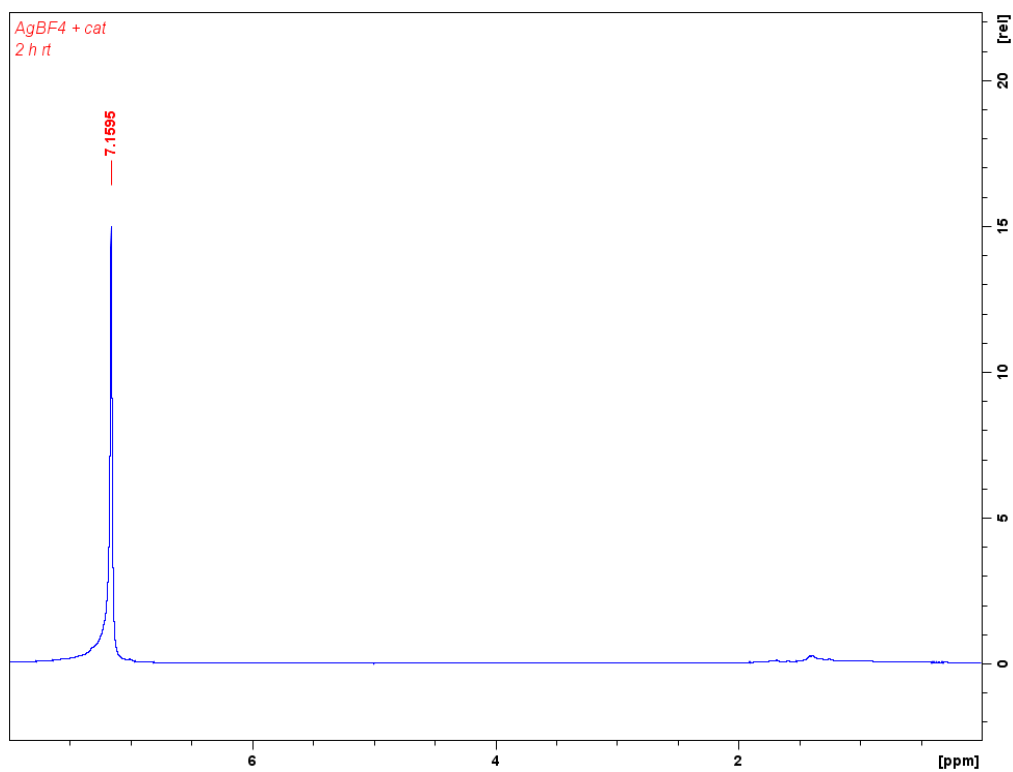


Figure B39. Table 2.3, entry 5. ¹H NMR (300 MHz, 25 °C, C₆D₆) spectrum of the oxidation of (salfan)Zr(O'Bu)₂ by AgBF₄.

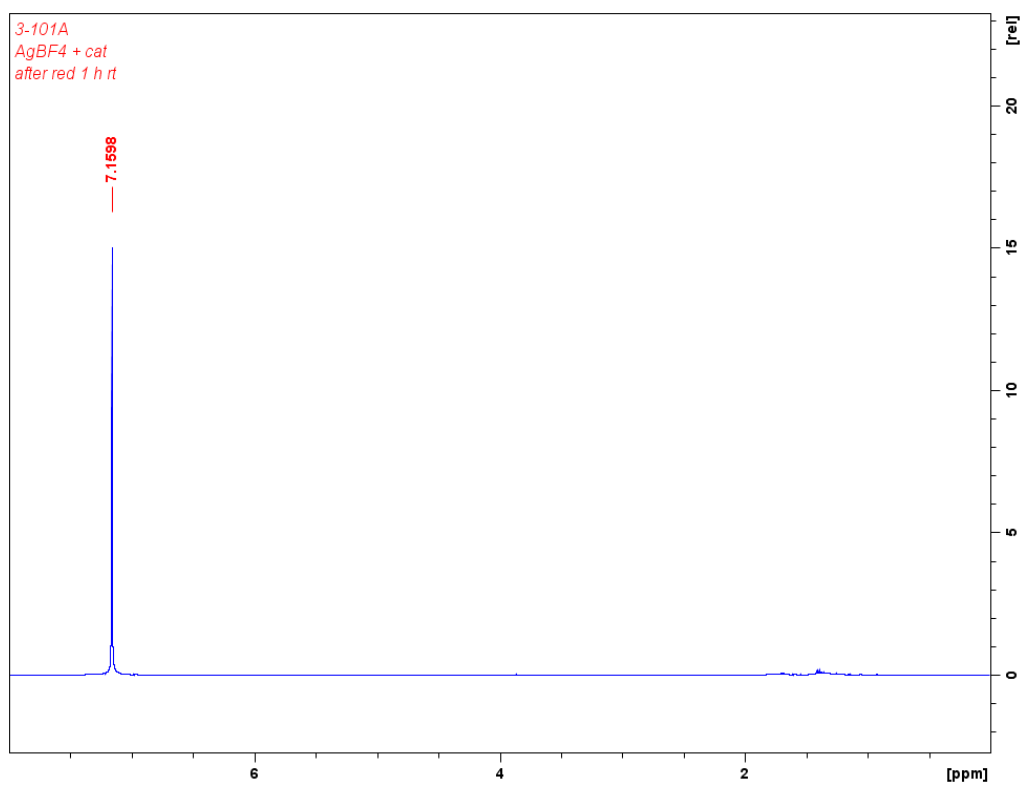


Figure B40. Table 2.3, entry 5. ¹H NMR (300 MHz, 25 °C, C₆D₆) spectrum of the oxidation of (salfan)Zr(O'Bu)₂ by AgBF₄ and subsequent reduction by CoCp₂.

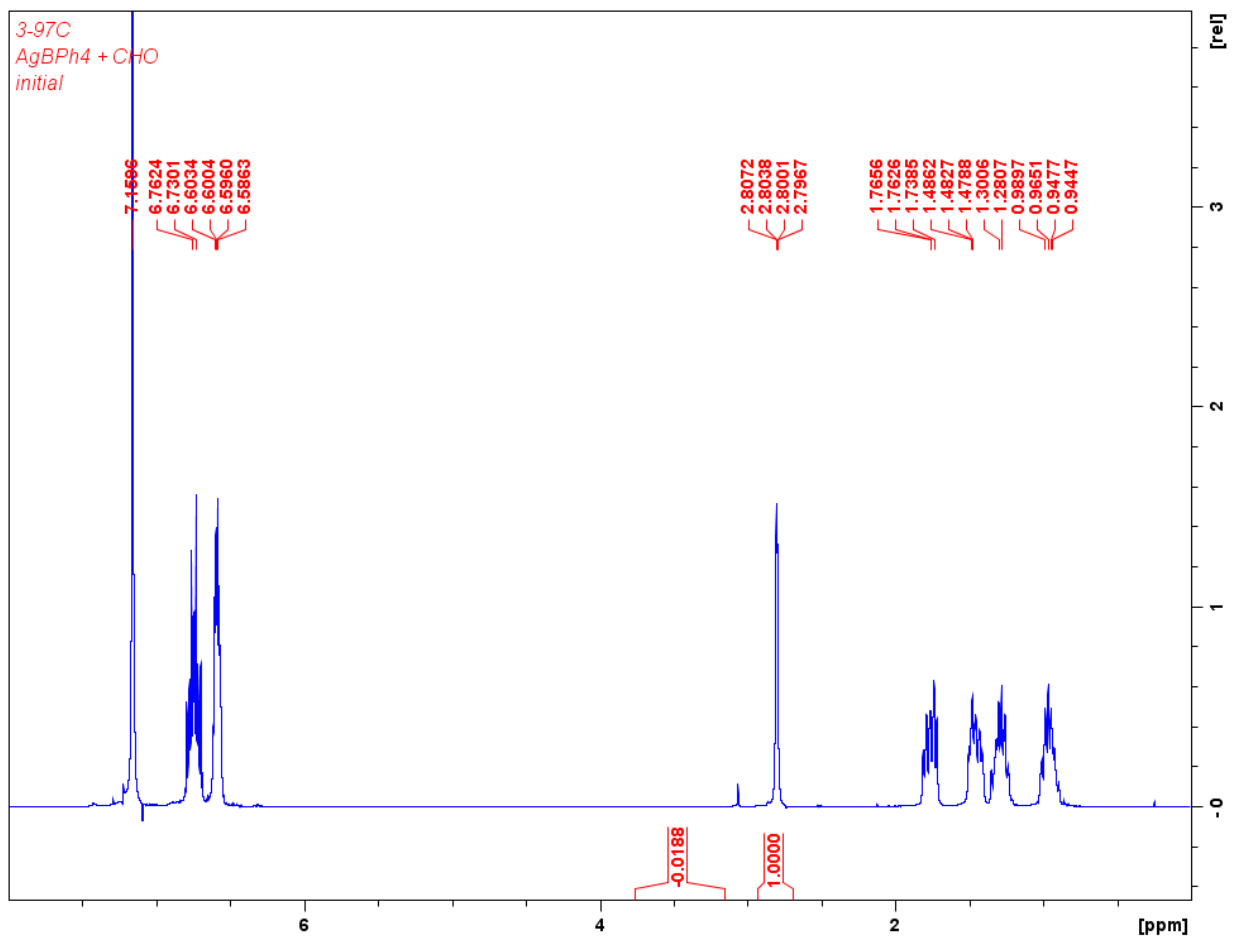


Figure B41. Table 2.3, entry 6. Polymerization of 100 equivalents of cyclohexene oxide by AgBPh₄ at ambient temperature. ¹H NMR (300 MHz, 25 °C, C₆D₆), δ (ppm): 6.71 (CFCH 1,2-difluorobenzene), 6.55 (CFCHCH 1,2-difluorobenzene), 3.60 (m, 2H, COCH PCHO), 2.80 (s, 2H, COCH₂ CHO), 1.76 (m, 2H, COCHCH₂ CHO), 1.48 (m, 2H, COCHCH₂ CHO), 1.29 (m, 2H, COCHCH₂CH₂ CHO), 0.95 (m, 2H, COCHCH₂CH₂ CHO).

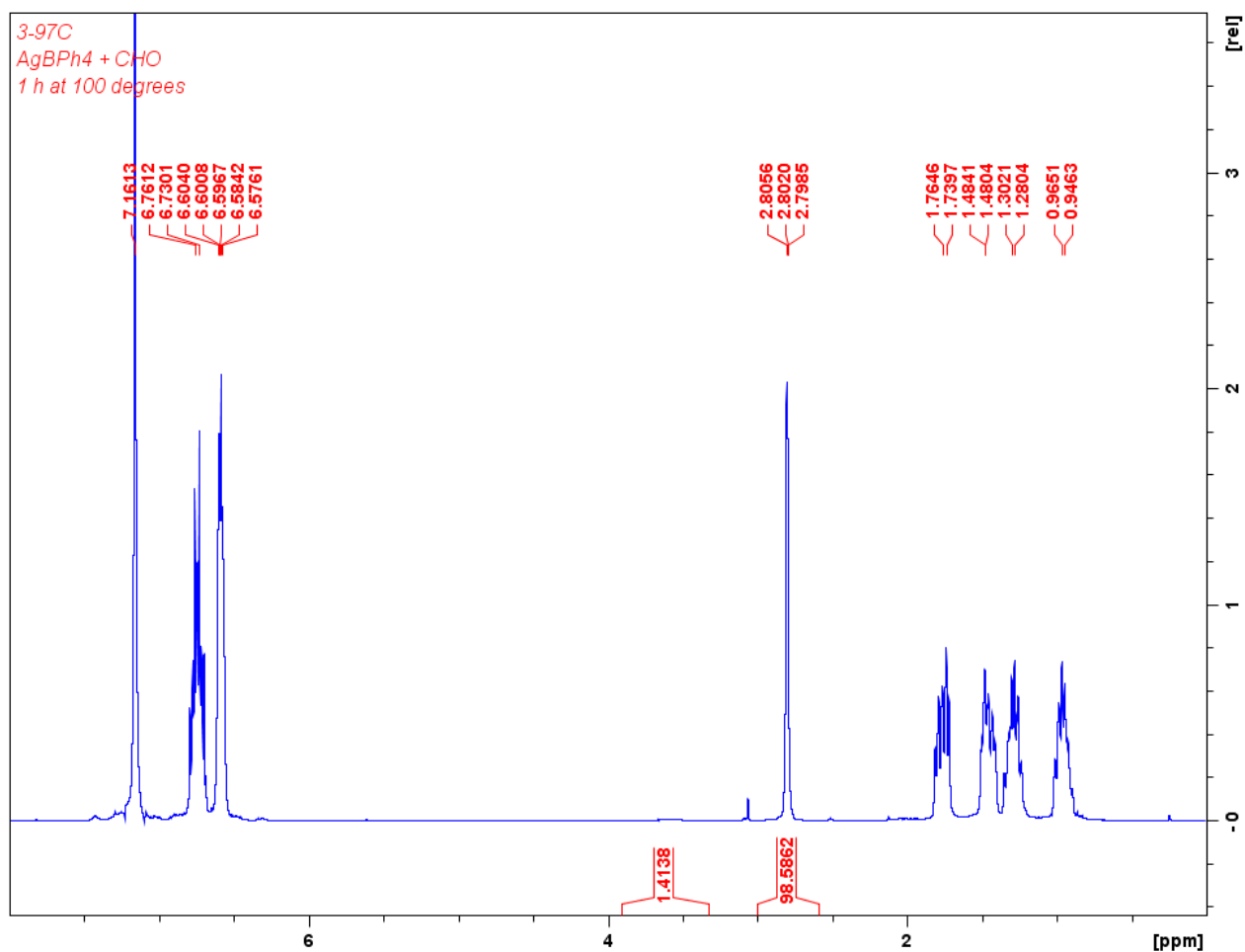


Figure B42. Table 2.3, entry 6. Polymerization of 100 equivalents of cyclohexene oxide by AgBPh₄ after 1 h at 100 °C. ¹H NMR (300 MHz, 25 °C, C₆D₆) δ (ppm): 6.73 (CFCH 1,2-difluorobenzene), 6.60 (CFCHCH 1,2-difluorobenzene), 3.62 (m, 2H, COCH PCHO), 2.80 (s, 2H, COCH₂ CHO), 1.75 (m, 2H, COCHCH₂ CHO), 1.48 (m, 2H, COCHCH₂ CHO), 1.29 (m, 2H, COCHCH₂CH₂ CHO), 0.95 (m, 2H, COCHCH₂CH₂ CHO).

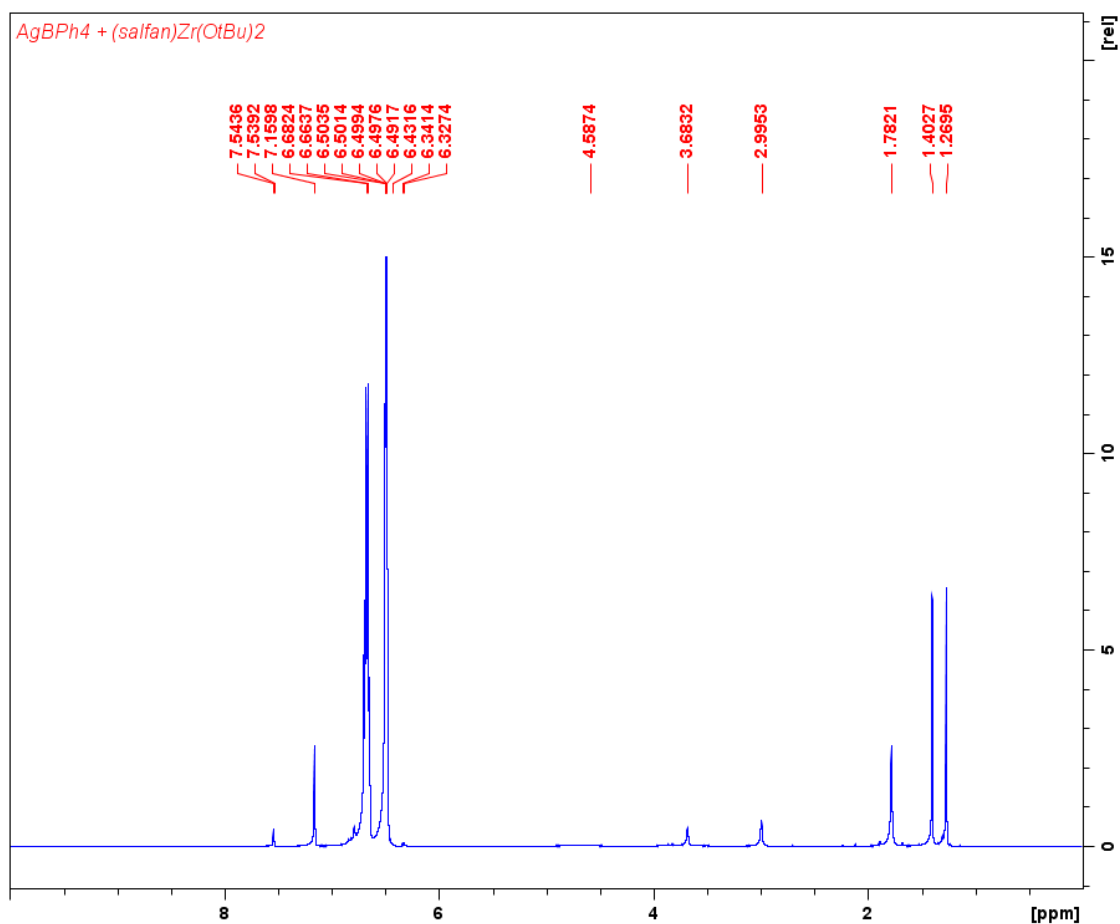


Figure B43. Table 2.3, entry 6. Oxidation of (salfan)Zr(O^tBu)₂ by AgBPh₄. ¹H NMR (300 MHz, 25 °C, C₆D₆), δ (ppm): 7.54 (d, J = 2.5 Hz, 2H, PhH), 6.79 (d, J = 2.5 Hz, 2H, PhH), 6.67 (CFCH 1,2-difluorobenzene), 6.50 (CFCHCH 1,2-difluorobenzene), 4.59 (br, 2H, CpH), 3.68 (s, 4H, NCH₂), 2.99 (s, 6H, NCH₃), 1.78 (s, 18H, C(CH₃)₃), 1.40 (s, 18H, C(CH₃)₃), 1.27 (s, 18H, C(CH₃)₃).

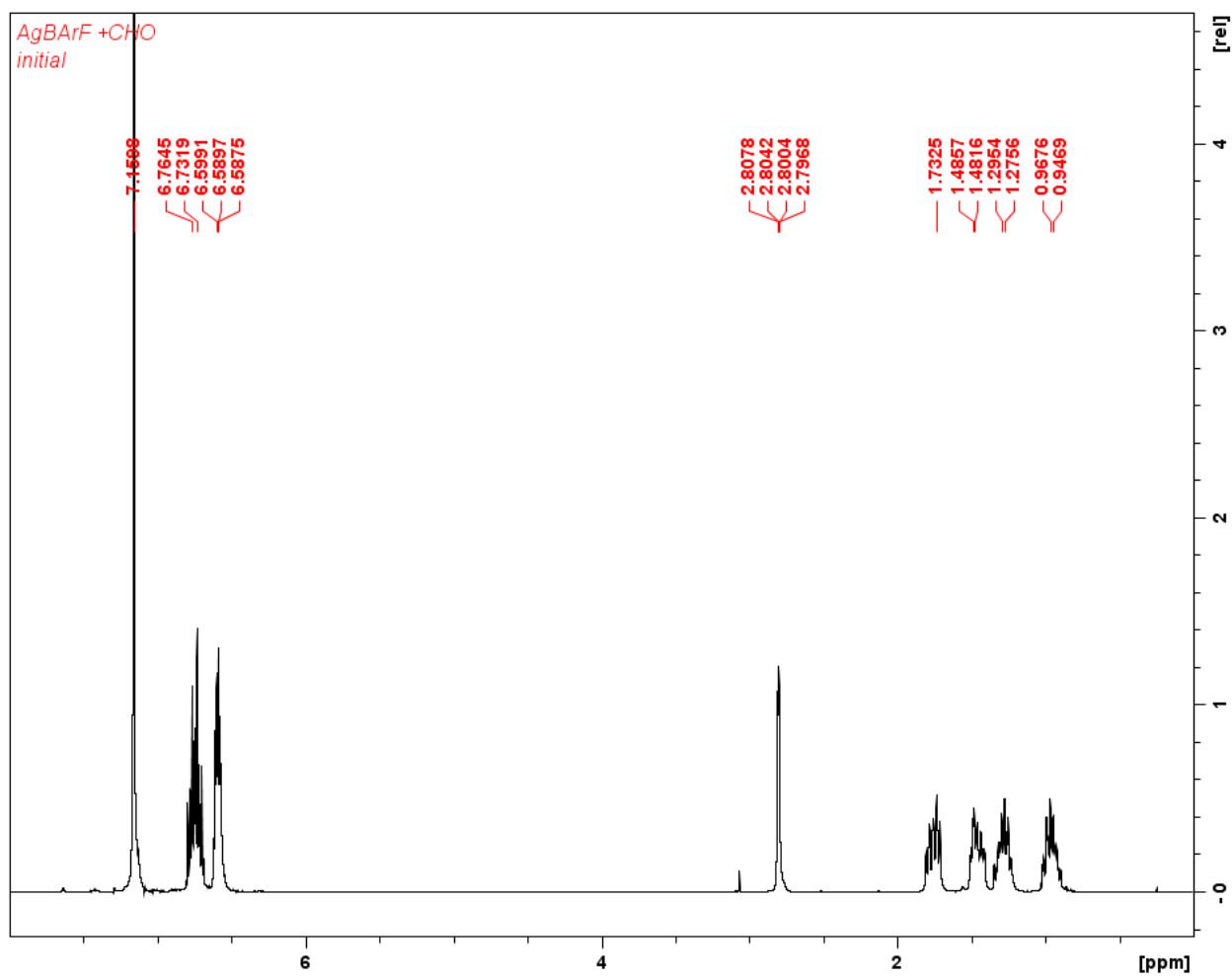


Figure B44. Table 2.3, entry 7. Polymerization of 100 equivalents of cyclohexene oxide by Ag[BAr^F₄] at ambient temperature. ¹H NMR (300 MHz, 25 °C, C₆D₆), δ (ppm): 6.76 (CFCH 1,2-difluorobenzene), 6.59 (CFCHCH 1,2-difluorobenzene), 2.80 (s, 2H, COCH₂ CHO), 1.73 (m, 2H, COCHCH₂ CHO), 1.48 (m, 2H, COCHCH₂ CHO), 1.28 (m, 2H, COCHCH₂CH₂ CHO), 0.95 (m, 2H, COCHCH₂CH₂ CHO).

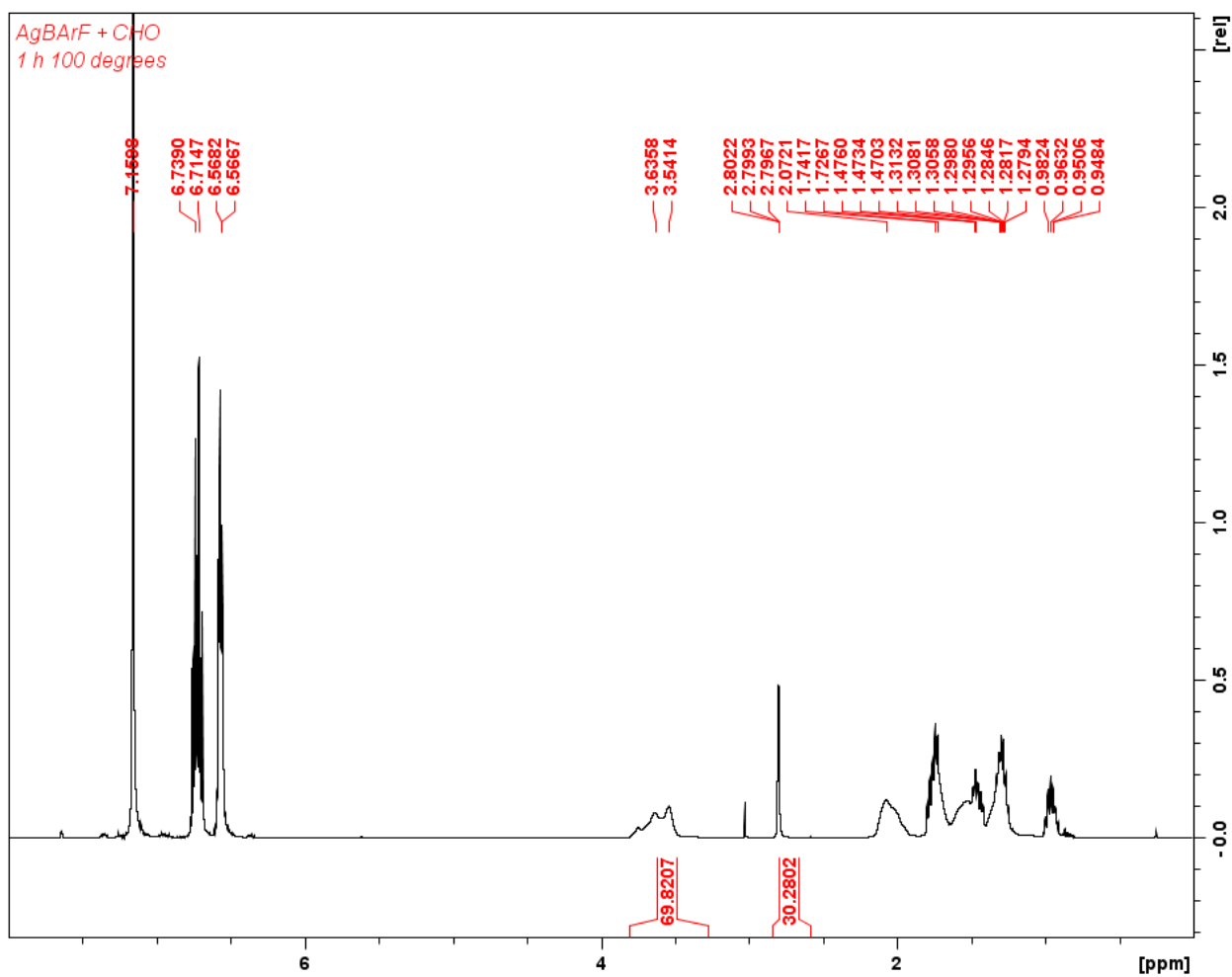


Figure B45. Table 2.3, entry 7. Polymerization of 100 equivalents of cyclohexene oxide by Ag[BAr^F₄] after 1 h at 100 °C. ¹H NMR (300 MHz, 25 °C, C₆D₆), δ (ppm): 6.72 (CFCH 1,2-difluorobenzene), 6.57 (CFCHCH 1,2-difluorobenzene), 3.62 (m, 2H, COCH PCHO), 2.80 (s, 2H, COCH₂ CHO), 2.07 (m, 2H, COCHCH₂ PCHO), 1.74 (m, 2H, COCHCH₂ CHO), 1.47 (m, 2H, COCHCH₂ CHO), 1.28 (m, 2H, COCHCH₂CH₂ CHO), 0.95 (m, 2H, COCHCH₂CH₂ CHO).

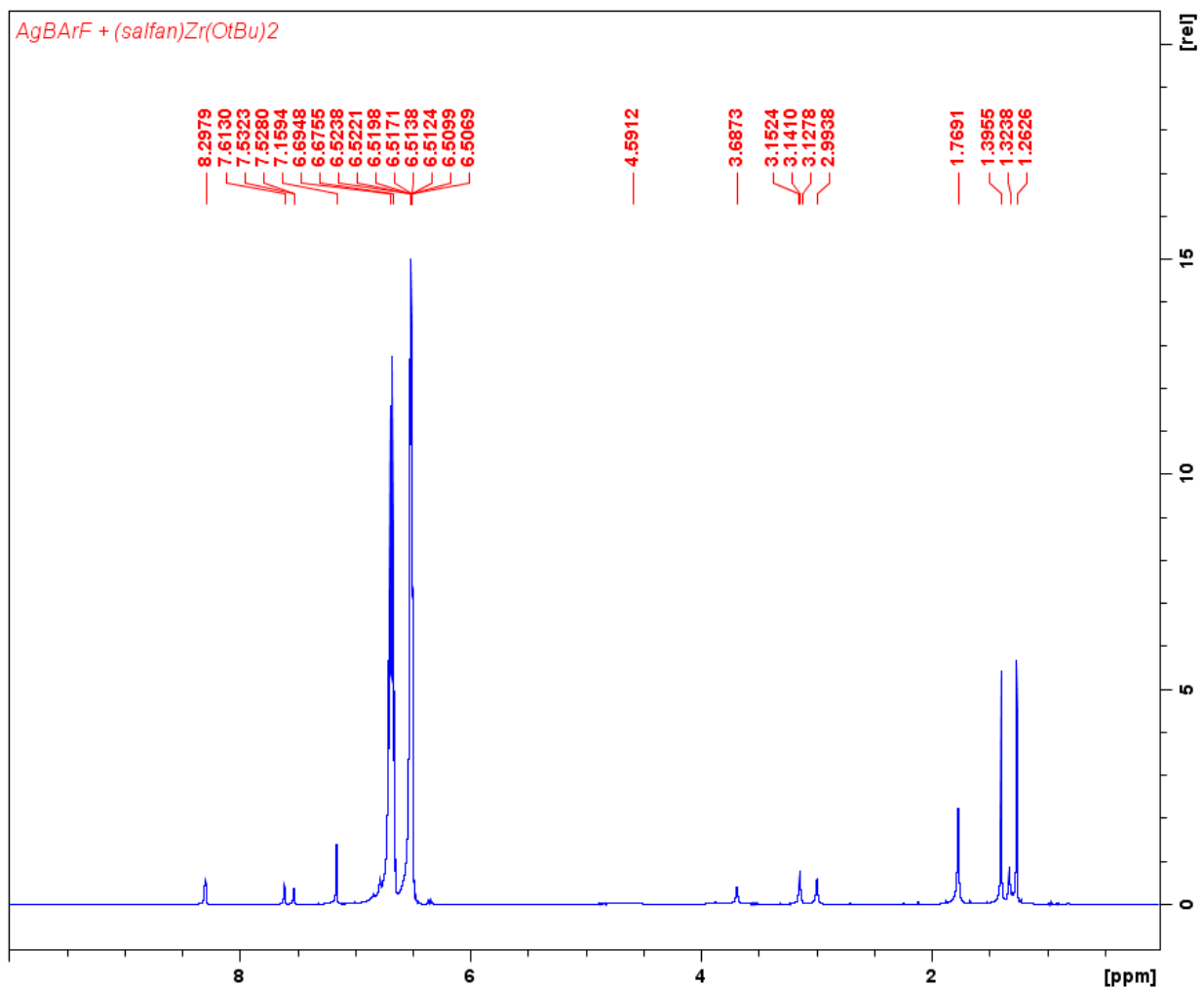


Figure B46. Table 2.3, entry 7. Oxidation of (salfan)Zr(O^tBu)₂ by Ag[BAr^F₄]. ¹H NMR (300 MHz, 25 °C, C₆D₆), δ (ppm): 8.30 (s, 2H, -OH), 7.61 (d, 2H, PhH), 7.53 (d, 2H, PhH), 6.69 (CFCH 1,2-difluorobenzene), 6.52 (CFCHCH 1,2-difluorobenzene), 4.59 (br, 2H, CpH), 3.69 (t, 4H, CpH), 3.14 (s, 8H, CpH), 2.99 (s, 6H, NCH₂), 1.77 (s, 18H, NCH₃), 1.40 (s, 18H, C(CH₃)₃), 1.26 (s, 18H, C(CH₃)₃).

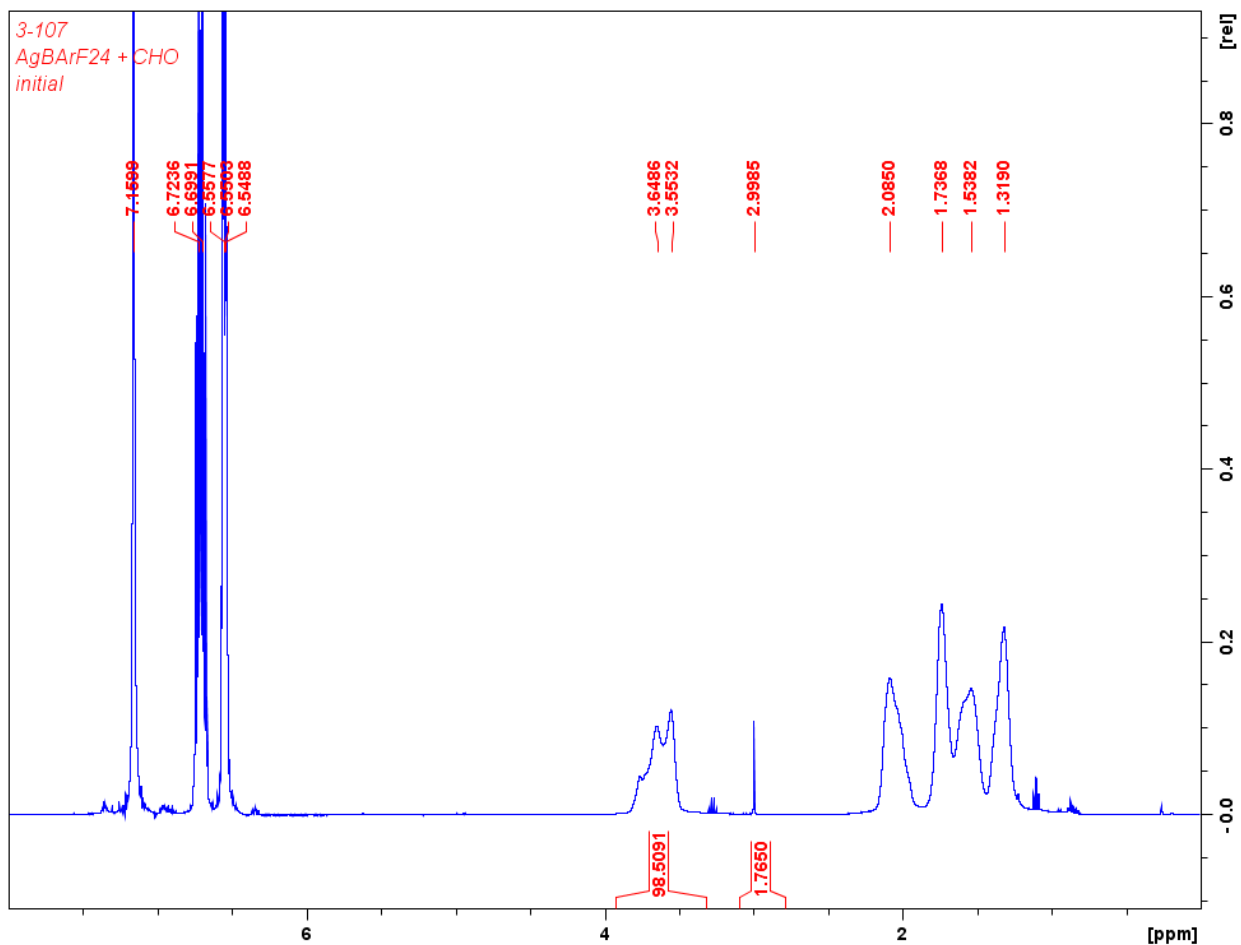


Figure B47. Table 2.3, entry 8. Polymerization of 100 equivalents of cyclohexene oxide by $\text{AgB}(\text{C}_6\text{F}_5)_4$ at ambient temperature. ^1H NMR (300 MHz, 25 °C, C_6D_6), δ (ppm): 6.71 (CFCH 1,2-difluorobenzene), 6.55 (CFCHCH 1,2-difluorobenzene), 3.60 (m, 2H, COCH PCHO), 3.00 (s, 2H, COCH₂ CHO), 2.08 (m, 2H, COCHCH₂ PCHO), 1.74 (m, 2H, COCHCH₂ PCHO), 1.54 (m, 2H, COCHCH₂CH₂ PCHO), 1.31 (m, 2H, COCHCH₂CH₂ PCHO).

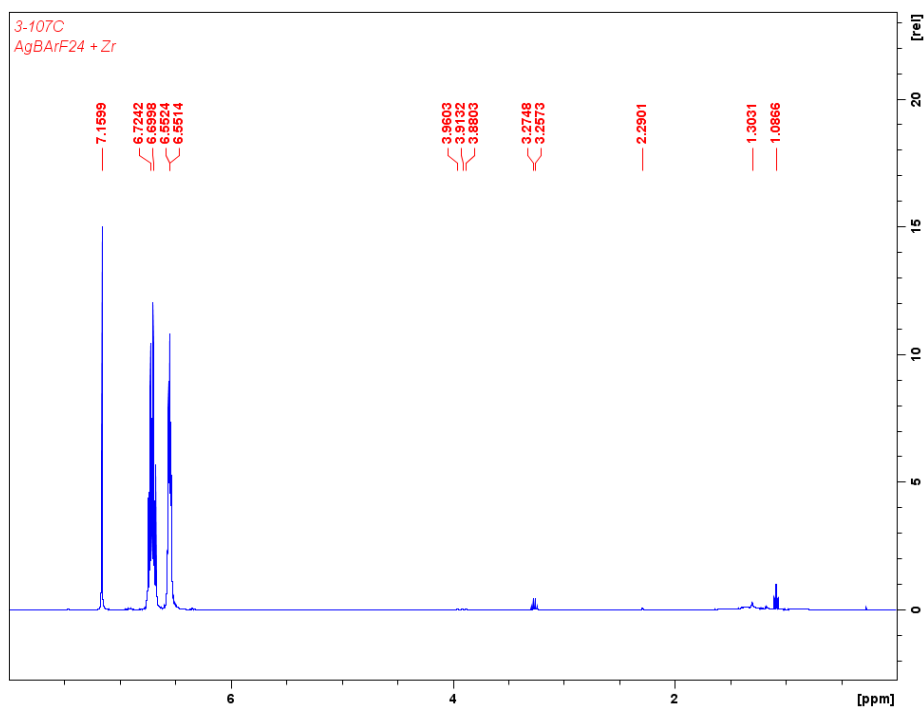


Figure B48. Table 2.3, entry 8. ^1H NMR (300 MHz, 25 °C, C_6D_6) spectrum of the oxidation of (salfan)Zr(O t Bu) $_2$ by AgB(C $_6$ F $_5$) $_4$.

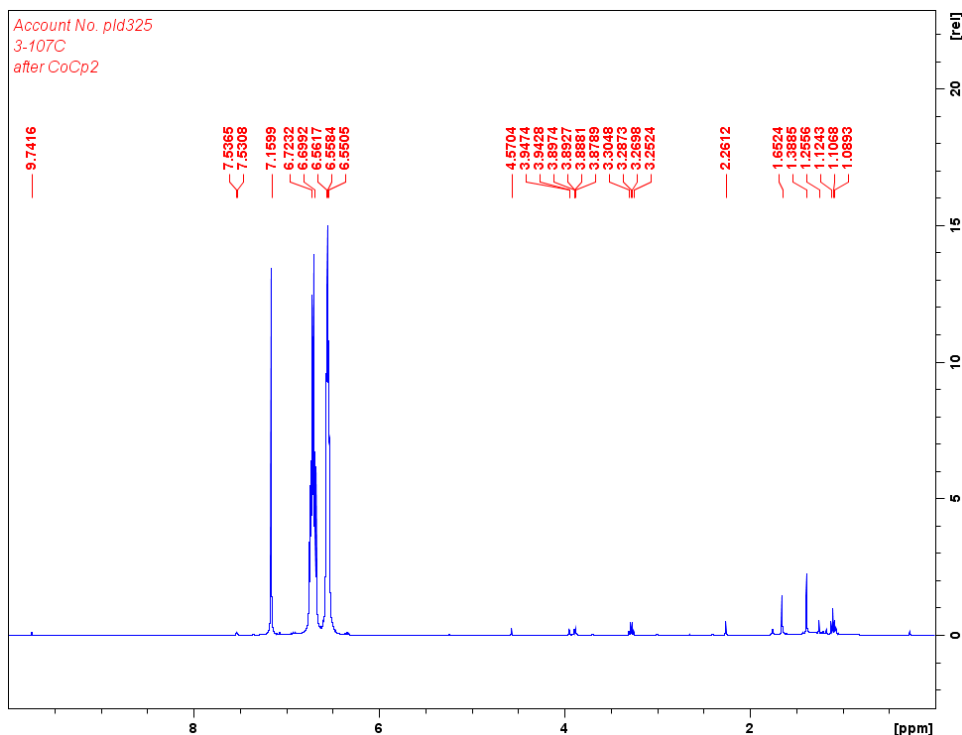


Figure B49. Table 2.3, entry 8. Oxidation of (salfan)Zr(O t Bu) $_2$ by AgB(C $_6$ F $_5$) $_4$ and subsequent reduction by CoCp $_2$. ^1H NMR (300 MHz, 25 °C, C_6D_6), δ (ppm): 9.74 (s, 2H, -OH), 7.53 (d, J = 2.3 Hz, 2H, PhH), 6.69 (CFCH 1,2-difluorobenzene), 6.55 (CFCHCH 1,2-difluorobenzene), 3.91 (t, J = 1.8 Hz, 4H, CpH), 3.86 (br, 8H, overlapping CpH and NCH $_2$), 2.26 (s, 4H, NCH $_3$), 1.65 (s, 18H, C(CH $_3$) $_3$), 1.38 (s, 18H, C(CH $_3$) $_3$).

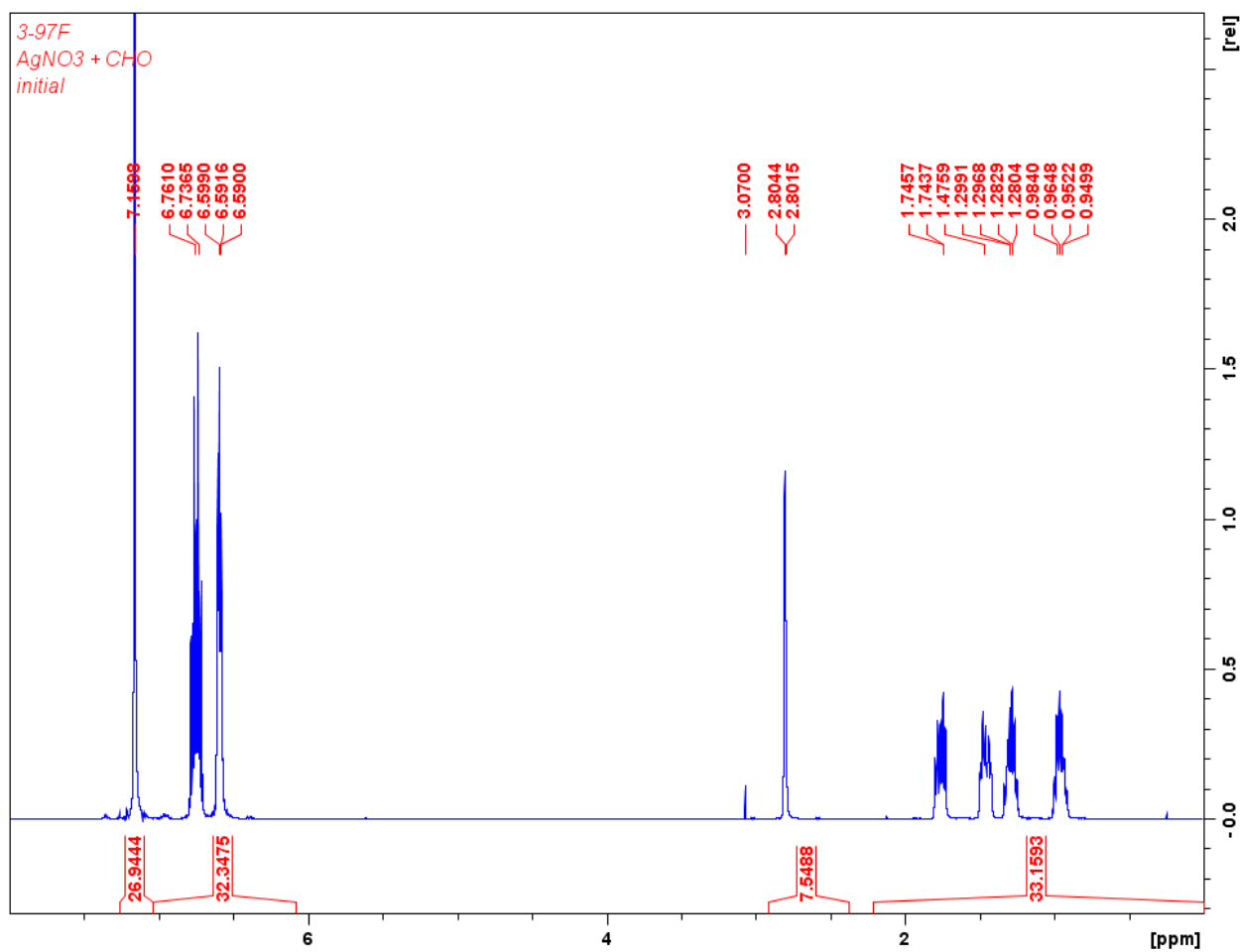


Figure B50. Table 2.3, entry 9. Polymerization of 100 equivalents of cyclohexene oxide by AgNO₃ at ambient temperature. ¹H NMR (300 MHz, 25 °C, C₆D₆), δ (ppm): 6.74 (CFCH 1,2-difluorobenzene), 6.59 (CFCHCH 1,2-difluorobenzene), 2.80 (s, 2H, COCH₂ CHO), 1.75 (m, 2H, COCHCH₂ CHO), 1.48 (m, 2H, COCHCH₂ CHO), 1.29 (m, 2H, COCHCH₂CH₂ CHO), 0.96 (m, 2H, COCHCH₂CH₂ CHO).

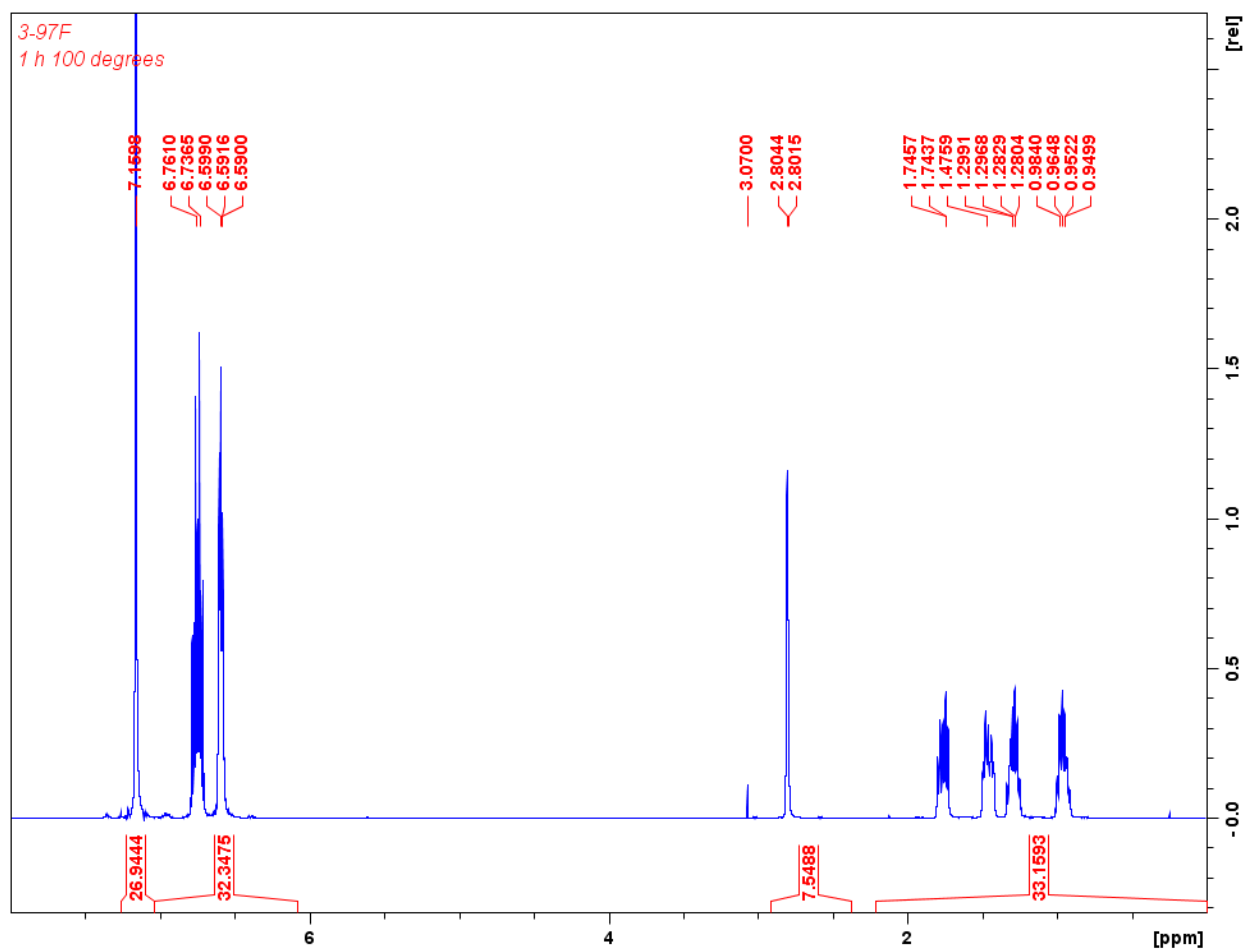


Figure B51. Table 2.3, entry 9. Polymerization of 100 equivalents of cyclohexene oxide by AgNO_3 after 1 hour at 100 °C. ^1H NMR (300 MHz, 25 °C, C_6D_6), δ (ppm): 6.76 (CFCH 1,2-difluorobenzene), 6.59 (CFCHCH 1,2-difluorobenzene), 2.80 (s, 2H, COCH₂ CHO), 1.74 (m, 2H, COCHCH₂ CHO), 1.47 (m, 2H, COCHCH₂ CHO), 1.28 (m, 2H, COCHCH₂CH₂ CHO), 0.96 (m, 2H, COCHCH₂CH₂ CHO).

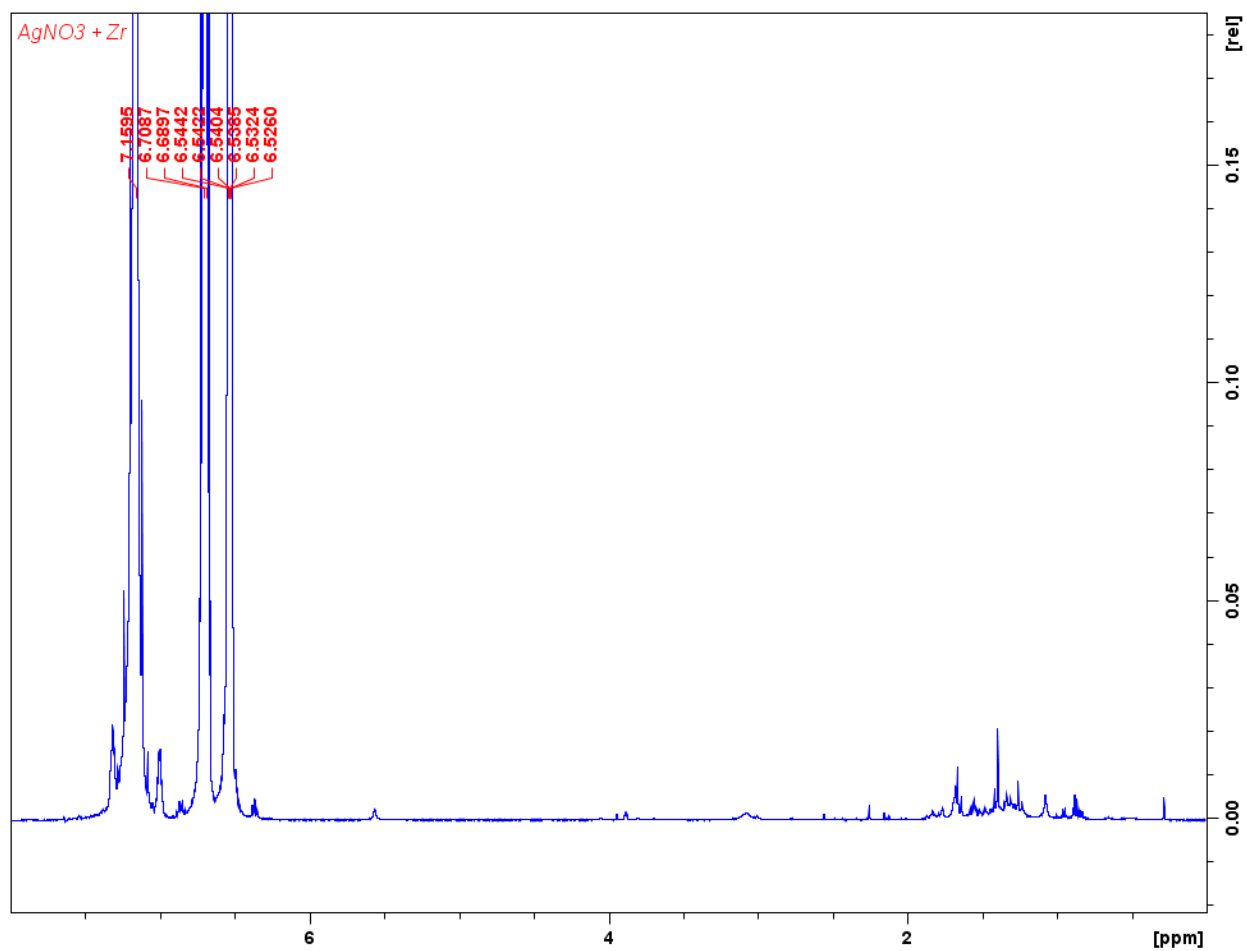


Figure B52. Table 2.3, entry 9. ¹H NMR (300 MHz, 25 °C, C₆D₆) spectrum of the oxidation of (salfan)Zr(O^tBu)₂ by AgNO₃.

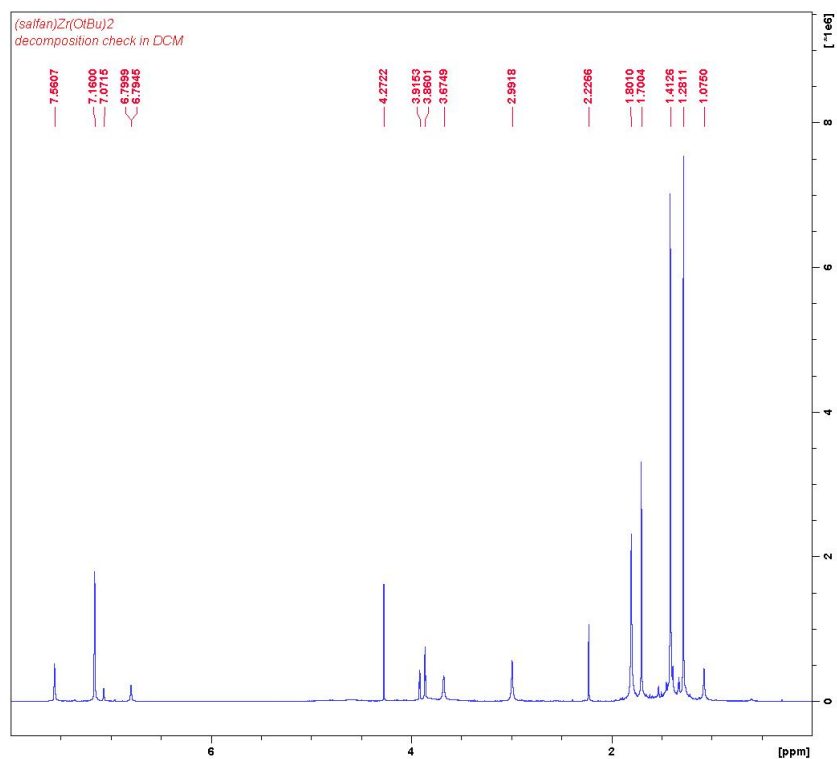


Figure B53. ¹H NMR (300 MHz, 25 °C, C₆D₆) spectrum of the decomposition of (salfan)Zr(O^tBu)₂ in CH₂Cl₂.

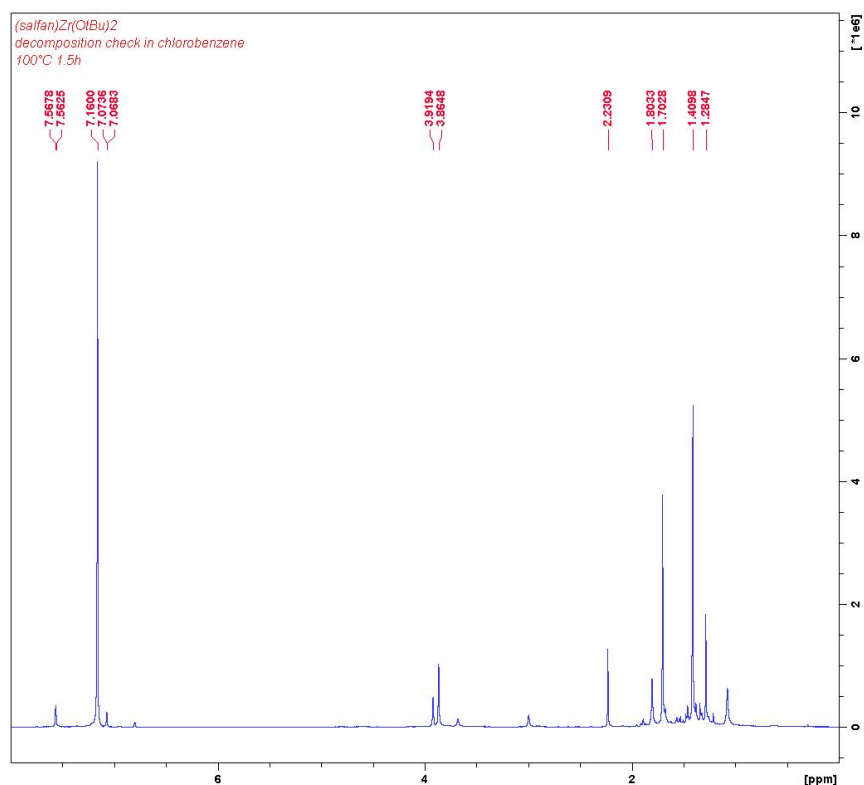


Figure B54. ¹H NMR (300 MHz, 25 °C, C₆D₆) spectrum of the decomposition of (salfan)Zr(O^tBu)₂ in chlorobenzene after 1.5 hours at 100 °C.

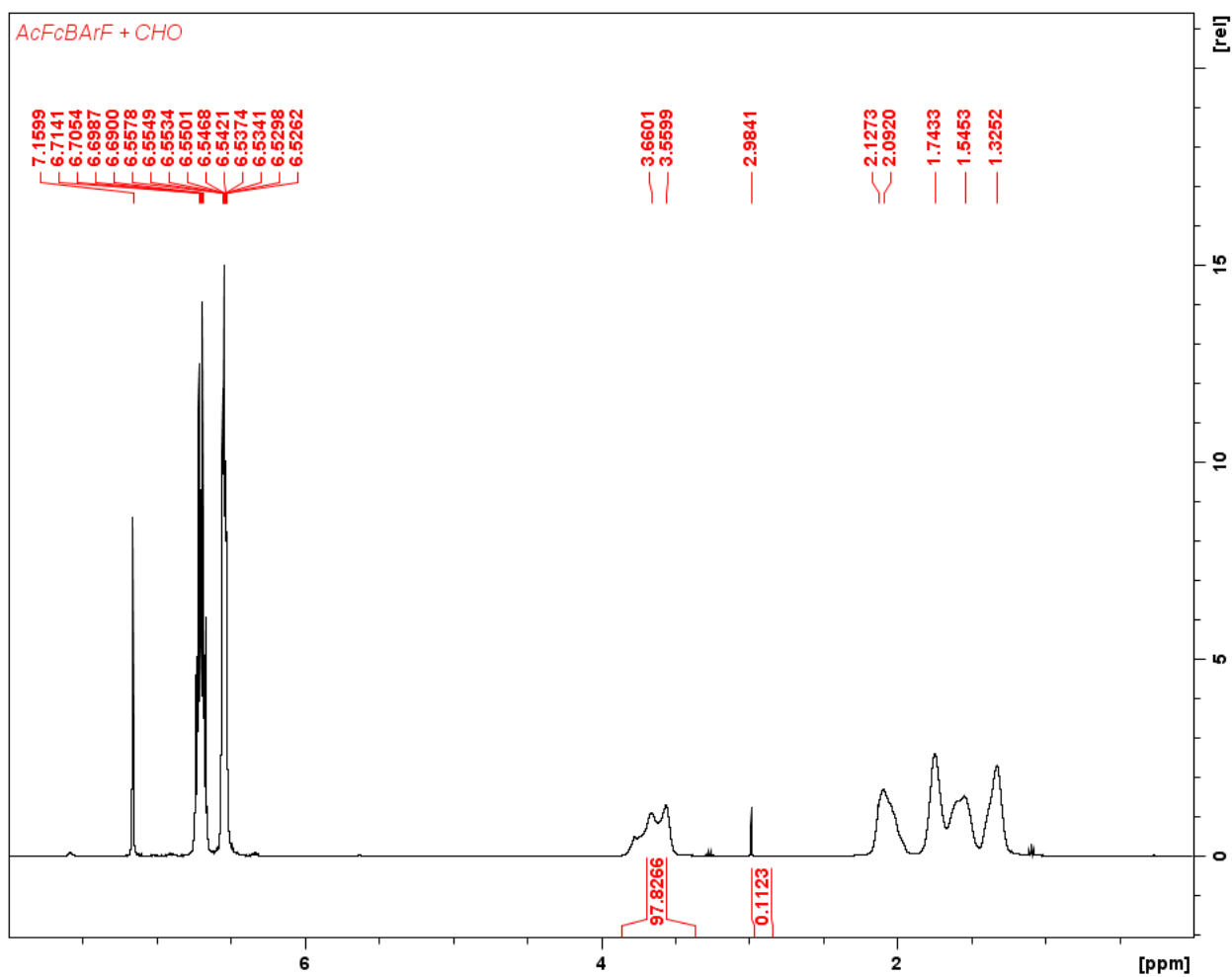


Figure B55. Polymerization of cyclohexene oxide by ${}^{\text{Ac}}\text{FcBAr}^{\text{F}}$. ${}^1\text{H}$ NMR (300 MHz, 25 °C, C_6D_6), δ (ppm): 6.70 (CFCH 1,2-difluorobenzene), 6.55 (CFCHCH 1,2-difluorobenzene), 3.62 (m, 2H, COCH PCHO), 2.98 (s, 2H, COCH₂ CHO), 2.10 (m, 2H, COCHCH₂ PCHO), 1.74 (m, 2H, COCHCH₂ PCHO), 1.54 (m, 2H, COCHCH₂CH₂ PCHO), 1.33 (m, 2H, COCHCH₂CH₂ PCHO).

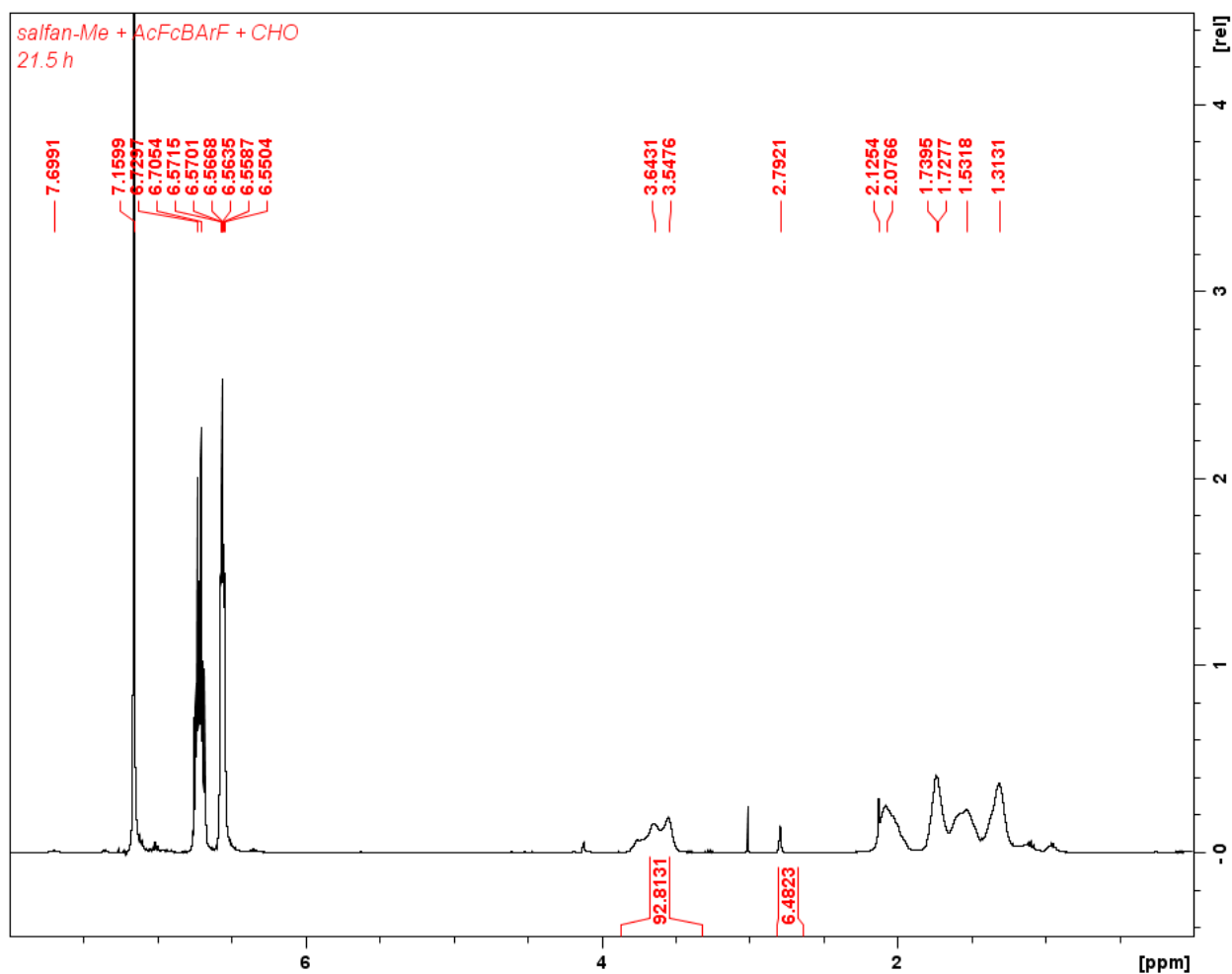


Figure B56. Polymerization of cyclohexene oxide by [salfan][BAr^F]. ¹H NMR (300 MHz, 25 °C, C₆D₆), δ (ppm): 6.71 (CFCH 1,2-difluorobenzene), 6.56 (CFCHCH 1,2-difluorobenzene), 3.59 (m, 2H, COCH PCHO), 2.80 (s, 2H, COCH₂ CHO), 2.07 (m, 2H, COCHCH₂ PCHO), 1.73 (m, 2H, COCHCH₂ PCHO), 1.53 (m, 2H, COCHCH₂CH₂ PCHO), 1.31 (m, 2H, COCHCH₂CH₂ PCHO).

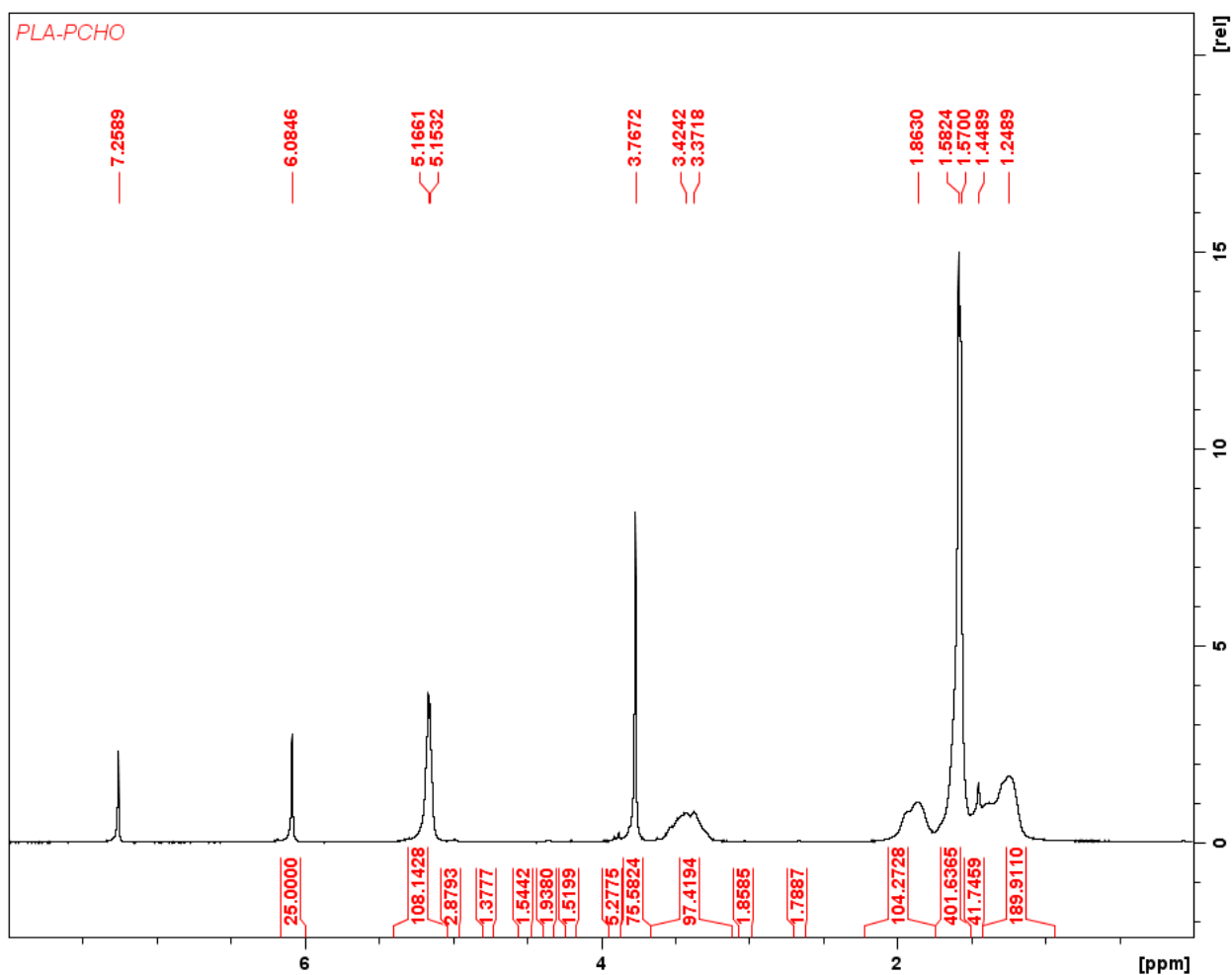


Figure B57. Table 2.4, entry 1. Table B2, entry 1. Polymerization of 100 equivalents of L-lactide, and cyclohexene oxide, monomers added sequentially, using initiator redox switch “red-ox”. ^1H NMR (300 MHz, 25 °C, CDCl_3), δ (ppm): 6.08 (s, 3H, PhH TMB), 5.16 (q, 2H, CHCH_3 PLA), 3.77 (s, 9H, CH_3 TMB), 3.40 (m, 2H, COCHPCHO), 1.86 (m, 2H, COCHCH_2 PCHO), 1.57 (d, 6H, CHCH_3 PLA), 1.25 (m, 2H, $\text{COCHCH}_2\text{CH}_2$ PCHO). Small peaks that may be related to the end group or junctions were integrated.

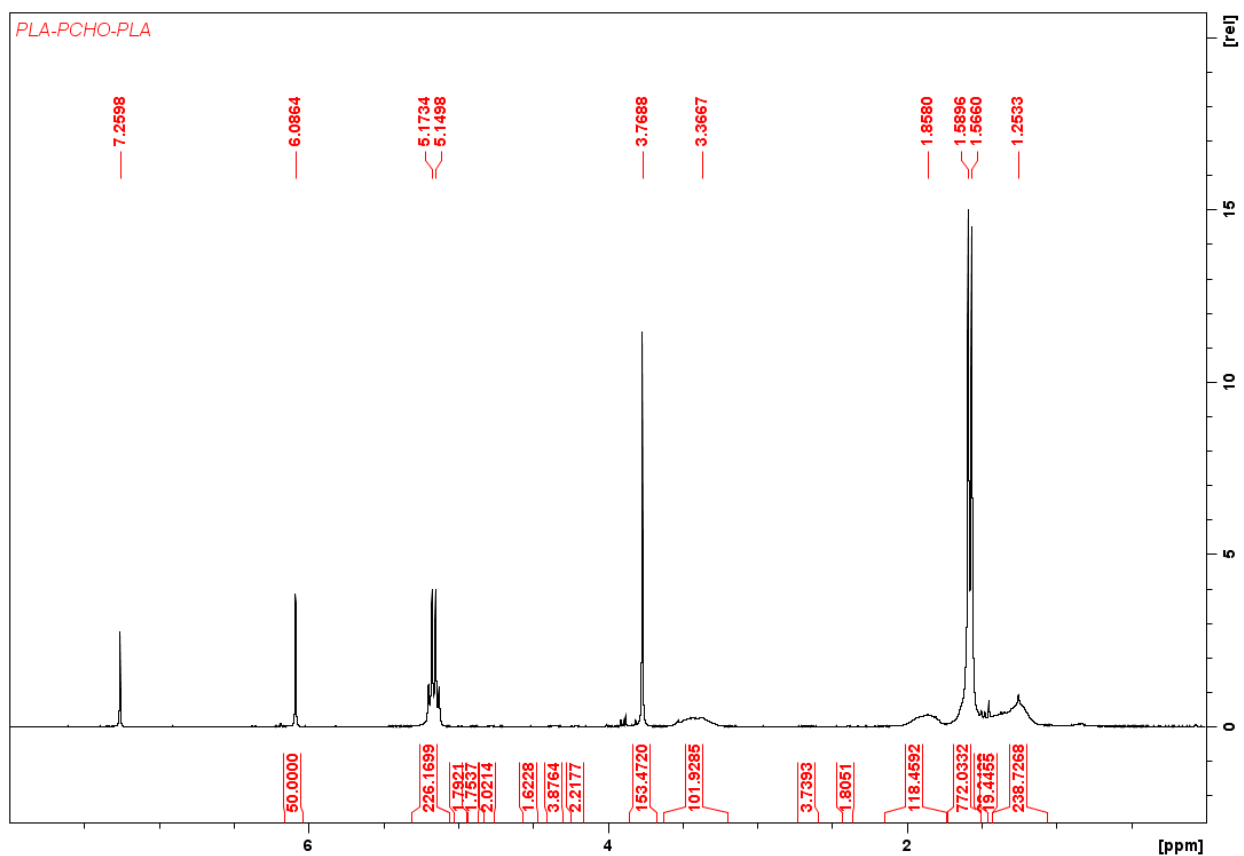


Figure B58. Table 2.4, entry 2. Table B3, entry 1. Polymerization of 100 equivalents of L-lactide, cyclohexene oxide and L-lactide monomers added sequentially, using initiator redox switch “red-ox-red”. ^1H NMR (300 MHz, 25 °C, CDCl_3), δ (ppm): 6.08 (s, 3H, PhH TMB), 5.16 (q, 2H, CHCH_3 PLA), 3.77 (s, 9H, CH_3 TMB), 3.37 (m, 2H, COCH PCHO), 1.86 (m, 2H, COCHCH_2 PCHO), 1.57 (d, 6H, CHCH_3 PLA), 1.25 (m, 2H, $\text{COCHCH}_2\text{CH}_2$ PCHO). Small peaks that may be related to the end group or junctions were integrated.

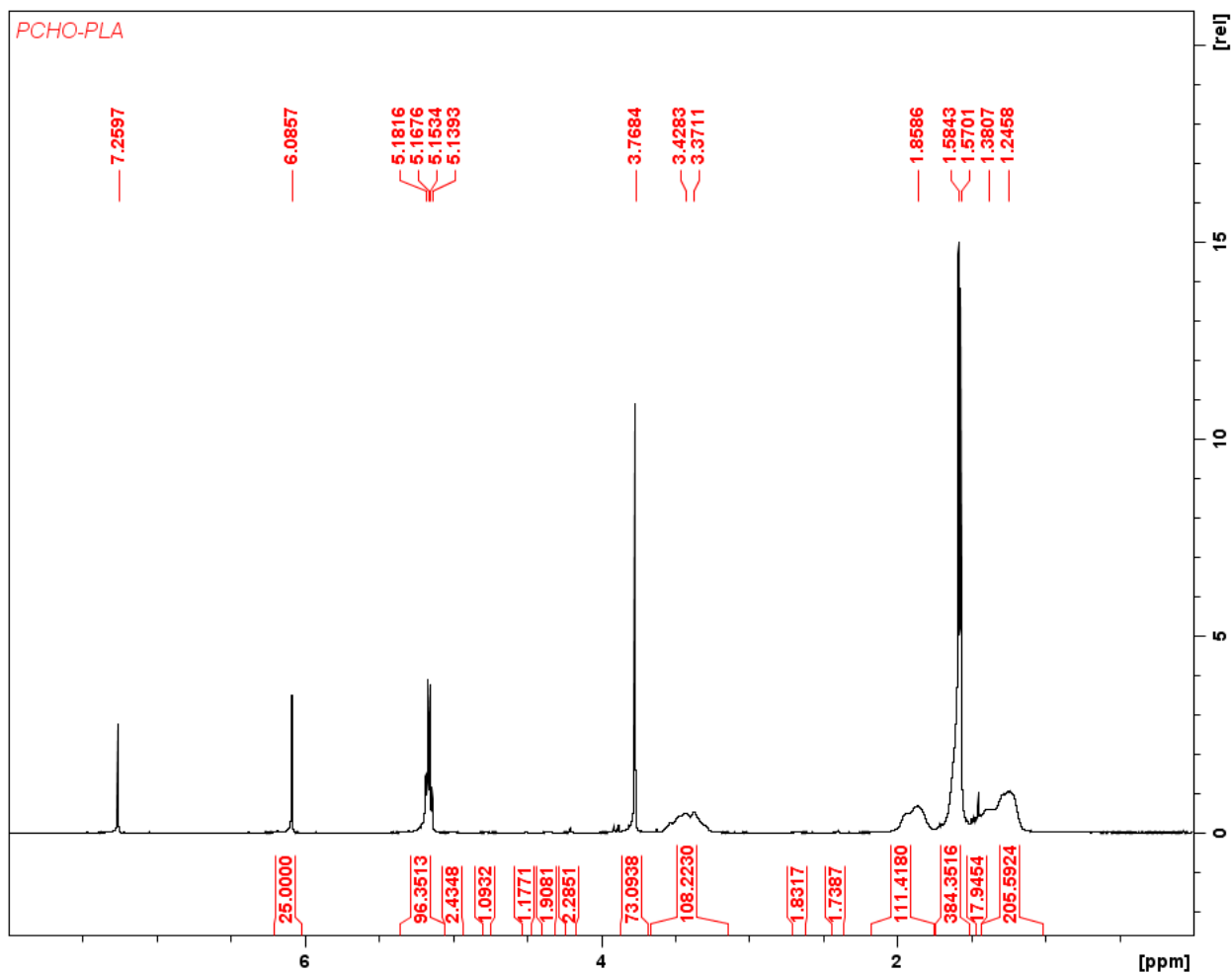


Figure B59. Table 2.4, entry 3. Table B4, entry 1. Polymerization of 100 equivalents of cyclohexene oxide and L-lactide, monomers added sequentially, using initiator redox switch “ox-red” ^1H NMR (300 MHz, 25 °C, CDCl_3), δ (ppm): 6.09 (s, 3H, PhH TMB), 5.16 (q, 2H, CHCH_3 PLA), 3.77 (s, 9H, CH_3 TMB), 3.40 (m, 2H, COCHPCHO), 1.86 (m, 2H, COCHCH_2 PCHO), 1.57 (d, 6H, CHCH_3 PLA), 1.38-1.25 (m, 2H, $\text{COCHCH}_2\text{CH}_2$ PCHO). Small peaks that may be related to the end group or junctions were integrated.

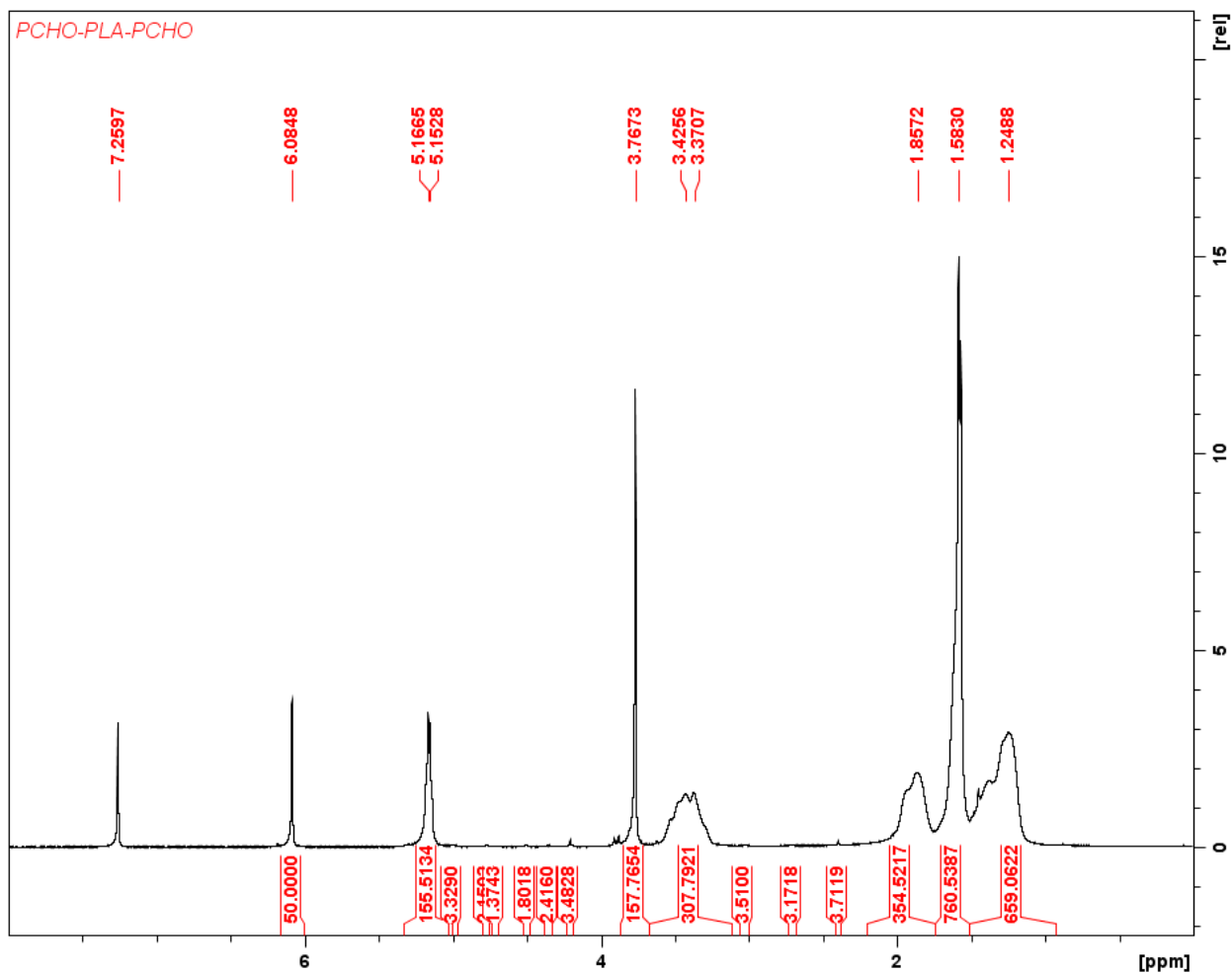


Figure B60. Table 2.4, entry 4. Table B5, entry 1. Polymerization of 100 equivalents of cyclohexene oxide, L-lactide, and cyclohexene oxide, monomers added sequentially, using initiator redox switch “ox-red-ox”. ^1H NMR (300 MHz, 25 °C, CDCl_3), δ (ppm): 6.08 (s, 3H, PhH TMB), 5.16 (q, 2H, CHCH_3 PLA), 3.77 (s, 9H, CH_3 TMB), 3.40 (m, 2H, COCH PCHO), 1.86 (m, 2H, COCHCH_2 PCHO), 1.57 (d, 6H, CHCH_3 PLA), 1.25 (m, 2H, $\text{COCHCH}_2\text{CH}_2$ PCHO). Small peaks that may be related to the end group or junctions were integrated.

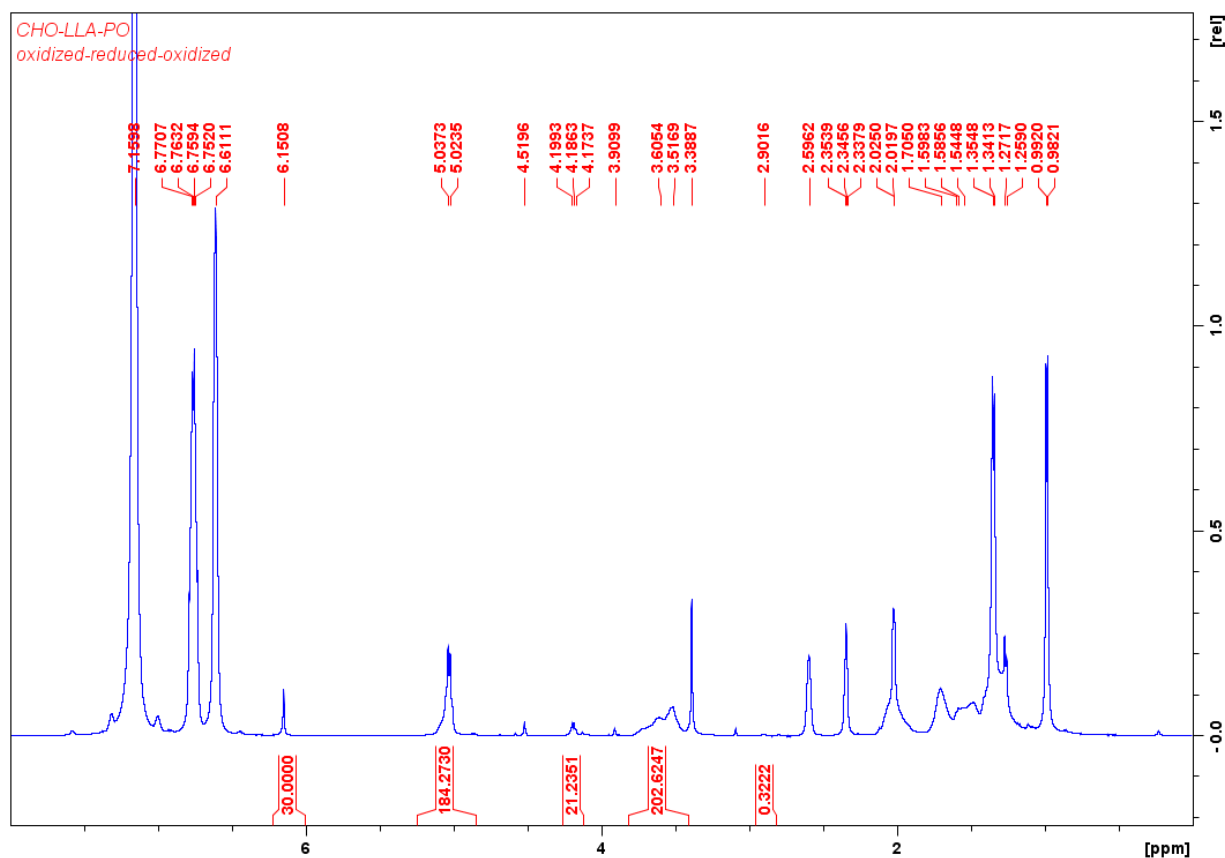


Figure B61. Table 2.4, entry 5. Polymerization of 100 equivalents of cyclohexene oxide, L-lactide, and propylene oxide, monomers added sequentially, using initiator redox switch “ox-red-ox”. ^1H NMR (300 MHz, 25 °C, C_6D_6), δ (ppm): 6.77 (CFCH 1,2-difluorobenzene), 6.61 (CFCHCH 1,2-difluorobenzene), 6.15 (s, 3H, PhH TMB), 5.03 (q, 2H, CHCH₃ PLA), 4.19 (q, 2H, CHCH₃ LA), 3.55 (m, 2H, COCH PCHO), 3.39 (s, 9H, CH₃ TMB), 2.90 (m, 1H, COCHCH₃ PPO), 2.60 (m, 1H, COCHCH₃ PO), 2.34 (m, 1H, COCH₂ PO), 2.02 (m, 2H, COCHCH₂ PCHO), 1.70-1.54 (m, 2H, COCHCH₂ PCHO), 1.35 (d, 3H, CH₃ PLA), 1.26 (m, 2H, COCHCH₂CH₂ CHO), 0.99 (d, 3H, COCHCH₃ PO).

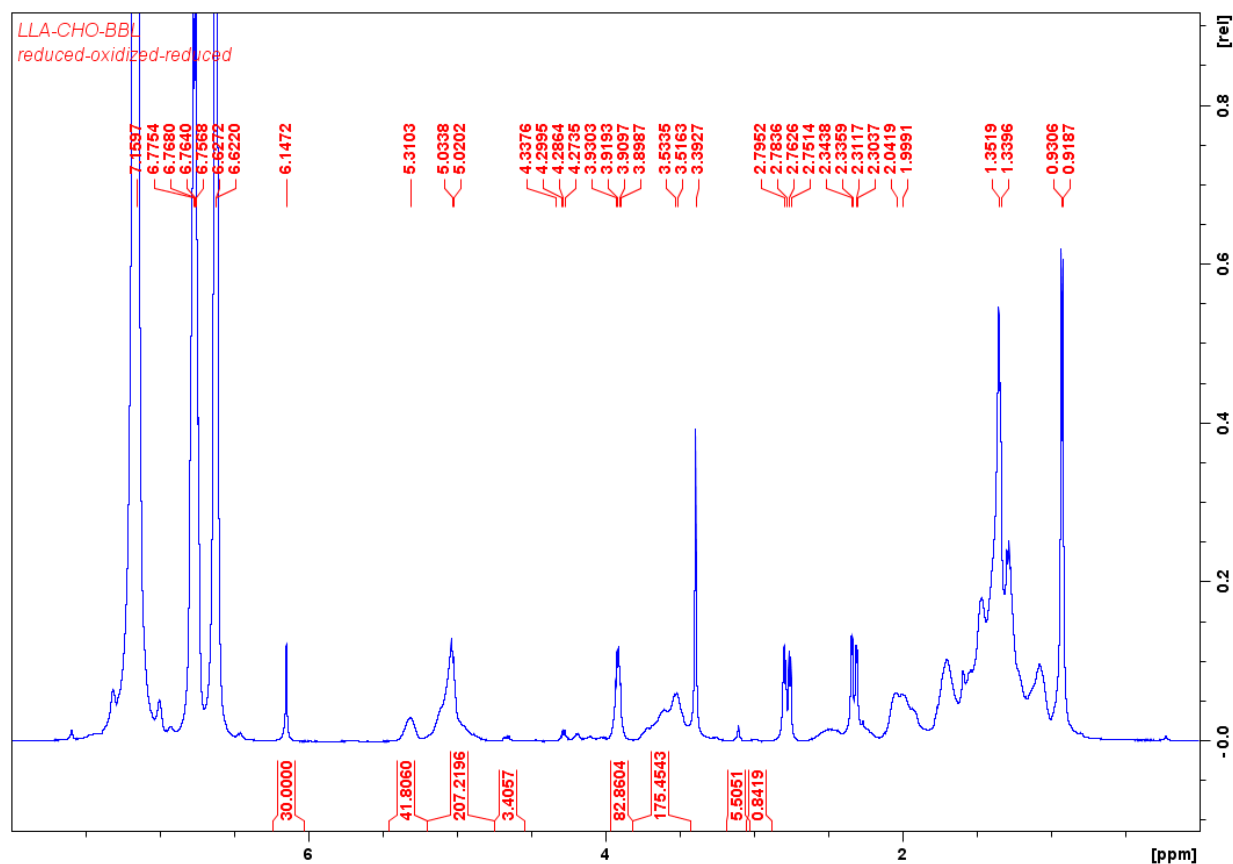


Figure B62. Table 2.4, entry 6. Polymerization of 100 equivalents of L-lactide, cyclohexene oxide, and β -butyrolactone, monomers added sequentially, using initiator redox switch “red-ox-red”. ^1H NMR (300 MHz, 25 °C, C_6D_6), δ (ppm): 6.76 (CFCH 1,2-difluorobenzene), 6.63 (CFCHCH 1,2-difluorobenzene), 6.15 (s, 3H, PhH TMB), 5.31 (m, 1H, OCHCH₃ PHB), 5.03 (q, 2H, CHCH₃ PLA), 4.30 (m, 1H, OCHCH₃ BBL), 3.91 (q, 2H, CHCH₃ LA), 3.52 (m, 2H, COCH PCHO), 3.39 (s, 9H, CH₃ TMB), 2.77 (m, 2H, COCH₂ BBL), 2.32 (m, 2H, COCH₂ BBL), 2.02 (m, 2H, COCHCH₂ PCHO), 1.34 (d, 6H, CHCH₃ PLA), 0.92 (t, 3H, OCHCH₃ BBL).

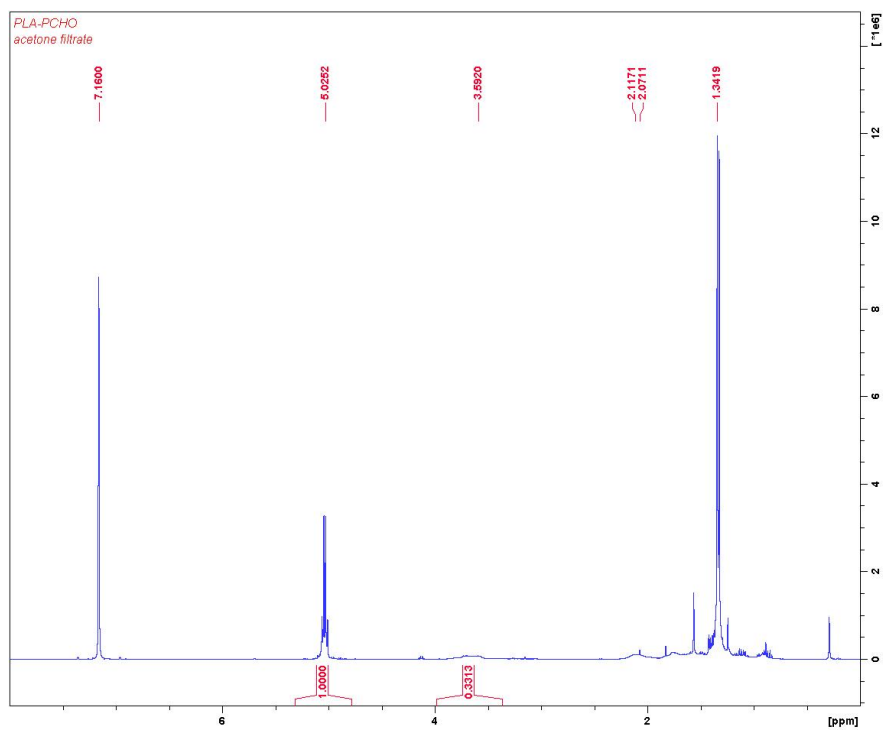


Figure B63. Table B2, entry 2. Acetone filtrate from selective precipitation of PLA-PCHO. ^1H NMR (300 MHz, 25 °C, C_6D_6), δ (ppm): 5.03 (q, 2H, CHCH_3 PLA), 3.59 (m, 2H, COCH PCHO), 2.11-2.07 (m, 2H, COCHCH_2 PCHO), 1.34 (d, 6H, CHCH_3 PLA).

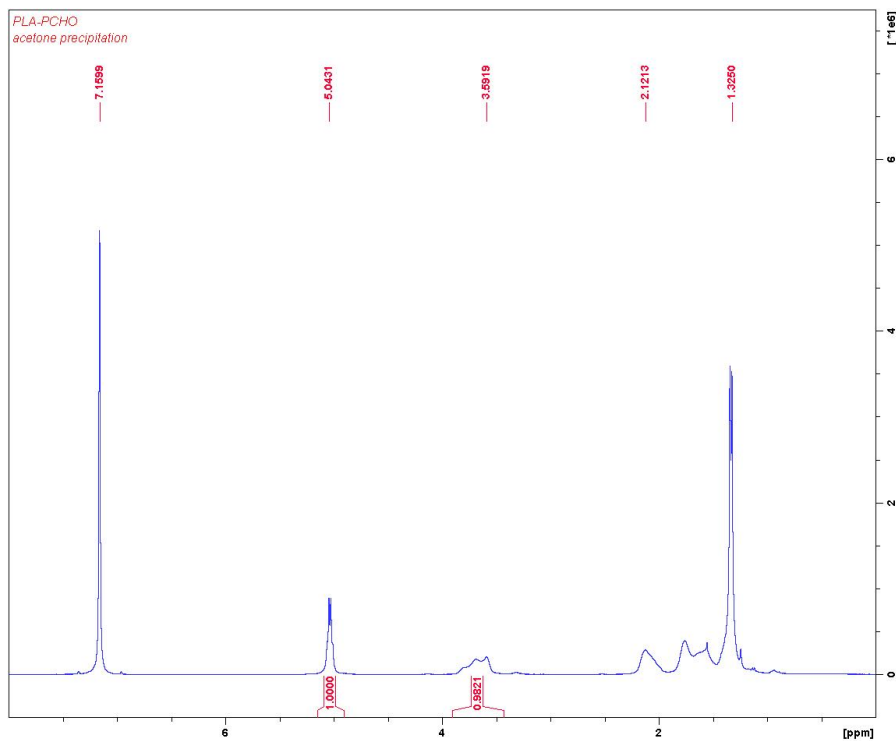


Figure B64. Table B2, entry 3. Acetone precipitate from selective precipitation of PLA-PCHO. ^1H NMR (300 MHz, 25 °C, C_6D_6), δ (ppm): 5.04 (q, 2H, CHCH_3 PLA), 3.59 (m, 2H, COCH PCHO), 2.12 (m, 2H, COCHCH_2 PCHO), 1.33 (m, 2H, $\text{COCHCH}_2\text{CH}_2$ PCHO).

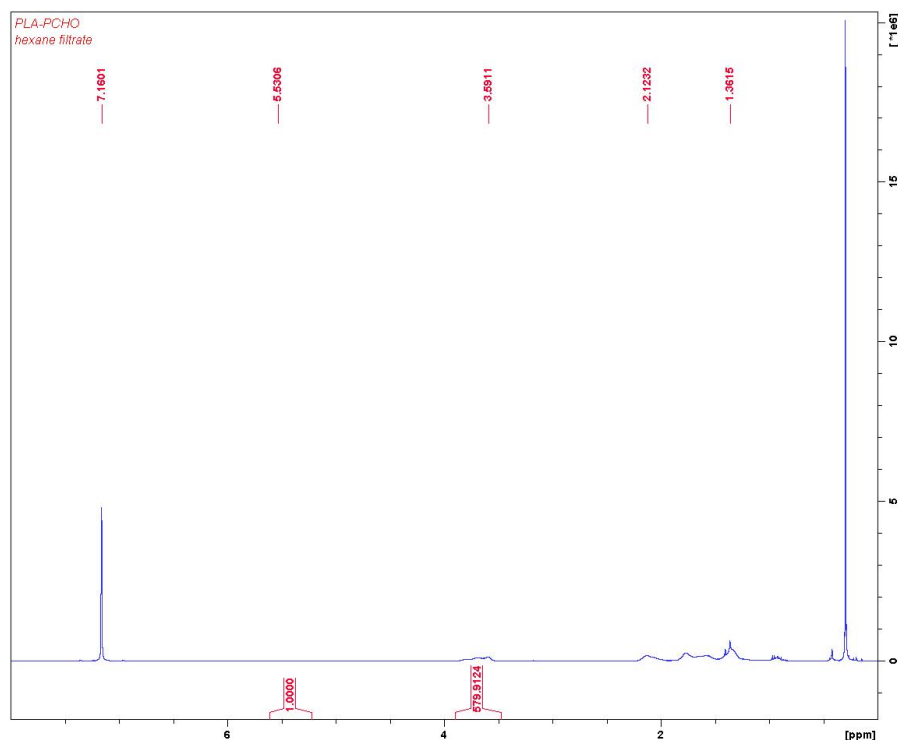


Figure B65. Table B2, entry 4. Hexanes filtrate from selective precipitation of PLA-PCHO. ^1H NMR (300 MHz, 25 °C, C_6D_6), δ (ppm): 5.53 (q, 2H, CHCH_3 PLA), 3.59 (m, 2H, COCH PCHO), 2.12 (m, 2H, COCHCH_2 PCHO), 1.36 (d, 6H, CHCH_3 PLA).

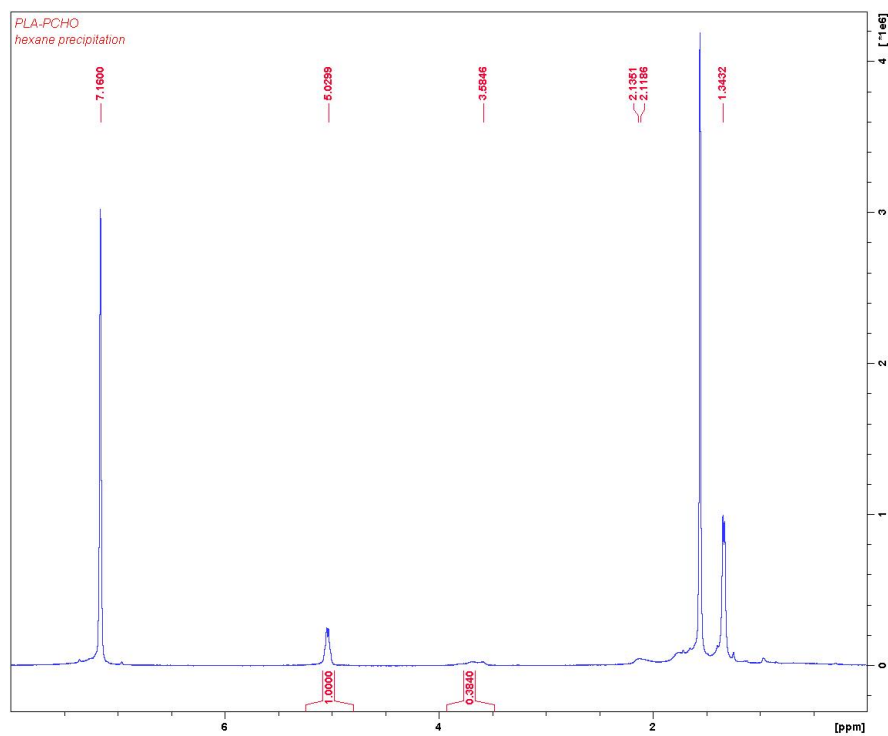


Figure B66. Table B2, entry 5. Hexanes precipitate from selective precipitation of PLA-PCHO. ^1H NMR (300 MHz, 25 °C, C_6D_6), δ (ppm): 5.03 (q, 2H, CHCH_3 PLA), 3.58 (m, 2H, COCH PCHO), 2.12 (m, 2H, COCHCH_2 PCHO), 1.34 (d, 6H, CHCH_3 PLA).

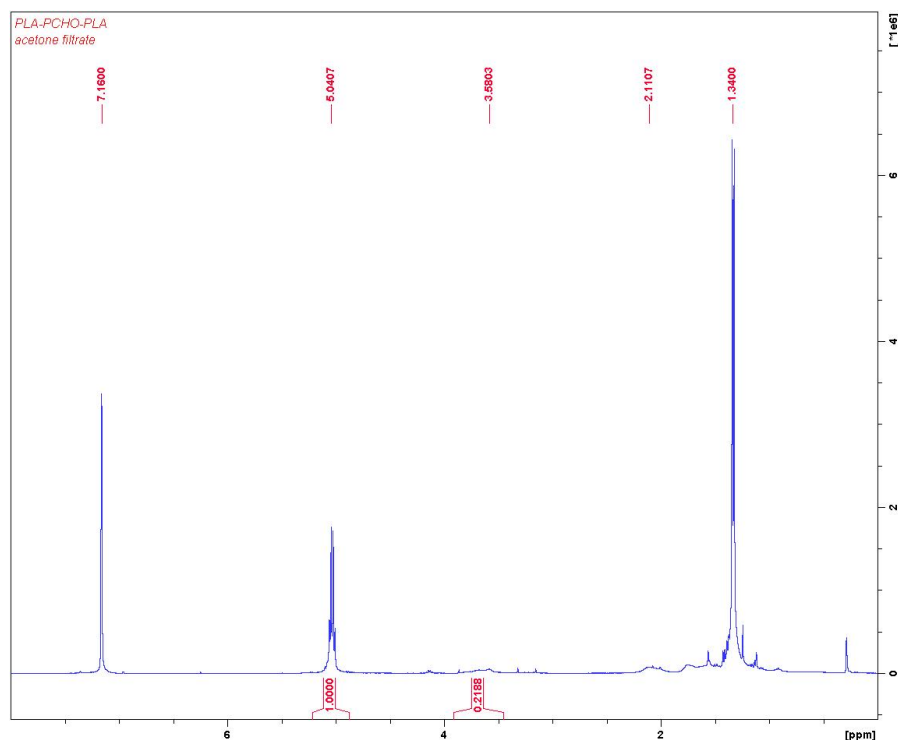


Figure B67. Table B3, entry 2. Acetone filtrate from selective precipitation of PLA-PCHO-PLA. ^1H NMR (300 MHz, 25 °, C_6D_6), δ (ppm): 5.04 (q, 2H, CHCH_3 PLA), 3.58 (m, 2H, COCH PCHO), 2.11 (m, 2H, COCHCH_2 PCHO), 1.34 (d, 6H, CHCH_3 PLA).

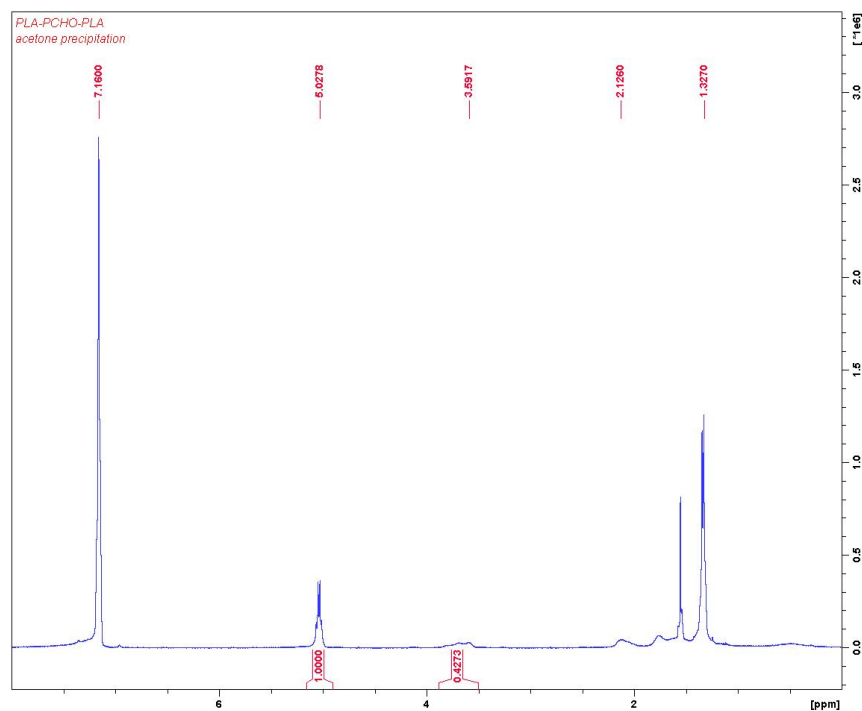


Figure B68. Table B3, entry 3. Acetone precipitate from selective precipitation of PLA-PCHO-PLA. ^1H NMR (300 MHz, 25 °C, C_6D_6), δ (ppm): 5.03 (q, 2H, CHCH_3 PLA), 3.58 (m, 2H, COCH PCHO), 2.12 (m, 2H, COCHCH_2 PCHO), 1.33 (d, 6H, CHCH_3 PLA).

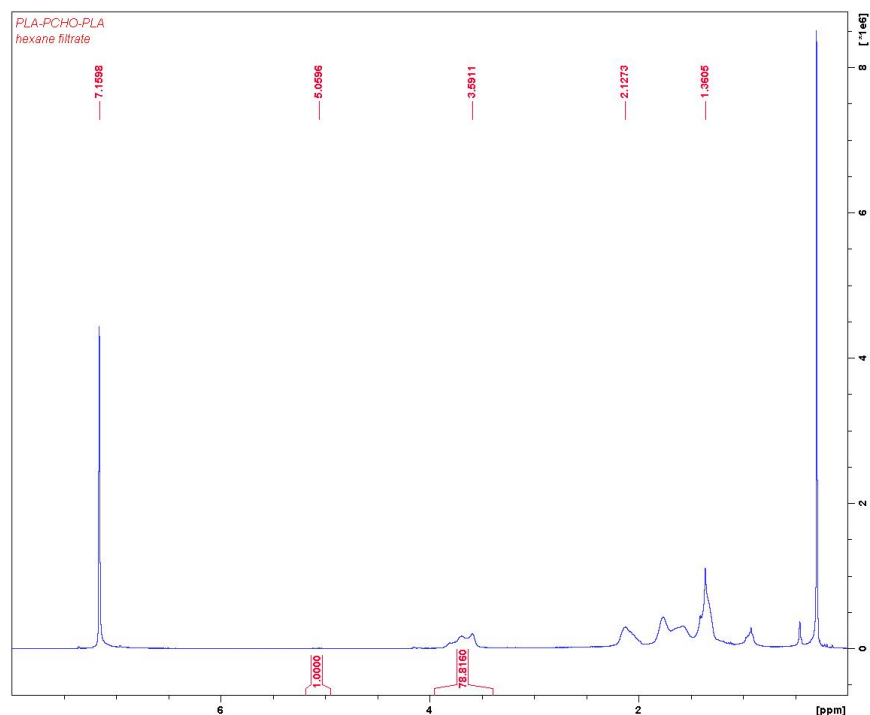


Figure B69. Table B3, entry 4. Hexanes filtrate from selective precipitation of PLA-PCHO-PLA. ^1H NMR (300 MHz, 25 °C, C_6D_6), δ (ppm): 5.06 (q, 2H, CHCH_3 PLA), 3.58 (m, 2H, COCH PCHO), 2.13 (m, 2H, COCHCH_2 PCHO), 1.36 (d, 6H, CHCH_3 PLA).

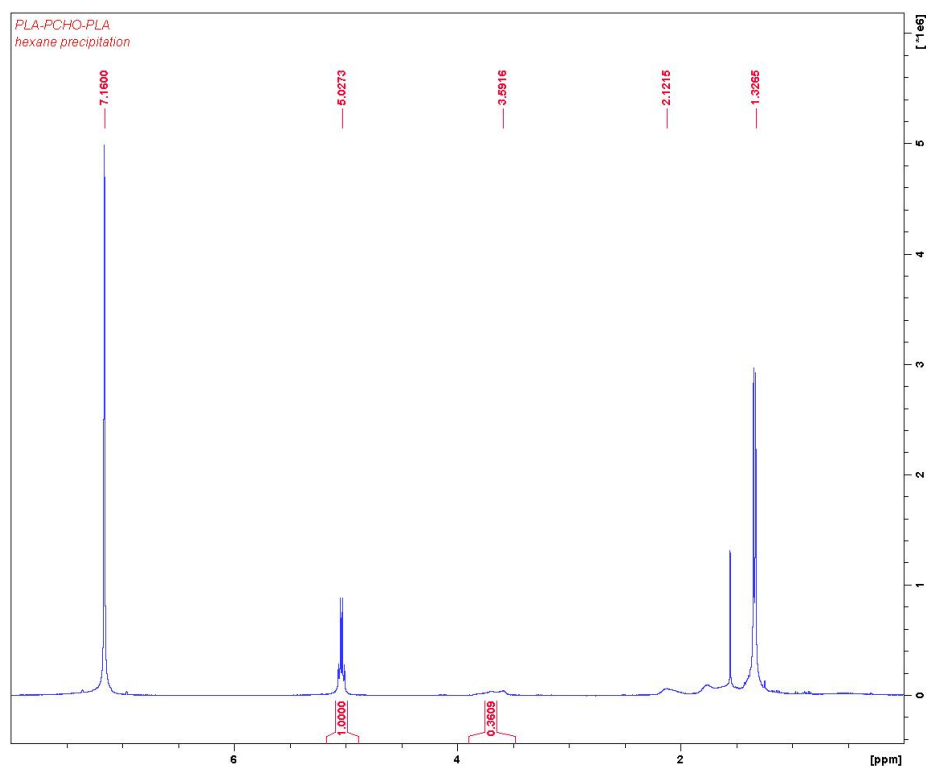


Figure B70. Table B3, entry 5. Hexanes precipitate from selective precipitation of PLA-PCHO-PLA. ^1H NMR (300 MHz, 25 °C, C_6D_6), δ (ppm): 5.03 (q, 2H, CHCH_3 PLA), 3.59 (m, 2H, COCH PCHO), 2.12 (m, 2H, COCHCH_2 PCHO), 1.33 (d, 6H, CHCH_3 PLA).

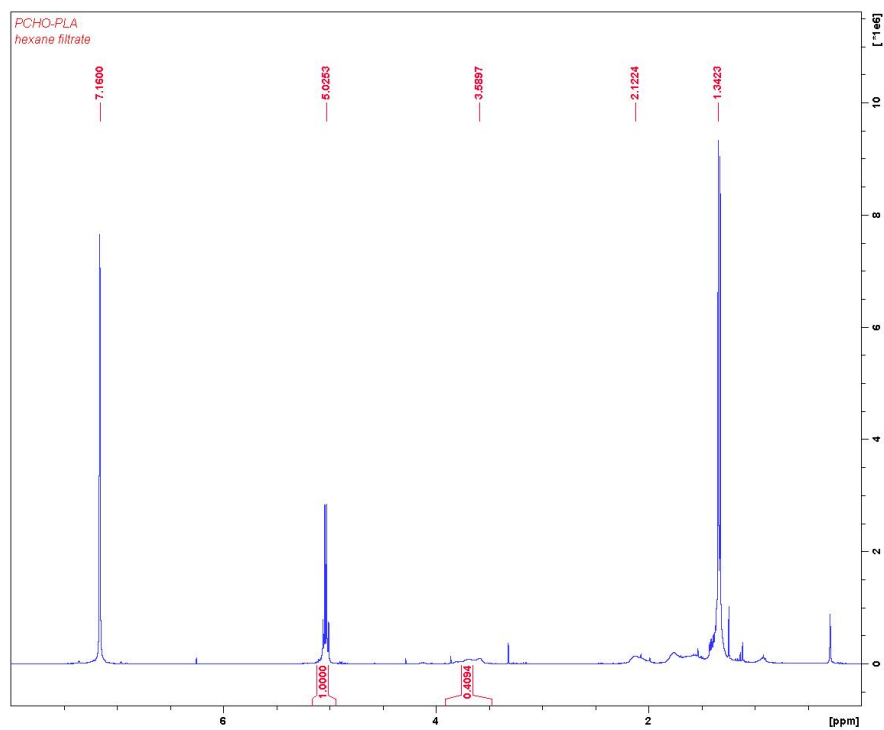


Figure B71. Table B4, entry 2. Acetone filtrate from selective precipitation of PCHO-PLA. ^1H NMR (300 MHz, 25 °C, C_6D_6), δ (ppm): 5.03 (q, 2H, CHCH_3 PLA), 3.58 (m, 2H, COCH PCHO), 2.12 (m, 2H, COCHCH_2 PCHO), 1.34 (d, 6H, CHCH_3 PLA).

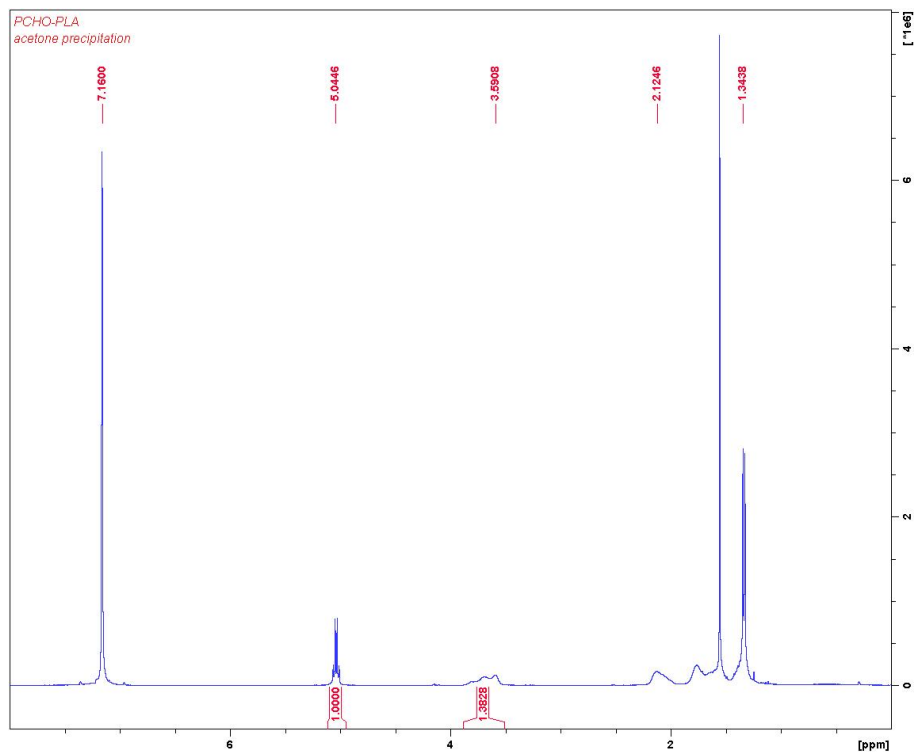


Figure B72. Table B4, entry 3. Acetone precipitate from selective precipitation of PCHO-PLA. ^1H NMR (300 MHz, 25 °C, C_6D_6), δ (ppm): 5.04 (q, 2H, CHCH_3 PLA), 3.59 (m, 2H, COCH PCHO), 2.12 (m, 2H, COCHCH_2 PCHO), 1.34 (d, 6H, CHCH_3 PLA).

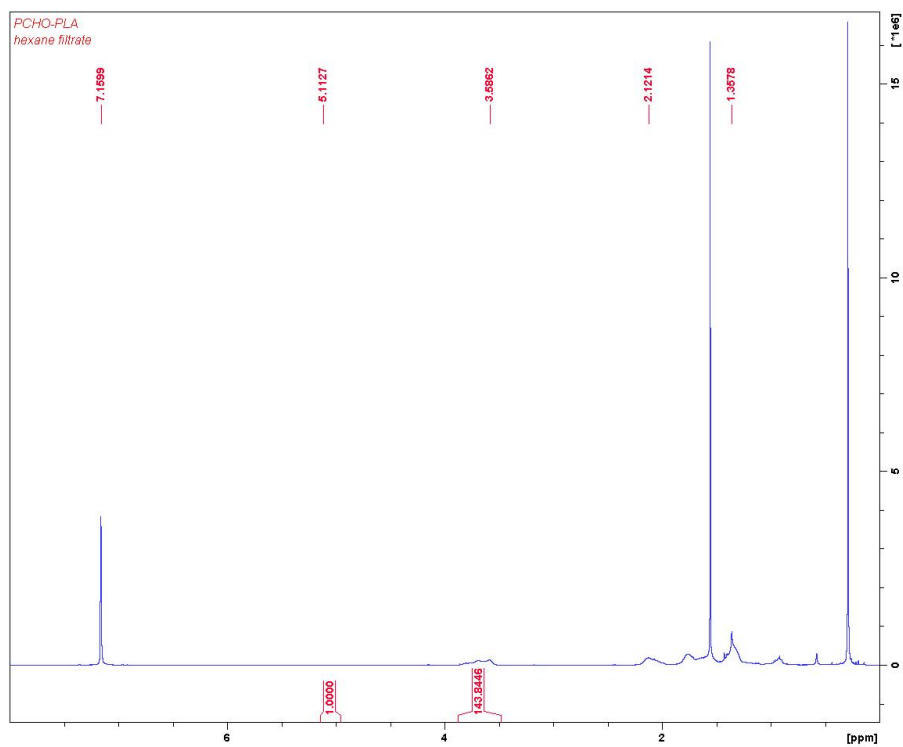


Figure B73. Table B4, entry 4. Hexanes filtrate from selective precipitation of PCHO-PLA. ^1H NMR (300 MHz, 25 °C, C_6D_6), δ (ppm): 5.11 (q, 2H, CHCH_3 PLA), 3.59 (m, 2H, COCH PCHO), 2.12 (m, 2H, COCHCH_2 PCHO), 1.36 (d, 6H, CHCH_3 PLA).

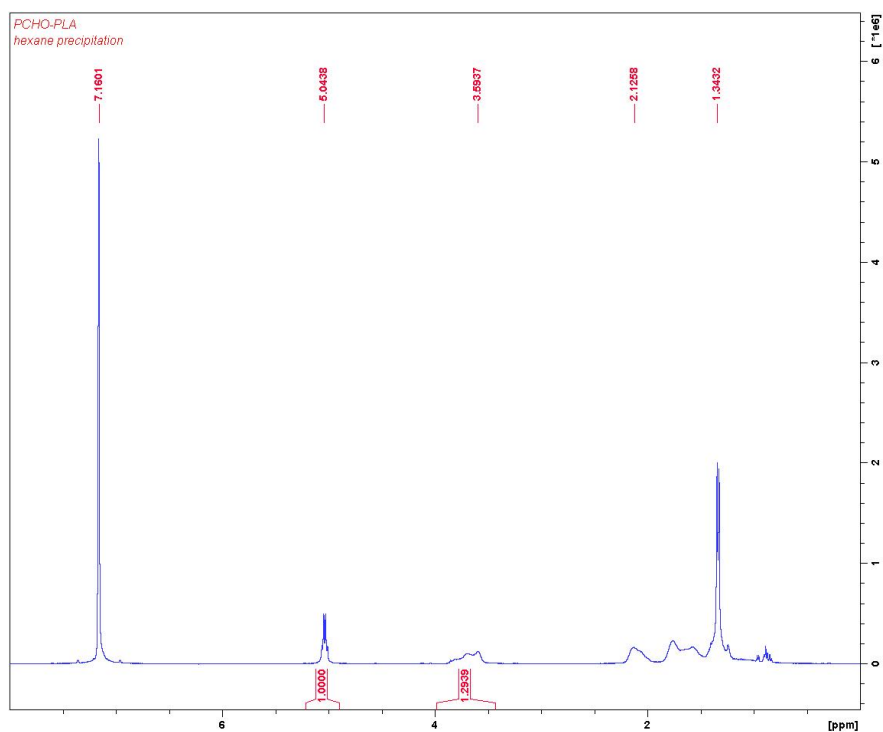


Figure B74. Table B4, entry 5. Hexanes precipitate from selective precipitation of PCHO-PLA. ^1H NMR (300 MHz, 25 °C, C_6D_6), δ (ppm): 5.03 (q, 2H, CHCH_3 PLA), 3.58 (m, 2H, COCH PCHO), 2.13 (m, 2H, COCHCH_2 PCHO), 1.34 (d, 6H, CHCH_3 PLA).

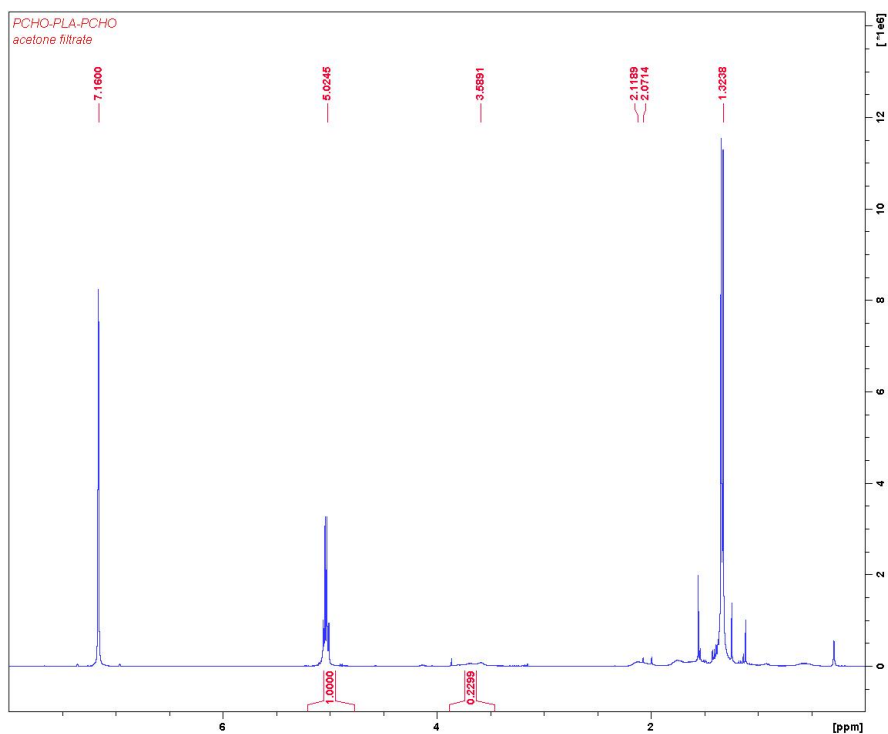


Figure B75. Table B5, entry 2. Acetone filtrate from selective precipitation of PCHO-PLA-PCHO. ^1H NMR (300 MHz, 25 °C, C_6D_6), δ (ppm): 5.02 (q, 2H, CHCH_3 PLA), 3.59 (m, 2H, COCH PCHO), 2.11-2.07 (m, 2H, COCHCH_2 PCHO), 1.33 (d, 6H, CHCH_3 PLA).

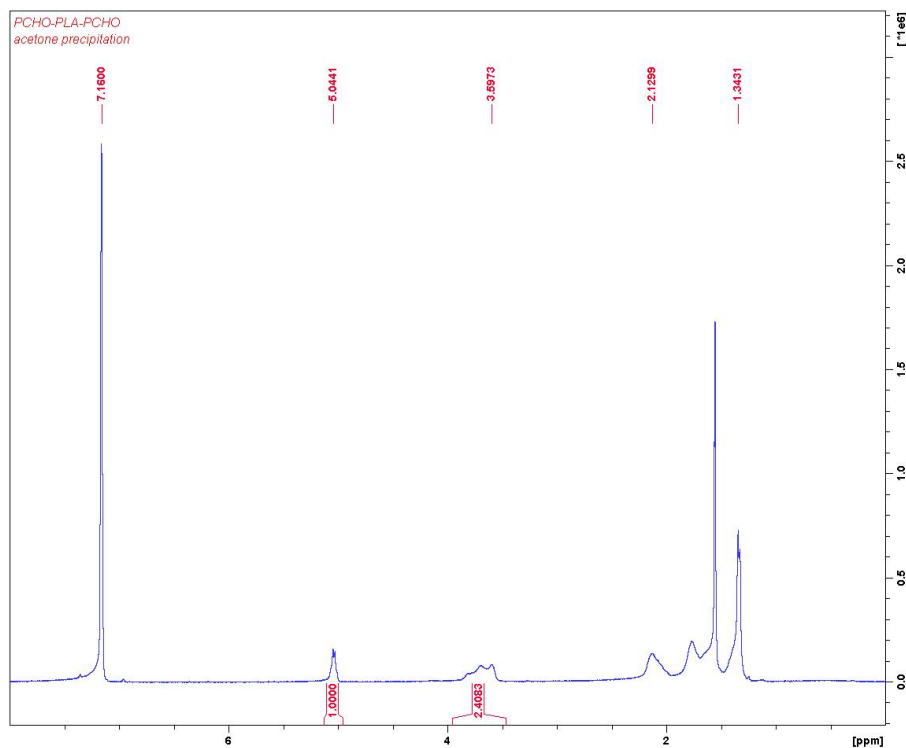


Figure B76. Table B5, entry 3. Acetone precipitate from selective precipitation of PCHO-PLA-PCHO. ^1H NMR (300 MHz, 25 °C, C_6D_6), δ (ppm): 5.04 (q, 2H, CHCH_3 PLA), 3.60 (m, 2H, COCH PCHO), 2.13 (m, 2H, COCHCH_2 PCHO), 1.34 (d, 6H, CHCH_3 PLA).

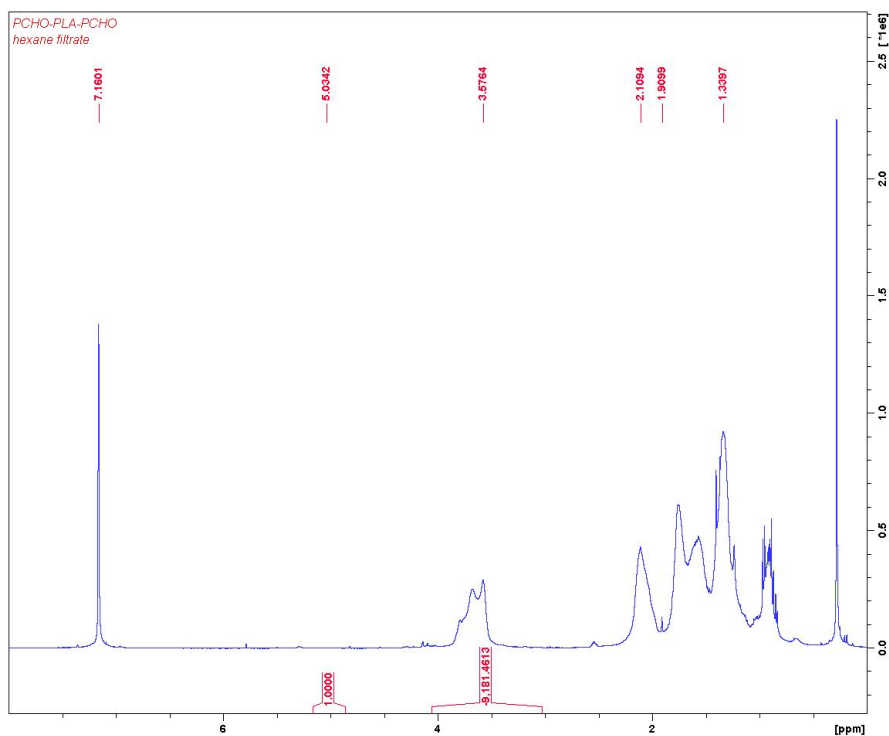


Figure B77. Table B5, entry 4. Hexanes filtrate from selective precipitation of PCHO-PLA-PCHO. ^1H NMR (300 MHz, 25 °C, C_6D_6), δ (ppm): 5.03 (q, 2H, CHCH_3 PLA), 3.58 (m, 2H, COCH PCHO), 2.11 (m, 2H, COCHCH_2 PCHO), 1.91 (m, 2H, COCHCH_2 PCHO), 1.34 (d, 6H, CHCH_3 PLA).

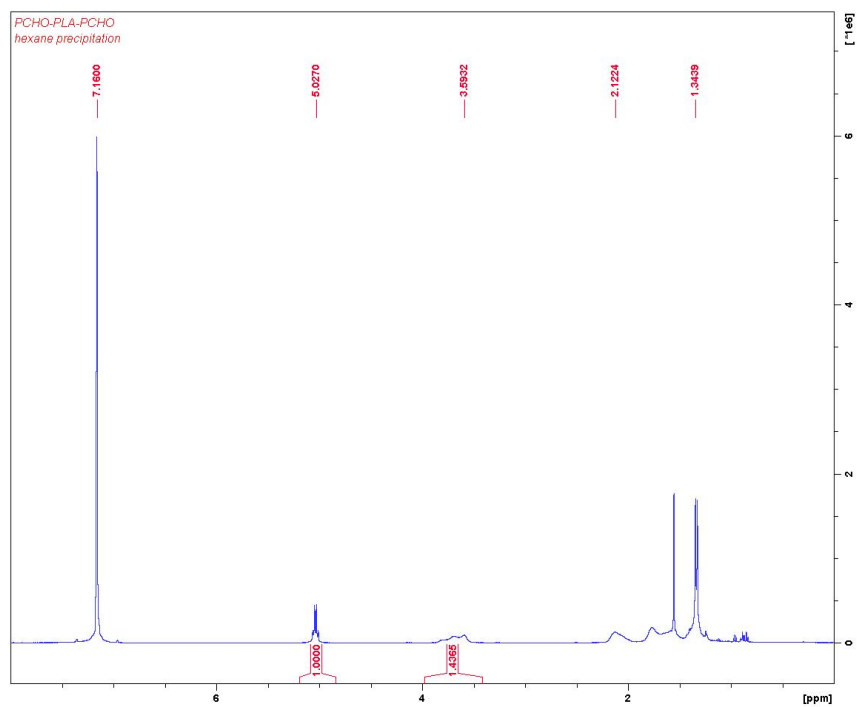


Figure B78. Table B5, entry 5. Hexanes precipitate from selective precipitation of PCHO-PLA-PCHO. ^1H NMR (300 MHz, 25 °C, C_6D_6), δ (ppm): 5.03 (q, 2H, CHCH_3 PLA), 3.59 (m, 2H, COCH PCHO), 2.12 (m, 2H, COCHCH_2 PCHO), 1.35 (d, 6H, CHCH_3 PLA).

DOSY Experiments

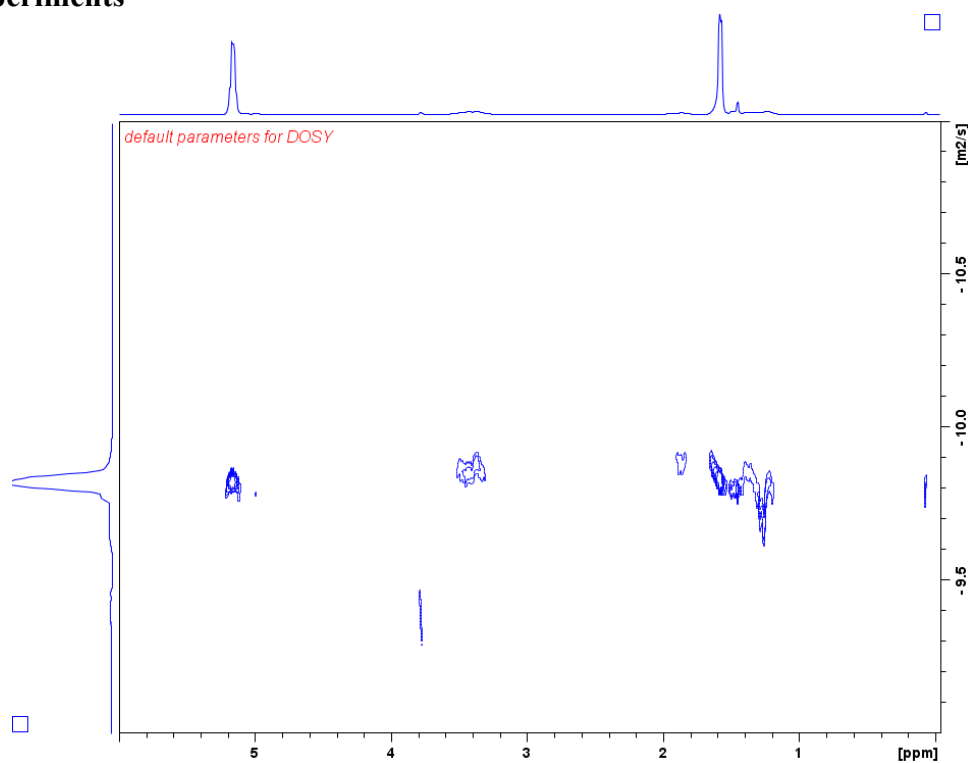


Figure B79. DOSY ¹H NMR (500 MHz, 25 °C, C₆D₆) spectrum of PLA and PCHO homopolymers; $D = 1.53 \times 10^{-10} \text{ m}^2 \text{ s}^{-1}$ (PLA) and $1.27 \times 10^{-10} \text{ m}^2 \text{ s}^{-1}$ (PCHO). Residual methanol at 3.8 ppm.

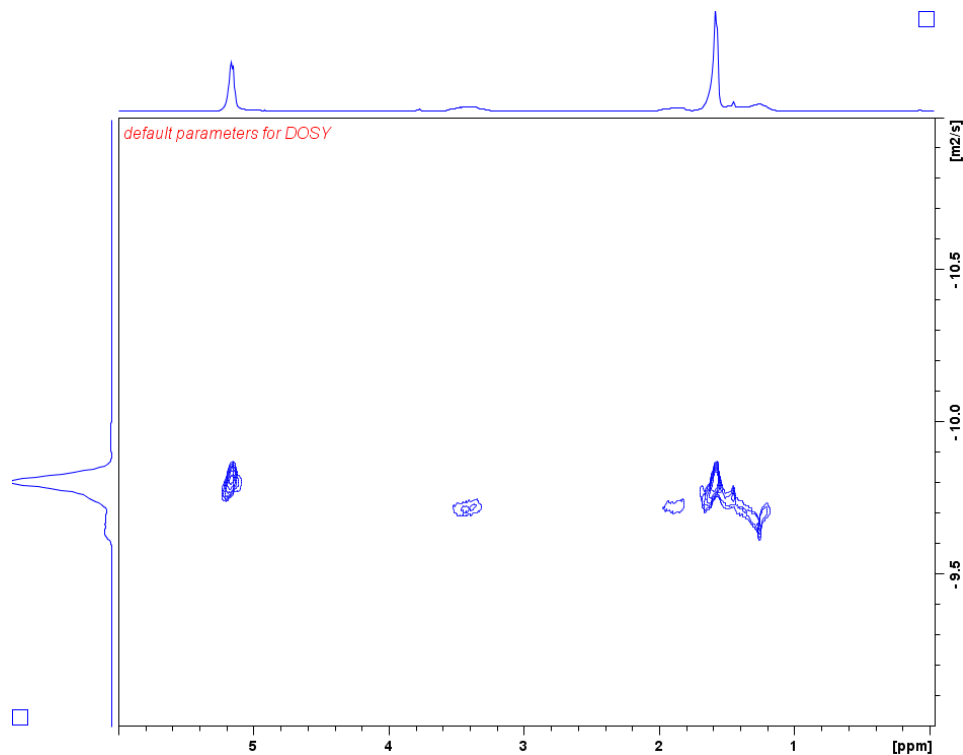


Figure B80. DOSY ¹H NMR (500 MHz, 25 °C, C₆D₆) spectrum of a PLA-PCHO diblock copolymer; $D = 1.76 \times 10^{-10} \text{ m}^2 \text{ s}^{-1}$.

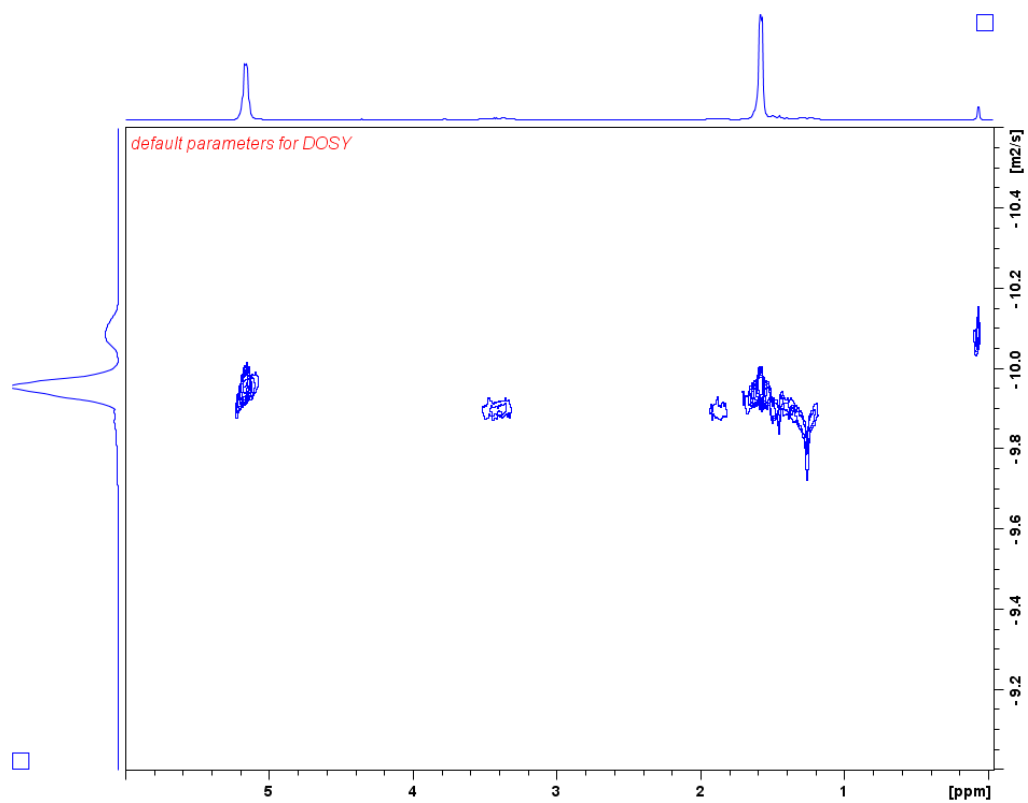


Figure B81. DOSY ^1H NMR (500 MHz, 25 $^\circ\text{C}$, C_6D_6) spectrum of a PLA-PCHO-PLA triblock copolymer; $D = 1.18 \times 10^{-10} \text{ m}^2\text{s}^{-1}$.

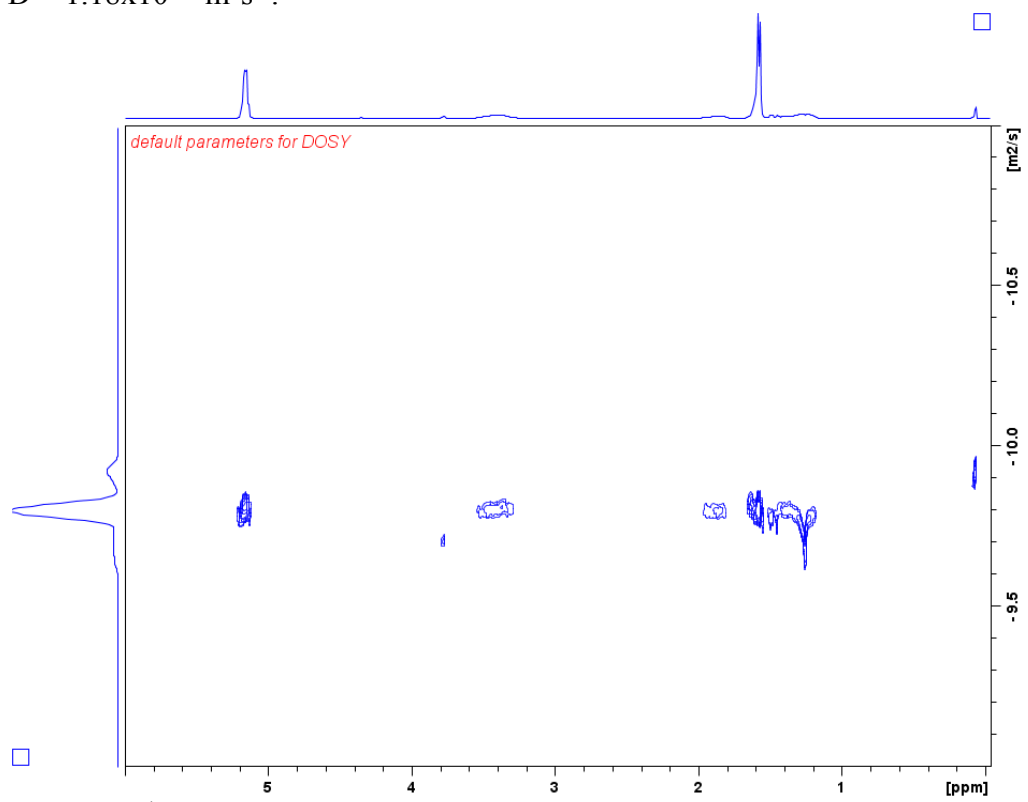


Figure B82. DOSY ^1H NMR (500 MHz, 25 $^\circ\text{C}$, C_6D_6) spectrum of PCHO-PLA diblock copolymer; $D = 1.57 \times 10^{-10} \text{ m}^2\text{s}^{-1}$.

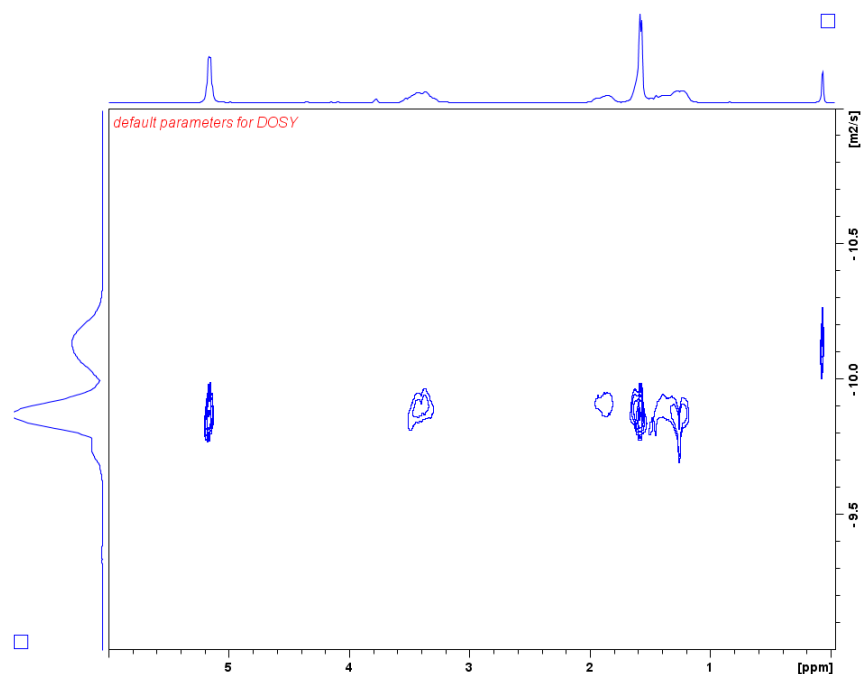


Figure B83. DOSY ^1H NMR (500 MHz, 25 °C, C_6D_6) spectrum of a PCHO-PLA-PCHO triblock copolymer; $D = 1.31 \times 10^{-10} \text{ m}^2 \text{ s}^{-1}$.

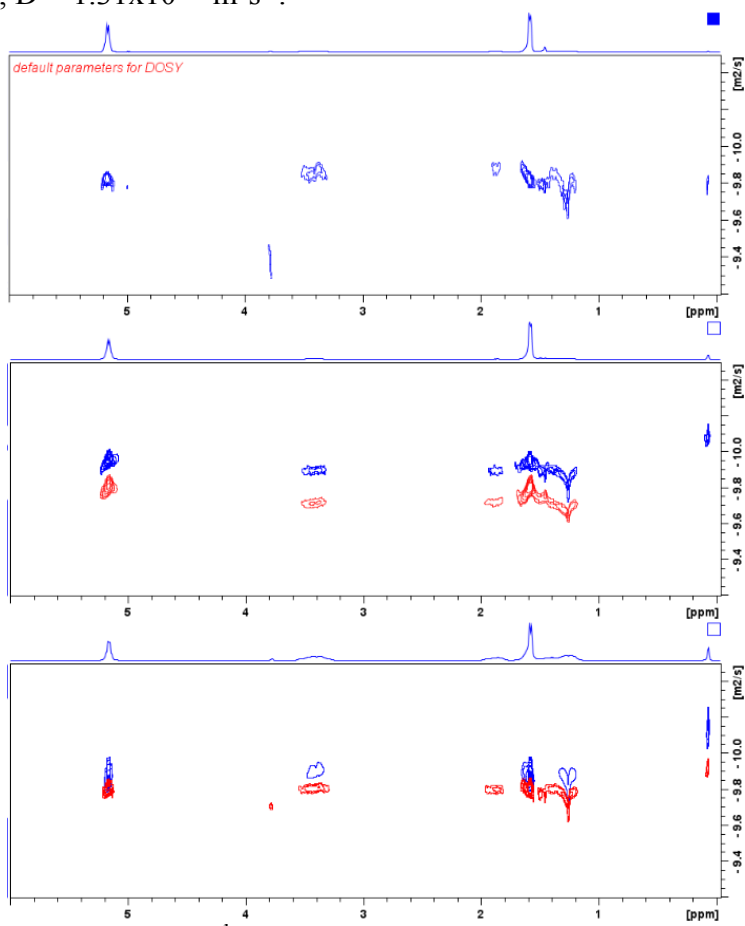


Figure B84. Comparison of DOSY ^1H NMR (500 MHz, 25 °C, C_6D_6). PLA, PCHO blend (top), PLA-CHO and PLA-PCHO-PLA (middle), PCHO-PLA and PCHO-PLA-PCHO (bottom).

Gel Permeation Chromatography (data from UCSB GPC or UCLA GPC-MALS)

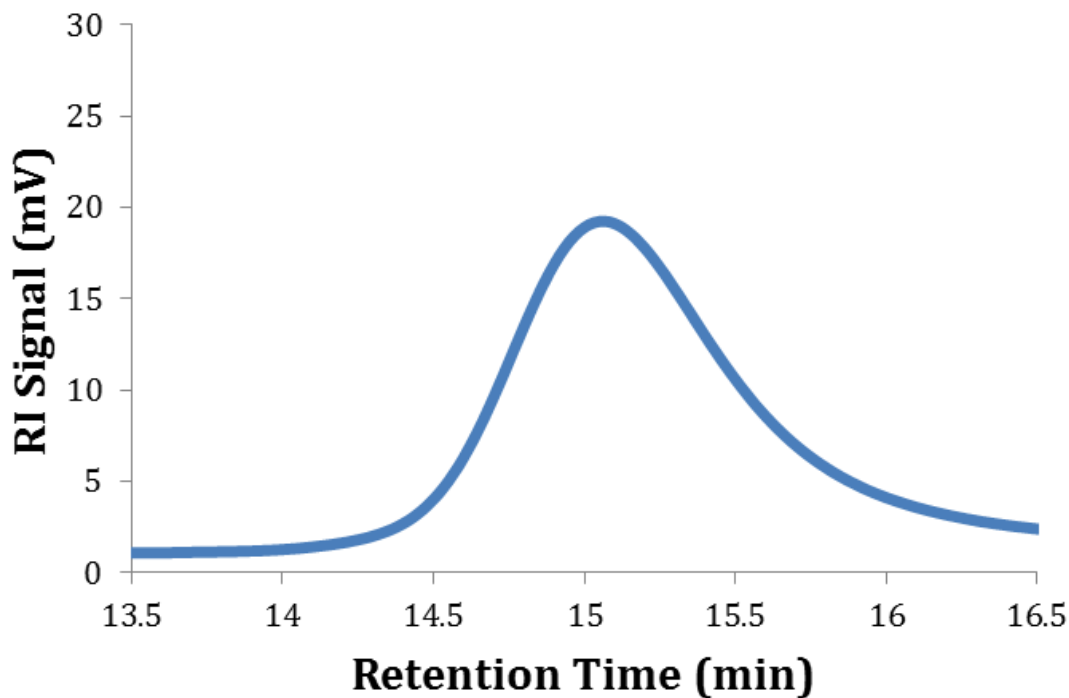


Figure B85. Table 2.2, entry 1: Polymerization of 100 equivalents of β -butyrolactone in the presence of 100 equivalents of cyclohexene oxide with initiator in the reduced state; $M_n = 9500$ Da, $M_w = 10800$ Da, $D = 1.13$.

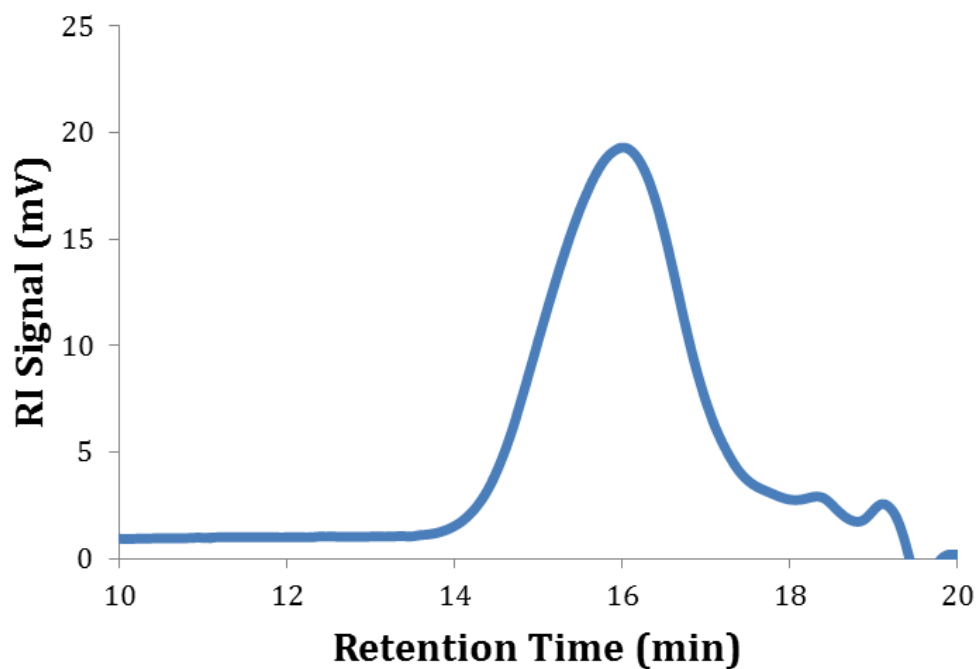


Figure B86. Table 2.2, entry 2: Polymerization of 100 equivalents of cyclohexene oxide in the presence of 100 equivalents of β -butyrolactone with initiator in the reduced state and subsequently oxidized; $M_n = 3900$ Da, $M_w = 6000$ Da, $D = 1.54$.

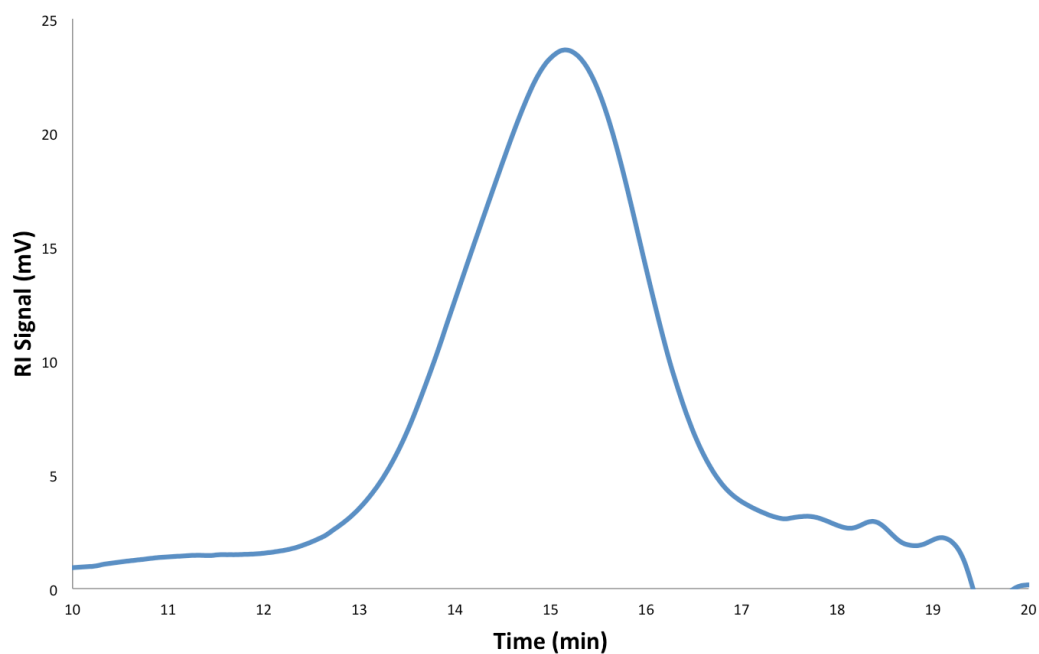


Figure B87. Table 2.2, entry 3: Polymerization of 100 equivalents of β -butyrolactone in the presence of 100 equivalents of cyclohexene oxide with initiator in the oxidized state; $M_n = 8300$ Da, $M_w = 12600$ Da, $D = 1.51$.

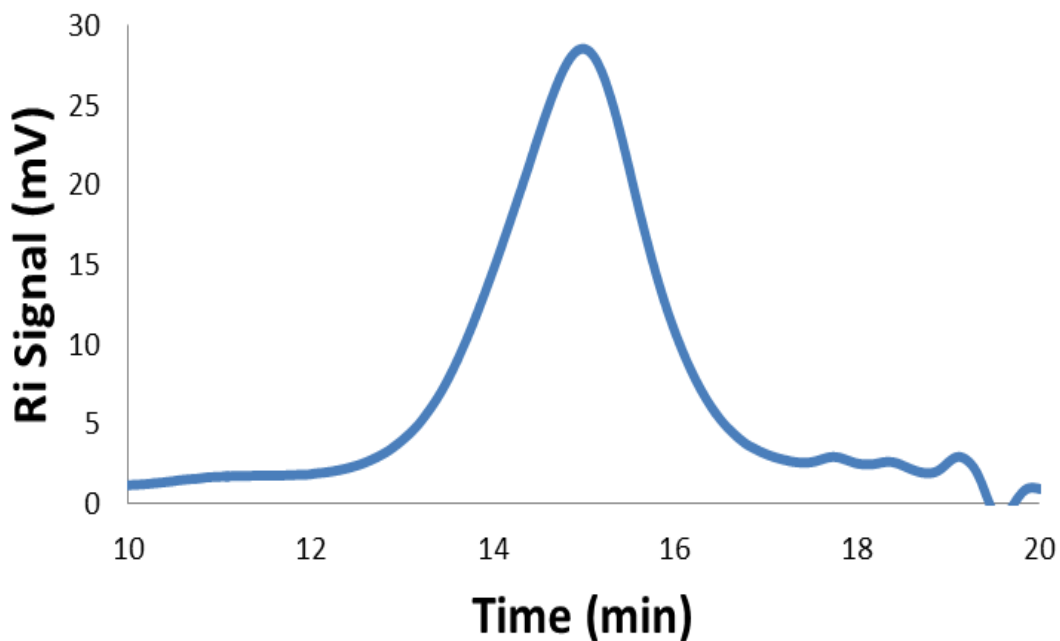


Figure B88. Table 2.2, entry 4: Polymerization of 100 equivalents of β -butyrolactone in the presence of 100 equivalents of cyclohexene oxide with initiator in the oxidized state and subsequently reduced; $M_n = 9700$ Da, $M_w = 15000$ Da, $D = 1.55$.

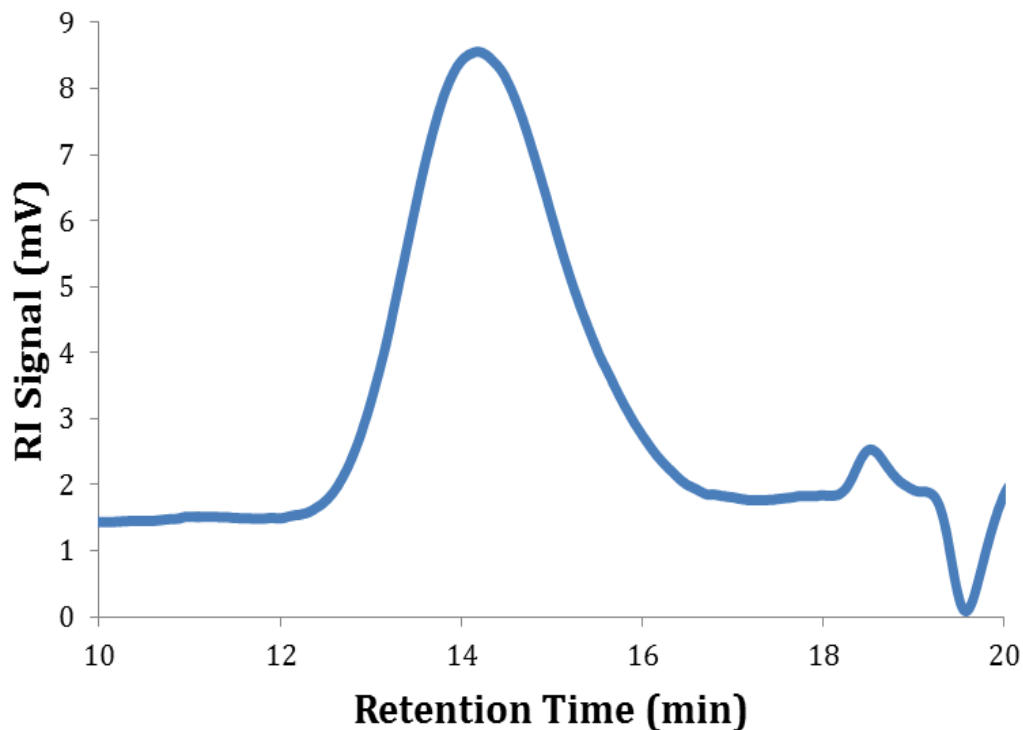


Figure B89. Table 2.2, entry 6: Polymerization of 100 equivalents of propylene oxide in the presence of 100 equivalents of L-lactide with initiator in the oxidized state and subsequently reduced; $M_n = 16400$ Da, $M_w = 27000$ Da, $D = 1.65$.

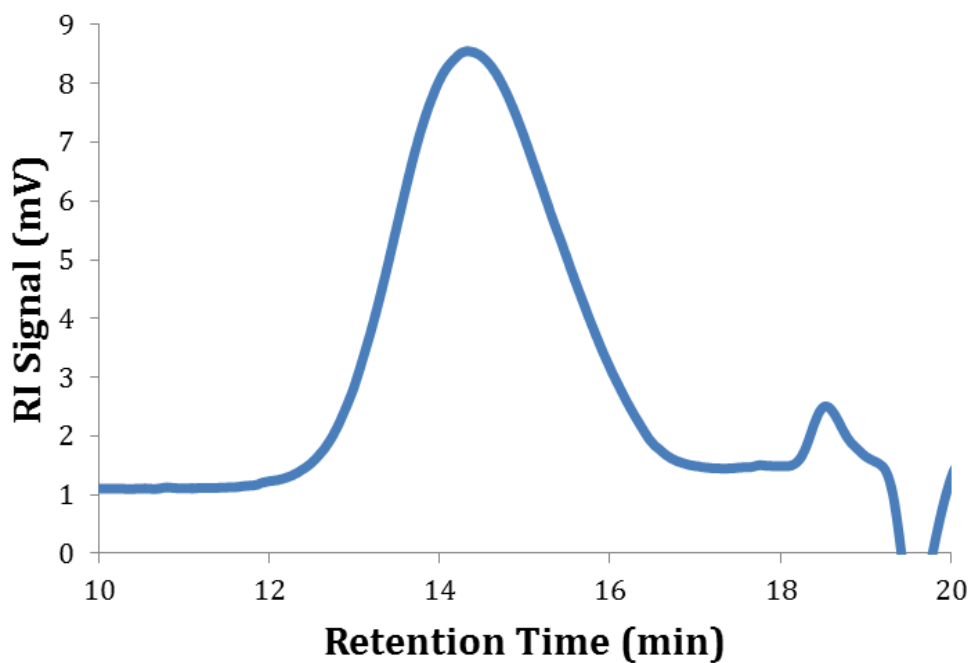


Figure B90. Table 2.2, entry 8: Polymerization of 100 equivalents of L-lactide in the presence of 100 equivalents of oxetane with initiator in the oxidized state and subsequently reduced; $M_n = 14100$ Da, $M_w = 23300$ Da, $D = 1.66$.

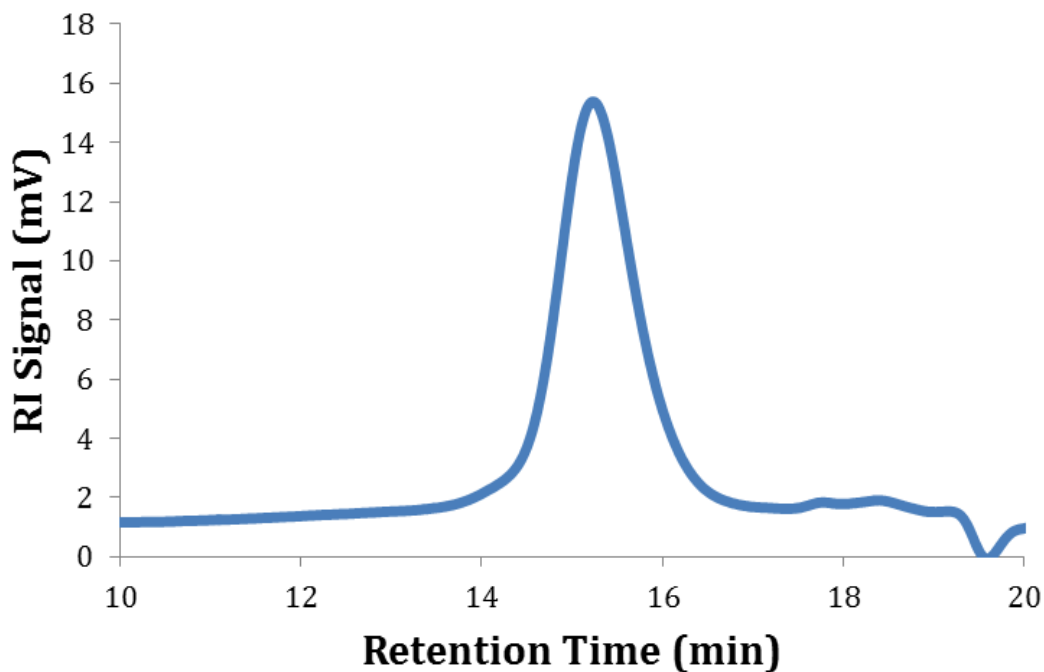


Figure B91. Table 2.2, entry 9: Polymerization of 100 equivalents of L-lactide in the presence of 100 equivalents of cyclohexene oxide with initiator in the reduced state; $M_n = 7900$ Da, $M_w = 9200$ Da, $D = 1.15$.

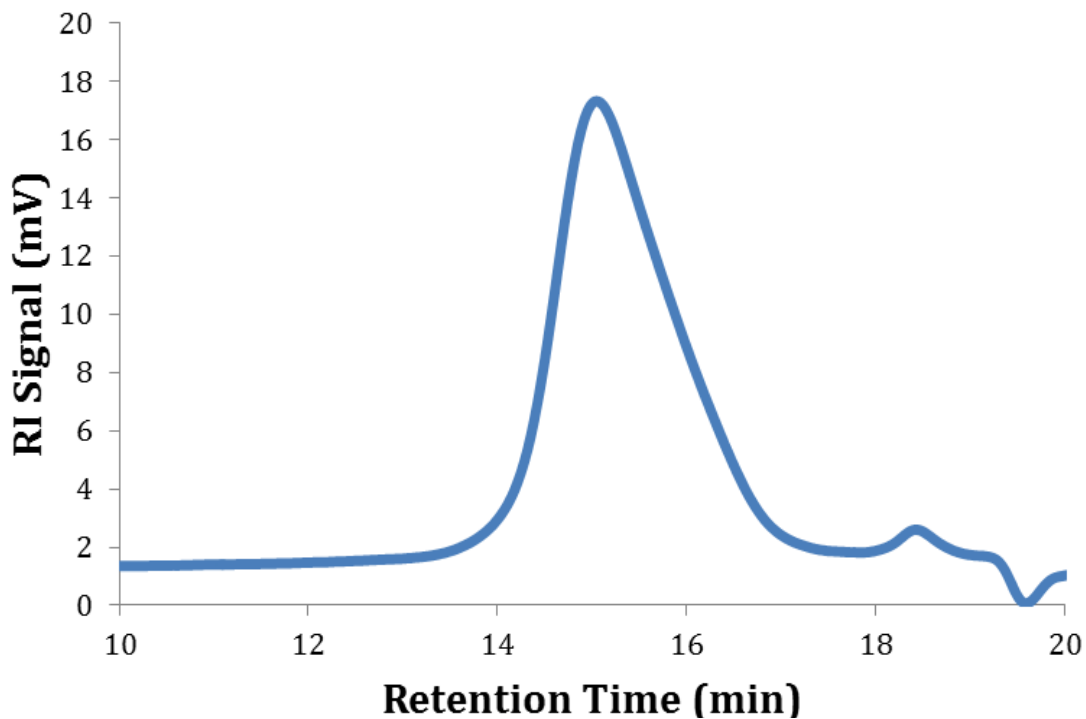


Figure B92. Table 2.2, entry 10: Polymerization of 100 equivalents of cyclohexene oxide in the presence of 100 equivalents of L-lactide with initiator in the reduced state and subsequently oxidized; $M_n = 7600$ Da, $M_w = 9900$ Da, $D = 1.30$.

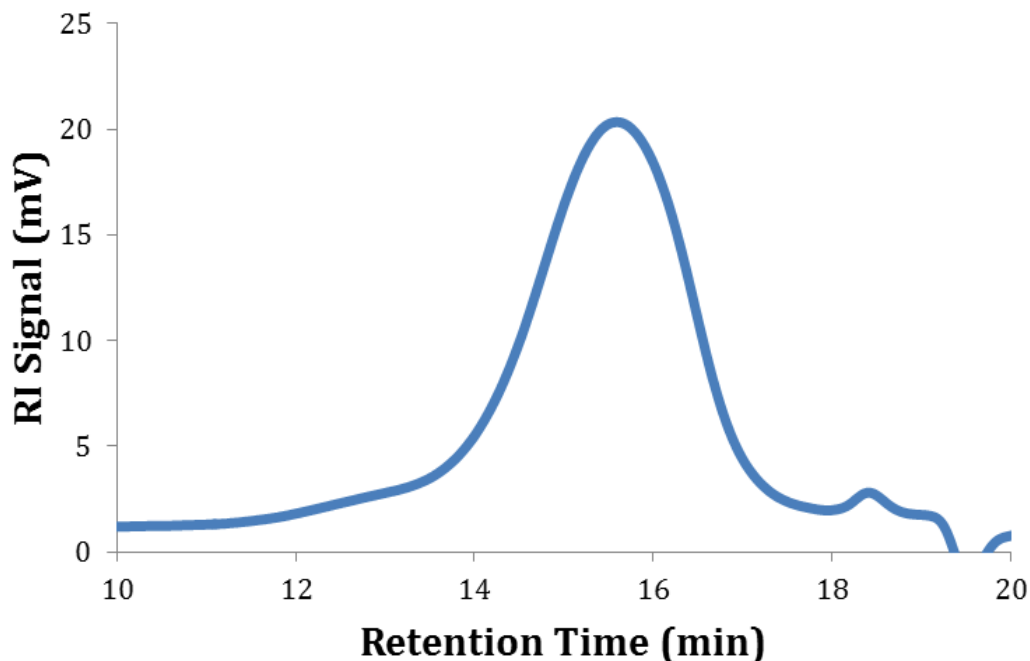


Figure B93. Table 2.2, entry 11: Polymerization of 100 equivalents of cyclohexene oxide in the presence of 100 equivalents of L-lactide with initiator in the oxidized state; $M_n = 5500$ Da, $M_w = 8500$ Da, $\mathcal{D} = 1.54$.

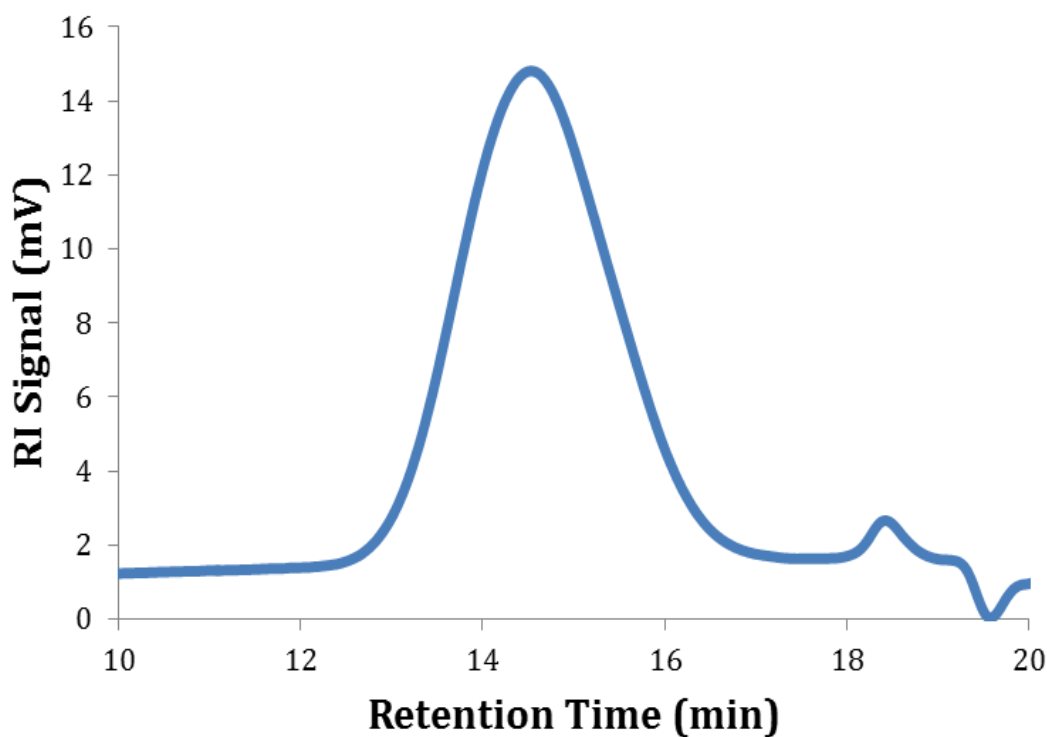


Figure B94. Table 2.2, entry 12: Polymerization of 100 equivalents of L-lactide in the presence of 100 equivalents of cyclohexene oxide with initiator in the oxidized state and subsequently reduced; $M_n = 12300$ Da, $M_w = 17800$ Da, $\mathcal{D} = 1.44$.

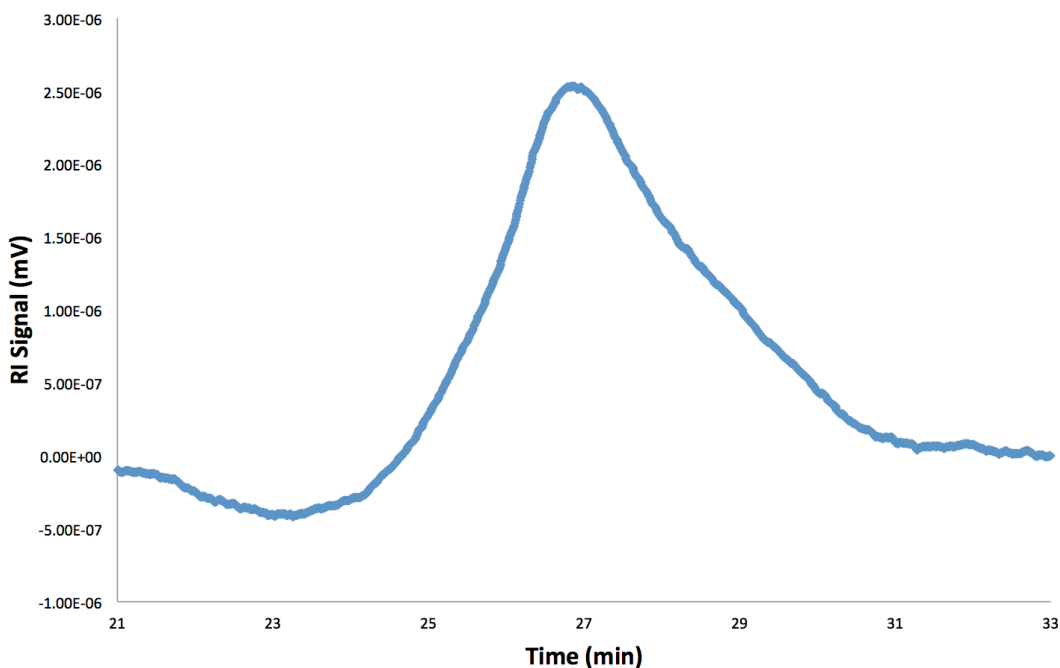


Figure B95. Table 2.4, entry 1. Table B1, entry 2. Table B2, entry 1: Polymerization of 100 equivalents of L-lactide and cyclohexene oxide, monomers added sequentially, using initiator redox switch “red-ox”; $M_n = 11400$ Da, $M_w = 15000$ Da, $D = 1.32$. Taken on GPC-MALS.

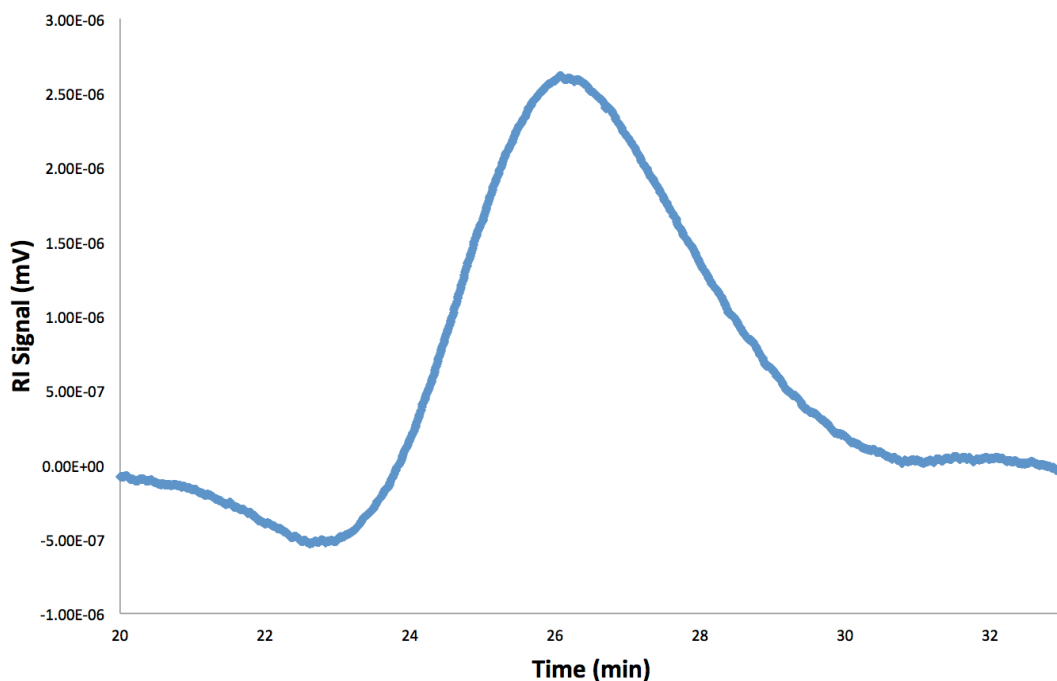


Figure B96. Table 2.4, entry 2. Table B1, entry 3. Table B3, entry 1: Polymerization of 100 equivalents of L-Lactide, cyclohexene oxide, and L-lactide, monomers added sequentially, using initiator redox switch “red-ox-red”; $M_n = 16900$ Da, $M_w = 21200$ Da, $D = 1.25$. Taken on GPC-MALS.

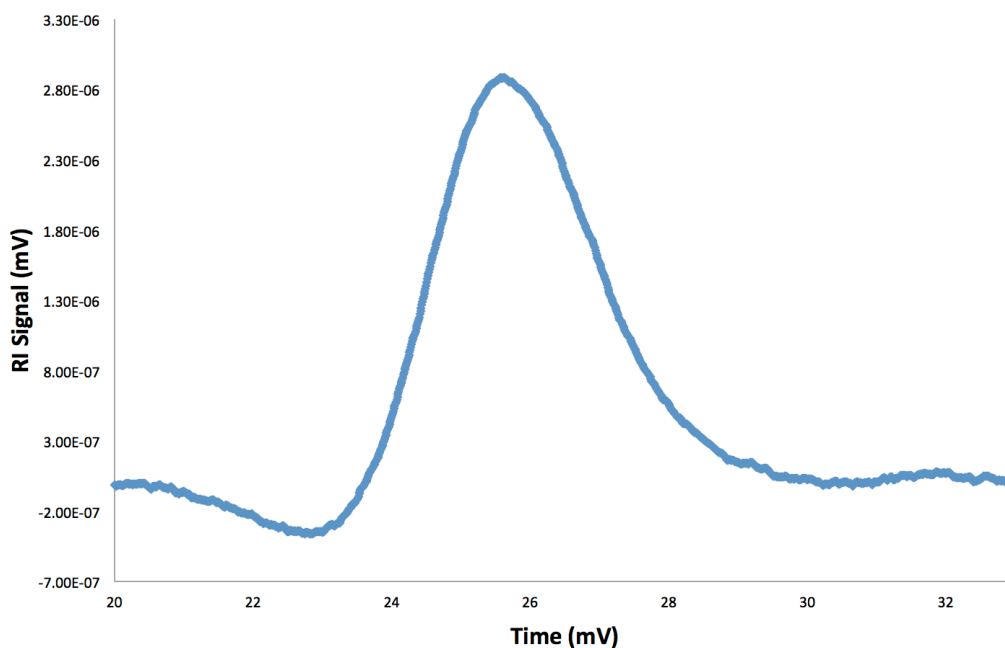


Figure B97. Table 2.4, entry 3. Table B1, entry 5. Table B4, entry 1: Polymerization of 100 equivalents of L-lactide, cyclohexene oxide, monomers added sequentially, using initiator redox switch “ox-red”; $M_n = 13900$ Da, $M_w = 23000$ Da, $D = 1.66$. Taken on GPC-MALS.

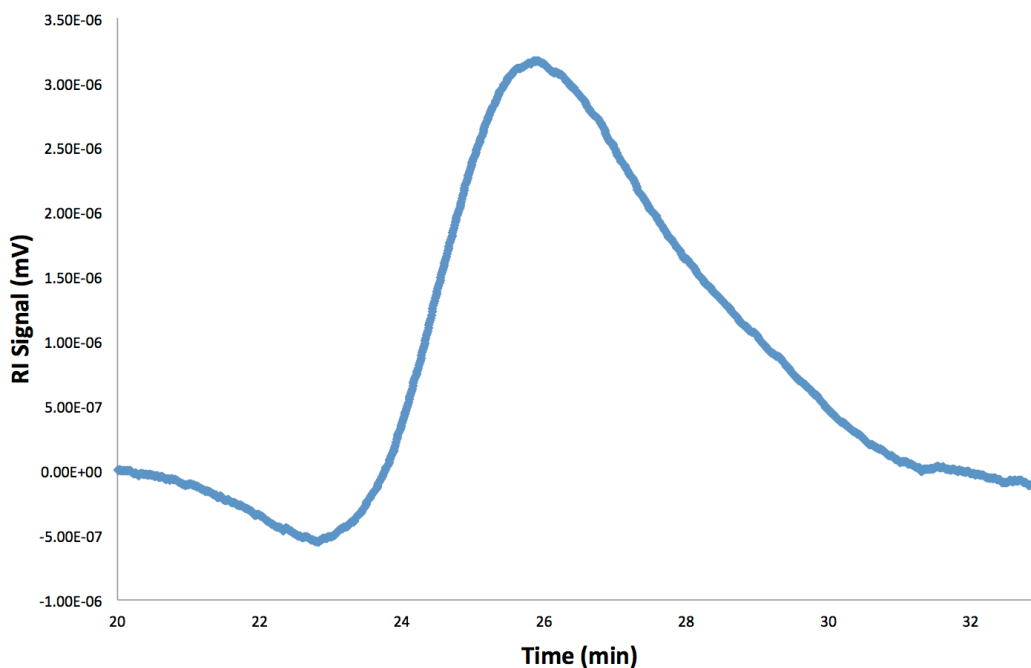


Figure B98. Table 2.4, entry 4. Table B1, entry 6. Table B5, entry 1: Polymerization of 100 equivalents of cyclohexene oxide, L-lactide, and cyclohexene oxide, monomers added sequentially, using initiator redox switch “ox-red-ox”; $M_n = 13300$ Da, $M_w = 20400$ Da, $D = 1.53$. Taken on GPC-MALS.

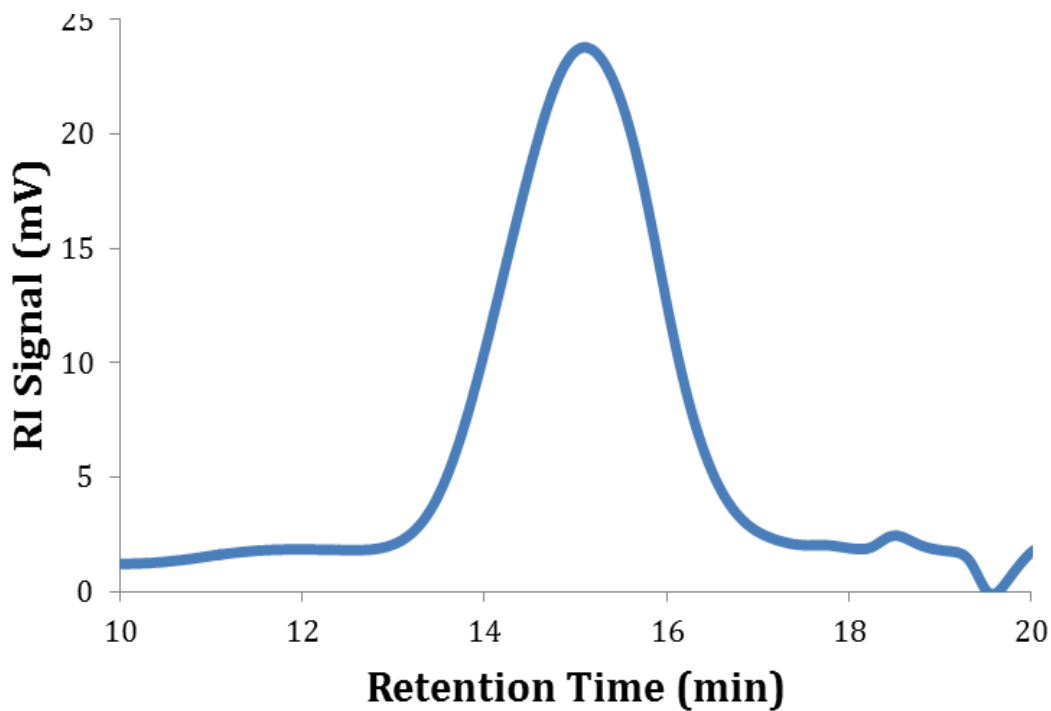


Figure B99. Table 2.4, entry 5: Polymerization of 100 equivalents of cyclohexene oxide, L-lactide, and propylene oxide, monomers added sequentially, using initiator redox switch “ox-red-ox”; $M_n = 9000$ Da, $M_w = 13800$ Da, $D = 1.54$.

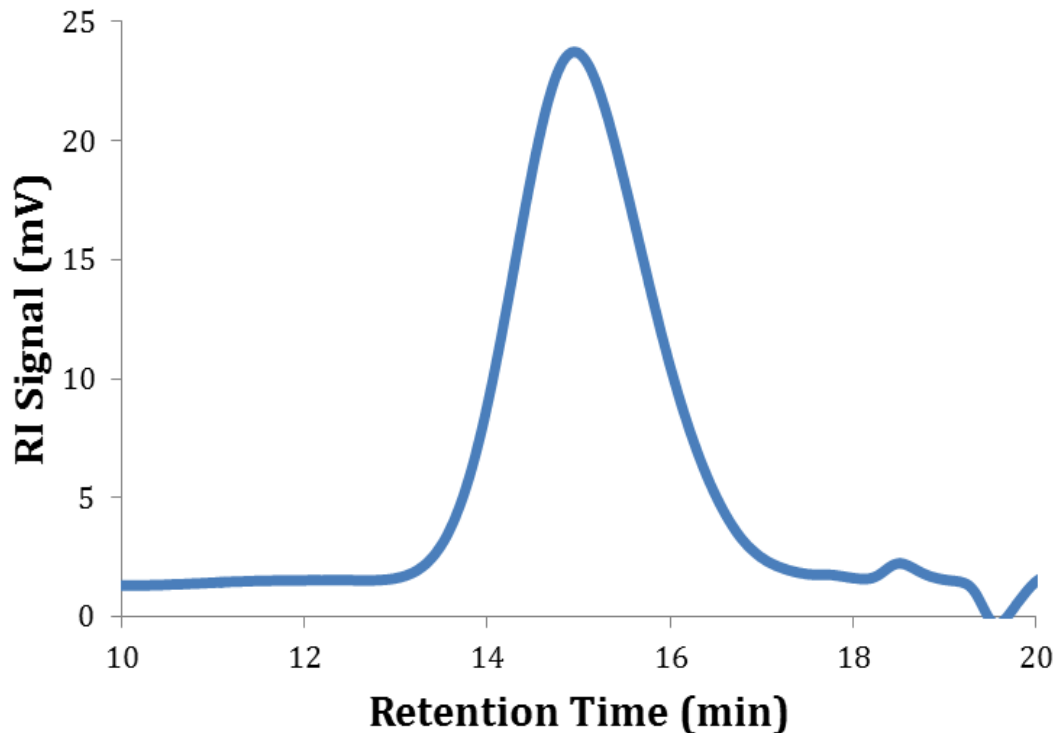


Figure B100. Table 2.4, entry 6: Polymerization of 100 equivalents of L-lactide, cyclohexene oxide, and β -butyrolactone, monomers added sequentially, using initiator redox switch “red-ox-red”; $M_n = 8900$ Da, $M_w = 13500$ Da, $D = 1.51$.

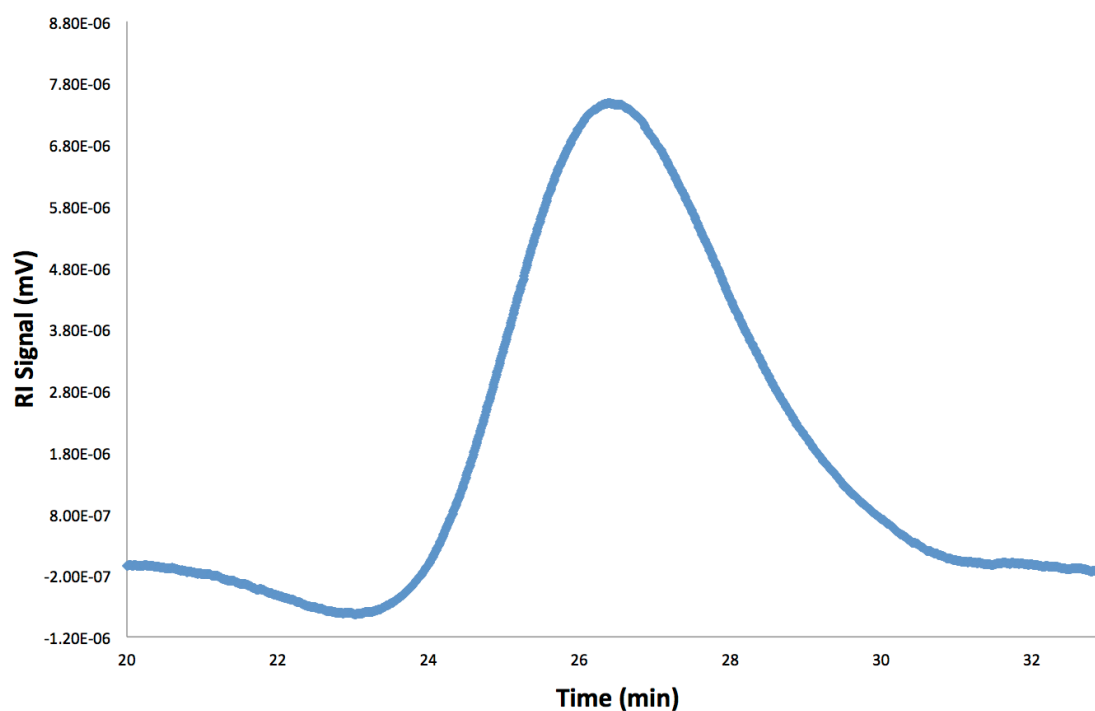


Figure B101. Polymerization of 100 equivalents of cyclohexene oxide by $[\text{H}_2(\text{salfan})][\text{BAr}^{\text{F}}]$; $M_n = 12900$ Da, $M_w = 17900$ Da, $D = 1.39$. Taken on GPC-MALS.

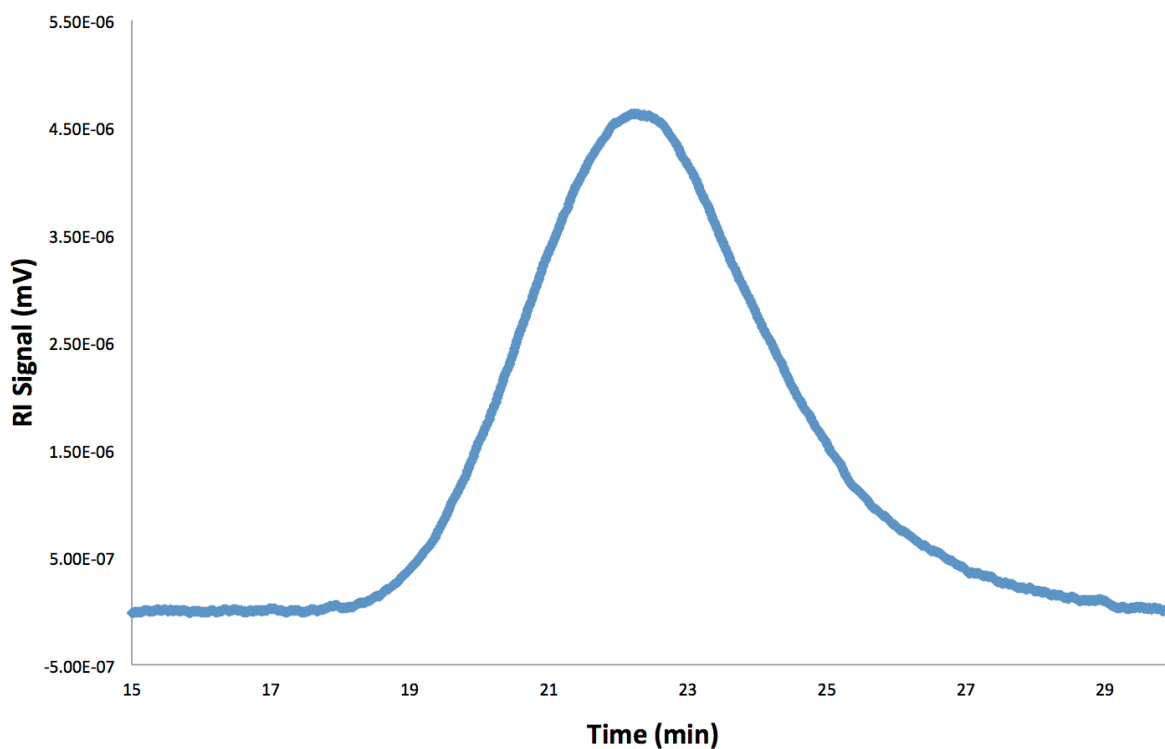


Figure B102. Polymerization of 100 equivalents of cyclohexene oxide by $^{\text{Ac}}\text{FcBAr}^{\text{F}}$; $M_n = 111400$ Da, $M_w = 158200$ Da, $D = 1.42$. Taken on GPC-MALS.

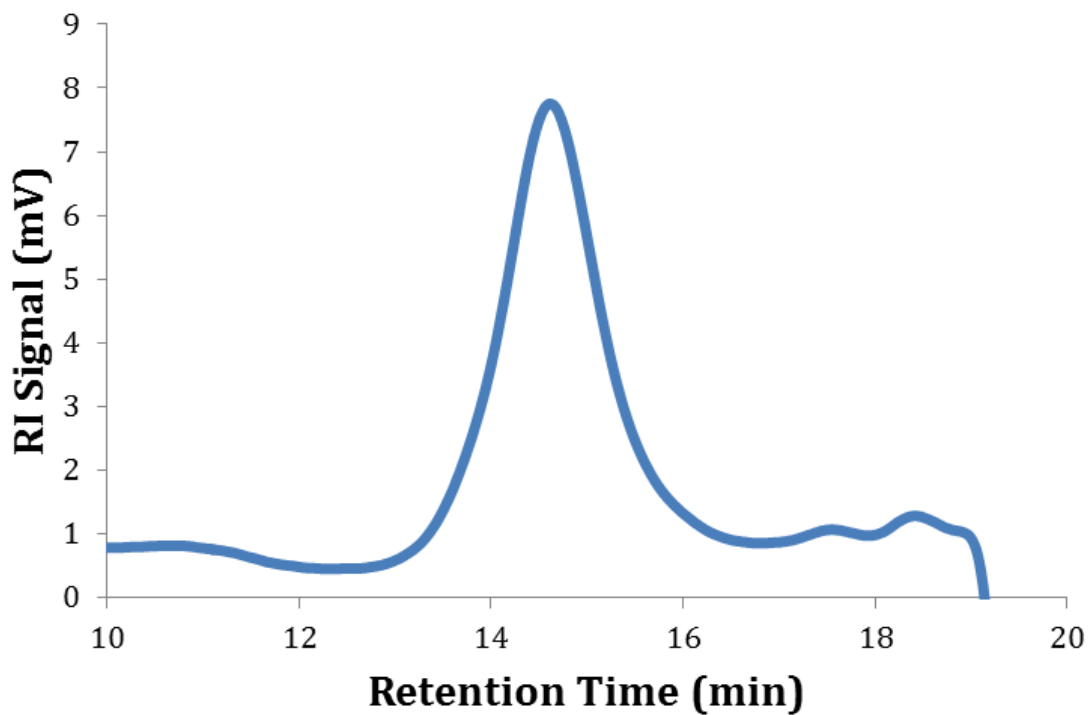


Figure B103. Table B1, entry 1: Polymerization of 100 equivalents of L-lactide with the initiator in the reduced state; $M_n = 12200$ Da, $M_w = 15900$ Da, $D = 1.30$.

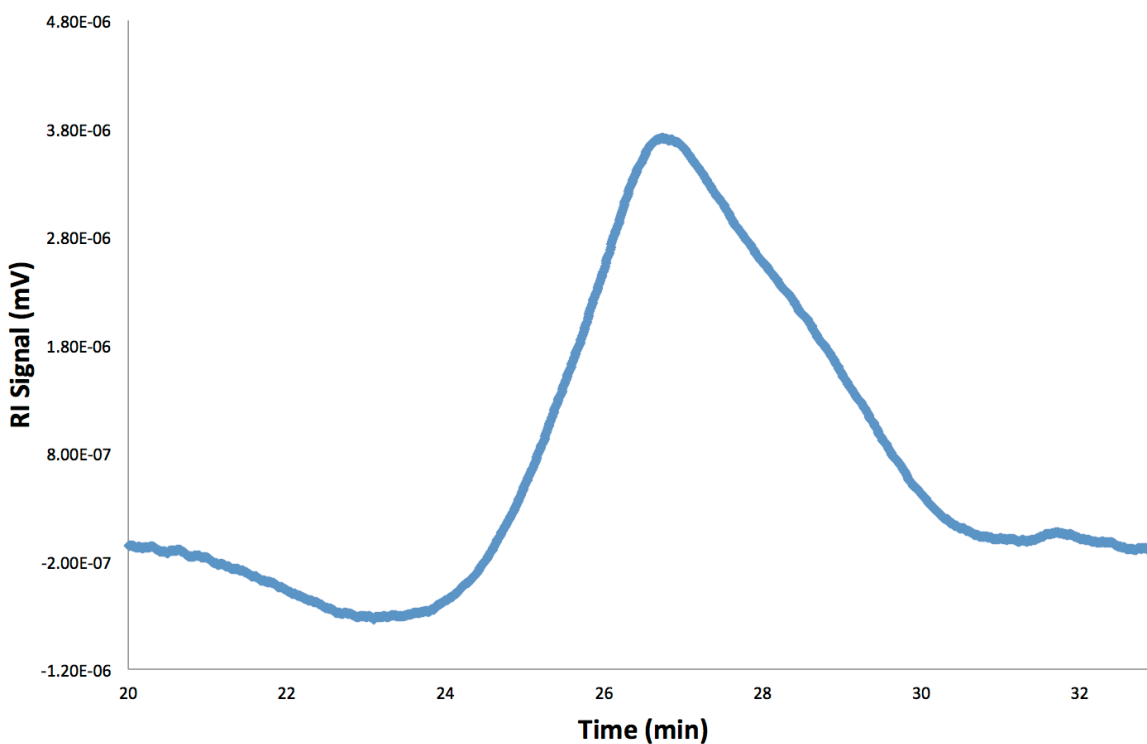


Figure B104. Table B2, entry 3: Acetone precipitate from selective precipitation of PLA-PCHO; $M_n = 12900$ Da, $M_w = 17200$ Da, $D = 1.33$. Taken on GPC-MALS.

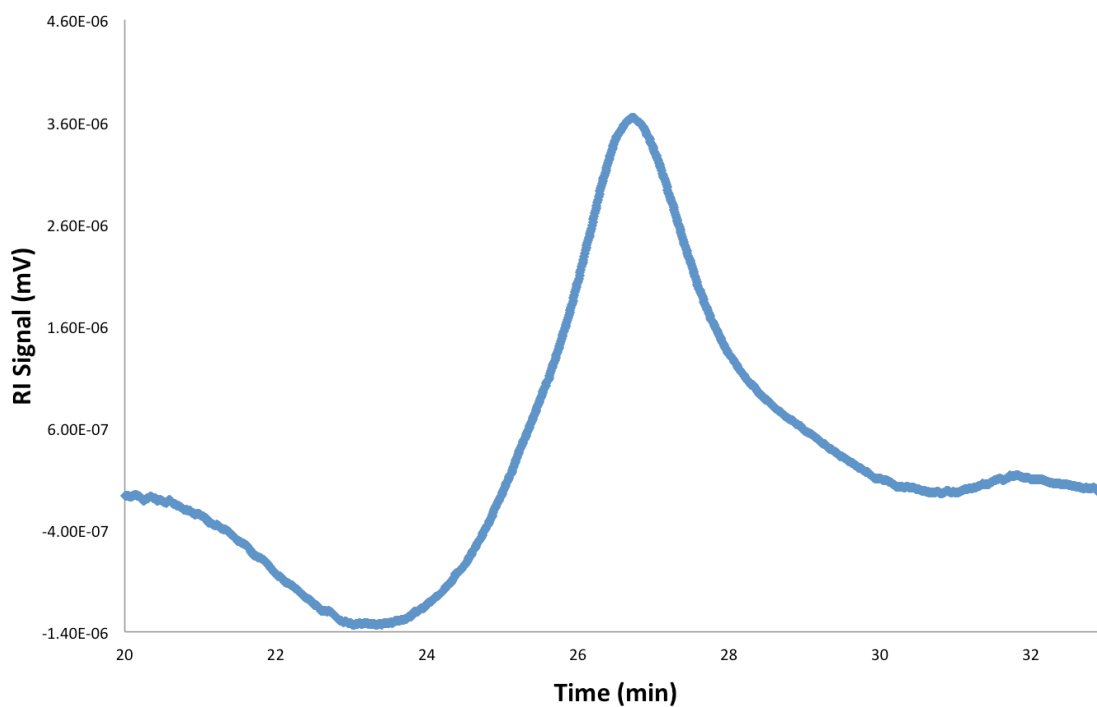


Figure B105. Table B2, entry 5: Hexanes precipitate from selective precipitation of PLA-PCHO; $M_n = 12800$ Da, $M_w = 16000$ Da, $D = 1.25$. Taken on GPC-MALS.

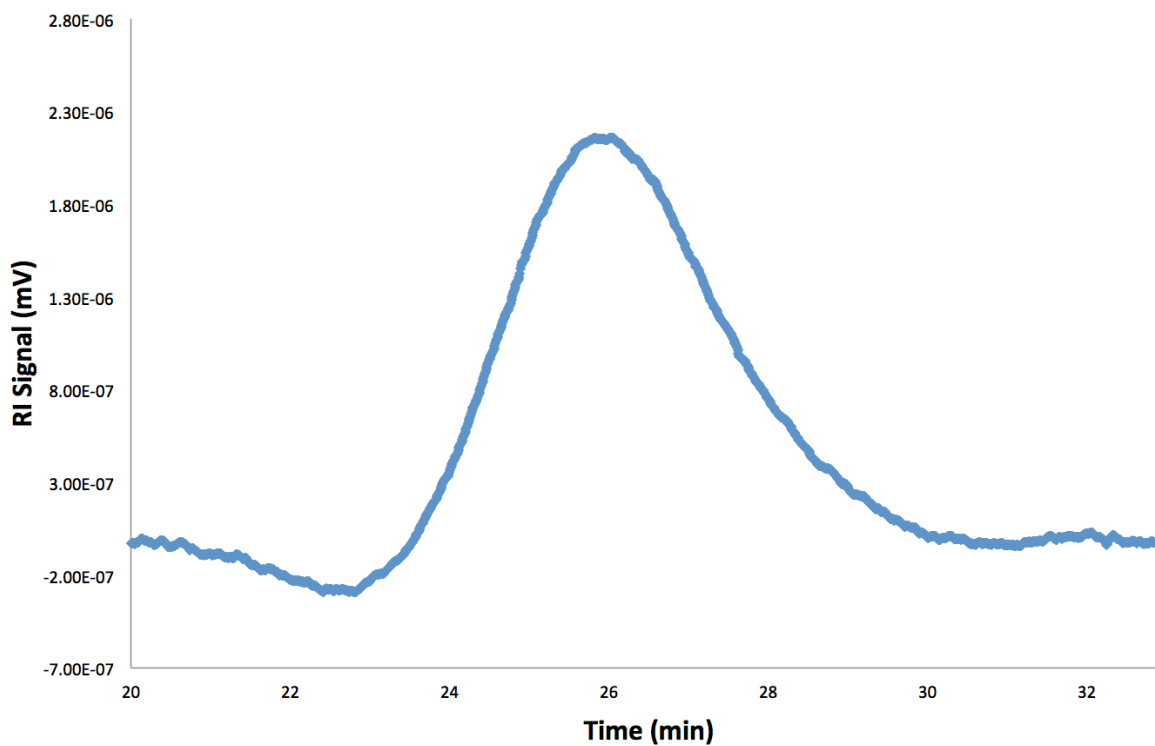


Figure B106. Table B3, entry 3: Acetone precipitate from selective precipitation of PLA-PCHO-PLA; $M_n = 17400$ Da, $M_w = 21400$ Da, $D = 1.23$. Taken on GPC-MALS.

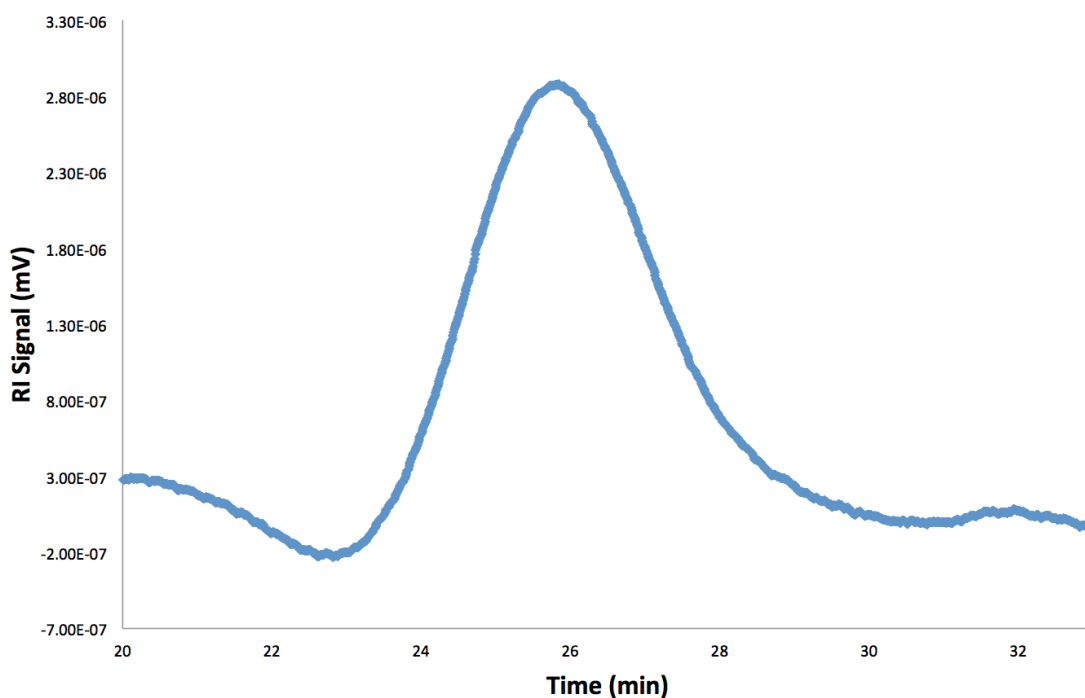


Figure B107. Table B3, entry 5: Hexanes precipitate from selective precipitation of PLA-PCHO-PLA; $M_n = 18100$ Da, $M_w = 25000$ Da, $\mathcal{D} = 1.38$. Taken on GPC-MALS.

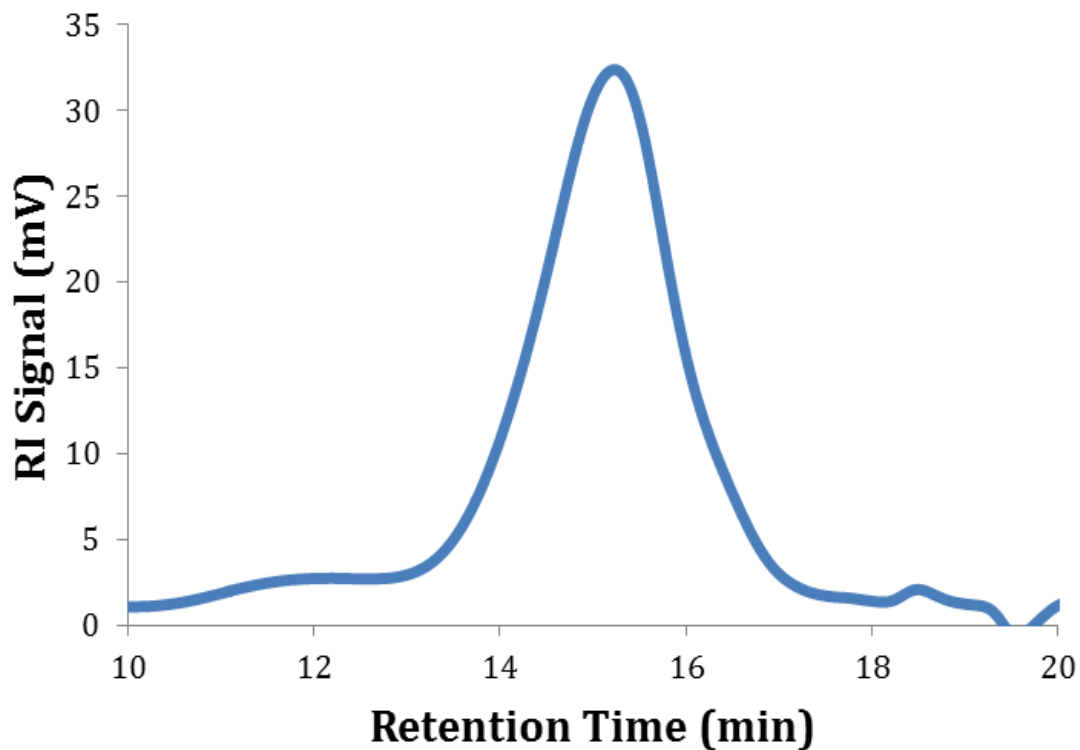


Figure B108. Table B1, entry 4: Polymerization of 100 equivalents of cyclohexene oxide with the initiator in the oxidized state; $M_n = 4000$ Da, $M_w = 5600$ Da, $\mathcal{D} = 1.38$.

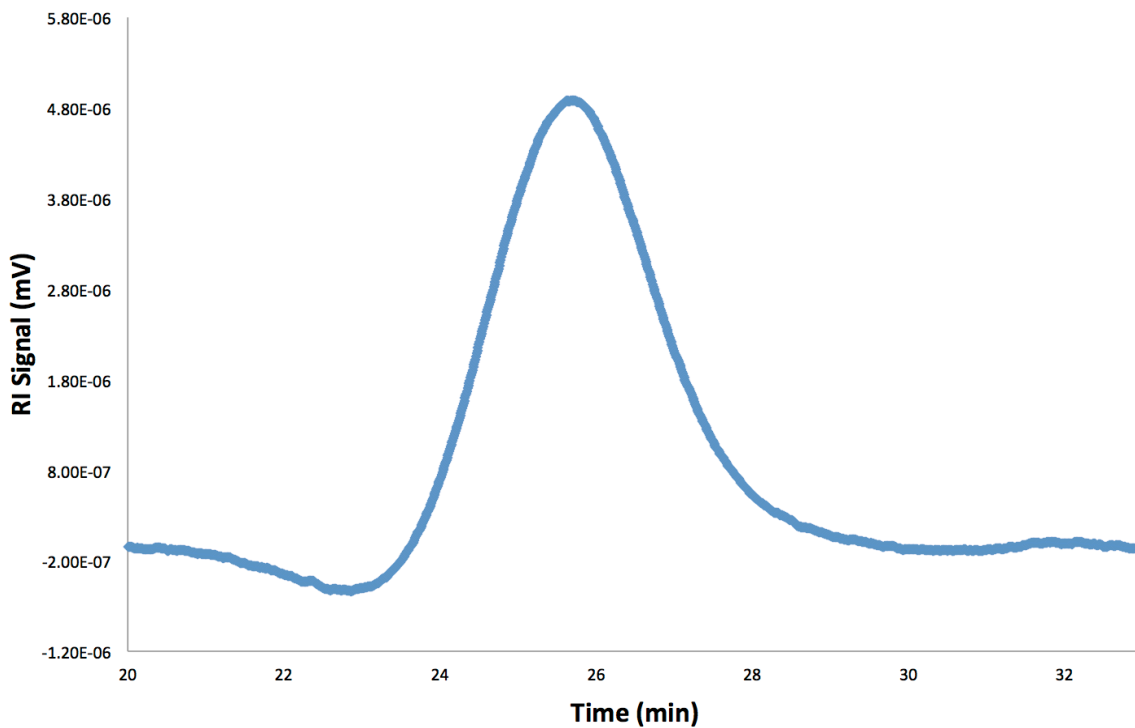


Figure B109. Table B4, entry 3: Acetone precipitate from selective precipitation of PCHO-PLA; $M_n = 18600$ Da, $M_w = 27400$ Da, $D = 1.48$. Taken on GPC-MALS.

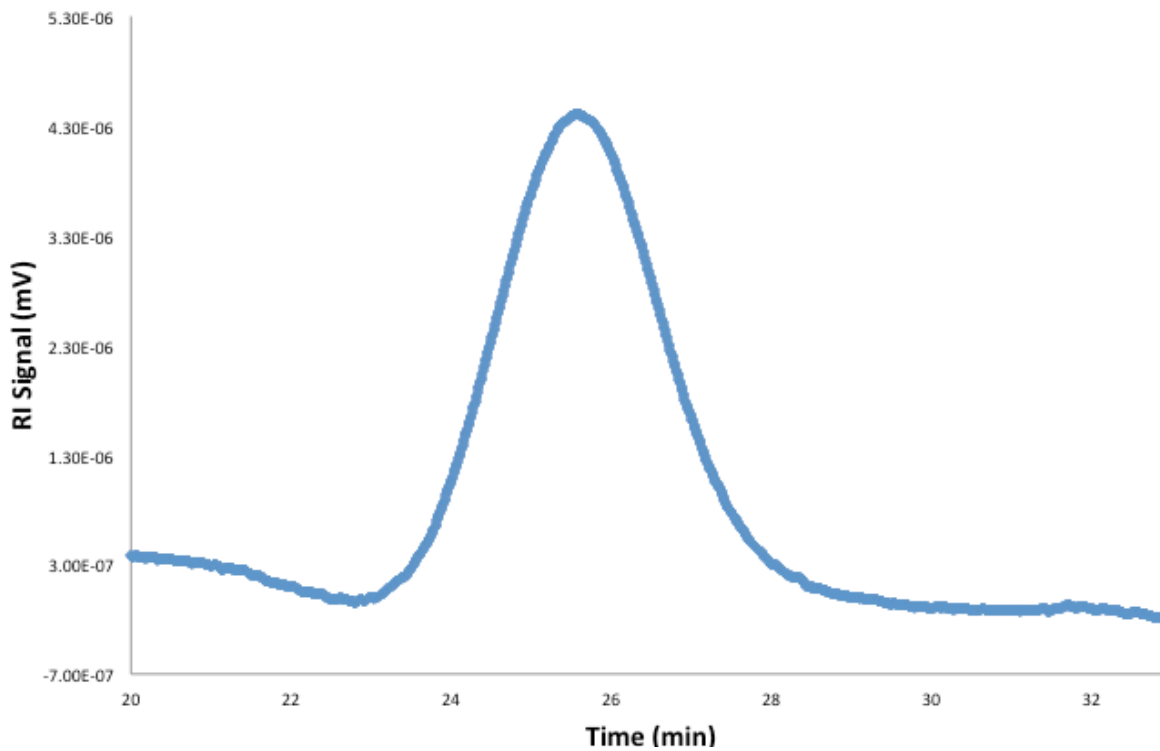


Figure B110. Table B4, entry 5: Hexanes precipitate from selective precipitation of PCHO-PLA; $M_n = 15800$ Da, $M_w = 25300$ Da, $D = 1.60$. Taken on GPC-MALS.

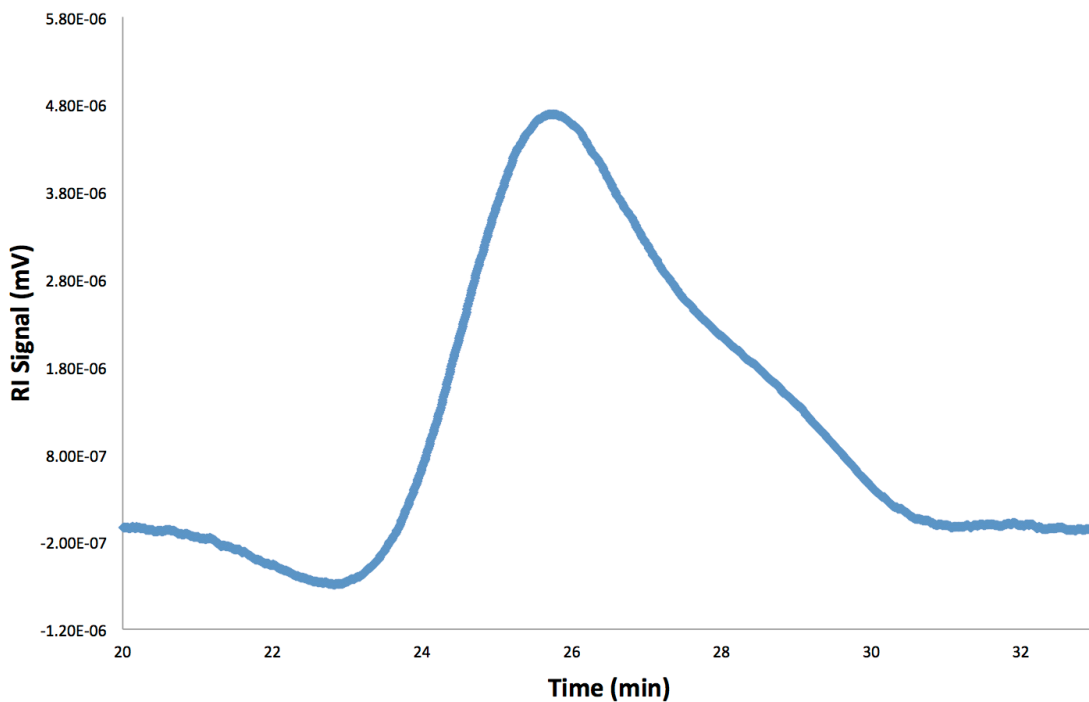


Figure B111. Table B5, entry 3: Acetone precipitate from selective precipitation of PCHO-PLA-PCHO; $M_n = 14000$ Da, $M_w = 20600$ Da, $\bar{D} = 1.47$. Taken on GPC-MALS.

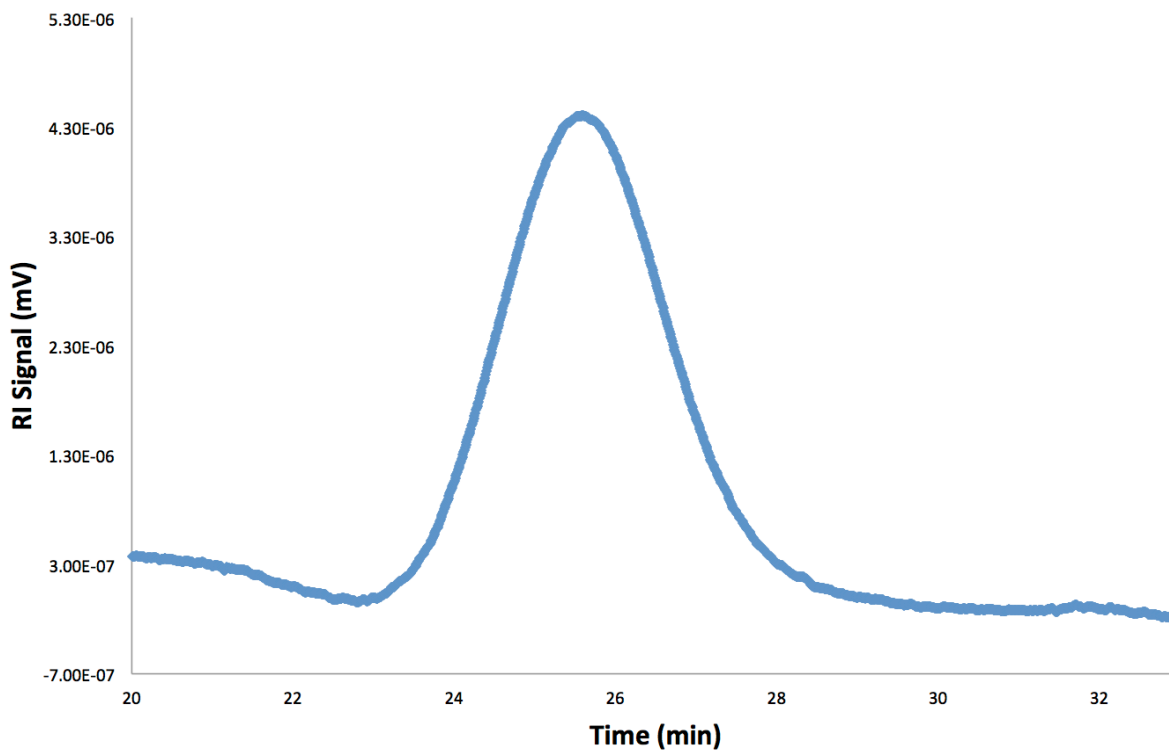


Figure B112. Table B5, entry 5: Hexanes precipitate from selective precipitation of PCHO-LA-PCHO; $M_n = 16800$ Da, $M_w = 25000$ Da, $\bar{D} = 1.49$. Taken on GPC-MALS.

References

1. (a) H. Tian, Z. Tang, X. Zhuang, X. Chen, X. Jing, *Prog. Polym. Sci.*, 2012, **37**, 237-280.
(b) B. D. Ulery, L. S. Nair, C. T. Laurencin, *J. Polym. Sci. B Polym. Phys.*, 2011, **49**, 832-864.
(c) A.-V. Ruzette, L. Leibler, *Nat. Mater.*, 2005, **4**, 19-31.
(d) F. Suriano, O. Coulembier, J. L. Hedrick, P. Dubois, *Polym. Chem.*, 2011, **2**, 528-533.
(e) M. Vert, *Biomacromolecules*, 2005, **6**, 538-546.
(f) L. S. Nair, C. T. Laurencin, *Prog. Polym. Sci.*, 2007, **32**, 762-798.
(g) E. S. Place, J. H. George, C. K. Williams, M. M. Stevens, *Chem. Soc. Rev.*, 2009, **38**, 1139-1151.
(h) I. Vroman, L. Tighzert, *Materials*, 2009, **2**, 307.
(i) C. Oerlemans, W. Bult, M. Bos, G. Storm, J. F. W. Nijsen, W. E. Hennink, *Pharm. Res.*, 2010, **27**, 2569-2589.
2. (a) T. Iwata, *Angew. Chem. Int. Ed.*, 2015, **54**, 3210-3215.
(b) D. J. Darensbourg, *Chem. Rev.*, 2007, **107**, 2388-2410.
3. Abetz, V.; Simon, P. F. W., Phase Behaviour and Morphologies of Block Copolymers. In *Block Copolymers I*, Abetz, V., Ed. Springer Berlin Heidelberg: Berlin, Heidelberg, 2005; pp 125-212.
4. J.-F. Lutz, M. Ouchi, D. R. Liu, M. Sawamoto, *Science*, 2013, **341**, 123-149.
5. (a) V. Tamboli, G. P. Mishra, A. K. Mitra, *Colloid Polym. Sci.*, 2012, **291**, 1235-1245.
(b) S. M. Guillaume, *Eur. Polym. J.*, 2013, **49**, 768-779.
6. (a) Y. Wang, M. A. Hillmyer, *Macromolecules*, 2000, **33**, 7395-7403.
(b) R. Jing, G. Wang, Y. Zhang, J. Huang, *Macromolecules*, 2011, **44**, 805-810.
7. (a) N. Chagneux, S. Camerlynck, E. Hamilton, F. M. L. Vilela, D. C. Sherrington, *Macromolecules*, 2007, **40**, 3183-3189.

- (b) D. Mecerreyes, G. Moineau, P. Dubois, R. Jérôme, J. L. Hedrick, C. J. Hawker, E. E. Malmström, M. Trollsas, *Angew. Chem. Int. Ed.*, 1998, **37**, 1274-1276.
- (c) T. He, D. Li, X. Sheng, B. Zhao, *Macromolecules*, 2004, **37**, 3128-3135.
- (d) W. Guerin, M. Helou, J.-F. Carpentier, M. Slawinski, J.-M. Brusson, S. M. Guillaume, *Polym. Chem.*, 2013, **4**, 1095-1106.
- (e) G.-P. Wu, D. J. Darensbourg, X.-B. Lu, *J. Am. Chem. Soc.*, 2012, **134**, 17739-17745.
- (f) G.-P. Wu, D. J. Darensbourg, *Macromolecules*, 2016, **49**, 807-814.
8. (a) C. Romain, C. K. Williams, *Angew. Chem. Int. Ed.*, 2014, **53**, 1607-1610.
- (b) X. Wang, A. Thevenon, J. L. Brosmer, I. Yu, S. I. Khan, P. Mehrkhodavandi, P. L. Diaconescu, *J. Am. Chem. Soc.*, 2014, **136**, 11264-11267.
9. (a) S. M. Guillaume, E. Kirillov, Y. Sarazin, J.-F. Carpentier, *Chem. Eur. J.*, 2015, **21**, 7988-8003.
- (b) V. Blanco, D. A. Leigh, V. Marcos, *Chem. Soc. Rev.*, 2015, **44**, 5341-5370.
- (c) A. Thevenon, J. A. Garden, A. J. P. White, C. K. Williams, *Inorg. Chem.*, 2015, **54**, 11906-11915.
- (d) Y. Zhu, C. Romain, C. K. Williams, *J. Am. Chem. Soc.*, 2015, **137**, 12179-12182.
- (e) S. Paul, C. Romain, J. Shaw, C. K. Williams, *Macromolecules*, 2015, **48**, 6047-6056.
10. (a) A. B. Biernesser, B. Li, J. A. Byers, *J. Am. Chem. Soc.*, 2013, **135**, 16553-16560.
- (b) L. A. Brown, J. L. Rhinehart, B. K. Long, *ACS Catal.*, 2015, **5**, 6057-6060.
- (c) C. K. A. Gregson, V. C. Gibson, N. J. Long, E. L. Marshall, P. J. Oxford, A. J. P. White, *J. Am. Chem. Soc.*, 2006, **128**, 7410-7411.
- (d) A. Sauer, J.-C. Buffet, T. P. Spaniol, H. Nagaie, K. Mashima, J. Okuda, *Chem. Cat. Chem.*, 2013, **5**, 1088-1091.
- (e) F. A. Leibfarth, K. M. Mattson, B. P. Fors, H. A. Collins, C. J. Hawker, *Angew. Chem. Int. Ed.*, 2013, **52**, 199-210.
- (f) S. M. Quan, P. L. Diaconescu, *Chem. Commun.*, 2015, **51**, 9643-9646.

- (g) E. M. Broderick, N. Guo, T. Wu, C. S. Vogel, C. Xu, J. Sutter, J. T. Miller, K. Meyer, T. Cantat, P. L. Diaconescu, *Chem. Commun.*, 2011, **47**, 9897-9899.
- (h) E. M. Broderick, N. Guo, C. S. Vogel, C. Xu, J. Sutter, J. T. Miller, K. Meyer, P. Mehrkhodavandi, P. L. Diaconescu, *J. Am. Chem. Soc.*, 2011, **133**, 9278-9281.
- (i) M. Abubekеров, S. M. Shepard, P. L. Diaconescu, *Eur. J. Inorg. Chem.*, 2016, **2016**, 2634-2640.
- (j) M. Abubekеров, P. L. Diaconescu, *Inorg. Chem.*, 2015, **54**, 1778-1784.
- (k) X. Wang, J. L. Brosmer, A. Thevenon, P. L. Diaconescu, *Organometallics*, 2015, **34**, 4700-4706.
- (l) J. L. Brosmer, P. L. Diaconescu, *Organometallics*, 2015, **34**, 2567-2572.
- (m) B. M. Upton, R. M. Gipson, S. Duhovic, B. R. Lydon, N. M. Matsumoto, H. D. Maynard, P. L. Diaconescu, *Inorg. Chem. Front.*, 2014, **1**, 271-277.
- (n) S. M. Shepard, P. L. Diaconescu, *Organometallics*, 2016, **35**, 2446-2453.
- (o) W. Huang, P. L. Diaconescu, *Inorg. Chem.*, 2016, **55**, 10013-10023.
11. A. B. Biernesser, K. R. Delle Chiaie, J. B. Curley, J. A. Byers, *Angew. Chem. Int. Ed.*, 2016, **55**, 5251-5254.
12. Y. Sarazin, J.-F. Carpentier, *Chem. Rev.*, 2015, **115**, 3564-3614.
13. J. Xiong, J. Zhang, Y. Sun, Z. Dai, X. Pan, J. Wu, *Inorg. Chem.*, 2015, **54**, 1737-1743.
14. Y. Bakkour, V. Darcos, S. Li, J. Coudane, *Polym. Chem.*, 2012, **3**, 2006-2010.
15. I. Yu, T. Ebrahimi, S. G. Hatzikiriakos, P. Mehrkhodavandi, *Dalton Trans.*, 2015, **44**, 14248-14254.
16. (a) H. Abe, Y. Doi, Y. Hori, T. Hagiwara, *Polymer*, 1998, **39**, 59-67.
- (b) J. Fagerland, A. Finne-Wistrand, D. Pappalardo, *New J. Chem.*, 2016, **40**, 7671-7679.
17. S. Y. Lee, P. Valtchev, F. Dehghani, *Green Chem.*, 2012, **14**, 1357-1366.
18. I. Bayram, A. Oral, K. Şirin, *J. Chem.*, 2013, **2013**, 6.
19. X. Shi, G. Zhang, T. Phuong, A. Lazzeri, *Molecules*, 2015, **20**, 1579.

20. Y. Y. Durmaz, M. Kukul, N. Moszner, Y. Yagci, *J. Polym. Sci. A Polym. Chem.*, 2009, **47**, 4793-4799.
21. A. B. Pangborn, M. A. Giardello, R. H. Grubbs, R. K. Rosen, F. J. Timmers, *Organometallics*, 1996, **15**, 1518-1520.
22. K. J. Miller, T. T. Kitagawa, M. M. Abu-Omar, *Organometallics*, 2001, **20**, 4403-4412.
23. M. Kuprat, M. Lehmann, A. Schulz, A. Villinger, *Organometallics*, 2010, **29**, 1421-1427.

Chapter 3: One-pot versus Sequential Monomer Addition in Redox-switchable Copolymerization

3.1 Introduction

Switchable catalysis¹ has emerged over the past few years as an increasingly viable method toward achieving controlled block copolymer synthesis.^{2,3,4,5,6,10} Redox switches for polymerization reactions are particularly useful and have shown good applicability so far.^{5-7,9} In 2014, our group reported a one-pot synthesis of polylactide-polycaprolactone (PLA-PCL) using (thiolfan*)Ti(O^{*i*}Pr), (thiolfan* = 1,1'-di(2-*tert*-butyl-6-thiophenoxy)ferrocene).⁷ This compound polymerized lactide (LA) in its reduced state, then, after an *in situ* redox switch, polymerized ϵ -caprolactone (CL) in its oxidized state. This represented a proof of concept, however, the initiator could only polymerize 17% of CL in the oxidized state before the lactide in solution began to polymerize as well. In 2016, concurrently with Byers et al., who used a bis(imino)pyridine iron complex, Fe(PDI)(4-methoxyphenoxy)₂, PDI = 2,6-(2,6-Me₂-C₆H₃N=CMe)₂C₅H₃N,⁹ the monomer scope of redox-switchable polymerization was expanded beyond cyclic esters to include cyclic ethers; the copolymerization of cyclohexene oxide (CHO) and LA was achieved either with a zirconium complex, (salfan)Zr(O^{*t*}Bu)₂ (salfan = 1,1'-di(2-*tert*-butyl-6-*N*-methylmethylenephenoxy)ferrocene),⁶ or the iron complex. Although one-pot reactions were contaminated by side reactions⁷ and homopolymer fragments,⁹ the homopolymers could be removed by an advantageous selective precipitation procedure.

When using (salfan)Zr(O^{*t*}Bu)₂ as a preinitiator, we found that we needed to employ a sequential addition of LA and CHO (Figure 3.1) because of a background reaction between the oxidant, ^{A_c}FcBAr^F (acetylferrocenium tetrakis[3,5-bis(trifluoromethyl)phenyl]borate), and CHO occurred. Nonetheless, ABA and BAB type triblock copolymers were successfully synthesized

and characterized.⁶ In the following chapter, the extent of the side reaction between the oxidant and CHO in a one-pot polymerization will be examined. In addition, various mechanistic aspects of lactide and cyclohexene oxide polymerization by $[(\text{salfan})\text{Zr}(\text{O}^t\text{Bu})_2][\text{BAR}^F]$ will be discussed.

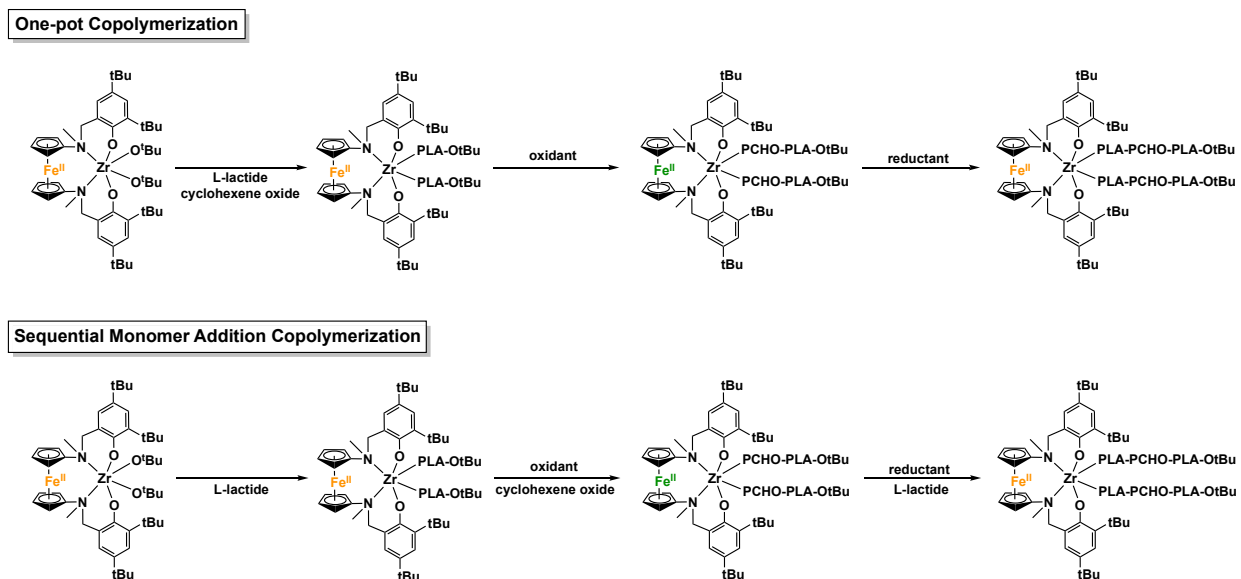


Figure 3.1. One-pot versus sequential monomer addition copolymerization.

3.2 Results and Discussion

Precipitation studies for one-pot copolymerization. In order to determine to what extent the side reaction with the oxidant affected the formation of triblock copolymers in one pot, we turned to selective precipitation methods developed by Byers et al.⁹ to separate homopolymer impurities from copolymer products. Copolymer mixtures were precipitated into acetone to remove polycyclohexene oxide homopolymers, then hexanes to remove polylactide homopolymers.

Table 3.1. Selective precipitation of PLA-PCHO-PLA copolymer synthesized by the one-pot method.

PLA-PCHO-PLA	PLA:PCHO ^a	Weight (mg)	M _n ^b (kDa)	Đ ^b
Crude	1 : 0.41	100	7.7	1.25
Acetone filtrate	1 : 0.51	75	9.7	2.22
Acetone ppt.	1 : 0.67	trace	-	-
Hexanes filtrate	1 : 3.12	7	-	-
Hexanes ppt.	1 : 0.37	58	6.5	1.82

^a Determined by integration of PLA methine region versus PCHO in the corresponding ¹H NMR spectra.

^b Determined by GPC-MALS. Đ = M_w/M_n

Table 3.2. Selective precipitation of PCHO-PLA-PCHO copolymer synthesized by the one-pot method.

PCHO-PLA-PCHO	PLA:PCHO ^a	Weight (mg)	M _n ^b (kDa)	Đ ^b
Crude	1 : 2.00	100	8.2	1.41
Acetone filtrate	1 : 1.83	68	5.7	1.33
Acetone ppt.	1 : 8.30	16	-	-
Hexanes filtrate	1 : 2.62	33	4.1	1.55
Hexanes ppt.	1 : 0.30	10	3.2	1.47

^a Determined by integration of PLA methine region versus PCHO in the corresponding ¹H NMR spectra.

^b Determined by GPC-MALS. Đ = M_w/M_n

The triblock copolymer PLA-PCHO-PLA was insoluble in hexanes (Table 3.1). The ¹H NMR spectrum of the purified polymer yielded an integration of 1:0.37 PLA:PCHO that showed a smaller percentage PCHO in the final polymer than the crude polymer mixture. M_n dropped from 7.7 to 6.5 kDa and the dispersity increased from 1.25 to 1.82, suggesting that the removal of some higher molecular weight impurities occurred. When analyzing the reverse triblock copolymer, PCHO-PLA-PCHO (Table 3.2), we found out that most of the mass remained in the hexanes filtrate. The lower molecular weight (4.1 versus 8.2 kDa), slight increase in dispersity (1.41 to 1.55), and much lower percentage of retained mass (33 mg from 100 mg) suggests that

the additional oxidation processes lead to more side reactions between the oxidant and CHO and thus more homopolymer fragments synthesis.

Compared to our triblock copolymers synthesized by sequential addition and purified by the same selective precipitation process (Chapter 2),⁶ the copolymers synthesized by the one-pot method have lower molecular weights and larger dispersities, consistent with a lower level of control over the polymerization and the generation of many smaller polymer fragments. While this is most pronounced in the PCHO-PLA-PCHO copolymer, where additional oxidations increased the percentage of side products and drastically changed the mass of the purified polymer, interestingly, the PLA-PCHO-PLA copolymer has a similar composition whether generated in one pot or by sequential addition, albeit a lower M_n in the former case.

Mechanism of CHO polymerization. The polymerization of epoxides is often via an anionic or cationic mechanism.⁸ Since the generation of PCHO by $^{Ac}FcBAR^F$ was likely the result of an ionic polymerization mechanism, we considered the possibility that CHO polymerization by $[(salfan)Zr(O^tBu)_2][BAR^F]$ might occur by a cationic mechanism. We observed that, in the presence of both CHO and LA, $[(salfan)Zr(O^tBu)_2][BAR^F]$ polymerized 83% of CHO in one hour and then began to polymerize LA, reaching 50% in four hours (Table 3.3, entry 1). When the initiator was instead reduced after one hour, LA polymerization reached 96% in three hours (Table 3.3, entry 2). The polymerization of LA after CHO by the oxidized complex was unusual because the oxidized initiator cannot polymerize LA alone (Table 3.3, entry 3). If a cationic mechanism was in place, the positive charge would be moved away from the metal center, thereby decreasing its electrophilicity to a state close to that of the reduced compound (Figure 3.2).

Table 3.3. Polymerization of LA and CHO by [(salfan)Zr(O^tBu)₂][BAR^F].

Entry	Monomer 1	Monomer 2	Initiator state	Time (h)	Conv. ^a
1	CHO	LA	ox	1	83-0
			ox	4	83-50
2	CHO	LA	ox	1	82-0
			red	3	85-96
3	LA	-	ox	25	8

Conditions: [M]/[I] = 100, [I] = 0.01 mM, 100 °C, (4:1) benzene-d₆: 1,2-difluorobenzene as solvent, 1,3,5-trimethoxybenzene as an internal standard, ^{Ac}FcBAR^F as oxidant, CoCp₂ as reductant. LA = L-lactide, CHO = cyclohexene oxide. ^a Determined by ¹H NMR spectroscopy. Conversion calculated by integration of polymer peaks versus internal standard. The first number indicates conversion of monomer 1, while the second number indicates conversion of monomer 2.

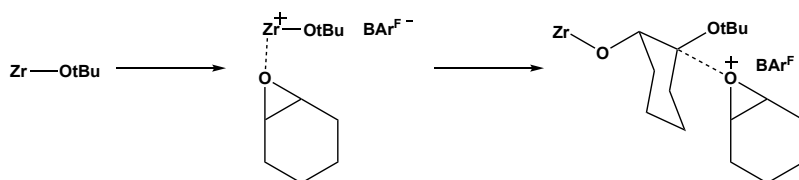


Figure 3.2. Potential reaction scheme of CHO cationic polymerization. “Zr” represents (salfan)Zr(O^tBu)₂, “Zr⁺” represents [(salfan)Zr(O^tBu)₂][BAR^F].

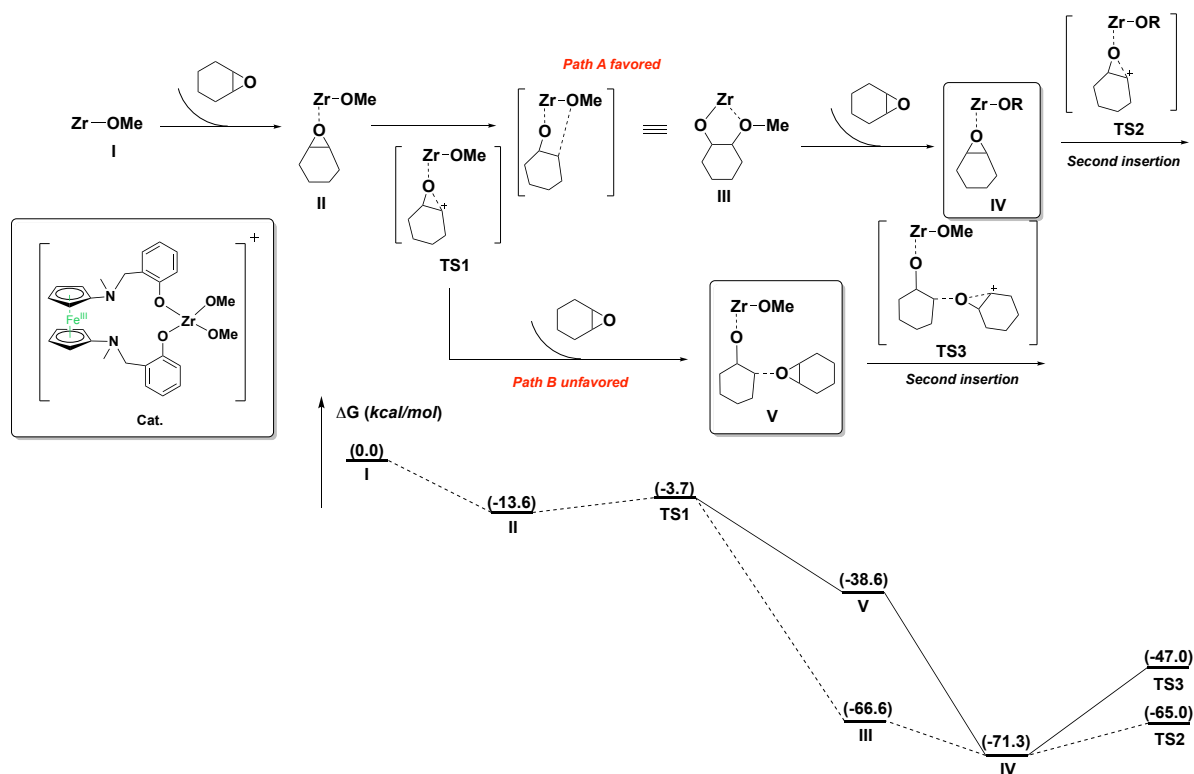


Figure 3.3. Potential energy surfaces of the ROP of CHO by $[(\text{salfan})\text{Zr}(\text{O}^t\text{Bu})_2][\text{BAR}^F]$.

To consider this possibility, DFT calculations for the coordination insertion and cationic ring opening mechanism of CHO were performed by Junnian Wei (Figure 3.3). Although both pathways are overall energetically favorable, intermediate **III**, on the coordination insertion pathway, was found to be 26 kcal/mol more stable than intermediate **V**, found on the cationic pathway. Likewise, **TS2**, corresponding to the second insertion during the first mechanism, was 18 kcal/mol lower in energy than **TS3**, which corresponds to the second insertion during the latter mechanism. Therefore, path A, a coordination insertion mechanism, seems to be favored. A similar mechanism was proposed by Byers et al.,³³ although a detailed mechanistic study has not been reported.

In addition, we examined the one-pot copolymerization activity of $[(\text{salfan})\text{Zr}(\text{O}^t\text{Bu})_2][\text{BAR}^F]$ at different temperatures. At room temperature, the copolymerization of LA and CHO showed only a 3% conversion of LA after 18 hours (Figure 3.4). At 100 °C, the

conversion of LA rose to 81.5% in the same amount of time (Figure 3.4). Without CHO, at 100 °C, LA polymerization reached eight percent after 25 hours (Table 3.3, entry 3). Therefore, the polymerization of LA by $[(\text{salfan})\text{Zr}(\text{O}^t\text{Bu})_2][\text{BAR}^{\text{F}}]$ seems to require both high temperatures as well as the presence of CHO to proceed at a significant rate. This may be explained by the coordination of CHO to the oxidized complex to form the low energy intermediate **III**, which allows the polymerization of LA more easily than initiator **I**.

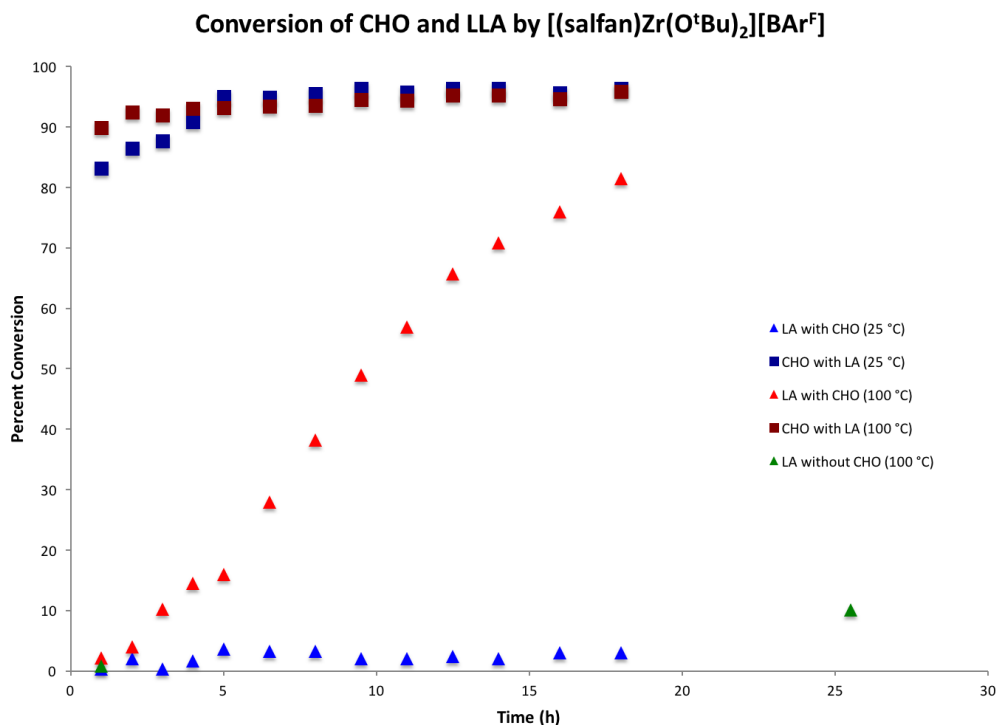


Figure 3.4. Polymerization of LA and CHO by $[(\text{salfan})\text{Zr}(\text{O}^t\text{Bu})_2][\text{BAR}^{\text{F}}]$.

To verify this theory, Junnian Wei calculated the energy barriers for the polymerization of LA (Figure 3.5). For the $(\text{salfan})\text{Zr}(\text{O}^t\text{Bu})_2$, the first insertion of LA is favorable. The final product $\mathbf{V}^{\text{red}}\text{-LA}$ has a similar structure to the initial initiator $\mathbf{I}^{\text{red}}\text{-LA}$ and is more stable by 8.9 kcal/mol. Therefore, the propagation step should have a similar energy barrier as the initiation step and LA polymerization should proceed smoothly.

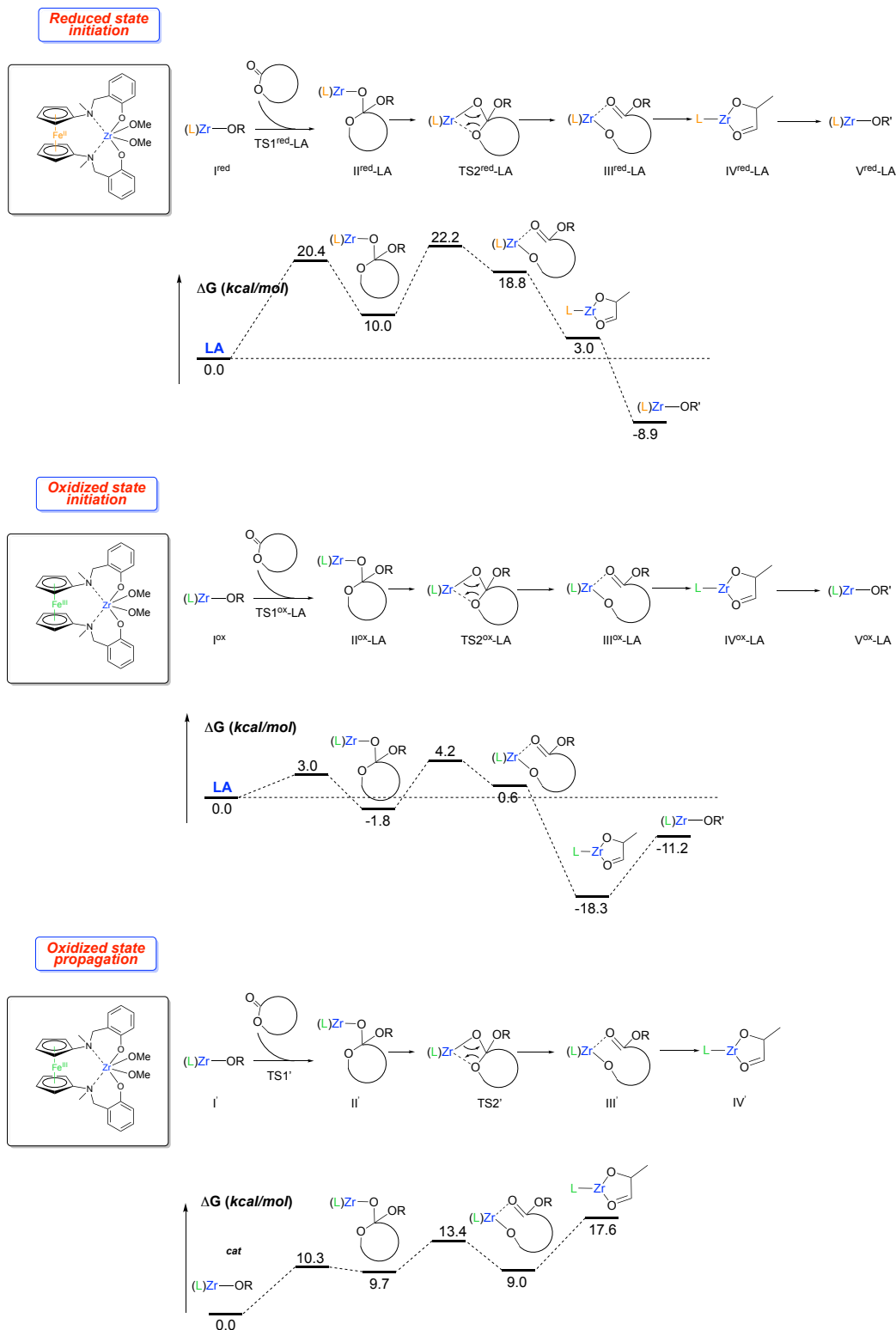


Figure 3.5. Potential energy surfaces of the ROP of LA by (salfan)Zr(O'Bu)₂ (top) and [(salfan)Zr(O'Bu)₂][BAR^F] (middle and bottom).

For the $[(\text{salfan})\text{Zr}(\text{O}^t\text{Bu})_2][\text{BAR}^{\text{F}}]$, after the insertion of LA, the carbonyl group coordinates to the Zr tightly, making the five-membered ring structure **IV^{ox}-LA** the favored product. Product **V^{ox}-LA** is less stable by 7.1 kcal/mol, which makes the following propagation thermodynamically unfavorable. However, it is likely that the insertion of CHO decreases the energy of the LA polymerization product in agreement with the calculations shown for the initiation step (Figure 3.5).

Block dependent polymerization rates. Since the presence of CHO showed an effect on the polymerization of LA by $[(\text{salfan})\text{Zr}(\text{O}^t\text{Bu})_2][\text{BAR}^{\text{F}}]$, we decided to investigate the influence of one monomer on the other's polymerization. Previously, we had observed different polymerization rates of LA and CHO for different blocks of the block copolymer.²³ To probe whether changes in the rate of polymerization was concentration, block length, or switch dependent, we synthesized a series of diblock copolymers under different conditions (Table 3.4).

Table 3.4. LA and CHO diblock copolymers synthesized by redox-switchable catalysis.

Entry	Polymer	Conv. 1 st block ^a	Conv. 2 nd block ^a	Time 1 st block (h)	Time 2 nd block (h)	M _n , theo ^b	M _n , GPC ^c	D ^d
1	LA ₅₀ -CHO ₅₀	90	73	7	19	11.5	13.0	1.22
2	CHO ₅₀ -LA ₅₀	91	90	6	4	12.9	13.8	1.53
3	LA ₅₀ -CHO ₅₀ [*]	94	79	3	21	11.7	13.6	1.29
4	CHO ₅₀ -LA ₅₀ [*]	90	95	3	2	13.2	15.5	1.26
5	LA ₂₅ -CHO ₂₅	90	84	5	20	5.2	7.4	1.20
6	CHO ₂₅ -LA ₂₅	90	88	6	3	5.9	8.7	1.23
7	LA ₁₂ -CHO ₁₂	88	47	3	5	2.6	3.8	1.06
8	CHO ₁₂ -LA ₁₂	84	77	2	3	4.4	8.8	1.17
9	LA ₂₅ -CHO ₂₅ - LA ₂₅ -CHO ₂₅	90 95	57 89	5 1	19 39	12.9	12.1	1.31
10	CHO ₂₅ -LA ₂₅ - CHO ₂₅ -LA ₂₅	94 86	97 99	4 13	2 1	9.6	9.7	1.16

Conditions: [M]/[I] = 100, [I] = 0.01 mM, 100 °C in reduced state, 25 °C in oxidized state, (4:1) benzene-d₆: 1,2-difluorobenzene as solvent, 1,3,5-trimethoxybenzene as an internal standard, ^{Ac}FcBAR^F as oxidant, CoCp₂ as reductant. LA = L-lactide, CHO = cyclohexene oxide. ^a Conversion calculated by integration of polymer and monomer peaks versus internal standard in ¹H NMR. ^b Determined by integration of PLA methine region and PCHO versus internal standard in ¹H NMR. ^c Determined by GPC-MALS. ^d D = M_w/M_n. * Concentration was doubled.

LA was polymerized more quickly as a second block than as a first block (Table 3.4, entries 1 and 2), while CHO was polymerized more slowly as a second block than as a first block (Table 3.4, entries 1 and 2). Increasing the concentration of the reaction made the polymerizations faster, but did not change the relative increases or decreases in time to achieve full conversion for the second block (Table 3.4, entries 3 and 4). Similarly, decreasing the number of equivalents from 100 to 50 (Table 3.4, entries 5 and 6) did not significantly change the relative rates of polymerization. Decreasing the number of equivalents to 25 (Table 3.4, entries 7 and 8) shortened the polymerization times of the first blocks and significantly increased the polymerization time of CHO as a second block. An additional two redox switches with two more copolymer blocks (Table 3.4, entries 9 and 10), showed that the increases and decreases in CHO and LA polymerization time established in the second blocks continued to further blocks, but did

not change appreciably. To visualize these changes, the changes in percent conversion were plotted against time (Figure 3.6). The polymerization of LA changed from five hours for 90% conversion in the first block to two hours for 89% conversion in the second block, two hours for 95% conversion in the third block and two hours for 95% conversion in the fourth block. For CHO, it took five hours to reach 89% conversion in the first block, 20 hours to reach 86% conversion in the second block, 20 hours to reach 75% conversion in the third block, and 20 hours to reach 98% conversion in the fourth block. These polymerization rates did not reveal a trend of polymerization time relative to position in the tetrablock copolymer. However, the rates did roughly correlate to the percentage of monomer left from the previous block (Table 3.5).

Table 3.5. Conversion of LA or CHO and percentage of residual monomer in tetrablock copolymer.

Entry	Monomer	% residual monomer^a	Conv. of block	Time (h)
1	LA	25	95	2
2	LA	14	95	2
3	LA	11	89	2
4	LA	0	90	5
5	CHO	11	75	20
6	CHO	9	86	20
7	CHO	5	98	20
8	CHO	0	89	5

Data from Table 2, entries 9 and 10. ^aDetermined by subtracting previous block's conversion from 100.

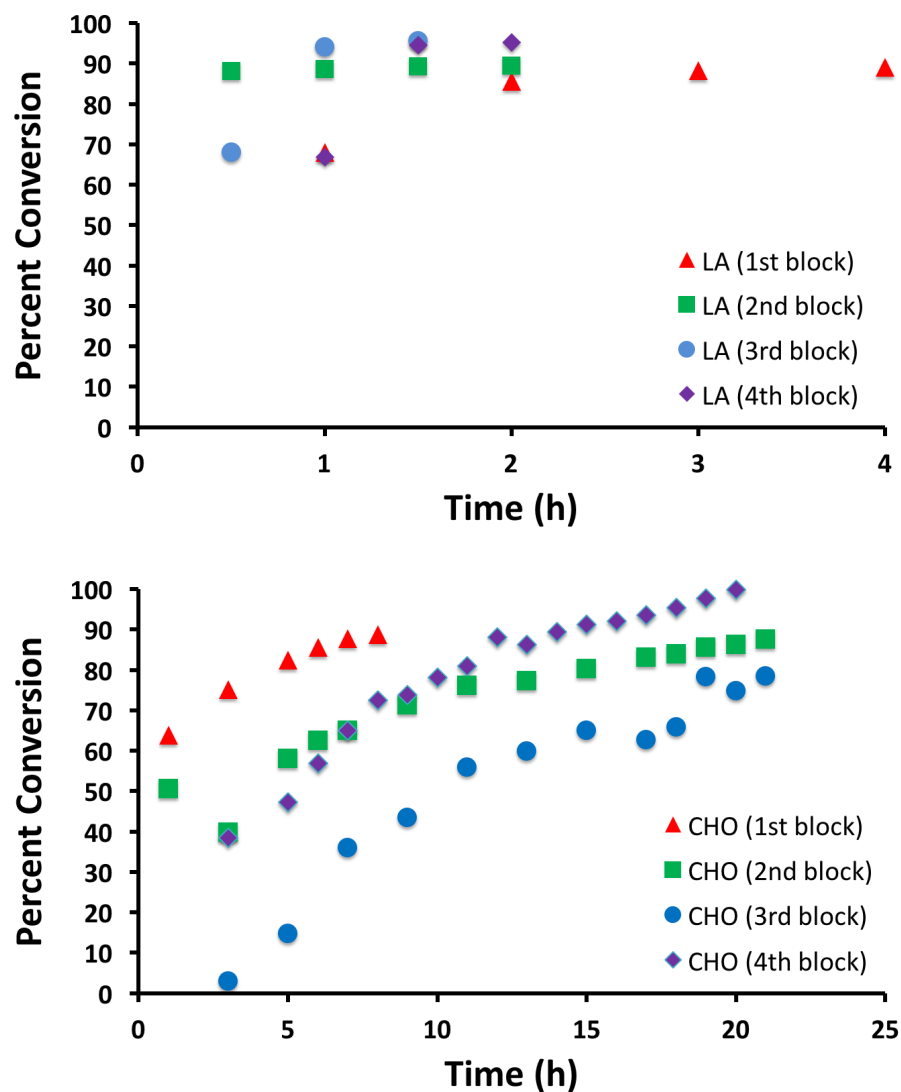


Figure 3.6. Percent conversion versus time, with position in tetrablock copolymer for LA (top) and CHO (bottom).

Previously, we found that $(\text{salfan})\text{Zr}(\text{O}^t\text{Bu})_2$ polymerized LA more quickly in the presence of CHO than without CHO. Conversely, $[(\text{salfan})\text{Zr}(\text{O}^t\text{Bu})_2][\text{BAr}^F]$ polymerized CHO more slowly in the presence of LA than in its absence (Figure 3.7).²³ Qualitative comparison of the rate of polymerization of LA and CHO as a first or second block (Figure 3.8) showed a similar trend. LA was polymerized more quickly as a second block when there was a small amount of CHO left over. CHO was polymerized much more slowly as a second block when

there was a small quantity of LA were left over. Therefore, we attribute the change in the rate to the polymerization of each monomer in the presence of residual monomer from the previous block.

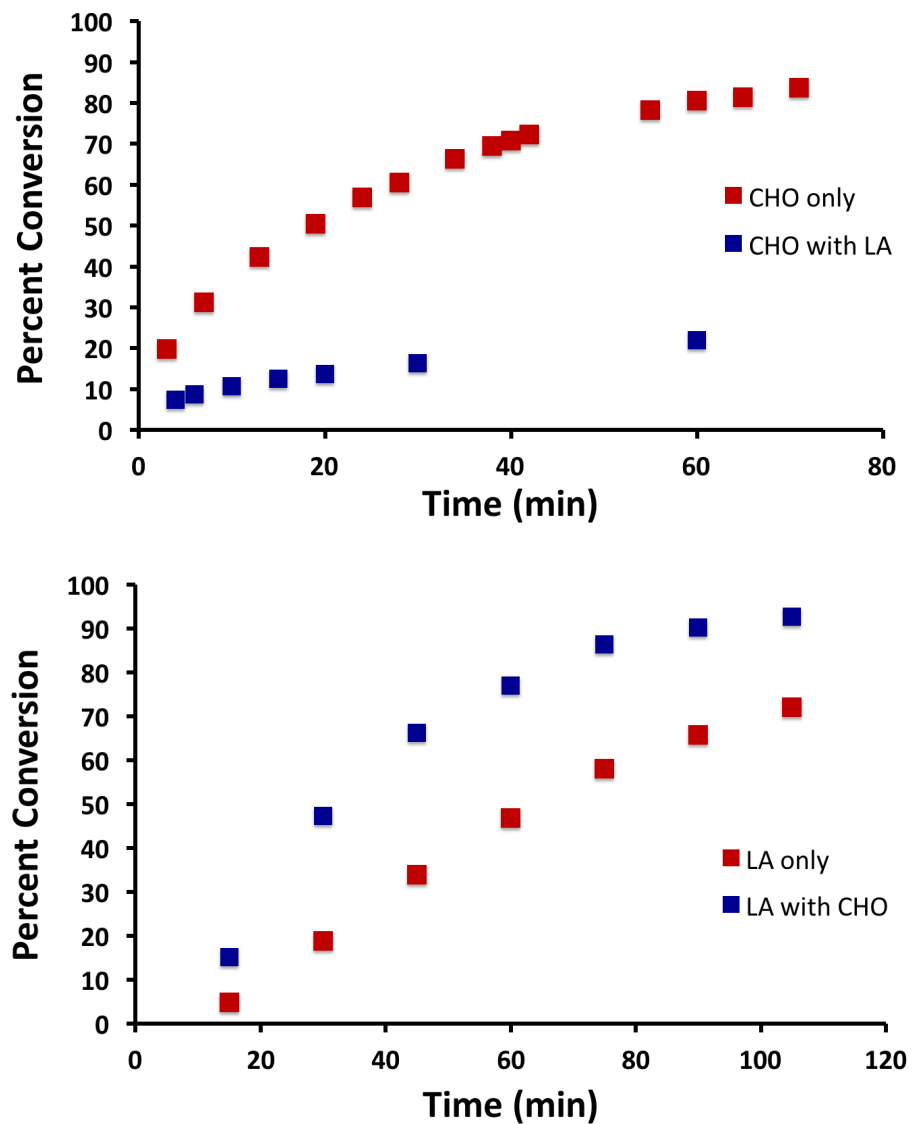


Figure 3.7. Comparison of polymerization rates of LA (top) and CHO (bottom) with and without the presence of the other monomer.

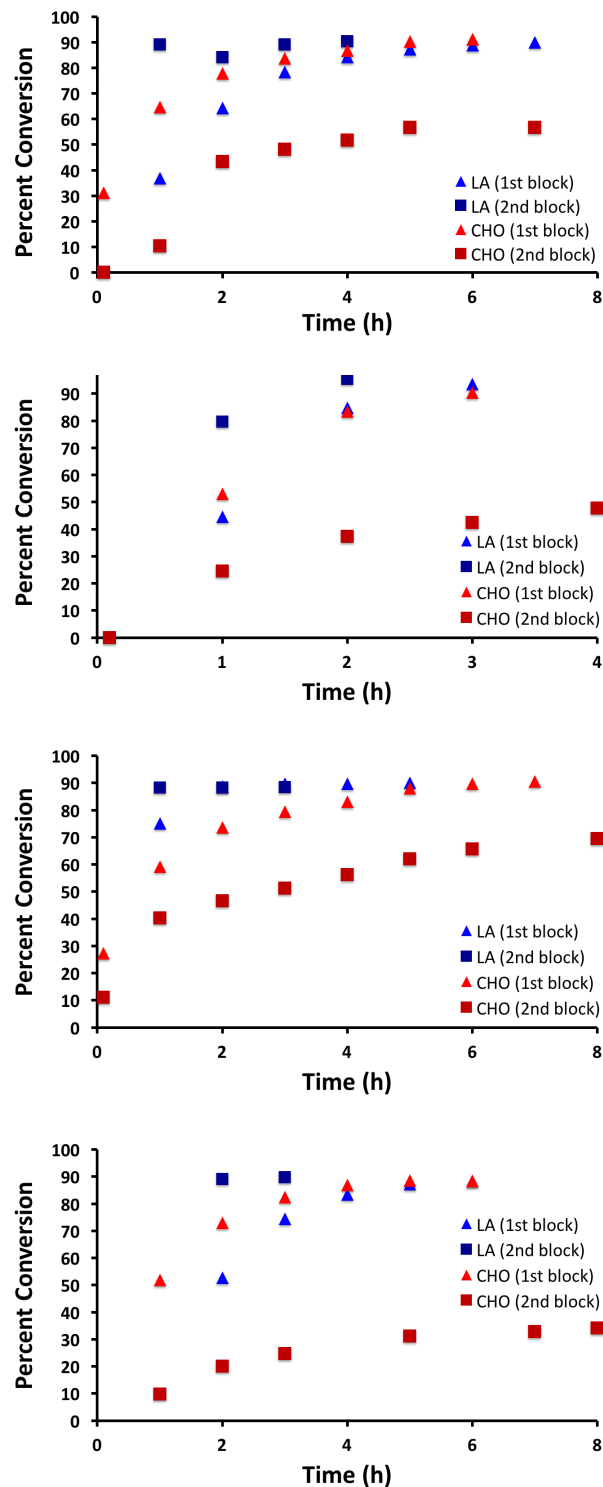


Figure 3.8. Comparison of LA and CHO polymerization rates as first and second blocks in the synthesis of diblock copolymers made of 100 equivalents (top), 100 equivalents concentrated (upper middle), 50 equivalents (lower middle), and 25 equivalents (bottom) of each monomer.

3.3 Conclusions

Comparison of the one-pot copolymerization method with the sequential monomer addition copolymerization using selective precipitations showed an increase in homopolymer impurities with one-pot copolymerization due to the side reaction of oxidant and CHO. The redox-switchable copolymerization mechanism of (salfan)Zr(O^tBu)₂ was examined using experimental methods and DFT calculations. [(salfan)Zr(O^tBu)₂][BAR^F] was found to polymerize CHO using an unusual mechanism for epoxides, coordination insertion. Polymerization of LA by [(salfan)Zr(O^tBu)₂][BAR^F] was found to be thermodynamically unfavored by calculations, but possible at 100 °C following the polymerization of CHO. It is likely that the polymerization of CHO lowers the energy of the LA polymerization product, but more studies are needed to fully understand this. The influence of one monomer on the polymerization of another was also evidenced by the different polymerization rates of LA and CHO in different blocks of block copolymers. LA is polymerized more quickly after CHO, CHO is polymerized more slowly after LA. These relative changes occurred regardless of monomer concentration or number of equivalents and roughly correlate with the percentage of leftover monomer in solution.

3.4 Experimental

General considerations

All experiments were performed under a dry nitrogen atmosphere using standard Schlenk techniques or an MBraun inert-gas glovebox. Solvents were purified using a two-column solid-state purification system by the method of Grubbs⁹ and transferred to the glove box without exposure to air. NMR solvents were obtained from Cambridge Isotope Laboratories, degassed and stored over activated molecular sieves prior to use. ¹H NMR spectra were recorded on

Bruker 300, Bruker 400 or Bruker 500 spectrometers at room temperature in C_6D_6 or $CDCl_3$. Chemical shifts are reported with respect to internal solvent, 7.16 ppm (C_6D_6) and 7.26 ppm ($CDCl_3$) for 1H NMR spectra. Cyclohexene oxide and 1,2-difluorobenzene were distilled over CaH_2 and brought into the glove box without exposure to air. L-lactide and 1,3,5-trimethoxybenzene were recrystallized from toluene at least twice before use. 2,4-di-*tert*-butylphenol, *n*-BuLi, cobaltocene, and $Zr(O^tBu)_4$ were purchased from Sigma Aldrich and used as received. $[^{Ac}Fc][BAr^F_4]$, $TPA[BAr^F_4]$, and $(salfan)Zr(O^tBu)_2$ were synthesized following previously published procedures.⁷ Molecular weights of the polymers were determined by GPC-MALS instrument at UCLA. GPC-MALS uses a Shimadzu Prominence-i LC 2030C 3D equipped with an autosampler, two MZ Analysentechnik MZ-Gel SDplus LS 5 μm , 300×8 mm linear columns, Wyatt DAWN HELEOS-II and Wyatt Optilab T-rEX. The column temperature was set at 40 °C. A flow rate of 0.70 mL/min was used and samples were dissolved in chloroform. dn/dc values were calculated for PLA and PCHO by creating 5 solutions of increasing concentration (0.1 - 1.0 mg/mL), directly injecting them into the RI detector sequentially, and using the batch dn/dc measurement methods in the Astra software. The dn/dc value for PLA and PCHO were calculated to be 0.024 mL/g and 0.086 mL/g over three trials.

General procedure for the polymerization of two monomers by $(salfan)Zr(O^tBu)_2$ or $[(salfan)Zr(O^tBu)_2][BAr^F_4]$ with two redox switches (one pot) for Tables 3.1 and 3.2.

Copolymerization of LA and CHO by $(salfan)Zr(O^tBu)_2$ (red-ox-red). To a C_6D_6 (0.30 mL) solution of $(salfan)Zr(O^tBu)_2$ (9.2 mg, 10 μmol) in a J-Young NMR tube, a solution of 1,3,5-trimethoxybenzene (33.6 mg, 100 μmol) in C_6D_6 (0.30 mL), 0.20 mL of $F_2C_6H_4$ and a

C_6D_6 (0.20 mL) solution of cyclohexene oxide (98.0 mg, 1.0 mmol) and L-lactide (288.0 mg, 2.0 mmol) were added. The reaction was heated to 100 °C and periodically removed from the oil bath every 30 min to be analyzed by 1H NMR spectroscopy until 50% conversion of LA was reached. A solution of $[^{13}C]Fc[BAr^F_4]$ (11.0 mg, 10 μ mol) in $F_2C_6H_4$ (0.20 mL) was added to oxidize the initiator. After two hours, the reaction was heated to 100 °C again for one hour and analyzed by 1H NMR spectroscopy to ensure CHO polymerization. A solution of $CoCp_2$ (1.9 mg, 10 μ mol) in C_6D_6 (0.60 mL) was added to reduce the initiator. After two hours, the solution was heated to 100 °C again and monitored until LA conversion reached over 90% by 1H NMR spectroscopy. At the end, the reaction mixture was dissolved in CH_2Cl_2 and poured into cold methanol; a white solid polymer precipitated and was filtered.

Copolymerization of LA and CHO by (salfan)Zr(O^tBu)₂ (ox-red-ox). To a C_6D_6 (0.30 mL) solution of (salfan)Zr(O^tBu)₂ (9.2 mg, 10 μ mol) in a J-Young NMR tube, a solution of 1,3,5-trimethoxybenzene (33.6 mg, 100 μ mol) in C_6D_6 (0.30 mL), 0.20 mL of $F_2C_6H_4$ and a solution of $[^{13}C]Fc[BAr^F_4]$ (11.0 mg, 10 μ mol) in $F_2C_6H_4$ (0.20 mL) was added. After two hours, a C_6D_6 (0.40 mL) solution of cyclohexene oxide (196.0 mg, 2.0 mmol) and L-lactide (144 mg, 1.0 mmol) was added. The reaction was heated to 100 °C and removed from the bath every 30 min to be analyzed by 1H NMR spectroscopy until 50% conversion of CHO was reached. A solution of $CoCp_2$ (1.9 mg, 10 μ mol) in C_6D_6 (0.20 mL) was added to reduce the initiator. After two hours, the reaction was heated to 100 °C again and analyzed by 1H NMR spectroscopy to ensure LLA polymerization. A solution of $[^{13}C]Fc[BAr^F_4]$ (11.0 mg, 10 μ mol) in $F_2C_6H_4$ (0.20 mL) was added. After two hours, the reaction was heated to 100 °C again and monitored until CHO conversion

reached over 90% by ^1H NMR spectroscopy. At the end, the reaction mixture was dissolved in CH_2Cl_2 and poured into cold methanol; a white solid polymer precipitated and was filtered.

Procedure for precipitation of homopolymers from copolymers. A polymerization reaction mixture was dissolved in minimal CH_2Cl_2 and poured into 10 mL of cold methanol. The mixture was centrifuged and the supernatant was poured off. The resulting crude polymer was dried, dissolved in minimal CH_2Cl_2 , and precipitated in 10 mL cold methanol two more times. To isolate the copolymer from any resulting homopolymer fragments selectively, 100 mg of the crude polymer was dissolved in minimal CH_2Cl_2 and poured into 10 mL of cold acetone. The mixture was centrifuged and filtered through a 0.20 micron FTPE filter. The isolated precipitate was dried, dissolved in minimal CH_2Cl_2 and poured into 10 mL of cold hexanes. The mixture was centrifuged and then filtered through a 0.20 micron FTPE filter. Filtrates and precipitates from each precipitation were dried, weighed, and analyzed by ^1H NMR spectroscopy and GPC.

General procedure for the polymerization of LA and CHO by $[(\text{salfan})\text{Zr}(\text{O}^t\text{Bu})_2][\text{BAR}^{\text{F}}_4]$ (1 pot) for Table 3.3, entries 1a and 1b, and Figure 3.5.

To a C_6D_6 (0.15 mL) solution of $(\text{salfan})\text{Zr}(\text{O}^t\text{Bu})_2$ (4.6 mg, 5 μmol) in a J-Young NMR tube, a solution of 1,3,5-trimethoxybenzene (16.8 mg, 50 μmol) in C_6D_6 (0.15 mL), 0.10 mL $\text{F}_2\text{C}_6\text{H}_4$ and a solution of $[\text{AcFc}][\text{BAR}^{\text{F}}_4]$ (5.5 mg, 5 μmol) in $\text{F}_2\text{C}_6\text{H}_4$ (0.10 mL) was added and the reaction was left at room temperature for two hours. A solution of cyclohexene oxide (49.0 mg, 0.5 mmol) in C_6D_6 (0.10 mL) and L-lactide (72.0 mg, 0.5 mmol) was added. The reaction was heated to 100 $^\circ\text{C}$ or left at room temperature and monitored by ^1H NMR spectroscopy. At the

end, the reaction was dissolved in CH₂Cl₂ and poured into cold methanol; a white solid precipitated briefly and was filtered.

General procedure for the polymerization of LA and CHO by [(salfan)Zr(O^tBu)₂][BAr^F₄] with one redox switch for Table 3.3, entries 2a and 2b.

To a C₆D₆ (0.15 mL) solution of (salfan)Zr(O^tBu)₂ (4.6 mg, 5 μmol) in a J-Young NMR tube, a solution of 1,3,5-trimethoxybenzene (16.8 mg, 50 μmol) in C₆D₆ (0.15 mL), 0.10 mL F₂C₆H₄ and a solution of [^{Ac}Fc][BAr^F₄] (5.5 mg, 5 μmol) in F₂C₆H₄ (0.10 mL) was added and the reaction was left at room temperature for two hours. A solution of cyclohexene oxide (49.0 mg, 0.5 mmol) in C₆D₆ (0.10 mL) and L-lactide (72.0 mg, 0.5 mmol) was added. After one hour, a solution of CoCp₂ (5.5 mg, 5 μmol) in C₆D₆ (0.10 mL) was then added and the reaction was left at room temperature for two hours. The reaction was heated to 100 °C and monitored by ¹H NMR spectroscopy. At the end, the reaction was dissolved in CH₂Cl₂ and poured into cold methanol; a white solid precipitated briefly and was filtered.

General procedure for the polymerization of LA by (salfan)Zr(O^tBu)₂ or [(salfan)Zr(O^tBu)₂][BAr^F₄] for Table 3.3, entry 3 and Figure 3.5.

To a C₆D₆ (0.15 mL) solution of (salfan)Zr(O^tBu)₂ (4.6 mg, 5 μmol) in a J-Young NMR tube, a solution of 1,3,5-trimethoxybenzene (16.8 mg, 50 μmol) in C₆D₆ (0.15 mL), 0.10 mL F₂C₆H₄ and a solution of [^{Ac}Fc][BAr^F₄] (5.5 mg, 5 μmol) in F₂C₆H₄ (0.10 mL) was added and the reaction was left at room temperature for two hours. L-lactide (72.0 mg, 0.5 mmol) was added.

The reaction was heated to 100 °C and monitored by ^1H NMR spectroscopy. At the end, the reaction was dissolved in CH_2Cl_2 and poured into cold methanol; a white solid precipitated briefly and was filtered.

General procedure for the sequential polymerization of LA and CHO by $(\text{salfan})\text{Zr}(\text{O}^t\text{Bu})_2$ or $[(\text{salfan})\text{Zr}(\text{O}^t\text{Bu})_2][\text{BAR}^{\text{F}}_4]$ with one redox switch for Table 3.4.

Copolymerization of LA and CHO by $(\text{salfan})\text{Zr}(\text{O}^t\text{Bu})_2$ (red-ox). To a C_6D_6 (0.15 mL) solution of $(\text{salfan})\text{Zr}(\text{O}^t\text{Bu})_2$ (4.6 mg, 5 μmol) in a J-Young NMR tube, a solution of 1,3,5-trimethoxybenzene (16.8 mg, 50 μmol) in C_6D_6 (0.15 mL), 0.20 mL of $\text{F}_2\text{C}_6\text{H}_4$, 0.50 mL C_6D_6 and L-lactide (72.0 mg, 0.5 mmol) were added. The reaction was heated to 100 °C and removed from the oil bath every hour to be analyzed by ^1H NMR spectroscopy until about 90% conversion occurred. A solution of $[\text{AcFc}][\text{BAR}^{\text{F}}_4]$ (5.5 mg, 5 μmol) in $\text{F}_2\text{C}_6\text{H}_4$ (0.10 mL) was then added and the reaction was left at room temperature for two hours. The volume of the solution was reduced to 0.90 mL and a solution of cyclohexene oxide (49.0 mg, 0.5 mmol) in C_6D_6 (0.10 mL) was added. The reaction was left at room temperature and analyzed by ^1H NMR spectroscopy until about 90% conversion occurred. At the end, the reaction mixture was dissolved in CH_2Cl_2 and poured into cold methanol; a white solid precipitated briefly and was filtered.

Copolymerization of LA and CHO by $[(\text{salfan})\text{Zr}(\text{O}^t\text{Bu})_2][\text{BAR}^{\text{F}}_4]$ (ox-red). To a C_6D_6 (0.15 mL) solution of $(\text{salfan})\text{Zr}(\text{O}^t\text{Bu})_2$ (4.6 mg, 5 μmol) in a J-Young NMR tube, a solution of 1,3,5-trimethoxybenzene (16.8 mg, 50 μmol) in C_6D_6 (0.15 mL), 0.4 mL C_6D_6 , 0.10

mL $F_2C_6H_4$ and a solution of $[^{Ac}Fc][BAR^F_4]$ (5.5 mg, 5 μ mol) in $F_2C_6H_4$ (0.10 mL) was added and the reaction was left at room temperature for two hours. A solution of cyclohexene oxide (49.0 mg, 0.5 mmol) in C_6D_6 (0.10 mL) was added. The reaction was monitored at room temperature by 1H NMR spectroscopy until about 90% conversion occurred. A solution of $CoCp_2$ (5.5 mg, 5 μ mol) in C_6D_6 (0.10 mL) was then added and the reaction was left at room temperature for two hours. The volume of the solution was reduced to 1.0mL and L-lactide (72.0 mg, 0.5 mmol) was added. The reaction was heated to 100 $^{\circ}C$ and removed from the oil bath every hour to be analyzed by 1H NMR spectroscopy. At the end, the reaction was dissolved in CH_2Cl_2 and poured into cold methanol; a white solid precipitated briefly and was filtered.

When using 50 equivalents or 25 equivalents, the volume of the overall solution was scaled down from 1.00 mL to 0.50 mL or 0.25 mL. When doubling the concentration, the overall concentration was scaled down to 0.50 mL. Solvent ratio of 4:1 $F_2C_6H_4$: C_6D_6 was maintained in all trials.

3.5 Appendix C

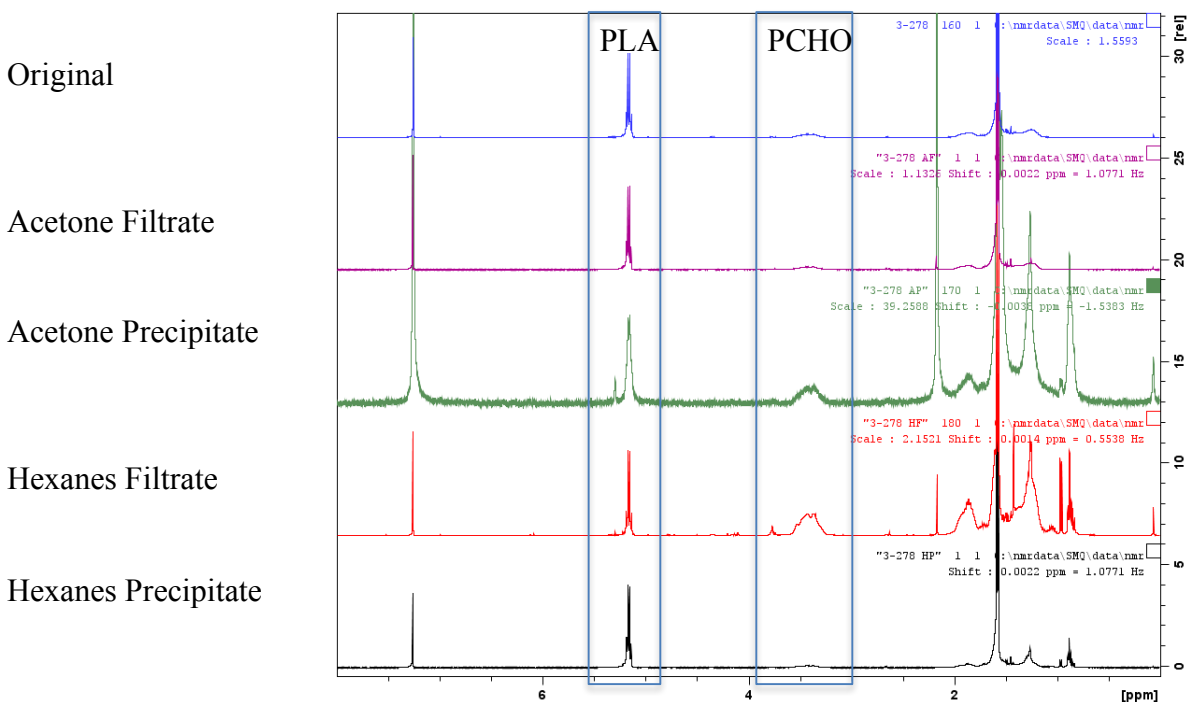


Figure C1. Overlaid ¹H NMR spectra of PLA-PCHO-PLA polymer through selective precipitation process. Quartet at 5.02 ppm corresponds to PLA methine protons, the broad peak at 3.60 ppm corresponds to PCHO alkyl protons.

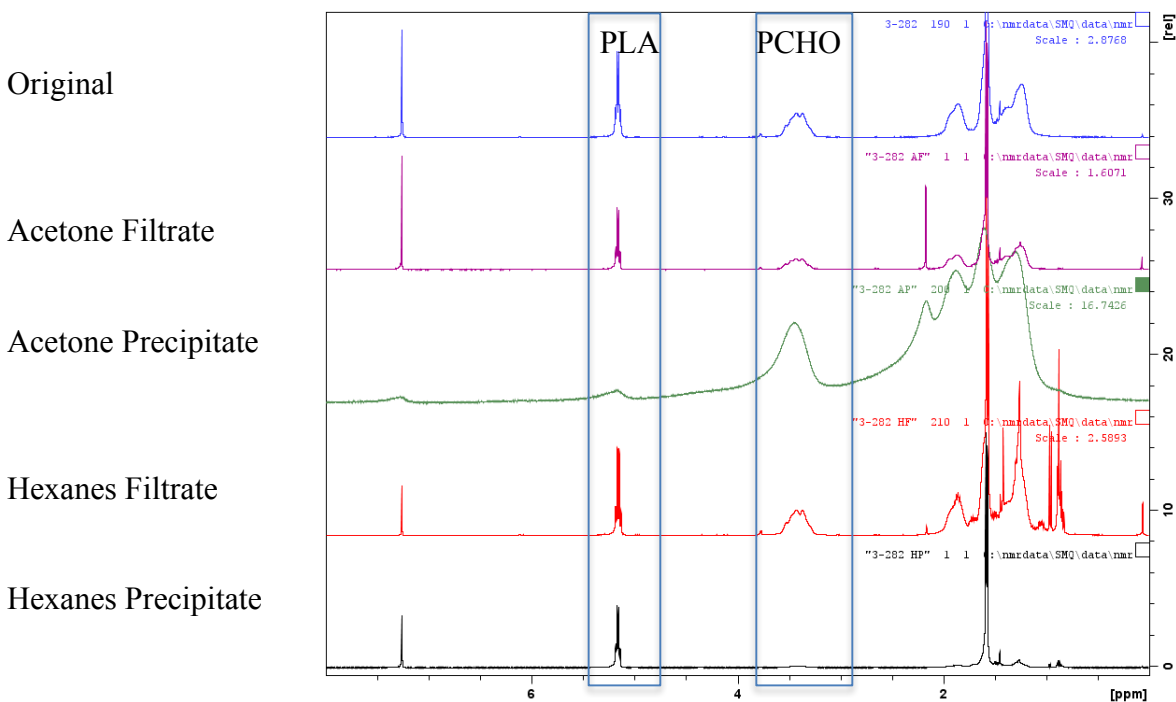


Figure C2. Overlaid ¹H NMR spectra of PCHO-PLA-PCHO polymer through selective precipitation process. Quartet at 5.02 ppm corresponds to PLA methine protons, the broad peak at 3.60 ppm corresponds PCHO alkyl protons.

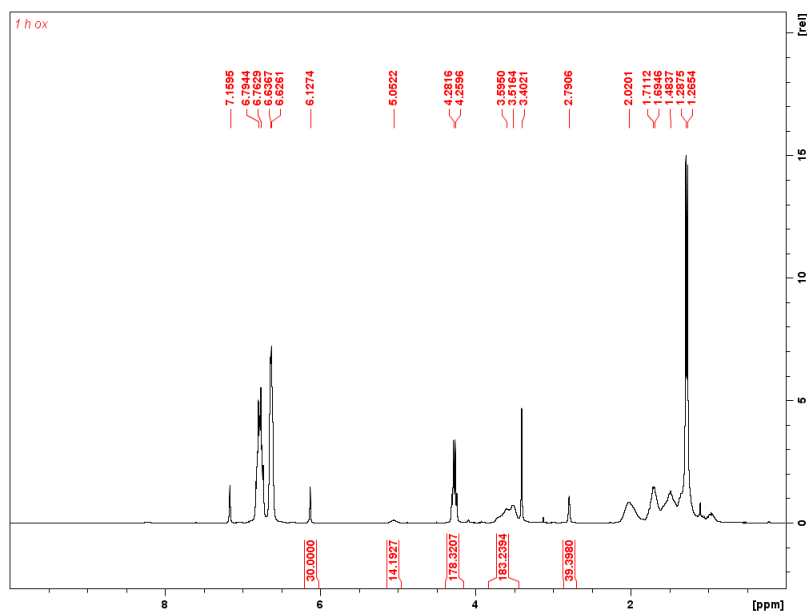


Figure C3. ^1H NMR spectrum of $[(\text{salfan})\text{Zr}(\text{O}'\text{Bu})_2][\text{BAR}^{\text{F}}]$ in presence of CHO and LA after one hour. ^1H NMR (300 MHz, 25 °C, C_6D_6), δ (ppm): 6.77 (m, $o\text{-F}_2\text{C}_6\text{H}_4$), 6.63 (m, $o\text{-F}_2\text{C}_6\text{H}_4$), 6.13 (s, 3H, PhH TMB), 5.05 (q, 2H, CHCH_3 PLA), 4.27 (q, 2H, CHCH_3 LA), 3.55 (b, 2H, COCH PCHO), 3.40 (s, 9H, CH_3 TMB), 2.79 (s, 2H, COCH CHO), 2.02 (m, 2H, COCHCH₂ PCHO), 1.70 (m, 2H, COCHCH₂CH₂ PCHO), 1.48 (m, 2H, COCHCH₂CH₂ PCHO), 1.27 (d, 6H, CHCH_3 LA).

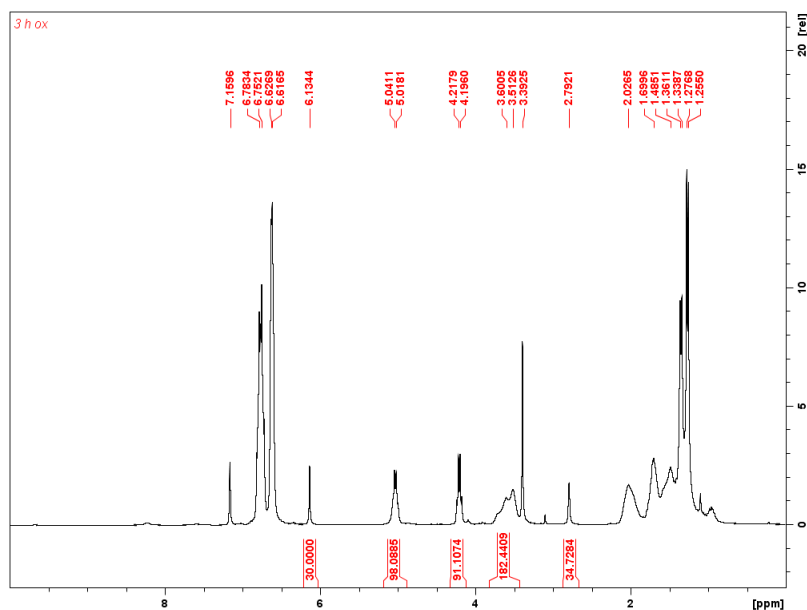


Figure C4. ^1H NMR spectrum of $[(\text{salfan})\text{Zr}(\text{O}'\text{Bu})_2][\text{BAR}^{\text{F}}]$ in presence of CHO and LA after 4 hours. ^1H NMR (300 MHz, 25 °C, C_6D_6), δ (ppm): 6.77 (m, $o\text{-F}_2\text{C}_6\text{H}_4$), 6.63 (m, $o\text{-F}_2\text{C}_6\text{H}_4$), 6.13 (s, 3H, PhH TMB), 5.05 (q, 2H, CHCH_3 PLA), 4.27 (q, 2H, CHCH_3 LA), 3.55 (b, 2H, COCH PCHO), 3.40 (s, 9H, CH_3 TMB), 2.79 (s, 2H, COCH CHO), 2.02 (m, 2H, COCHCH₂ PCHO), 1.70 (m, 2H, COCHCH₂CH₂ PCHO), 1.48 (m, 2H, COCHCH₂CH₂ PCHO), 1.34 (d, 6H, CHCH_3 PLA), 1.27 (d, 6H, CHCH_3 LA).

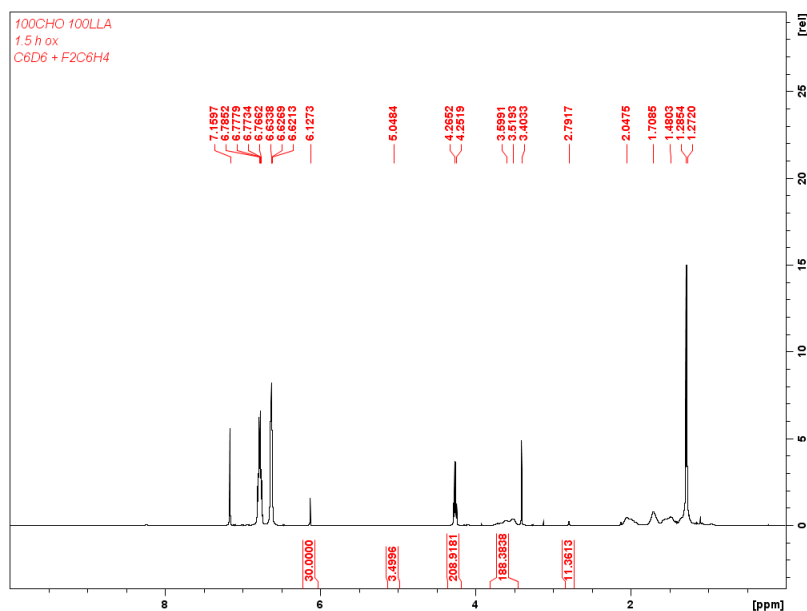


Figure C5. ^1H NMR spectrum of $[(\text{salfan})\text{Zr}(\text{O}'\text{Bu})_2][\text{BAr}^{\text{F}}]$ in presence of CHO and LA after one hour. ^1H NMR (300 MHz, 25 °C, C_6D_6), δ (ppm): 6.77 (m, $o\text{-F}_2\text{C}_6\text{H}_4$), 6.63 (m, $o\text{-F}_2\text{C}_6\text{H}_4$), 6.13 (s, 3H, PhH TMB), 5.05 (q, 2H, CHCH_3 PLA), 4.27 (q, 2H, CHCH_3 LA), 3.55 (b, 2H, COCH PCHO), 3.40 (s, 9H, CH_3 TMB), 2.79 (s, 2H, COCH CHO), 2.05 (m, 2H, COCHCH₂ PCHO), 1.71 (m, 2H, COCHCH₂CH₂ PCHO), 1.48 (m, 2H, COCHCH₂CH₂ PCHO), 1.27 (d, 6H, CHCH_3 LA).

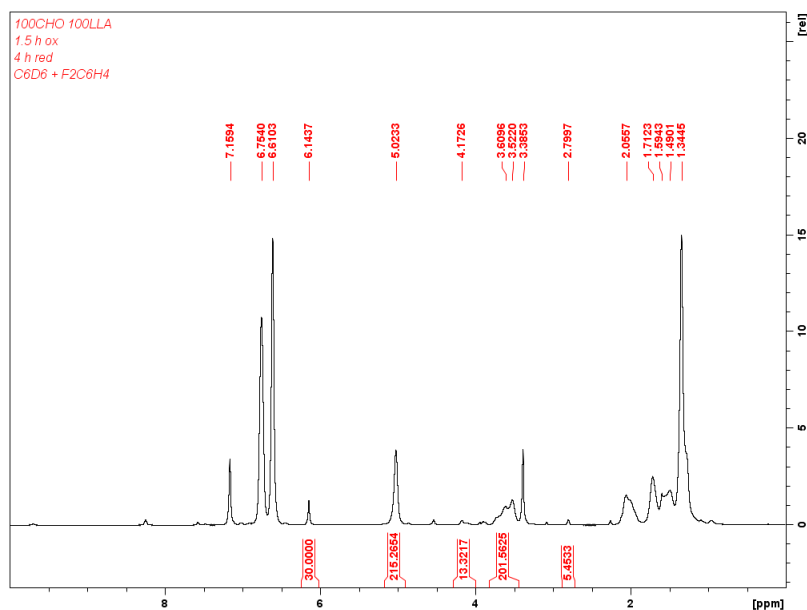


Figure C6. ^1H NMR spectrum of $[(\text{salfan})\text{Zr}(\text{O}'\text{Bu})_2][\text{BAr}^{\text{F}}]$ in presence of CHO and LA after one hour then reduced for 4 hours. ^1H NMR (300 MHz, 25 °C, C_6D_6), δ (ppm): 6.77 (m, $o\text{-F}_2\text{C}_6\text{H}_4$), 6.63 (m, $o\text{-F}_2\text{C}_6\text{H}_4$), 6.13 (s, 3H, PhH TMB), 5.02 (q, 2H, CHCH_3 PLA), 4.17 (q, 2H, CHCH_3 LA), 3.55 (b, 2H, COCH PCHO), 3.39 (s, 9H, CH_3 TMB), 2.80 (s, 2H, COCH CHO), 2.06 (m, 2H, COCHCH₂ PCHO), 1.71 (m, 2H, COCHCH₂CH₂ PCHO), 1.55 (m, 2H, COCHCH₂CH₂ PCHO), 1.34 (d, 6H, CHCH_3 PLA).

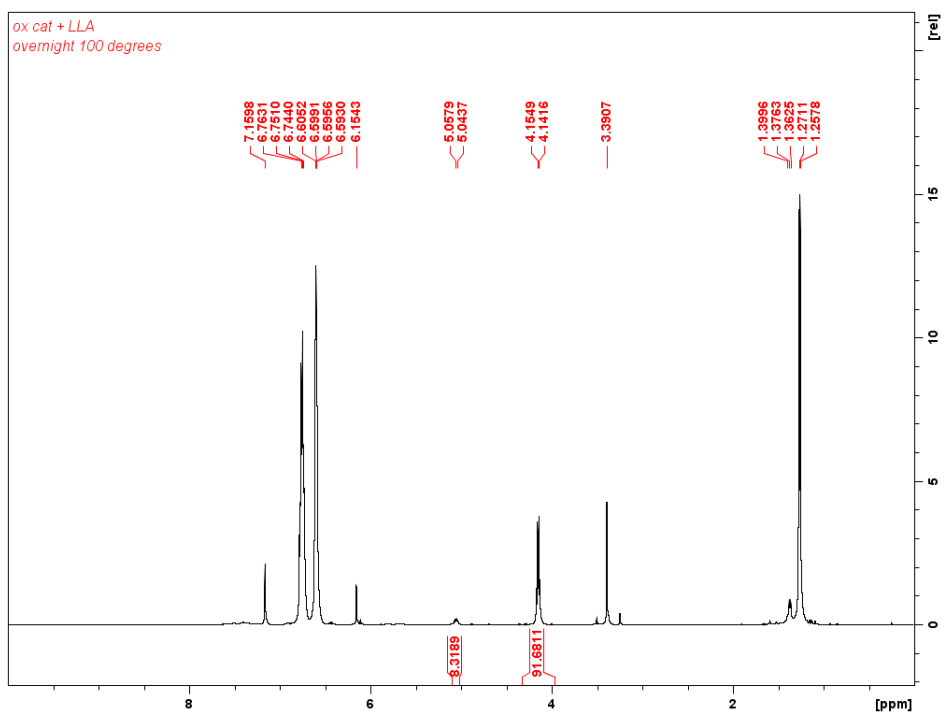


Figure C7. ^1H NMR spectrum of $[(\text{salan})\text{Zr}(\text{O}'\text{Bu})_2][\text{BAR}^{\text{F}}]$ in presence of LA after 24 hours.

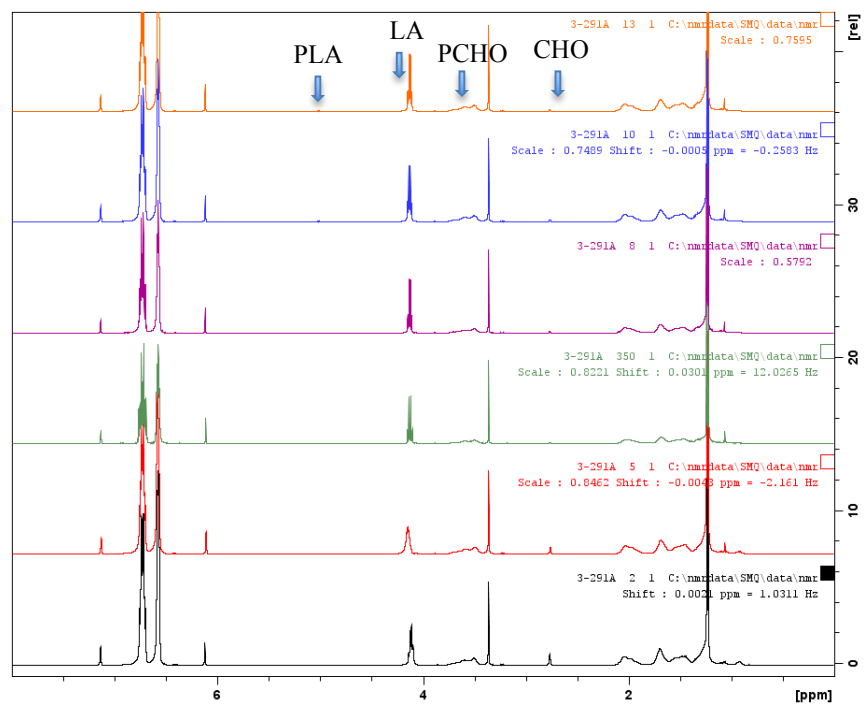


Figure C8. Overlaid ^1H NMR spectra of $[(\text{salan})\text{Zr}(\text{O}'\text{Bu})_2][\text{BAR}^{\text{F}}]$ in presence of CHO and LA at room temperature over 18 hours.

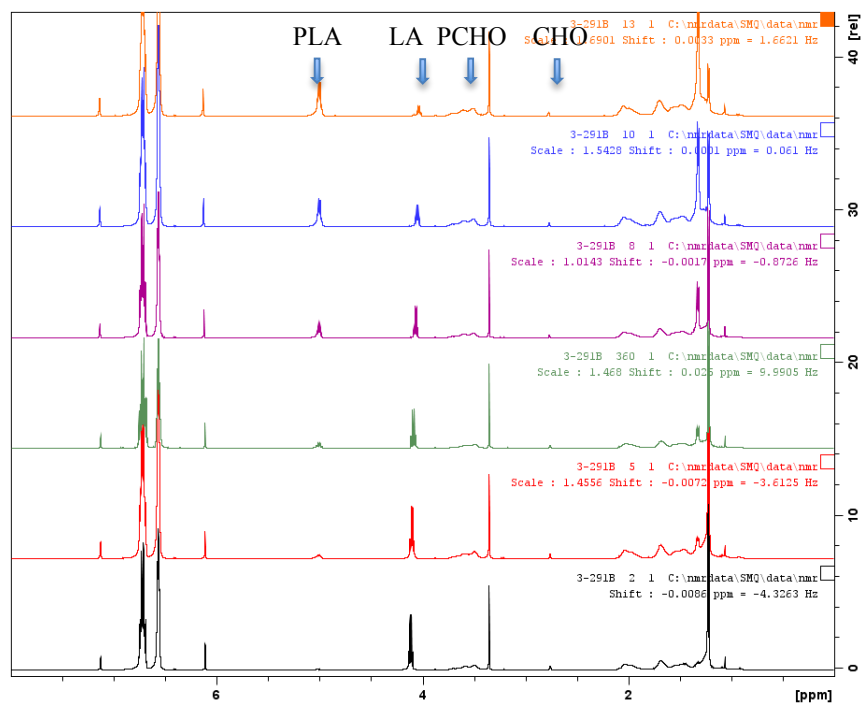


Figure C9. Overlaid ^1H NMR spectra of $[(\text{salfan})\text{Zr}(\text{O}'\text{Bu})_2][\text{BAR}^{\text{F}}]$ in presence of CHO and LA at 100 degrees over 18 hours.

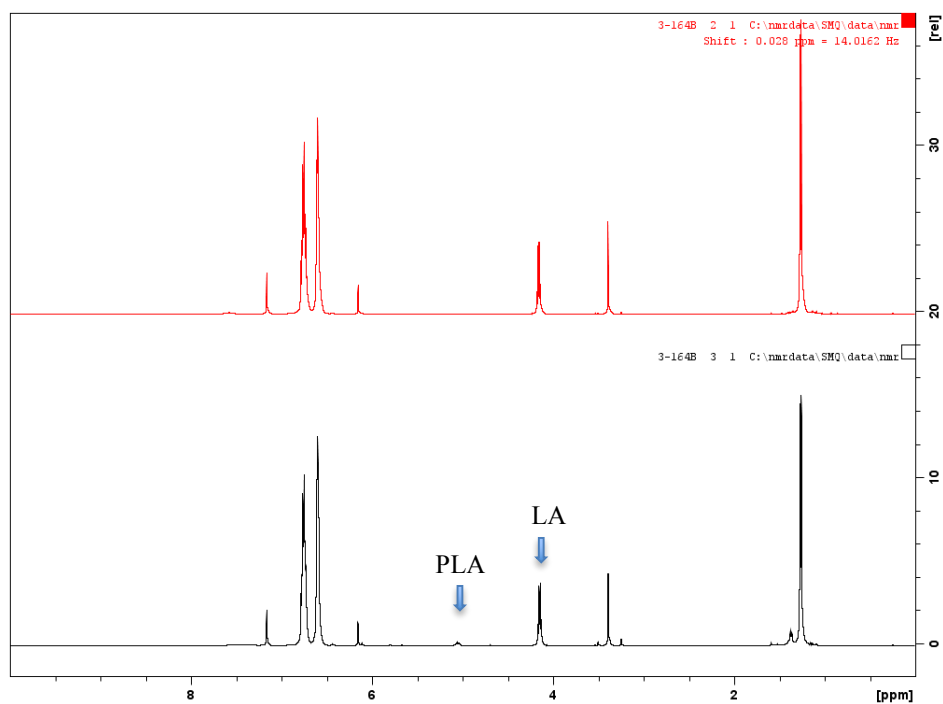


Figure C10. Overlaid ^1H NMR spectrum of $[(\text{salfan})\text{Zr}(\text{O}'\text{Bu})_2][\text{BAR}^{\text{F}}]$ in presence of LA at room temperature over 25 hours.

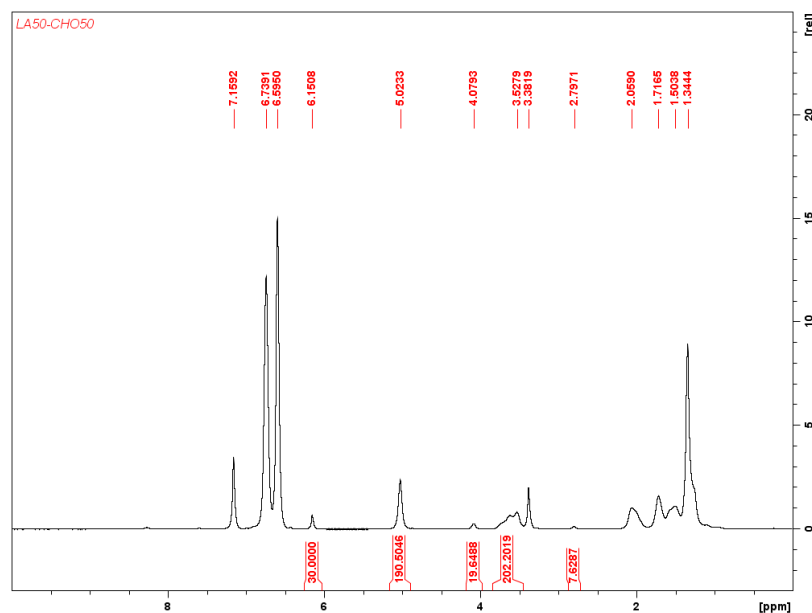


Figure C11. ^1H NMR spectrum of LA₅₀-CHO₅₀ (Table 3.4, entry 1). Polymerization of 100 equivalents of L-lactide, and cyclohexene oxide, monomers added sequentially, using initiator redox switch “red-ox”. ^1H NMR (300 MHz, 25 °C, C₆D₆), δ (ppm): 6.74 (m, *o*-F₂C₆H₄), 6.60 (m, *o*-F₂C₆H₄), 6.15 (s, 3H, PhH TMB), 5.02 (q, 2H, CHCH₃ PLA), 4.08 (q, 2H, CHCH₃ LA), 3.53 (b, 2H, COCH PCHO), 3.38 (s, 9H, CH₃ TMB), 2.80 (s, 2H, COCH CHO), 2.06 (m, 2H, COCHCH₂ PCHO), 1.71 (m, 2H, COCHCH₂CH₂ PCHO), 1.50 (m, 2H, COCHCH₂CH₂ PCHO), 1.34 (d, 6H, CHCH₃ PLA).

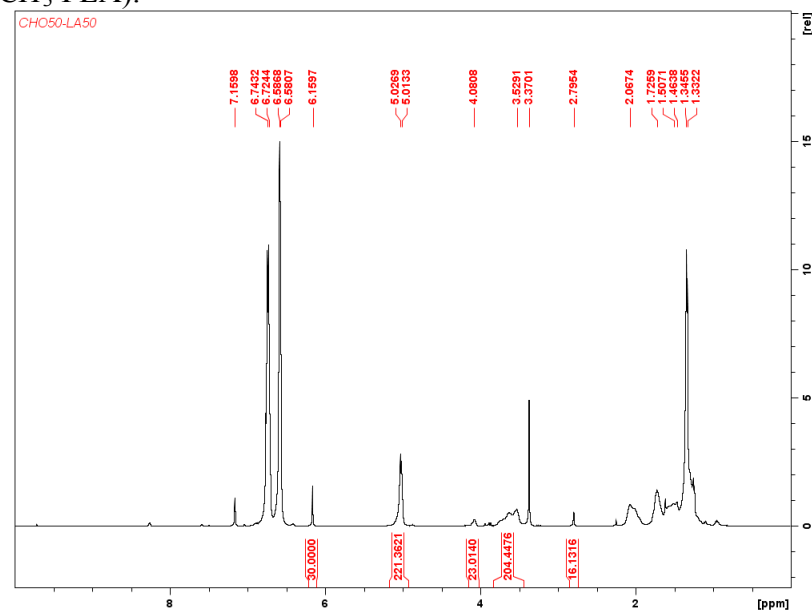


Figure C12. ^1H NMR spectrum of LA₅₀-CHO₅₀ (Table 3.4, entry 2). Polymerization of 100 equivalents of L-lactide, and cyclohexene oxide, monomers added sequentially, using initiator redox switch “ox-red”. ^1H NMR (300 MHz, 25 °C, C₆D₆), δ (ppm): 6.73 (m, *o*-F₂C₆H₄), 6.58 (m, *o*-F₂C₆H₄), 6.16 (s, 3H, PhH TMB), 5.02 (q, 2H, CHCH₃ PLA), 4.08 (q, 2H, CHCH₃ LA), 3.45 (b, 2H, COCH PCHO), 3.37 (s, 9H, CH₃ TMB), 2.80 (s, 2H, COCH CHO), 2.07 (m, 2H, COCHCH₂ PCHO), 1.73 (m, 2H, COCHCH₂CH₂ PCHO), 1.48 (m, 2H, COCHCH₂CH₂ PCHO), 1.34 (d, 6H, CHCH₃ PLA).

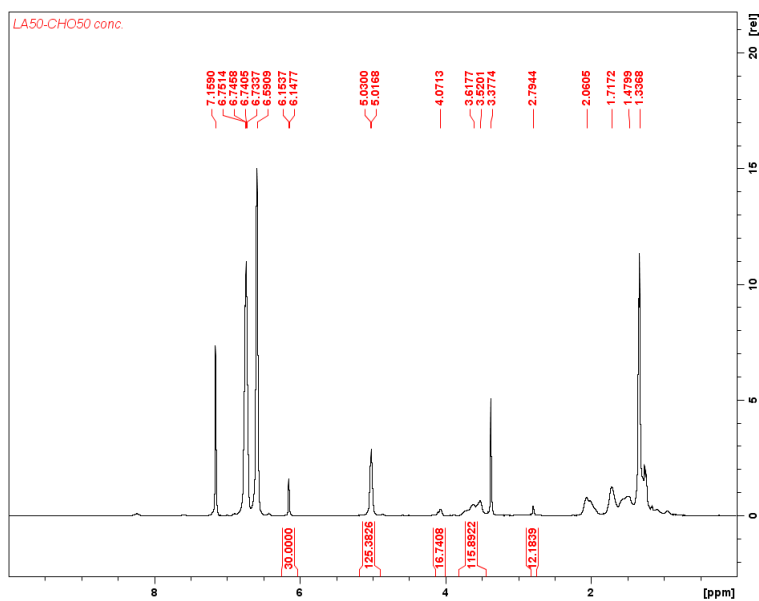


Figure C13. ^1H NMR spectrum of LA₅₀-CHO₅₀ (Table 3.4, entry 3). Polymerization of 100 equivalents of L-lactide, and cyclohexene oxide, monomers added sequentially, using initiator redox switch “red-ox”. ^1H NMR (300 MHz, 25 °C, C₆D₆), δ (ppm): 6.74 (m, *o*-F₂C₆H₄), 6.59 (m, *o*-F₂C₆H₄), 6.15 (s, 3H, PhH TMB), 5.02 (q, 2H, CHCH₃ PLA), 4.07 (q, 2H, CHCH₃ LA), 3.57 (b, 2H, COCH PCHO), 3.38 (s, 9H, CH₃ TMB), 2.79 (s, 2H, COCH CHO), 2.06 (m, 2H, COCHCH₂ PCHO), 1.71 (m, 2H, COCHCH₂CH₂ PCHO), 1.48 (m, 2H, COCHCH₂CH₂ PCHO), 1.34 (d, 6H, CHCH₃ PLA).

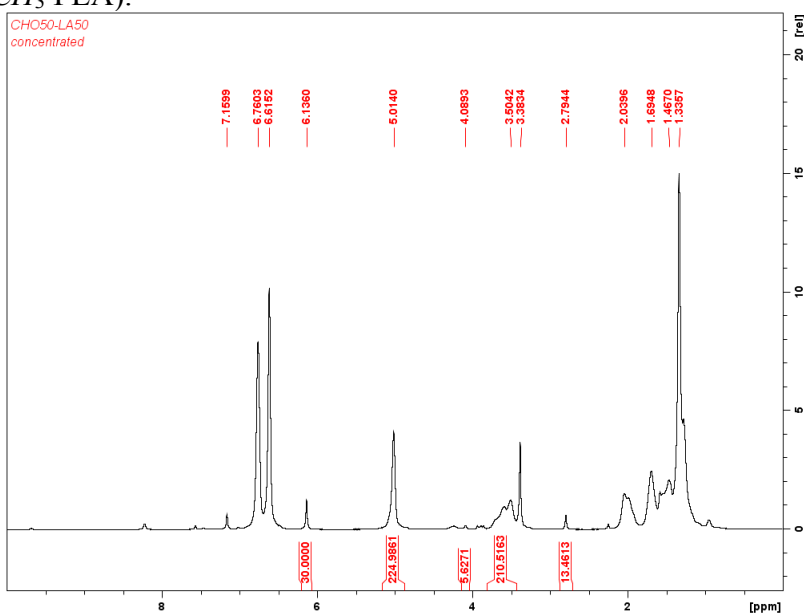


Figure C14. ^1H NMR spectrum of LA₅₀-CHO₅₀ (Table 3.4, entry 4). Polymerization of 100 equivalents of L-lactide, and cyclohexene oxide, monomers added sequentially, using initiator redox switch “ox-red”. ^1H NMR (300 MHz, 25 °C, C₆D₆), δ (ppm): 6.76 (m, *o*-F₂C₆H₄), 6.62 (m, *o*-F₂C₆H₄), 6.14 (s, 3H, PhH TMB), 5.01 (q, 2H, CHCH₃ PLA), 4.09 (q, 2H, CHCH₃ LA), 3.50 (b, 2H, COCH PCHO), 3.38 (s, 9H, CH₃ TMB), 2.79 (s, 2H, COCH CHO), 2.04 (m, 2H, COCHCH₂ PCHO), 1.69 (m, 2H, COCHCH₂CH₂ PCHO), 1.47 (m, 2H, COCHCH₂CH₂ PCHO), 1.34 (d, 6H, CHCH₃ PLA).

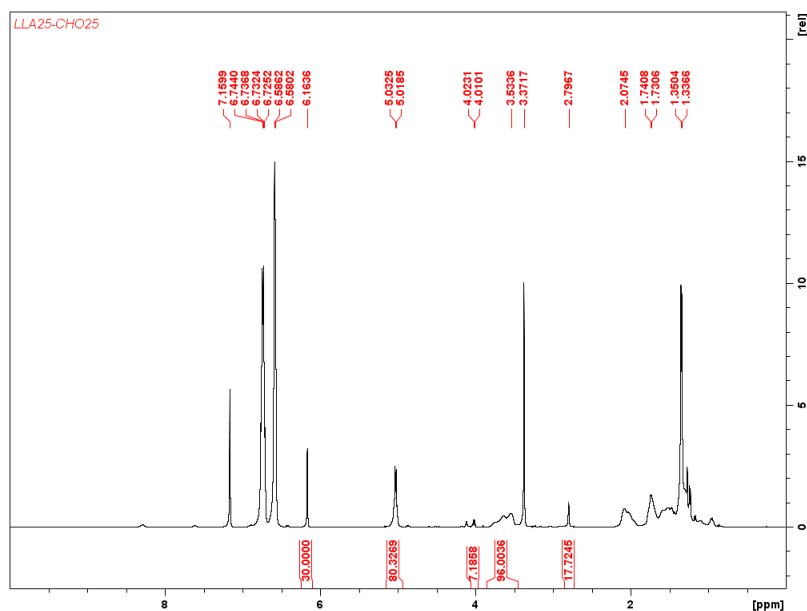


Figure C15. ^1H NMR spectrum of LA₂₅-CHO₂₅ (Table 3.4, entry 5). Polymerization of 50 equivalents of L-lactide, and cyclohexene oxide, monomers added sequentially, using initiator redox switch “red-ox”. ^1H NMR (300 MHz, 25 °C, C₆D₆), δ (ppm): 6.73 (m, *o*-F₂C₆H₄), 6.58 (m, *o*-F₂C₆H₄), 6.16 (s, 3H, PhH TMB), 5.02 (q, 2H, CHCH₃ PLA), 4.02 (q, 2H, CHCH₃ LA), 3.53 (b, 2H, COCH PCHO), 3.37 (s, 9H, CH₃ TMB), 2.80 (s, 2H, COCH CHO), 2.07 (m, 2H, COCHCH₂ PCHO), 1.74 (m, 2H, COCHCH₂CH₂ PCHO), 1.34 (d, 6H, CHCH₃ PLA).

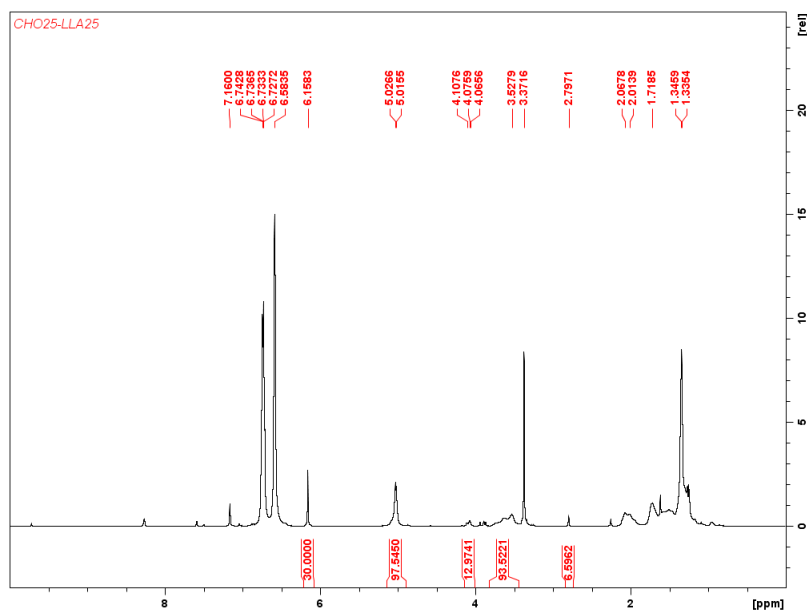


Figure C16. ^1H NMR spectrum of CHO₂₅-LA₂₅ (Table 3.4, entry 6). Polymerization of 50 equivalents of L-lactide, and cyclohexene oxide, monomers added sequentially, using initiator redox switch “ox-red”. ^1H NMR (300 MHz, 25 °C, C₆D₆), δ (ppm): 6.74 (m, *o*-F₂C₆H₄), 6.58 (m, *o*-F₂C₆H₄), 6.16 (s, 3H, PhH TMB), 5.02 (q, 2H, CHCH₃ PLA), 4.08 (q, 2H, CHCH₃ LA), 3.53 (b, 2H, COCH PCHO), 3.37 (s, 9H, CH₃ TMB), 2.80 (s, 2H, COCH CHO), 2.04 (m, 2H, COCHCH₂ PCHO), 1.72 (m, 2H, COCHCH₂CH₂ PCHO), 1.34 (d, 6H, CHCH₃ PLA).

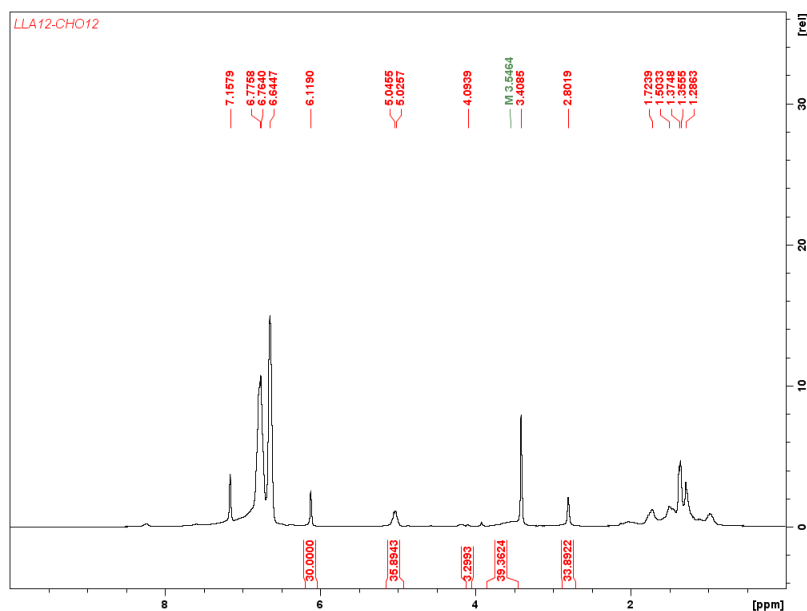


Figure C17. ^1H NMR spectrum of LA₁₂-CHO₁₂ (Table 3.4, entry 7). Polymerization of 25 equivalents of L-lactide, and cyclohexene oxide, monomers added sequentially, using initiator redox switch “red-ox”. ^1H NMR (300 MHz, 25 °C, C₆D₆), δ (ppm): 6.77 (m, *o*-F₂C₆H₄), 6.64 (m, *o*-F₂C₆H₄), 6.12 (s, 3H, PhH TMB), 5.03 (q, 2H, CHCH₃ PLA), 4.09 (q, 2H, CHCH₃ LA), 3.55 (b, 2H, COCH PCHO), 3.41 (s, 9H, CH₃ TMB), 2.80 (s, 2H, COCH CHO), 1.73 (m, 2H, COCHCH₂CH₂ PCHO), 1.50 (m, 2H, COCHCH₂CH₂ PCHO), 1.36 (d, 6H, CHCH₃ PLA).

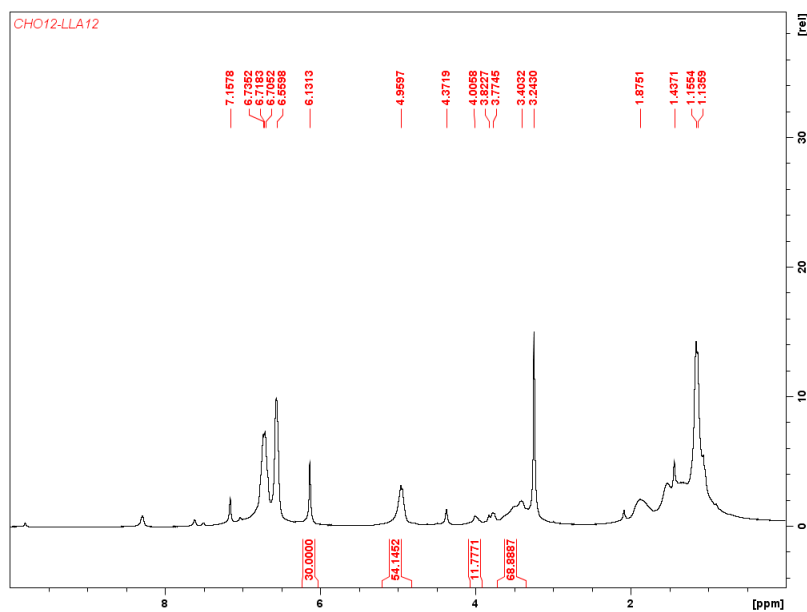


Figure C18. ^1H NMR spectrum of CHO₁₂-LA₁₂ (Table 3.4, entry 8). Polymerization of 25 equivalents of L-lactide, and cyclohexene oxide, monomers added sequentially, using initiator redox switch “ox-red”. ^1H NMR (300 MHz, 25 °C, C₆D₆), δ (ppm): 6.72 (m, *o*-F₂C₆H₄), 6.56 (m, *o*-F₂C₆H₄), 6.13 (s, 3H, PhH TMB), 4.96 (q, 2H, CHCH₃ PLA), 4.01 (q, 2H, CHCH₃ LA), 3.40 (b, 2H, COCH PCHO), 3.24 (s, 9H, CH₃ TMB), 1.88 (m, 2H, COCHCH₂ PCHO), 1.44 (m, 2H, COCHCH₂CH₂ PCHO), 1.15 (d, 6H, CHCH₃ PLA).

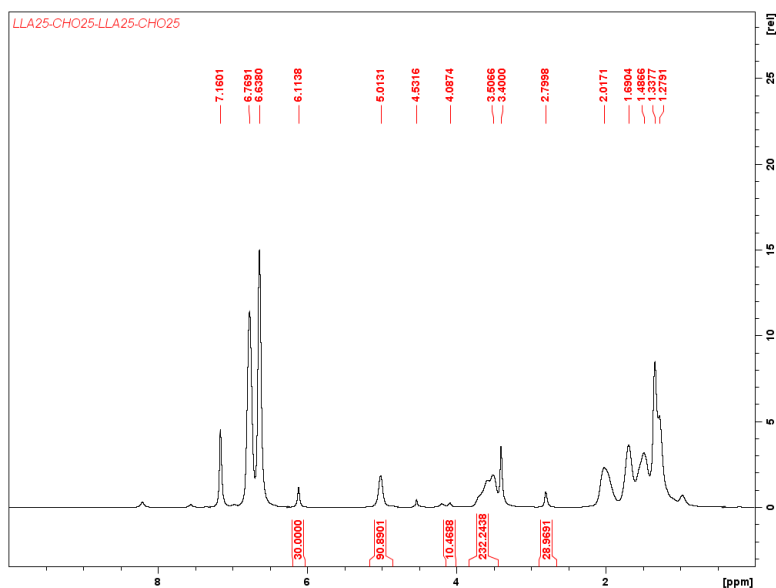


Figure C19. ^1H NMR spectrum of $\text{LA}_{25}\text{-CHO}_{25}\text{-LA}_{25}\text{-CHO}_{25}$ (Table 3.4, entry 9). Polymerization of 100 equivalents of L-lactide, and cyclohexene oxide, monomers added sequentially, using initiator redox switch “red-ox-red-ox”. ^1H NMR (300 MHz, 25 °C, C_6D_6), δ (ppm): 6.77 (m, $o\text{-F}_2\text{C}_6\text{H}_4$), 6.64 (m, $o\text{-F}_2\text{C}_6\text{H}_4$), 6.11 (s, 3H, PhH TMB), 5.01 (q, 2H, CHCH_3 PLA), 4.09 (q, 2H, CHCH_3 LA), 3.50 (b, 2H, COCH PCHO), 3.40 (s, 9H, CH_3 TMB), 2.80 (s, 2H, COCH CHO), 2.02 (m, 2H, COCHCH_2 PCHO), 1.69 (m, 2H, $\text{COCHCH}_2\text{CH}_2$ PCHO), 1.49 (m, 2H, $\text{COCHCH}_2\text{CH}_2$ PCHO), 1.34 (d, 6H, CHCH_3 PLA).

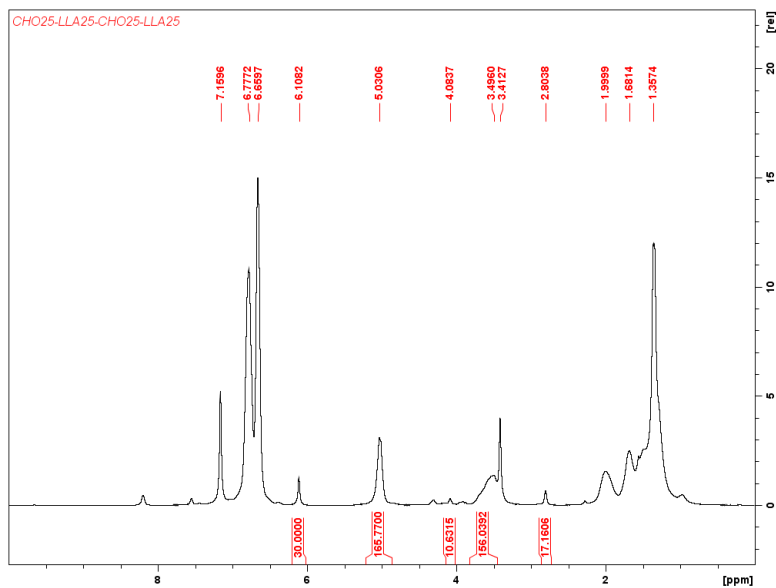


Figure C20. ^1H NMR spectrum of $\text{CHO}_{25}\text{-LA}_{25}\text{-CHO}_{25}\text{-LA}_{25}$ (Table 3.4, entry 10). Polymerization of 100 equivalents of L-lactide, and cyclohexene oxide, monomers added sequentially, using initiator redox switch “ox-red-ox-red”. ^1H NMR (300 MHz, 25 °C, C_6D_6), δ (ppm): 6.78 (m, $o\text{-F}_2\text{C}_6\text{H}_4$), 6.56 (m, $o\text{-F}_2\text{C}_6\text{H}_4$), 6.11 (s, 3H, PhH TMB), 5.03 (q, 2H, CHCH_3 PLA), 4.08 (q, 2H, CHCH_3 LA), 3.50 (b, 2H, COCH PCHO), 3.41 (s, 9H, CH_3 TMB), 2.80 (s, 2H, COCH CHO), 2.00 (m, 2H, COCHCH_2 PCHO), 1.68 (m, 2H, $\text{COCHCH}_2\text{CH}_2$ PCHO), 1.36 (d, 6H, CHCH_3 PLA).

Gel Permeation Chromatography

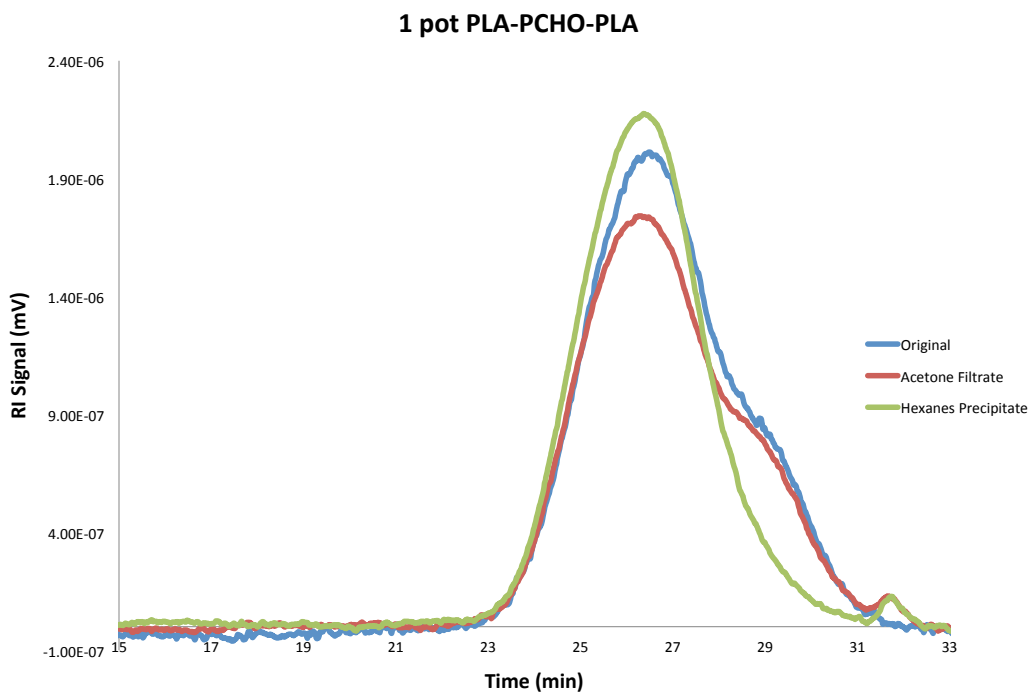


Figure C21. GPC traces of PLA-PCHO-PLA during selective precipitation process (Table 3.1).

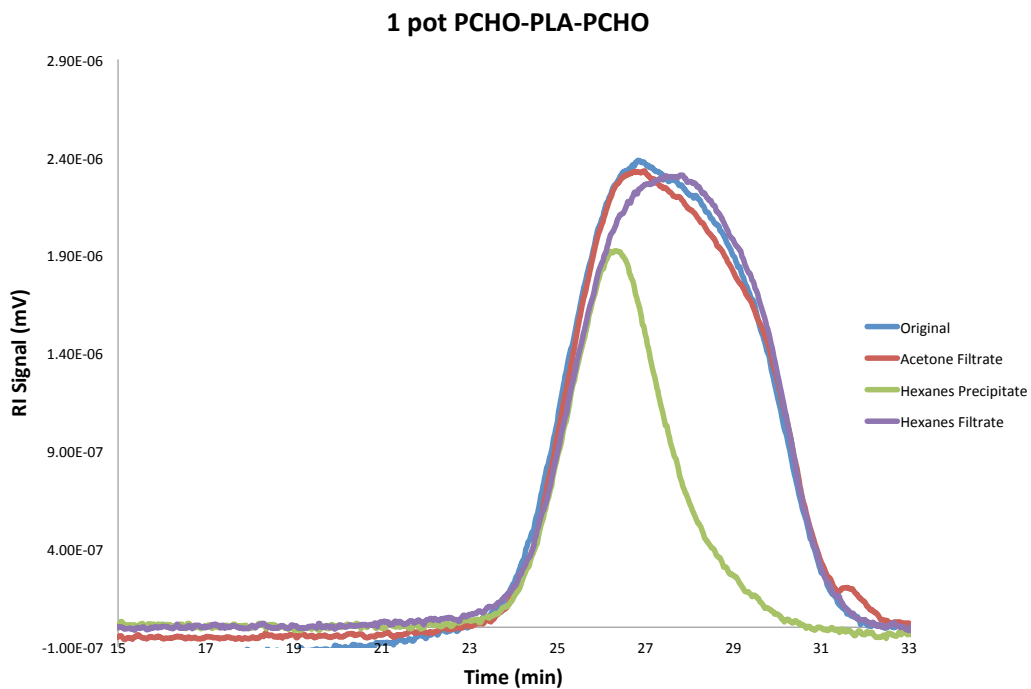


Figure C22. GPC traces of PLA-PCHO-PLA during selective precipitation process (Table 3.2).

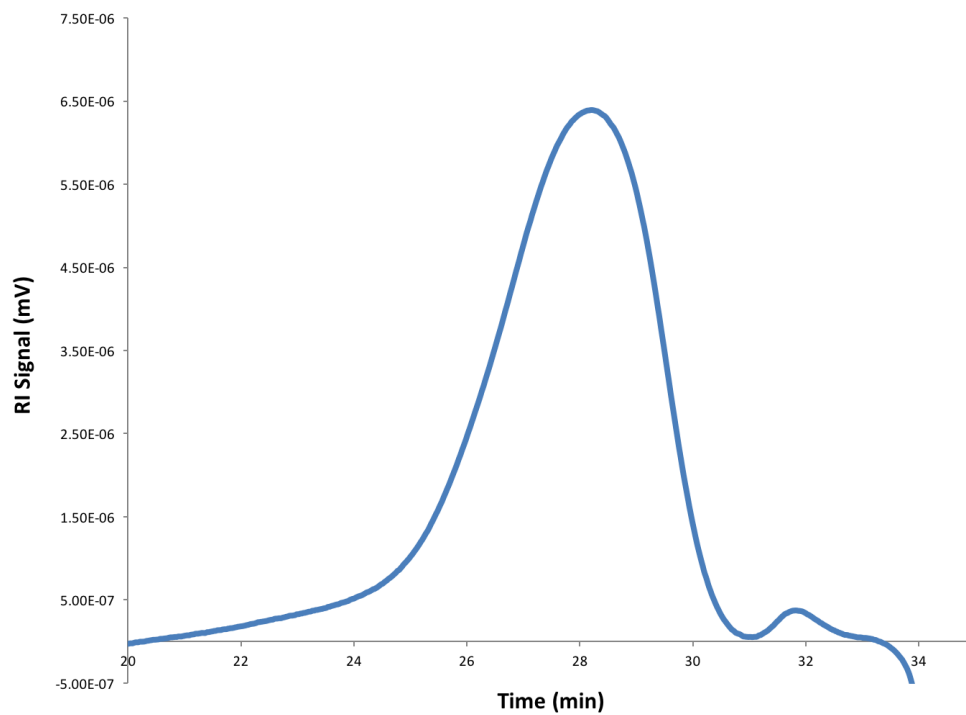


Figure C23. GPC trace of LA₅₀-CHO₅₀ (Table 3.4, entry 1). $M_n = 10900$ Da, $M_w = 13200$ Da, $\mathcal{D} = 1.21$.

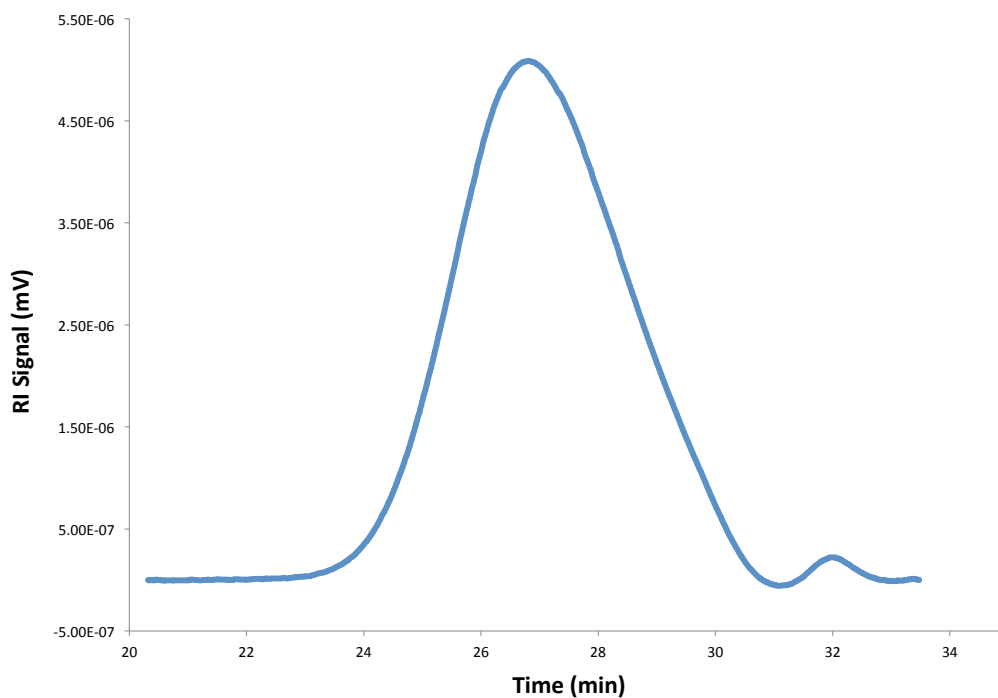


Figure C24. GPC trace of CHO₅₀-LA₅₀ (Table 3.4, entry 2). $M_n = 13800$ Da, $M_w = 21100$ Da, $\mathcal{D} = 1.53$.

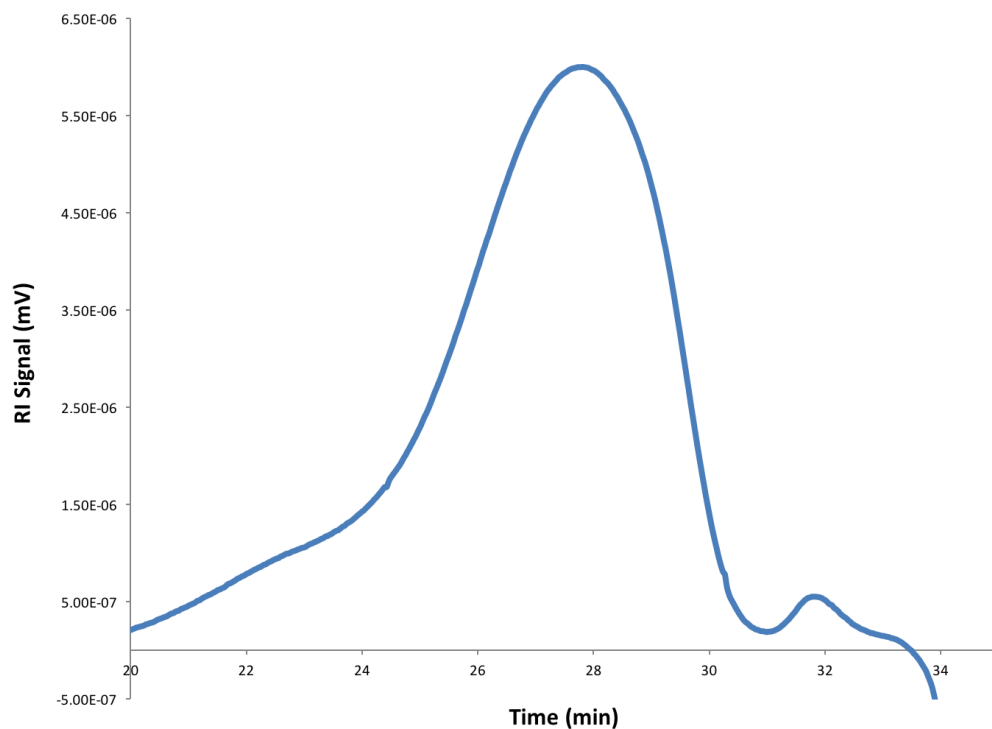


Figure C25. GPC trace of LA₅₀-CHO₅₀ (Table 3.4, entry 3). $M_n = 13600$ Da, $M_w = 17500$ Da, $\mathcal{D} = 1.29$.

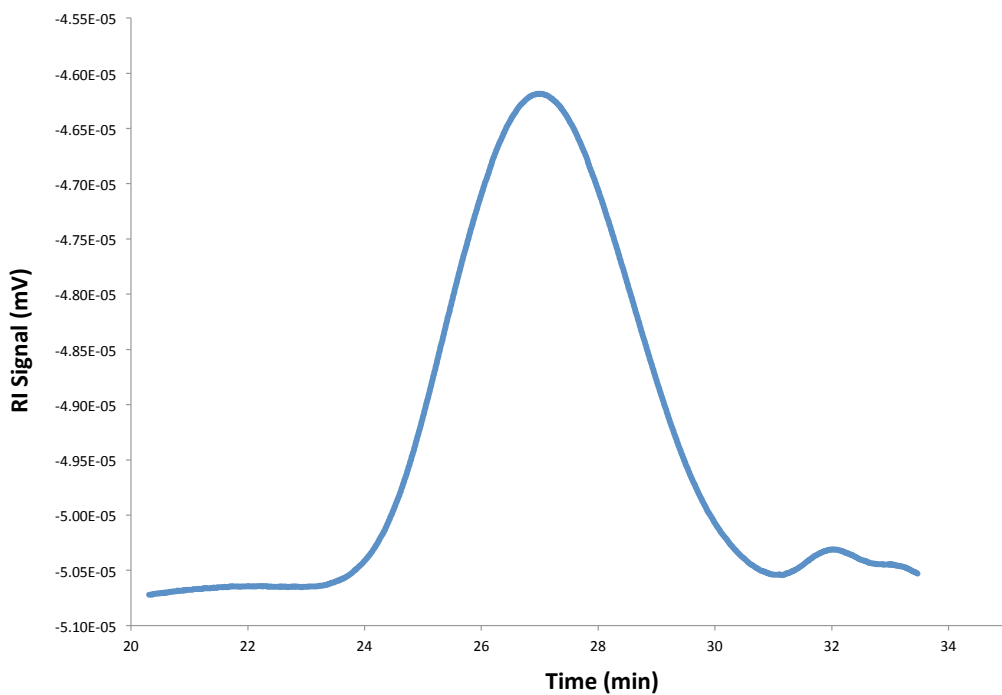


Figure C26. GPC trace of CHO₅₀-LA₅₀ (Table 3.4, entry 4). $M_n = 15500$ Da, $M_w = 19500$ Da, $\mathcal{D} = 1.26$.

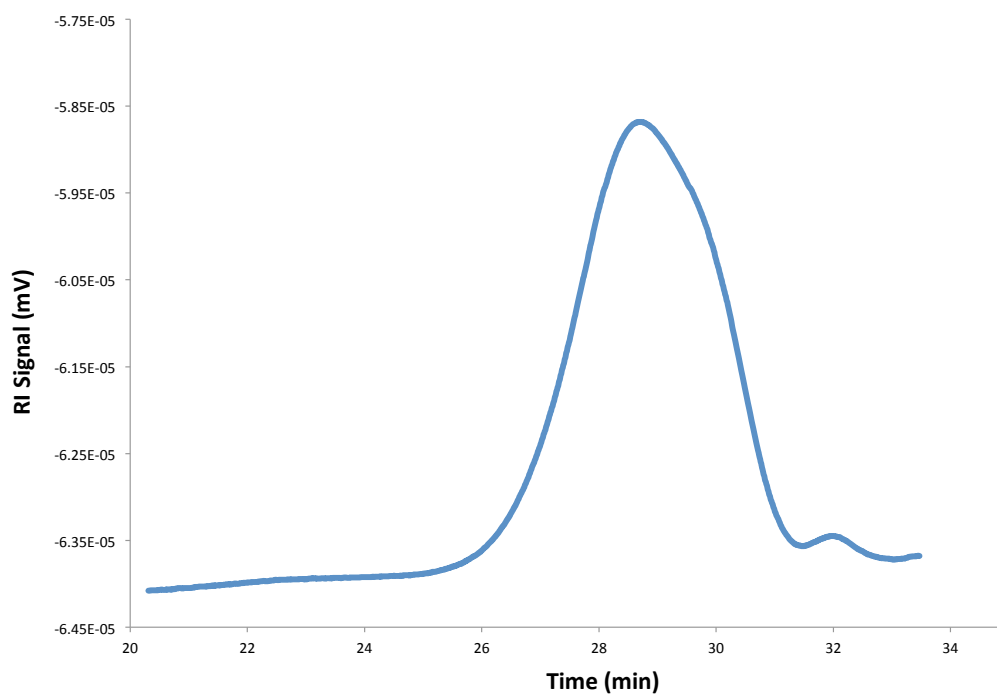


Figure C27. GPC trace of LA₂₅-CHO₂₅ (Table 3.4, entry 5). $M_n = 7400$ Da, $M_w = 8900$ Da, $D = 1.20$.

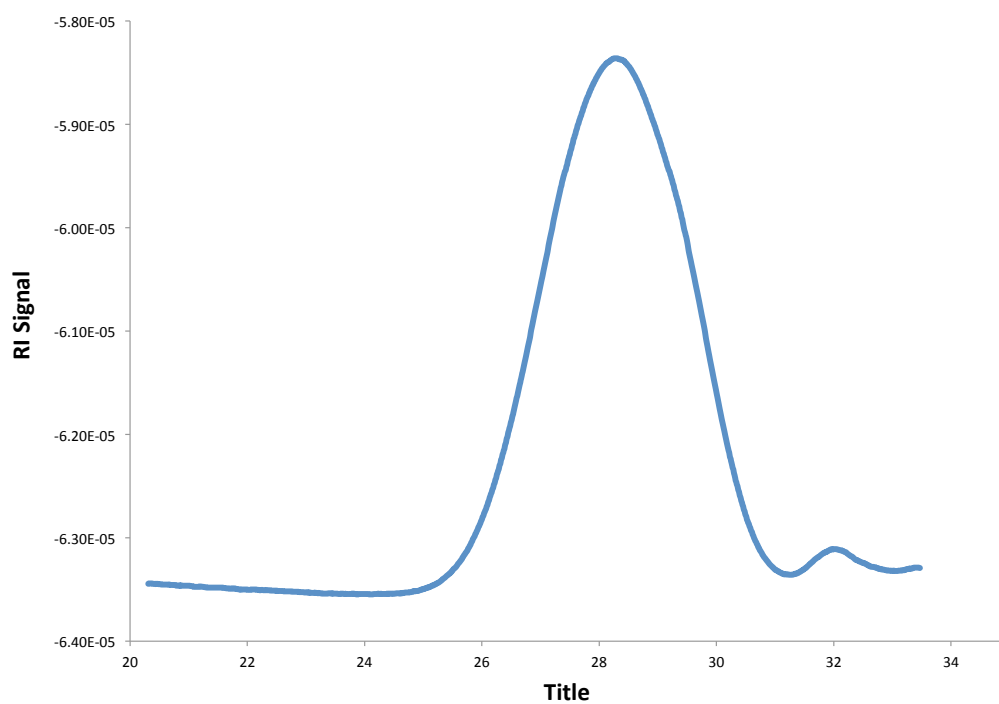


Figure C28. GPC trace of CHO₂₅-LA₂₅ (Table 3.4, entry 6). $M_n = 8700$ Da, $M_w = 10700$ Da, $D = 1.23$.

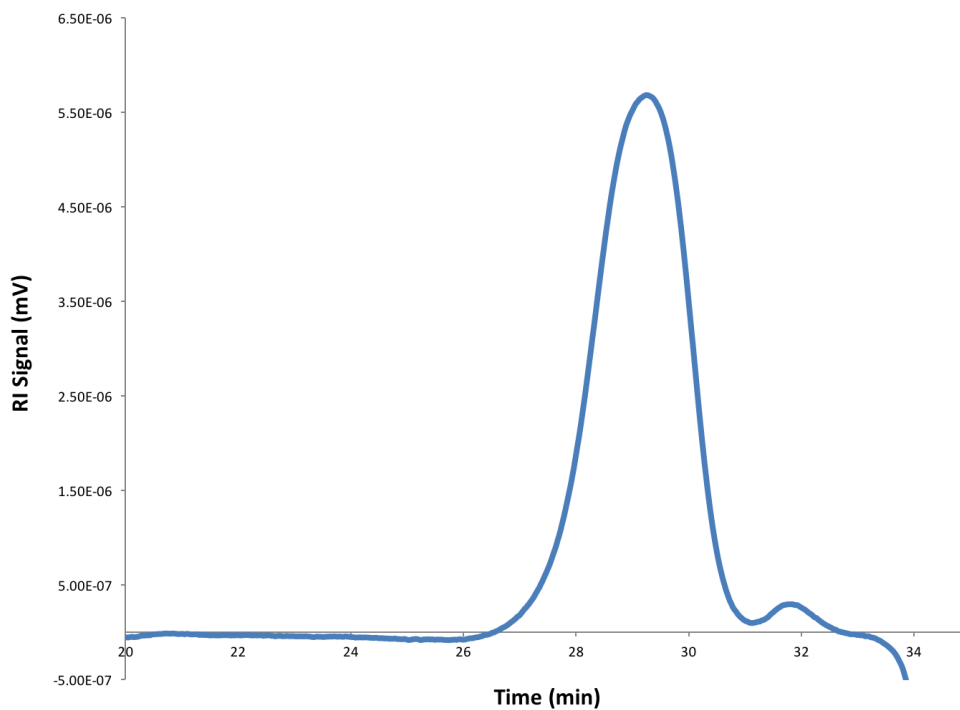


Figure C29. GPC trace of LA₁₂-CHO₁₂ (Table 3.4, entry 7). $M_n = 3800$ Da, $M_w = 4028$ Da, $D = 1.06$.

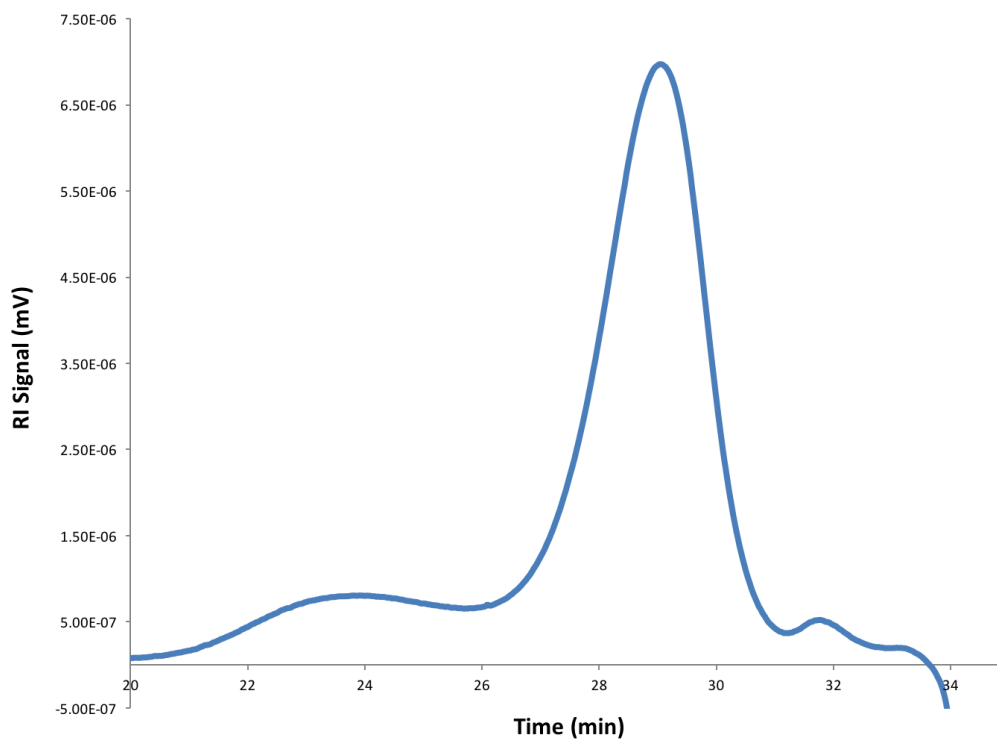


Figure C30. GPC trace of CHO₁₂-LA₁₂ (Table 3.4, entry 8). $M_n = 8800$ Da, $M_w = 10300$ Da, $D = 1.17$.

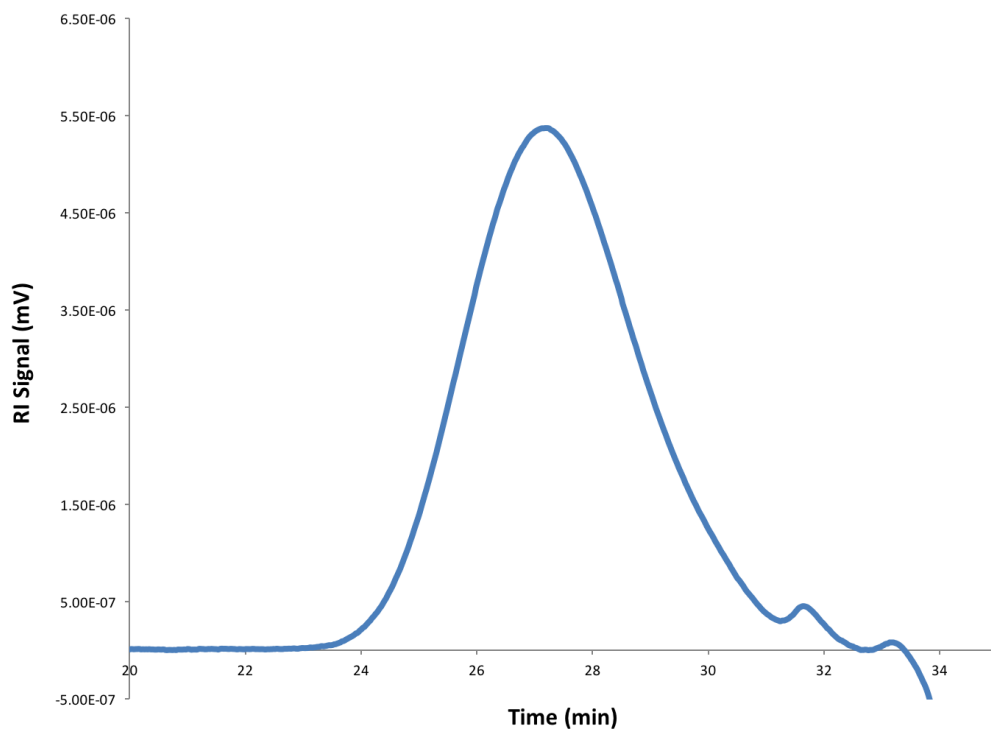


Figure C31. GPC trace of LA₂₅-CHO₂₅-LA₂₅-CHO₂₅ (Table 3.4, entry 9). $M_n = M_n = 12100$ Da, $M_w = 15900$ Da, $\mathcal{D} = 1.31$.

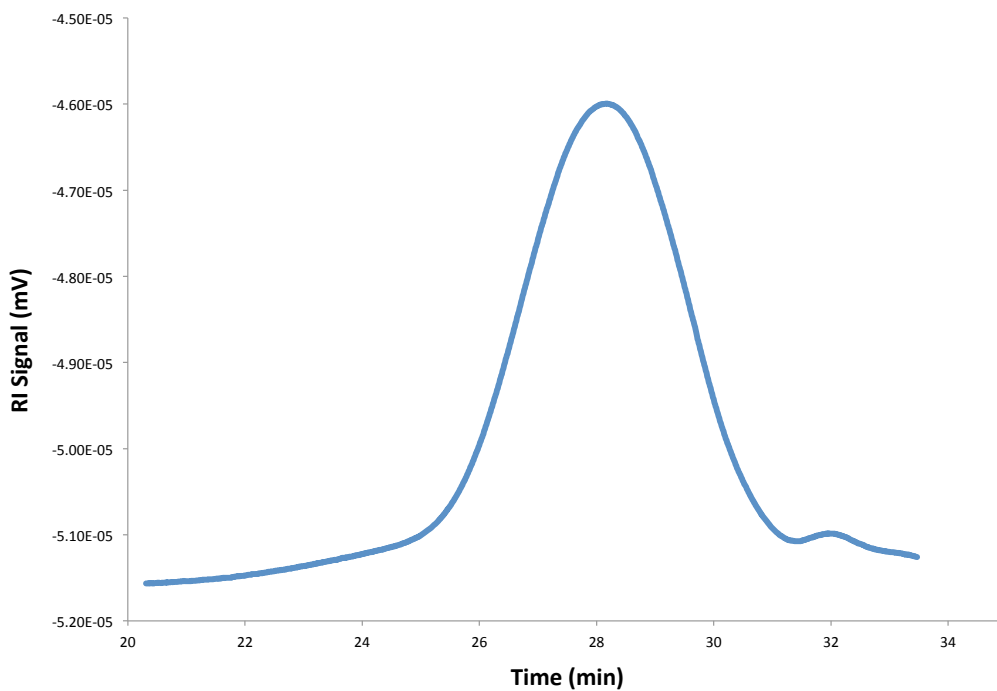


Figure C32. GPC trace of CHO₂₅-LA₂₅-CHO₂₅-LA₂₅ (Table 3.4, entry 10). $M_n = 9700$ Da, $M_w = 11300$ Da, $\mathcal{D} = 1.16$.

DFT Calculations

All calculations were carried out by Junnian Wei with the GAUSSIAN 09 program package¹⁰ on the Extreme Science and Engineering Discovery Environment (XSEDE).¹¹ The ^tBu groups on the benzene rings are replaced by H atoms and the ZrO^tBu groups are replaced by ZrOMe groups to simplify the calculations. It should be noted that using a dispersion correction is important and the D3 version of Grimme's dispersion¹² was applied.

Table S1. Energies, enthalpies, and free energies of the structures calculated at the PBE1PBE/SDD, 6-311+G(d,p) (PCM, GD3, benzene)//B3LYP/LANL2DZ, 6-31G(d) level.

Structures	correction of H	correction of G	G	E with corrections	new G with corrections
lactide	0.151554	0.105907	-534.250539	-533.935059	-533.829152
cyclohexene oxide	0.158689	0.122532	-309.664403	-309.516963	-309.394431
I^{red} (initiator)	0.587655	0.485362	-1666.372396	-1666.502833	-1666.017471
I^{ox} (initiator)	0.588406	0.479747	-1666.171515	-1666.309904	-1665.830157
II^{ox}-CHO	0.749101	0.615668	-1975.856085	-1975.86191	-1975.246242
TS1^{ox}-CHO	0.747391	0.62125	-1975.838504	-1975.851758	-1975.230508
III^{ox}-CHO	0.751521	0.622593	-1975.937727	-1975.95339	-1975.330797
IV^{ox}-CHO	0.913225	0.773089	-2285.59277	-2285.505788	-2284.732699
V^{ox}-CHO	0.910638	0.764821	-2285.540016	-2285.445315	-2284.680494
TS2^{ox}-CHO	0.910643	0.769705	-2285.582823	-2285.492283	-2284.722578
TS3^{ox}-CHO	0.909782	0.766979	-2285.556187	-2285.460886	-2284.693907
TS1^{red}-LA	0.73905	0.605425	-2200.589108	-2200.419507	-2199.814082
II^{red}-LA	0.740715	0.603911	-2200.60214	-2200.434596	-2199.830685
TS2^{red}-LA	0.739124	0.60819	-2200.579681	-2200.419356	-2199.811166
III^{red}-LA	0.740294	0.60748	-2200.586012	-2200.424113	-2199.816633
IV^{red}-LA	0.74073	0.605276	-2200.618465	-2200.447092	-2199.841816
V^{red}-LA	0.74218	0.613229	-2200.62201	-2200.474105	-2199.860876
TS1^{ox}-LA	0.74111	0.606918	-2200.410945	-2200.261514	-2199.654596
II^{ox}-LA	0.742477	0.606644	-2200.416685	-2200.268902	-2199.662258
TS2^{ox}-LA	0.740598	0.606484	-2200.40446	-2200.259137	-2199.652653
III^{ox}-LA	0.741145	0.608287	-2200.412567	-2200.266644	-2199.658357
IV^{ox}-LA	0.742425	0.603117	-2200.452774	-2200.291655	-2199.688538
V^{ox}-LA	0.742247	0.608517	-2200.384382	-2200.285657	-2199.67714

I'	0.665293	0.539118	-1933.328843	-1933.31054	-1932.771422
TS1'	0.818052	0.67355	-2467.54084	-2467.25774	-2466.58419
II'	0.819143	0.673284	-2467.541145	-2467.25841	-2466.585126
TS2'	0.817662	0.673041	-2467.532126	-2467.252263	-2466.579222
III'	0.818745	0.669277	-2467.539179	-2467.255449	-2466.586172
IV'	0.819589	0.669263	-2467.539565	-2467.24172	-2466.572457

References

1. (a) A. J. Teator, H. Shao, G. Lu, P. Liu, C. W. Bielawski, *Organometallics*, 2017, **36**, 490-497.
(b) S. Klenk, S. Rupf, L. Suntrup, M. van der Meer, B. Sarkar, *Organometallics*, 2017, **36**, 2026-2035.
(c) A. Feyrer, F. Breher, *Inorg. Chem. Front.*, 2017, **4**, 1125-1134.
(d) Blanco, V.; Leigh, D. A.; Marcos, V., *Chem. Soc. Rev.* 2015, **44**, 5341-5370.
(e) U. Lüning, *Angew. Chem. Int. Ed.*, 2012, **51**, 8163-8165.
(f) H. J. Yoon, J. Kuwabara, J.-H. Kim, C. A. Mirkin, *Science*, 2010, **330**, 66-69.
(g) S. M. Shepard, P. L. Diaconescu, *Organometallics*, 2016, **35**, 2446–2453.
(h) W. Huang, P. L. Diaconescu, *Inorg. Chem.*, 2016, **55**, 10013–10023.
(i) B. Liu, D. Cui, T. Tang, *Angew. Chem. Int. Ed.*, 2016, **55**, 11975-11978.
(j) A. J. Teator, D. N. Lastovickova, C. W. Bielawski, *Chem. Rev.*, 2016, **116**, 1969-1992.
(k) S. M. Guillaume, E. Kirillov, Y. Sarazin, J.-F. Carpentier, *Chem. Eur. J.*, 2015, **21**, 7988-8003.
(l) L. A. Brown, J. L. Rhinehart, B. K. Long, *ACS Catal.*, 2015, **5**, 6057-6060.
(m) B. M. Neilson, C. W. Bielawski, *Chem. Commun.*, 2013, **49**, 5453-5455.
(n) M. Abubekеров, S. M. Shepard, P. L. Diaconescu, *Eur. J. Inorg. Chem.*, 2016, **2016**, 2634-2640.
(o) E. M. Broderick, N. Guo, T. Wu, C. S. Vogel, C. Xu, J. Sutter, J. T. Miller, K. Meyer, T. Cantat, P. L. Diaconescu, *Chem. Commun.*, 2011, **47**, 9897-9899.
(p) E. M. Broderick, N. Guo, C. S. Vogel, C. Xu, J. Sutter, J. T. Miller, K. Meyer, P. Mehrkhodavandi, P. L. Diaconescu, *J. Am. Chem. Soc.*, 2011, **133**, 9278–9281.
2. J. Wei, M. N. Riffel, P. L. Diaconescu, *Macromolecules*, 2017, **50**, 1847-1861.
3. S. M. Quan, X. Wang, R. Zhang, P. L. Diaconescu, *Macromolecules*, 2016, **49**, 6768-6778.
4. X. Wang, A. Thevenon, J. L. Brosmer, I. Yu, S. I. Khan, P. Mehrkhodavandi, P. L. Diaconescu, *J. Am. Chem. Soc.*, 2014, **136**, 11264-11267.

8. (a) D. J. Darensbourg, *Inorg. Chem. Front.*, 2017, **4**, 412-419.
- (b) C. Romain, Y. Zhu, P. Dingwall, S. Paul, H. S. Rzepa, A. Buchard, C. K. Williams, *J. Am. Chem. Soc.*, 2016, **138**, 4120-4131.
- (c) Y. Zhu, C. Romain, C. K. Williams, *J. Am. Chem. Soc.*, 2015, **137**, 12179-12182.
- (d) S. Paul, C. Romain, J. Shaw, C. K. Williams, *Macromolecules*, 2015, **48**, 6047-6056.
- (e) C. Romain, C. K. Williams, *Angew. Chem. Int. Ed.*, 2014, **53**, 1607-1610.
6. A. B. Biernesser, K. R. Delle Chiaie, J. B. Curley, J. A. Byers, *Angew. Chem. Int. Ed.*, 2016, **55**, 5251-5254.
7. A. B. Biernesser, B. Li, J. A. Byers, *J. Am. Chem. Soc.*, 2013, **135**, 16553-16560.
8. (a) O. Nuyken, S. D. Pask, *Polymers*, 2013, **5**, 361-403.
- (b) J. Herzberger, K. Niederer, H. Pohlitz, J. Seiwert, M. Worm, F. R. Wurm, J. Frey, *Chem. Rev.*, 2016, **116**, 2170-2243
9. A. B. Pangborn, M. A. Giardello, R. H. Grubbs, R. K. Rosen and F. J. Timmers, *Organometallics*, 1996, **15**, 1518-1520.
10. M. J. Frisch, Gaussian 09 (Revision D.01). Gaussian Inc.: Wallingford, CT, 2010.
11. J. Towns, T. Cockerill, M. Dahan, I. Foster, K. Gaither, A. Grimshaw, V. Hazlewood, S. Lathrop, D. Lifka, G. D. Peterson, R. Roskies, J. R. Scott, N. Wilkins-Diehr, *Computing in Science and Engineering*, 2014, **16**, 62-74.
12. S. Grimme, J. Antony, S. Ehrlich, H. Krieg, *J. Chem. Phys.*, 2010, **132**, 154104.

Chapter 4: Application of Bulk Electrolysis to Redox-switchable Copolymerization

4.1. Introduction

As discussed in Chapter 2, the complications of using chemical oxidants in redox-switchable copolymerization are multifold. In the ionic pair that comprises most chemical oxidants, the cation's role of oxidizing agent requires selectivity toward the initiator rather than the monomer, and the importance of choosing an appropriate counteranion cannot be understated.¹ Unwanted side reactions with monomers, irreversible oxidations, and the generation of an unreactive or unstable oxidized initiator are all shortcomings to be avoided. In our previous publication, the search for an ideal oxidant was extensive,² but ultimately unsuccessful. Sequential monomer addition was employed instead.

To circumvent the need for chemical oxidants and reductants entirely, investigations into bulk electrolysis were carried out. The application of electrochemical methods to polymerization was first used by Szarvasy in 1900 to prepare induline dyes.³ In the 1940s-1950s, electroinitiated polymerizations of olefins were explored extensively^{4,5} including the copolymerization of monomers.⁶ The shift toward utilizing a separate molecule that could be generated and utilized to polymerize styrene was first explored by Tidswell and Doughty in the 1960s.⁷ Several papers around this time also studied the cationic mechanism of these polymerizations.⁸ In the 1970s, the focus changed from using an electric current as a control toward monitoring electric potential,⁹ studying the formation of polymer on electrodes,^{10,11} and expanding the range of monomers.¹²

Recent examples of bulk electrolysis in polymerization initiator generation are rare. Group 3-6 metal or bimetallic lanthanide complexes in the presence of inert noncoordinating anions for the polymerization of ethylene¹³, 1-octene¹⁴, and propylene¹⁵ have been reported in

patents by the Dow Chemical Company. In another example of indirect electrochemical polymerization, titanium (III) dimethylglyoxime was found to mediate the polymerization of acrylonitrile in an aqueous sulfuric acid and methanol solution.¹⁶ Styrene's low solubility in aqueous and highly polar solvents poses a challenge to maintaining a conducting environment. By using a mixed biphasic system, Nayak and coworkers electropolymerized styrene and generated polymers between 44-47 kDa.¹⁷ In one of the few reports on the anodic polymerization of benzene, the use of $\text{BF}_3\text{O}(\text{C}_2\text{H}_5)_2$ as an electrolyte allowed the aromatic molecule be polymerized in nitrobenzene.¹⁸

4.2 Results and Discussion

As most bulk electrolysis cells are customized, there is currently a huge variety in cell designs. Taking inspiration from the Peters group and their work in electrocatalytic hydrogen evolution,¹⁹ we initially planned on using a separated cell with membranes or methyl cellulose plugs to serve as a salt bridge. However, methyl cellulose plugs rely on hydrogen bonding to create a gel network and require protic solvents, which degrade $(\text{salfan})\text{Zr}(\text{O}^t\text{Bu})_2$. Membranes like nafion degrade in our chosen electrolyte solution of tetrabutylammonium hexafluorophosphate (TBAPF_6) in *o*- $\text{F}_2\text{C}_6\text{H}_4$ which was evidenced by ^{19}F NMR spectroscopy (Figure 4.1). Due to these complications, we turned to an H-cell design used in the Yang group for CO_2 , CO , and H^+ reduction that employs a fine frit to separate the two halves of the bulk electrolysis cell.²⁰

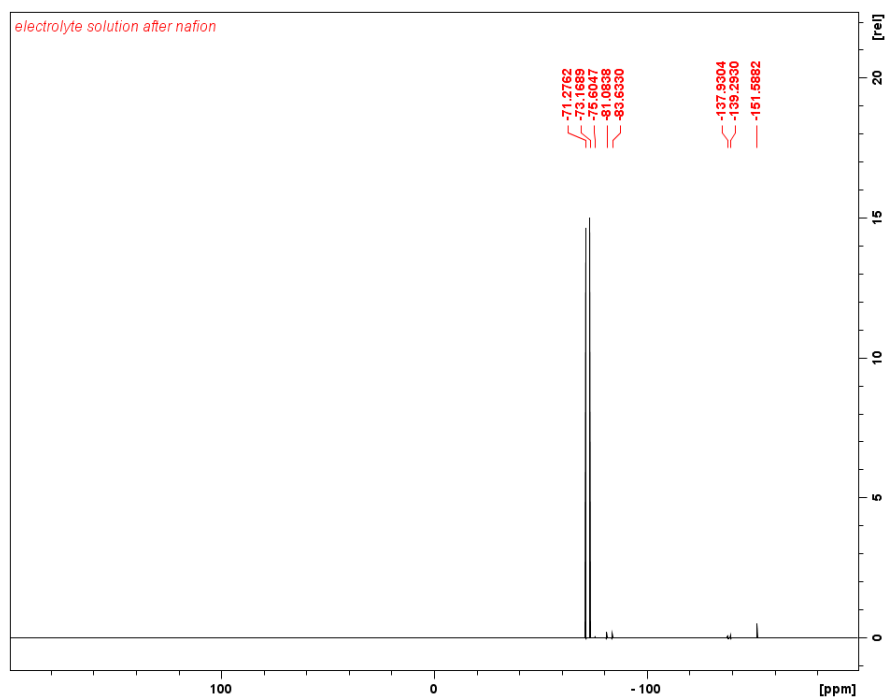


Figure 4.1. Electrolyte solution after nafion was immersed in it for 24 hours. ^{19}F NMR (400 MHz CDCl_3) ppm: -71.3 (TBAPF_6), -73.2 (TBAPF_6), -75.6 (OCF_2 , nafion), -81.1 (CF_3 , nafion), -83.6 (OCF_2 , nafion), -138.6 (ArF , difluorobenzene), -151.6 (unknown).

Initial control reactions were done to determine whether the electrolyte could polymerize cyclohexene oxide (CHO). CHO was not polymerized under these conditions (Figure 4.2). The addition of (salfan) $\text{Zr}(\text{O}^i\text{Bu})_2$ to a 100 mM solution of TBAPF_6 in $o\text{-F}_2\text{C}_6\text{H}_4$ led to the polymerization of LA at room temperature over six days (Figure 4.3). Self polymerization of the monomers in the electrolyte solution was shown not to occur as a cyclic voltammogram from 1.6 V to -1.6 V did not show redox events or changes in current (Figures 4.4-4.5).

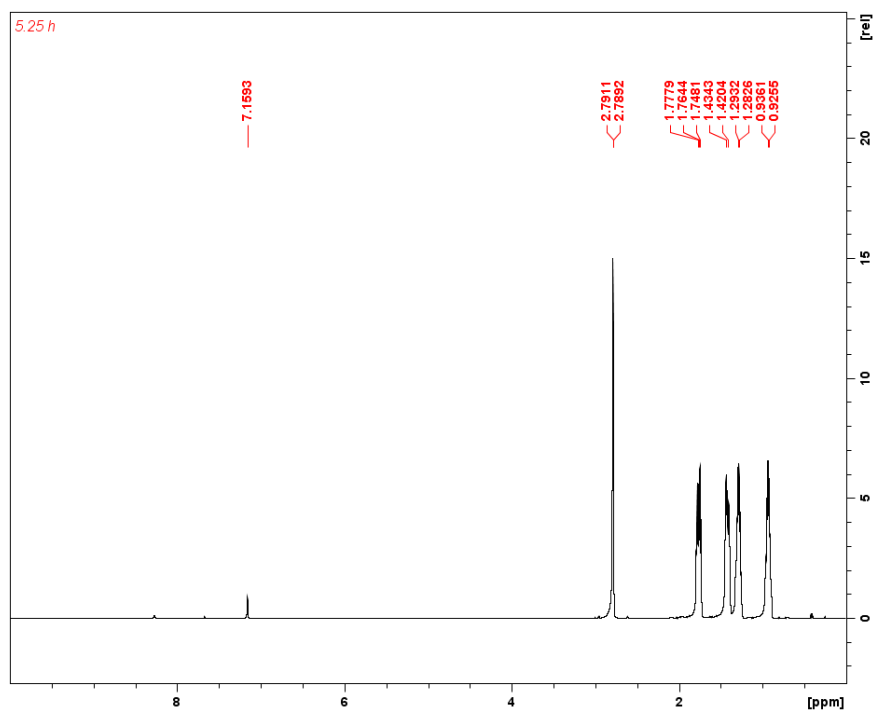


Figure 4.2. Cyclohexene oxide in the presence of TBAPF₆ for 5.25 hours. ¹H NMR (300 MHz, 25 °C, C₆D₆), δ (ppm): 2.79 (s, 2H, COCH CHO), 1.76 (m, 2H, COCHCH₂ PCHO), 1.43 (m, 2H, COCHCH₂ PCHO), 1.28 (m, 2H, COCHCH₂CH₂ PCHO), 0.93 (m, 2H, COCHCH₂CH₂ PCHO).

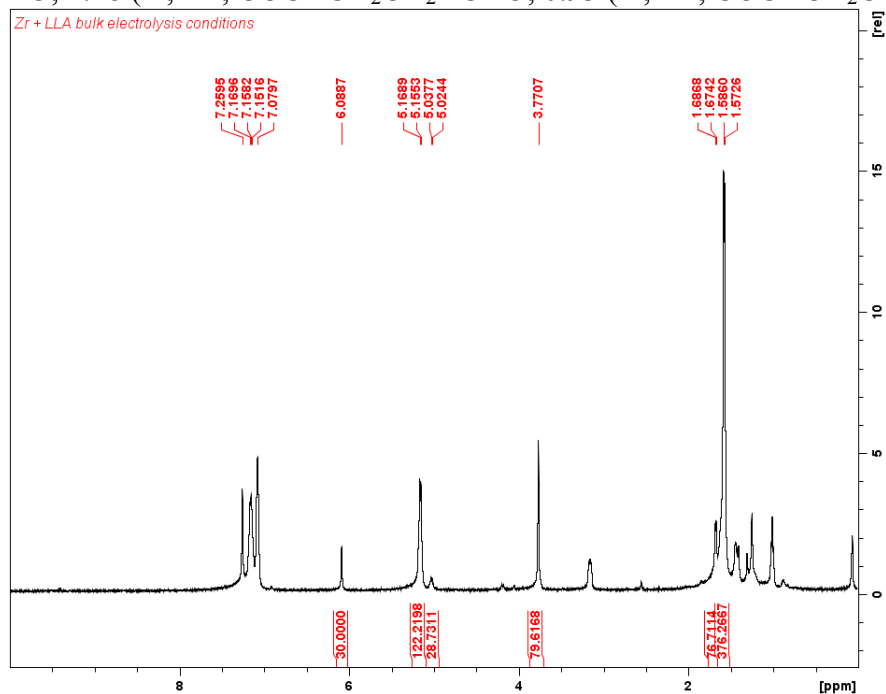


Figure 4.3. Polymerization of lactide by (salfan)Zr(O^{*t*}Bu)₂ under bulk electrolysis conditions. ¹H NMR (300 MHz, 25 °C, CDCl₃), δ (ppm): 7.16 (CFCH 1,2-difluorobenzene), 7.08 (CFCHCH 1,2-difluorobenzene), 6.09 (s, 3H, CH TMB), 5.16 (q, 3H, CH PLA), 5.03 (q, 3H, CH LA), 3.08 (s, 9H, CH₃ TMB), 1.69 (d, 6H, CH₃ LA), 1.58 (d, 6H, CH₃ PLA).

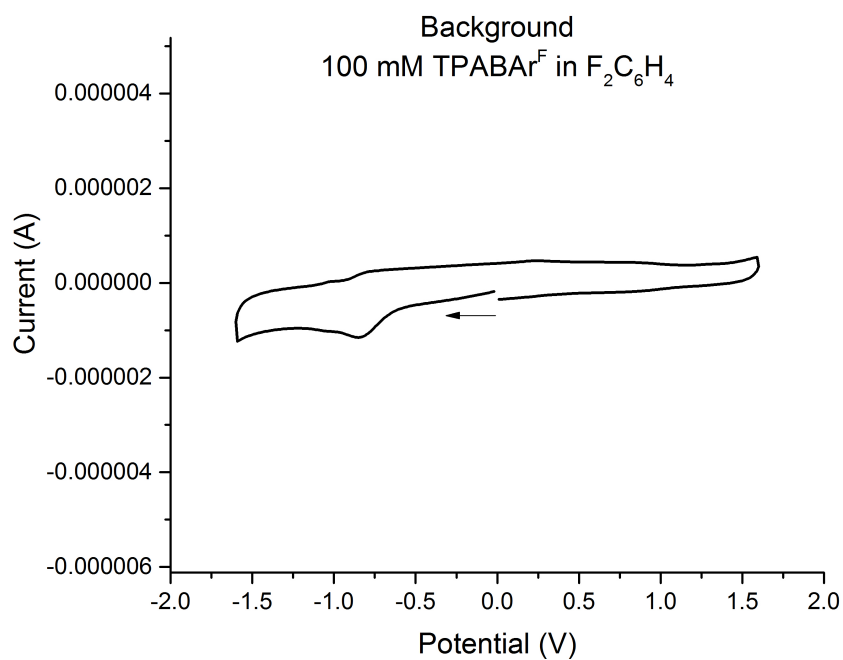


Figure 4.4. Background scan of 100 mM TPABAr^F in *o*-F₂C₆H₄.

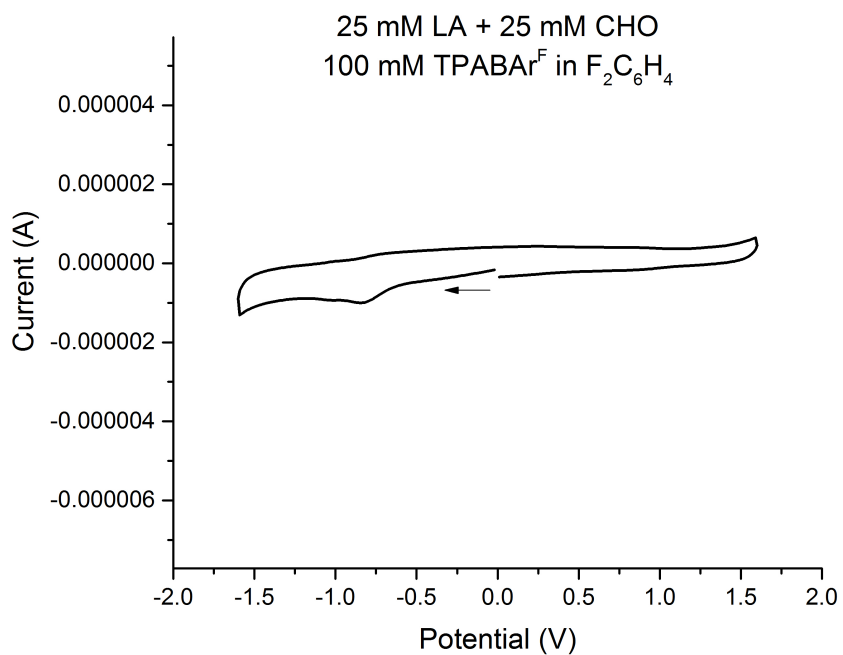


Figure 4.5. Cyclohexene oxide and lactide in 100 mM TPABAr^F in *o*-F₂C₆H₄.

(salfan)Zr(O^tBu)₂ was oxidized and reduced in the presence of LA and CHO, using TBAPF₆ as an electrolyte (100 mM) and *o*-F₂C₆H₄ as a solvent. Although a color change was noted as the initiator was oxidized and then reduced, no polymerization occurred (Figure 4.6). We attributed this to the PF₆⁻ anion binding too tightly to the oxidized initiator and preventing CHO from reaching the metal center. When screening oxidants, we noticed a similar phenomenon.² Both AgOTf and I₂ reversibly oxidized (salfan)Zr(O^tBu)₂ but the resulting oxidized complexes could not polymerize CHO. In fact, the importance of the counteranion for cationic initiators has been extensively discussed.¹

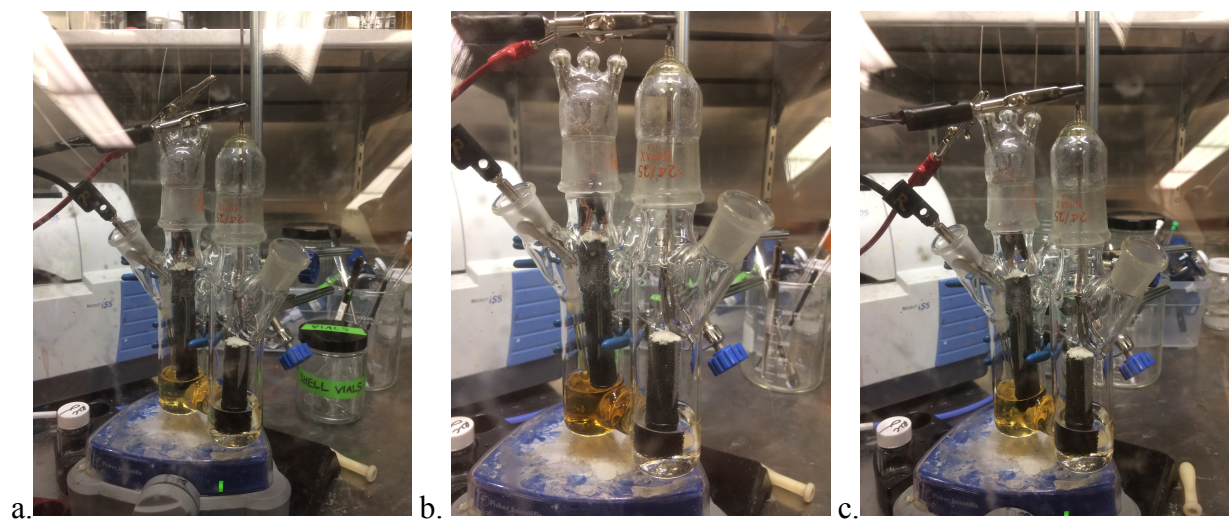


Figure 4.6. Color change from yellow to brown to yellow as (salfan)Zr(O^tBu)₂ (a) was oxidized (b) and reduced (c).

Repeating the bulk electrolysis experiment with TPABAr^F as the electrolyte provided a larger non-coordinating counteranion and allowed CHO polymerization by [(salfan)Zr(O^tBu)₂][BAr^F]. However upon the reduction of [(salfan)Zr(O^tBu)₂][BAr^F], no

polymerization of LA occurred, even after heating at 100 °C overnight. Salfen peaks in the resulting ^1H NMR spectra indicated a possible water or oxygen contamination of the system leading to decomposition. Following a rigorous exclusion of oxygen and water, we were able to repeat the bulk electrolysis and obtain 30% polymerization of LA with the re-reduced initiator after 48 hours at 100 °C (Table 4.1, Figure 4.7). The presence of free ligand in the corresponding ^1H NMR spectra still indicated decomposition in the reduction step that we attribute to either using too low of a potential, passing too many coulombs, or not a rigorous enough exclusion of water and oxygen. An independent control reaction of $\text{H}_2\text{salfen-Me}$ with TPABAr^{F} and LA in *o*- $\text{F}_2\text{C}_6\text{H}_4$ at 100 °C showed only 2% polymerization of LA after 24 hours and 3% after 48 hours (Figure 4.8). Therefore, we concluded that the resulting PLA was primarily synthesized by the re-reduced initiator rather than ligand generated from decomposition. The GPC trace of the initial PCHO polymer has a low molecular weight (7.2 kDa) and high dispersity (1.71), consistent with the fast polymerization and slow oxidation or initiation period. The subsequent diblock copolymer PCHO-PLA has a much higher molecular weight (25.0 kDa) and lower dispersity (1.38), consistent with a small percentage of active initiator polymerizing LA. There is a small unidentified peak between 15-20 minutes in the GPC trace of the polymer from the oxidized solution that is not present in the polymer from the reduced solution.

Table 4.1. Bulk electrolysis of (salfan)Zr(O^tBu)₂ in the presence of LA and CHO.

Entry	Polymer	Oxidation State of initiator	Conv. 1 st block	Conv. 2 nd block	Potential (V)	Time (h)	M _n , theo ^a	M _n , GPC ^b	D ^b
1	CHO ₅₀ -LA ₅₀	Oxidized	92	0	1.6	2.15	4.9	7.2	1.71
2	CHO ₅₀ -LA ₅₀	Reduced			-1.0	1.38			
3	CHO ₅₀ -LA ₅₀	Reduced			-1.2	0.58			
4	CHO ₅₀ -LA ₅₀	Reduced			-1.6	0.70			
5	CHO ₅₀ -LA ₅₀	Reduced	92	30	-	48	7.0	25.0	1.38

Conditions: 100 mM TPABAr^F, 1 mM (salfan)Zr(O^tBu)₂, 25 mM LA, 25 mM CHO, Solvent = *o*-F₂C₆H₄.

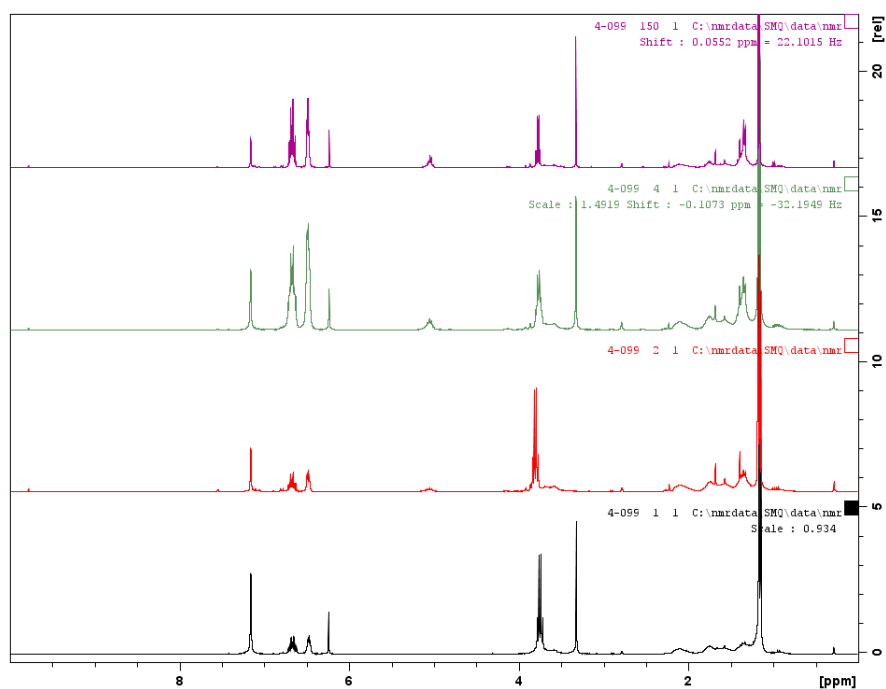


Figure 4.7. Polymerization of LA and CHO by (salfan)Zr(O^tBu)₂ oxidized and reduced by bulk electrolysis. From bottom to top: oxidized state, reduced state one day, reduced state two days, reduced state three days.

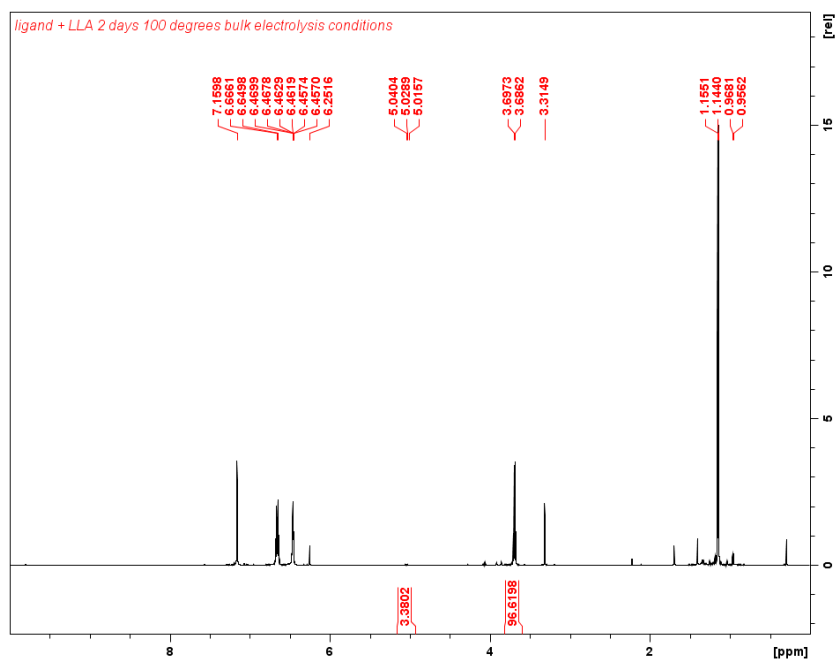


Figure 4.8. ^1H NMR of $\text{H}_2\text{salfan-Me}$ and LLA after 2 days at $100\text{ }^\circ\text{C}$. ^1H NMR (300 MHz, $25\text{ }^\circ\text{C}$, C_6D_6), δ (ppm): 6.67 (CFCH 1,2-difluorobenzene), 6.46 (CFCHCH 1,2-difluorobenzene), 6.25 (s, 3H, CH TMB), 5.03 (q, 3H, CH PLA), 3.69 (q, 3H, CH LA), 3.31 (s, 9H, CH_3 TMB), 1.15 (d, 6H, CH_3 PLA), 0.96 (d, 6H, CH_3 LA).

4.3 Conclusions

Preliminary studies of the bulk electrolysis application to redox-switchable polymerization are promising. Initial challenges in cell design and electrolyte choice were solved by utilizing a simple H-cell with a glass frit separator and choosing an electrolyte that can provide a non-coordinating BAr^{F} anion. Current obstacles include maintaining a rigorously water and oxygen free environment. A delayed monomer addition may also be helpful in lowering the dispersity of the final polymer as slow electrochemical oxidation of the initiator begets a long initiation period.

4.4 Experimental

General considerations

All experiments were performed under a dry nitrogen atmosphere using standard Schlenk techniques or an MBraun inert-gas glovebox. Solvents were purified using a two-column solid-state purification system by the method of Grubbs²¹ and transferred to the glove box without exposure to air. NMR solvents were obtained from Cambridge Isotope Laboratories, degassed and stored over activated molecular sieves prior to use. ¹H NMR spectra were recorded on Bruker 300, Bruker 400 or Bruker 500 spectrometers at room temperature in C₆D₆ or CDCl₃. Chemical shifts are reported with respect to internal solvent, 7.16 ppm (C₆D₆) and 7.26 ppm (CDCl₃) for ¹H NMR spectra. Cyclohexene oxide and 1,2-difluorobenzene were distilled over CaH₂ and brought into the glove box without exposure to air. L-lactide and 1,3,5-trimethoxybenzene were recrystallized from toluene at least twice before use. 2,4-di-*tert*-butylphenol, *n*-BuLi, cobaltocene, and Zr(O^{*t*}Bu)₄ were purchased from Sigma Aldrich and used as received. [^{Ac}Fc][BAR^F₄], TPA[BAR^F₄], and (salfan)Zr(O^{*t*}Bu)₂ were synthesized following previously published procedures.²² Molecular weights of the polymers were determined by GPC-MALS instrument at UCLA. GPC-MALS uses a Shimadzu Prominence-i LC 2030C 3D equipped with an autosampler, two MZ Analysentechnik MZ-Gel SDplus LS 5 μm, 300 × 8mm linear columns, Wyatt DAWN HELEOS-II and Wyatt Optilab T-rEX. The column temperature was set at 40 °C. A flow rate of 0.70 mL/min was used and samples were dissolved in chloroform. dn/dc values were calculated for PLA and PCHO by creating 5 solutions of increasing concentration (0.1 - 1.0 mg/mL), directly injecting them into the RI detector sequentially, and using the batch dn/dc measurement methods in the Astra software. The dn/dc value for PLA and PCHO were calculated to be 0.024 mL/g and 0.086 mL/g over three trials. TPABAR^F was synthesized by

combining TPACl and NaBAR^F in methanol and precipitating the product in water. NaBAR^F was synthesized²³ and purified²⁴ according to literature procedures. Electrolyte was recrystallized at least 3 times from dichloromethane and dried in a vacuum oven overnight before use.

Initial bulk electrolysis studies were carried out with the Yang Group at UCI. Controlled potential electrolyses were performed in a 50 mL H-Cell. Vitreous carbon foam rods were used for the working and counter electrodes, while a Ag wire electrode was used as the reference. The carbon foam rods were attached to copper wire leads using conductive silver epoxy (AI Technology Prima-Solder EG8050) under Loctite epoxy. The counter electrode was separated from the bulk solution by a 10 mm extra-fine (Ace glass porosity E) fritted glass. The working and reference electrodes were connected to the exterior of the cell via nickel sleeves joining the electrode leads to a tungsten wire that was sealed through a 14/20 ground-glass stopper.

Follow up bulk electrolysis experiments were carried out in in a 50 mL H-Cell purchased from Pine Instruments. Vitreous carbon foam rods were used for the working and counter electrodes, while a Ag wire electrode was used as the reference. The carbon foam rods were attached to copper wire leads using conductive silver epoxy (AI Technology Prima-Solder EG8050) under Loctite epoxy. The counter electrode was separated from the bulk solution by a 10 mm extra-fine (Ace glass porosity E) fritted glass. Setup pictured below.



4.5 Appendix D

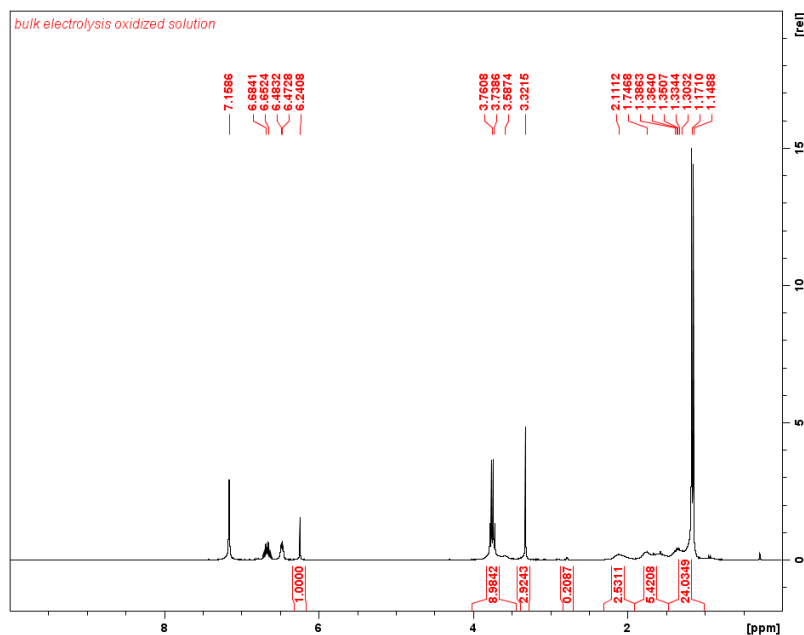


Figure D1. ^1H NMR of polymer formed after (salfan) $\text{Zr}(\text{O}^t\text{Bu})_2$ was oxidized. ^1H NMR (300 MHz, 25 °C, C_6D_6), δ (ppm): 6.67 (CFCH 1,2-difluorobenzene), 6.48 (CFCHCH 1,2-difluorobenzene), 6.24 (s, 3H, CH TMB), 3.75 (q, 3H, CH LA), 3.59 (m, 2H, COCH PCHO), 3.32 (s, 9H, CH_3 TMB), 2.80 (s, 2H, COCH CHO), 2.11 (m, 2H, COCHCH₂ PCHO), 1.75 (m, 2H, COCHCH₂ PCHO), 1.32 (m, 2H, COCHCH₂CH₂ PCHO), 1.16 (d, 6H, CH_3 LA).

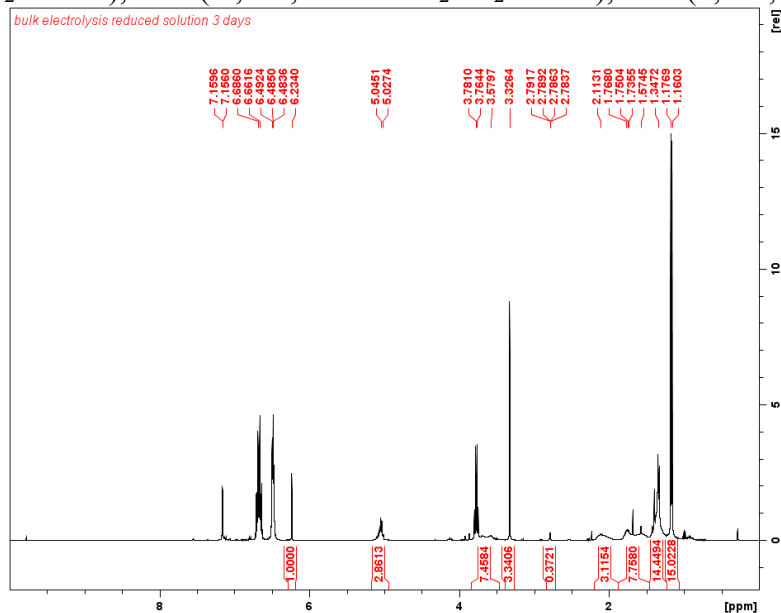


Figure D2. ^1H NMR of polymer formed after oxidized initiator was reduced. 2 days at 100 °C. ^1H NMR (300 MHz, 25 °C, C_6D_6), δ (ppm): 6.67 (CFCH 1,2-difluorobenzene), 6.49 (CFCHCH 1,2-difluorobenzene), 6.23 (s, 3H, CH TMB), 5.04 (q, 3H, CH LA), 3.77 (q, 3H, CH LA), 3.58 (m, 2H, COCH PCHO), 3.33 (s, 9H, CH_3 TMB), 2.79 (s, 2H, COCH CHO), 2.11 (m, 2H, COCHCH₂ PCHO), 1.75 (m, 2H, COCHCH₂ PCHO), 1.57 (m, 2H, COCHCH₂CH₂ PCHO), 1.35 (d, 6H CH_3 , PLA), 1.16 (d, 6H, CH_3 LA).

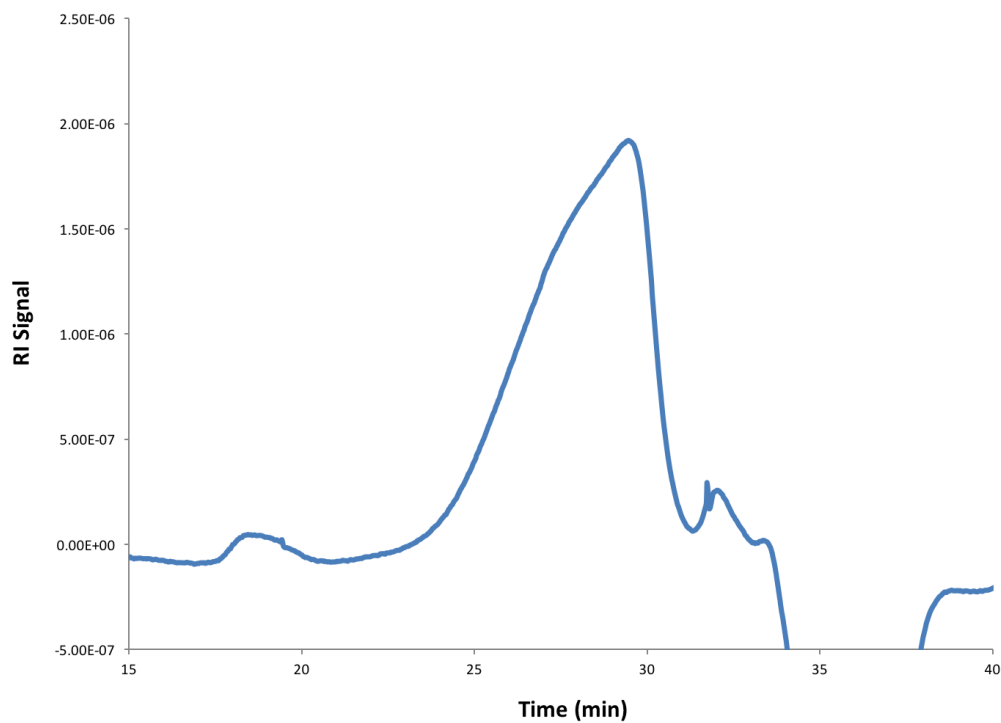


Figure D3. GPC trace of polymer after oxidation of initiator. $M_n = 7200$ Da, $M_w = 12300$ Da, $D = 1.71$.

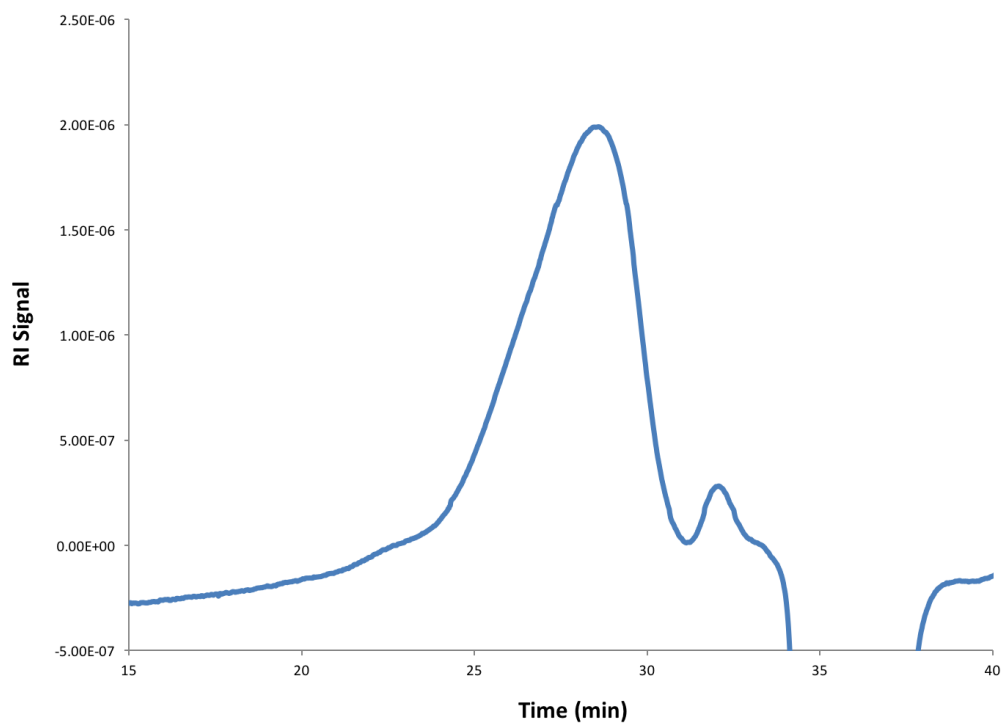


Figure D4. GPC trace of polymer after reduction of initiator. 2 days 100 °C. $M_n = 25000$ Da, $M_w = 34500$ Da, $D = 1.38$.

References

1. Y. Sarazin, J.-F. Carpentier, *Chem. Rev.*, 2015, **115**, 3564-3614.
2. S. M. Quan, X. Wang, R. Zhang, P. L. Diaconescu, *Macromolecules*, 2016, **49**, 6768-6778.
3. E. C. Szarvasy, *J. Chem. Soc., Trans.*, 1900, **77**, 207-212.
4. (a) B. M. Tidswell, *Rep. Prog. Appl. Chem.* 1968, **53**, 516.
(b) B. L. Funt, *Macromolecular Rev.* 1966, **1**, 35.
(c) T. Asahara, M. J. Sen, *Synth. Org. Chem., Japan* 1967, **25**, 719.
(d) N. Yamazaki, *Adv. in Polym. Sci.* 1969, **6**, 377.
(e) C. L. Wilson, *Rec. Chem. Prog.*, 1949, **10**, 25.
(f) J. W. Breitenbach C. Srna, *Pure Appl. Chem.* 1962, **4**, 245.
(g) C. F. Heins, *J. Polym. Sci. B*, 1969, **7**, 625.
(h) N. Yamazaki, *Adv. Polym. Sci.*, 1969, **6**, 377.
(i) J. W. Breitenbach, *Adv. Polym. Sci.*, 1972, **9**, 47.
(j) M. M. Baizer, *Nature*, 1969, **56**, 405.
5. (a) B. Nayak, R.C. Bhakta, *J. Applied Electrochem.*, 1983, **13**, 105-110.
(b) G. Pistoia, O. Bagnarelli, *J. Polym. Sci. Polym. Chem. Ed.* 1979, **17**, 1001.
(c) S. M. Jovanic, D. Sepa, M. V. Vojnovic, *Makromol. Chem.* 1970, **139**, 289.
(d) W. B. Smith, H. G. Gilde, *J. Amer. Chem. Soc.*, 1959, **81**, 5325.
(e) G. Parravano, *J. Amer. Chem. Soc.*, 1951, **73**, 628.
(f) E. Dineen, T. C. Schwan, C. L. Wilson, *J. Electrochem. Soc.*, 1949, **96**, 226.
6. J. W. Breitenbach C. Srna, *Pure Appl. Chem.* 1962, **4**, 245.
7. (a) B. L. Funt, S. W. Laurent, *Canadian J. Chem.*, 1964, **42**, 2728-2732.
(b) B. L. Funt, S. N. Bhadani, *Canadian J. Chem.*, 1964, **42**, 2733-2738.

8. (a) J. W. Breitenbach, *Makromol. Chem.*, 1960, **2**, 171.
(b) W. Strobel, R. C. Schulz, *Makromol. Chem.*, 1970, **133**, 303.
(c) B.L. Funt, T. J. Blain, *J. Polym. Sci. A-1*, 1970, **8**, 3339.
(d) B. L. Funt, T. J. Blain, *J. Polym. Sci.* 1971, **9**, 47.
9. U. Akbulut, J. E. Fernandez, R. L. Birke, *J. Polym. Sci. Polym. Chem.*, 1975, **13**, 133.
10. R. V. Subramanian, *Adv. Polym. Sci.*, 1979, **33**, 33.
11. N. Cheremisinoff, *Handbook of Polymer Science and Technology*, Marcel Dekker Inc., 1989.
12. G. Mengoli, G. Vidotto, *Macromolecular Chem. And Physics*, 1971, **142**, 121-129.
13. J. T. Patton, T. J. Marks, L. Li, Patent WO9914222 A1, 1999.
14. D. D. Graf, J. Klosin, P. N. Nickias, J. T. Patton, US Patent 6235917 B1, 2001.
15. F. J. Timmers, J. C. Stevens, D. D. Devore, R. K. Rosen, J. T. Patton, D. R. Neithamer, US Patent 6465384 B1, 2002.
16. B. S. Sherigara, M. P. Yashoda, Padmalatha, *J. Phys. Org. Chem.*, 1999, **12**, 605-611.
17. R. C. Bhakta, S. Sanyal, B. Nayak, *J. Macromol. Sci. A*, 1987, **24**, 493-505.
18. S. N. Bhadani, S. K. S. Gupta, M. Gupta, J. Prasad, *J. Appl. Polym. Sci.*, 1993, **47**, 1215-1218.
19. X. Hu, B. S. Brunshwig, J. C. Peters, *J. Am. Chem. Soc.*, 2007, **129**, 8988-8998.
20. D. W. Shaffer, S. I. Johnson, A. L. Rheingold, J. W. Ziller, W. A. Goddard, R. J. Nielsen, J. Y. Yang, *Inorg. Chem.*, 2014, **53**, 13031-13041.
21. A. B. Pangborn, M. A. Giardello, R. H. Grubbs, R. K. Rosen and F. J. Timmers, *Organometallics*, 1996, **15**, 1518-1520.
22. X. Wang, A. Thevenon, J. L. Brosmer, I. Yu, S. I. Khan, P. Mehrkhodavandi, P. L. Diaconescu, *J. Am. Chem. Soc.*, 2014, **136**, 11264-11267.
23. D. L. Reger, T. D. Wright, C. A. Little, J. J. S. Lamba, M. D. Smith, *Inorg. Chem.*, 2001, **40**, 3810-3814.
24. N. A. Yakelis, R. G. Bergman, *Organometallics*, 2005, **24**, 3579-3581.

Chapter 5: Polymerization of Epoxides by Dodecaborate Clusters

5.1 Introduction

As 3D-aromatic structures, boron-rich clusters such as carboranes and dodecaborates often serve as a bridge between inorganic and organic chemistry, finding use in many areas,¹ including materials science² and drug delivery.³ Icosahedral boron-rich clusters have been well studied since the 1960s.⁴ While carboranes are charge neutral, dodecaborates can exist in a number of oxidation states. Dodecaborate clusters were first theorized to be stable in the dianionic form in 1955.⁵ The first synthesis by Pitochelli and Hawthorne in 1960⁶ yielded 4% of the cluster from iodododecaborane. Since then, better syntheses with the yields up to 90% have been disclosed.⁷ In 2016, the Spokoyny group reported a facile and scalable method toward synthesizing the perfunctionalized derivatives of these molecules, isolating gram quantities in one pot and open-air conditions.⁸ Cyclic voltammetry showed distinct and reversible redox events for these compounds and many of the anionic and dianionic forms were easily isolated and characterized.⁹ Subsequent publications examined the photo-redox behavior of these compounds and their activity toward the polymerization of styrene monomers¹⁰ and the synthesis of atomically precise nanomolecules.¹¹

5.2 Results and Discussion

Based on oxidation potentials and ease of synthesis, we investigated several variations of these functionalized dodecaborates as oxidants for (salfan)Zr(O^tBu)₂ (Figure 5.1). Although these dodecaborate clusters were able to reversibly oxidize the zirconium complex (Figure E1), they also reacted with cyclohexene oxide (CHO), the target monomer of the oxidized complex.

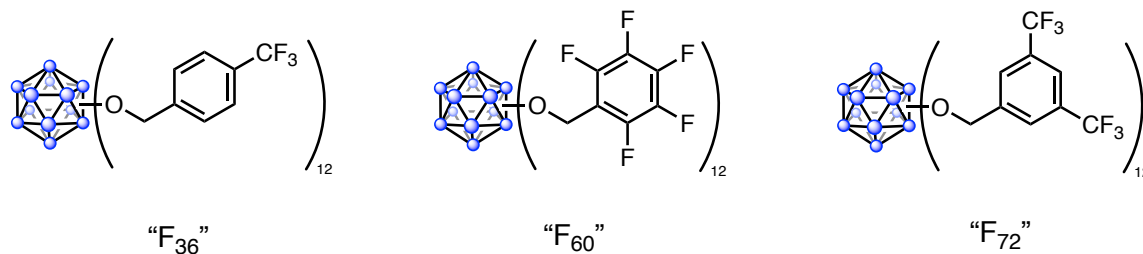
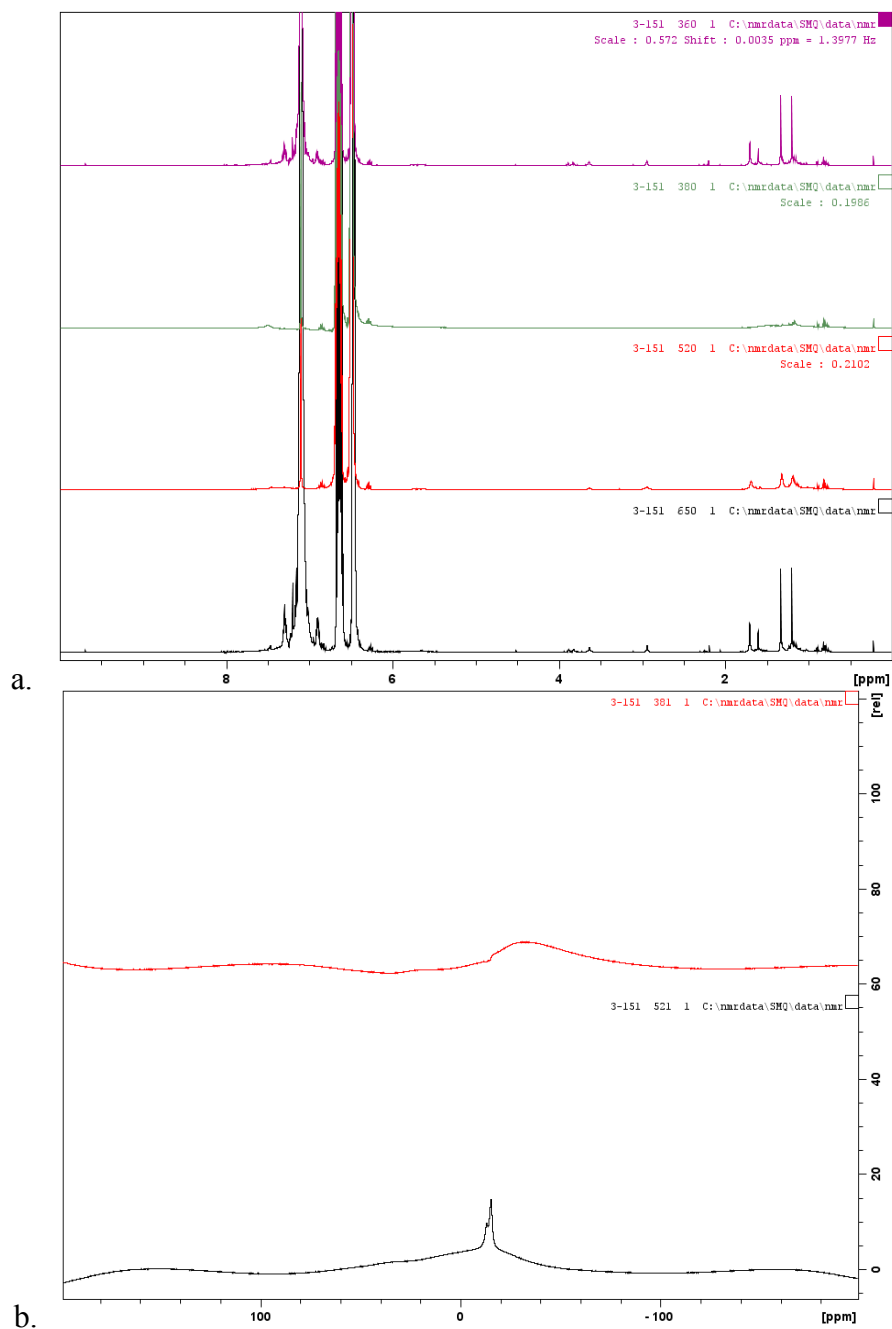


Figure 5.1. Dodecaborate derivatives described in this chapter. Blue ball = boron atom.

When a stoichiometric amount of dodecaborate F_{36} and $(\text{salfan})\text{Zr}(\text{O}^i\text{Bu})_2$ were combined, the solution turned from orange to pink, corresponding to a change in the cluster from the neutral to the anionic form. When left out at room temperature for a few hours, the solution became colorless, indicative of the dodecaborate's dianionic form. To determine whether a single cluster could oxidize two equivalents of $(\text{salfan})\text{Zr}(\text{O}^i\text{Bu})_2$, half an equivalent of F_{36} was combined with one equivalent of the zirconium complex. Indeed, the diamagnetic peaks of the compound disappeared and the ^{11}B NMR peaks of the anionic then dianionic F_{36} appeared over 24 hours. The addition of 0.5 equivalents of cobaltocene (CoCp_2) reduced some of the oxidized compound. An additional 0.5 equivalents of CoCp_2 returned $(\text{salfan})\text{Zr}(\text{O}^i\text{Bu})_2$ cleanly (Figure 5.2).



Conditions: [(salfen)Zr(O'Bu)₂] = 0.0083 M, [F₃₆] = 0.0042 M, inert, 25 °C, (4:1) benzene-d₆:1,2-difluorobenzene as solvent

Figure 5.2. (a) ¹H NMR spectrum of (salfen)Zr(O'Bu)₂ (top). Oxidation of (salfen)Zr(O'Bu)₂ by 0.5 equivalents of F₃₆ (second from top), then reduction by 0.5 equivalents of CoCp₂ (second from bottom) and then another 0.5 equivalents of CoCp₂ (bottom). (right) (b) ¹¹B NMR spectrum F₃₆⁻¹ (top) F₃₆⁻² (bottom). Neutral F₃₆ has a peak around 41 ppm.

GPC analysis of the polycyclohexene oxide (PCHO) obtained from an independent reaction of CHO and F₃₆ showed an unusually large molecular weight of 178 kDa (Table 5.1, entry 2). This polymerization was repeated under a number of conditions. Open-air conditions led to a lower molecular weight of 122 kDa (Table 5.1, entry 1). Raising the equivalents of monomer had no discernable effect on the molecular weight (Table 5.1, entries 2-5) but decreased polymerization times to 30 minutes and increased dispersity to 1.64. Repeating the reaction at 0 °C drastically prolonged the reaction time (20 h) and gave a slightly lower molecular weight of 147 kDa (Table 5.1, entry 6). A sequential addition of 100 equivalents and then another 100 equivalents of monomer over twelve hours raised the molecular weight slightly to 186 kDa (Table 5.1, entry 7). In the absence of light, the reaction time increased to 180 minutes and the resulting polymer weighed 150 kDa (Table 5.1, entry 8). Diluting the solution lowered the molecular weight to 106 kDa (Table 5.1, entry 9), while running the polymerization neat created a gel of polymer that still had a similar M_n as the original polymer (Table 5.1, entry 10). Using CDCl₃ as a solvent had the most dramatic effect, lowering the molecular weight to 28 kDa and raising its dispersity to 1.68 (Table 5.1, entry 11). Reactions in CH₂Cl₂ and *o*-F₂C₆H₄ gave lower molecular weights in the presence of LED lights (Table 5.1, entries 12-14).

Because most catalysts show limited activity, high molecular weight polymers are difficult to achieve. Most PCHO reported in the literature have molecular weights below 100 kDa.¹² Some noteworthy systems that can achieve higher molecular weight polymers used cationic and/or photoinitiated processes. *N*-alkoxy-pyridinium and *N*-alkoxy-quinolinium can generate 200 kDa PCHO in 180 minutes.¹³ A combination of benzoyltrimethylgermane, onium salt, and UV radiation can photoinitiate CHO polymerization to reach 151 kDa polymers.¹⁴ Boron compounds have been used to enhance polymerization activity¹⁵ and synthesize polymers

reaching up to 380 kDa.¹⁶ However, the highest molecular weights (up to 900 kDa) were reached using high monomer loadings¹⁷ (up to 100,000) or long reaction times¹⁸ (up to 45 h). By using an easily synthesized functionalized dodecaborate, we have been able to furnish large molecular weight polymers under a variety of conditions and without the need for high monomer loadings or long reaction times.

Table 5.1. Polymerization of CHO by F₃₆.

Entry	Monomer	Equiv.	Cond.	Time (min)	Conversion ^a	M _{n,theo} ^b	M _{n,exp} ^c	D ^d
1	CHO	100	air	120	98.3	9.6	121.8	1.31
2	CHO	100	[M] raised [I] same	120	98.7	9.7	177.9	1.28
3	CHO	200		120	99.3	19.5	189.3	1.30
4	CHO	500		60	98.3	48.2	121.7	1.62
5	CHO	1000	same	30	97.8	96.0	149.2	1.64
6	CHO	500	0 °C	20 h	99.9	9.8	147.4	1.55
7	CHO	100*2	seq. add.	12 h	99.9	19.5	185.6	1.24
8	CHO	100	dark	180	90.9	8.9	149.6	1.19
9	CHO	100	dilute	180	96.5	9.5	106.4	1.29
10	CHO	100	neat	120**	98.3	9.6	169.1	1.40
11	CHO	100	CDCl ₃	24 h	98.0	9.6	28.3	1.68
12	CHO	100	CH ₂ Cl ₂	120	98.3	9.6	176.6	1.45

Conditions: [M]/[I] = 100, [I] = 0.0083 M, inert, (4:1) benzene-d₆:1,2-difluorobenzene as solvent, CHO = cyclohexene oxide. ^a Conversion calculated by integration of polymer versus monomer peak. ^b Theoretical weight calculated by equivalents x conversion x molecular weight of monomer. Reported in 10³ g/mol. ^c M_n values are reported in 10³ g/mol. ^d D = M_w/M_n. **gelled immediately

Encouraged high activity of CHO, several other cyclic ether monomers were tested for activity with F₃₆ (Table 5.2). Disappointingly, propylene oxide (PO) and styrene oxide (SO) generated only small polymers of 2.2 kDa and oligomers of 600 Da (Table 5.2, entries 1 and 2) with very broad dispersities. Both of these reactions also showed minute amounts of aldehyde side products from the oxidation of the monomer (propionaldehyde from PO and

phenylacetaldehyde from SO) in their ^1H NMR spectra. Oxetane (OX) was polymerized to 85% and generated a polymer of 4.8 kDa with a dispersity of 1.36 (Table 5.2, entry 3).

Table 5.2. Polymerization of epoxide monomers by F_{36} .

Entry	Monomer	Equiv.	Cond.	Time (min)	Conversion ^a	$M_{n,theo}$ ^b	$M_{n,exp}$ ^c	D ^d
1	PO	100	inert	2 d	full	5.8	2.2	3.37*
2	SO	100	inert	2 d	full	12.0	0.6	2.06*
3	OX	100	inert	20 h	85.3	5.8	4.8	1.36

Conditions: $[\text{M}]/[\text{I}] = 100$, $[\text{I}] = 0.0083$ M, inert, $25\text{ }^\circ\text{C}$, (4:1) benzene- d_6 :1,2-difluorobenzene as solvent PO = propylene oxide, SO = styrene oxide, OX = oxetane. ^a Conversion calculated by integration of polymer versus monomer peak. “full” conversion = disappearance of monomer rather than complete conversion to polymer. ^b Theoretical weight calculated by equivalents x conversion x molecular weight of monomer. Reported in 10^3 g/mol. ^c M_n values are reported in 10^3 g/mol. ^d $D = M_w/M_n$. * Bimodal or multimodal distribution

F_{60} had a similar polymerization activity as F_{36} toward cyclic ethers (Table 5.3). Polymerization of CHO at room temperature and $0\text{ }^\circ\text{C}$ gave PCHO with molecular weights of 182 kDa and 142 kDa respectively (Table 5.3, entries 1 and 2). Interestingly, F_{60} generated larger polymers of SO than F_{36} (Table 5.3, entry 4), however polymerization activity with PO was lower (Table 5.3, entry 3). Reaction with limonene oxide (LO) was immediate, but several products were produced along with the polymer (Table 5.3, entry 5).

Table 5.3. Polymerization of cyclic ethers by F₆₀.

Entry	Monomer	Equiv.	Cond.	Time (min)	Conversion ^a	M _{n,theo} ^b	M _{n,exp} ^c	D ^d
1	CHO	100	inert	2 h	93.3	9.1	181.6	1.65
2	CHO	100	0 °C	19 h	98.7	9.7	142.1	1.51
3	PO	100	50 °C	1 d	full	5.8	1.6	1.07
4	SO	100	inert	1 h	full	12.0	3.6	1.30
5	LO	100	inert	2 min	full	15.2	2.5	1.16

Conditions: [M]/[I] = 100, [I] = 0.0083 M, inert, (4:1) benzene-d₆:1,2-difluorobenzene as solvent. CHO = cyclohexene oxide, PO = propylene oxide, SO = styrene oxide, LO = limonene oxide. ^a Conversion calculated by integration of polymer versus monomer peak. “full” conversion = disappearance of monomer rather than complete conversion to polymer. ^b Theoretical weight calculated by equivalents x conversion x molecular weight of monomer. Reported in 10³ g/mol. ^c M_n values are reported in 10³ g/mol. ^d D = M_w/M_n

Based on the Spokoiny group’s study of the electronic structure and photocatalytic behavior of dodecaborate clusters⁹, F₇₂, F₆₀, and F₃₆ were chosen to examine the effects of solvent and LED (450 nm) light on the polymerization of cyclic ethers (Table 5.4). CHO polymerizations in CH₂Cl₂ generated polymers with larger molecular weight polymers than in *o*-F₂C₆H₄. Most of these polymers had very high molecular weights, ranging from 35 to 120 kDa. Dispersity varied from 1.4 to 1.6. For PO, the resulting molecular weights were similar in both solvents and quite low. In addition, the generation of propionaldehyde from PO was prevalent.

For SO and LO, the generation of polymer was difficult to assess in the ¹H NMR since the growing polymer peaks overlapped with solvent peaks for SO and monomer peaks with both. It was noted though that significant amounts of the oxidized monomer in the form of phenylacetaldehyde for SO and dihydrocarvone for LO were found in the ¹H NMR. The polymerization of LO is uncommon¹⁹ and molecular weights above 3 kDa are not usually found unless copolymerization with phthalic anhydride²⁰ or CO₂²¹ is used.

Pinene oxide (PiO) has been known to be easily oxidized in a mixture of compounds, which has some use in the fragrance industry.²² Indeed, the ¹H NMR revealed a combination of compounds, primarily campholenic anhydride and starting material.

Table 5.4. Polymerization of cyclic ethers with functionalized dodecaborates.

Cluster	Monomer	Solvent	Light	Conversion ^a	M _{n,exp} ^b	D ^c
F ₇₂	CHO	<i>o</i> -F ₂ C ₆ H ₄	LED	99	106.0	1.54
F ₇₂	CHO	CH ₂ Cl ₂	LED	99	99.8	1.41
F ₇₂	CHO	<i>o</i> -F ₂ C ₆ H ₄	Dark	99	95.2	1.54
F ₇₂	LO	<i>o</i> -F ₂ C ₆ H ₄	LED	Full	1.3	1.18
F ₇₂	LO	CH ₂ Cl ₂	LED	Full	1.1	1.25
F ₇₂	SO	<i>o</i> -F ₂ C ₆ H ₄	LED	Full	1.7	1.18
F ₇₂	SO	CH ₂ Cl ₂	LED	Full	1.7	1.16
F ₇₂	PO	<i>o</i> -F ₂ C ₆ H ₄	LED	98	0.4	1.35*
F ₇₂	PO	CH ₂ Cl ₂	LED	37	0.3	1.05
F ₇₂	PiO	<i>o</i> -F ₂ C ₆ H ₄	LED	Full	1.5	2.86*
F ₇₂	PiO	CH ₂ Cl ₂	LED	Full	-	-
F ₆₀	CHO	<i>o</i> -F ₂ C ₆ H ₄	LED	99	35.6	1.54
F ₆₀	CHO	CH ₂ Cl ₂	LED	93	48.8	1.56
F ₆₀	CHO	<i>o</i> -F ₂ C ₆ H ₄	Dark	99	134.5	1.54
F ₆₀	LO	<i>o</i> -F ₂ C ₆ H ₄	LED	Full	0.9	1.38
F ₆₀	LO	CH ₂ Cl ₂	LED	Full	1.3	1.20
F ₆₀	SO	<i>o</i> -F ₂ C ₆ H ₄	LED	Full	1.6	1.06*
F ₆₀	SO	CH ₂ Cl ₂	LED	Full	1.5	1.19*
F ₆₀	PO	<i>o</i> -F ₂ C ₆ H ₄	LED	96	0.3	1.06*
F ₆₀	PO	CH ₂ Cl ₂	LED	9	0.3	1.05*
F ₆₀	PiO	<i>o</i> -F ₂ C ₆ H ₄	LED	Full	-	-
F ₆₀	PiO	CH ₂ Cl ₂	LED	Full	-	-
F ₃₆	CHO	<i>o</i> -F ₂ C ₆ H ₄	LED	99	62.2	1.60
F ₃₆	CHO	CH ₂ Cl ₂	LED	99	120.4	1.56
F ₃₆	CHO	<i>o</i> -F ₂ C ₆ H ₄	Dark	91	71.9	1.53
F ₃₆	LO	<i>o</i> -F ₂ C ₆ H ₄	LED	Full	1.2	1.25
F ₃₆	LO	CH ₂ Cl ₂	LED	Full	1.4	1.19
F ₃₆	SO	<i>o</i> -F ₂ C ₆ H ₄	LED	Full	1.5	1.17*
F ₃₆	SO	CH ₂ Cl ₂	LED	Full	1.6	1.16
F ₃₆	PO	<i>o</i> -F ₂ C ₆ H ₄	LED	68	0.3	1.27*
F ₃₆	PO	CH ₂ Cl ₂	LED	67	0.3	1.27*
F ₃₆	PiO	<i>o</i> -F ₂ C ₆ H ₄	LED	Full	-	-
F ₃₆	PiO	CH ₂ Cl ₂	LED	Full	-	-

Conditions: [M]/[I] = 100, [I] = 0.02 mM, inert, 25 °C. CHO = cyclohexene oxide. LO = limonene oxide, SO = styrene oxide, PO = propylene oxide, PiO = pinene oxide. ^a Conversion calculated by integration of polymer versus monomer peak. “full” conversion = disappearance of monomer rather than complete conversion to polymer. ^b M_n values are reported in 10³ g/mol. ^c D = M_w/ M_n. * part of bimodal or multimodal distribution

To determine whether the polymerization of CHO by dodecaborate clusters was living, we observed the polymerization of CHO by F_{36} over 6 hours (Figure 5.2). Aliquots at various time points were taken, quenched and analyzed (Table 5.5). Based on the non-linear relationship between conversion and molecular weight, we determined the polymerization to be non-living (Figure 5.3).

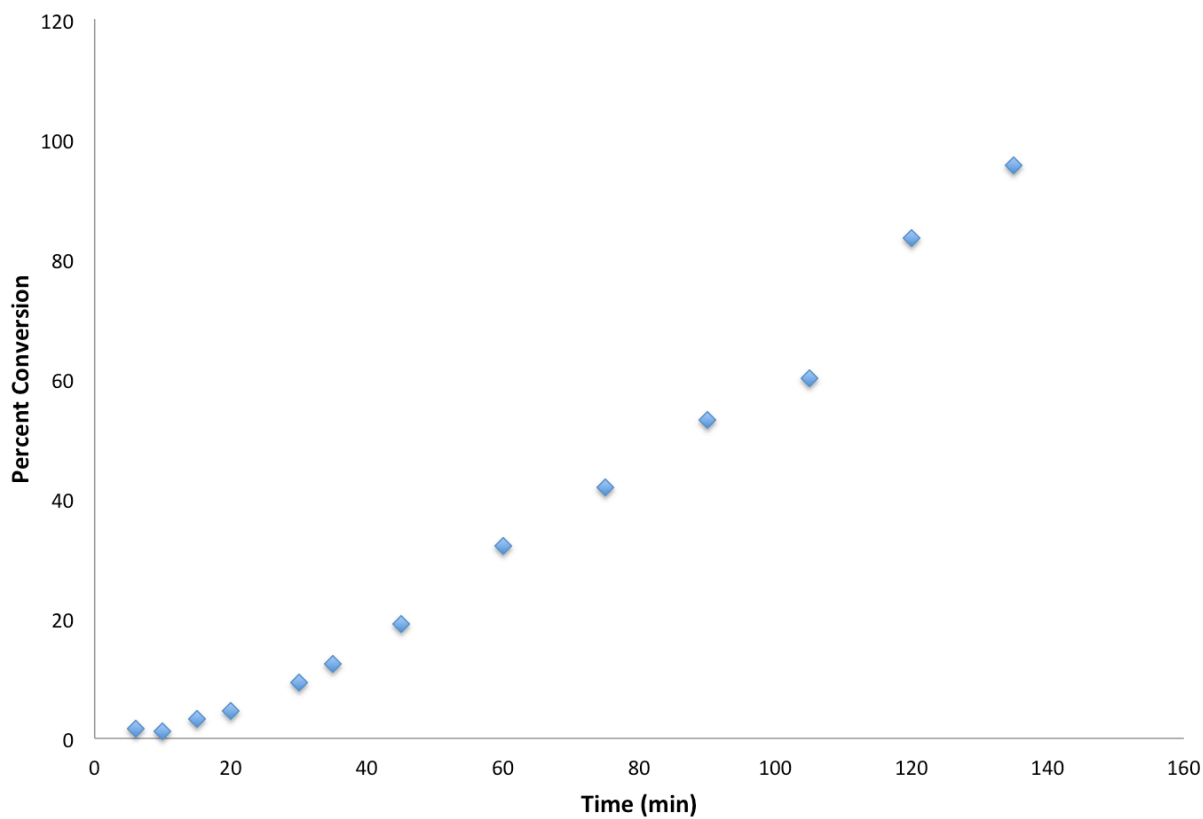


Figure 5.2. Conversion of CHO to PCHO over time by F_{36} .

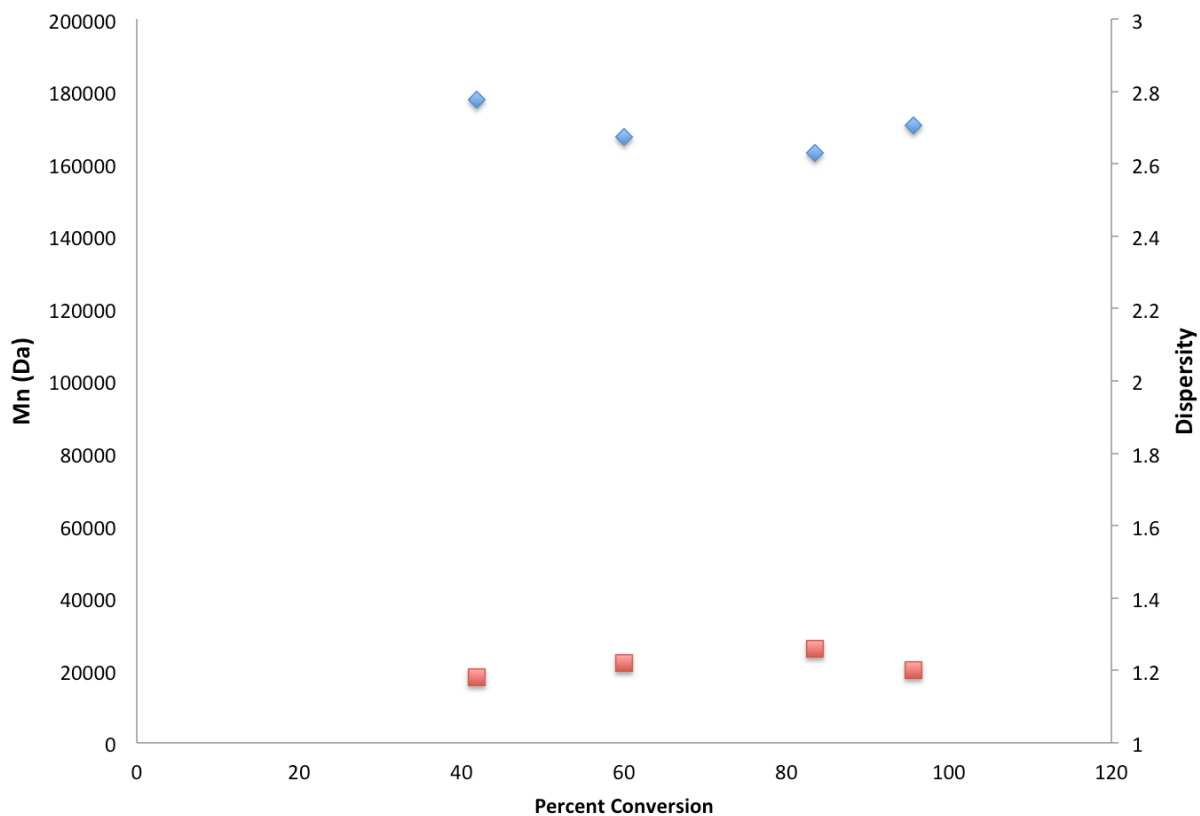


Figure 5.3. Molecular weight of PCHO versus conversion.

Table 5.5. Aliquots from polymerization of CHO by F₃₆.

Entry	Equiv. ^a	Time (min)	Conversion ^a	M _{n,theo} ^b	M _{n,exp} ^c	D ^d
1	100	75	41.82	4.1	177.7	1.18
2	100	105	60.00	5.9	167.3	1.22
3	100	120	83.52	8.2	162.9	1.26
4	100	135	95.65	9.4	170.6	1.20

Conditions: [M]/[I] = 100, [I]=0.0083, inert, 25 °C, (4:1) benzene-d₆:1,2-difluorobenzene as solvent. CHO = cyclohexene oxide. ^a Conversion calculated by integration of polymer versus monomer peak. “full” conversion = disappearance of monomer rather than complete conversion to polymer. ^b Theoretical weight calculated by equivalents x conversion x molecular weight of monomer. Reported in 10³ g/mol. ^c M_n values are reported in 10³ g/mol. ^d D = M_w/M_n

5.3 Conclusions

Functionalized dodecaborate cluster F_{36} has been shown to oxidize (salfan)Zr(O^tBu)₂ reversibly. One F_{36} cluster can oxidize two equivalents of (salfan)Zr(O^tBu)₂ by utilizing its high redox potentials. F_{36} , F_{60} , and F_{72} polymerized CHO to make very high molecular weight polymers, up to 190 kDa within two hours. These polymers may find use in industrial settings where low catalyst loadings and robust reaction conditions are practical. Polymerization of SO, LO, and PO were less successful. Polymers in the 1-3 kDa range were furnished alongside some side products due to oxidation. Attempted polymerizations of PiO generated a range of oxidation products, primarily campholenic aldehyde. The large PCHO polymers produced by F_{36} , F_{60} , and F_{72} are notable and promising. Other monomers are being explored.

5.4 Experimental

General considerations

All experiments were performed under a dry nitrogen atmosphere using standard Schlenk techniques or an MBraun inert-gas glovebox. Solvents were purified using a two-column solid-state purification system by the method of Grubbs²³ and transferred to the glove box without exposure to air. NMR solvents were obtained from Cambridge Isotope Laboratories, degassed and stored over activated molecular sieves prior to use. ¹H NMR spectra were recorded on Bruker 300, Bruker 400 or Bruker 500 spectrometers at room temperature in C₆D₆ or CDCl₃. Chemical shifts are reported with respect to internal solvent, 7.16 ppm (CDCl₃) and 7.26 ppm (CDCl₃) for ¹H NMR spectra. Liquid monomers and 1,2-difluorobenzene were distilled over CaH₂ and brought into the glove box without exposure to air. See below for more detail. Solid monomers and 1,3,5-trimethoxybenzene were recrystallized from toluene at least twice before

use. 2,4-di-*tert*-butylphenol, *n*-BuLi, cobaltocene, and Zr(O^{*t*}Bu)₄ were purchased from Sigma Aldrich and used as received. F₃₆⁸, F₆₀¹⁰, F₇₂²⁴ were synthesized following previously published procedures by Jon Axtell in the Spokoyny group. Molecular weights of the polymers were determined by GPC (Gel Permeation Chromatography). GPC MALS uses a Shimadzu Prominence-i LC 2030C 3D equipped with an autosampler, two MZ Analysentechnik MZ-Gel SDplus LS 5 μm, 300 × 8mm linear columns, Wyatt DAWN HELEOS-II and Wyatt Optilab T-rEX. The column temperature was set at 40 °C. A flow rate of 0.70 mL/min was used and samples were dissolved in chloroform. dn/dc values were calculated for PLA and PCHO by creating 5 solutions of increasing concentration (0.1 - 1.0 mg/mL), directly injecting them into the RI detector sequentially, and using the batch dn/dc measurement methods in the Astra software.

Polymerization procedure for Tables 5.1-5.3, 5.6

0.10 mL of a 50 mM dodecaborate solution in *o*-F₂C₆H₄ was put in a J-Young tube, followed by 0.30 mL C₆D₆ and 0.10 mL *o*-F₂C₆H₄. 0.10 mL of a 5.0 M solution of CHO was added, and the solution was shaken to mix the contents. Reaction was monitored by ¹H NMR until complete. Afterwards the mixture was quenched with ~3 mL cold MeOH to afford a white precipitate. The slurry was cooled at -40 °C overnight then centrifuged. Removal of the supernatant left isolated polymer behind.

Polymerization procedure for Tables 5.4 and 5.5

In a dark, nitrogen-filled glovebox, epoxide monomer (0.50 mmol) was charged to a dram vial followed by 0.15 mL of *o*-F₂C₆H₄ or CH₂Cl₂. 0.10 mL B₁₂(OCH₂C₆F₅) from a 5.0 × 10⁻² mM stock solution was then added to begin the polymerization. The mixture was brought out of the glovebox and set to stir at room temperature for two hours under blue (450 nm) LED

irradiation. After two hours, the mixture was quenched with ~3 mL cold MeOH to afford a white precipitate. The slurry was cooled at -40 °C overnight then centrifuged. Removal of the supernatant left isolated polymer behind.

For polymerizations run in the absence of light, vials were covered with aluminum foil and stirred without blue LED irradiation.

Purification of epoxides

Propylene oxide was refluxed with CaH₂ overnight and fractionally distilled under nitrogen at 34.5 °C.

Limonene oxide was distilled over NaH under vacuum at 164-167 °C under reduced pressure. Remaining hydroxyl impurities were methylated with MeI then the solution was redistilled.

Styrene oxide was distilled under a reduced pressure. Phenylacetylaldehyde impurity was (<1%). Reduction with PtO₂ then distillation removed the impurity.

5.5 Appendix E

^1H NMR Spectroscopy

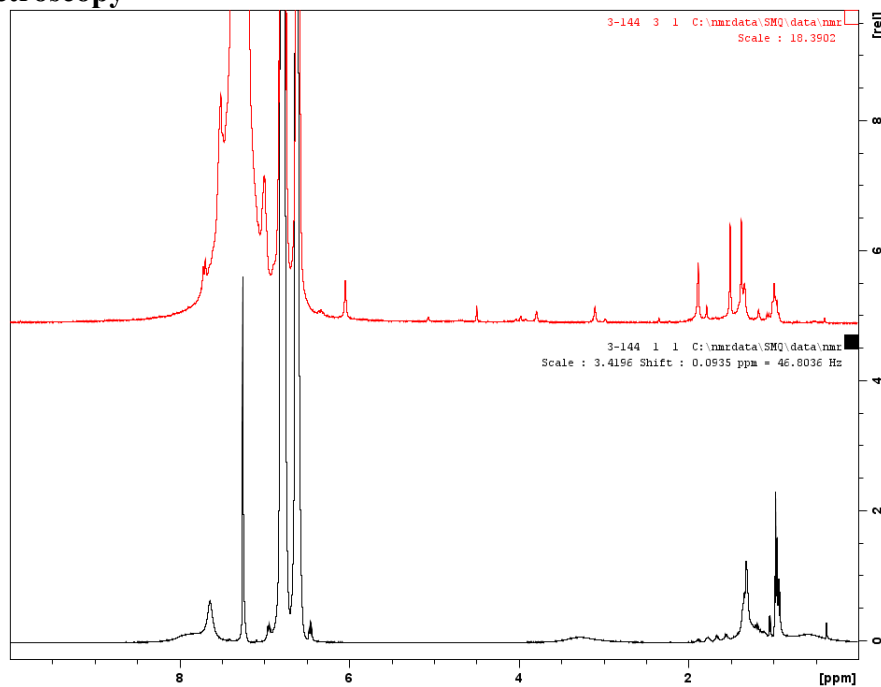


Figure E1. Oxidation of $(\text{salfan})\text{Zr}(\text{O}^t\text{Bu})_2$ by F_{36} (bottom) and subsequent reduction by CoCp_2 (top).

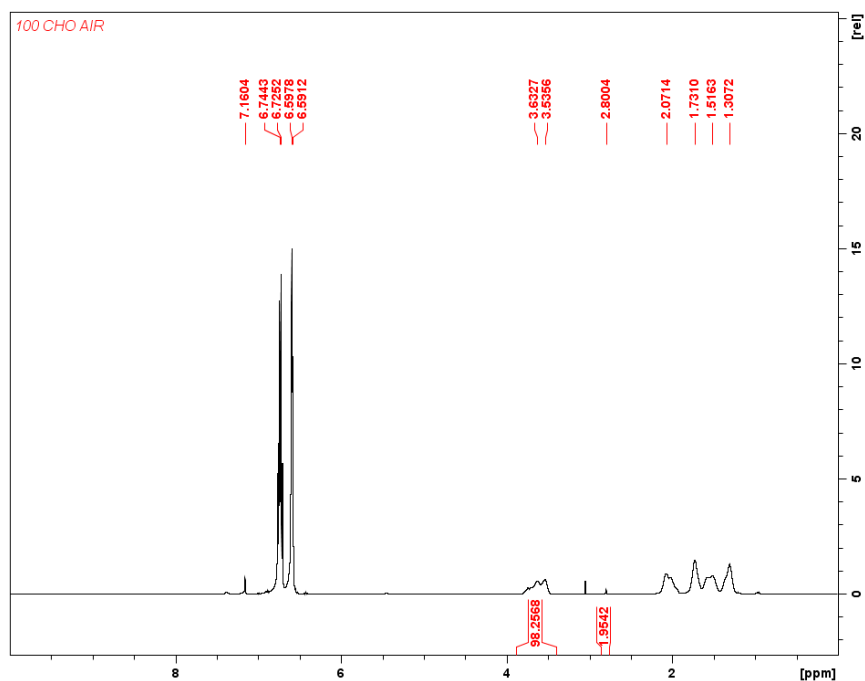


Figure E2. Table 5.1, entry 1. Polymerization of 100 equivalents of CHO by F_{36} in 4:1 $\text{F}_2\text{C}_6\text{H}_4:\text{C}_6\text{D}_6$ in open air. ^1H NMR (300 MHz, 25 $^\circ\text{C}$, C_6D_6), δ (ppm): 6.74 (CFCH 1,2-difluorobenzene), 6.59 (CFCHCH 1,2-difluorobenzene), 3.58 (m, 2H, COCH PCHO), 2.80 (s, 2H, COCH CHO), 1.73 (m, 2H, COCHCH₂ PCHO), 1.52 (m, 2H, COCHCH₂ PCHO), 1.31 (m, 2H, COCHCH₂CH₂ PCHO).

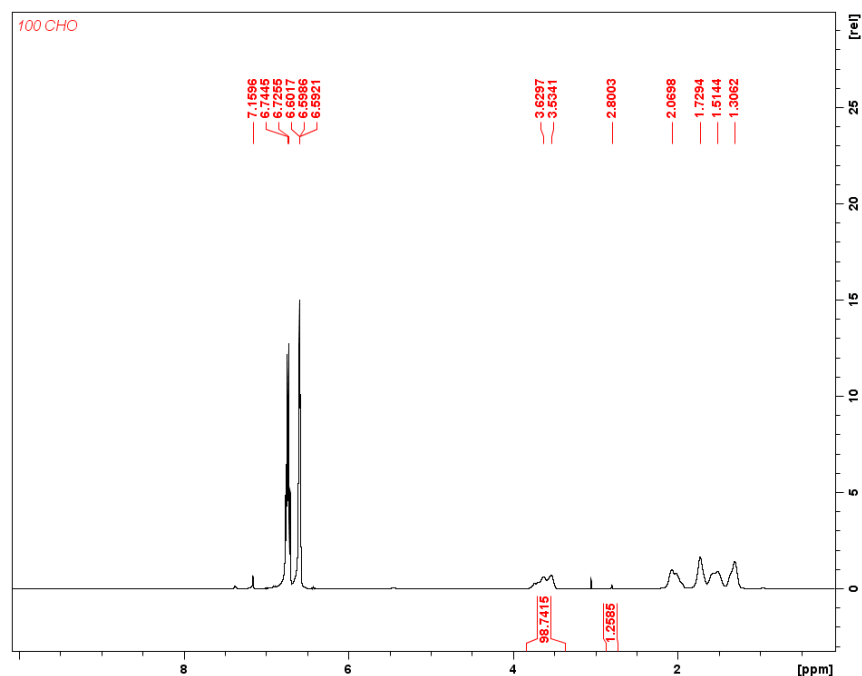


Figure E3. Table 5.1, entry 2. Polymerization of 100 equivalents of CHO by F₃₆ in 4:1 F₂C₆H₄:C₆D₆. ¹H NMR (300 MHz, 25 °C, C₆D₆), δ (ppm): 6.73 (CFCH 1,2-difluorobenzene), 6.60 (CFCHCH 1,2-difluorobenzene), 3.58 (m, 2H, COCH PCHO), 2.80 (s, 2H, COCH CHO), 2.07 (m, 2H, COCHCH₂ PCHO), 1.73 (m, 2H, COCHCH₂ PCHO), 1.51 (m, 2H, COCHCH₂CH₂ PCHO), 1.30 (m, 2H, COCHCH₂CH₂ PCHO).

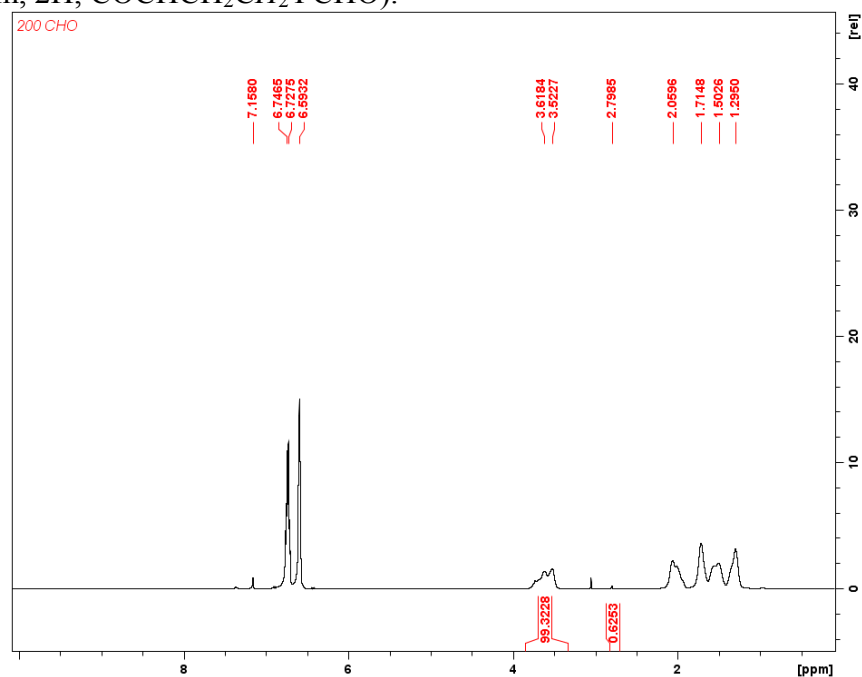


Figure E4. Table 5.1, entry 3. Polymerization of 200 equivalents of CHO by F₃₆ in 4:1 F₂C₆H₄:C₆D₆. ¹H NMR (300 MHz, 25 °C, C₆D₆), δ (ppm): 6.73 (CFCH 1,2-difluorobenzene), 6.59 (CFCHCH 1,2-difluorobenzene), 3.57 (m, 2H, COCH PCHO), 2.80 (s, 2H, COCH CHO), 2.06 (m, 2H, COCHCH₂ PCHO), 1.71 (m, 2H, COCHCH₂ PCHO), 1.50 (m, 2H, COCHCH₂CH₂ PCHO), 1.30 (m, 2H, COCHCH₂CH₂ PCHO).

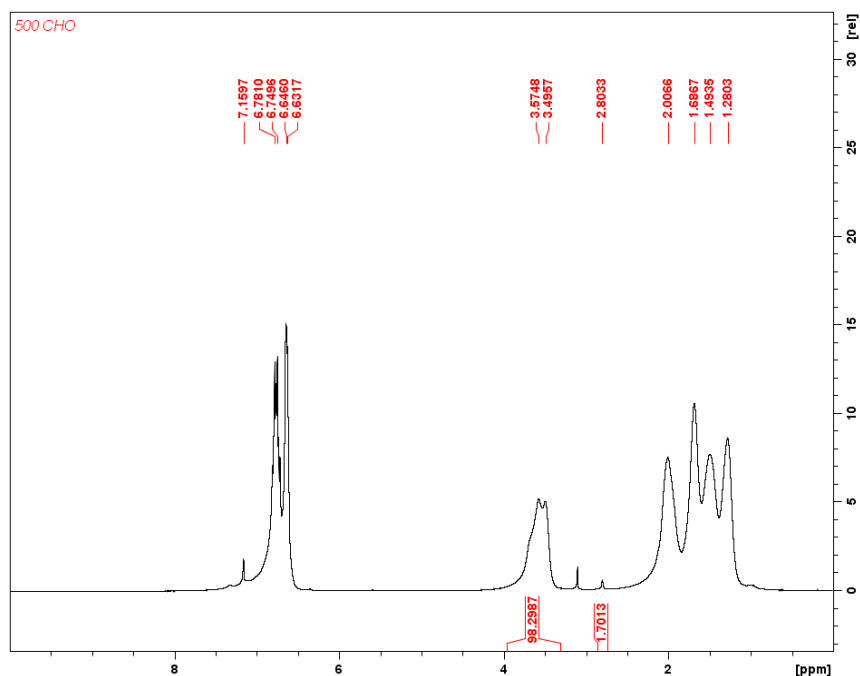


Figure E5. Table 5.1, entry 4. Polymerization of 500 equivalents of CHO by F_{36} in 4:1 $F_2C_6H_4:C_6D_6$. 1H NMR (300 MHz, 25 °C, C_6D_6), δ (ppm): 6.76 (CFCH 1,2-difluorobenzene), 6.64 (CFCHCH 1,2-difluorobenzene), 3.53 (m, 2H, COCH PCHO), 2.80 (s, 2H, COCH CHO), 2.00 (m, 2H, COCHCH₂ PCHO), 1.69 (m, 2H, COCHCH₂ PCHO), 1.49 (m, 2H, COCHCH₂CH₂ PCHO), 1.28 (m, 2H, COCHCH₂CH₂ PCHO).

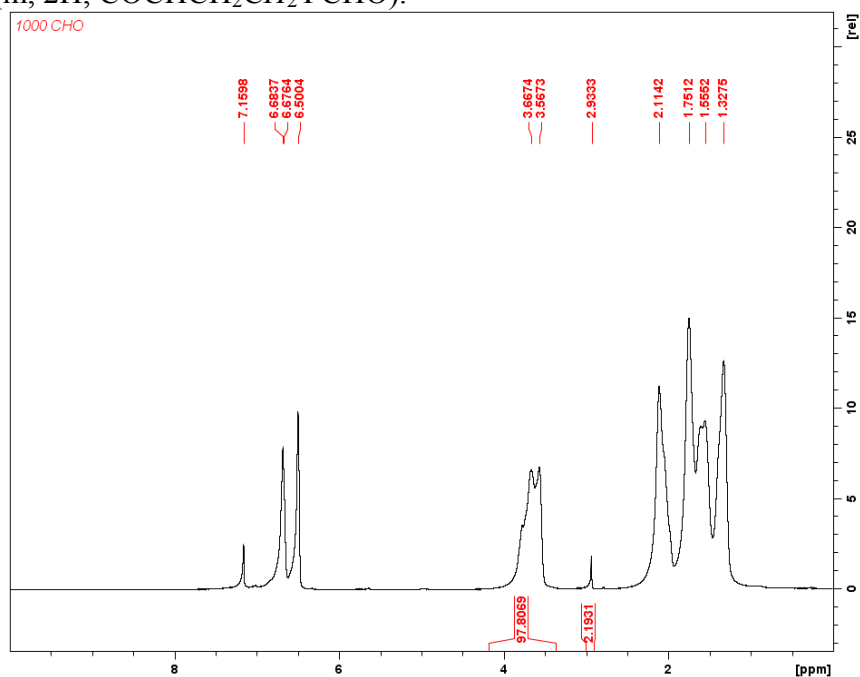


Figure E6. Table 5.1, entry 5. Polymerization of 1000 equivalents of CHO by F_{36} in 4:1 $F_2C_6H_4:C_6D_6$. 1H NMR (300 MHz, 25 °C, C_6D_6), δ (ppm): 6.68 (CFCH 1,2-difluorobenzene), 6.50 (CFCHCH 1,2-difluorobenzene), 3.59 (m, 2H, COCH PCHO), 2.93 (s, 2H, COCH CHO), 2.11 (m, 2H, COCHCH₂ PCHO), 1.75 (m, 2H, COCHCH₂ PCHO), 1.56 (m, 2H, COCHCH₂CH₂ PCHO), 1.33 (m, 2H, COCHCH₂CH₂ PCHO).

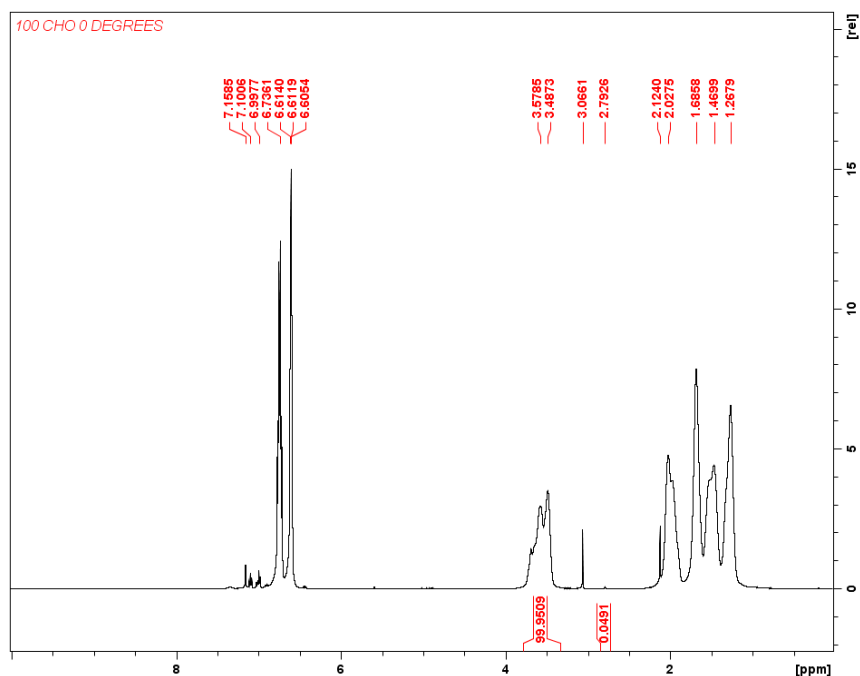


Figure E7. Table 5.1, entry 6. Polymerization of 100 equivalents of CHO by F_{36} in 4:1 $F_2C_6H_4:C_6D_6$ at 0 °C. 1H NMR (300 MHz, 25 °C, C_6D_6), δ (ppm): 6.74 (CFCH 1,2-difluorobenzene), 6.61 (CFCHCH 1,2-difluorobenzene), 3.52 (m, 2H, COCH PCHO), 2.79 (s, 2H, COCH CHO), 2.03 (m, 2H, COCHCH₂ PCHO), 1.69 (m, 2H, COCHCH₂ PCHO), 1.47 (m, 2H, COCHCH₂CH₂ PCHO), 1.27 (m, 2H, COCHCH₂CH₂ PCHO).

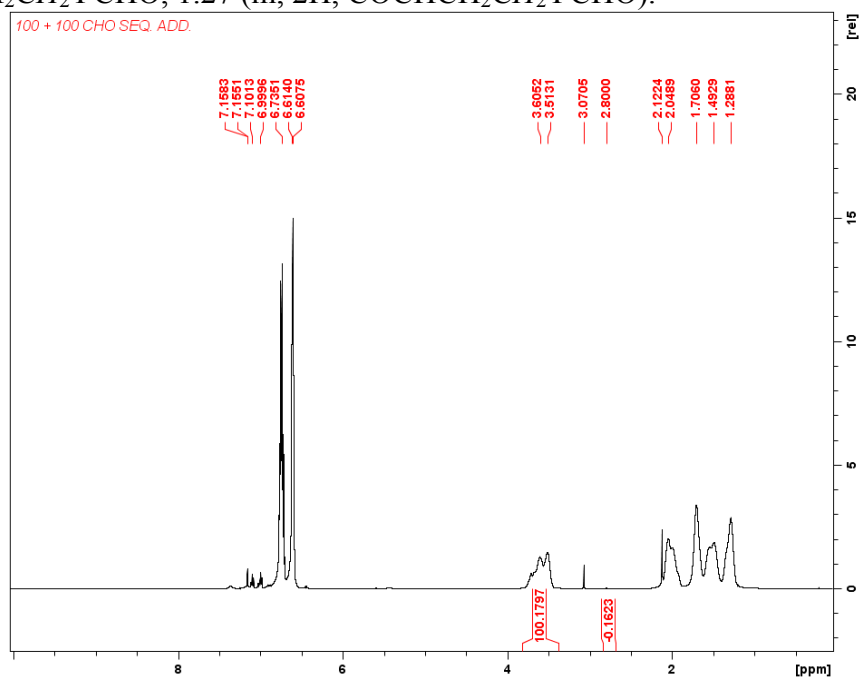


Figure E8. Table 5.1, entry 7. Polymerization of 100 equivalents of CHO followed by another 100 equivalents of CHO by F_{36} in 4:1 $F_2C_6H_4:C_6D_6$. 1H NMR (300 MHz, 25 °C, C_6D_6), δ (ppm): 6.74 (CFCH 1,2-difluorobenzene), 6.61 (CFCHCH 1,2-difluorobenzene), 3.56 (m, 2H, COCH PCHO), 2.80 (s, 2H, COCH CHO), 2.05 (m, 2H, COCHCH₂ PCHO), 1.71 (m, 2H, COCHCH₂ PCHO), 1.49 (m, 2H, COCHCH₂CH₂ PCHO), 1.29 (m, 2H, COCHCH₂CH₂ PCHO).

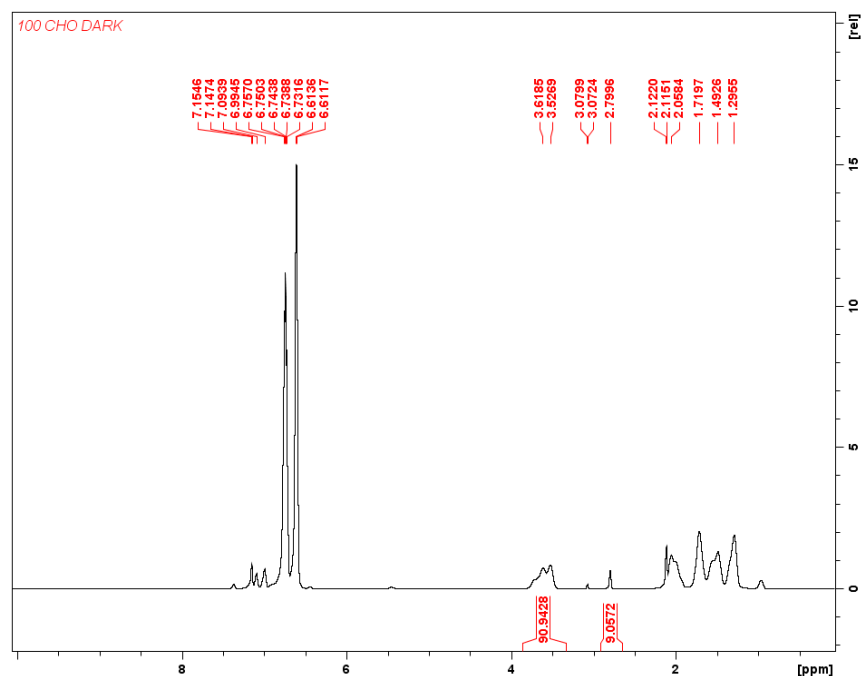


Figure E9. Table 5.1, entry 8. Polymerization of 100 equivalents of CHO by F_{36} in 4:1 $F_2C_6H_4:C_6D_6$ in the dark. 1H NMR (300 MHz, 25 °C, C_6D_6), δ (ppm): 6.74 (CFCH 1,2-difluorobenzene), 6.61 (CFCHCH 1,2-difluorobenzene), 3.57 (m, 2H, COCH PCHO), 2.80 (s, 2H, COCH CHO), 2.06 (m, 2H, COCHCH₂ PCHO), 1.72 (m, 2H, COCHCH₂ PCHO), 1.49 (m, 2H, COCHCH₂CH₂ PCHO), 1.30 (m, 2H, COCHCH₂CH₂ PCHO).

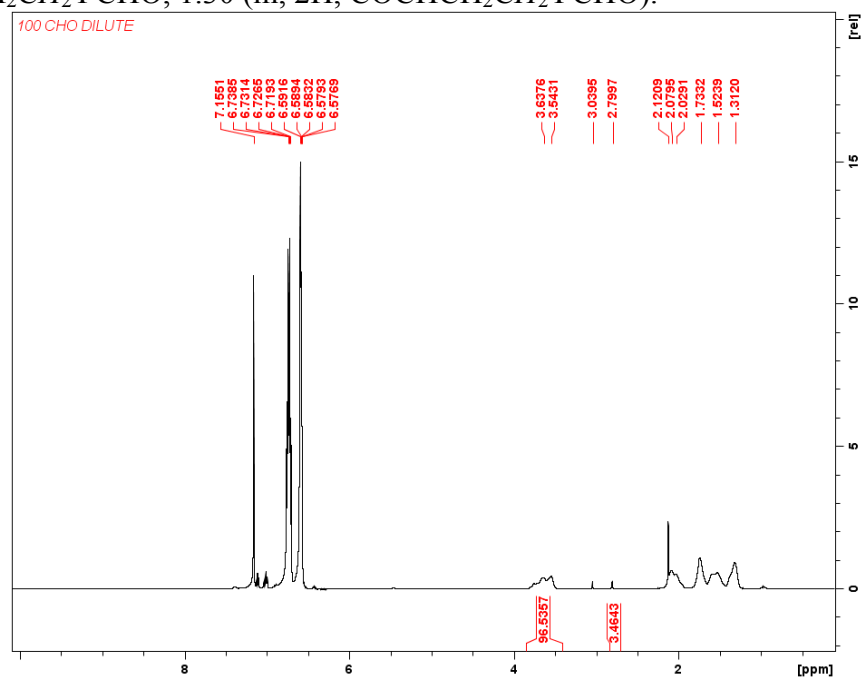


Figure E10. Table 5.1, entry 9. Polymerization of 100 equivalents of CHO by F_{36} in 4:1 $F_2C_6H_4:C_6D_6$ in a diluted solution. 1H NMR (300 MHz, 25 °C, C_6D_6), δ (ppm): 6.73 (CFCH 1,2-difluorobenzene), 6.58 (CFCHCH 1,2-difluorobenzene), 3.59 (m, 2H, COCH PCHO), 2.80 (s, 2H, COCH CHO), 2.08 (m, 2H, COCHCH₂ PCHO), 1.73 (m, 2H, COCHCH₂ PCHO), 1.52 (m, 2H, COCHCH₂CH₂ PCHO), 1.31 (m, 2H, COCHCH₂CH₂ PCHO).

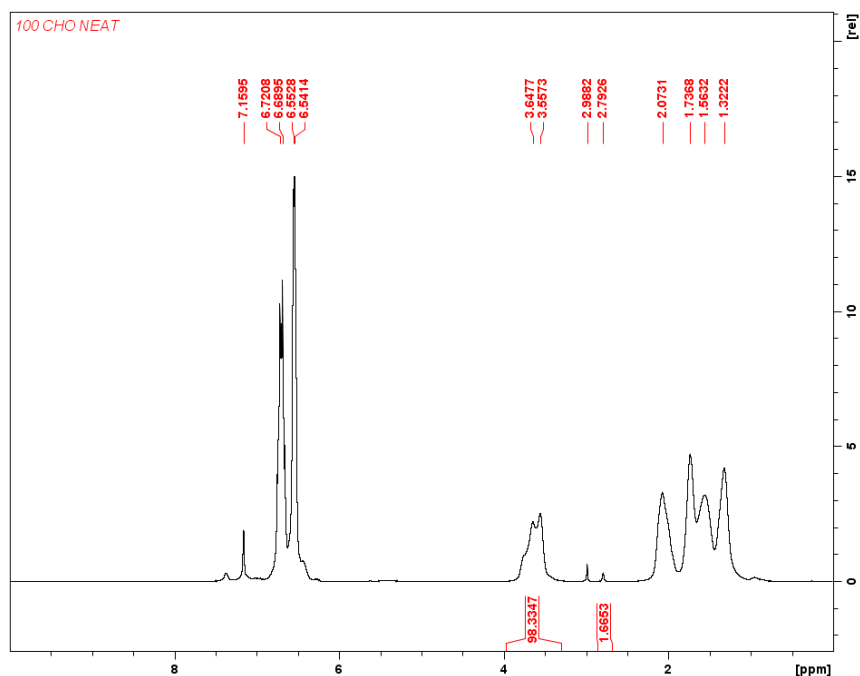


Figure E11. Table 5.1, entry 10. Polymerization of 100 equivalents of CHO by F_{36} neat. 1H NMR (300 MHz, 25 °C, C_6D_6), δ (ppm): 6.70 (CFCH 1,2-difluorobenzene), 6.55 (CFCHCH 1,2-difluorobenzene), 3.60 (m, 2H, COCH PCHO), 2.79 (s, 2H, COCH CHO), 2.07 (m, 2H, COCHCH₂ PCHO), 1.74 (m, 2H, COCHCH₂ PCHO), 1.56 (m, 2H, COCHCH₂CH₂ PCHO), 1.32 (m, 2H, COCHCH₂CH₂ PCHO).

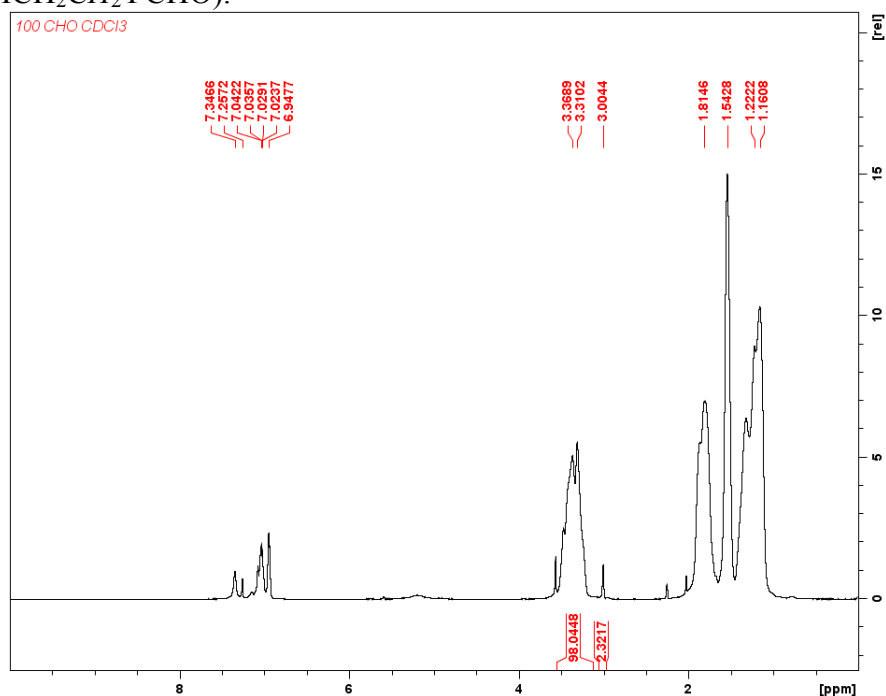


Figure E12. Table 5.1, entry 11. Polymerization of 100 equivalents of CHO by F_{36} in $CDCl_3$. 1H NMR (300 MHz, 25 °C, $CDCl_3$), δ (ppm): 7.03 (CFCH 1,2-difluorobenzene), 6.95 (CFCHCH 1,2-difluorobenzene), 3.34 (m, 2H, COCH PCHO), 3.00 (s, 2H, COCH CHO), 1.81 (m, 2H, COCHCH₂ PCHO), 1.54 (m, 2H, COCHCH₂ PCHO), 1.19 (m, 4H, COCHCH₂CH₂ PCHO).

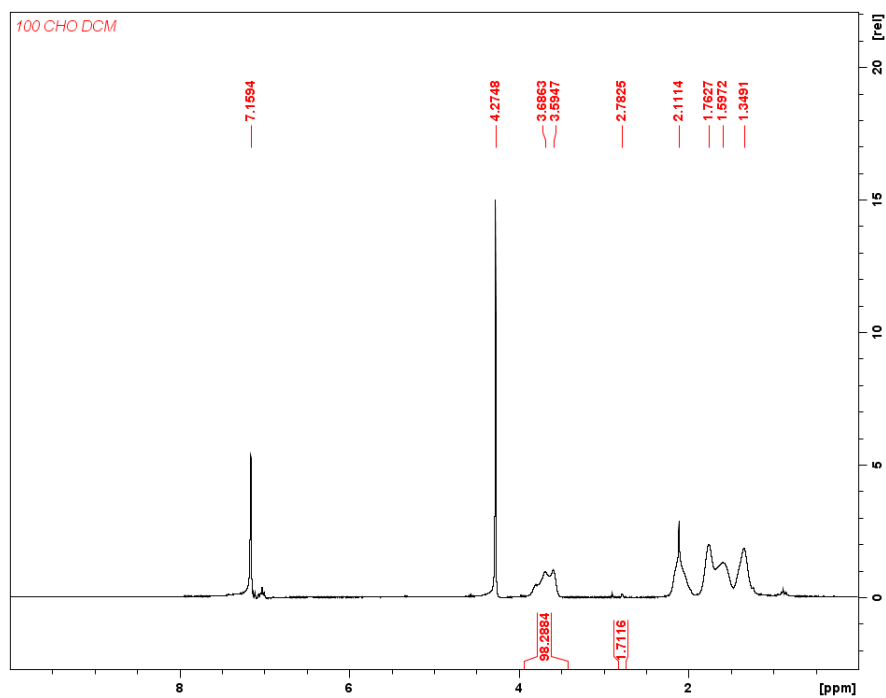


Figure E13. Table 5.1, entry 12. Polymerization of 100 equivalents of CHO by F_{36} in CH_2Cl_2 . 1H NMR (300 MHz, 25 °C, C_6D_6), δ (ppm): 4.27 (s, CH CH_2Cl_2), 3.63 (m, 2H, $COCH$ PCHO), 2.78 (s, 2H, $COCH$ CHO), 2.11 (m, 2H, $COCHCH_2$ PCHO), 1.76 (m, 2H, $COCHCH_2$ PCHO), 1.60 (m, 2H, $COCHCH_2CH_2$ PCHO), 1.35 (m, 2H, $COCHCH_2CH_2$ PCHO).

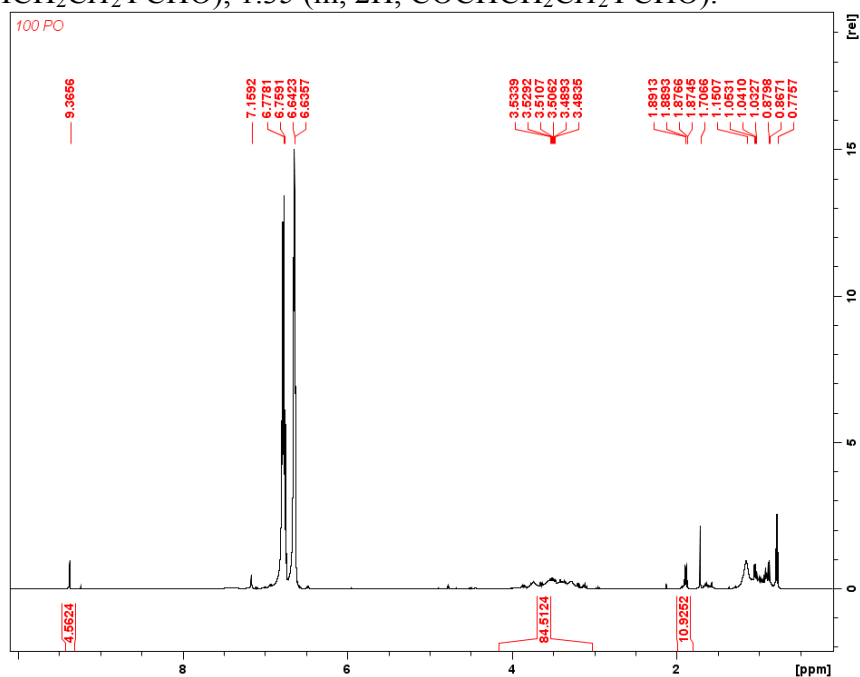


Figure E14. Table 5.2, entry 1. Polymerization of 100 equivalents of PO by F_{36} in 4:1 $F_2C_6H_4:C_6D_6$. 1H NMR (300 MHz, 25 °C, C_6D_6), δ (ppm): 9.37 (t, 1H, OCH propionaldehyde), 6.76 (CFCH 1,2-difluorobenzene), 6.64 (CFCHCH 1,2-difluorobenzene), 3.50 (m, 1H, OCH PPO), 1.89 (m, 1H, CH_2 PO), 1.15 (m, 3H, CH_3 PPO), 1.04 (m, 1H, CH_2 PO), 0.87 (d, 3H, CH_3 PO), 0.77 (m, 3H, CH_3 PO).

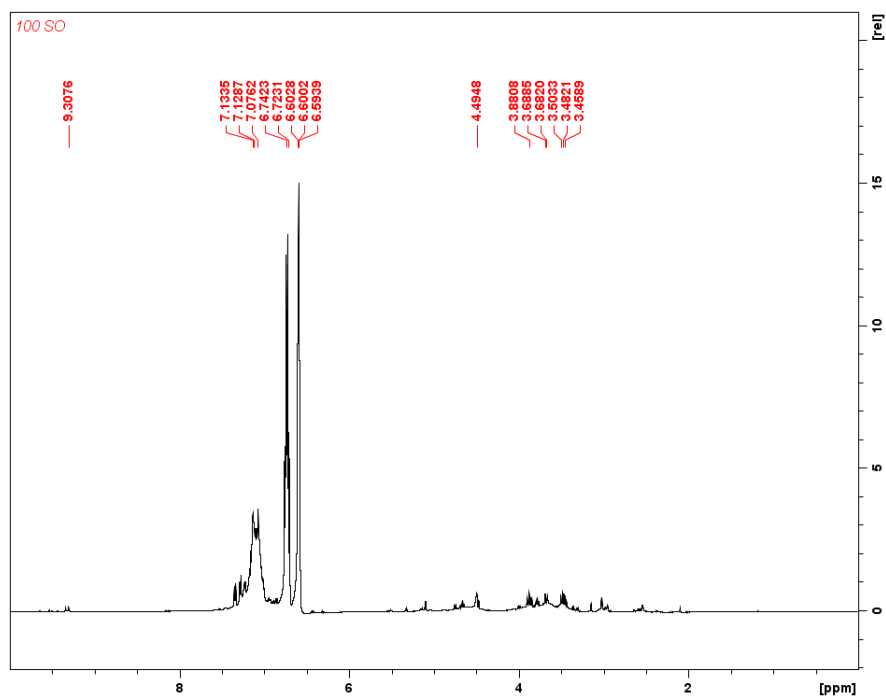


Figure E15. Table 5.2, entry 2. Polymerization of 100 equivalents of SO by F_{36} in 4:1 $F_2C_6H_4:C_6D_6$. 1H NMR (300 MHz, 25 °C, C_6D_6), δ (ppm): 9.30 (t, 1H, OCH phenylacetylaldehyde), 7.13 (m, 5H, ArH polystyrene oxide), 6.73 (CFCH 1,2-difluorobenzene), 6.60 (CFCHCH 1,2-difluorobenzene), 3.48 (m, 1H, CH_2 styrene oxide).

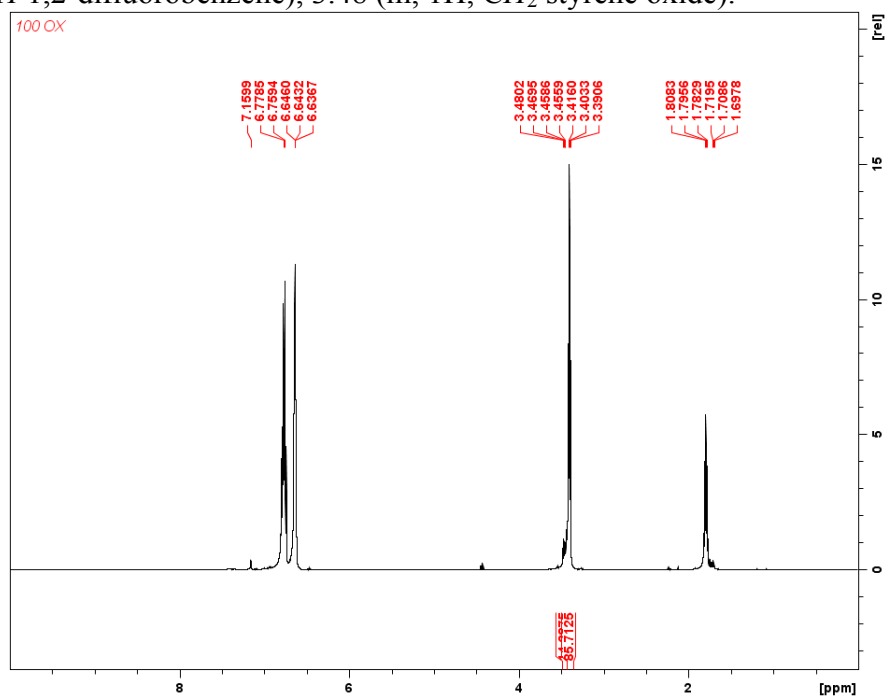


Figure E16. Table 5.2, entry 3. Polymerization of 100 equivalents of OX by F_{36} in 4:1 $F_2C_6H_4:C_6D_6$. 1H NMR (300 MHz, 25 °C, C_6D_6), δ (ppm): 6.73 (CFCH 1,2-difluorobenzene), 6.60 (CFCHCH 1,2-difluorobenzene), 3.46 (m, 4H, CH_2 OX), 3.40 (m, 4H, CH_2 POX), 1.80 (m, 2H, CH_2 POX), 1.71 (m, 2H, CH_2 OX).

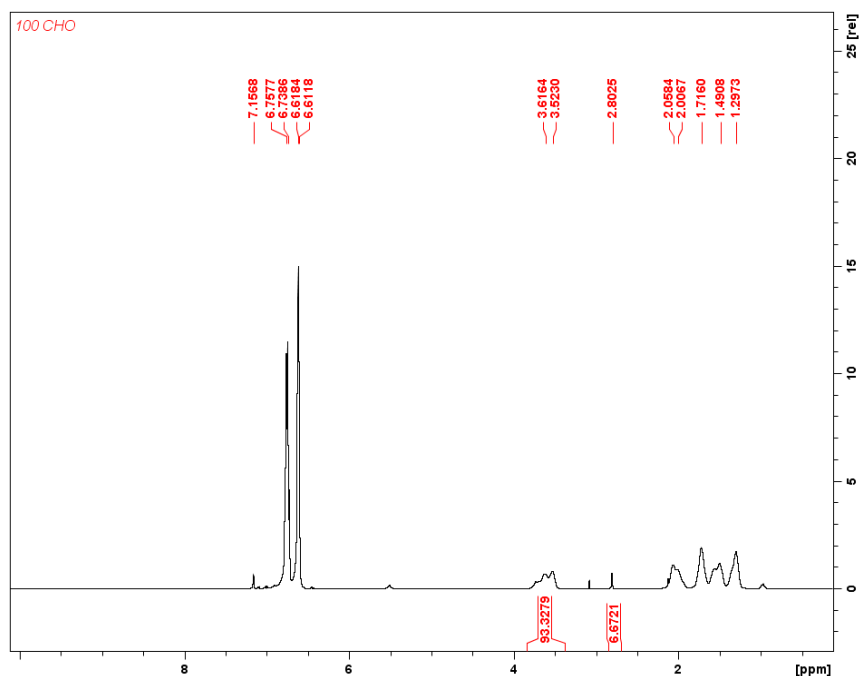


Figure E17. Table 5.3, entry 1. Polymerization of 100 equivalents of CHO by F₆₀ in 4:1 F₂C₆H₄:C₆D₆. ¹H NMR (300 MHz, 25 °C, C₆D₆), δ (ppm): 6.76 (CFCH 1,2-difluorobenzene), 6.61 (CFCHCH 1,2-difluorobenzene), 3.56 (m, 2H, COCH PCHO), 2.80 (s, 2H, COCH CHO), 2.03 (m, 2H, COCHCH₂ PCHO), 1.72 (m, 2H, COCHCH₂ PCHO), 1.49 (m, 2H, COCHCH₂CH₂ PCHO), 1.30 (m, 2H, COCHCH₂CH₂ PCHO).

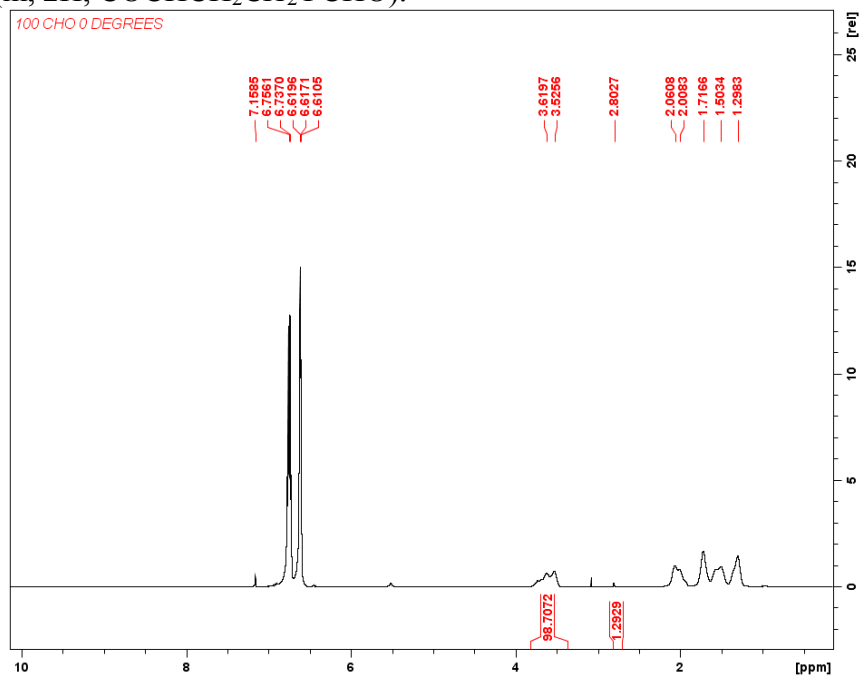


Figure E18. Table 5.3, entry 2. Polymerization of 100 equivalents of CHO by F₆₀ in 4:1 F₂C₆H₄:C₆D₆ at 0 °C. ¹H NMR (300 MHz, 25 °C, C₆D₆), δ (ppm): 6.76 (CFCH 1,2-difluorobenzene), 6.62 (CFCHCH 1,2-difluorobenzene), 3.56 (m, 2H, COCH PCHO), 2.80 (s, 2H, COCH CHO), 2.03 (m, 2H, COCHCH₂ PCHO), 1.72 (m, 2H, COCHCH₂ PCHO), 1.50 (m, 2H, COCHCH₂CH₂ PCHO), 1.30 (m, 2H, COCHCH₂CH₂ PCHO).

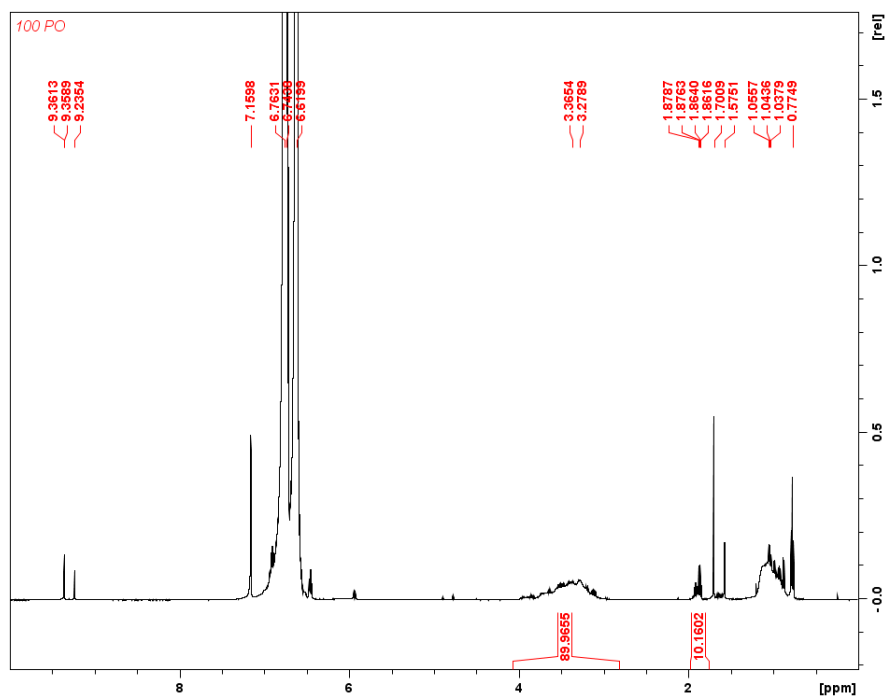


Figure E19. Table 5.3, entry 3. Polymerization of 100 equivalents of PO by F₆₀ in 4:1 F₂C₆H₄:C₆D₆. ¹H NMR (300 MHz, 25 °C, C₆D₆), δ (ppm): 9.36 (t, 1H, OCH propionaldehyde), 6.75 (CFCH 1,2-difluorobenzene), 6.62 (CFCHCH 1,2-difluorobenzene), 3.32 (m, 1H, OCH PPO), 1.87 (m, 1H, OCH PO), 1.04 (m, 3H, CH₃ PPO), 0.77 (d, 3H, CH₃ PO).

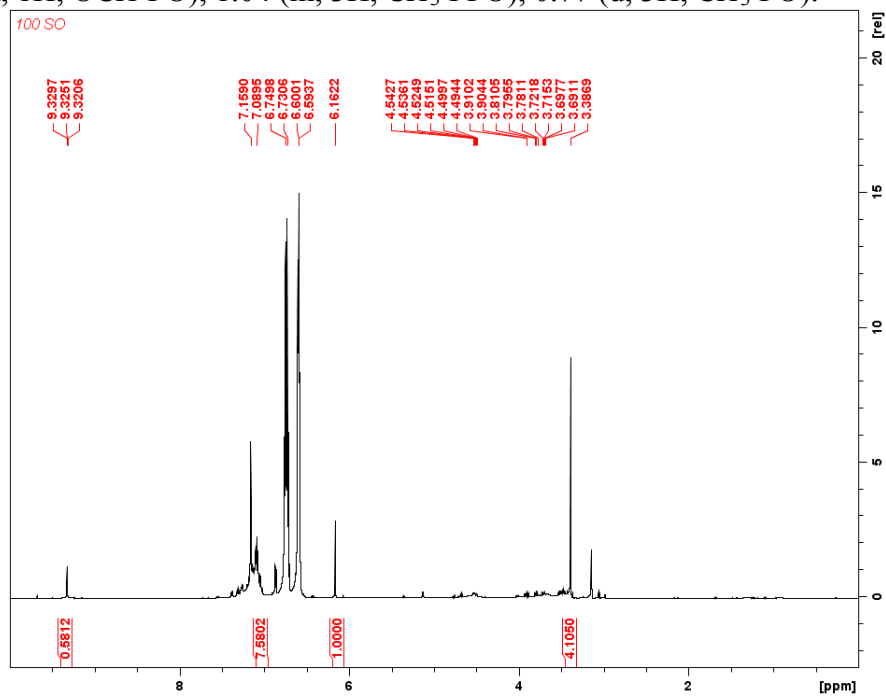


Figure E20. Table 5.3, entry 4. Polymerization of 100 equivalents of SO by F₆₀ in 4:1 F₂C₆H₄:C₆D₆. ¹H NMR (300 MHz, 25 °C, C₆D₆), δ (ppm): 9.33 (t, 1H, OCH phenylacetylaldehyde), 7.09 (m, 5H, ArH polystyrene oxide), 6.74 (CFCH 1,2-difluorobenzene), 6.60 (CFCHCH 1,2-difluorobenzene), 6.16 (s, 3H, PhH TMB), 3.38 (s, 9H, CH₃ TMB).

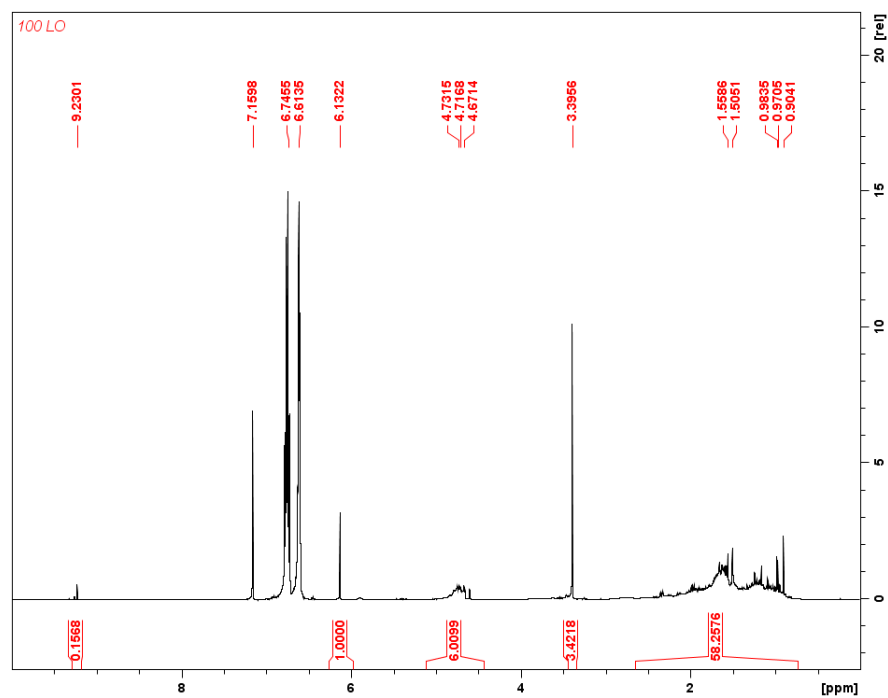


Figure E21. Table 5.3, entry 5. Polymerization of 100 equivalents of LO by F₆₀ in 4:1 F₂C₆H₄:C₆D₆. ¹H NMR (300 MHz, 25 °C, C₆D₆), δ (ppm): 9.51 (t, 1H, OCH campholenic aldehyde), 6.74 (CFCH 1,2-difluorobenzene), 6.61 (CFCHCH 1,2-difluorobenzene), 6.13 (s, 3H, PhH TMB), 4.72 (b, 1H, OCH polylimonene oxide), 3.40 (s, 9H, CH₃ TMB), 1.53 (s, 3H, CH₃ polylimonene oxide), 0.98 (s, 3H, CH₃ limonene oxide), 0.90 (s, 2H, CH₂ limonene oxide).

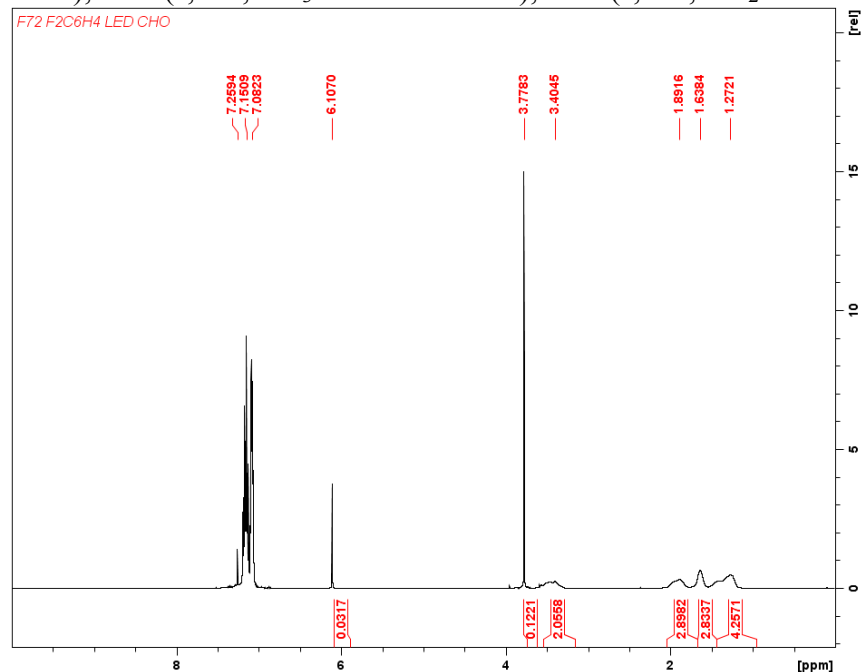


Figure E22. Table 5.4. Polymerization of CHO by F₇₂ in F₂C₆H₄ in the presence of blue LED light. ¹H NMR (300 MHz, 25 °C, CDCl₃), δ (ppm): 7.15 (CFCH 1,2-difluorobenzene), 7.08 (CFCHCH 1,2-difluorobenzene), 6.11 (s, 3H, PhH TMB), 3.78 (s, 9H, CH₃ TMB), 3.40 (m, 2H, COCH PCHO), 1.89 (m, 2H, COCHCH₂ PCHO), 1.64 (m, 2H, COCHCH₂ PCHO), 1.27 (m, 4H, COCHCH₂CH₂ PCHO).

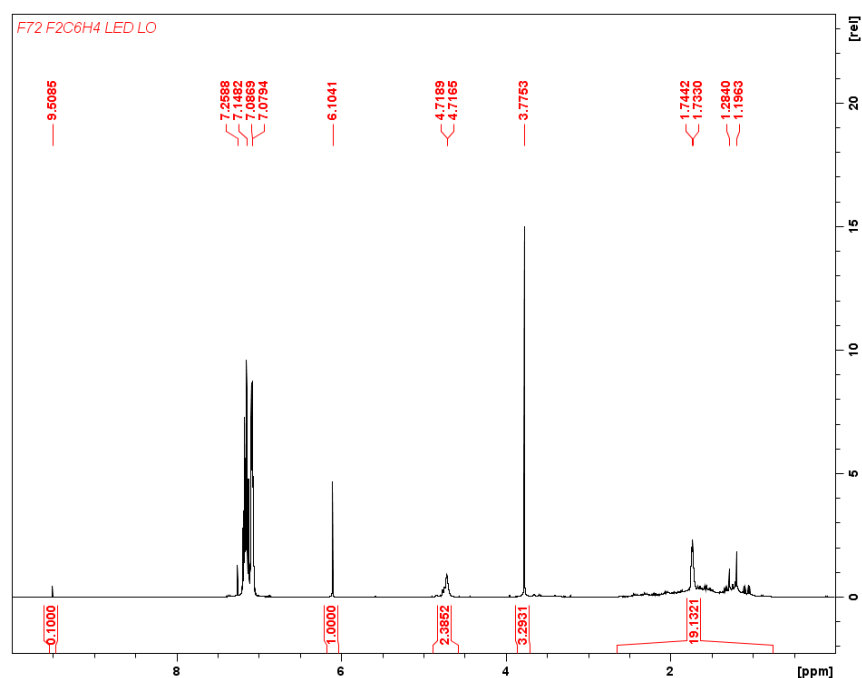


Figure E23. Table 5.4. Polymerization of LO by F_{72} in $F_2C_6H_4$ in the presence of blue LED light. 1H NMR (300 MHz, 25 °C, $CDCl_3$), δ (ppm): 9.51 (t, 1H, OCH xx), 7.15 (CFCH 1,2-difluorobenzene), 7.09 (CFCHCH 1,2-difluorobenzene), 6.10 (s, 3H, PhH TMB), 4.72 (b, 1H, OCH polylimonene oxide), 3.78 (s, 9H, CH_3 TMB), 1.74 (s, 3H, CH_3 polylimonene oxide), 1.28 (s, 3H, CH_3 limonene oxide), 1.20 (s, 2H, CH_2 limonene oxide).

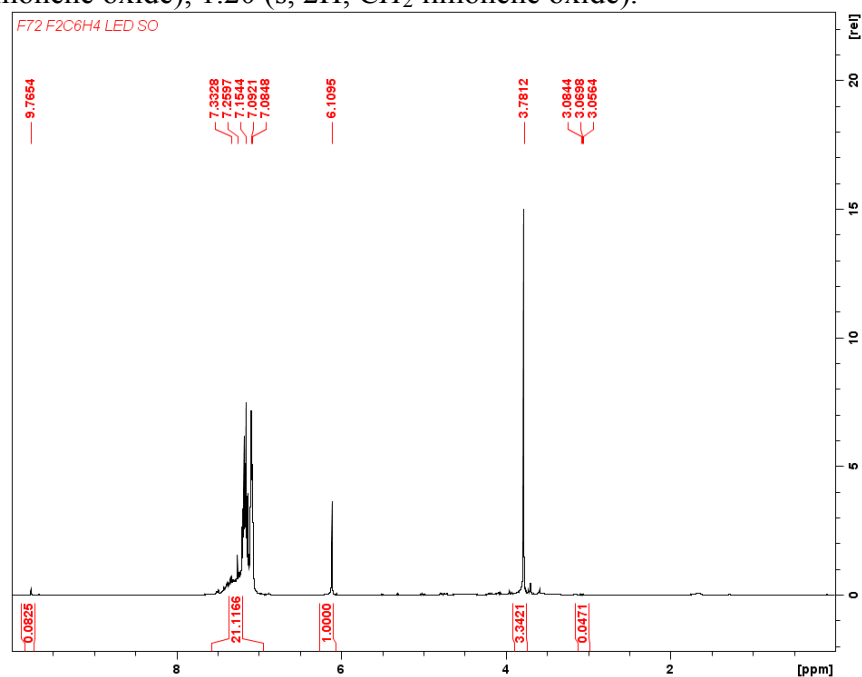


Figure E24. Table 5.4. Polymerization of SO by F_{72} in $F_2C_6H_4$ in the presence of blue LED light. 1H NMR (300 MHz, 25 °C, $CDCl_3$), δ (ppm): 9.77 (t, 1H, OCH phenylacetaldehyde), 7.33 (m, 5H, ArH polystyrene oxide), 7.15 (CFCH 1,2-difluorobenzene), 7.09 (CFCHCH 1,2-difluorobenzene), 6.11 (s, 3H, PhH TMB), 3.78 (s, 9H, CH_3 TMB), 3.07 (m, 1H, CH_2 styrene oxide).

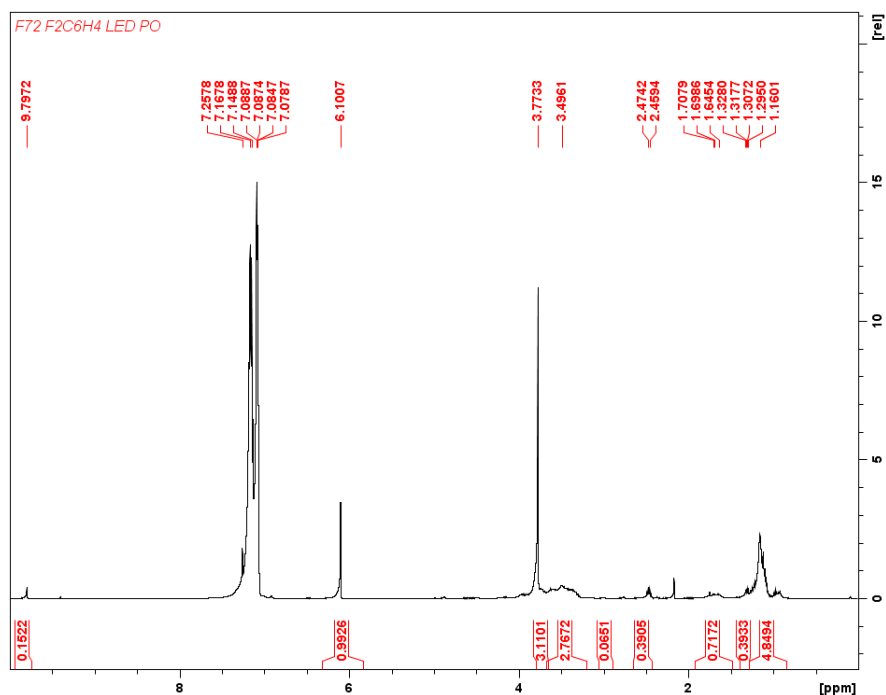


Figure E25. Table 5.4. Polymerization of PO by F₇₂ in F₂C₆H₄ in the presence of blue LED light. ¹H NMR (300 MHz, 25 °C, CDCl₃), δ (ppm): 9.80 (m, 1H, OCH propionaldehyde), 7.17 (CFCH 1,2-difluorobenzene), 7.08 (CFCHCH 1,2-difluorobenzene), 6.10 (s, 3H, PhH TMB), 3.77 (s, 9H, CH₃ TMB), 3.50 (m, 1H, OCH PPO), 2.99 (m, 1H, OCH PO), 2.44 (m, 1H, CH₂ propionaldehyde), 1.32 (d, 3H, CH₃ PPO), 1.14 (m, 3H, CH₃ propionaldehyde).

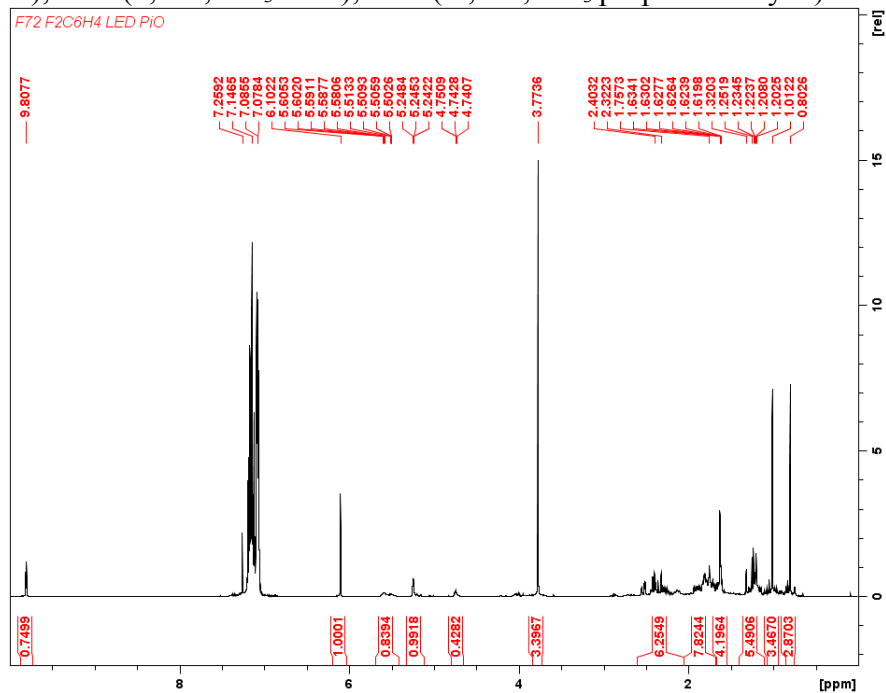


Figure E26. Table 5.4. Polymerization of PiO by F₇₂ in F₂C₆H₄ in the presence of blue LED light. ¹H NMR (300 MHz, 25 °C, CDCl₃), δ (ppm): 9.80 (t, 1H, OCH, campholenic aldehyde), 7.15 (CFCH 1,2-difluorobenzene), 7.08 (CFCHCH 1,2-difluorobenzene), 6.10 (s, 3H, PhH TMB), 5.58 (t, 1H, CH campholenic aldehyde), 3.77 (s, 9H, CH₃ TMB).

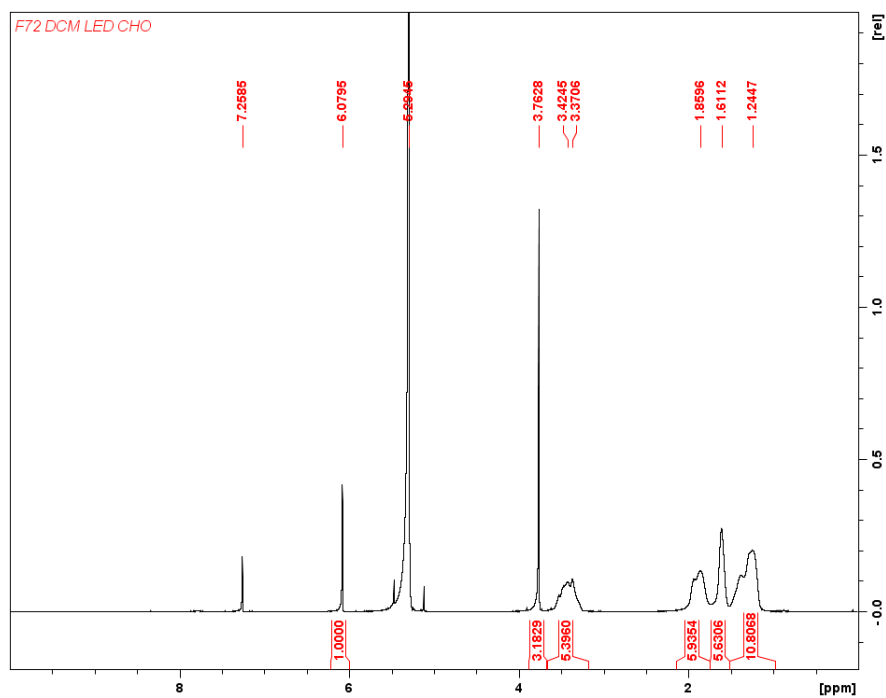


Figure E27. Table 5.4. Polymerization of CHO by F₇₂ in CH₂Cl₂ in the presence of blue LED light. ¹H NMR (300 MHz, 25 °C, CDCl₃), δ (ppm): 6.08 (s, 3H, PhH TMB), 5.30 (CH CH₂Cl₂), 3.76 (s, 9H, CH₃ TMB), 3.40 (m, 2H, COCHCH₂ PCHO), 1.86 (m, 2H, COCHCH₂ PCHO), 1.61 (m, 2H, COCHCH₂CH₂ PCHO), 1.24 (m, 2H, COCHCH₂CH₂ PCHO).

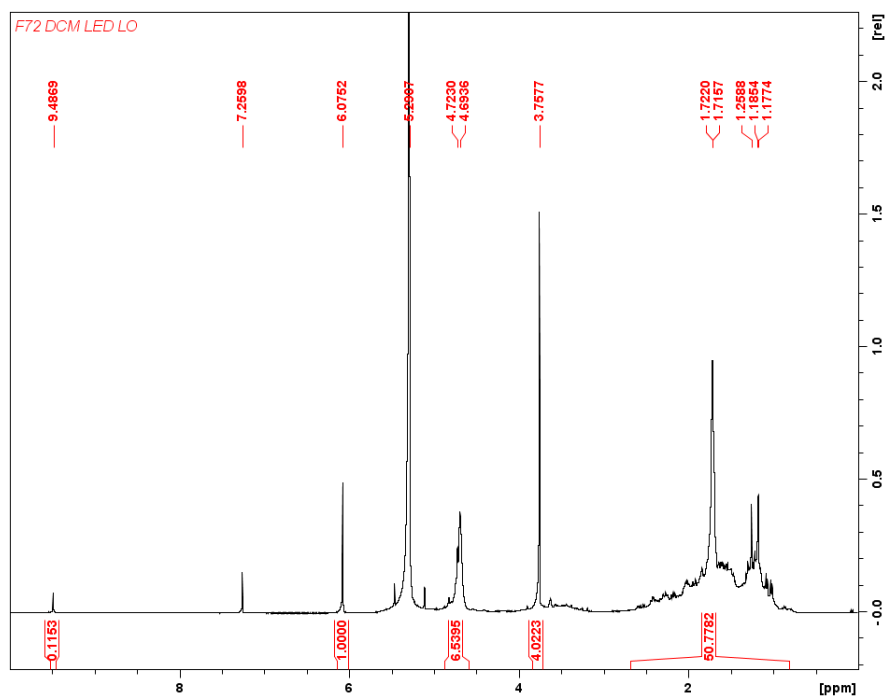


Figure E28. Table 5.4. Polymerization of LO by F₇₂ in CH₂Cl₂ in the presence of blue LED light. ¹H NMR (300 MHz, 25 °C, CDCl₃), δ (ppm): 9.49 (t, 1H, OCH xx), 6.08 (s, 3H, PhH TMB), 5.30 (CH CH₂Cl₂), 4.70 (b, 1H, OCH polylimonene oxide), 3.76 (s, 9H, CH₃ TMB), 1.72 (s, 3H, CH₃ polylimonene oxide), 1.26 (s, 3H, CH₃ limonene oxide), 1.19 (s, 2H, CH₂ limonene oxide).

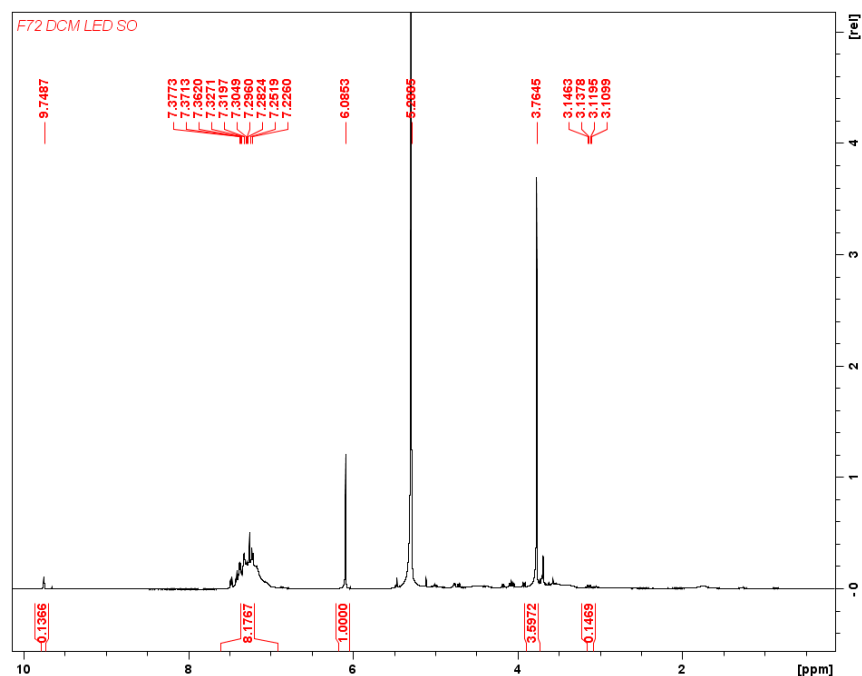


Figure E29. Table 5.4. Polymerization of SO by F_{72} in CH_2Cl_2 in the presence of blue LED light. ^1H NMR (300 MHz, 25 °C, CDCl_3), δ (ppm): 9.75 (t, 1H, OCH phenylacetylaldehyde), 7.33 (m, 5H, ArH polystyrene oxide), 6.09 (s, 3H, PhH TMB), 5.30 (CH CH_2Cl_2), 3.76 (s, 9H, CH_3 TMB), 3.12 (m, 1H, CH_2 styrene oxide).

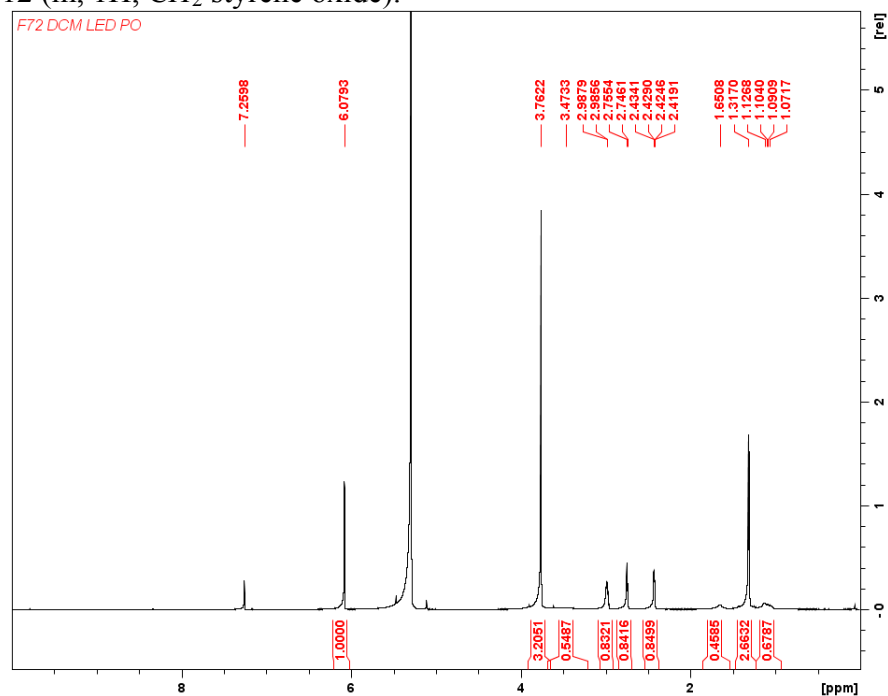


Figure E30. Table 5.4. Polymerization of PO by F_{72} in CH_2Cl_2 in the presence of blue LED light. ^1H NMR (300 MHz, 25 °C, CDCl_3), δ (ppm): 6.08 (s, 3H, PhH TMB), 5.30 (CH CH_2Cl_2), 3.76 (s, 9H, CH_3 TMB), 3.47 (m, 1H, OCH PPO), 2.99 (m, 1H, OCH PO), 2.75 (m, 1H, CH_2 PO), 2.43 (m, 1H, CH_2 PO), 1.32 (d, 3H, CH_3 PO and PPO), 1.14 (m, 3H, CH_3 propionaldehyde).

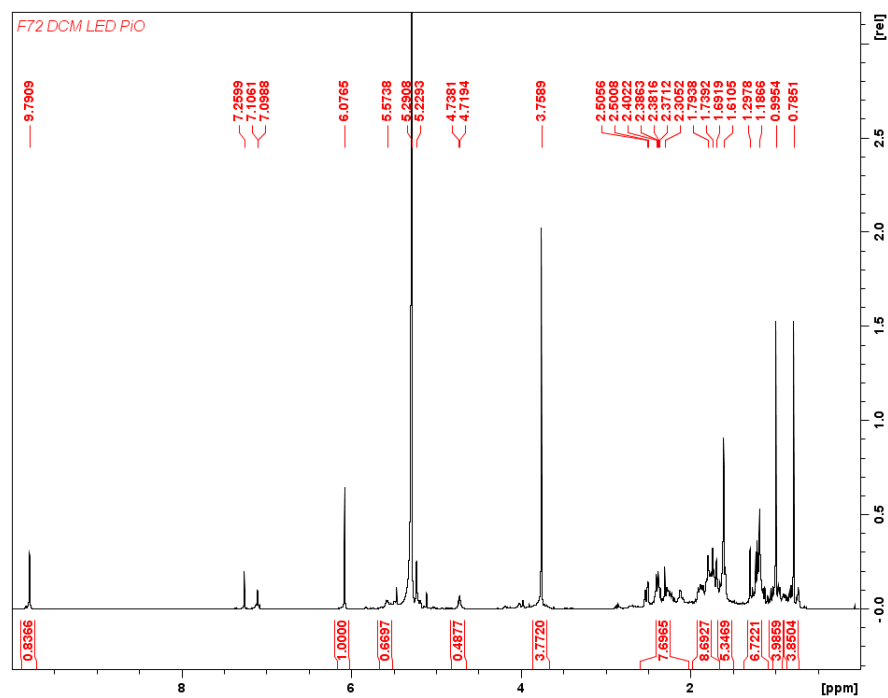


Figure E31. Table 5.4. Polymerization of PiO by F₇₂ in CH₂Cl₂ in the presence of blue LED light. ¹H NMR (300 MHz, 25 °C, CDCl₃), δ (ppm): 9.79 (t, 1H, OCH, campholenic aldehyde), 6.08 (s, 3H, PhH TMB), 5.57 (t, 1H, CH campholenic aldehyde), 5.29 (CH CH₂Cl₂), 3.76 (s, 9H, CH₃ TMB).

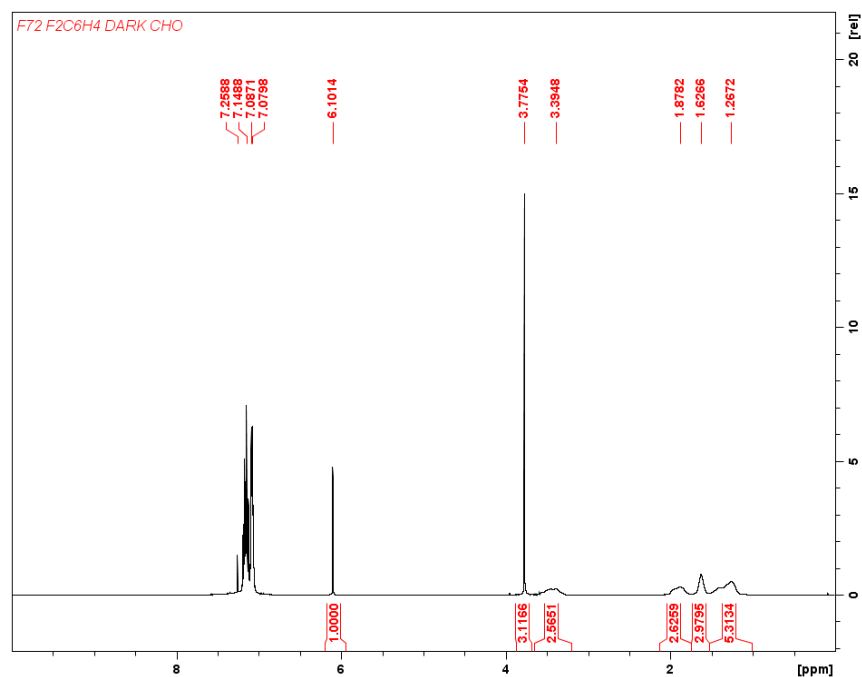


Figure E32. Table 5.4. Polymerization of CHO by F₇₂ in F₂C₆H₄ in the dark. ¹H NMR (300 MHz, 25 °C, CDCl₃), δ (ppm): 7.15 (CFCH 1,2-difluorobenzene), 7.08 (CFCHCH 1,2-difluorobenzene), 6.10 (s, 3H, PhH TMB), 3.78 (s, 9H, CH₃ TMB), 3.40 (m, 2H, COCH PCHO), 1.88 (m, 2H, COCHCH₂ PCHO), 1.63 (m, 2H, COCHCH₂ PCHO), 1.27 (m, 4H, COCHCH₂CH₂ PCHO).

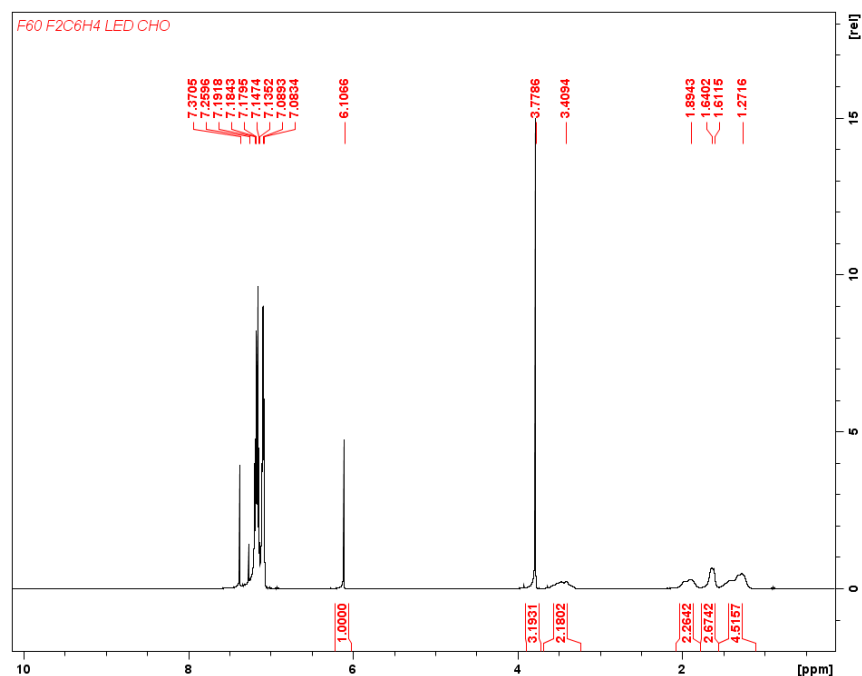


Figure E33. Table 5.4. Polymerization of CHO by F₆₀ in F₂C₆H₄ in the presence of blue LED light. ¹H NMR (300 MHz, 25 °C, CDCl₃), δ (ppm): 7.37 (ArH, benzene), 7.15 (CFCH 1,2-difluorobenzene), 7.09 (CFCHCH 1,2-difluorobenzene), 6.11 (s, 3H, PhH TMB), 3.78 (s, 9H, CH₃ TMB), 3.41 (m, 2H, COCH PCHO), 1.89 (m, 2H, COCHCH₂ PCHO), 1.63 (m, 2H, COCHCH₂ PCHO), 1.27 (m, 4H, COCHCH₂CH₂ PCHO).

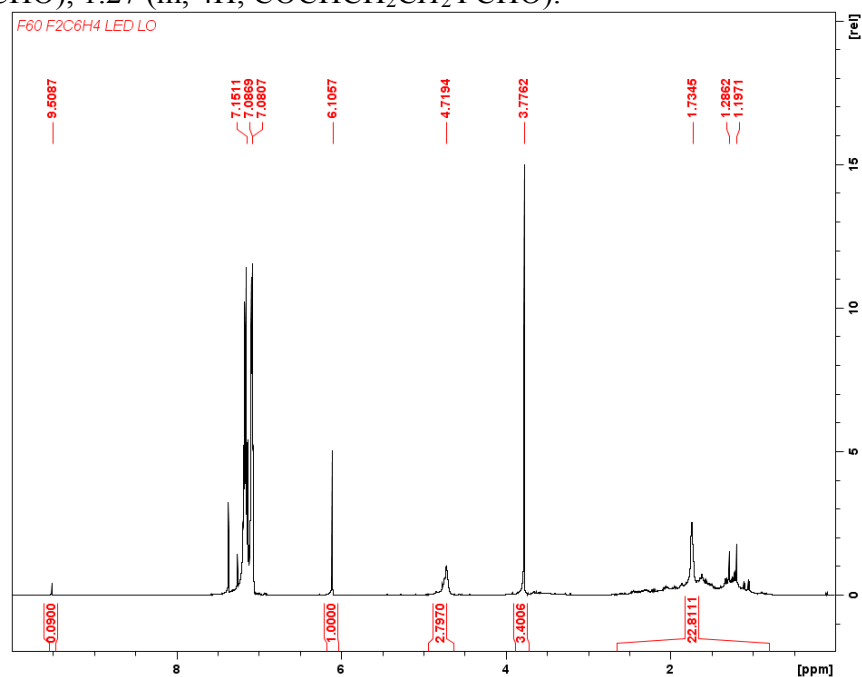


Figure E34. Table 5.4. Polymerization of LO by F₆₀ in F₂C₆H₄ in the presence of blue LED light. ¹H NMR (300 MHz, 25 °C, CDCl₃), δ (ppm): 9.51 (t, 1H, OCH xx), 7.15 (CFCH 1,2-difluorobenzene), 7.08 (CFCHCH 1,2-difluorobenzene), 6.11 (s, 3H, PhH TMB), 4.72 (b, 1H, OCH polylimonene oxide), 3.78 (s, 9H, CH₃ TMB), 1.73 (s, 3H, CH₃ polylimonene oxide), 1.29 (s, 3H, CH₃ limonene oxide), 1.20 (s, 2H, CH₂ limonene oxide).

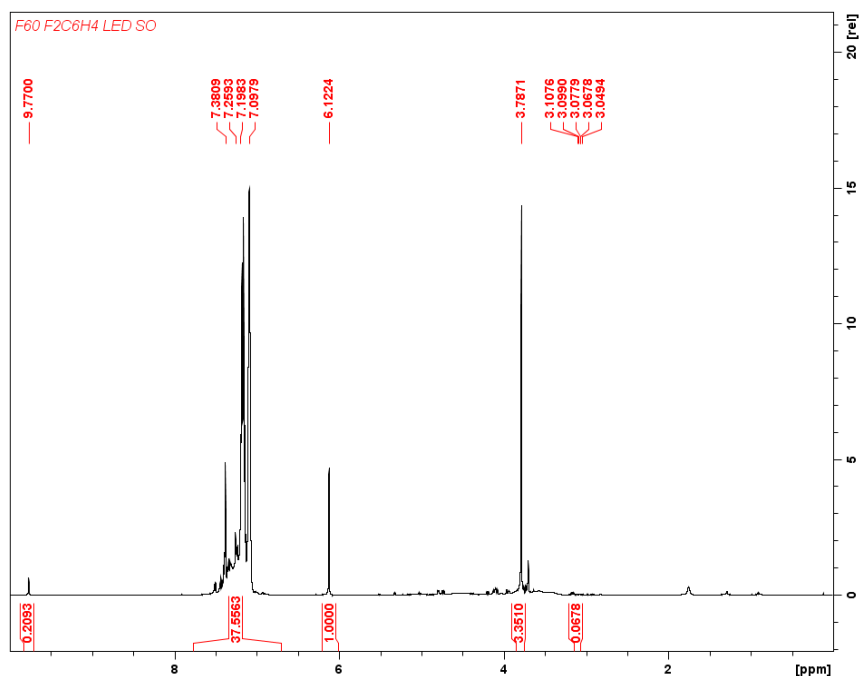


Figure E35. Table 5.4. Polymerization of SO by F₆₀ in F₂C₆H₄ in the presence of blue LED light. ¹H NMR (300 MHz, 25 °C, CDCl₃), δ (ppm): 9.77 (t, 1H, OCH phenylacetylaldehyde), 7.38 (ArH benzene), 7.31 (m, 5H, ArH polystyrene oxide), 7.20 (CFCH 1,2-difluorobenzene), 7.10 (CFCHCH 1,2-difluorobenzene), 6.12 (s, 3H, PhH TMB), 3.79 (s, 9H, CH₃ TMB), 3.08 (m, 1H, CH₂ styrene oxide).

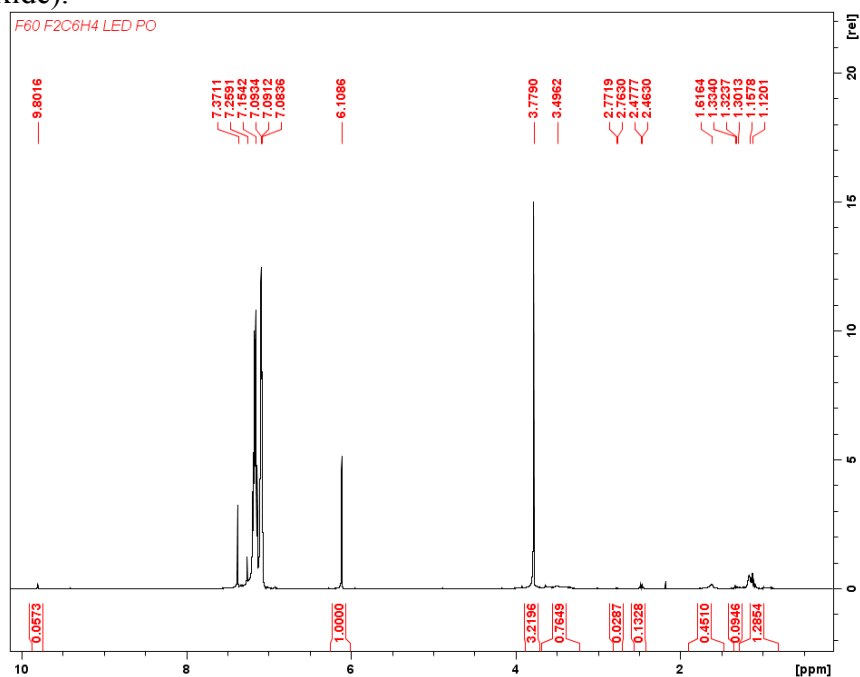


Figure E36. Table 5.4. Polymerization of PO by F₆₀ in F₂C₆H₄ in the presence of blue LED light. ¹H NMR (300 MHz, 25 °C, CDCl₃), δ (ppm): 9.80 (m, 1H, OCH propionaldehyde), 7.15 (CFCH 1,2-difluorobenzene), 7.09 (CFCHCH 1,2-difluorobenzene), 6.11 (s, 3H, PhH TMB), 3.78 (s, 9H, CH₃ TMB), 3.50 (m, 1H, OCH PPO), 2.99 (m, 1H, OCH PO), 2.76 (m, 1H, CH₂ PO), 2.47 (m, 1H, CH₂ PO), 1.32 (d, 3H, CH₃ PPO), 1.14 (m, 3H, CH₃ propionaldehyde).

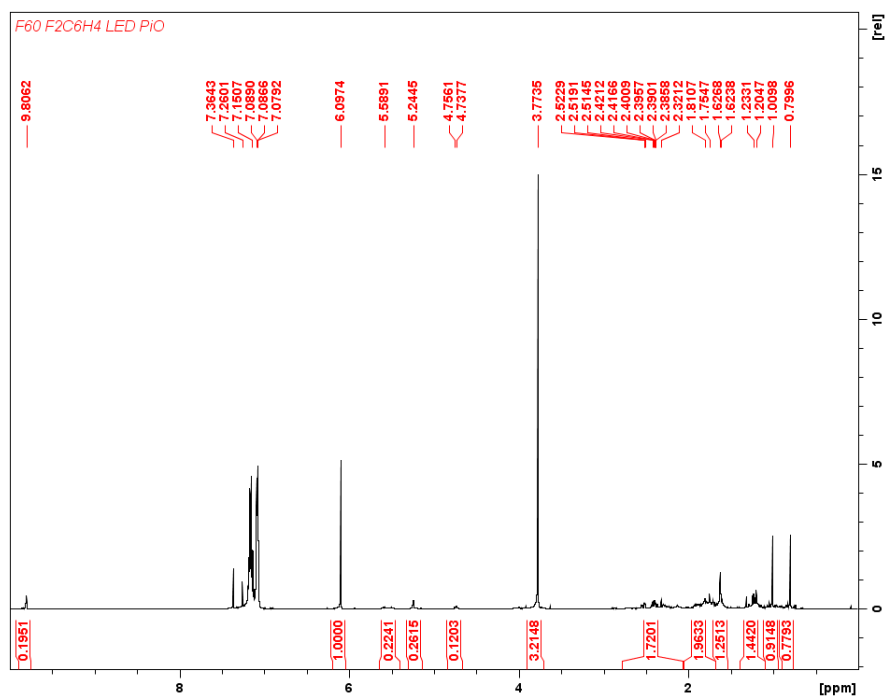


Figure E37. Table 5.4. Polymerization of PiO by F₆₀ in F₂C₆H₄ in the presence of blue LED light. ¹H NMR (300 MHz, 25 °C, CDCl₃), δ (ppm): 9.80 (t, 1H, OCH, campholenic aldehyde), 7.15 (CFCH 1,2-difluorobenzene), 7.08 (CFCHCH 1,2-difluorobenzene), 6.10 (s, 3H, PhH TMB), 5.59 (t, 1H, CH campholenic aldehyde), 3.77 (s, 9H, CH₃ TMB).

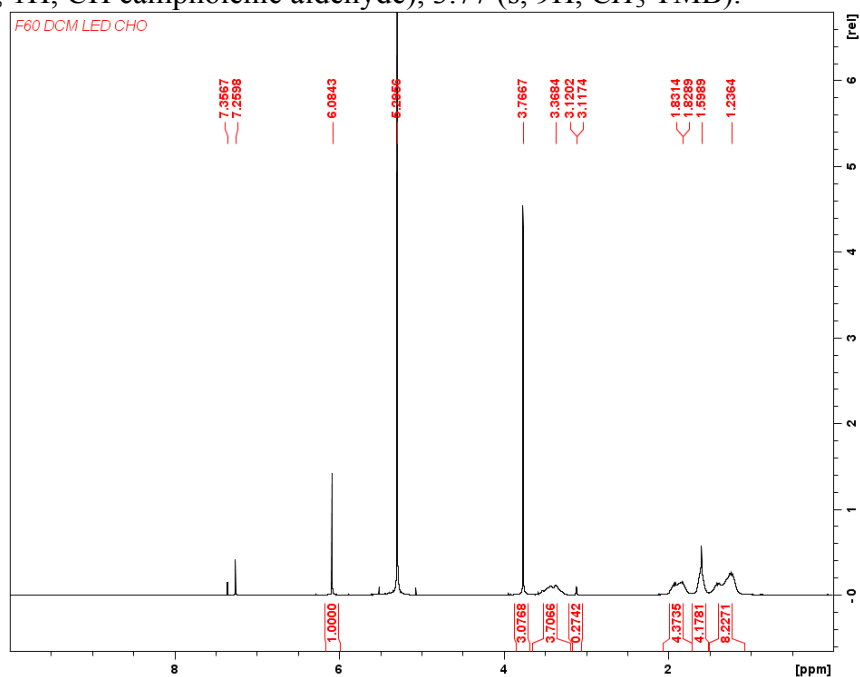


Figure E38. Table 5.4. Polymerization of CHO by F₆₀ in CH₂Cl₂ in the presence of blue LED light. ¹H NMR (300 MHz, 25 °C, CDCl₃), δ (ppm): 7.36 (ArH benzene), 6.08 (s, 3H, PhH TMB), 5.30 (CH CH₂Cl₂), 3.77 (s, 9H, CH₃ TMB), 3.37 (m, 2H, COCH PCHO), 3.12 (s, 2H, COCH CHO), 1.83 (m, 2H, COCHCH₂ PCHO), 1.60 (m, 2H, COCHCH₂ PCHO), 1.24 (m, 4H, COCHCH₂CH₂ PCHO).

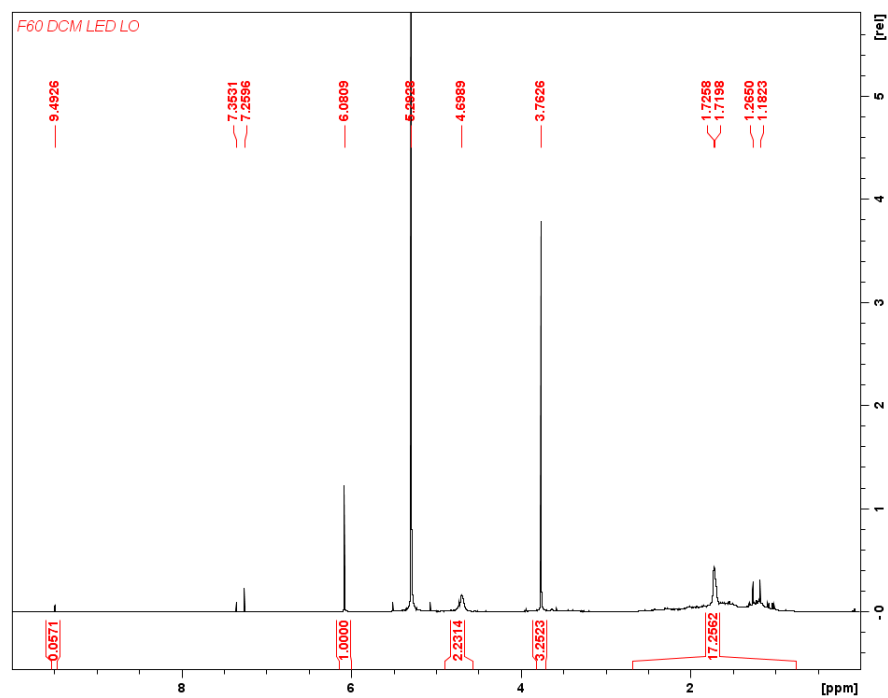


Figure E39. Table 5.4. Polymerization of LO by F₆₀ in CH₂Cl₂ in the presence of blue LED light. ¹H NMR (300 MHz, 25 °C, CDCl₃), δ (ppm): 9.49 (t, 1H, OCH xx), 7.35 (ArH benzene), 6.08 (s, 3H, PhH TMB), 5.30 (CH CH₂Cl₂), 4.70 (b, 1H, OCH polylimonene oxide), 3.76 (s, 9H, CH₃ TMB), 1.72 (s, 3H, CH₃ polylimonene oxide), 1.27 (s, 3H, CH₃ limonene oxide), 1.18 (s, 2H, CH₂ limonene oxide).

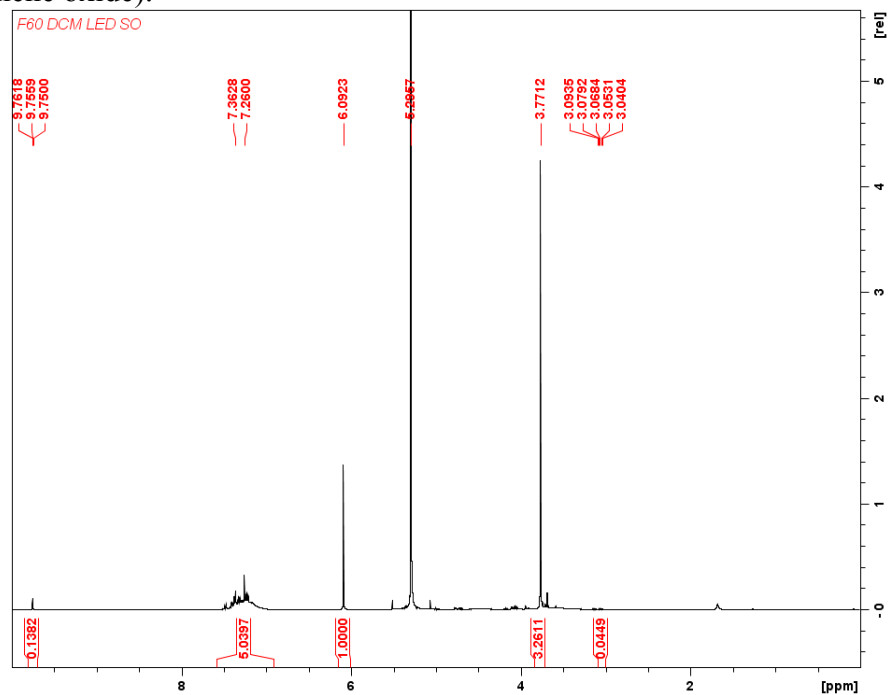


Figure E40. Table 5.4. Polymerization of SO by F₆₀ in CH₂Cl₂ in the presence of blue LED light. ¹H NMR (300 MHz, 25 °C, CDCl₃), δ (ppm): 9.76 (t, 1H, OCH phenylacetylaldehyde), 7.36 (m, 5H, ArH polystyrene oxide), 6.09 (s, 3H, PhH TMB), 5.30 (CH CH₂Cl₂), 3.77 (s, 9H, CH₃ TMB), 3.07 (m, 1H, CH₂ styrene oxide).

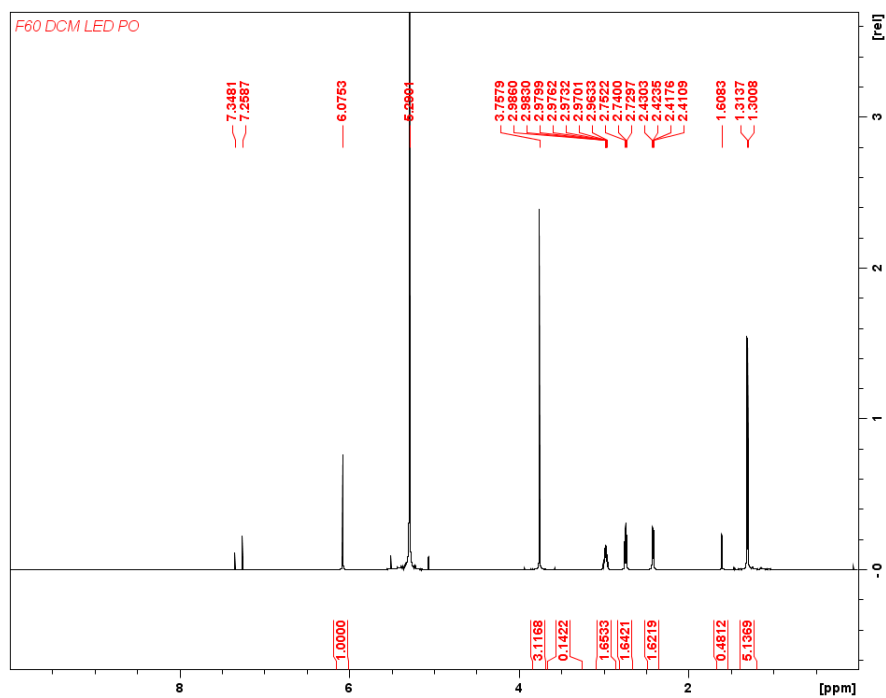


Figure E41. Table 5.4. Polymerization of PO by F₆₀ in CH₂Cl₂ in the presence of blue LED light. ¹H NMR (300 MHz, 25 °C, CDCl₃), δ (ppm): 7.35 (ArH benzene), 6.08 (s, 3H, PhH TMB), 5.30 (CH CH₂Cl₂), 3.76 (s, 9H, CH₃ TMB), 3.47 (m, 1H, OCH PPO), 2.99 (m, 1H, OCH PO), 2.74 (m, 1H, CH₂ PO), 2.42 (m, 1H, CH₂ PO), 1.32 (d, 3H, CH₃ PO).

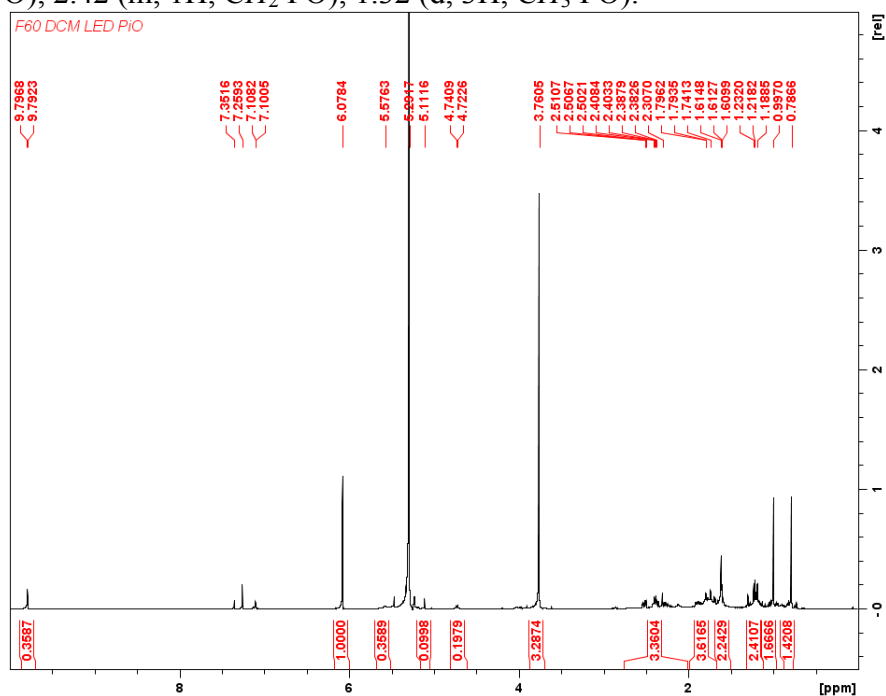


Figure E42. Table 5.4. Polymerization of PiO by F₆₀ in CH₂Cl₂ in the presence of blue LED light. ¹H NMR (300 MHz, 25 °C, CDCl₃), δ (ppm): 9.80 (t, 1H, OCH, campholenic aldehyde), 6.08 (s, 3H, PhH TMB), 5.58 (t, 1H, CH campholenic aldehyde), 5.29 (CH CH₂Cl₂), 3.76 (s, 9H, CH₃ TMB).

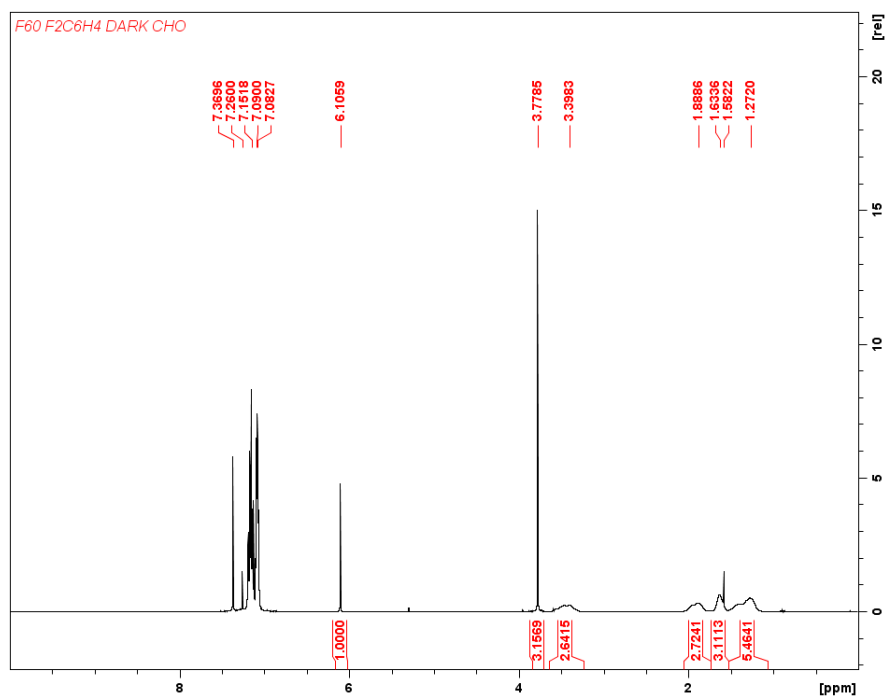


Figure E43. Table 5.4. Polymerization of CHO by F₆₀ in F₂C₆H₄ in the dark. ¹H NMR (300 MHz, 25 °C, CDCl₃), δ (ppm): 7.37 (ArH, benzene), 7.15 (CFCH 1,2-difluorobenzene), 7.09 (CFCHCH 1,2-difluorobenzene), 6.11 (s, 3H, PhH TMB), 3.78 (s, 9H, CH₃ TMB), 3.40 (m, 2H, COCH PCHO), 1.89 (m, 2H, COCHCH₂ PCHO), 1.60 (m, 2H, COCHCH₂ PCHO), 1.27 (m, 4H, COCHCH₂CH₂ PCHO).

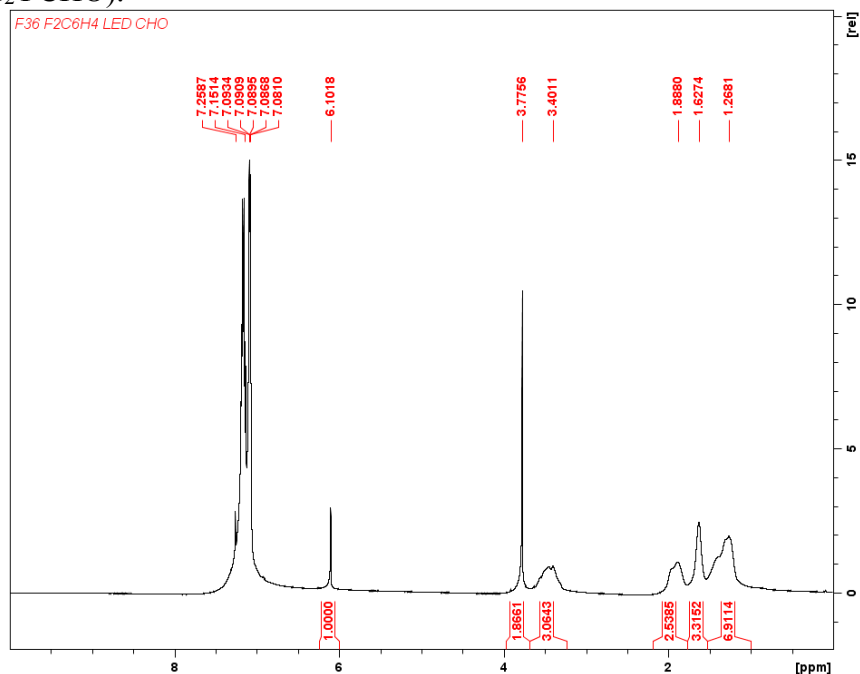


Figure E44. Table 5.4. Polymerization of CHO by F₃₆ in F₂C₆H₄ in the presence of blue LED light. ¹H NMR (300 MHz, 25 °C, CDCl₃), δ (ppm): 7.15 (CFCH 1,2-difluorobenzene), 7.09 (CFCHCH 1,2-difluorobenzene), 6.10 (s, 3H, PhH TMB), 3.78 (s, 9H, CH₃ TMB), 3.40 (m, 2H, COCH PCHO), 3.13 (s, 2H, COCH CHO), 1.89 (m, 2H, COCHCH₂ PCHO), 1.63 (m, 2H, COCHCH₂ PCHO), 1.27 (m, 4H, COCHCH₂CH₂ PCHO).

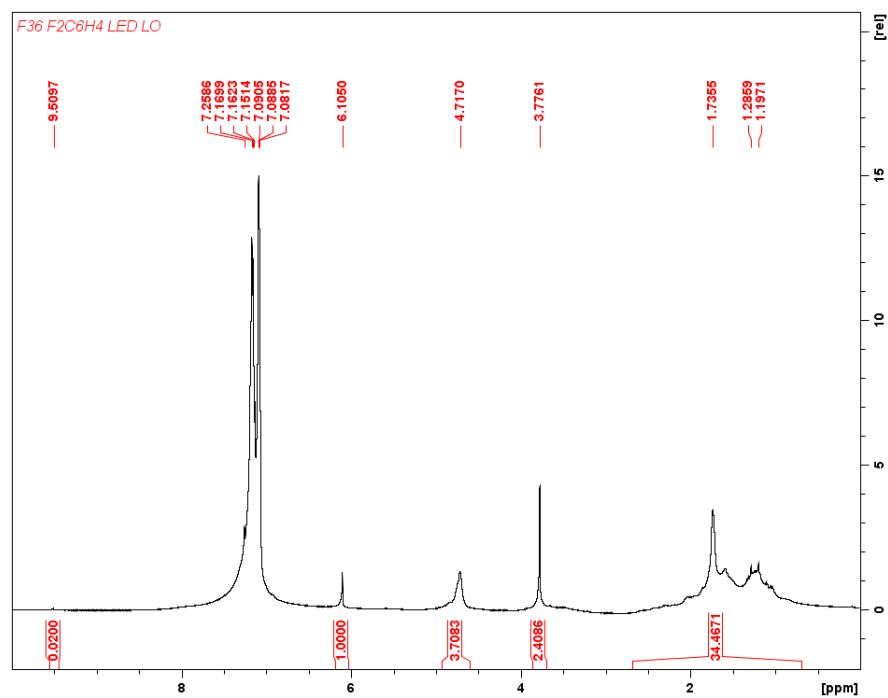


Figure E45. Table 5.4. Polymerization of LO by F₃₆ in F₂C₆H₄ in the presence of blue LED light. ¹H NMR (300 MHz, 25 °C, CDCl₃), δ (ppm): 9.51 (t, 1H, OCH xx), 7.15 (CFCH 1,2-difluorobenzene), 7.09 (CFCHCH 1,2-difluorobenzene), 6.11 (s, 3H, PhH TMB), 4.72 (b, 1H, OCH polylimonene oxide), 3.78 (s, 9H, CH₃ TMB), 1.74 (s, 3H, CH₃ polylimonene oxide), 1.29 (s, 3H, CH₃ limonene oxide), 1.20 (s, 2H, CH₂ limonene oxide).

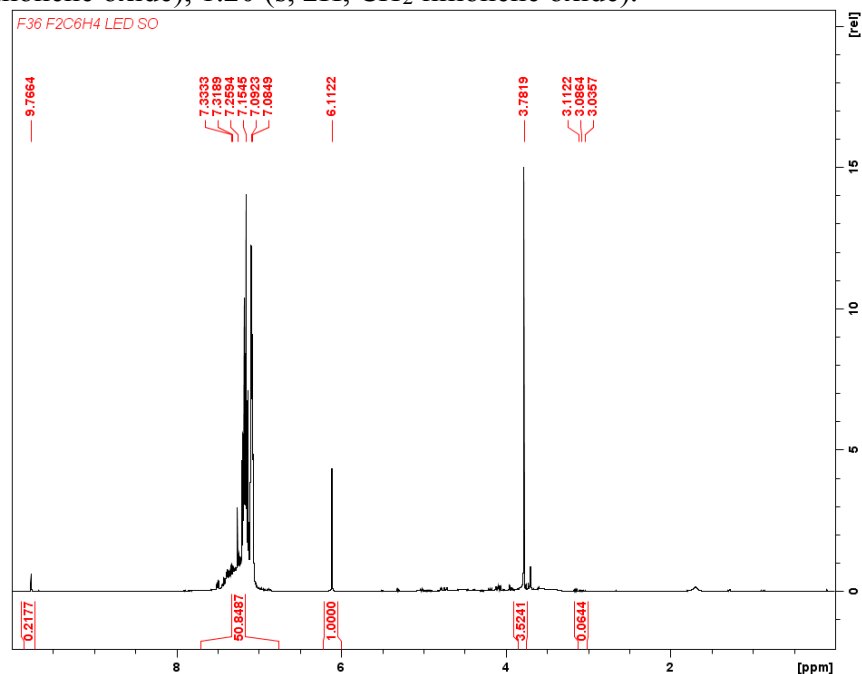


Figure E46. Table 5.4. Polymerization of SO by F₃₆ in F₂C₆H₄ in the presence of blue LED light. ¹H NMR (300 MHz, 25 °C, CDCl₃), δ (ppm): 9.75 (t, 1H, OCH phenylacetaldehyde), 7.33 (m, 5H, ArH polystyrene oxide), 7.15 (CFCH 1,2-difluorobenzene), 7.09 (CFCHCH 1,2-difluorobenzene), 6.11 (s, 3H, PhH TMB), 3.78 (s, 9H, CH₃ TMB), 3.09 (m, 1H, CH₂ styrene oxide).

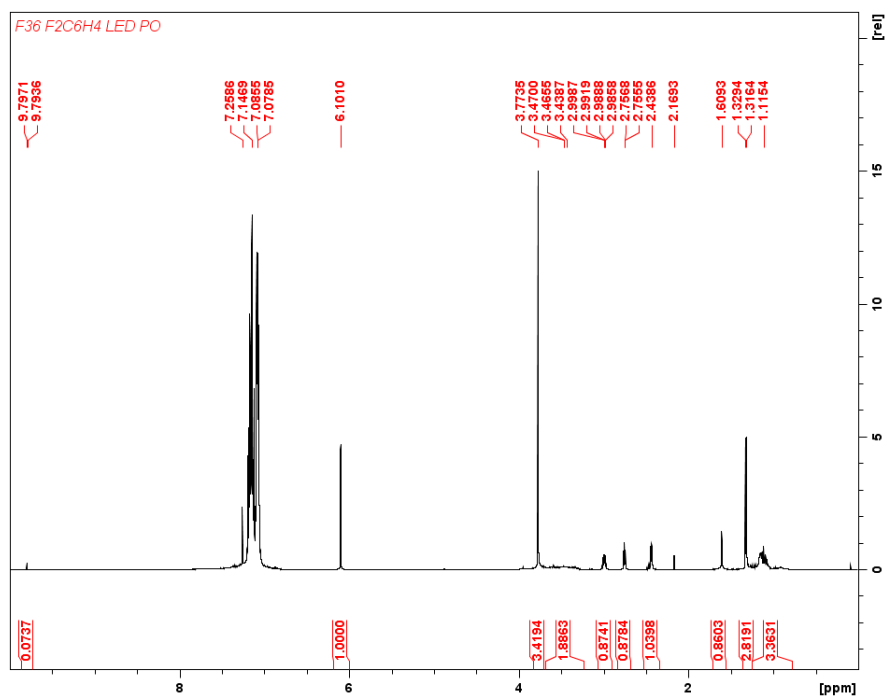


Figure E47. Table 5.4. Polymerization of PO by F₃₆ in F₂C₆H₄ in the presence of blue LED light. ¹H NMR (300 MHz, 25 °C, CDCl₃), δ (ppm): 9.79 (m, 1H, OCH propionaldehyde), 7.15 (CFCH 1,2-difluorobenzene), 7.08 (CFCHCH 1,2-difluorobenzene), 6.10 (s, 3H, PhH TMB), 3.81 (s, 9H, CH₃ TMB), 3.47 (m, 1H, OCH PPO), 2.99 (m, 1H, OCH PO), 2.76 (m, 1H, CH₂ PO), 2.44 (m, 1H, CH₂ PO), 1.32 (d, 3H, CH₃ PO and PPO), 1.14 (m, 3H, CH₃ propionaldehyde).

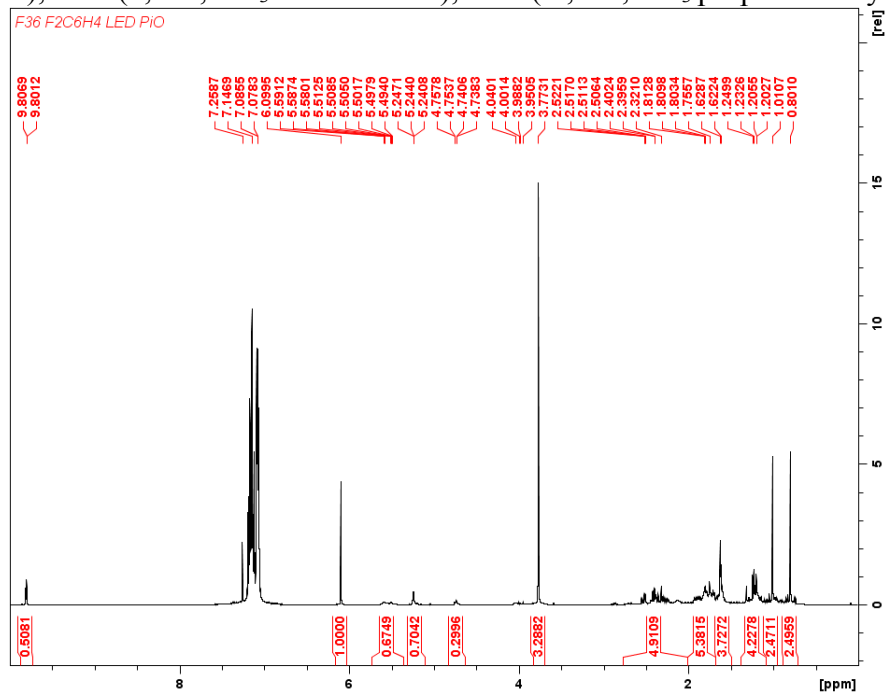


Figure E48. Table 5.4. Polymerization of PiO by F₃₆ in F₂C₆H₄ in the presence of blue LED light. ¹H NMR (300 MHz, 25 °C, CDCl₃), δ (ppm): 9.80 (t, 1H, OCH, campholenic aldehyde), 7.15 (CFCH 1,2-difluorobenzene), 7.08 (CFCHCH 1,2-difluorobenzene), 6.10 (s, 3H, PhH TMB), 5.58 (t, 1H, CH campholenic aldehyde), 3.77 (s, 9H, CH₃ TMB).

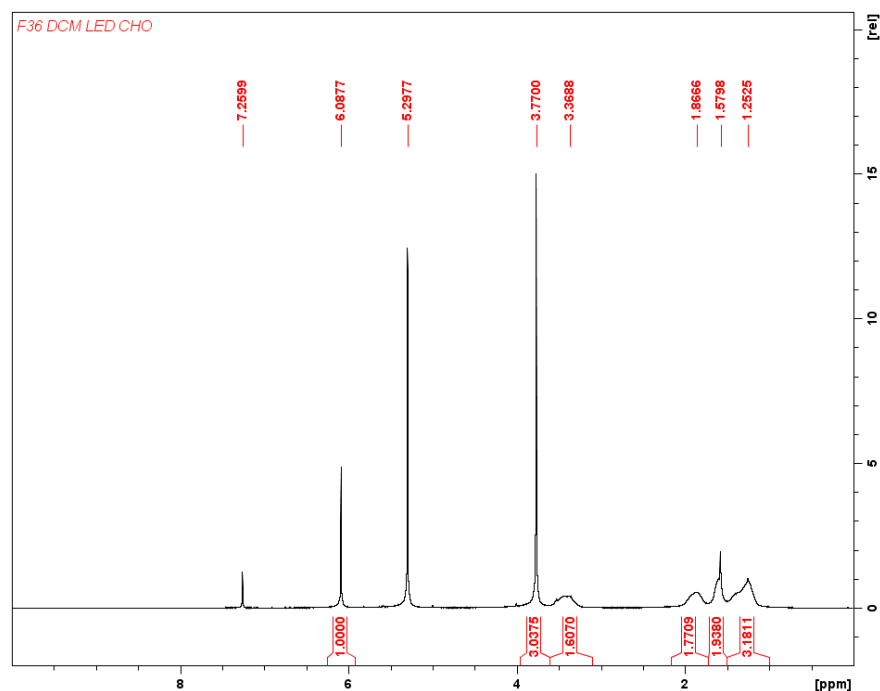


Figure E49. Table 5.4. Polymerization of CHO by F₃₆ in CH₂Cl₂ in the presence of blue LED light. ¹H NMR (300 MHz, 25 °C, CDCl₃), δ (ppm): 6.09 (s, 3H, PhH TMB), 5.30 (CH CH₂Cl₂), 3.77 (s, 9H, CH₃ TMB), 3.37 (m, 2H, COCHCH₂ PCHO), 1.87 (m, 2H, COCHCH₂ PCHO), 1.58 (m, 2H, COCHCH₂CH₂ PCHO), 1.25 (m, 2H, COCHCH₂CH₂ PCHO).

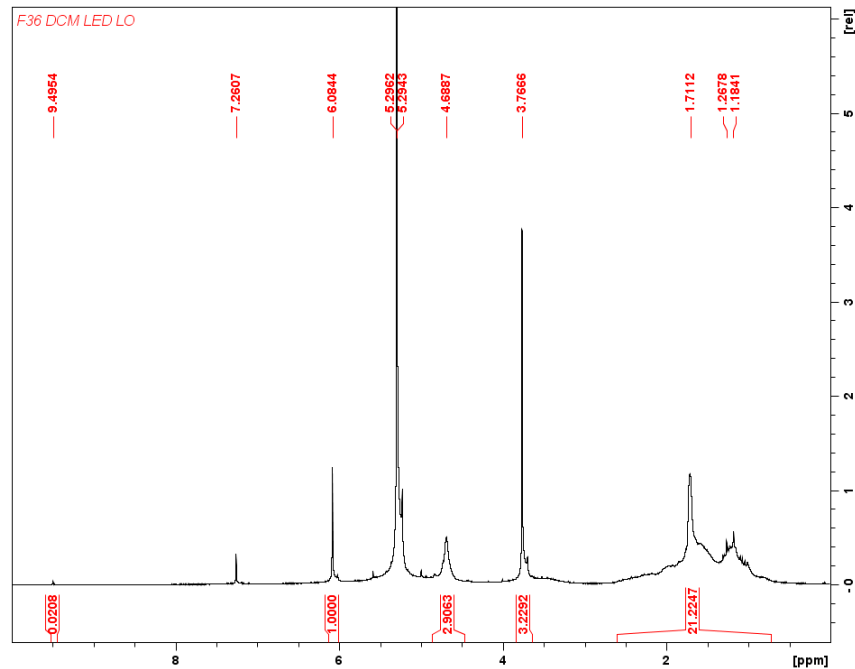


Figure E50. Table 5.4. Polymerization of LO by F₃₆ in CH₂Cl₂ in the presence of blue LED light. ¹H NMR (300 MHz, 25 °C, CDCl₃), δ (ppm): 9.50 (t, 1H, OCH xx), 6.08 (s, 3H, PhH TMB), 5.30 (CH CH₂Cl₂), 4.49 (b, 1H, OCH polylimonene oxide), 3.77 (s, 9H, CH₃ TMB), 1.71 (s, 3H, CH₃ polylimonene oxide), 1.27 (s, 3H, CH₃ limonene oxide), 1.18 (s, 2H, CH₂ limonene oxide).

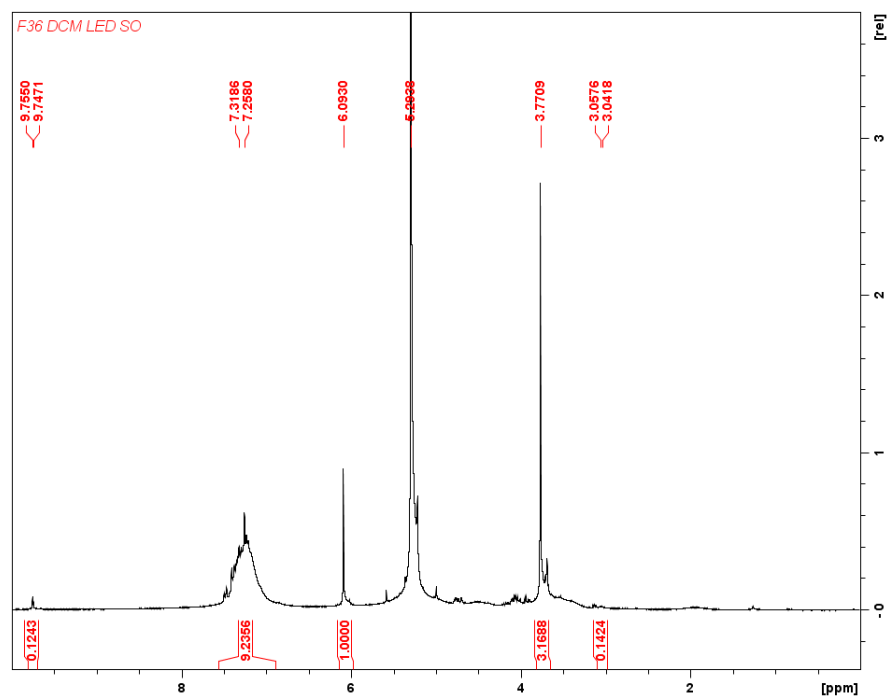


Figure E51. Table 5.4. Polymerization of SO by F₃₆ in CH₂Cl₂ in the presence of blue LED light. ¹H NMR (300 MHz, 25 °C, CDCl₃), δ (ppm): 9.75 (t, 1H, OCH phenylacetylaldehyde), 7.31 (m, 5H, ArH polystyrene oxide), 6.09 (s, 3H, PhH TMB), 5.30 (CH CH₂Cl₂), 3.77 (s, 9H, CH₃ TMB), 3.09 (m, 1H, CH₂ styrene oxide).

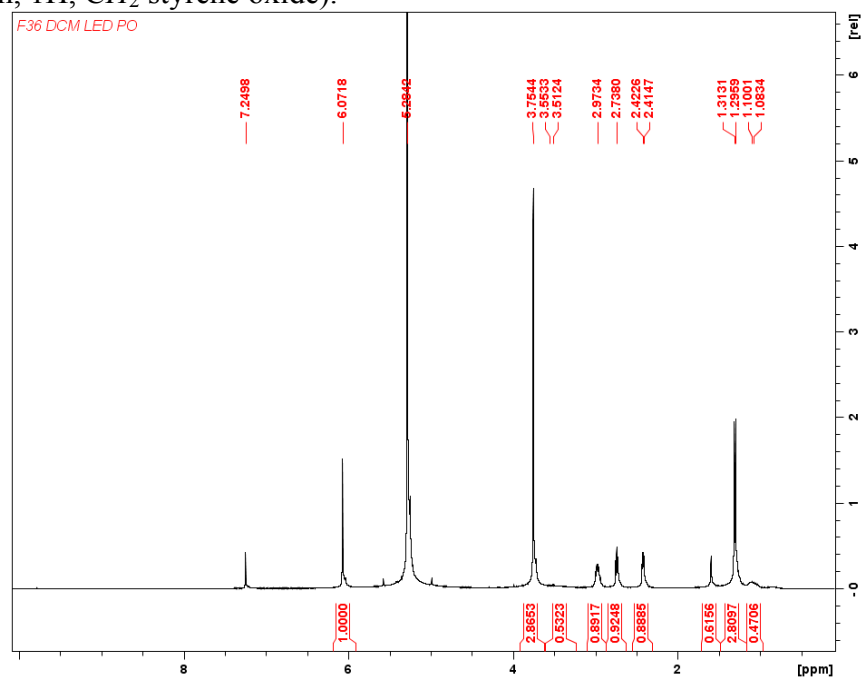


Figure E52. Table 5.4. Polymerization of PO by F₃₆ in CH₂Cl₂ in the presence of blue LED light. ¹H NMR (300 MHz, 25 °C, CDCl₃), δ (ppm): 6.07 (s, 3H, PhH TMB), 5.30 (CH CH₂Cl₂), 3.75 (s, 9H, CH₃ TMB), 3.51 (m, 1H, OCH PPO), 2.97 (m, 1H, OCH PO), 2.74 (m, 1H, CH₂ PO), 2.42 (m, 1H, CH₂ PO), 1.31 (d, 3H, CH₃ PO), 1.09 (m, 3H, CH₃ propionaldehyde).

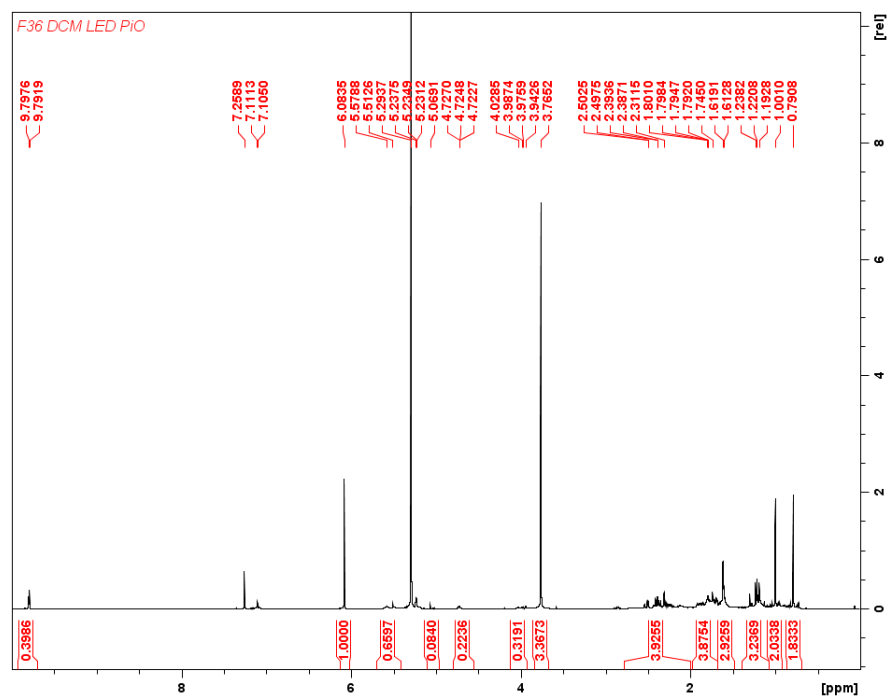


Figure E53. Table 5.4. Polymerization of PiO by F₃₆ in CH₂Cl₂ in the presence of blue LED light. ¹H NMR (300 MHz, 25 °C, CDCl₃), δ (ppm): 9.80 (t, 1H, OCH, campholenic aldehyde), 6.08 (s, 3H, PhH TMB), 5.58 (t, 1H, CH campholenic aldehyde), 5.30 (CH CH₂Cl₂), 3.77 (s, 9H, CH₃ TMB).

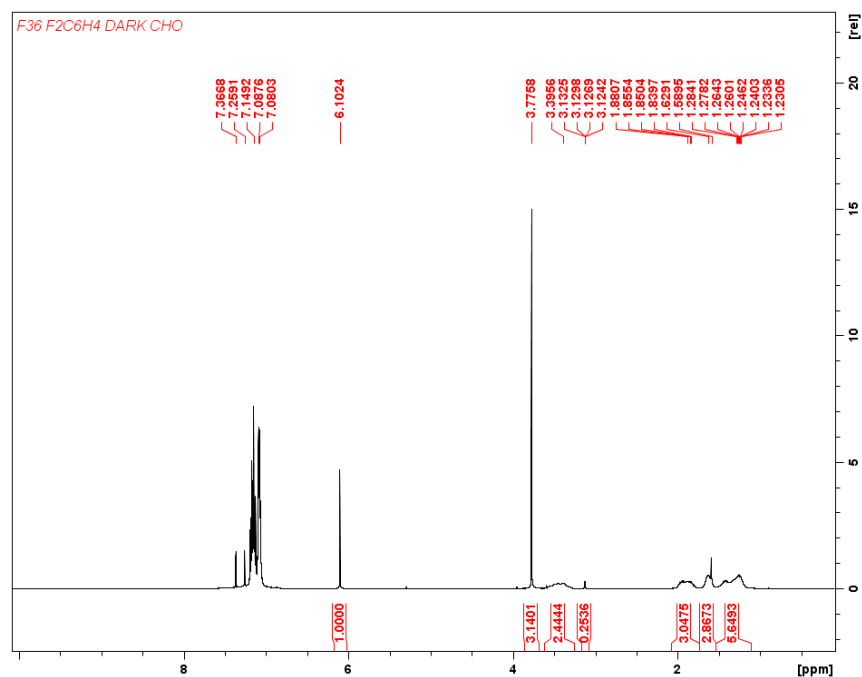


Figure E54. Table 5.4. Polymerization of CHO by F₃₆ in F₂C₆H₄ in the dark. ¹H NMR (300 MHz, 25 °C, CDCl₃), δ (ppm): 7.37 (ArH, benzene), 7.15 (CFCH 1,2-difluorobenzene), 7.09 (CFCHCH 1,2-difluorobenzene), 6.10 (s, 3H, PhH TMB), 3.78 (s, 9H, CH₃ TMB), 3.40 (m, 2H, COCH PCHO), 3.13 (s, 2H, COCH CHO), 1.87 (m, 2H, COCHCH₂ PCHO), 1.60 (m, 2H, COCHCH₂ PCHO), 1.25 (m, 4H, COCHCH₂CH₂ PCHO).

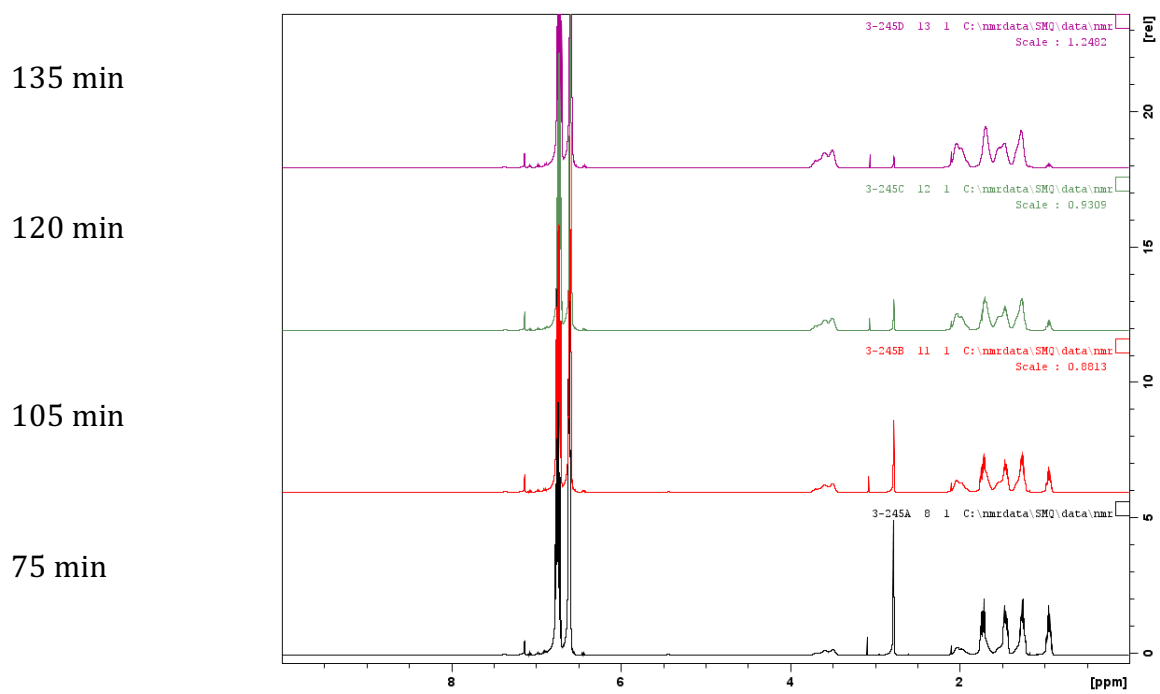


Figure E55. Conversion of CHO to PCHO by F₃₆ over time.

Gel Permeation Chromatography

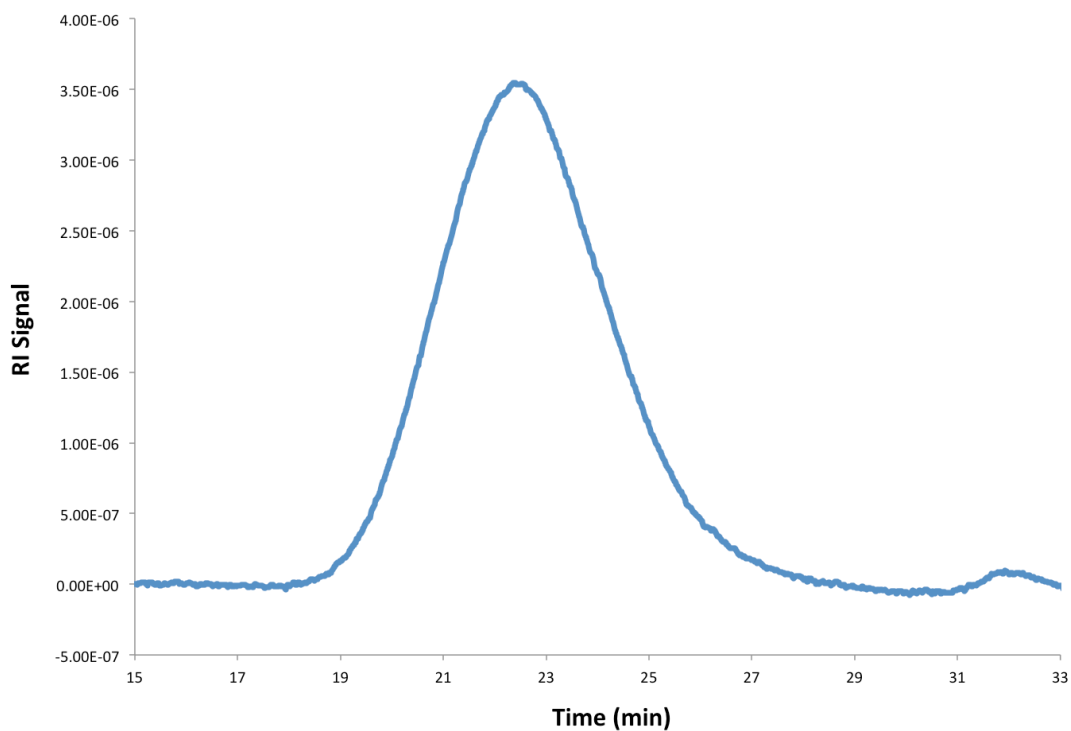


Figure E56. Table 5.1, entry 1. Polymerization of 100 equivalents of CHO by F₃₆ in 4:1 F₂C₆H₄:C₆D₆ in open air. M_n = 121800 Da, M_w = 159600 Da, \mathcal{D} = 1.31.

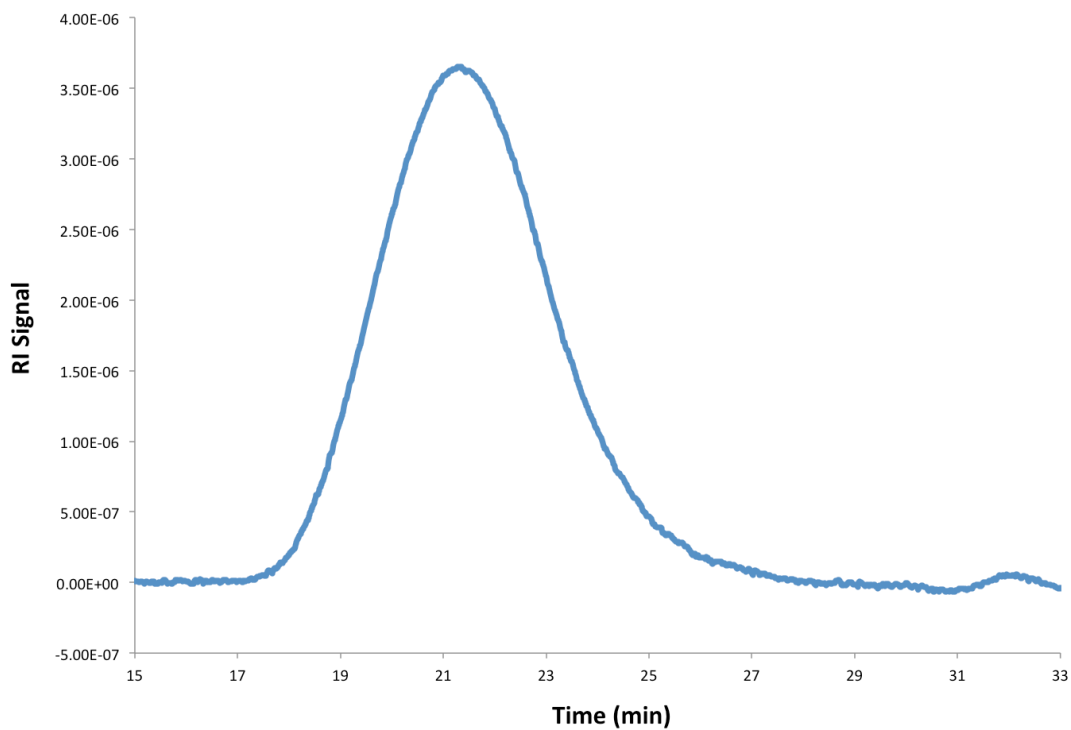


Figure E57. Table 5.1, entry 2. Polymerization of 100 equivalents of CHO by F₃₆ in 4:1 F₂C₆H₄:C₆D₆. M_n = 177900 Da, M_w = 227700 Da, \mathcal{D} = 1.28.

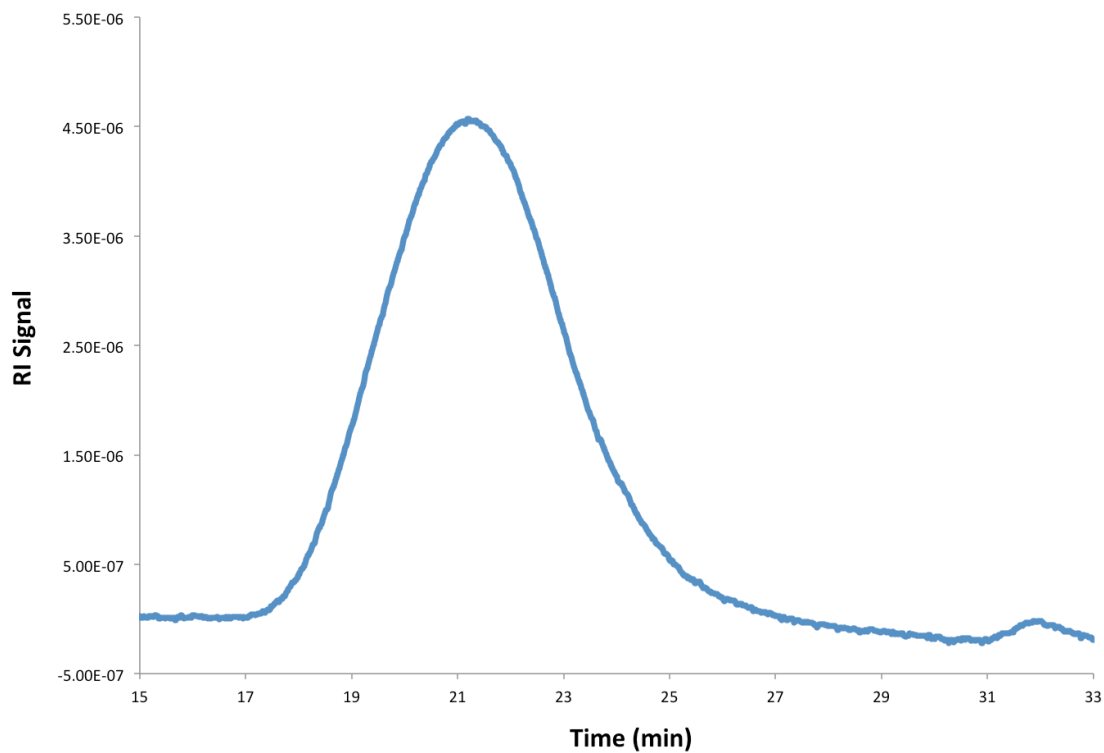


Figure E58. Table 5.1, entry 3. Polymerization of 200 equivalents of CHO by F_{36} in 4:1 $F_2C_6H_4:C_6D_6$. $M_n = 189300$ Da, $M_w = 246100$ Da, $D = 1.30$.

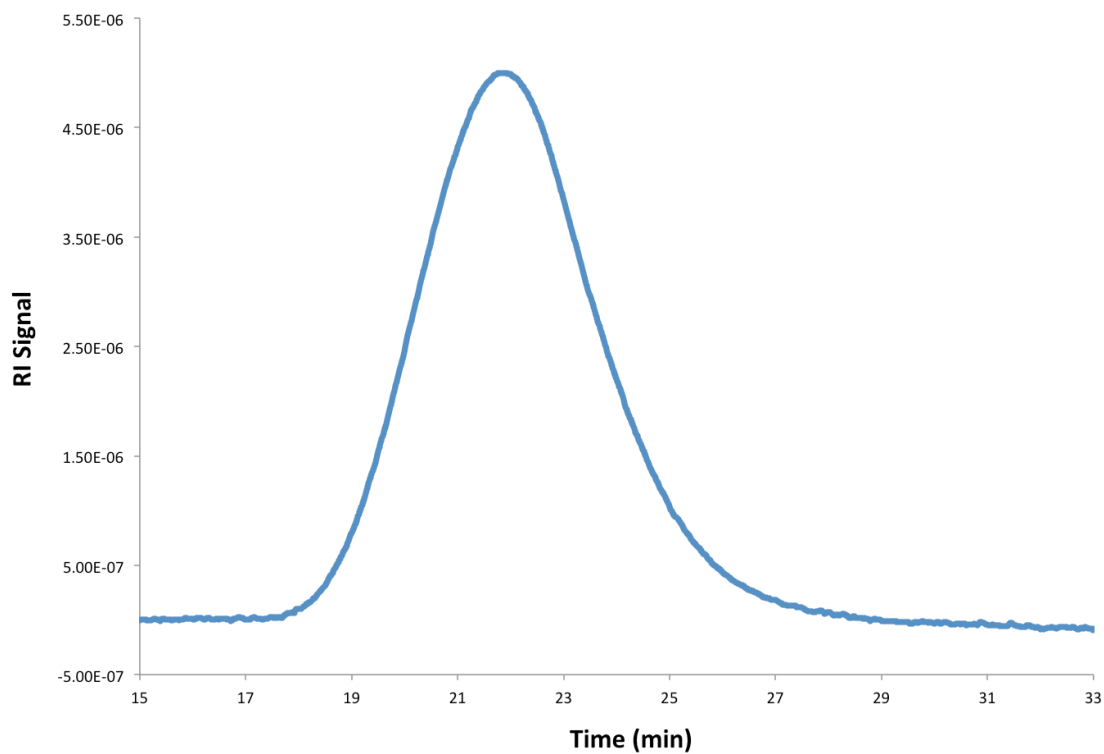


Figure E59. Table 5.1, entry 4. Polymerization of 500 equivalents of CHO by F_{36} in 4:1 $F_2C_6H_4:C_6D_6$. $M_n = 121700$ Da, $M_w = 197200$ Da, $D = 1.62$.

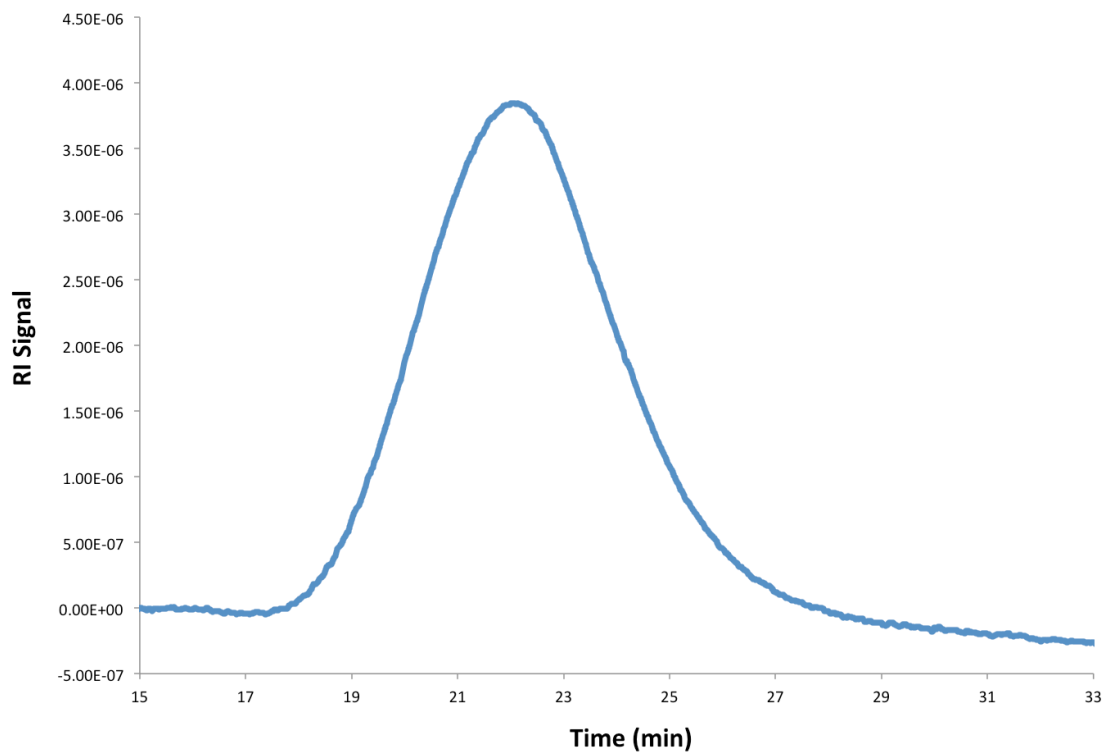


Figure E60. Table 5.1, entry 5. Polymerization of 1000 equivalents of CHO by F_{36} in 4:1 $F_2C_6H_4:C_6D_6$. $M_n = 149200$ Da, $M_w = 244700$ Da, $\mathcal{D} = 1.64$.

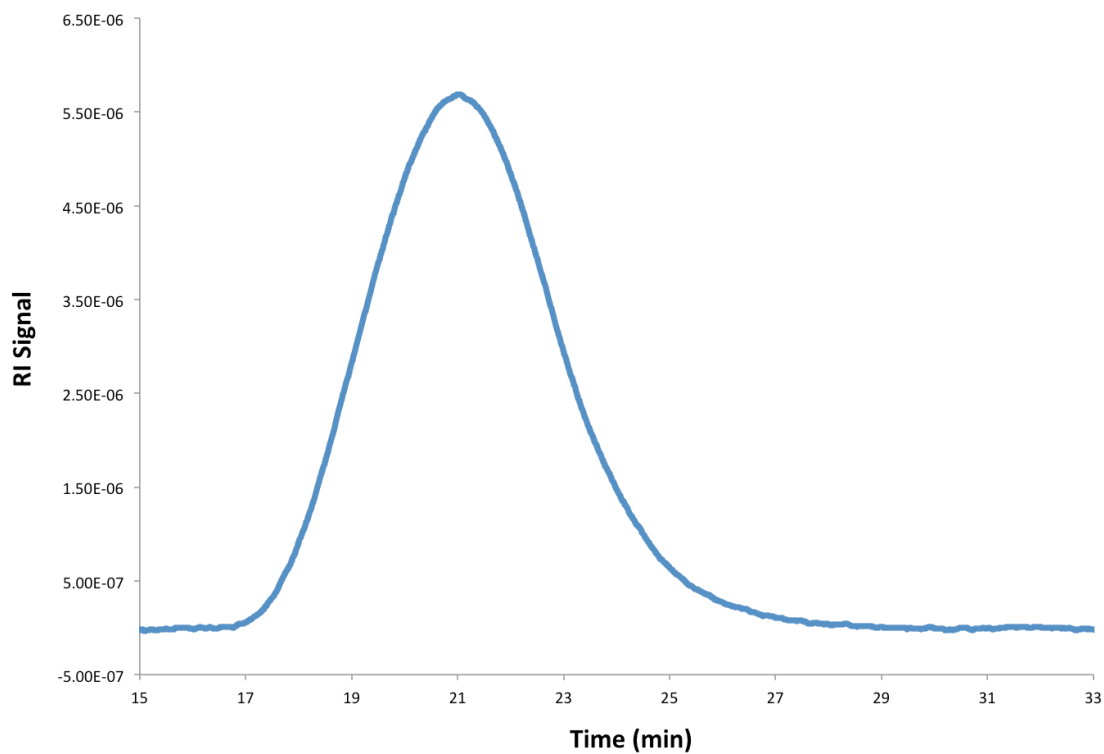


Figure E61. Table 5.1, entry 6. Polymerization of 100 equivalents of CHO by F_{36} in 4:1 $F_2C_6H_4:C_6D_6$ at 0 °C. $M_n = 147400$ Da, $M_w = 228500$ Da, $\mathcal{D} = 1.55$.

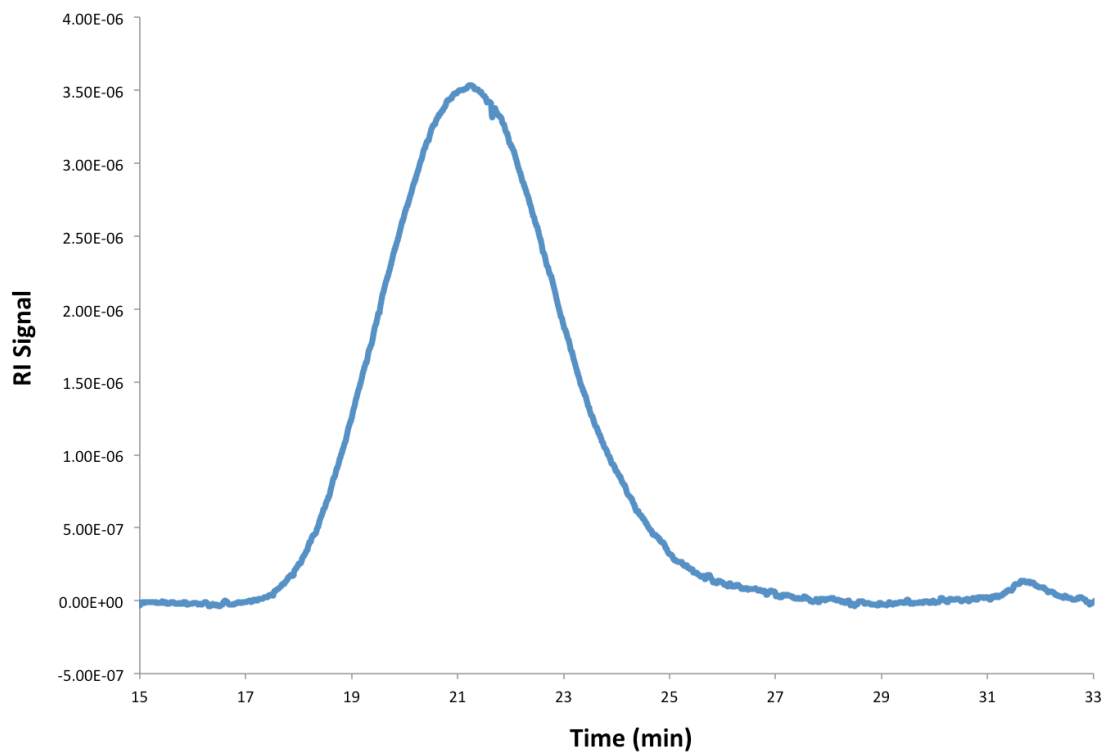


Figure E62. Table 5.1, entry 7. Polymerization of two sequential additions of 100 equivalents of CHO by F_{36} in 4:1 $F_2C_6H_4:C_6D_6$. $M_n = 185600$ Da, $M_w = 230100$ Da, $\bar{D} = 1.24$.

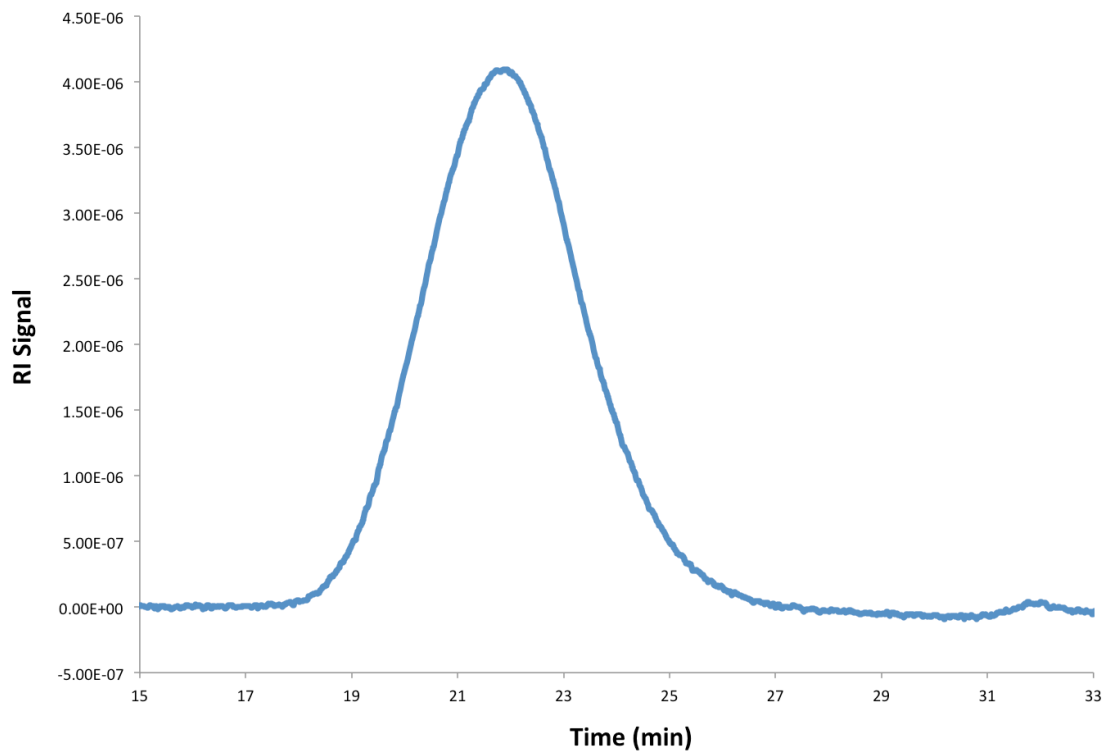


Figure E63. Table 5.1, entry 8. Polymerization of 100 equivalents of CHO by F_{36} in 4:1 $F_2C_6H_4:C_6D_6$ in the dark. $M_n = 149600$ Da, $M_w = 178000$ Da, $\bar{D} = 1.18$.

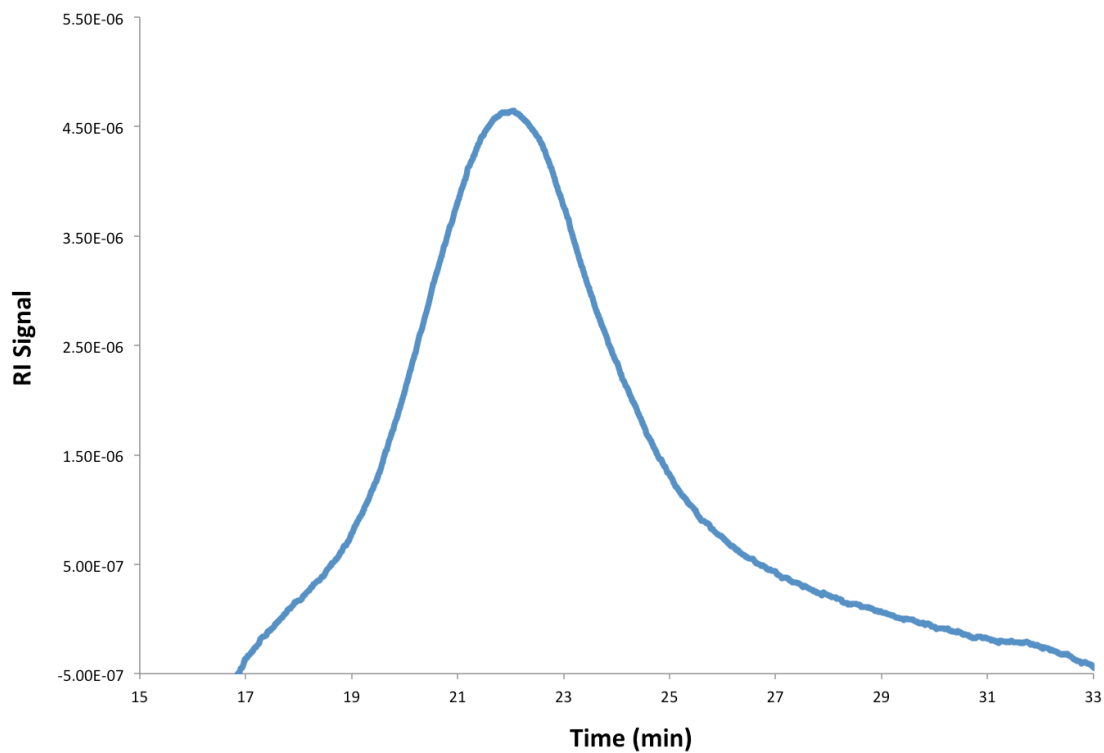


Figure E64. Table 5.1, entry 9. Polymerization of 100 equivalents of CHO by F_{36} in 4:1 $F_2C_6H_4:C_6D_6$ in a diluted solution. $M_n = 106400$ Da, $M_w = 137300$ Da, $D = 1.29$.

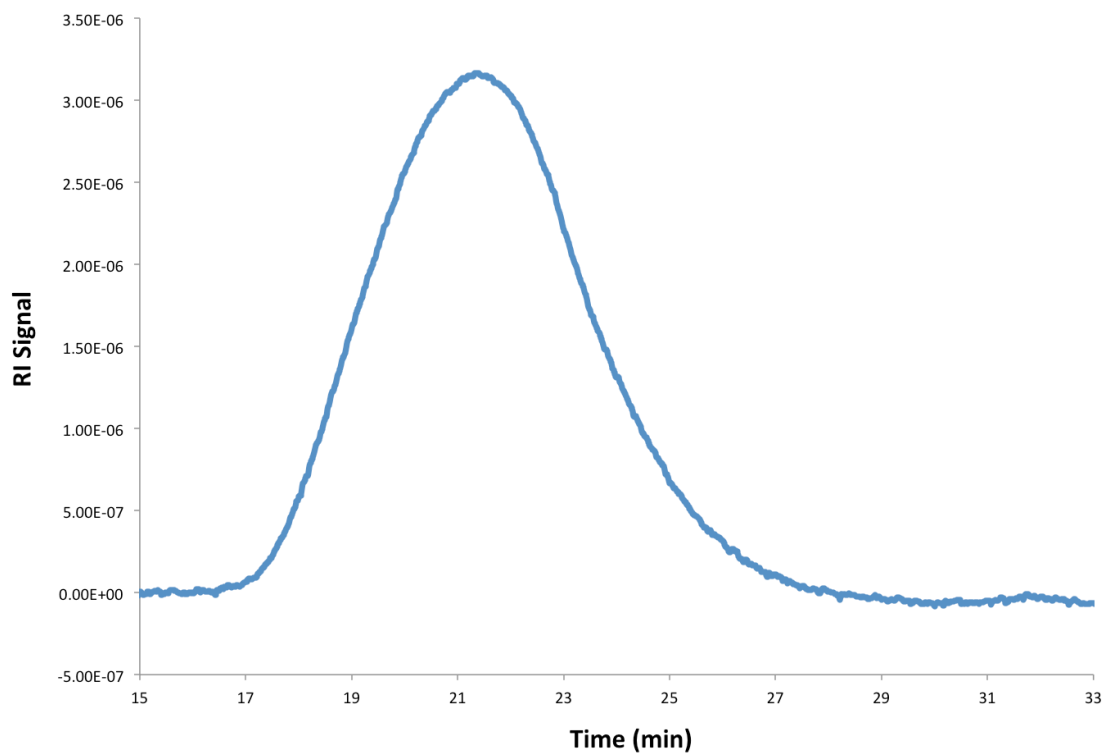


Figure E65. Table 5.1, entry 10. Polymerization of 100 equivalents of CHO by F_{36} neat. $M_n = 169100$ Da, $M_w = 236700$ Da, $D = 1.40$.

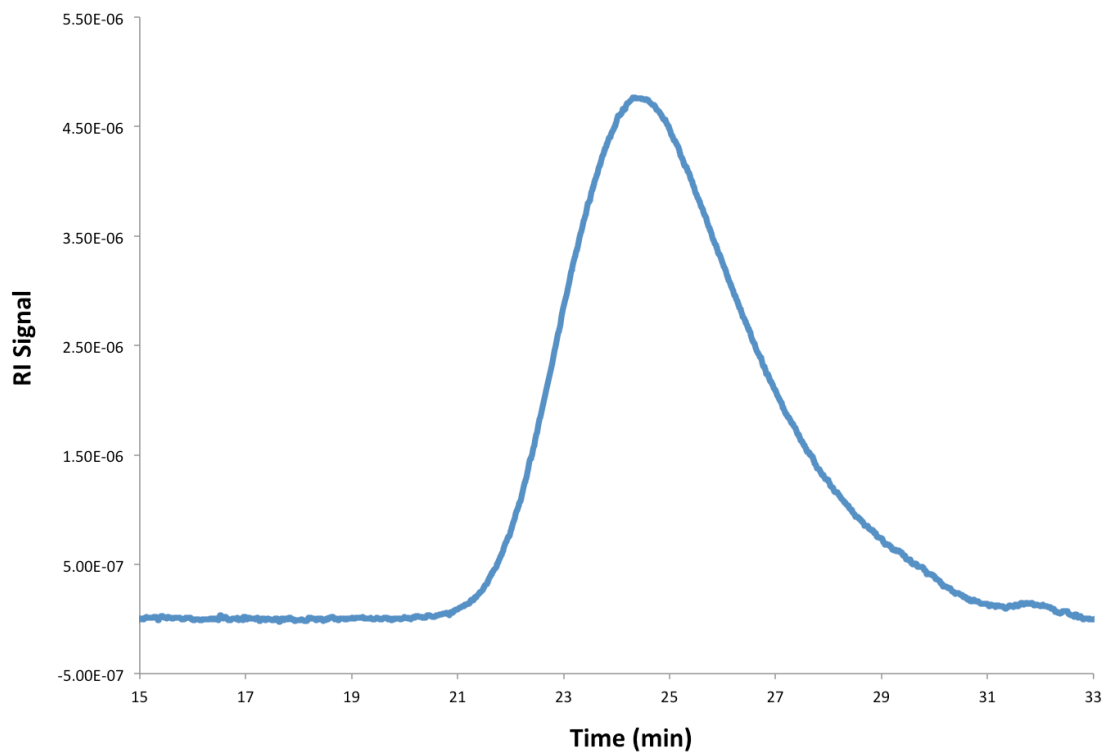


Figure E66. Table 5.1, entry 11. Polymerization of 100 equivalents of CHO by F_{36} in $CDCl_3$. $M_n = 28300$ Da, $M_w = 47500$ Da, $D = 1.68$.

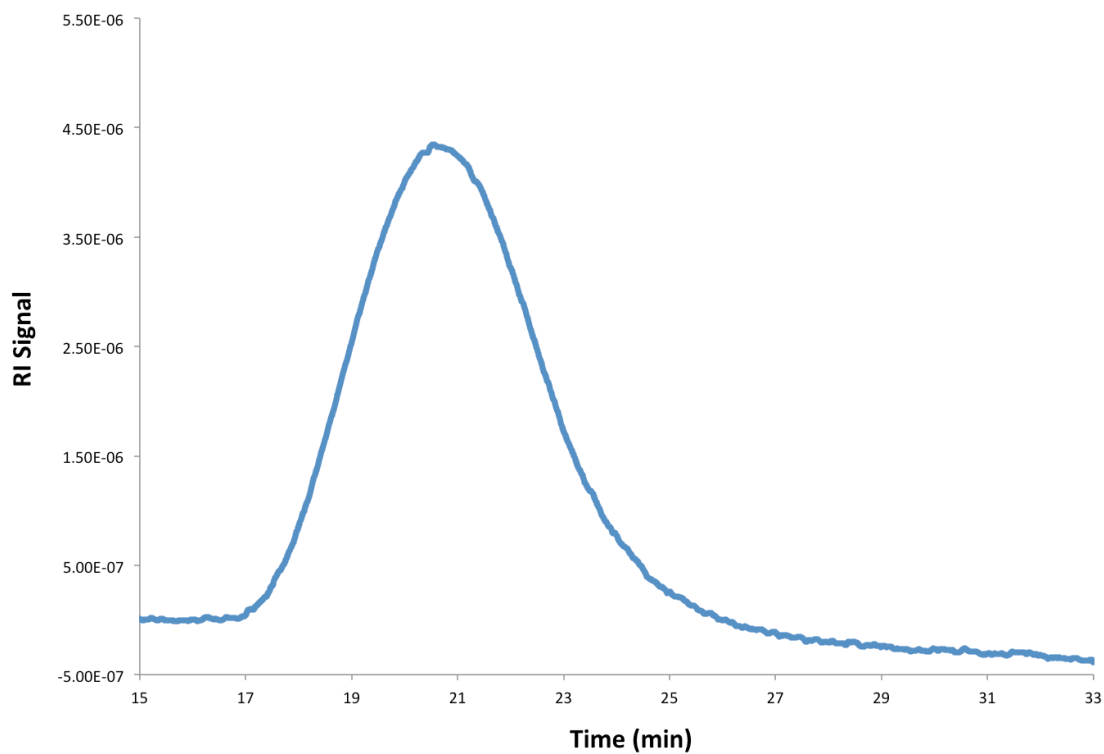


Figure E67. Table 5.1, entry 12. Polymerization of 100 equivalents of CHO by F_{36} in CH_2Cl_2 . $M_n = 176600$ Da, $M_w = 256000$ Da, $D = 1.45$.

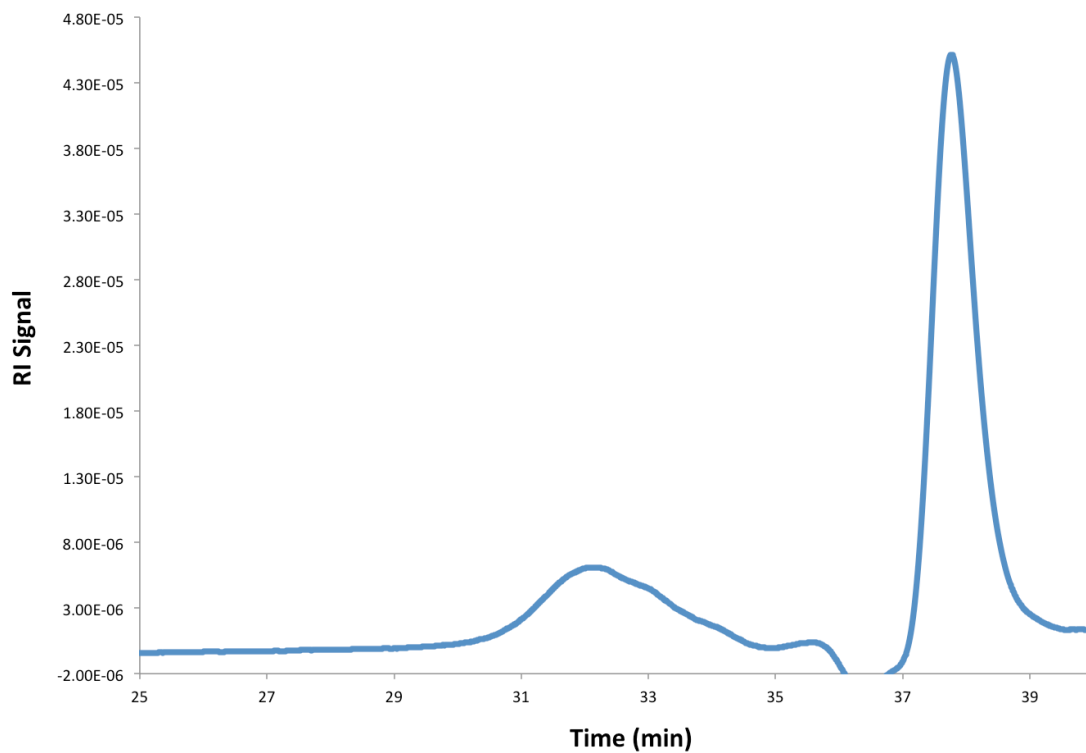


Figure E68. Table 5.2, entry 1. Polymerization of 100 equivalents of PO by F₃₆ in 4:1 F₂C₆H₄:C₆D₆. $M_n = 2200$ Da, $M_w = 7400$ Da, $\mathcal{D} = 3.37$.

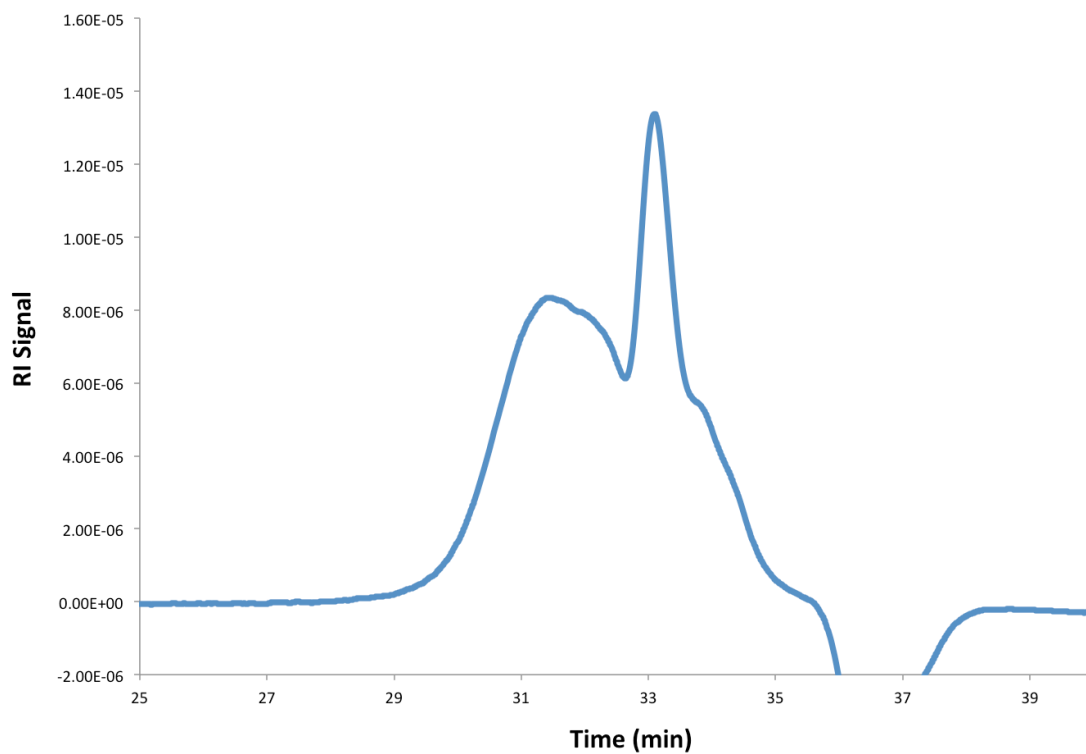


Figure E69. Table 5.2, entry 2. Polymerization of 100 equivalents of SO by F₃₆ in 4:1 F₂C₆H₄:C₆D₆. $M_n = 600$ Da, $M_w = 1200$ Da, $\mathcal{D} = 2.06$.

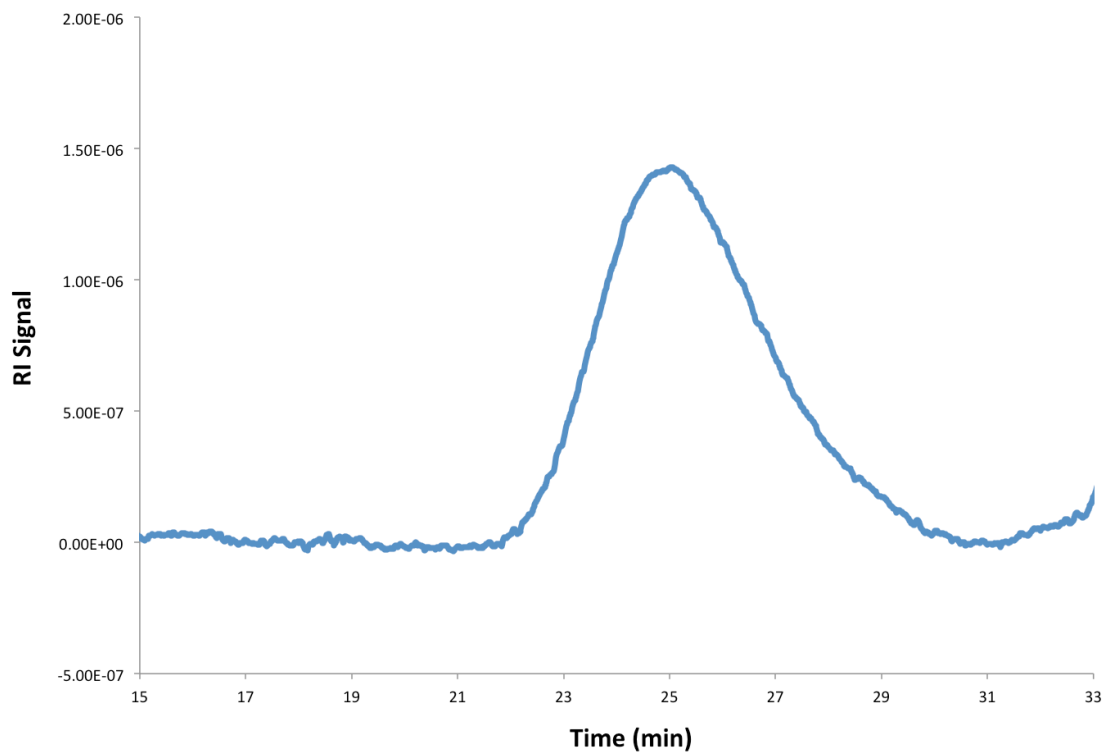


Figure E70. Table 5.2, entry 3. Polymerization of 100 equivalents of OX by F₃₆ in 4:1 F₂C₆H₄:C₆D₆. $M_n = 4800$ Da, $M_w = 6500$ Da, $\mathcal{D} = 1.36$.

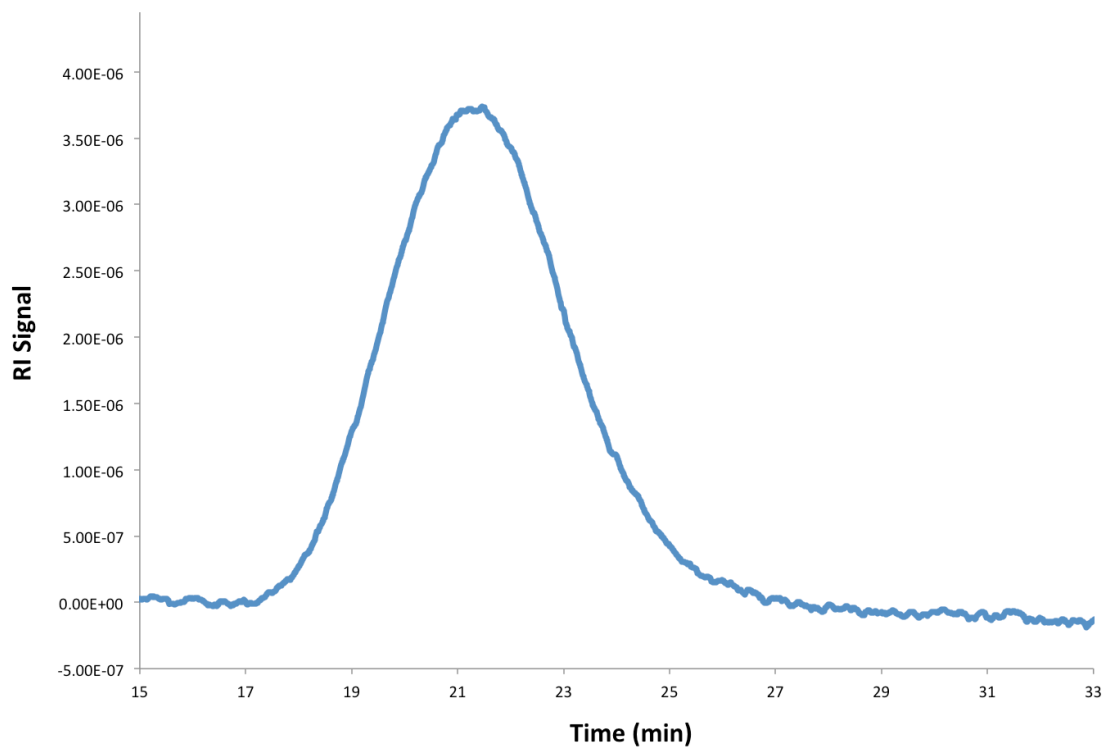


Figure E71. Table 5.3, entry 1. Polymerization of 100 equivalents of CHO by F₆₀ in 4:1 F₂C₆H₄:C₆D₆. $M_n = 181600$ Da, $M_w = 299600$ Da, $\mathcal{D} = 1.65$.

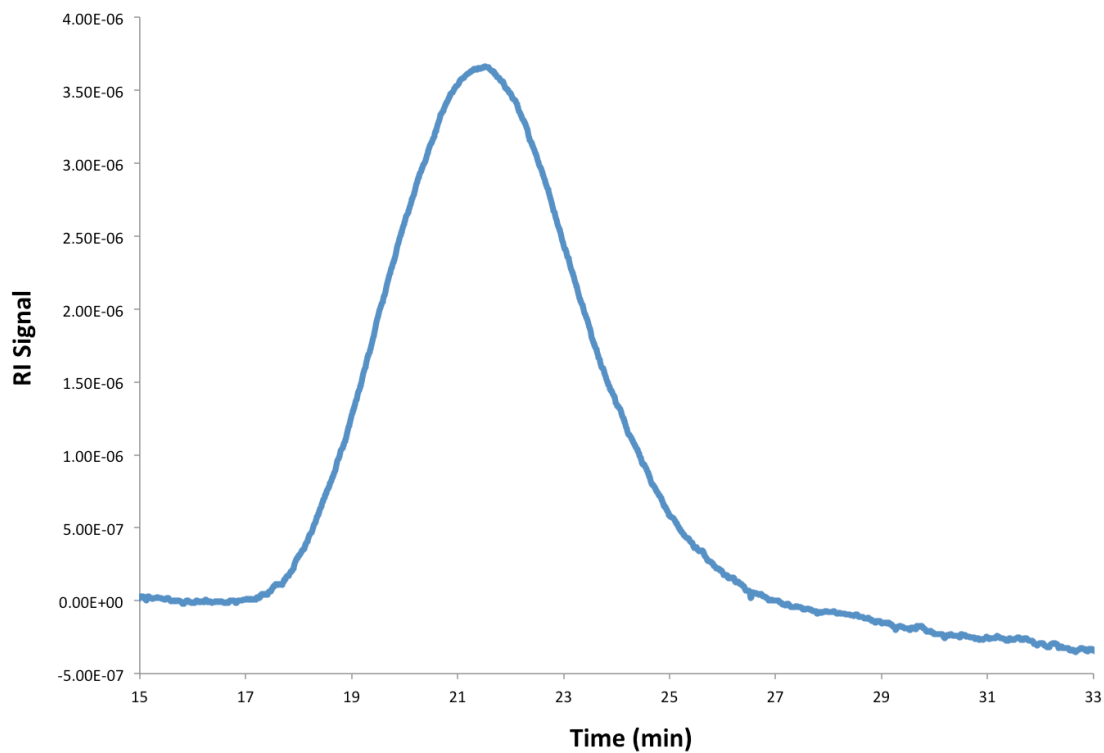


Figure E72. Table 5.3, entry 2. Polymerization of 100 equivalents of CHO by F₆₀ in 4:1 F₂C₆H₄:C₆D₆ at 0 °C. M_n = 142100 Da, M_w = 214600 Da, *D* = 1.51.

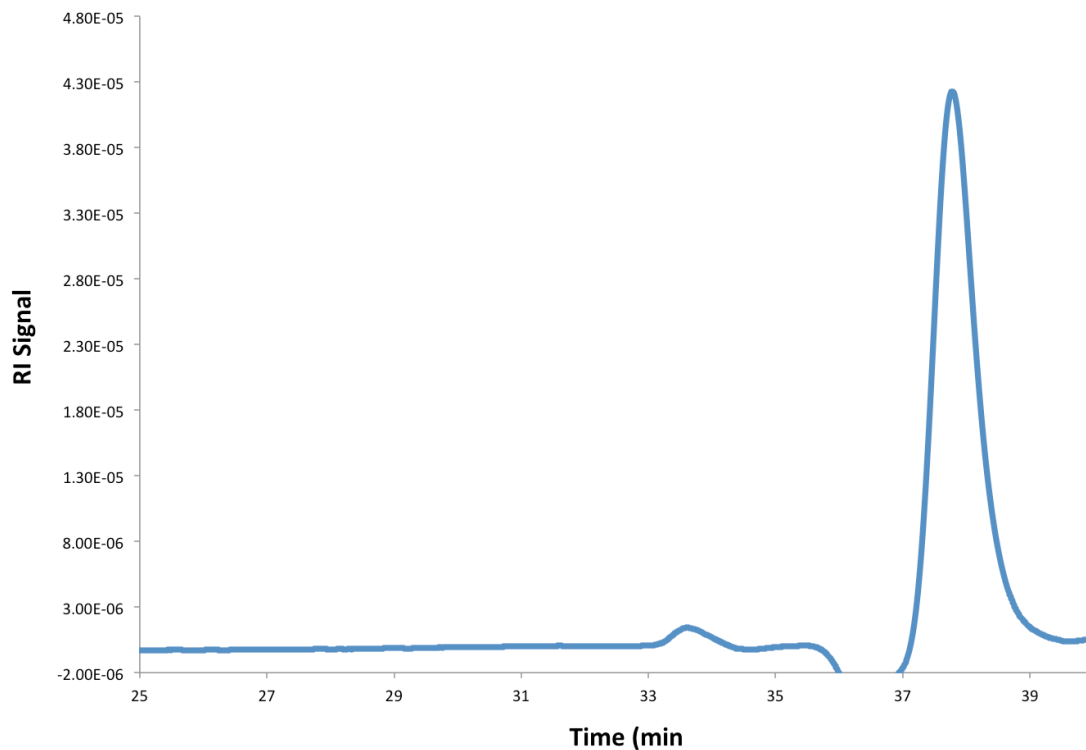


Figure E73. Table 5.3, entry 3. Polymerization of 100 equivalents of PO by F₆₀ in 4:1 F₂C₆H₄:C₆D₆. M_n = 1600 Da, M_w = 1700 Da, *D* = 1.07.

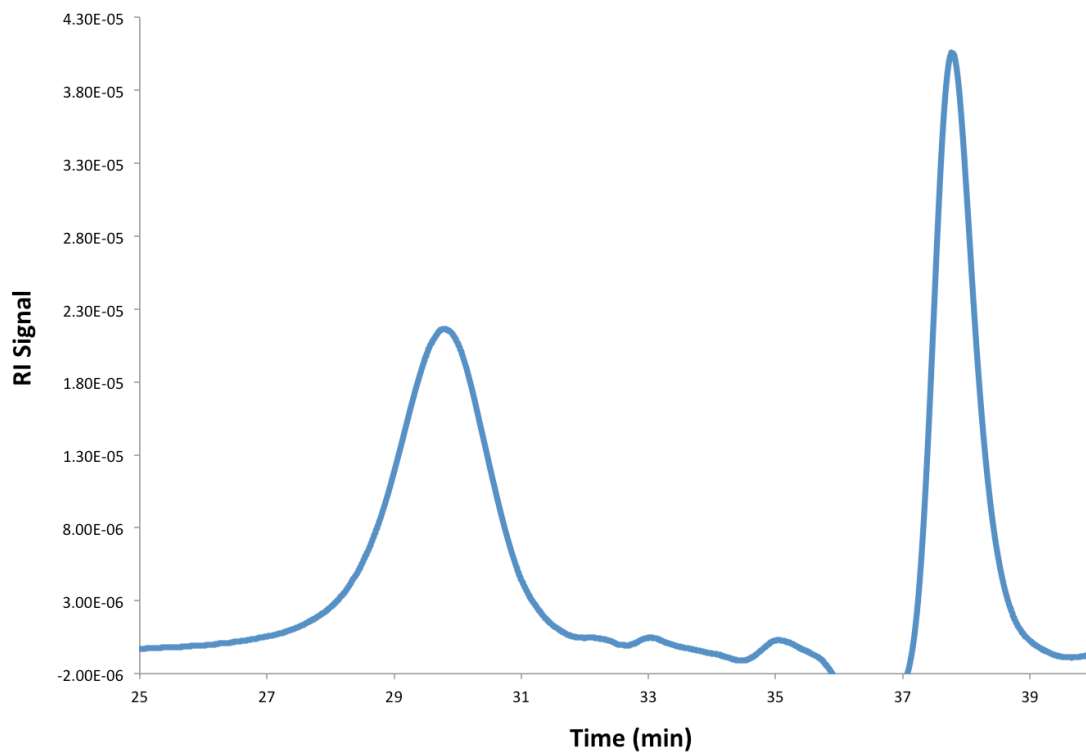


Figure E74. Table 5.3, entry 4. Polymerization of 100 equivalents of SO by F₆₀ in 4:1 F₂C₆H₄:C₆D₆. M_n = 3600 Da, M_w = 4700 Da, *D* = 1.3.

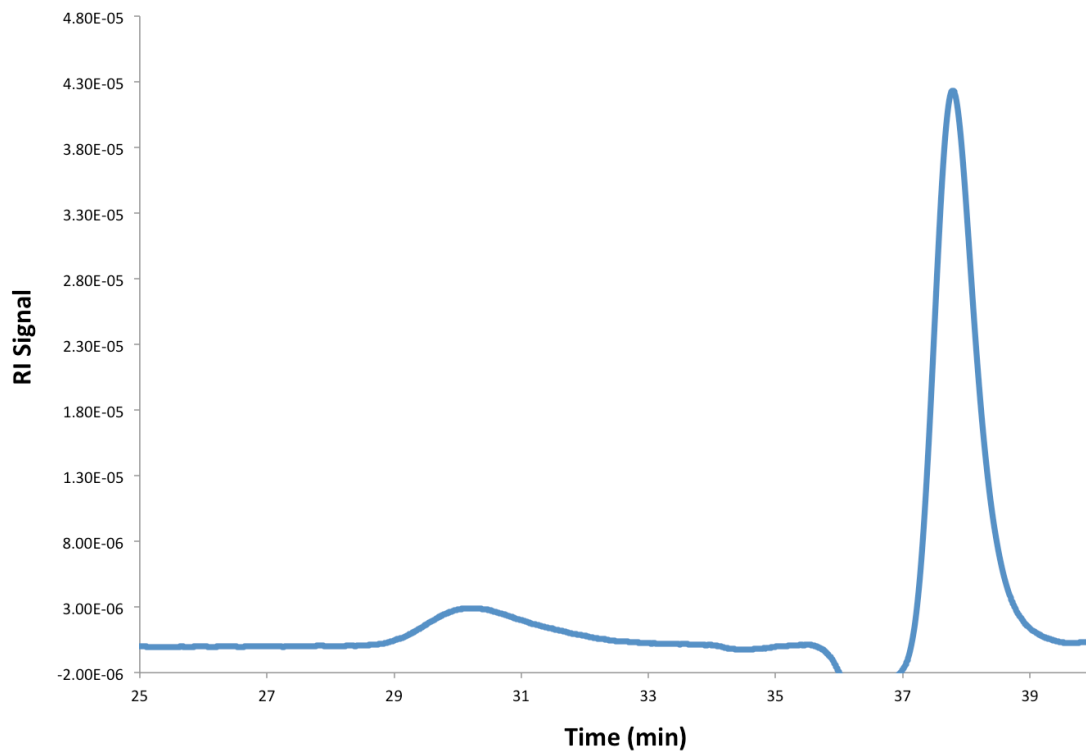


Figure E75. Table 5.3, entry 5. Polymerization of 100 equivalents of LO by F₆₀ in 4:1 F₂C₆H₄:C₆D₆. M_n = 2500 Da, M_w = 2900 Da, *D* = 1.16.

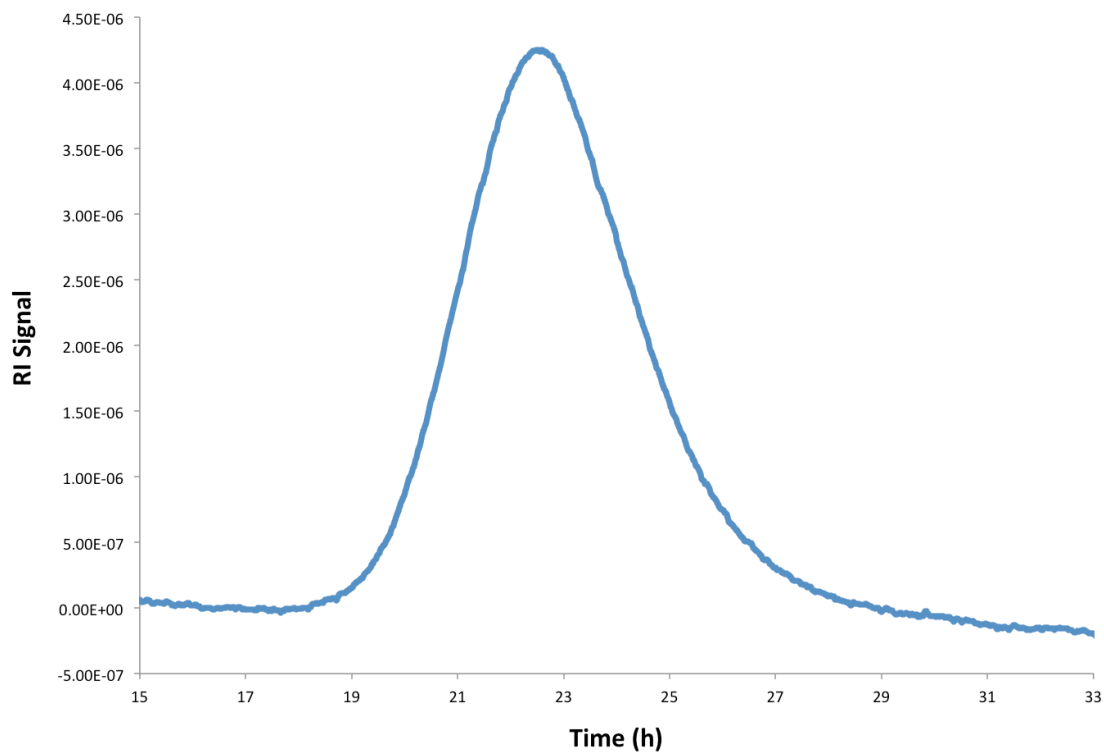


Figure E76. Table 5.5. Polymerization of CHO by F_{72} in $F_2C_6H_4$ in the presence of blue LED light. $M_n = 106000$ Da, $M_w = 163200$ Da, $D = 1.54$.

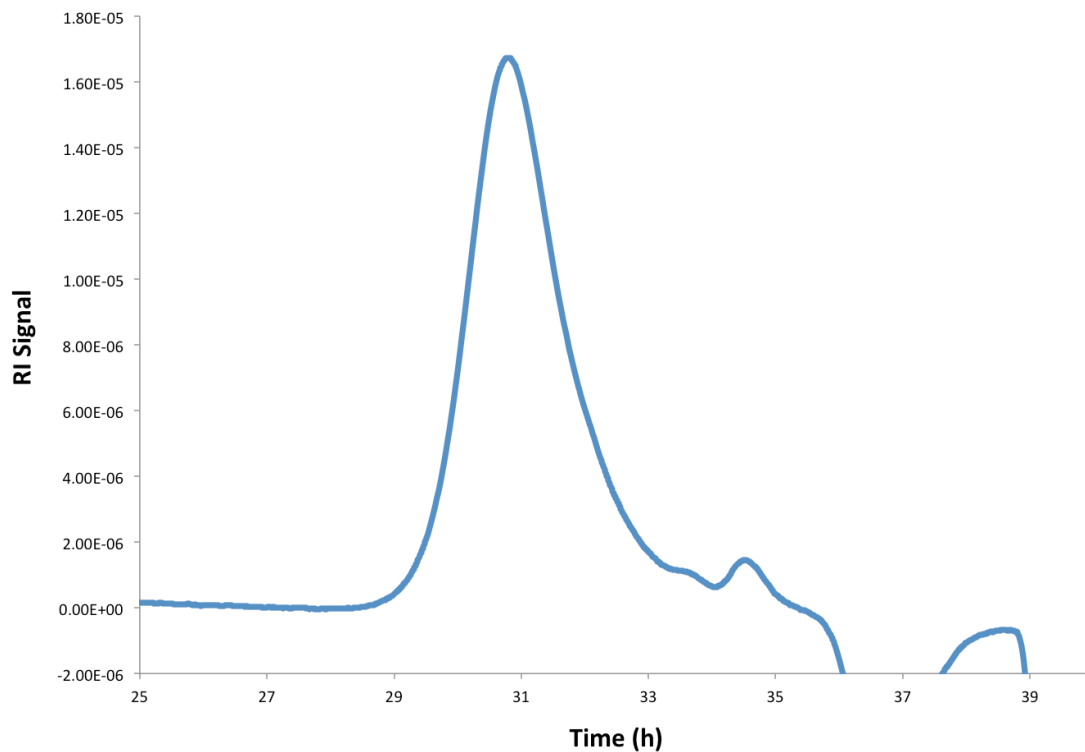


Figure E77. Table 5.5. Polymerization of LO by F_{72} in $F_2C_6H_4$ in the presence of blue LED light. $M_n = 1300$ Da, $M_w = 1500$ Da, $D = 1.18$.

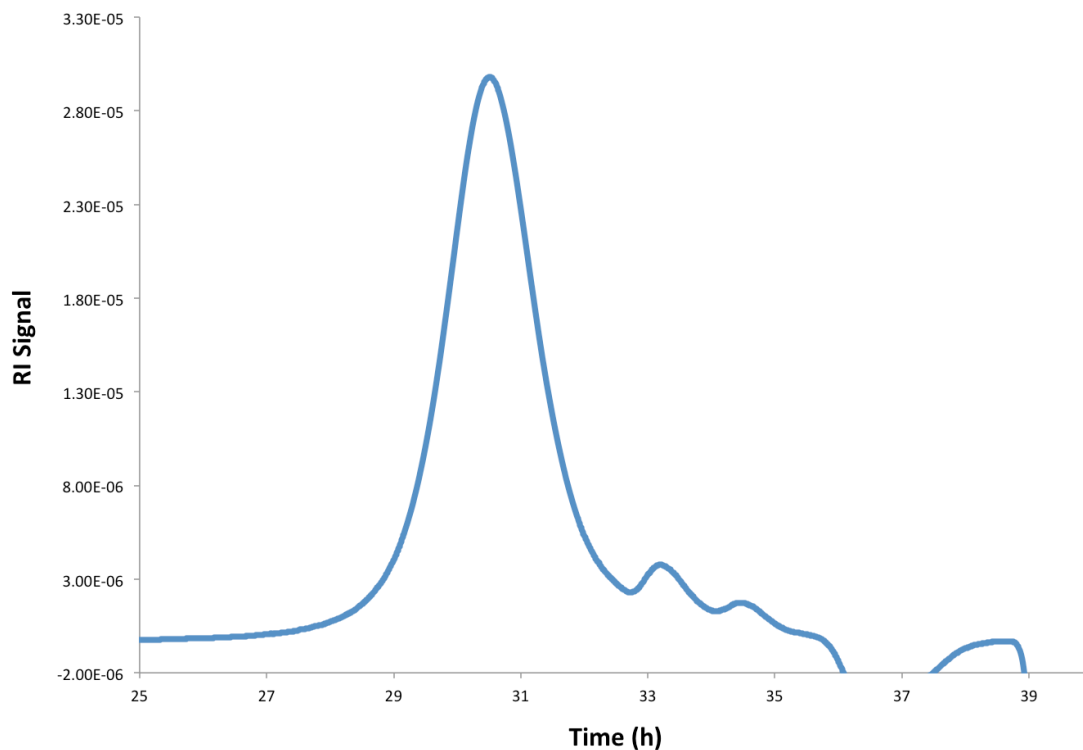


Figure E78. Table 5.5. Polymerization of SO by F_{72} in $F_2C_6H_4$ in the presence of blue LED light. $M_n = 1700$ Da, $M_w = 2000$ Da, $D = 1.18$.

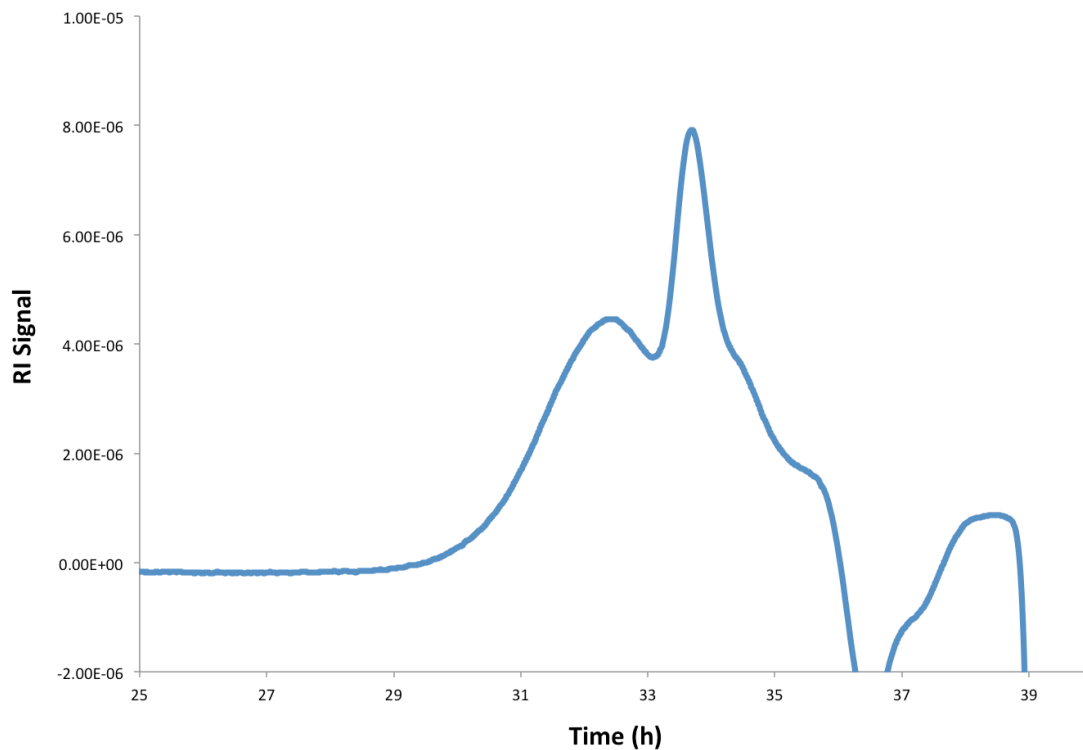


Figure E79. Table 5.5. Polymerization of PO by F_{72} in $F_2C_6H_4$ in the presence of blue LED light. $M_n = 426$ Da, $M_w = 575$ Da, $D = 1.35$.

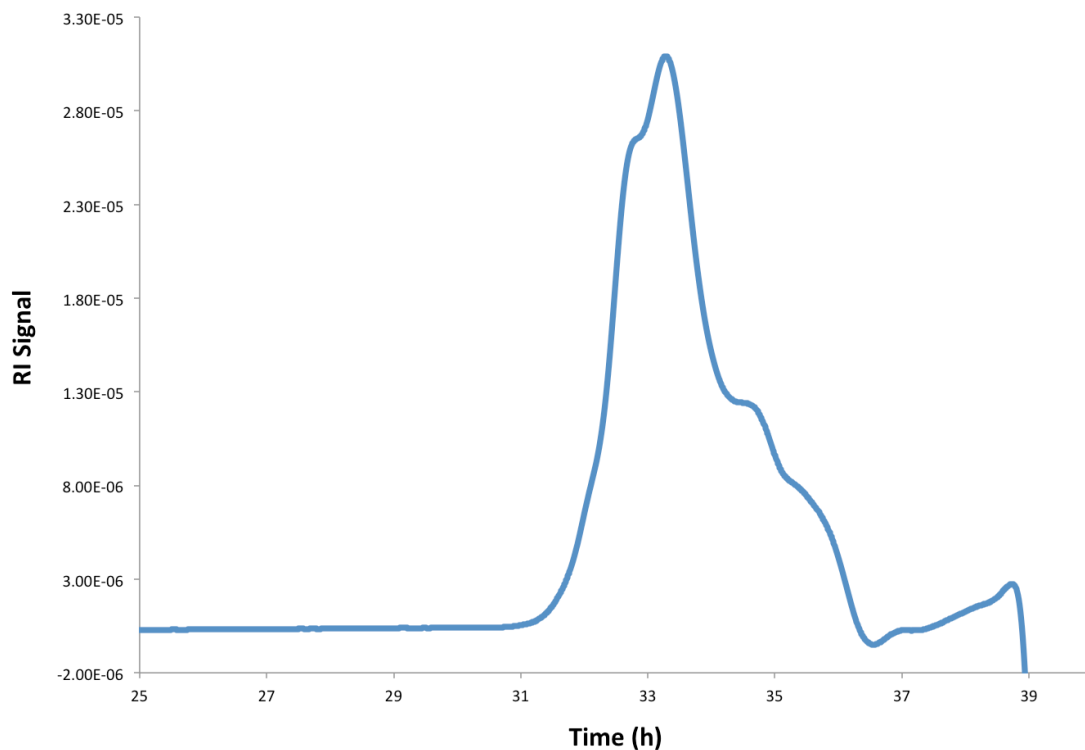


Figure E80. Table 5.5. Polymerization of PiO by F_{72} in $F_2C_6H_4$ in the presence of blue LED light.

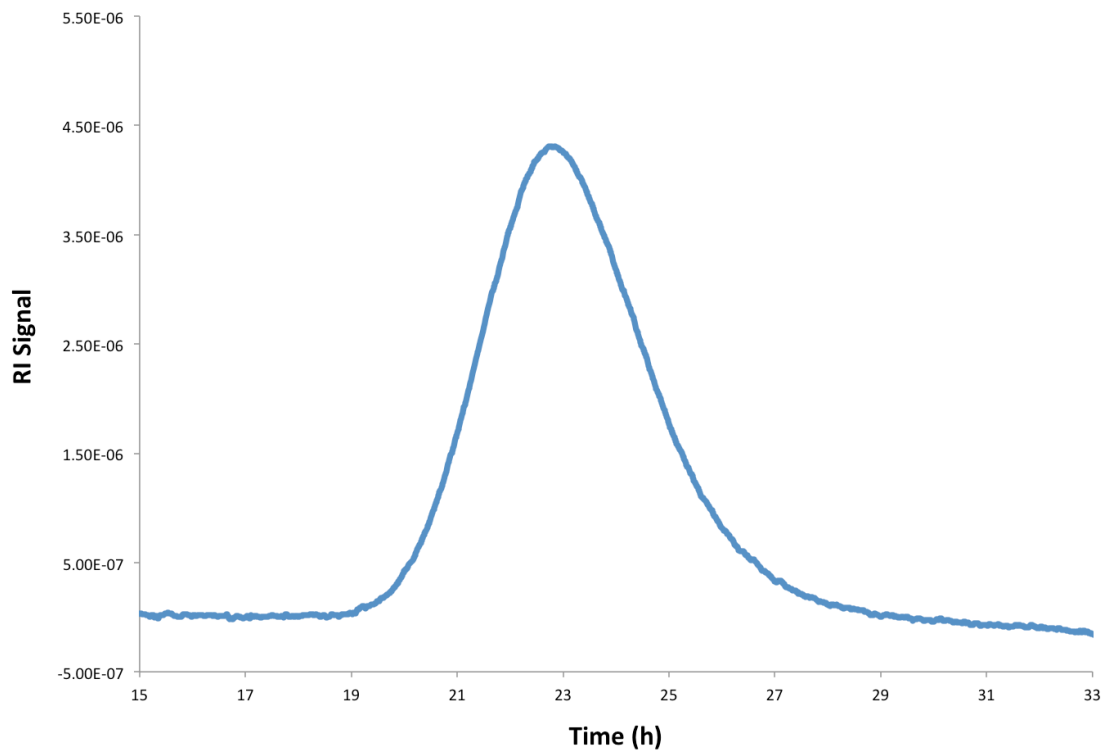


Figure E81. Table 5.5. Polymerization of CHO by F_{72} in CH_2Cl_2 in the presence of blue LED light. $M_n = 99800$ Da, $M_w = 140700$ Da, $D = 1.41$.

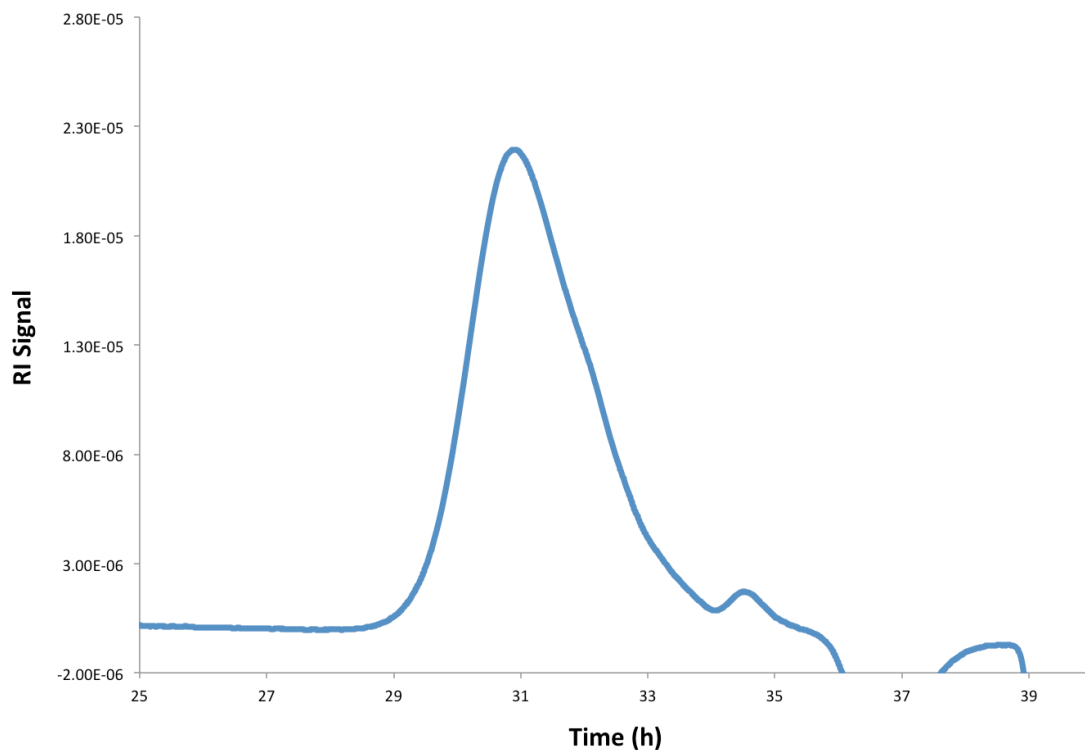


Figure E82. Table 5.5. Polymerization of LO by F_{72} in CH_2Cl_2 in the presence of blue LED light. $M_n = 1100$ Da, $M_w = 1400$ Da, $D = 1.25$.

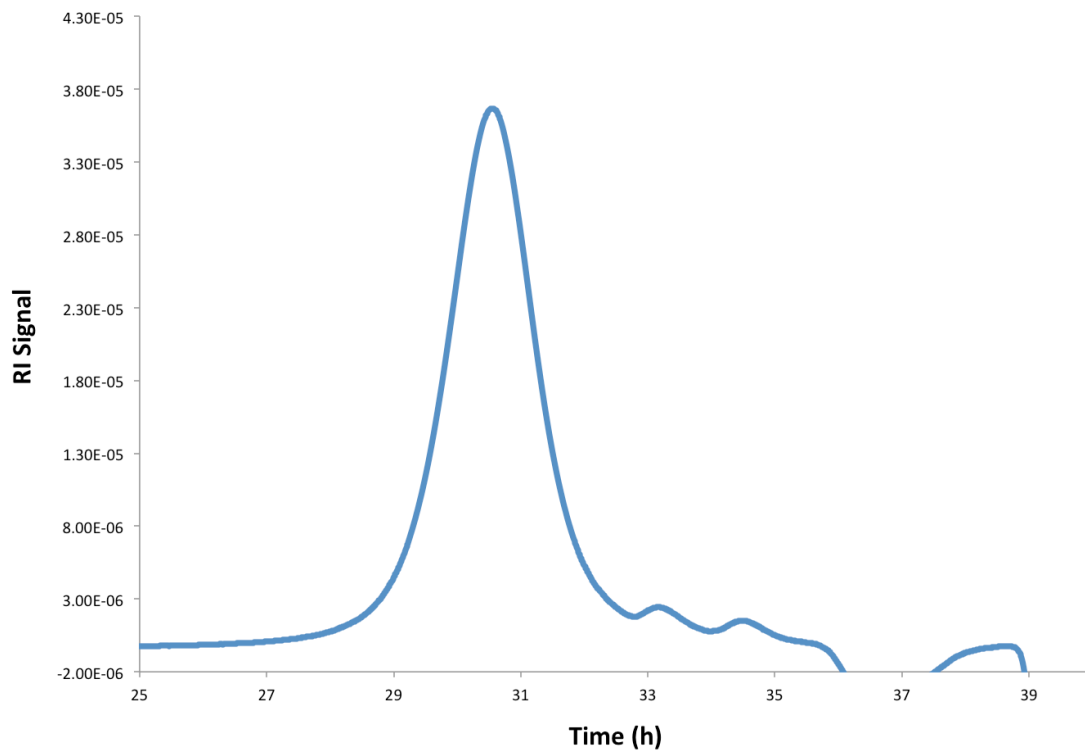


Figure E83. Table 5.5. Polymerization of SO by F_{72} in CH_2Cl_2 in the presence of blue LED light. $M_n = 1700$ Da, $M_w = 1900$ Da, $D = 1.16$.

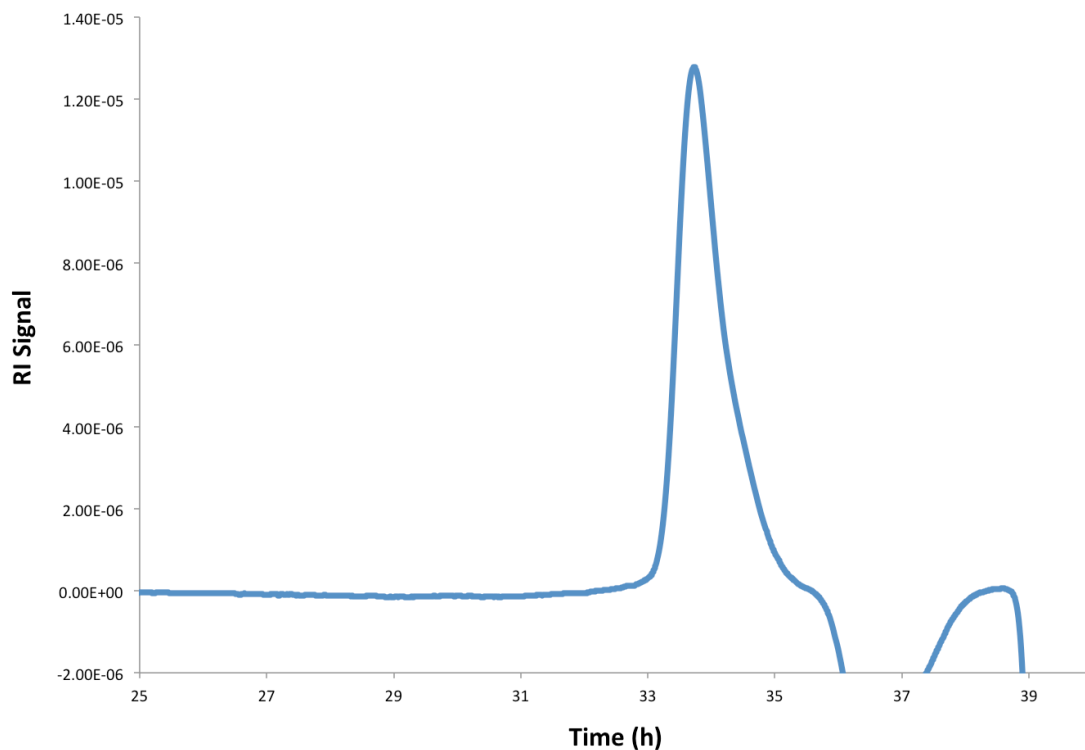


Figure E84. Table 5.5. Polymerization of PO by F_{72} in CH_2Cl_2 in the presence of blue LED light. $M_n = 321$ Da, $M_w = 337$ Da, $D = 1.05$.

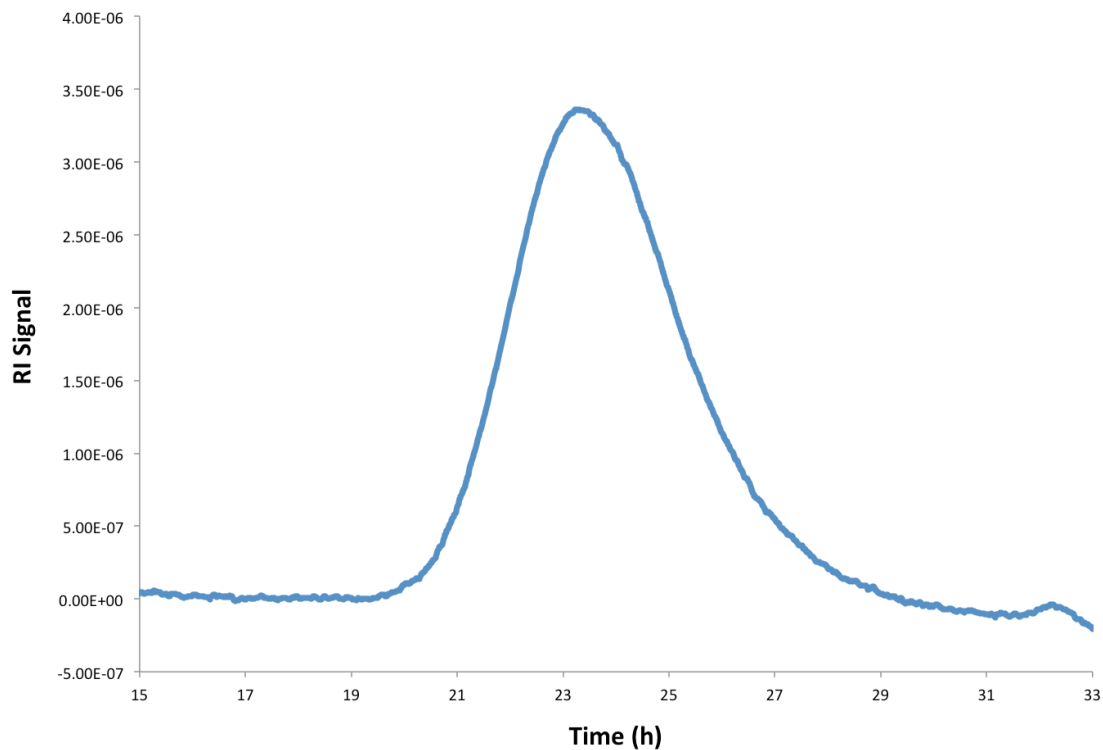


Figure E85. Table 5.5. Polymerization of CHO by F_{72} in $F_2C_6H_4$ in the dark. $M_n = 95200$ Da, $M_w = 146500$ Da, $D = 1.54$.

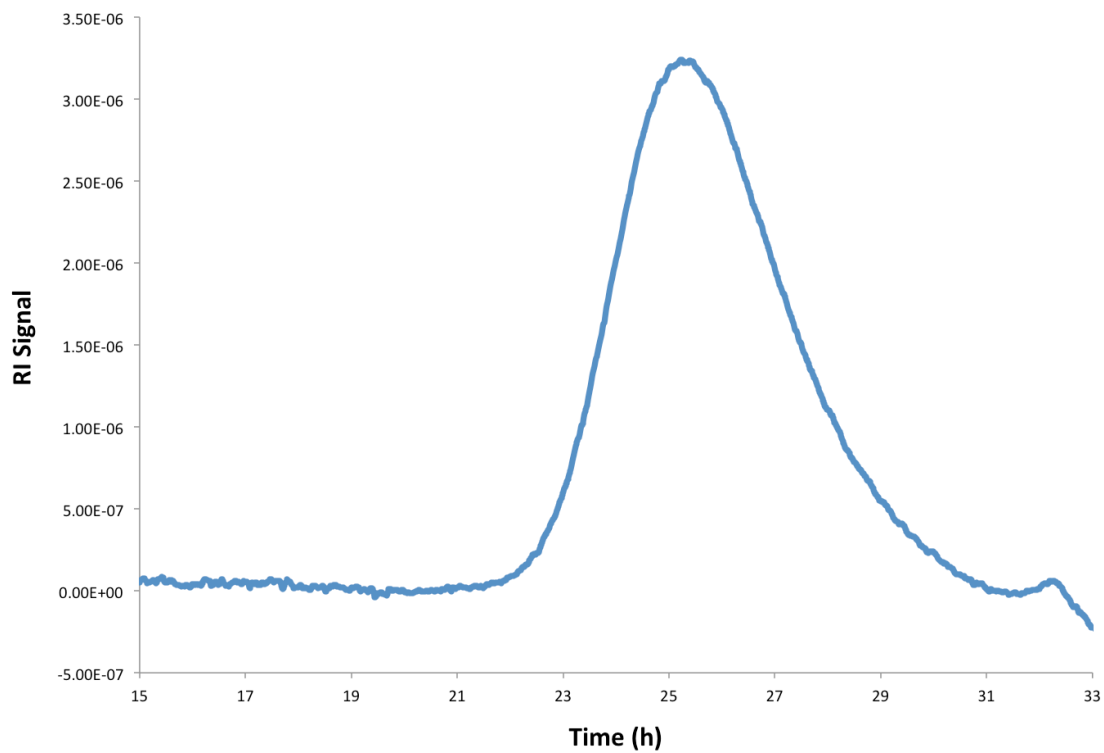


Figure E86. Table 5.5. Polymerization of CHO by F₆₀ in F₂C₆H₄ in the presence of blue LED light. $M_n = 35600$ Da $M_w = 54900$ Da, $\bar{D} = 1.54$.

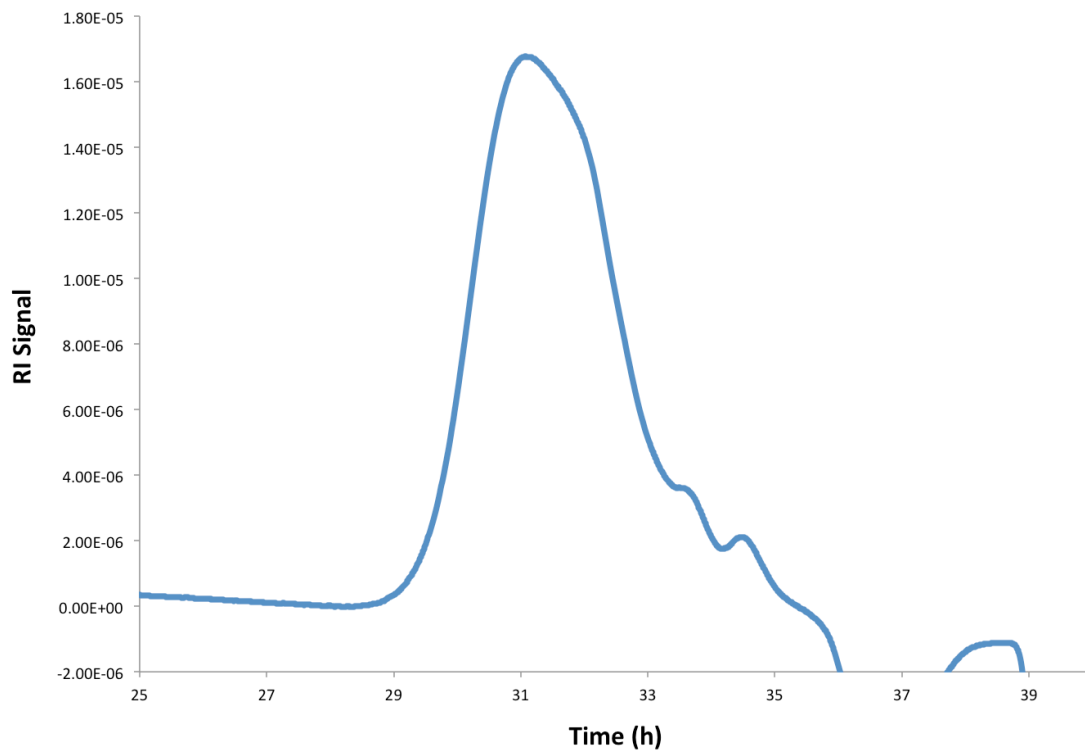


Figure E87. Table 5.5. Polymerization of LO by F₆₀ in F₂C₆H₄ in the presence of blue LED light. $M_n = 894$ Da, $M_w = 1200$ Da, $\bar{D} = 1.38$.

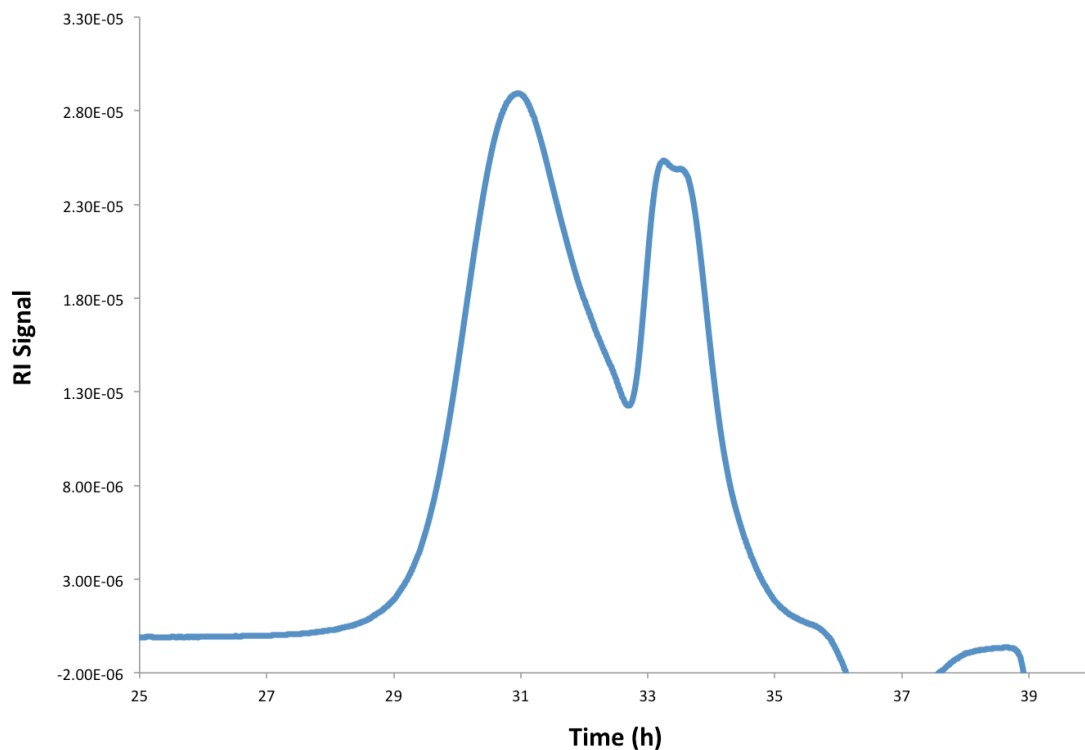


Figure E88. Table 5.5. Polymerization of SO by F_{60} in $F_2C_6H_4$ in the presence of blue LED light. $M_n = 1600$ Da, $M_w = 1700$ Da, $D = 1.06$.

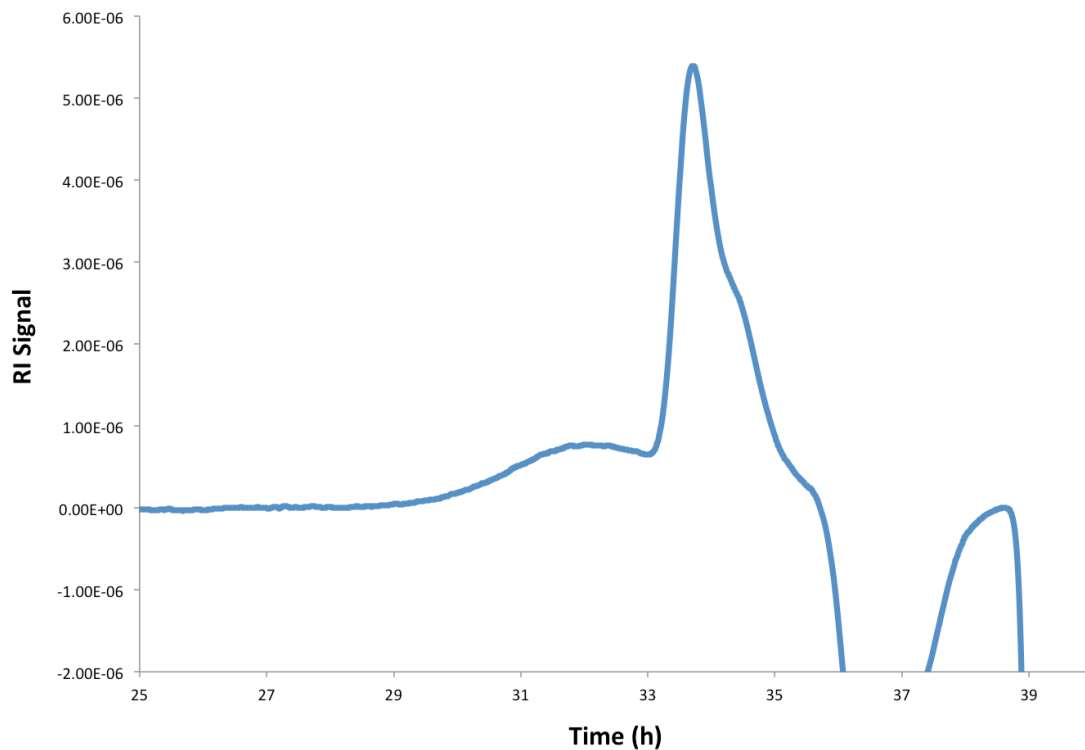


Figure E89. Table 5.5. Polymerization of PO by F_{60} in $F_2C_6H_4$ in the presence of blue LED light. $M_n = 305$ Da, $M_w = 323$ Da, $D = 1.05$.

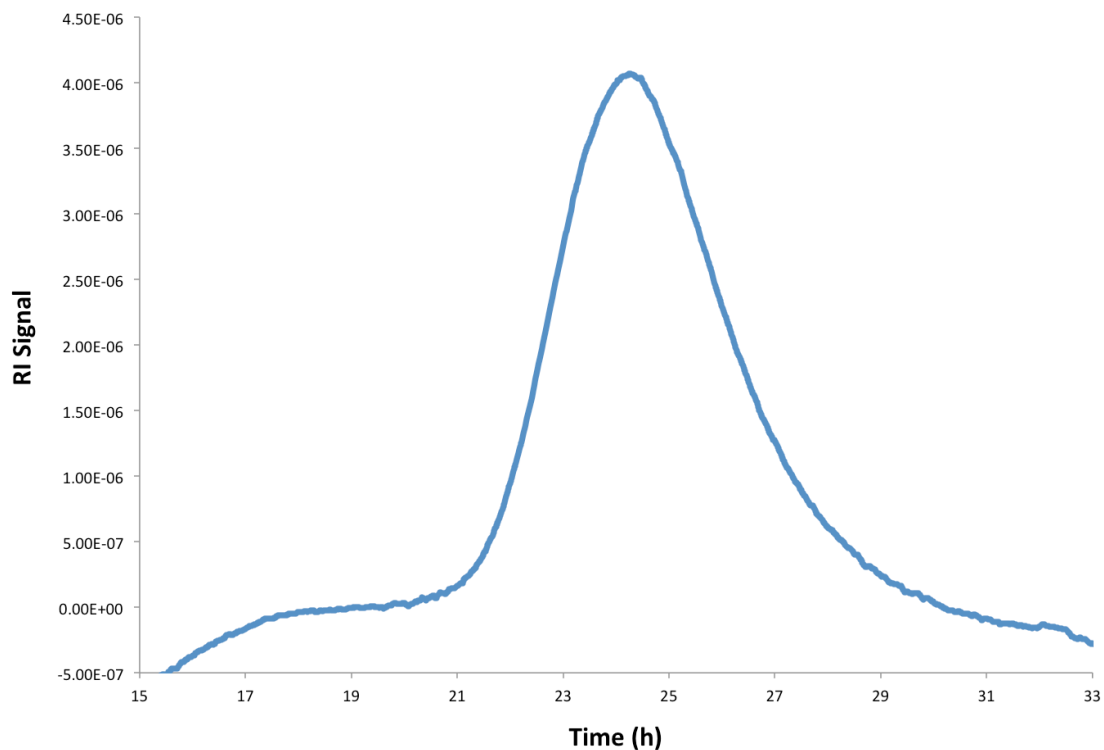


Figure E90. Table 5.5. Polymerization of CHO by F₆₀ in CH₂Cl₂ in the presence of blue LED light. $M_n = 48800$ Da, $M_w = 76200$ Da, $D = 1.56$.

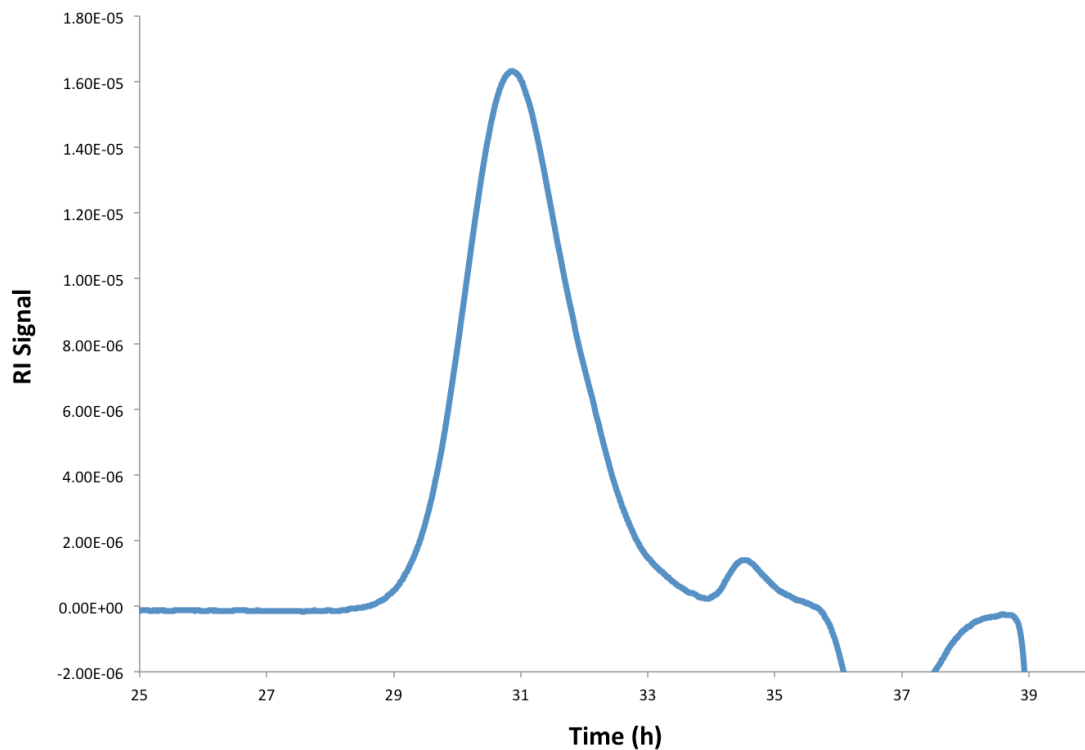


Figure E91. Table 5.5. Polymerization of LO by F₆₀ in CH₂Cl₂ in the presence of blue LED light. $M_n = 1300$ Da, $M_w = 1500$ Da, $D = 1.20$.

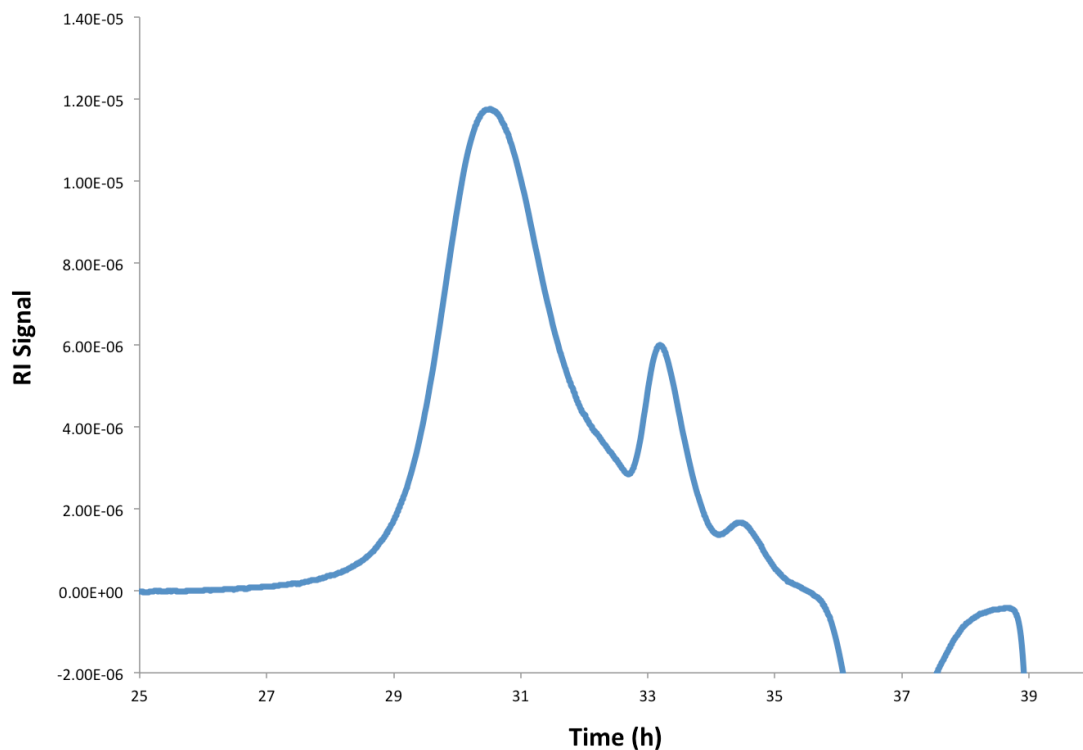


Figure E92. Table 5.5. Polymerization of SO by F_{60} in CH_2Cl_2 in the presence of blue LED light. $M_n = 1500$ Da, $M_w = 1800$ Da, $D = 1.19$.

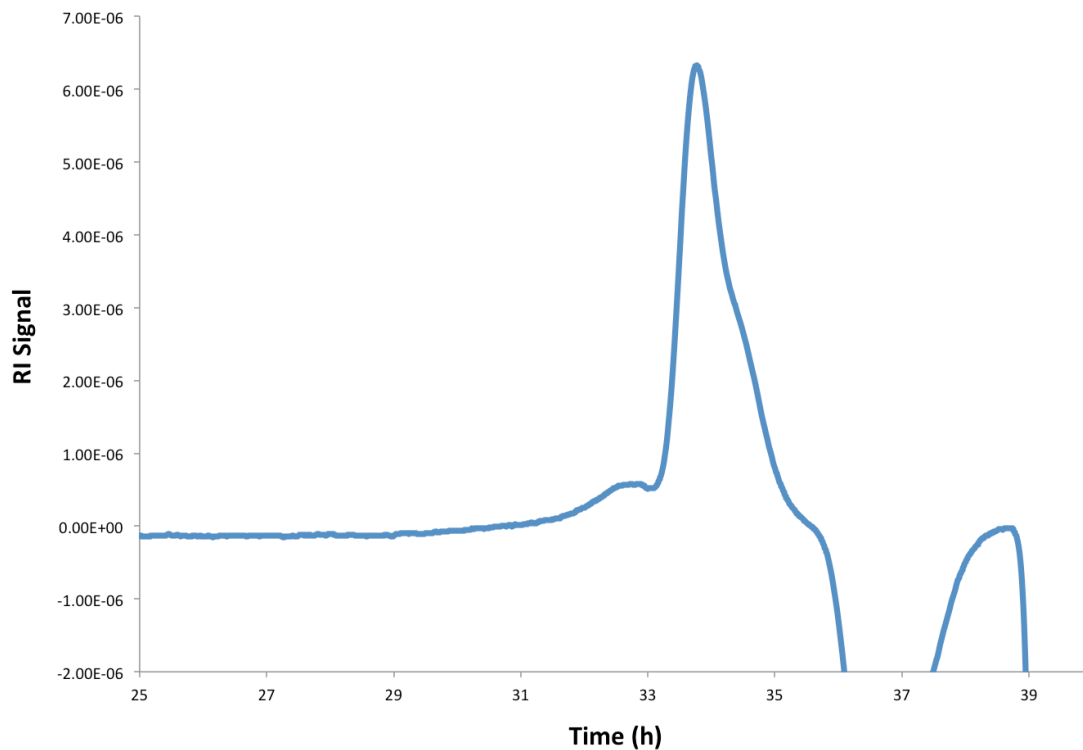


Figure E93. Table 5.5. Polymerization of PO by F_{60} in CH_2Cl_2 in the presence of blue LED light. $M_n = 307$ Da, $M_w = 322$ Da, $D = 1.05$.

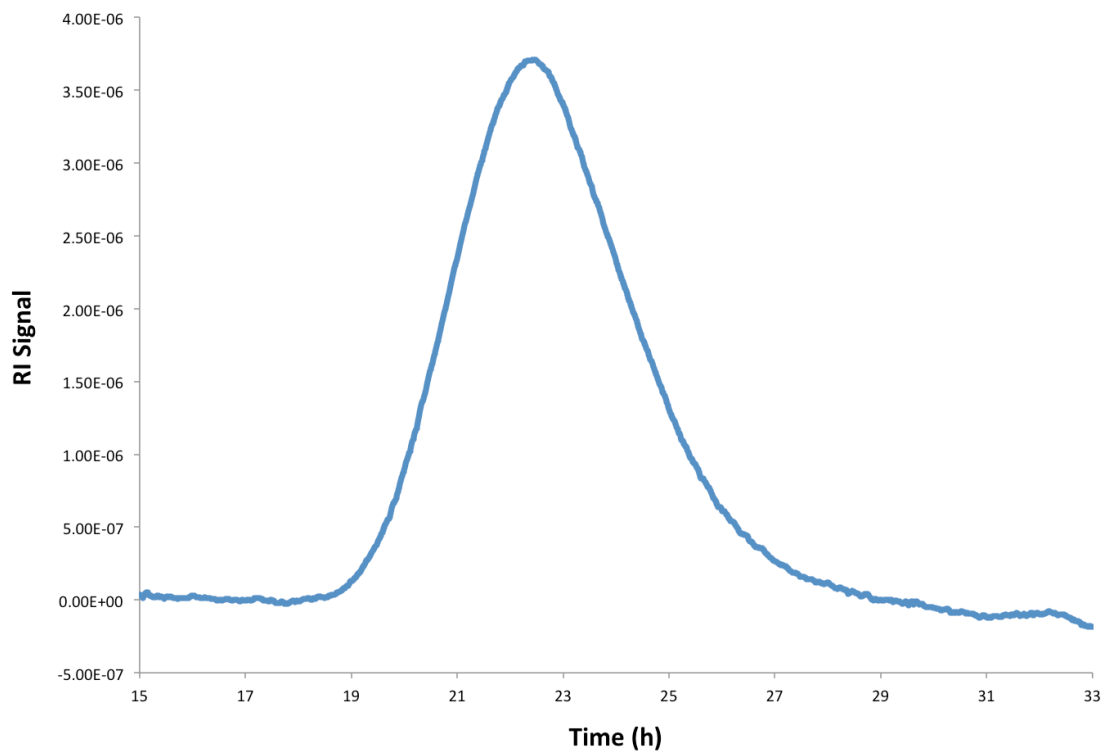


Figure E94. Table 5.5. Polymerization of CHO by F₆₀ in F₂C₆H₄ in the dark. M_n = 134500 Da, M_w = 207100 Da, \mathcal{D} = 1.54.

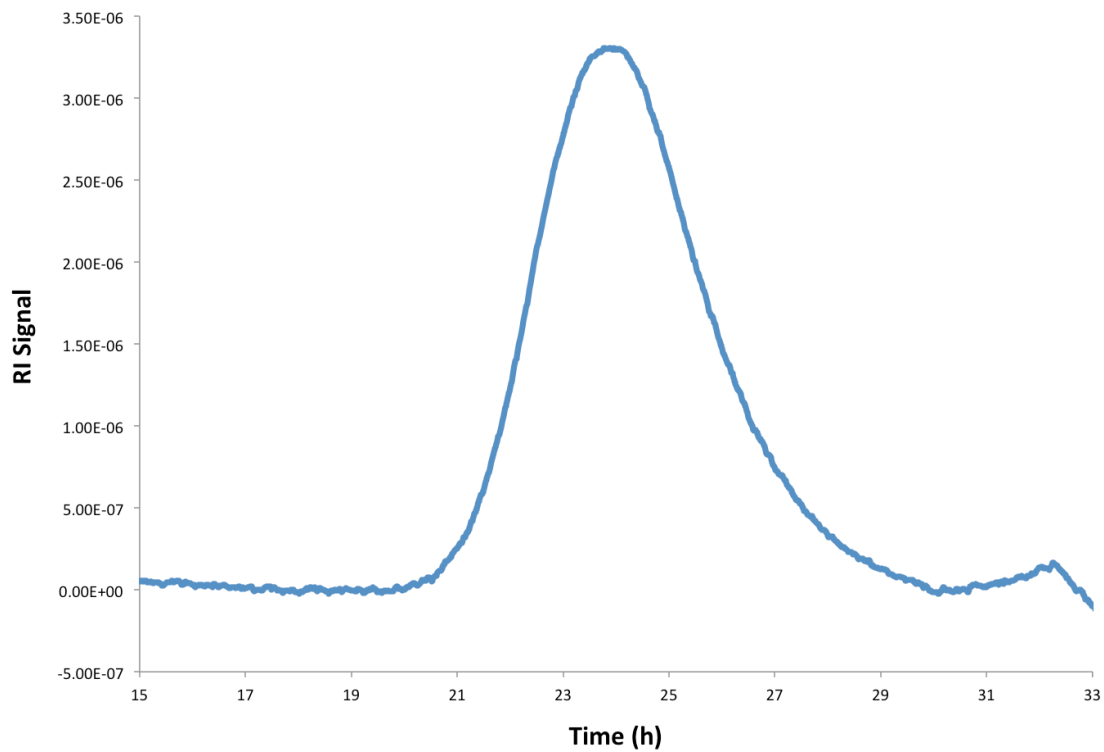


Figure E95. Table 5.5. Polymerization of CHO by F₃₆ in F₂C₆H₄ in the presence of blue LED light. M_n = 62200 Da, M_w = 99400 Da, \mathcal{D} = 1.60.

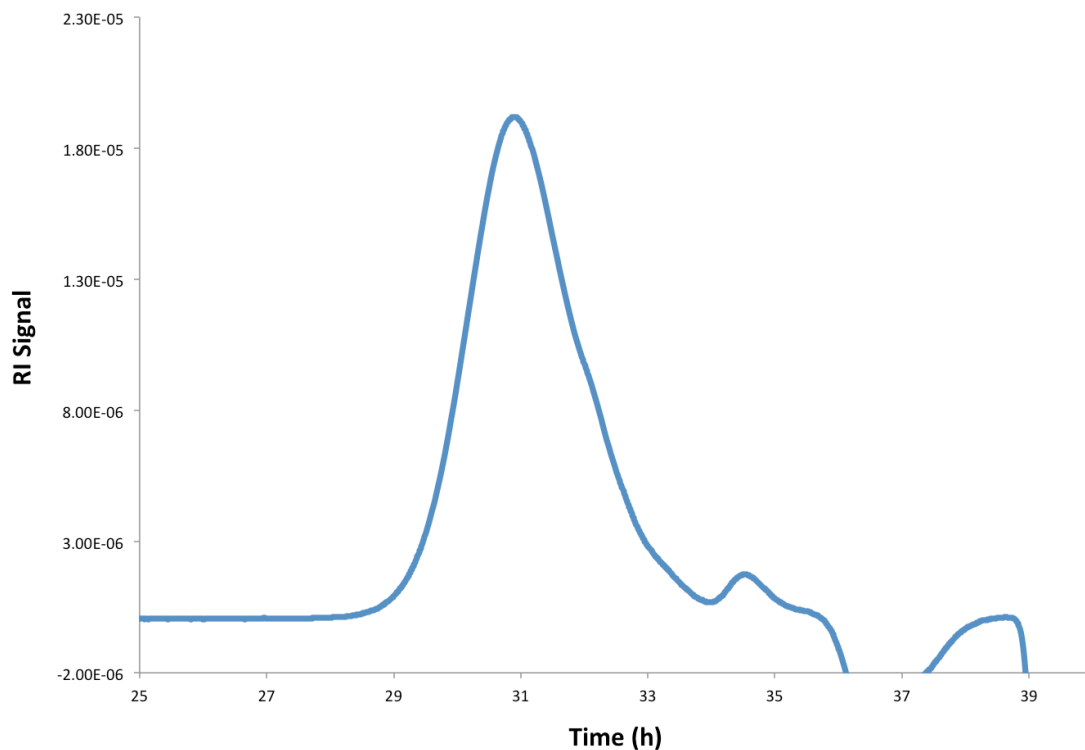


Figure E96. Table 5.5. Polymerization of LO by F_{36} in $F_2C_6H_4$ in the presence of blue LED light. $M_n = 1200$ Da, $M_w = 1500$ Da, $D = 1.25$.

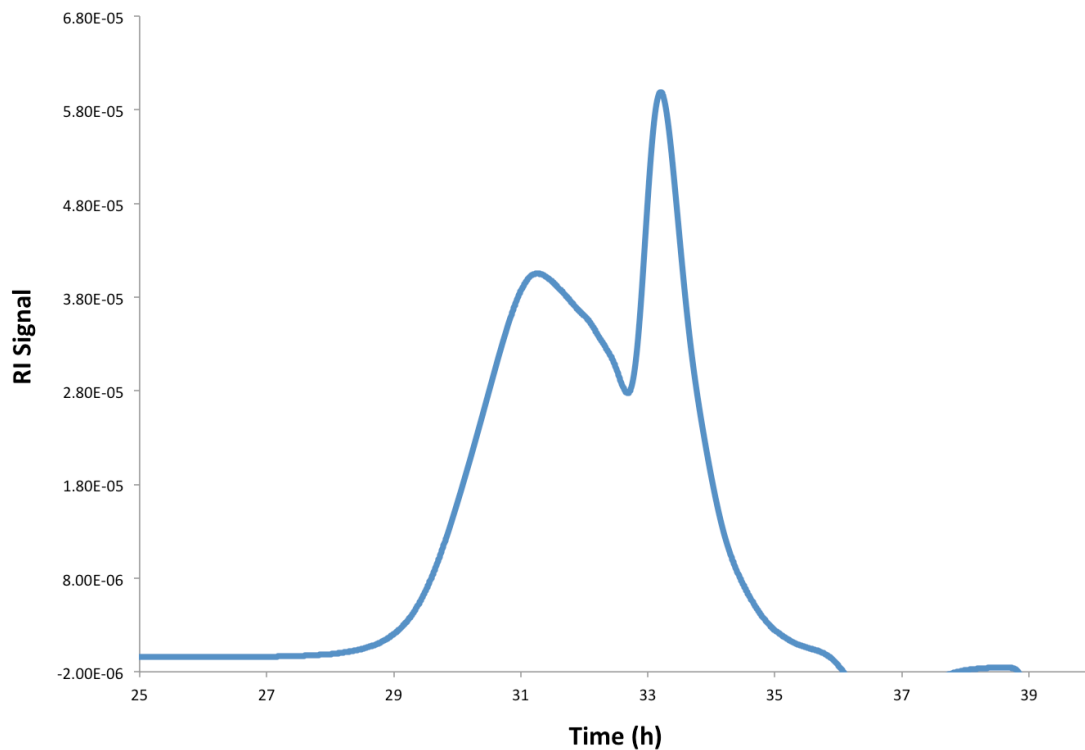


Figure E97. Table 5.5. Polymerization of SO by F_{36} in $F_2C_6H_4$ in the presence of blue LED light. $M_n = 1500$ Da, $M_w = 1800$ Da, $D = 1.17$.

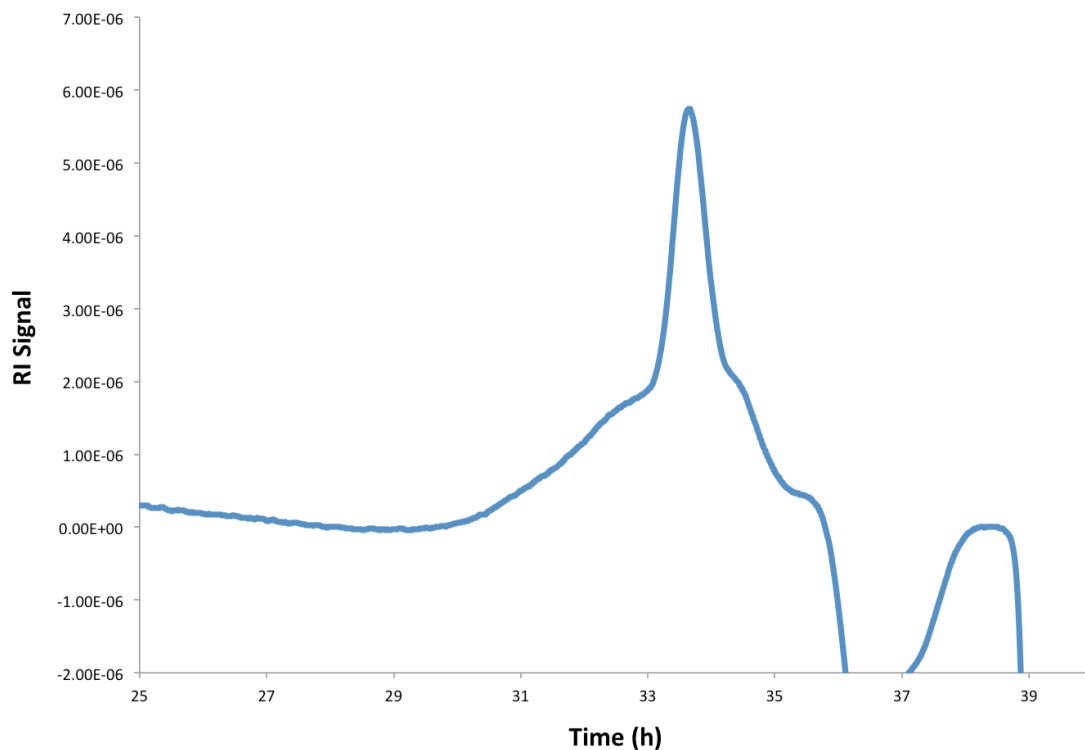


Figure E98. Table 5.5. Polymerization of PO by F_{36} in $F_2C_6H_4$ in the presence of blue LED light. $M_n = 390$ Da, $M_w = 495$ Da, $D = 1.27$.

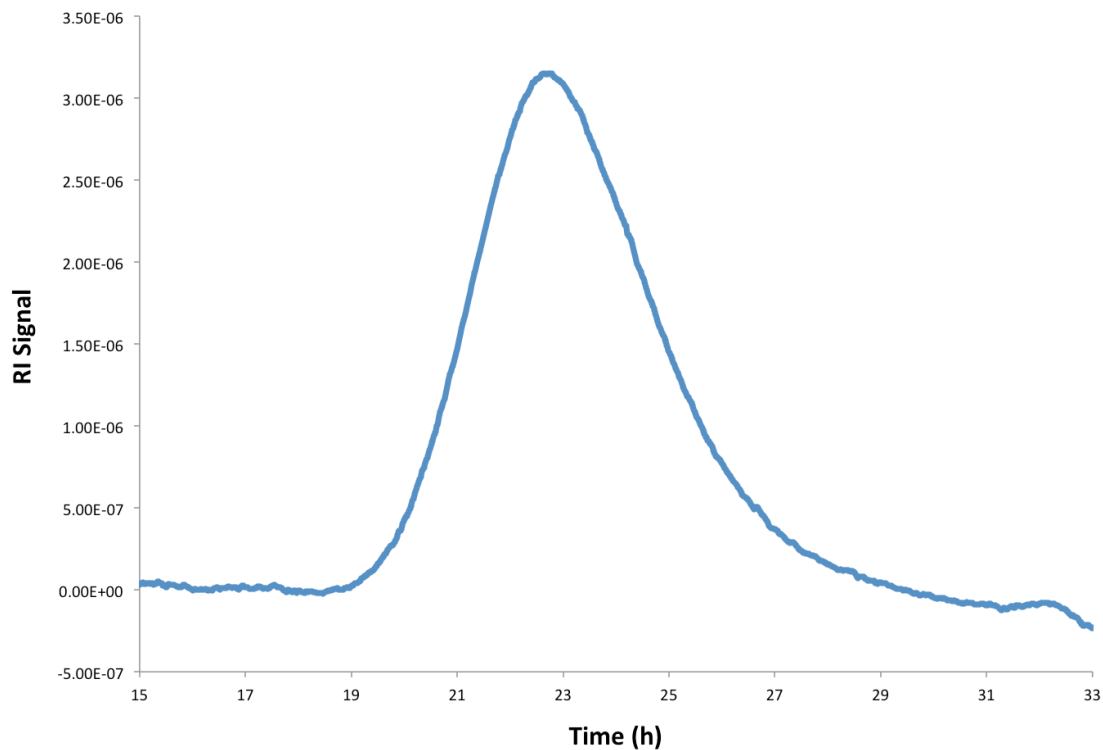


Figure E99. Table 5.5. Polymerization of CHO by F_{36} in CH_2Cl_2 in the presence of blue LED light. $M_n = 120400$ Da, $M_w = 187800$ Da, $D = 1.56$.

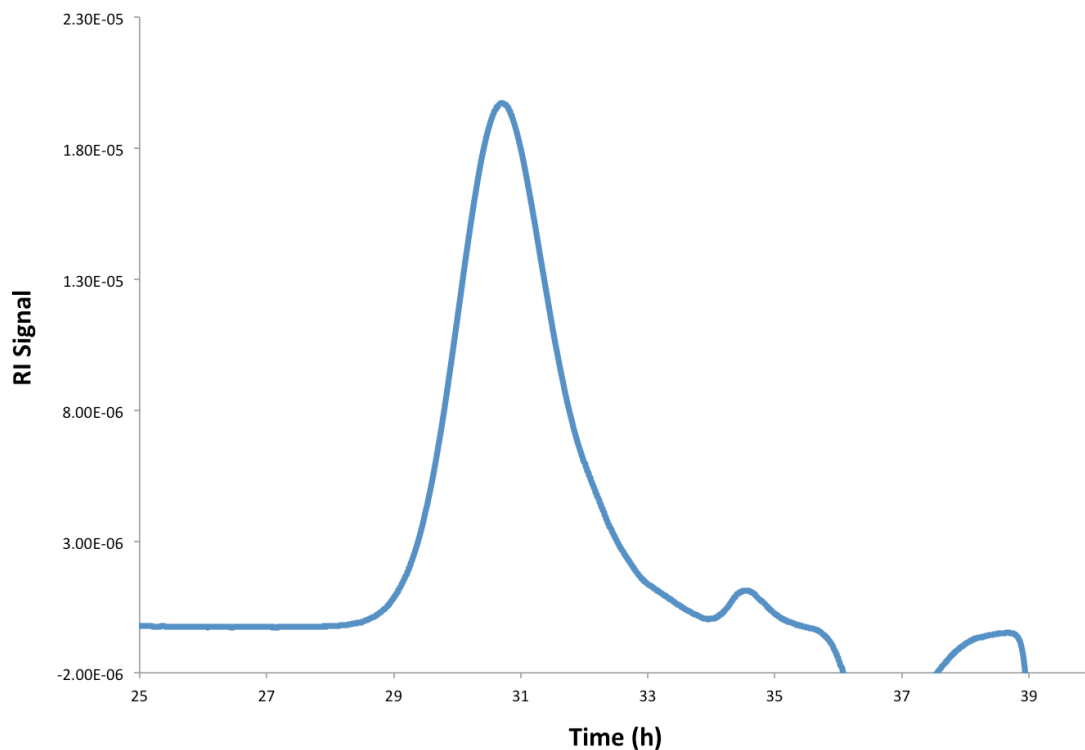


Figure E100. Table 5.5. Polymerization of LO by F_{36} in CH_2Cl_2 in the presence of blue LED light. $M_n = 1400$ Da, $M_w = 1700$ Da, $\mathcal{D} = 1.19$.

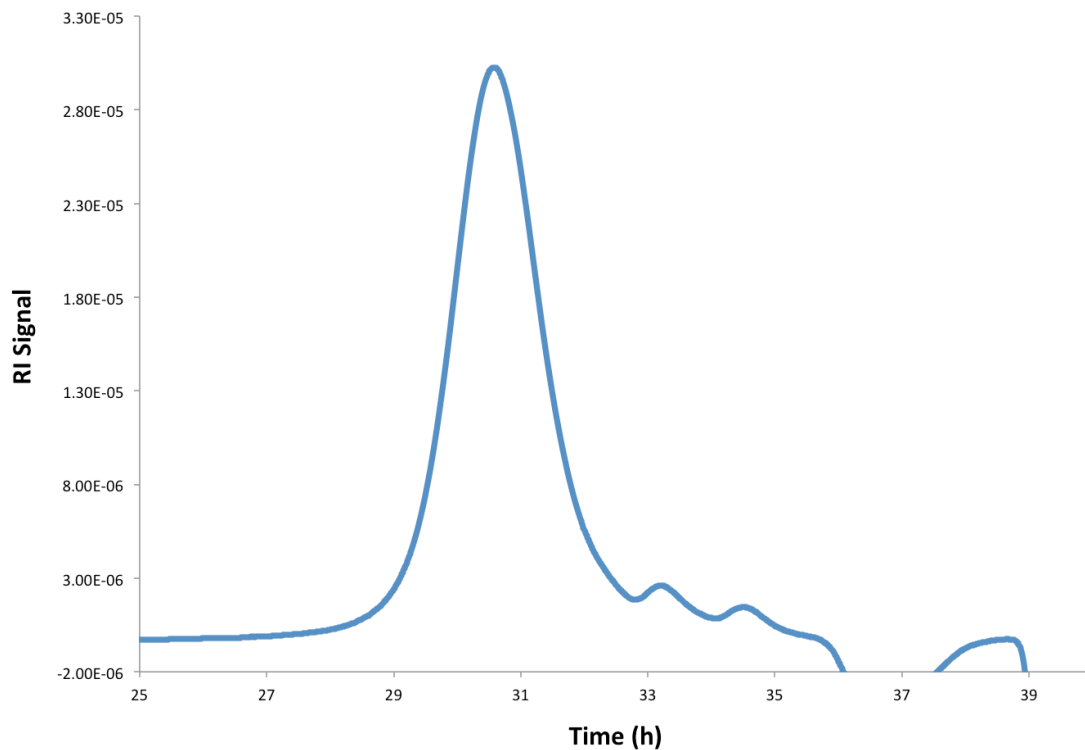


Figure E101. Table 5.5. Polymerization of SO by F_{36} in CH_2Cl_2 in the presence of blue LED light. $M_n = 1600$ Da, $M_w = 1800$ Da, $\mathcal{D} = 1.16$.

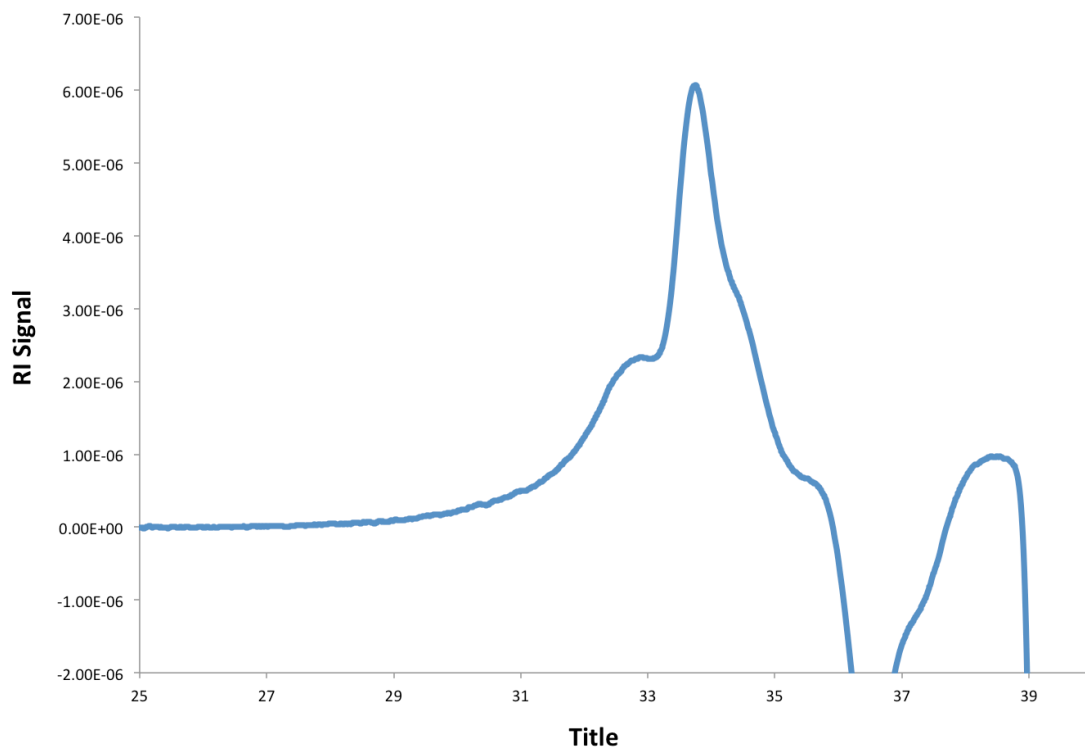


Figure E102. Table 5.5. Polymerization of PO by F₃₆ in CH₂Cl₂ in the presence of blue LED light. M_n = 372 Da, M_w = 472 Da, \mathcal{D} = 1.27.

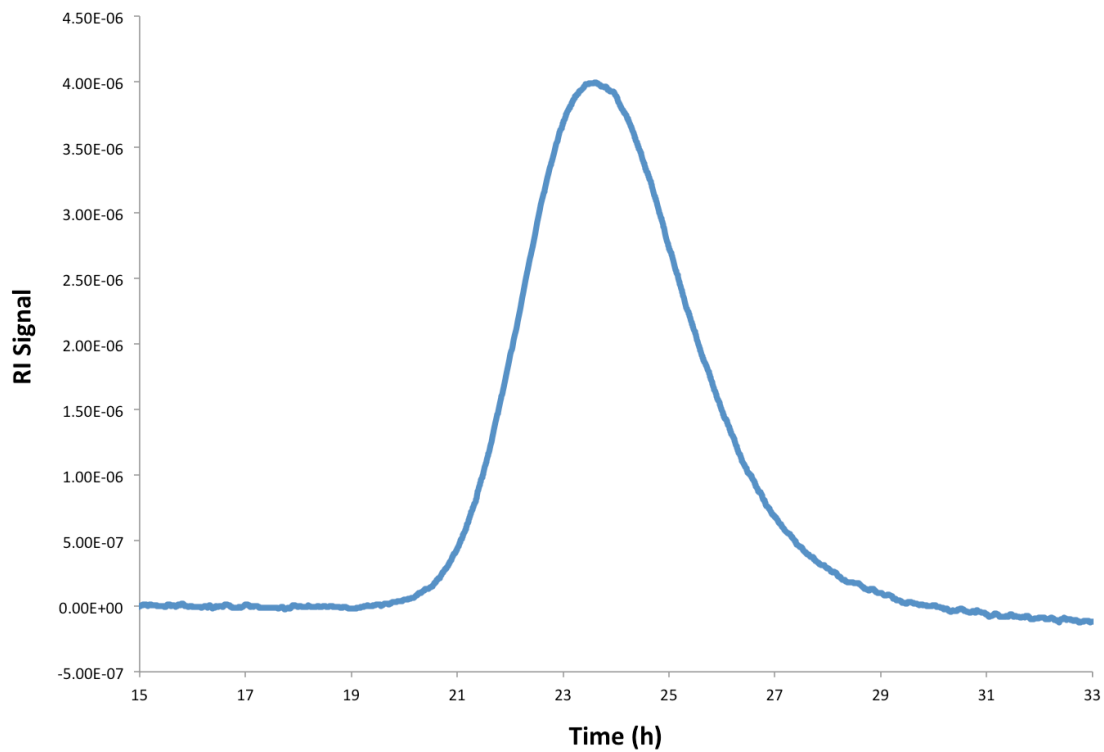


Figure E103. Table 5.5. Polymerization of CHO by F₃₆ in F₂C₆H₄ in the dark. M_n = 71900 Da, M_w = 110000 Da, \mathcal{D} = 1.53.

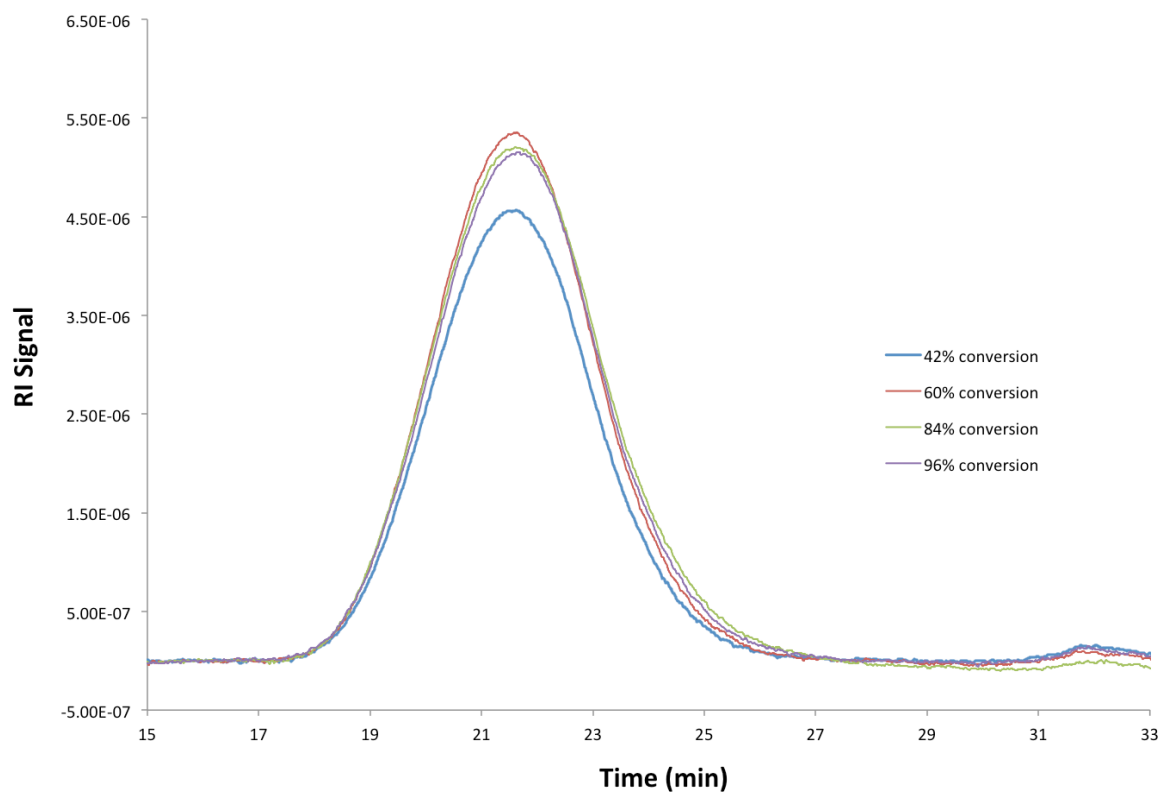


Figure E104. Table 5.5. Molecular weight of PCHO at different points of conversion.

References

1. Grimes, R., *J. Chem. Educ.*, 2004, **81**, 657.
2. B. Dash, R. Satapathy, J. Maguire, N. Hosmane, *New J. Chem.*, 2011, **35**, 1955-1972.
3. Z. Lesnikowski, *J. Med. Chem.*, 2016, **59**, 7738–7758.
4. R. Grimes, *Carboranes*, Academic Press, 2016.
5. H. C. Longuet-Higgins, M. de V. Roberts, *Proc. R. Soc. London, Ser. A*, 1955, **230**, 110–119.
6. A. R. Pitochelli and F. M. Hawthorne, *J. Am. Chem. Soc.*, 1960, **82**, 3228–3229.
7. (a) I. B. Sivaev, V. I. Bregadze and S. Sjöberg, *Collect. Czech. Chem. Commun.*, 2002, **67**, 679–727.
(b) M. Davidson, A. K. Hughes, T. B. Marder, K. Wade, *Contemporary Boron Chemistry*, Royal Chemistry Society, 2000, vol. 253.
(c) N. S. Hosmane, *Boron Science: New Technologies and Applications*, Taylor & Francis, 2011.
(d) C. Knapp, *Comprehensive Inorganic Chemistry II*, Elsevier, 2013, pp. 651–679.
(e) D. Olid, R. Núñez, C. Viñas and F. Teixidor, *Chem. Soc. Rev.*, 2013, **42**, 3318-3336.
(f) V. Geis, K. Guttsche, C. Knapp, H. Scherer and R. Uzun, *Dalton Trans.*, 2009, **15**, 2687-2694.
8. A. I. Wixtrom, Y. Shao, D. Jung, C. W. Machan, S. N. Kevork, E. A. Qian, J. C. Axtell, S. I. Khan, C. P. Kubiak, A. M. Spokoyny, *Inorg. Chem. Front.*, 2016, **3**, 711.
9. T. Peymann, C. B. Knobler, S. I. Khan and M. F. Hawthorne, *Angew. Chem., Int. Ed.*, 2001, **40**, 1664–1667.
10. M. S. Messina, J. C. Axtell, Y. Wang, P. Chong, A. I. Wixtrom, K. O. Kirlikovali, B. M. Upton, B. M. Hunter, O. S. Shafaat, S. I. Khan, J. R. Winkler, H. B. Gray, A. N. Alexandrova, H. D. Maynard, A. M. Spokoyny, *J. Am. Chem. Soc.*, 2016, **138**, 6952–6955.
11. E. A. Qian, A. I. Wixtrom, J. C. Axtell, A. Saebi, D. Jung, P. Rehak, Y. Han, E. H. Mouilly, D. Mosallaei, S. Chow, M. Messina, J.-Y. Wang, A. T. Royappa, A. L. Rheingold, H. D. Maynard, P. Kral, A. M. Spokoyny, *Nature Chem.*, 2017, **9**, 333-340.
12. (a) M. Thiam, N. Spassky, *Macromol. Chem. Phys.*, 1999, 200, **9**, 2107-2110.

- (b) M. G. Mikhael, A. B. Padias, H. K. Hall Jr., *Macromolecules*, 1995, **28**, 5951–5954.
- (c) A. Aouissi, Z. A. Al-Othman, A. Salhabi, *Int. J. Polym. Sci.*, 2015, **2015**, 826512.
- (d) D. Chakraborty, D. Mandal, V. Ramkumar, V. Subramanian, J. V. Sundar, *Polym. J.*, 2015, **56**, 157-170.
- (e) K. C. Kim, C. A. Reed. *J. Am. Chem. Soc.*, 2002, **124**, 7662–7663.
13. Y. Yagci, A. Kornowski, W. Schnabel, *J. Polym. Sci., Part A: Polym. Chem.*, 1992, **30**, 9, 1987-1991.
14. Y. Y. Durmaz, N. Moszner, Y. Yagci, *Macromolecules*, 2008, **41**, 6714–6718.
15. Y. Sarazin, M. Schormann, M. Bochmann, *Organometallics*, 2004, **23**, 3296–3302.
16. N. Merle, K. W. Tornroos, V. R. Jensen, E. J. Le Roux, *J. Organomet. Chem.*, 2011, **696**, 1691-1697.
17. H. Plommer, I. Reim, F. M. Kerton, *Dalton Trans.*, 2015, **44**, 12098-12102.
18. S. Pappuru, R. Chokkapu, D. Chakraborty, V. Ramkumar, *Dalton Trans.*, 2013, **42**, 16412-16427.
19. (a) J. A. Aikins, F. Williams, *Ring-Opening Polymerization*, 1985, **24**, 335-359.
- (b) H. J. Park, C. Y. Ryu, J. V. Crivello, *J. Polym. Sci., Part A: Polym Chem.*, 2013, **51**, 109-117.
20. E. H. Nejad, A. Paoniasari, C. G. W. van Melis, C. E. Koning, R. Duchateau, *Macromolecules*, 2013, **46**, 631–637.
21. (a) C. M. Byrne, S. D. Allen, E. B. Lobkovsky, G. W. Coates *J. Am. Chem. Soc.*, 2004, **126**, 11404–11405.
- (b) L. P. Carrodegua, J. Gonzalez-Fabra, F. Castro-Gomez, C. Bo, A. W. Kleij, *Chem. Eur. J.*, 2015, **21**, 6115-6122.
- (c) O. Hauenstein, M. Reiter, S. Agarwal, B. Rieger, A. Greiner, *Green Chem.*, 2016, **18**, 760-770.
- (d) O. Hauenstein, S. Agarwal, A. Greiner, *Nat. Commun.*, 2016, **7**, 11862.
22. (a) A. Corma, S. Iborra, A. Velty, *Chem. Rev.*, 2007, **107**, 2411-2502.

- (b) G. Neri, G. Rizzo, C. Crisafulli, L. De Luca, A. Donato, M. G. Musolino, R. Pietropaolo, *Appl. Cat., A*, 2005, **295**, 116-125
- (c) M. Vicevic, K. V. K. Boodhoo, K. Scott, *Chem. Eng. J.*, 2007, **133**, 43-57
23. A. B. Pangborn, M. A. Giardello, R. H. Grubbs, R. K. Rosen and F. J. Timmers, *Organometallics*, 1996, **15**, 1518-1520.
24. Private communication

Conclusions and Outlook

The field of redox-switchable polymerization has developed in the last ten years to include a number of examples of on-off polymerization switches^{1,2,3,4,5} and a few examples of switchable copolymerization with orthogonal selectivity toward two monomers.^{6,7,8,9} Our group's efforts in this area have yielded Ce,² Y,³ In,³ Pd,⁴ Al,⁵ Ti,⁶ and Zr⁶ complexes capable of redox-switchable polymerizations with olefins, cyclic esters and cyclic ethers. The work presented in this dissertation illustrates the challenges in studying these systems, difficulties in honing the polymerization conditions, and the ways in which developing a redox-switchable initiator can be rewarding.

In Chapter 1, (salfen)In(O^tBu) was initially conceived to be an improvement on the redox-switchable (phosfen)In(OPh), but had an irreversible reversible event. Fortunately, it was discovered to have extremely high polymerization activity with lactones, producing some of the fastest polymerization rates for ϵ -caprolactone, δ -valerolactone, and β -butyrolactone of group 13 metals initiators and was the first indium initiator for δ -valerolactone polymerization.

The redox-switchable copolymerization of L-lactide (LA) and cyclohexene oxide (CHO) was achieved in Chapter 2 using (salfan)Zr(O^tBu)₂. ABA and BAB type block copolymers were synthesized. Though, due to the complicated role of the oxidant, sequential monomer additions were needed. GPC analysis indicated an increase in the hydrodynamic volume of the copolymers after the addition of a PLA block and a decrease after the addition of a PCHO block. However, sequential precipitations, 2D NMR experiments, and DOSY experiments confirmed the formation of block copolymers and indicated that no significant homopolymer impurities are present.

Chapter 3 probed the mechanistic details of redox-switchable copolymerization. One-pot copolymerization methods were found generate significant fractions of homopolymer impurities, which could be separated to some extent by selective precipitations. DFT methods revealed that [(salfan)Zr(O^tBu)₂][BAR^F]'s polymerization of CHO favors a coordination insertion mechanism rather than a cationic mechanism. [(salfan)Zr(O^tBu)₂][BAR^F]'s polymerization of LA was found to be thermodynamically unfavored according to DFT calculations, but experimentally possible after CHO polymerization at 100 °C. We hypothesize that this is an effect of CHO lowering the energy of the LA polymerization product, but more studies are needed. Lastly, the influence of one monomer on the polymerization of another was seen in the different polymerization rates of LA and CHO in different blocks of block copolymers. LA is polymerized more quickly after CHO. CHO is polymerized more slowly after LA. We currently attribute these changes in polymerization rate to effects from residual monomer from the previous block.

In Chapter 4, electrochemical methods were applied to redox-switchable polymerization in order to circumvent the need for chemical oxidants and reductants. The initial studies into the bulk electrolysis of (salfan)Zr(O^tBu)₂ revealed challenges in cell design and electrolyte choice. Employing an H-cell and TPABAR^F as an electrolyte has resolved these issues and allowed for the synthesis of block copolymers. However, maintaining a rigorously water and oxygen free environment remains an obstacle toward improving control over these polymerizations.

In a departure from ferrocene-based ligand complexes, Chapter 5 surveyed functionalized dodecaborate clusters as oxidants for (salfan)Zr(O^tBu)₂ and initiators for epoxide polymerization. One equivalent of dodecaborate F₃₆ was shown to oxidize two equivalents of (salfan)Zr(O^tBu)₂ by utilizing its high redox potentials. Very high molecular weight polymers of CHO were

synthesized by F₃₆, F₆₀, and F₇₂, up to 190 kDa within two hours. The polymerization of other epoxides was less successful.

Although there has been a significant progress in the field of redox-switchable copolymerization, there is still much room for improvement. Monomer scopes are currently limited within classes of molecules (lactones, olefins, etc). Expansion beyond these classes is necessary to synthesize novel materials with unique physical properties. *In situ* redox-switchable copolymerizations often suffer from competing side reactions between the oxidant and monomer. Elimination of these side reactions via bulk electrolysis or judicious choice of oxidant can offer greater control over these polymerizations. Lastly, the chemistry that governs the selectivity of an initiator toward a monomer in the oxidized or reduced state is still unsolved. DFT and various statistical methods may be helpful in drawing conclusions, finding trends, and hopefully one day predicting new redox-switchable polymerization initiators.

Below are a number of short studies that may be useful in initiating future projects.

Appendix F.

F1. Synthesis of (salfen)InOAr

In Chapter 1, it was found that (salfen)In(O^tBu) has high activity in the polymerization of lactones, but shows irreversible redox behavior. The redox-switchable indium complex that was previously published by our group, (phosfen)In(OPh),³ utilized a phenoxide instead of an alkoxide group. Therefore, we attempted to synthesize several indium aryloxide variations of (salfen)In(O^tBu) to find a redox-switchable highly active indium compound.

Potassium aryloxides were prepared from potassium hydride and phenols (Figure F1.1). Afterwards, the potassium salts were combined with (salfen)InCl to yield (salfen)InOAr (Figure F1.2). Although the synthesis of (salfen)InOAr^{2,6-di-Me} and (salfen)InOAr^{2,4-di-tBu} were successful,

(salfen)InOPh could not be made cleanly. Cyclic voltammetry was used to assess the redox behavior of these compounds. (salfen)InOAr^{2,4-di-tBu} showed a quasi-reversible redox event around 0.45 V and an irreversible oxidation event at 1.6 V (Figure F1.5). (salfen)InOAr^{2,6-di-Me} showed a reversible event around 0.20 V and an ill-defined event at -1.4 V (Figure F1.6). Both of these compounds have yet to be studied for the polymerization lactide and lactones. (salfen)InOAr^{2,6-di-Me} in particular may be a good candidate for redox-switchable catalysis.

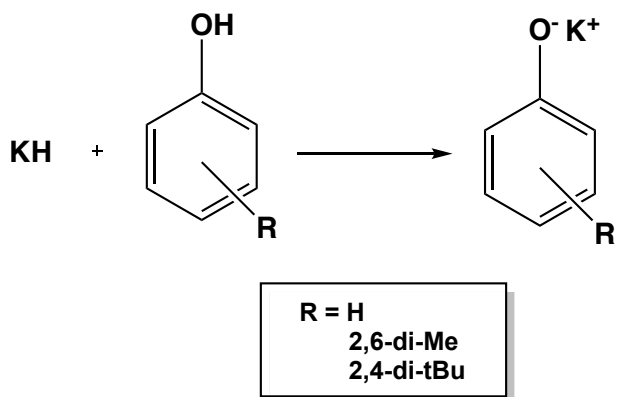


Figure F1.1. Synthesis of potassium aryloxide (R = Me, H).

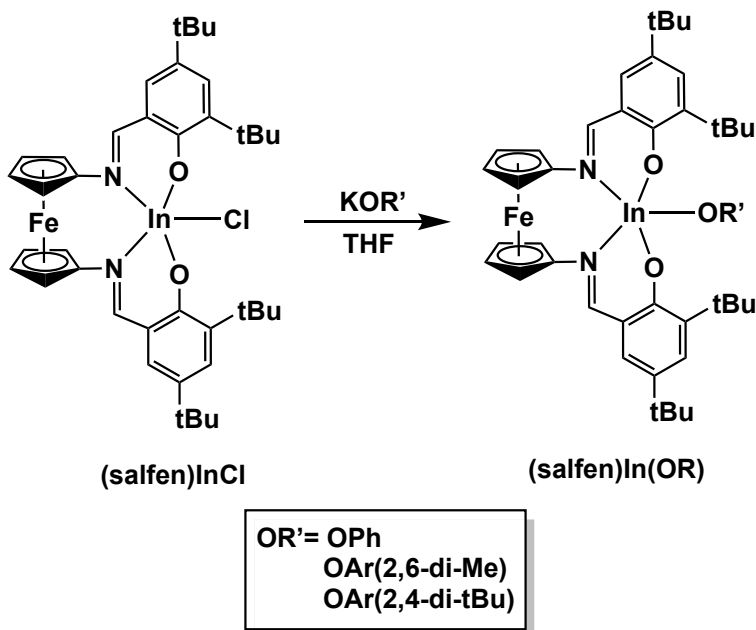


Figure F1.2. Synthesis of (salfen)InOAr variations.

Synthesis of KOPh

Phenol was dissolved in THF. A THF slurry of KH was added dropwise. Bubbling indicated the release of hydrogen gas. Solution turned clear over an hour. Solution was filtered, concentrated and layered with hexanes. Crystals formed overnight and were collected for KOPh(2,6-di-methyl) (97.8mg, 72.6%). Very few crystals formed for KOPh.

Synthesis of (salfen)InOAr^(2,4-di-tBu)

KOPh(2,4-di-tBu) was washed with hexanes and recrystallized in tetrahydrofuran. (salfen)InCl was recrystallized from diethyl ether. (salfen)InCl (50.0 mg, 0.0628 mmol) was dissolved in THF. A THF solution of KOPh(2,4-di-tBu) (19.6 mg, 0.0690 mmol) was added dropwise. Reaction was stirred for 45 minutes. Volatiles were removed. Crude product was dissolved in hexanes. Solution was filtered through Celite. Solvent was removed in vacuo.

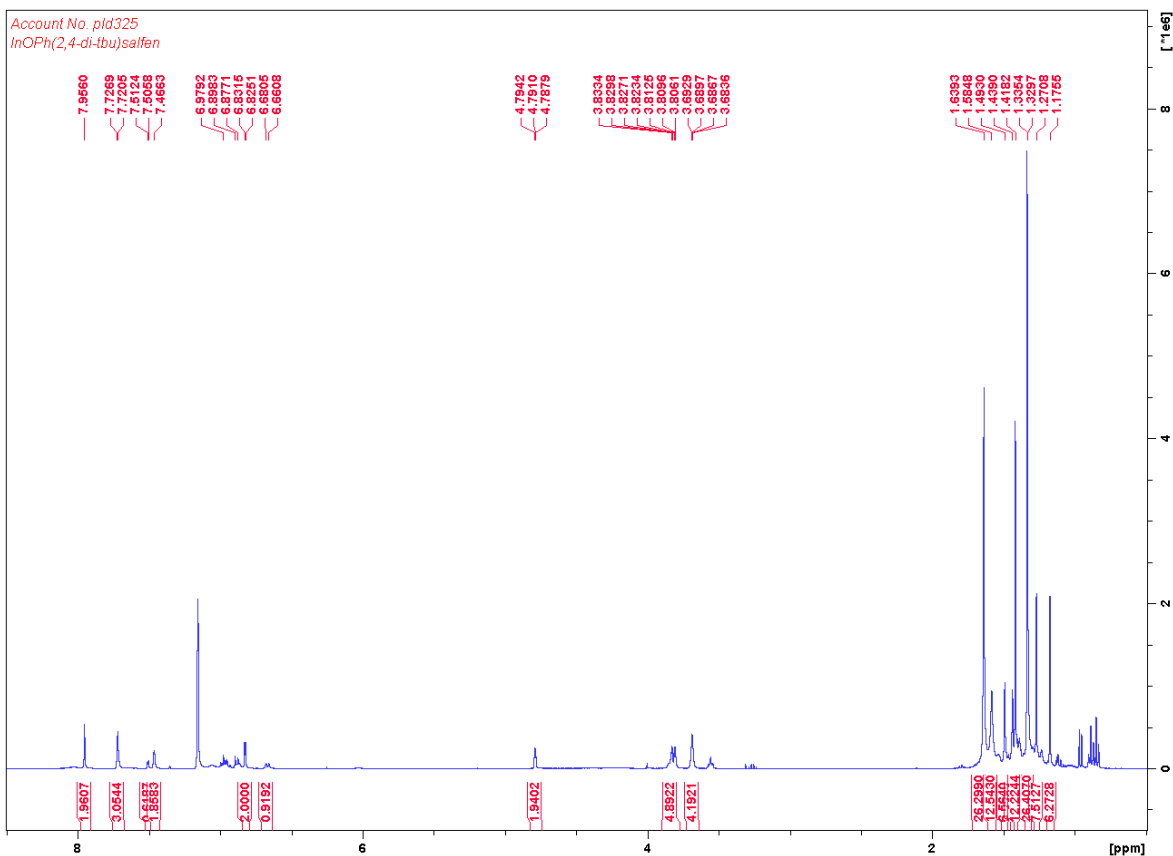


Figure F1.3. ^1H NMR spectrum (300 MHz, C_6D_6) of $(\text{salfen})\text{InOAr}^{(2,4\text{-di-tBu})}$ ppm: 7.96 (s, 2H, ArH), 7.72 (d, 2H, ArH), 7.46 (d, 1H, ArH), 6.88 (dd, 1H, ArH), 6.83 (d, 2H, NCH), 6.67 (d, 1H, ArH), 4.76 (q, 2H, fcH), 3.81 (dq, 4H, fcH), 3.69 (q, 2H, fcH), 1.64 (s, 27H, CH_3), 1.34 (s, 27H, CH_3).

Synthesis of $(\text{salfen})\text{InOAr}^{(2,6\text{-di-Me})}$

$(\text{salfen})\text{InCl}$ was dissolved in diethyl ether. $\text{KOAr}(2,6\text{-di-Me})$ was dissolved separately in diethyl ether. $\text{KOAr}(2,6\text{-di-Me})$ was added to $(\text{salfen})\text{InCl}$ and stirred for one hour. Solution was filtered through Celite, concentrated and layered with hexanes.

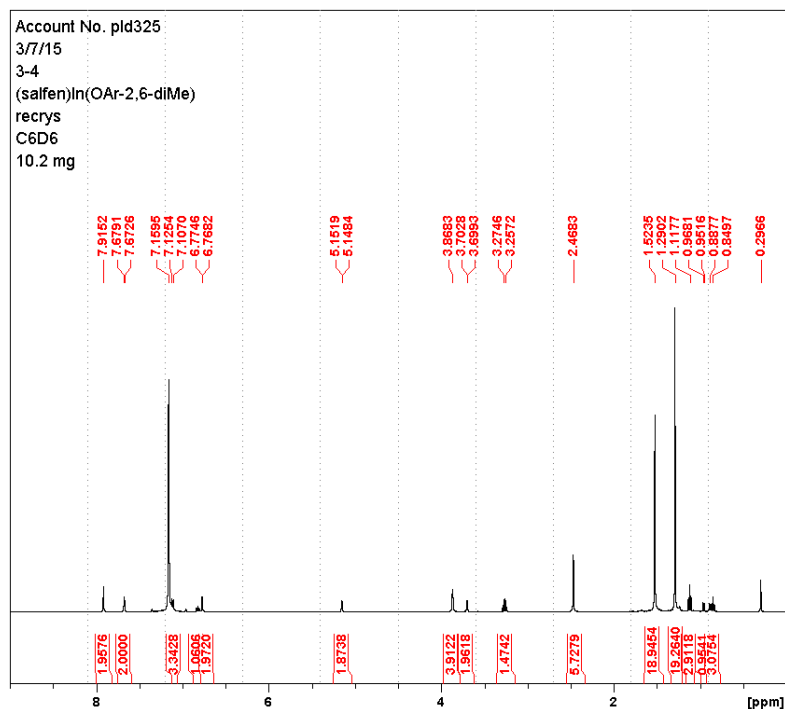


Figure F1.4. ^1H NMR spectrum of (salfen)InOAr^(2,6-di-Me) (300 MHz, C_6D_6) ppm: 7.91 (s, 2H, ArH), 7.68 (d, 2H, ArH), 7.12 (d, 2H, ArH), 6.81 (t, 1H, ArH), 6.77 (d, 2H, NCH), 5.15 (s, 2H, fcH), 3.87 (s, 4H, fcH), 3.69 (s, 2H, fcH), 2.47 (s, 6H, CH_3), 1.53 (s, 18H, CH_3), 1.29 (s, 18H, CH_3).

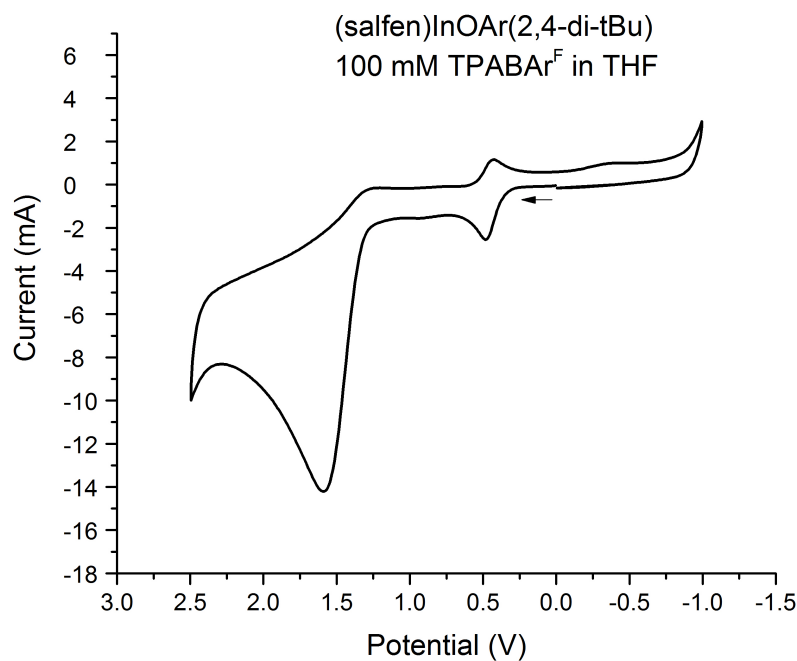


Figure F1.5. Cyclic voltammogram of 1.0 mM (salfen)InOAr^(2,4-di-tBu) recorded with a glassy carbon electrode at 100 mV/s in THF, 0.010 M $[(\text{C}_3\text{H}_7)_4\text{N}][\text{BAr}_4^{\text{F}}]$. $E_{1/2} = 0.45$ V.

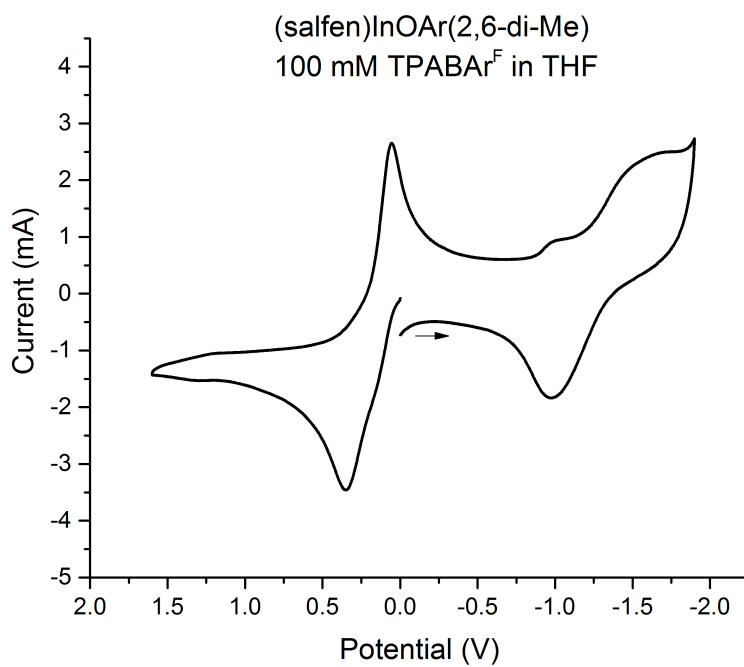


Figure F1.6. Cyclic voltammogram of 1.0 mM (salfen)InOAr^(2,6-di-Me) recorded with a glassy carbon electrode at 100 mV/s in THF, 0.010 M [(C₃H₇)₄N][BAr^F₄]. $E_{1/2} = 0.20$ V.

F2. Radical ring-opening polymerization by (salfen)In(O^tBu)

As noted in Chapter 1, attempts to oxidize (salfen)In(O^tBu) with AgOTf resulted in the cleavage of the In-O bond and replacement of O^tBu with OTf. One can take advantage of this bond cleavage to initiate a radical polymerization.

(salfen)In(O^tBu) (4.2 mg, 0.005 mmol) in 0.15 mL C₆H₆ and 1,3,5-trimethoxybenzene (8.4 mg, 0.005 mmol) in 0.15 mL C₆H₆ were added to a J-Young tube. The solution was dried and 0.40 mL C₆D₆ was added followed by 0.10 mL of 50 mM solution of cyclohexene oxide. The reaction was heated to 100 degrees for 21 hours with no change. AgOTf (1.3 mg, 0.005 mmol) was added and the solution turned brown. After 3.5 h at room temperature 26% of the CHO polymerized. After heating to 100 degrees overnight, the polymerization reached 30%. Excess CoCp₂ was added. No additional polymerization occurred.

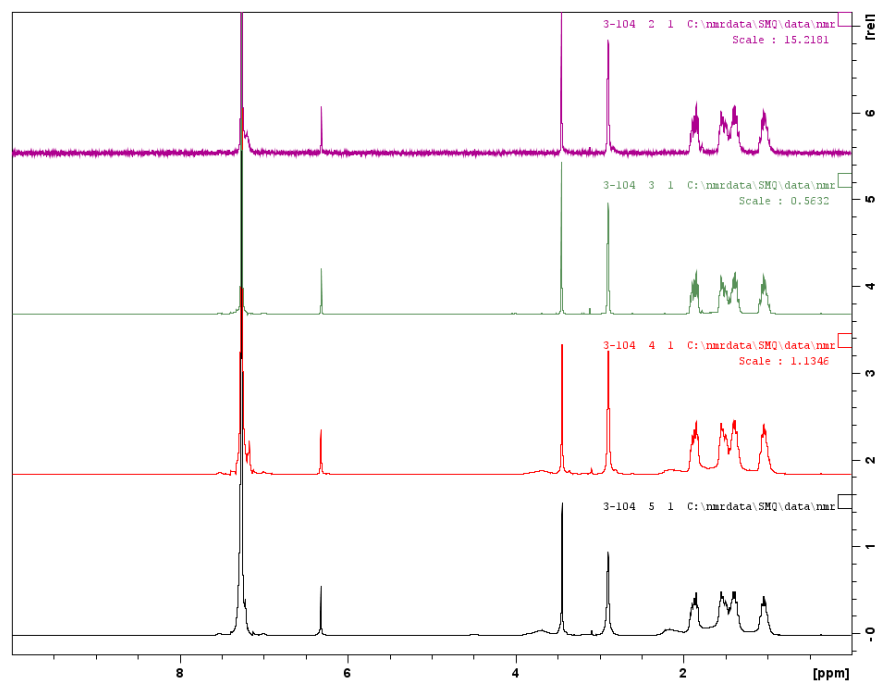


Figure F2.1. Polymerization of CHO by oxidation of (salfen)In(O^tBu). Initial mixture of (salfen)In(O^tBu), 1,3,5-trimethoxybenzene and CHO after 1 hour at 100 °C (top), after 1 day at 100 °C (second from top), after addition of AgOTf (second from bottom), and after 4 hours at room temperature (bottom). For a more detailed version of the bottom spectrum, see Figure F2.2.

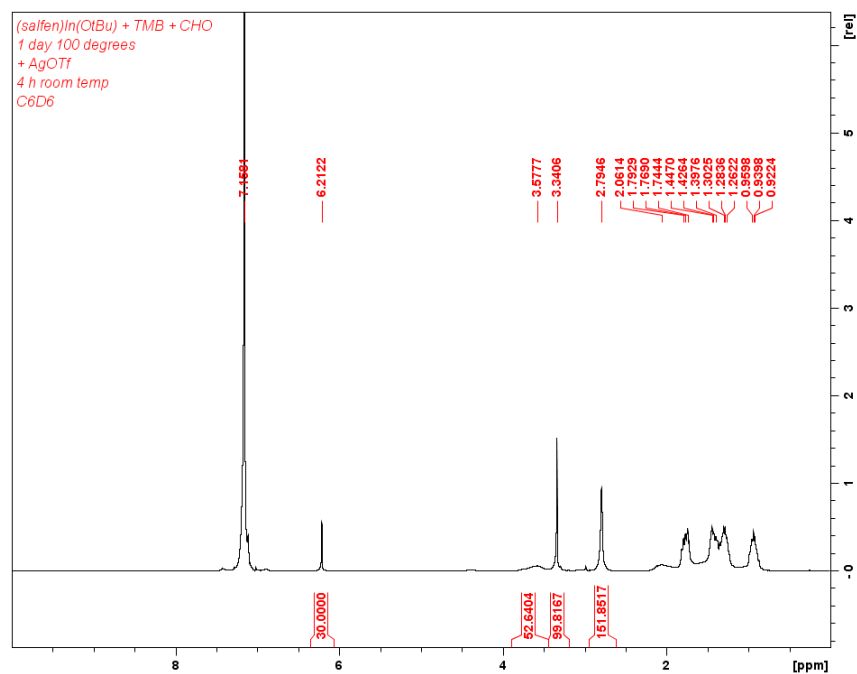


Figure F2.2. Polymerization of CHO by oxidation of (saifen)In(O^tBu) after 1 day. ¹H NMR spectrum (300 MHz, C₆D₆) ppm: 6.21 (s, 3H, CH TMB), 3.58 (b, 2H, CH PCHO), 3.41 (s, 9H, CH₃ TMB), 2.79 (s, 2H, CH CHO), 2.06 (m, 2H, CH₂ PCHO), 1.78 (m, 2H, OCHCH₂ CHO), 1.43 (m, 2H, OCHCH₂ CHO), 1.28 (m, 2H, OCHCH₂CH₂ CHO), 0.94 (m, 2H, OCHCH₂CH₂ CHO).

F3. Copolymerization of lactones by (salfen)In(O^tBu)

As described in Chapter 1, (salfen)In(O^tBu) was found to be extremely active toward a number of cyclic esters. To take advantage of this reactivity, large block copolymers were synthesized using sequential monomer additions (Table F.3.1).

Table F3.1. Block copolymers made by (salfen)In(O^tBu)

Monomer 1	Monomer 2	Monomer 3	Time (h)	Conversion ^a	M _{n,theo} ^b	M _{n,exp} ^c	D ^d
LA	CL	LA	4-15-4.5	99.5-94-100	19.7	16.5	1.28
LA	TMC	LA	2-24-4	97.1-98.8-99	19.5	21.2	1.04

Conditions: [M]/[I] = 100, [M] = 0.50 mM, 25 °C, C₆D₆ as solvent, 1,3,5-trimethoxybenzene as an internal standard. LA = lactide, CL = ε-caprolactone, TMC = trimethylene carbonate. ^a Determined by integration of polymer versus monomer peak. ^b Calculated by integrating internal standard against polymer peaks. ^c Determined by GPC-MALS. ^d D = M_w/M_n.

(salfen)In(O^tBu) (4.2 mg, 0.005 mmol) in 0.15 mL C₆H₆ was added to an J-Young tube and dried. 0.35 mL C₆D₆ was added. Monomers (0.25 mmol) were added and the reaction was monitored to near completion before the next monomer was added. LA = 36 mg, CL = 28.5 mg, TMC = 25.7 mg. 1,3,5-trimethoxybenzene was added at the end to determine theoretical molecular weight. Polymer was precipitated in cold methanol and collected as a solid.

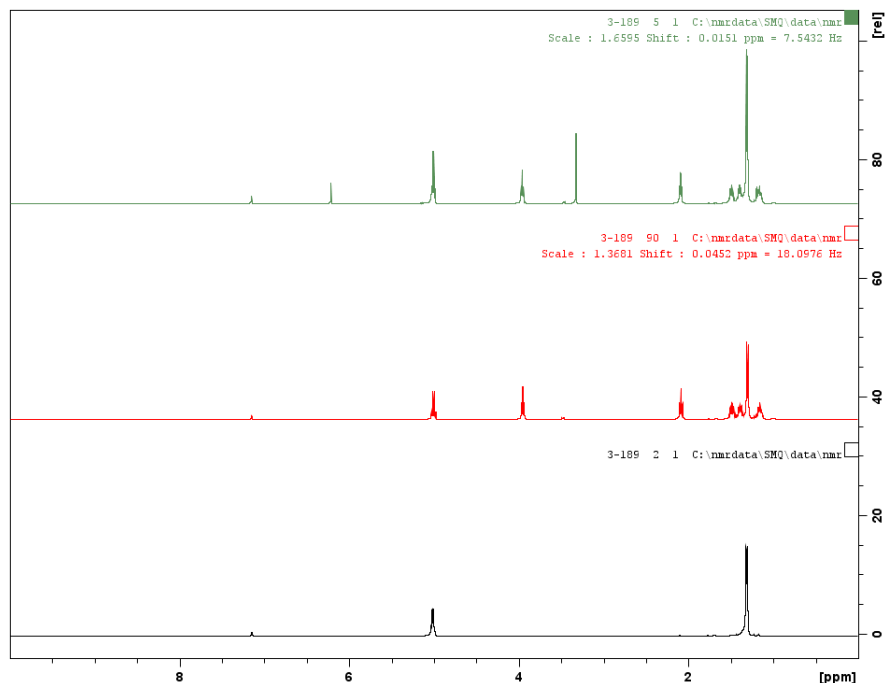


Figure F3.1. Table F3.1, entry 1. Overlay of ^1H NMR spectra from sequential polymerization of LA-CL-LA. LA first block (bottom) CL second block (middle) LA third block (top).

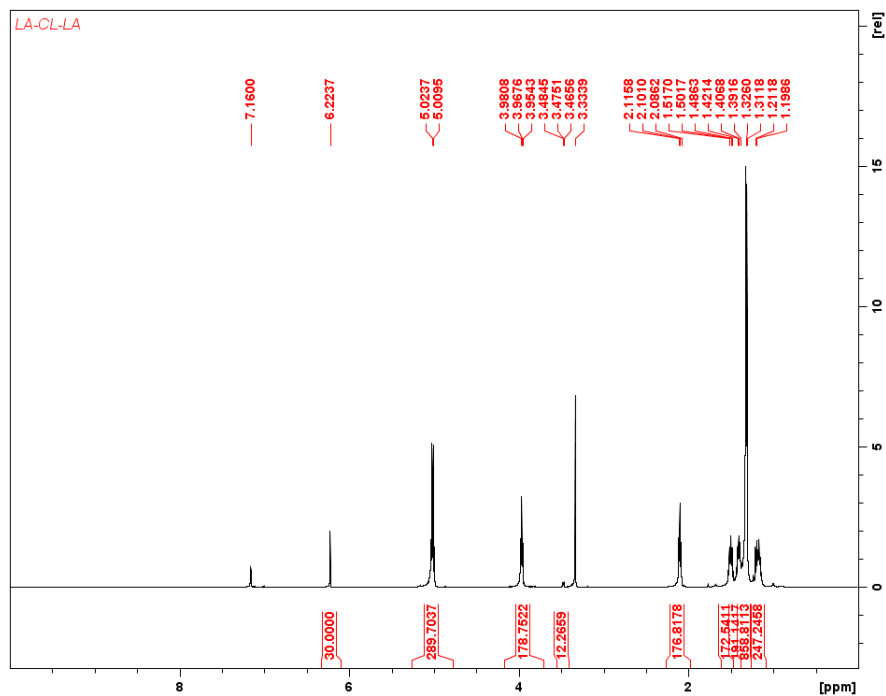


Figure F3.2. Table F3.1, entry 1. LA-CL-LA. ^1H NMR (300 MHz, 25 °C, C_6D_6), δ (ppm): 6.22 (s, 3H, CH TMB), 5.01 (q, 3H, CH PLA), 3.97 (q, 2H, CH₂ PCL), 3.33 (s, 9H, CH₃ TMB), 2.11 (q, 2H, CH₂ PCL), 1.51 (m, 2H, CH₂ PCL), 1.41 (m, 2H, CH₂ PCL), 1.32 (d, 6H, CH₃ PLA), 1.20 (m, 2H, CH₂ PCL).

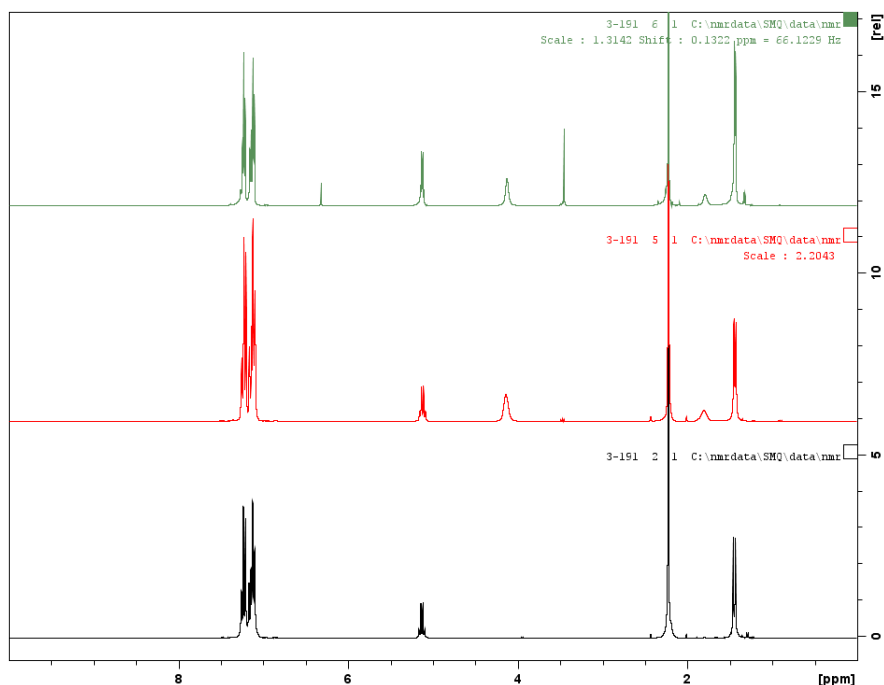


Figure F3.3. Table F3.1, entry 2. Overlay of ^1H NMR spectra from sequential polymerization of LA-TMC-LA. LA first block (bottom), TMC second block (middle), LA third block (top).

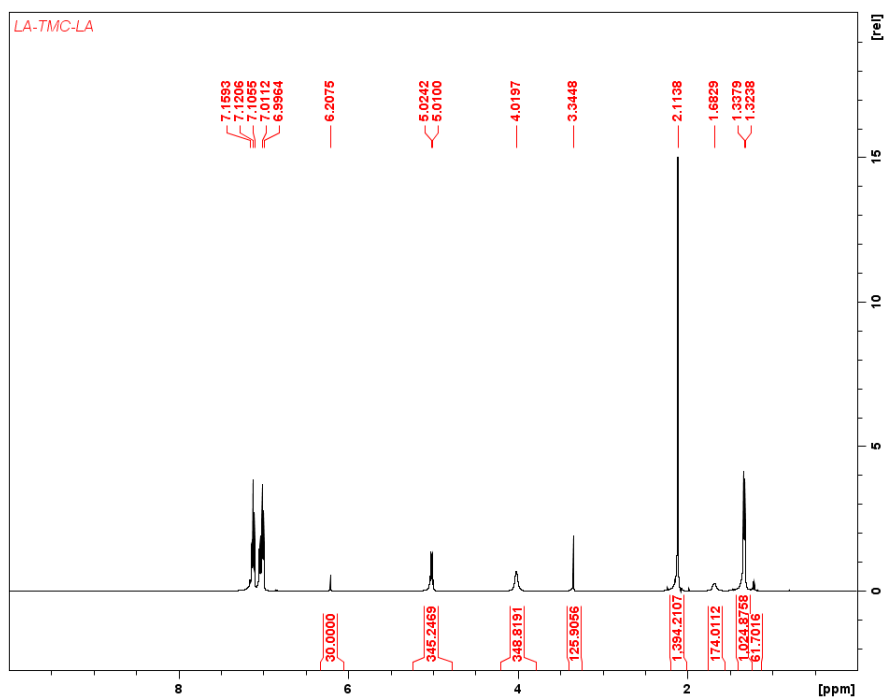


Figure F3.4. Table F3.1, entry 2. LA-TMC-LA. ^1H NMR spectrum (300 MHz, 25 °C, C_6D_6), δ (ppm): 7.12 (toluene), 7.00 (toluene), 6.21 (s, 3H, CH TMB), 5.02 (q, 3H, CH PLA), 4.02 (m, 4H, CH_2 PTMC), 3.34 (s, 9H, CH_3 TMB), 2.11 (toluene), 1.68 (m, 2H, CH_2 PTMC), 1.33 (d, 6H, CH_3 PLA).

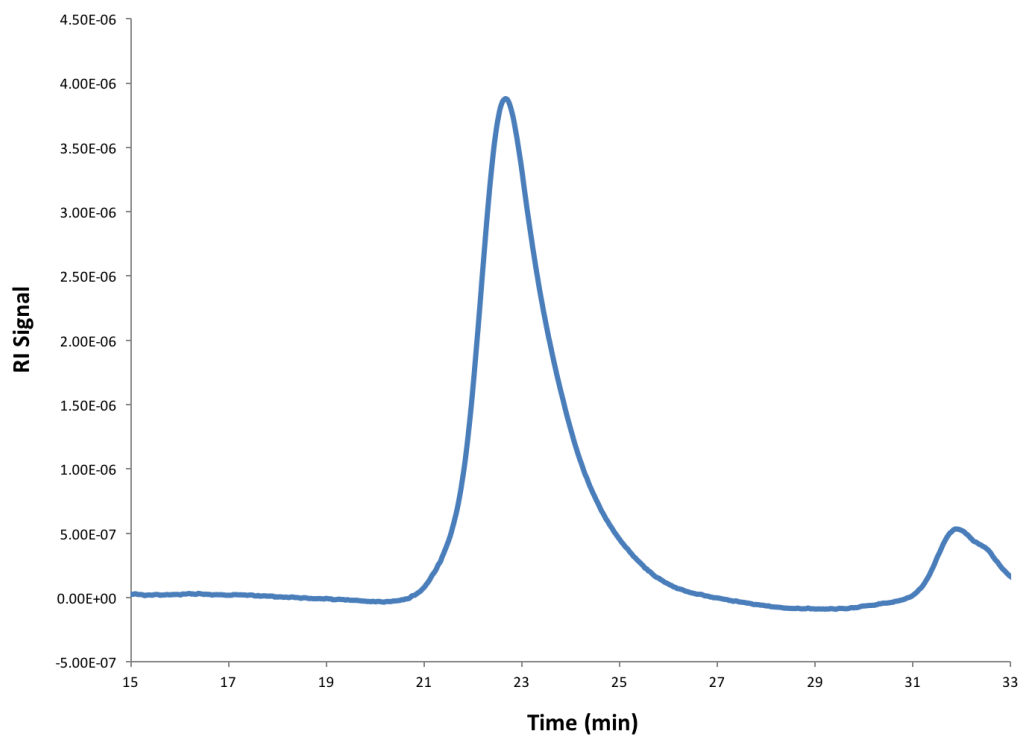


Figure F3.5. Table F3.1, entry 1. GPC trace of LA-CL-LA. $M_n = 16500$ Da, $M_w = 21100$ Da, $D = 1.28$.

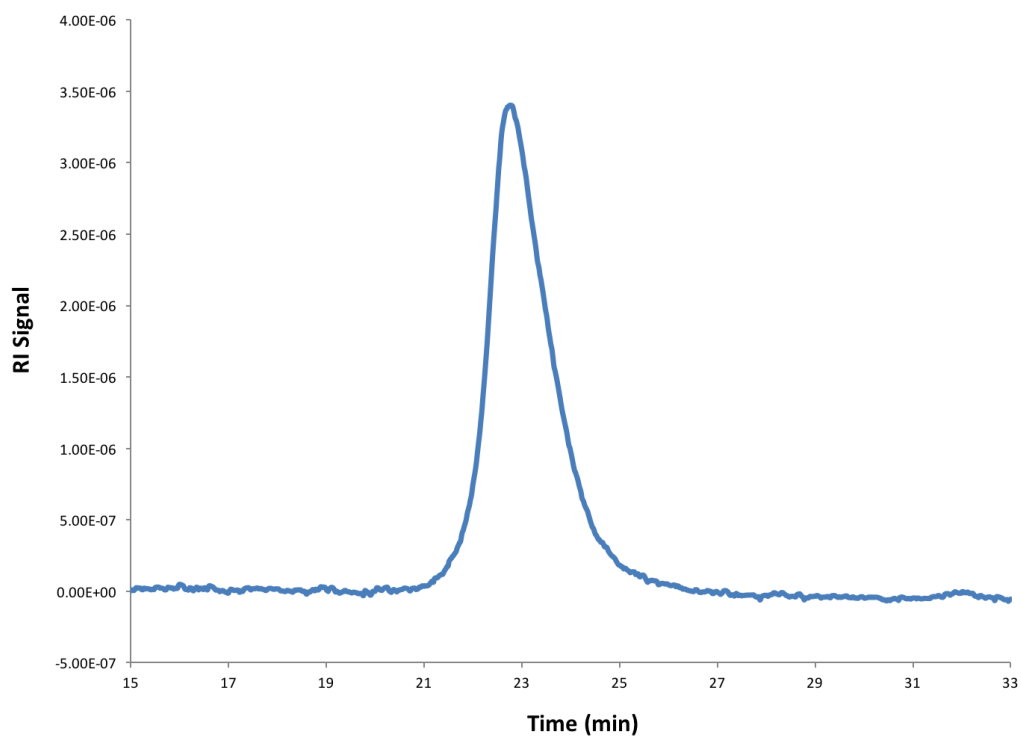


Figure F3.6. Table F3.1, entry 2. GPC trace of LA-TMC-LA. $M_n = 20400$ Da, $M_w = 21200$ Da, $D = 1.04$.

F4. Asymmetric salen ligands

Asymmetric ligand frameworks are sometimes employed to synthesize isotactic polymers by favoring an orientation for the incoming monomer. Non-planar M(ONNO) complexes are a common design for these polymerization catalysts and can be synthesized with salen, salalen, or salalen type ligands (Figure F4.1).¹⁰

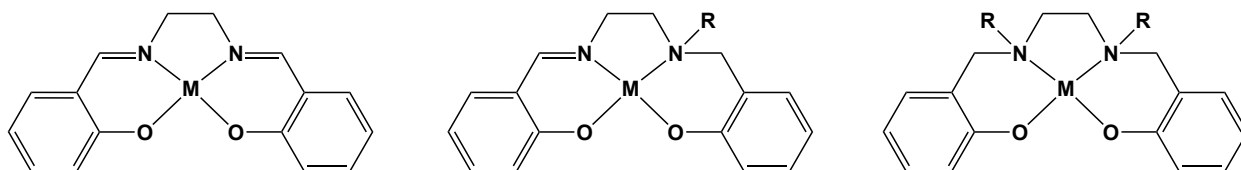


Figure F4.1. M(ONNO) complexes with salen (left) salalen (middle) and salalen (right) ligands.

The following ligands were made accidentally.

Synthesis of H₂salfan (H and Me)

salfan*(OBn)₂ (134.8 mg, 1.67 mmol) in THF was added to a slurry of NaH (71 mg, 1.67 mmol) in THF. Reaction was stirred for one minute. MeI (237.7 mg, 1.67 mmol) in THF was added. Reaction was stirred for one minute then sealed and heated to 60 °C for 24 h. It was likely that the NaH batch was not pure and thus only half of the ligand was methylated.

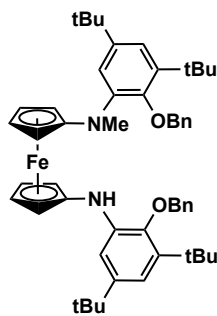


Figure F4.2. H₂salfan (H and Me).

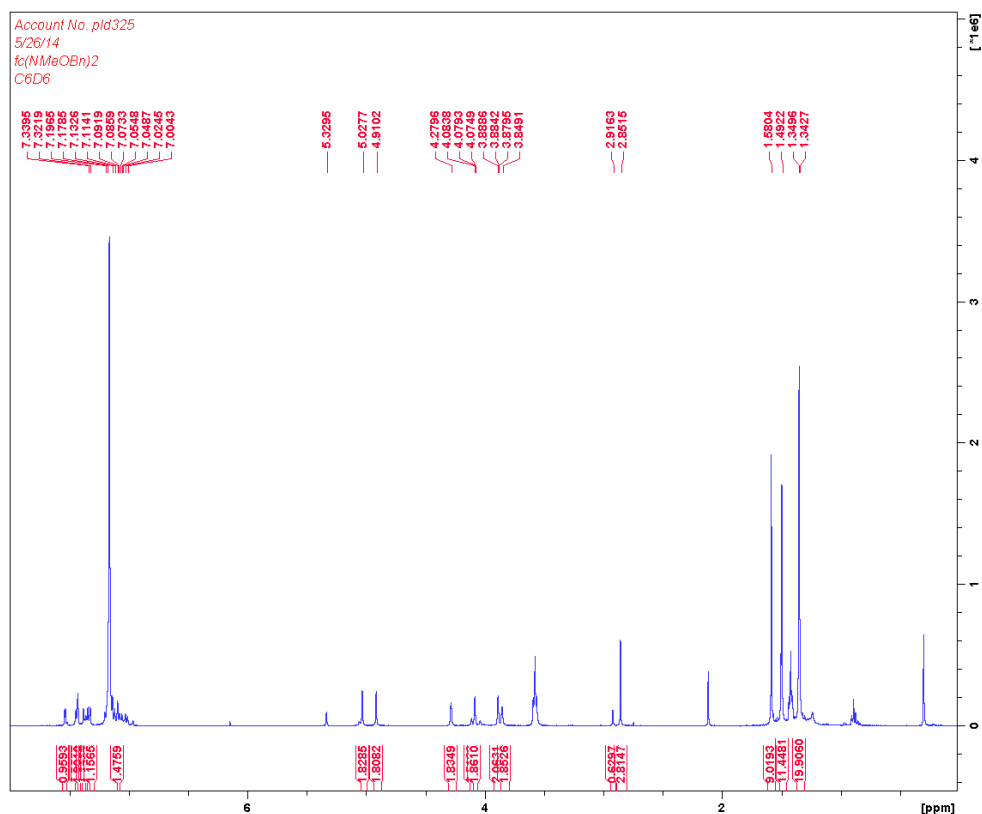


Figure F4.3. H₂salfan (H and Me). ¹H NMR spectrum (400 MHz, C₆D₆) ppm: 7.53 (1H, ArH), 7.44 (1H, ArH), 7.42 (2H, ArH), 7.37 (1H, ArH), 7.35 (1H, ArH), 7.34 (1H, ArH), 7.32 (1H, ArH), 7.09 (2H, ArH), 5.02 (2H, PhCH₂), 4.91 (2H, PhCH₂), 4.28 (2H, CpH), 4.08 (2H, CpH), 3.88 (2H, CpH), 3.85 (2H, CpH), 2.85 (3H, CH₃), 1.58 (9H, CH₃), 1.49 (9H, CH₃), 1.35 (9H, CH₃), 1.34 (9H, CH₃).

Synthesis of fcNH₂(NH-aryl-OBn)

Pd(dba)₂ (26.6mg, .0463 mmol) was added to dppf (25.8 mg, 0.0463 mmol) in a vial. Reaction was stirred for 30 minutes [color changed from dark orange red to light orange]. Diaminoferrocene (200 mg, 0.926 mmol) in toluene was added to a Schlenk tube, followed by NaO^tBu (266.6 mg, 2.777 mmol), and then benzyl protected 6-bromo-2,4-di-tertbutyl-phenol (695 mg, 1.85 mmol). Pd solution was then added to the Schlenk tube. Reaction was stirred for 15-30 min to relieve pressure, then heated to 100 °C for 24 hours. Solution was filtered over Celite, dried and recrystallized in toluene and hexanes. Solid was collected and washed with hexanes. It is not clear how fcNH₂(NH-aryl-OBn) became mono-substituted.

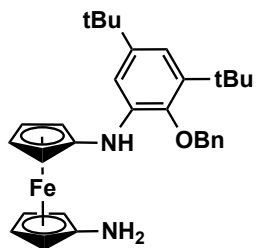


Figure F4.4. fcNH₂(NH-aryl-OBn)

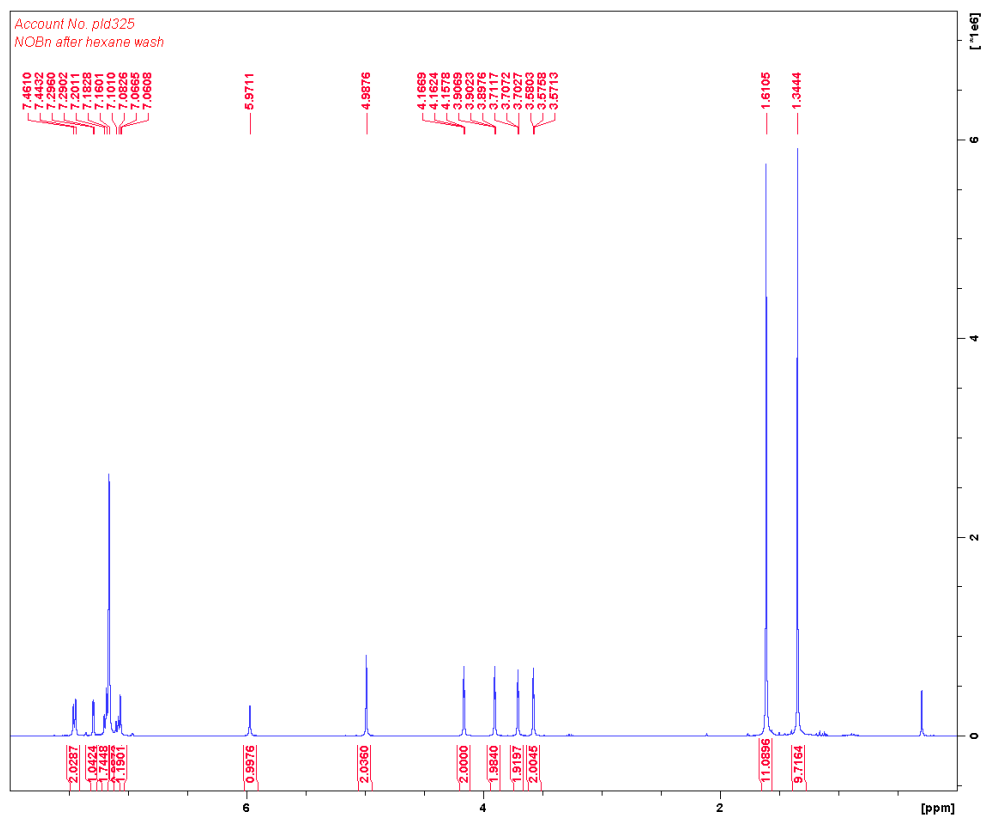


Figure F4.5. fcNH₂(NH-aryl-OBn). ¹H NMR spectrum (400 MHz, C₆D₆) ppm: 7.45 (2H, ArH), 7.29 (1H, ArH), 7.18 (2H, ArH), 7.07 (1H, ArH), 5.97 (1H, NH), 4.99 (2H, PhCH₂), 4.16 (2H, CpH), 3.90 (2H, CpH), 3.71 (2H, CpH), 3.58 (2H, CpH), 1.61 (9H, CH₃), 1.34 (9H, CH₃).

Synthesis of fc(SH)

Fc(Li)₂ (5.00 g, 0.0159 mol) was dissolved in about 100 mL of THF:toluene (1:1) in 250 mL. S₈ (1.01 g, 0.316 mol) was mixed in about 20 mL of THF:toluene (1:1) to create a slurry

then added dropwise over 15 minutes. Reaction was stirred for 2 hours, taken out of the box then quenched with about 50 mL water. About 32 mL of a 1 M HCl solution was added. The product was extracted with diethyl ether. About 8 mL of a 33% KOH solution was added. Product was extracted with water. About 50 mL of 1 M HCl was added. Product was extracted with diethyl ether. Solution was dried with MgSO₄, filtered and dried. Solid was recrystallized in hexanes. It is unclear how fc(SH) became only singly substituted. It is likely that the fc(Li)₂ was not pure.

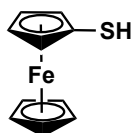


Figure F4.6. fc(SH)

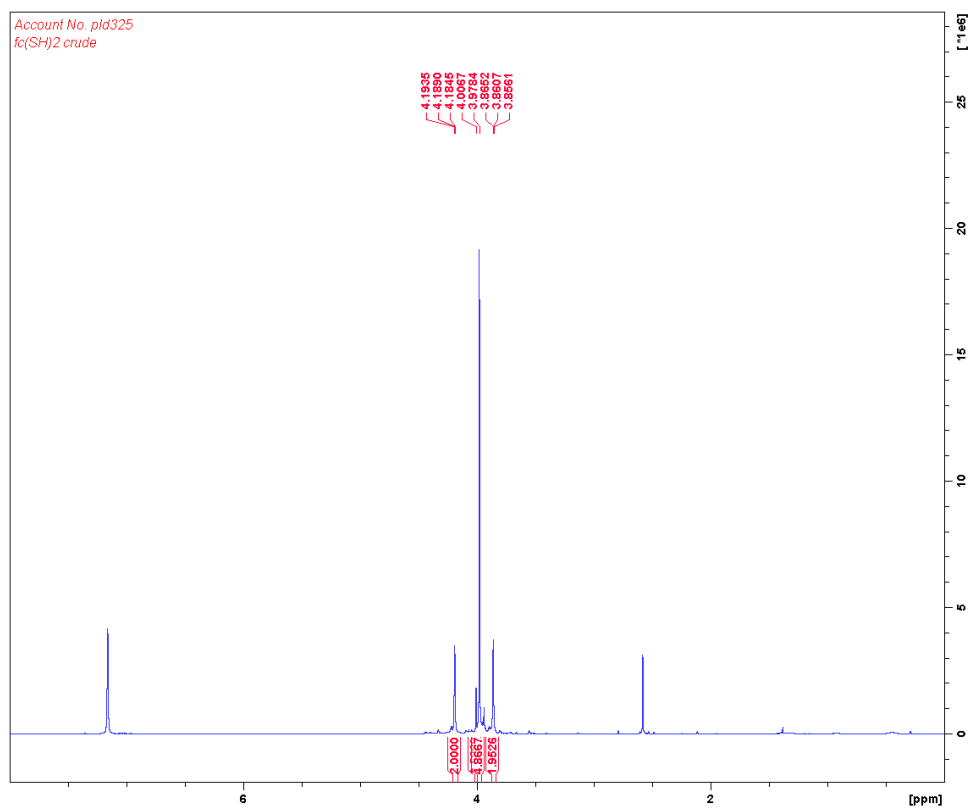


Figure F4.7. fc(SH). ¹H NMR spectrum (400 MHz, C₆D₆) ppm: 4.18 (t, 2H, CpH), 4.00 (ferrocene), 3.98 (s, 5H, CpH), 3.86 (t, 2H, CpH).

F5. Alternating Copolymers of Anhydrides and Epoxides by (salfan)Zr(O^tBu)₂

In the last decade, polyester synthesis from the copolymerization of epoxides and anhydrides has gained much traction.¹¹ Since [(salfan)Zr(O^tBu)₂][BAR^F] showed fast activity with cyclohexene oxide (CHO), several zirconium compounds were tested for copolymerization activity with CHO and succinic anhydride (SA). Gratifyingly, (salfan)Zr(O^tBu)₂ produced an alternating copolymer (Figure F.5.1). As many different types of epoxide and anhydride combinations have been shown to produce polyester copolymers, this is a promising area for future research.

(salfan)Zr(O^tBu)₂ (4.9 mg, 0.005 mmol) in 0.15 mL C₆D₆ was put in a J-Young tube. 0.30 mL C₆D₆ and 0.10 mL o-F₂C₆H₄ were added followed by succinic anhydride (50 mg, 0.50 mmol) and cyclohexene oxide (49 mg, 0.50 mmol). After two days at room temperature, CHO proton signals disappeared. Polymer was precipitated in hexanes and analyzed by ¹H NMR spectroscopy. The signals were consistent with the formation of SA/CHO alternating copolymers.¹²

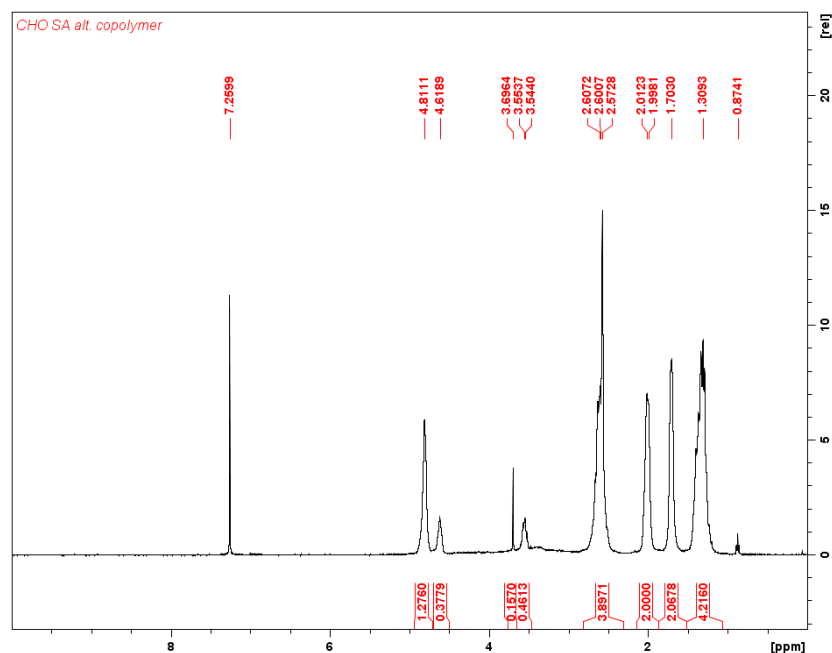


Figure F5.1. SA and CHO copolymer. ^1H NMR spectrum (CDCl_3 300 MHz) ppm: 4.81(m, 2H, OCH PCHO alternating copolymer), 4.62(m, 1H, OCH PCHO end group), 3.70 (m, 4H, CH_2 SA), 3.55 (m, 1H, OCH PCHO end group), 3.40 (m, 2H, OCH PCHO homopolymer), 2.61 (m, 4H, CH_2 PSA alternating copolymer), 2.00 (b, 2H, OCH CH_2 PCHO alternating copolymer), 1.70 (b, 2H, OCH CH_2 PCHO alternating copolymer), 1.31(b, 4H, PCHO OCH CH_2CH_2 alternating copolymer).

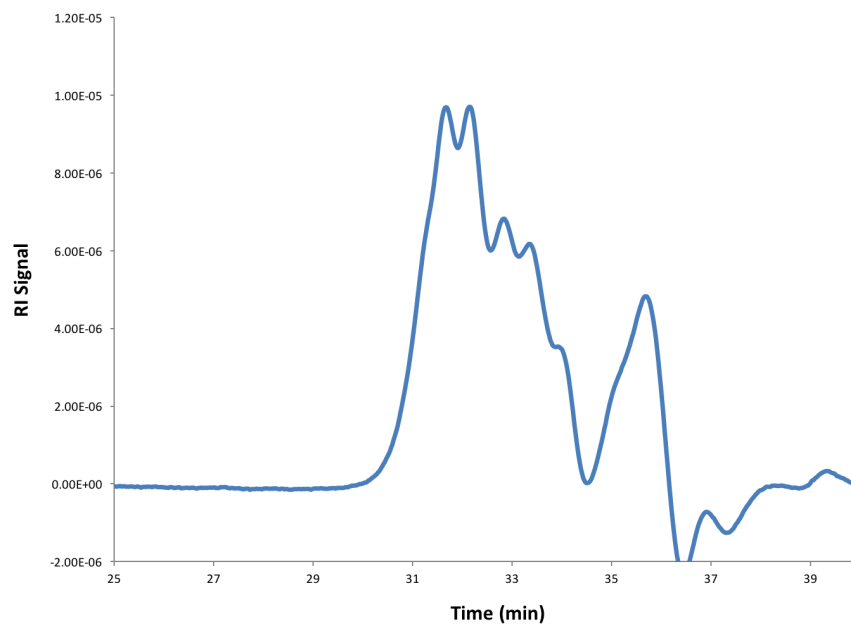


Figure F5.2. GPC trace of SA and CHO copolymer. $M_n = 1069$ Da, $M_w = 2565$, $D = 2.40$.

F6. Polymerization of allyl-CL

The Maynard group has recently produced a new set of biocompatible polymers by installing pendant side groups to allyl-caprolactone (allyl-CL) polymers via a thiol-ene reaction.¹³ Given the high activity of some compounds studied by us toward cyclic esters, we tested (salfen)Zr(O^tBu)₂ and [(salfan)Zr(O^tBu)₂][BAr^F] with allyl-CL.

(salfan)Zr(O^tBu)₂ (0.15 mL, 0.005 mmol) was charged to a J-Young tube followed by 0.10 mL C₆D₆ and TMB (0.15 mL 0.005 mmol). 0.07 mL of allyl-CL (0.5 mmol) was added. No polymer was formed initially (Figure F6.1). The reaction was checked after one hour at room temperature then one hour at 50 °C. After heating at 50 °C overnight there was still no conversion. After monitoring for one day, ^{Ac}FcBAr^F (0.10 mL, 0.005 mmol) was added. When ^{Ac}FcBAr^F was added, a small percentage of polymer formed (Figure F6.2). Heating overnight at 75 °C converted the remaining allyl-CL to polymer (Figure F6.3).

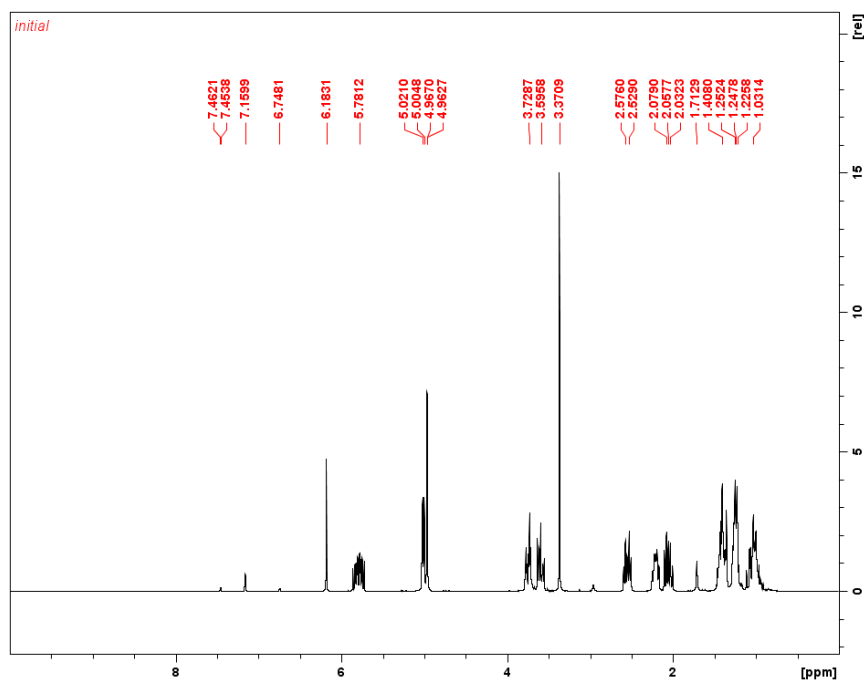


Figure F6.1. (salfen)Zr(O^tBu)₂ and allyl-CL initially. ¹H NMR spectrum (C₆D₆ 300 MHz) ppm: 5.78 (m, 1H, CH₂=CH), 4.98 (m, 2H, CH₂=CH), 3.66 (m, 2H, OCH₂), 2.35 (m, 2H, O=CCHCH₂CH), 2.01 (m, 1H, O=CCH), 1.37 (m, 4H, CH₂CH₂CH₂CH₂O), 1.03 (m, 2H, CH₂CH₂CH₂CH₂O).

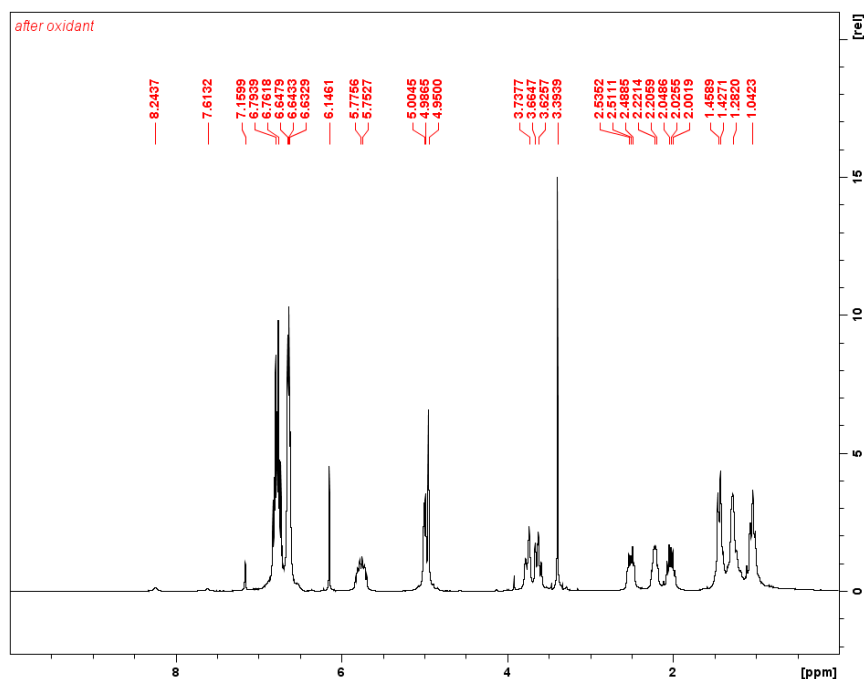


Figure F6.2. (salfan)Zr(O^tBu)₂ and allyl-CL after addition of A^cFcBar^F. ¹H NMR spectrum (C₆D₆ 300 MHz) ppm: 6.78 (difluorobenzene), 6.64 (difluorobenzene), 6.15 (TMB), 5.76 (m, 1H, CH₂=CH), 4.98 (m, 2H, CH₂=CH), 3.66 (m, 2H, OCH₂), (3.39 (TMB), 2.35 (m, 2H, O=CCHCH₂CH), 2.01 (m, 1H, O=CCH), 1.37 (m, 4H, CH₂CH₂CH₂CH₂O), 1.04 (m, 2H, CH₂CH₂CH₂CH₂O).

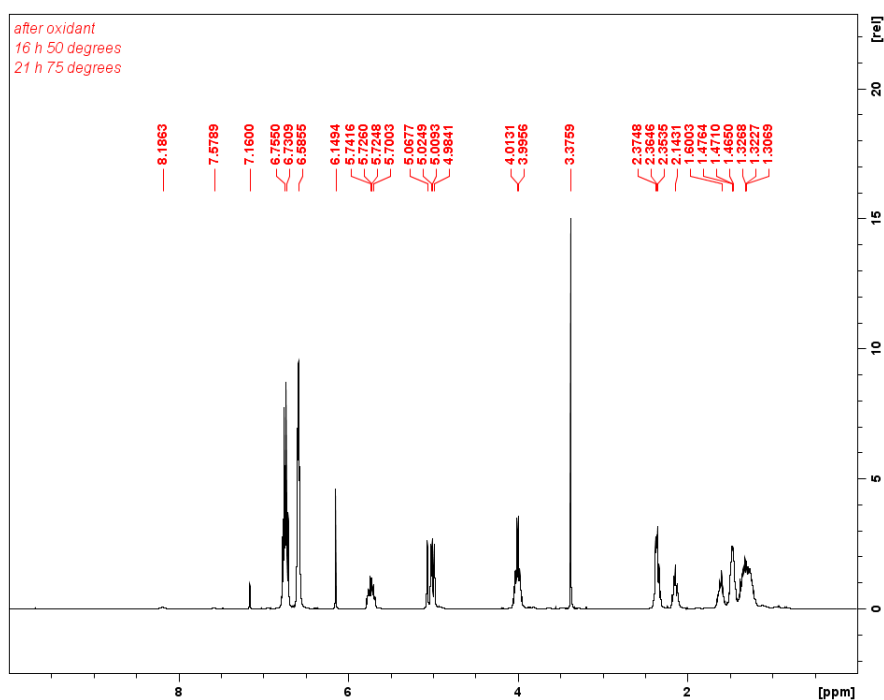


Figure F6.3. [(salfan)Zr(O'Bu)₂][BAR^F] and allyl-CL after heating overnight. ¹H NMR spectrum (C₆D₆ 300 MHz) ppm: 6.76 (difluorobenzene), 6.59 (difluorobenzene), 6.15 (TMB), 5.73 (m, 1H, CH₂=CH), 5.02 (m, 2H, CH₂=CH), 4.00 (m, 2H, OCH₂), 3.38 (TMB), 2.36 (m, 2H, O=CCHCH₂CH), 2.14 (m, 1H, O=CCH), 1.55 (m, 4H, CH₂CH₂CH₂CH₂O), 1.32 (m, 2H, CH₂CH₂CH₂CH₂O)

For comparison, [(salfan)Zr(O'Bu)₂][BAR^F] was generated independently and tested with allyl-CL as well as caprolactone (CL). CL showed complete conversion after one hour at 75 °C. Allyl-CL showed 90% conversion after 17 hours at 75 °C.

(salfan)Zr(O'Bu)₂ (0.15 mL, 0.005 mmol) was charged to a J-Young tube followed by ^{Ac}FcBAR^F (0.10 mL, 0.005 mmol) and TMB (0.15 mL 0.005 mmol). 0.07 mL of allyl CL (0.5 mmol) or 57 mg of CL was the added. Reaction was monitored to completion. Polymer was precipitated in cold methanol.

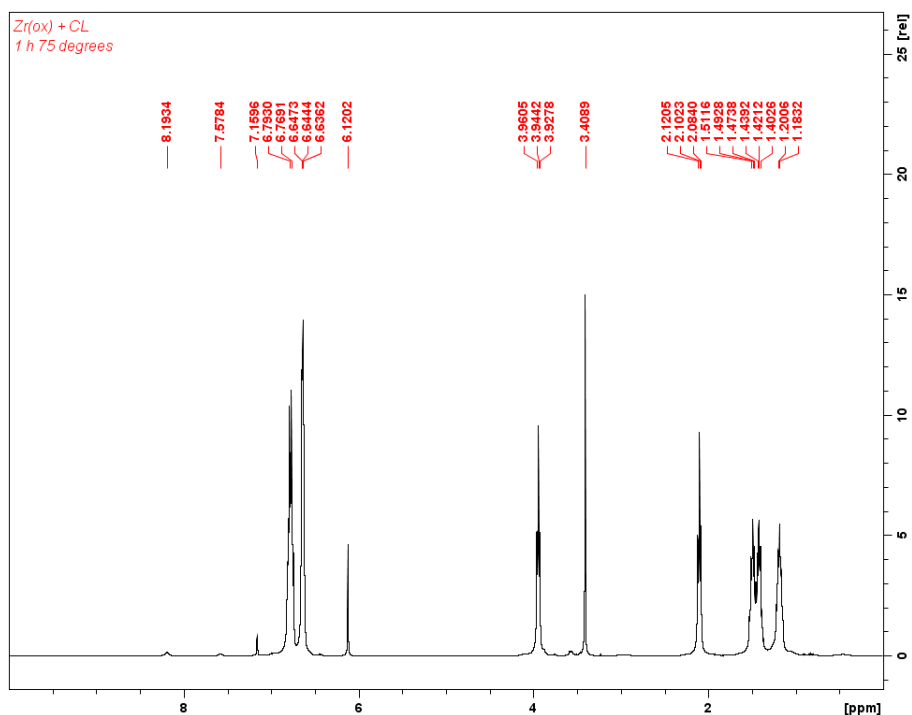


Figure F6.4. [(salfan)Zr(O'Bu)₂][BAR^F] and CL. ¹H NMR spectrum (C₆D₆ 300 MHz) ppm: 6.78 (difluorobenzene), 6.64 (difluorobenzene), 6.12 (TMB), 3.94 (m, 2H, OCH₂), 3.41 (TMB), 2.10 (m, 2H, O=CCH₂), 1.45 (m, 4H, OCH₂CH₂CH₂CH₂), 1.19 (m, 2H, OCH₂CH₂CH₂).

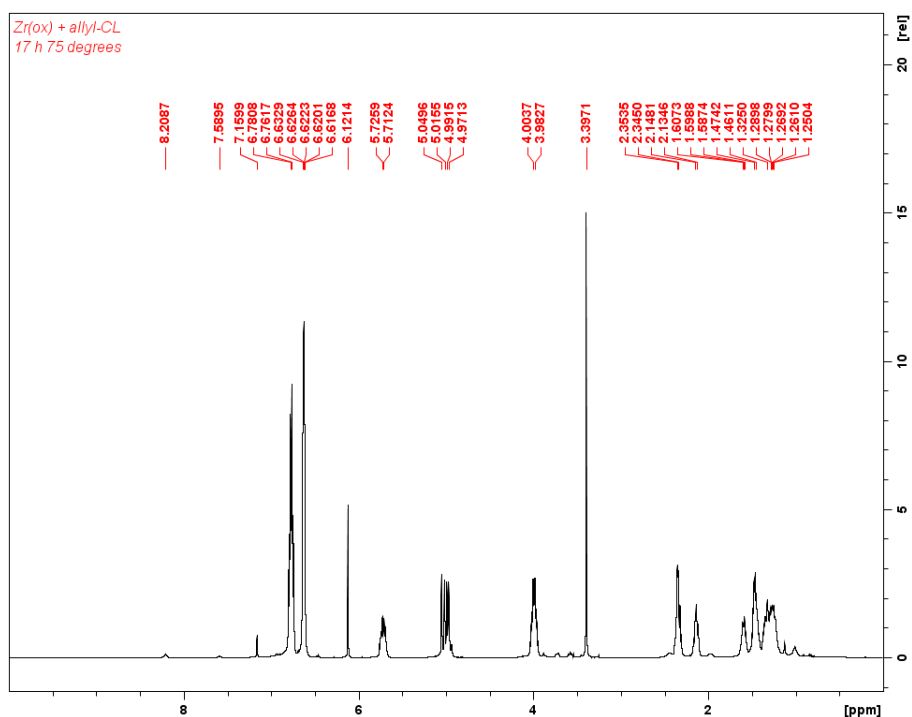


Figure F6.5. [(salfan)Zr(O'Bu)₂][BAR^F] and allyl-CL. ¹H NMR spectrum (C₆D₆ 300 MHz) ppm: 6.78 (difluorobenzene), 6.62 (difluorobenzene), 6.12 (TMB), 5.72 (m, 1H, CH₂=CH), 5.00 (m, 2H, CH₂=CH), 3.99 (m, 2H, OCH₂), 3.40 (TMB), 2.35 (m, 2H, O=CCHCH₂CH), 2.14 (m, 1H, O=CCH), 1.53 (m, 4H, CH₂CH₂CH₂CH₂O), 1.27 (m, 2H, CH₂CH₂CH₂CH₂O)

References

1. (a) R. Savka, S. Foro, M. Gallei, M. Rehahn, H. Plenio, *Chem. - Eur. J.*, 2013, **19**, 10655–10662.
(b) C. D. Varnado Jr., E. L. Rosen, M. S. Collins, V. M. Lynch, C. W. Bielawski, *Dalton Trans.* 2013, **42**, 13251–13264.
(c) A. Sauer, J.-C. Buffet, T. P. Spaniol, H. Nagaie, K. Mashima, J. Okuda, *Chem. Cat. Chem.*, 2013, **5**, 1088–1091.
2. E. M. Broderick, N. Guo, T. Wu, C. S. Vogel, C. Xu, J. Sutter, J. T. Miller, K. Meyer, T. Cantat, P. L. Diaconescu, *Chem. Commun.*, 2011, **47**, 9897–9899.
3. E. M. Broderick, N. Guo, C. S. Vogel, C. Xui, J. Sutter, J. T. Miller, K. Meyer, P. Mehrkhodavandi, P. L. Diaconescu, *J. Am. Chem. Soc.*, 2011, **133**, 9278–9281.
4. M. Abubekеров, S. M. Shepard, P. L. Diaconescu, *Eur. J. Inorg. Chem.*, 2016, **15**, 2634–2640.
5. J. Wei, M. N. Riffel, P. L. Diaconescu, *Macromolecules*, 2017, **50**, 1847–1861.
6. X. Wang, A. Thevenon, J. L. Brosmer, I. Yu, S. I. Khan, P. Mehrkhodavandi, P. L. Diaconescu, *J. Am. Chem. Soc.*, 2014, **136**, 11264–11267.
7. A. B. Biernesser, K. R. Delle Chiaie, J. B. Curley, J. A. Byers, *Angew. Chem.*, 2016, **55**, 5251–5254.
8. K. R. Delle Chiaie, L. M. Yablon, A. B. Biernesser, G. R. Michalowski, A. W. Sudyn, J. A. Byers, *Polym. Chem.*, 2016, **7**, 4675–4681.
9. S. M. Quan, X. Wang, R. Zhang, P. L. Diaconescu, *Macromolecules*, 2016, **49**, 6768–6778.
10. K. Matsumoto, B. Saito, T. Katsuki, *Chem Commun.*, 2007, **0**, 3619–3627.
11. (a) A. M. DiCiccio, G. W. Coates, *J. Am. Chem. Soc.*, 2011, **133**, 10724–10727.
(b) E. H. Nejad, C. G. W. Melis, T. J. Vermeer, C. E. Koning, R. Duchateau, *Macromolecules*, 2012, **45**, 1779–1776.
(c) J. M. Longo, M. J. Sanford, G. W. Coates, *Chem. Rev.*, 2016, **116**, 15167–15197.
12. F. Isnard, M. Lamberti, C. Pellicchia, M. Mazzeo, *Chem. Cat. Chem.*, 2017, **9**, 2972–2979.
13. E. M. Pelegri-O’Day, S. J. Paluck, H. D. Maynard, *J. Am. Chem. Soc.*, 2017, **139**, 1145–1154.